

EAS Publications Series, Volume 46, 2011



**PAHs and the Universe: A Symposium to
Celebrate the 25th Anniversary of the PAH
Hypothesis**

Toulouse, France
31 May - 04 June, 2010

Edited by: *C. Joblin and A.G.G.M. Tielens*



17 avenue du Hoggar, PA de Courtabœuf, B.P. 112, 91944 Les Ulis cedex A, France

First pages of all issues in the series and full-text articles
in PDF format are available to registered users at:

<http://www.eas-journal.org>

Sponsors

Centre National de la Recherche Scientifique (CNRS-INSU, INP, INC)

Université Toulouse III - Paul Sabatier (UPS)

Centre National d'Études Spatiales (CNES)

Région Midi-Pyrénées

Ministère de l'Enseignement Supérieur et de la Recherche

European Space Agency (ESA)

IRSAMC-UPS

Réseau de Chimie Théorique

Département de la Haute Garonne

Scientific Organizing Committee

V. Bierbaum, University of Boulder, USA

L. d'Hendecourt, IAS, Paris, France

T. Geballe, Gemini Observatory, Hawaii, USA

K. Gordon, STScI, Baltimore, USA

T. Henning, MPIA, Heidelberg, Germany

E. Herbst, Ohio State University, USA

C. Joblin (co-chair), CESR, Toulouse, France

R. Kennicutt, University of Cambridge, USA

D. Lutz, MPE, Garching, Germany

T. Onaka, University of Tokyo, Japan

J.-L. Puget, IAS, Paris, France

F. Salama, NASA ARC, USA

S. Schlemmer, University of Cologne, Germany

F. Spiegelman, LCPQ, Toulouse, France

A. Tielens (co-chair), Leiden Observatory, The Netherlands

Cover Figure

New light on and from PAHs: From Orion to Le Pont de Toulouse. Image credits: Orion as seen by Spitzer, NASA/JPL-Caltech/S.T. Megeath (University of Toledo, Ohio); Toulouse, L. Montier.

Indexed in: ADS, Current Contents Proceedings – Engineering & Physical Sciences, ISTEP®/ISI Proceedings, ISTEP/ISI CDROM Proceedings.

ISBN 978-2-7598-0624-9

EDP Sciences Les Ulis

ISSN 1633-4760

e-ISSN 1638-1963

This work is subject to copyright. All rights are reserved, whether the whole or part of the material is concerned, specifically the rights of translation, reprinting, re-use of illustrations, recitation, broad-casting, reproduction on microfilms or in other ways, and storage in data banks. Duplication of this publication or parts thereof is only permitted under the provisions of the French Copyright law of March 11, 1957. Violations fall under the prosecution act of the French Copyright Law.

© EAS, EDP Sciences 2011

Printed in UK

Foreword

Some twenty five years ago, driven by ground-based, airborne, and IRAS observations, the PAH hypothesis was first formulated to explain the strong emission features that dominate the mid-infrared spectra of most bright astronomical sources. In this hypothesis, the well-known infrared emission features – at 3.3, 6.2, 7.7, 8.6, and 11.2 μm – were attributed to large (<50 C-atom) Polycyclic Aromatic Hydrocarbon (PAH) molecules that are pumped by the strong far-ultraviolet photon flux from nearby stars. Since then, spectroscopy using the Short Wavelength Spectrometer and ISOCAM on the Infrared Space Observatory launched by the European Space Agency in 1995, the InfraRed Spectrograph on the Spitzer Space Telescope launched by NASA in 2005 and the InfraRed Camera onboard the Japanese AKARI satellite launched in 2006 have revealed the richness of the interstellar infrared emission spectrum and the variations therein. These spectral variations reflect variations in the molecular characteristics of the PAH family, reflecting the local physical and chemical conditions of the emitting regions. Parallel to these observational developments, experimental and theoretical studies of the physical and chemical properties of astrophysically relevant PAHs have really taken off. Such studies aim at elucidating the intrinsic infrared, visible, and ultraviolet properties of large PAH molecules and their dependence on molecular characteristics. In addition, dedicated experiments are performed to study the origin, evolution, and chemical role of PAHs in the interstellar medium. It is clear that this field has really taken off and the PAH hypothesis has evolved into the reigning paradigm.

Observations have shown that PAH molecules are abundant and ubiquitous in the interstellar medium. Conversely, PAHs may also be a dominant “force” in the interstellar medium, dominating the photoelectric heating of interstellar gas and may be important for the ionization balance inside dense molecular cloud cores. While much progress has been made, still more remains to be discovered including the role of derivative species such as nitrogenated PAHs, PAH clusters and PAH complexes with metals, and the relationship between PAH molecules and carbonaceous grains including Hydrogenated Amorphous Carbon and diamond. PAHs may also provide a catalytic surface for the formation of, for example, molecular hydrogen. Furthermore, photolysis of PAH related species may provide a source of small hydrocarbons particularly in regions rich in UV photons.

We are now reaching a stage where we can start to use the observations of the IR emission spectrum as diagnostic tools to determine the physical conditions in the emitting regions of, in particular, regions of star and planet formation. Because the IR emission features dominate the IR spectrum of regions of massive star formation, these bands are also often used as proxies to determine the importance of star formation on galactic scales. Specifically, the importance of star formation versus AGN activity for the luminosity source of (Ultra)Luminous InfraRed Galaxies is based upon a quantitative interpretation of the observed PAH emission from galactic nuclei. At this moment, the Herschel and Planck ESA space missions are geared towards probing the low frequency bending modes of PAHs

and the rotational transitions of this spinning dust component. The James Webb Space Telescope and the Stratospheric Observatory for Infrared Astronomy, and the possible SPICA mission will provide in the coming years spectral imaging at high resolution and increased sensitivity. The future for the PAH universe looks bright.

We considered it therefore timely to organize a scientific meeting “*PAHs and the universe: A Symposium to celebrate the 25th anniversary of the PAH hypothesis*” with the goal to bring together experts in the area of astronomical observations, laboratory studies, and astronomical modeling of interstellar PAHs to discuss the state-of-the-art and to chart the future. Moreover, and more importantly, two of the pioneers of the interstellar PAH hypothesis – Lou Allamandola and Alain Léger – are reaching a milestone in their life – they soon will be 65 years young – and this meeting provided a good occasion to celebrate their accomplishments in opening up and driving this field.

The symposium was hosted in Toulouse (France) by the CESR and LCPQ (University of Toulouse and CNRS), May 31 through June 4th, 2010. We are very grateful for their hospitality and want to acknowledge the hard work by the local organizing committee that was instrumental in making this symposium such a resounding success. This symposium would not have been possible without the generous financial support by INSU-CNRS, Université Paul Sabatier (UPS), CNES, Région Midi-Pyrénées, Ministère de l’Enseignement Supérieur et de la Recherche, ESA, IRSAMC-UPS, INC-CNRS, Réseau de chimie théorique, INP-CNRS, and Département de la Haute Garonne. We would like to thank the Scientific Organizing Committee for the well-conceived scientific program, which highlighted all aspects of interstellar PAHs. We also thank the participants for the reviews, contributed papers, and poster papers and the stimulating discussions. The PAH symposium was attended by some 130 scientists from 18 different countries and 5 continents, all united in their quest for the molecular Universe.

This is the first time in 25 years that a symposium was organized on this important topic and we felt that this warranted the publication of proceedings. The goal of the proceedings paralleled those of the symposium: to publish a lasting legacy of this meeting summarizing the field and charting the future. We have asked the reviewers to write review chapters at a graduate level pedagogical fashion to yield a reference text for years to come. In addition, these proceedings include the contributed papers, which provide a cross cut of the field as it is today. In reading these papers, we have been impressed by the hard work and care with which they were written. A symposium and its proceedings are only as good as the participants and speakers make it and, from that perspective, this meeting was top-notch.

Mountain View & Toulouse
Xander Tielens & Christine Joblin

December 9, 2010

List of Participants

ACKE	Bram	Instit. Astronomy, K.U. Leuven, Belgium
ALATA	Ivan	Centre Laser, Univ. Paris Sud 11, France
ALLAMANDOLA	Louis	NASA Ames Research Center, CA, USA
ALVARO GALUE	Hector	FOM Rijnhuizen, The Netherlands
BAOUCHE	SAOUD	Paris Observatory, France
BARTHEL	Robert	Instit. Phys. Chem., KIT, Karlsruhe, Germany
BASIRE	Marie	ISMO, Univ. Paris Sud/CNRS, France
BEARPARK	Michael	Imperial College London, UK
BECKER	Luann	Johns Hopkins Univ., Baltimore, USA
BERNARD	Jean-Philippe	CESR, Univ. Toulouse/CNRS, France
BERNE	Olivier	Leiden Observatory, The Netherlands
BIENNIER	Ludovic	IPR, Univ. Rennes 1/CNRS, France
BIERBAUM	Veronica	Univ. Colorado, Boulder, USA
BLANCHET	Valérie	LCAR-IRSAMC, Univ. Toulouse/CNRS, France
BOERSMA	Christiaan	NASA Ames Research Center, CA, USA
BOGGIO-PASQUA	Martial	LCPQ, Univ. Toulouse/CNRS, France
BOULANGER	François	IAS, Univ. Paris Sud/CNRS, France
BOUWMAN	Jordy	Leiden Observatory, The Netherlands
BRECHIGNAC	Philippe	ISMO, Univ. Paris Sud/CNRS, France
BRYSON	Kathryn	NASA Ames Research Center, CA, USA
CALZETTI	Daniela	Astronomy Dept., Univ. Massachusetts, USA
CAMI	Jan	Univ. Western Ontario & SETI Institut., Canada
CANDIAN	Alessandra	University of Nottingham, UK
CARPENTIER	Yvain	Max-Planck-Institut. Astron., Jena, Germany
CERNICHARO	Jose	Centro de Astrobiologia INTA-CSIC, Spain
CHANDRASEKARAN	Vijayanand	ISM, Univ. Bordeaux 1/CNRS, France
CHERCHNEFF	Isabelle	Universitaet Basel, Switzerland
CONTRERAS	Cesar	NASA Ames Research Center, CA, USA
COUPEAUD	Anne	CESR, Univ. Toulouse/CNRS, France
COX	Nick	Instit. Astronomy, K.U. Leuven, Belgium
D'HENDECOURT	Louis	IAS, Univ. Paris Sud/CNRS, France
DALLE ORE	Cristina	SETI Institute/ NASA Ames, CA, USA
DARTOIS	Emmanuel	IAS, Univ. Paris Sud/CNRS, France
DEDONDER	Claude	CNRS/Univ. Paris-Sud 11, France
DEMYK	Karine	CESR, Univ. Toulouse/CNRS, France
DOPFER	Otto	TU Berlin, Germany
DRAINE	Bruce	Princeton University, USA
ELLINGER	Yves	LCT - Univ. Pierre et Marie Curie/ CNRS, France
FERAUD	Géraldine	ISMO, Univ. Paris Sud/CNRS, France
FRIHA	Hela	ISMO, Univ. Paris Sud/CNRS, France
GADALLAH	Kamel	University of Jena, Germany
GADEA	Florent Xavier	LCPQ, Univ. Toulouse/CNRS, France
GADALLAH	Kamel	University of Jena, Germany

GADEA	Florent Xavier	LCPQ, Univ. Toulouse/CNRS, France
GALLIANO	Frédéric	AIM, CEA/Saclay, France
GEBALLE	Tom	Gemini Observatory, Hawaii, USA
GEPPERT	Wolf	Stockholm University, Sweden
GIARD	Martin	CESR, Univ. Toulouse/CNRS, France
GODARD	Marie	IAS, Univ. Paris Sud/CNRS, France
GORDON	Karl	Space Telescope Science Instit., Baltimore, USA
GUENNOUN	Zohra	ISM, Univ. Bordeaux 1/CNRS, France
HAMMONDS	Mark	University of Nottingham, UK
HANNACHI	Yacine	ISM, Univ. Bordeaux 1/CNRS, France
HARAGUCHI	Kentaro	Nagoya University, Japan
HEBDEN	Kerry	University of Manchester, UK
HELTON	L. Andrew	University of Minnesota, Minneapolis, USA
HERBST	Eric	Ohio State University, Columbus, USA
HOLM	Anne I. S.	Stockholm University, Sweden
HONY	Sacha	AIM, CEA/Saclay, France
HORNEKAER	Liv	Aarhus University, Denmark
HUNT	Leslie	INAF-Osserv. Astrof. Arcetri, Italy
IGLESIAS-GROTH	Susana	Instit. Astrofísica de Canarias, Spain
IVANOVSKAYA	Viktoria	ISMO, Univ. Paris Sud/CNRS, France
JÄGER	Cornelia	Friedrich Schiller Univ., Jena, Germany
JOALLAND	Baptiste	CESR/LCPQ - Univ. Toulouse/CNRS, France
JOBLIN	Christine	CESR, Univ. Toulouse/CNRS, France
JØRGENSEN	Bjarke	Aarhus University, Denmark
JOUVET	Christophe	ISMO, Univ. Paris Sud/CNRS, France
KAMP	Inga	Kapteyn Astron. Institut., Groningen, The Netherlands
KANEDA	Hidehiro	Nagoya University, Japan
KAZMIERCZAK	Maja	Nicolaus Copernicus Univ., Torun, Poland
KIM	Ji Hoon	Seoul National Univ., Republic of Korea
KLÆRKE	Benedikte	Aarhus University, Denmark
KRELOWSKI	Jacek	Nicolaus Copernicus Univ., Torun, Poland
LAGACHE	Guilaine	IAS, Univ. Paris Sud/CNRS, France
LAWICKI	Arkadiusz	CIMAP - GANIL, France
LE BOURLOT	Jacques	Univ. Paris-Diderot, Paris 7 & Obs. Paris, France
LE PADELLEC	Arnaud	CESR, Univ. Toulouse/CNRS, France
LE PAGE	Valéry	Univ. Colorado, Boulder, USA
LEE	Timothy	NASA Ames Research Center, CA, USA
LEGER	Alain	IAS, Univ. Paris Sud/CNRS, France
LI	Aigen	University of Missouri, Columbia, USA
MAHADEVAPPA	Naganathappa	Swami Ramanand Teerth Marathwada Univ., India
MARBLE	Andy	Steward Observatory, Tucson, USA
MASCETTI	Joëlle	ISM, Univ. Bordeaux 1/CNRS, France
MASON	Rachel	Gemini Observatory, Hawaii, USA
MAURETTE	Michel	CSNSM, Univ. Paris Sud/CNRS, France
MAYER	Paul	Chemistry Dep., Univ. Ottawa, Canada
MENNELLA	Vito	INAF-Osserv. Astron. Capodimonte, Italy
MISSELT	Karl	Steward Observatory, Tucson, USA

MONTILLAUD	Julien	CESR, Univ. Toulouse/CNRS, France
MULAS	Giacomo	INAF - Osserv. Astron. Cagliari, Italy
NILSSON	Louis	Aarhus University, Denmark
O'DOWD	Matt	Columbia University, New York, USA
OHSAWA	Ryou	Grad. School of Science, Univ. Tokyo, Japan
OKADA	Yoko	I. Physik. Institut, Univ. Köln, Germany
OMONT	Alain	IAP, Univ. Pierre et Marie Curie/CNRS, France
ONAKA	Takashi	University of Tokyo, Japan
OOMENS	Jos	FOM Rijnhuizen, The Netherlands
OTAGURO	Jacqueline	Western Ontario Univ., London, Canada
PARNEIX	Pascal	ISMO, Univ. Paris Sud/CNRS, France
PATHAK	Amit	Indian Instit. Astrophysics, Bangalore, India
PAUZAT	Françoise	LCT - Univ. Pierre et Marie Curie/ CNRS, France
PEETERS	Els	Univ. Western Ontario & SETI Instit., Canada
PILLERI	Paolo	CESR, Univ. Toulouse/CNRS, France
PINO	Thomas	ISMO, Univ. Paris Sud/CNRS, France
PUGET	Jean-Loup	IAS, Univ. Paris Sud/CNRS, France
RAPACIOLI	Mathias	LCPQ, Univ. Toulouse/CNRS, France
RASTOGI	Shantanu	Physics Dept., DDU Gorakhpur Univ., India
RHO	Jeonghee	California Institute of Technology, USA
RICKETTS	Claire	NASA Ames Research Center, CA, USA
RISTORCELLI	Isabelle	CESR, Univ. Toulouse/CNRS, France
ROUILLE	Gaël	Universität Jena, Germany
ROUSSEAU	Patrick	CIMAP - GANIL, France
SAKON	Itsuki	University of Tokyo, Japan
SALAMA	Farid	NASA Ames Research Center, CA, USA
SALES	Dinalva Aires	Univer. Federal Rio Grande do Sul, Porto Alegre, Brazil
SANDSTROM	Karin	Max-Planck-Instit. Astron., Heidelberg, Germany
SARRE	Peter	University of Nottingham, UK
SELLGREN	Kris	Ohio State University, Columbus, USA
SHENOY	Sachindev	NASA Ames Research Center, CA, USA
SIEBENMORGEN	Ralf	ESO, Garching. Germany
SIMON	Aude	LCPQ, Univ. Toulouse/CNRS, France
SMITH	Erin	NASA Ames Research Center, CA, USA
SMOLDERS	Kristof	Instit. Astronomy, K.U. Leuven, Belgium
SNOW	Theodore	Univ. Colorado, Boulder, USA
SPIEGELMAN	Fernand	LCPQ, Univ. Toulouse/CNRS, France
STEGLICH	Mathias	Universität Jena, Germany
TALBI	Dahbia	GRAAL, Univ. Montpellier 2/CNRS, France
TEILLET-BILLY	Dominique	ISMO, Univ. Paris Sud/CNRS, France
THROWER	John	Aarhus University, Denmark
TIELENS	Alexander	Leiden Observatory, The Netherlands
VERSTRAETE	Laurent	IAS, Univ. Paris Sud/CNRS, France
WALKER	Mark	Manly Astrophysics, Australia
WOODS	Paul	University of Manchester, UK

Contents

<i>Foreword</i>	III
<i>List of participants</i>	V
Introduction	
25 Years of PAH Hypothesis A.G.G.M. Tielens	3
Rich IR Spectra of Interstellar PAHs	
Astronomical Observations of the PAH Emission Bands E. Peeters	13
Astronomical Models of PAHs and Dust B.T. Draine	29
Dialectics of the PAH Abundance Trend with Metallicity F. Galliano	43
The Shape of Mid-IR PAH Bands in the Universe O. Berné, P. Pilleri and C. Joblin	49
AKARI Near-Infrared Spectroscopy of 3 Micron PAH and 4 Micron PAD Features T. Onaka, I. Sakon, R. Ohsawa, T. Shimonishi, Y. Okada, M. Tanaka and H. Kaneda	55
Laboratory Infrared Spectroscopy of PAHs J. Oomens	61
Computational IR Spectroscopy for PAHs: From the Early Years to the Present Status F. Pauzat	75

Modeling the Anharmonic Infrared Emission Spectra of PAHs: Application to the Pyrene Cation M. Basire, P. Parneix, T. Pino, Ph. Bréchnignac and F. Calvo	95
Laboratory Spectroscopy of Protonated PAH Molecules Relevant For Interstellar Chemistry O. Dopfer	103
The NASA Ames PAH IR Spectroscopic Database and the far-IR C. Boersma, L.J. Allamandola, C.W. Bauschlicher, Jr., A. Ricca, J. Cami, E. Peeters, F. Sánchez de Armas, G. Puerta Saborido, A.L. Mattioda and D.M. Hudgins	109
Analyzing Astronomical Observations with the NASA Ames PAH Database J. Cami	117
Search for far-IR PAH Bands with Herschel: Modelling and Observational Approaches C. Joblin, G. Mulas, G. Mallocci and E. Bergin & the HEXOS consortium	123

PAHs and Star Formation in the Near and Far Universe

Polycyclic Aromatic Hydrocarbons as Star Formation Rate Indicators D. Calzetti	133
PAHs and the ISM in Metal-Poor Starbursts L.K. Hunt, Y.I. Izotov, M. Sauvage and T.X. Thuan	143
Introduction to AMUSES: AKARI Survey with a Window of Opportunity J.H. Kim, M. Im, H.M. Lee, M.G. Lee and the AMUSES team	149

The Lifecycle of PAHs in Space

PAH Evolution in the Harsh Environment of the ISM H. Kaneda, T. Onaka, I. Sakon, D. Ishihara, A. Mouri, M. Yamagishi and A. Yasuda	157
PAH and Dust Processing in Supernova Remnants J. Rho, M. Andersen, A. Tappe, W.T. Reach, J.P. Bernard and J. Hewitt	169

The Formation of Polycyclic Aromatic Hydrocarbons in Evolved Circumstellar Environments	
I. Cherchneff.....	177
Insights into the Condensation of PAHs in the Envelope of IRC +10216	
L. Biennier, H. Sabbah, S.J. Klippenstein, V. Chandrasekaran, I.R. Sims and B.R. Rowe.....	191
Formation and Evolution of Circumstellar and Interstellar PAHs: A Laboratory Study	
C.S. Contreras, C.L. Ricketts and F. Salama.....	201
Confirmation of C ₆₀ in the Reflection Nebula NGC 7023	
K. Sellgren, M.W. Werner, J.G. Ingalls, J.D.T. Smith, T.M. Carleton and C. Joblin.....	209
The Spitzer Surveys of the Small Magellanic Cloud: Insights into the Life-Cycle of Polycyclic Aromatic Hydrocarbons	
K.M. Sandstrom, A.D. Bolatto, B.T. Draine, C. Bot and S. Stanimirovic.....	215
PAH-related Very Small Grains in Photodissociation Regions: Implications from Molecular Simulations	
M. Rapacioli, F. Spiegelman, B. Joalland, A. Simon, A. Mirtschink, C. Joblin, J. Montillaud, O. Berné and D. Talbi.....	223
The Formation of Benzene in Dense Environments	
P.M. Woods.....	235
Experimental Studies of the Dissociative Recombination Processes for the C ₆ D ₆ ⁺ and C ₆ D ₇ ⁺ Ions	
M. Hamberg, E. Vigren, R.D. Thomas, V. Zhaunerchyk, M. Zhang, S. Trippel, M. Kaminska, I. Kashperka, M. af Ugglas, A. Källberg, A. Simonsson, A. Paál, J. Semaniak, M. Larsson and W.D. Geppert.....	241
VUV Photochemistry of PAHs Trapped in Interstellar Water Ice	
J. Bouwman, H.M. Cuppen, L.J. Allamandola and H. Linnartz.....	251
PAHs in Regions of Planet Formation	
Observations of Hydrocarbon Emission in Disks Around Young Stars	
B. Acke.....	259
Evolution of PAHs in Protoplanetary Disks	
I. Kamp.....	271

PAH in Vectorized Three Dimensional Monte Carlo Dust Radiative Transfer Models R. Siebenmorgen, F. Heymann and E. Krügel.....	285
--	-----

PAHs and Carbonaceous Grains & Solar System Materials

From PAHs to Solid Carbon C. Jäger, H. Mutschke, T. Henning and F. Huisken.....	293
PAHs and Astrobiology L.J. Allamandola.....	305
Solid State Molecular Reactors in Space M. Maurette.....	319
Polycyclic Aromatic Hydrocarbons and the Extinction Curve G. Mulas, G. Mallocci, C. Joblin and C. Cecchi-Pestellini.....	327
The Diffuse Interstellar Bands in History and in the UV T.P. Snow and J.D. Destree.....	341
The PAH-DIB Hypothesis N.L.J. Cox.....	349
Electronic Spectroscopy of PAHs T. Pino, Y. Carpentier, G. Féraud, H. Friha, D.L. Kokkin, T.P. Troy, N. Chalyavi, Ph. Bréchnignac and T.W. Schmidt.....	355
Spectroscopy of Protonated and Deprotonated PAHs M. Hammonds, A. Pathak, A. Candian and P.J. Sarre.....	373
Observations of Interstellar Carbon Compounds E. Dartois.....	381
Interaction of Atomic Hydrogen with Carbon Grains V. Mennella.....	393
Near-Infrared Spectroscopy of Interstellar Dust F. Boulanger, T. Onaka, P. Pilleri and C. Joblin.....	399
Atypical Dust Species in the Ejecta of Classical Novae L.A. Helton, A. Evans, C.E. Woodward and R.D. Gehrz.....	407

The Role of PAHs in the Interstellar Medium

The Role of PAHs in the Physics of the Interstellar Medium L. Verstraete	415
PAHs and the Chemistry of the ISM V.M. Bierbaum, V. Le Page and T.P. Snow	427
[FePAH] ⁺ Complexes and [Fe _x PAH _y] ⁺ Clusters in the Interstellar Medium: Stability and Spectroscopy A. Simon, M. Rapacioli, F. Spiegelman and C. Joblin	441
Modelling the Physical and Chemical Evolution of PAHs and PAH-related Species in Astrophysical Environments J. Montillaud, C. Joblin and D. Toublanc	447
Superhydrogenated PAHs: Catalytic Formation of H ₂ J.D. Thrower, L. Nilsson, B. Jørgensen, S. Baouche, R. Balog, A.C. Luntz, I. Stensgaard, E. Rauls and L. Hornekær	453

Summary of the Meeting

Summary of the Meeting A. Omont	463
Author Index	469
Astronomical Object Index	471
Chemical Compound Index	473
Subject Index	475

Introduction

25 YEARS OF PAH HYPOTHESIS

A.G.G.M. Tielens¹

Abstract. Strong IR emission features at 3.3, 6.2, 7.7, 8.6, and 11.2 μm are a common characteristic of the interstellar medium of the Milky Way and nearby galaxies and out to redshifts of ~ 3 . Here, we review the history of the PAH hypothesis which attributes these emission features to vibrational fluorescence of large (~ 50 carbon-atom Polycyclic Aromatic Hydrocarbon molecules pumped by ultraviolet photons from nearby stars or the average interstellar radiation field. Over the last 25 years, our insight in the characteristics of these molecules and their role in the Universe has greatly improved and the PAH hypothesis is alive and well; not in the least due a remarkable adaptability. Not surprisingly, the precise characteristics of these species remains to be defined.

1 The early years

Over the last three decades our understanding of the interstellar medium has increased dramatically. To a large extent this has been driven by rapid developments in infrared detector technology driven by the Cold War. Sensitive infrared spectrometers operating in all the infrared windows are now standard on all major ground-based infrared observatories and major infrared space missions have probed the Universe at all infrared wavelengths. As soon as the infrared sky opened up for spectroscopy in the early 70ies, Gillett *et al.* (1973) discovered broad emission features in the L (3 μm) and N (10 μm) band windows (Fig. 1). While a good fit could be obtained to the profile and peak position of the 11.3 μm band with carbonates, air-borne observatories refuted this identification since the strong band at 6.85 μm was not detected (Russell *et al.* 1977; Willner *et al.* 1979). Instead, these observations revealed that the the 3.3 and 11.3 μm bands were part of a set of strong bands – together with bands at 6.2, 7.7, and 8.6 μm – that occurred together. These and subsequent observations established that these broad

¹ Leiden Observatory, Leiden University, PO Box 9513, Leiden, The Netherlands

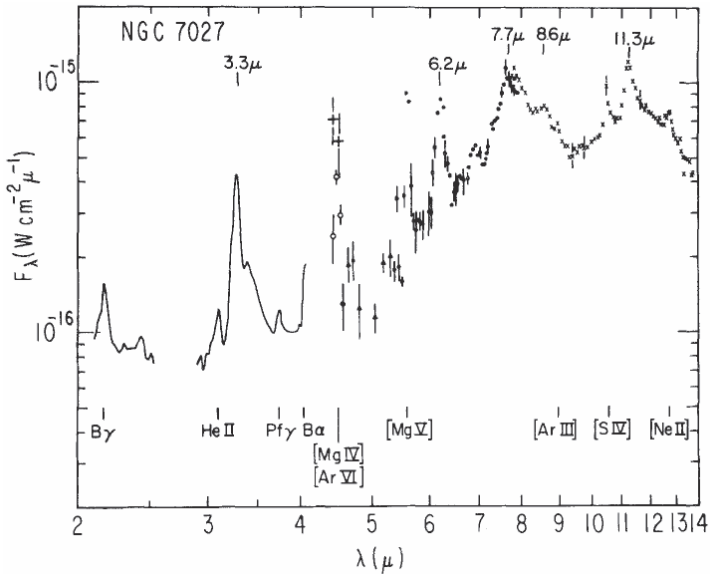


Fig. 1. The first overview spectrum of the PAH emission bands obtained from the ground in the L and N band windows and from the Kuiper Airborne Observatory (5–8 μm). Taken from the review by Willner *et al.* (1979).

IR emission features were a common characteristic of all objects where strong ultraviolet (UV) photons illuminated nearby material. Surprisingly, the nature of the objects seemed irrelevant: planetary nebulae, HII regions, reflection nebulae, and starburst galaxies all showed the same set of emission features. For almost a decade, identification of the carrier remained mysterious and these bands were collectively called the Unidentified InfraRed (UIR) bands. In the early 80ies, Duley & Williams (1981) realized that the peak positions of the UIR bands were very characteristic for aromatic materials and they proposed Hydrogenated Amorphous Carbon grains as the carriers. This proposal highlighted, however, an energetic issue inherent to all “bulk” grain approaches for the UIR bands: The emission originated far from the illuminating star where the radiative equilibrium temperature of grains is much too low ($T_d \sim 10 - 75$ K) to account for emission in the near- and mid-IR range. The next – and key step – was provided by Kris Sellgren 1984 who studied the IR emission from reflection nebula where this “energy” crisis was particularly rampant. She realized that the limited heat capacity of very small grains would result in large temperature excursions upon absorption of a single UV photon. Assuming a typical UV photon energy of 10 eV, a size of 50 C-atoms was implied. Independently, Léger & Puget (1984) and Allamandola *et al.* (1985) put these concepts together and the PAH hypothesis was born: the IR emission features at 3.3, 6.2, 7.7, and 11.3 μm are carried by large Polycyclic Aromatic Hydrocarbon molecules containing some 50 C-atoms and with a drived abundance

of 5–10% of the elemental carbon, these molecules – as a class – are the most abundant organic molecules in space.

In these early years, there was much discussion on the character of the carriers of the UIR bands and a plentitude of materials were proposed including PAH molecules, HAC grains, Quenched Carbonaceous Composite, and coal. At the Santa Clara conference at the end of the 80ies, the situation was summarized by the title of the session on the IR emission bands: “the Overidentified InfraRed bands” (Allamandola & Tielens 1989). All of these materials shared however the basic molecular structure of PAH molecules: benzene rings fused together into aromatic structures decorated with hydrogen at the edge, although many of these materials also contained other molecular structures often with other elements besides C and H. While the idea that the IR emission bands are carried by large molecules rather than grains is now undisputed, the exact structure of the species and in particular the presence of heteroatoms are still widely and vividly debated.

2 The PAH hypothesis

This heralded an exciting period where new ideas were announced at a rapid pace. In particular, at about the same time Kris Sellgren performed her breakthrough study, the IRAS mission discovered widespread emission at 12 and 25 μm in the diffuse interstellar medium of the Milky Way and other galaxies (Low *et al.* 1984). While there was no spectrum, it was quickly surmised that this emission was, in essence, the UIR bands at 7.7, 8.6, and 11.3 μm in combination with a continuum steeply rising towards longer wavelengths and all pumped by the interstellar radiation field (Puget *et al.* 1985). Hence, PAH molecules had to be ubiquitous throughout the interstellar medium. It was also realized that such molecules would also have absorption bands in the visible and UV range. In fact, the well-known Diffuse Interstellar Bands (DIBs) in the visible region of the spectrum might well be due to ionized or “radical” members of the PAH family (van der Zwet & Allamandola 1985; Crawford *et al.* 1985; Leger *et al.* 1985) and these bands may well hold important clues for the identification of individual interstellar PAHs. Because of their high abundance, it was also quickly clear that PAH molecules would have an enormous influence on the energy and ionization balance of interstellar gas both in the diffuse and dense media and hence on the phase structure, gas phase composition, and ambipolar diffusion of clouds (Verstraete *et al.* 1990; Lepp & Dalgarno 1988). Many of these ideas are summarized in the first reviews (Leger & Puget 1989; Allamandola *et al.* 1989). At this point, the PAH hypothesis can be summarized as:

- A substantial fraction of the carbon in the universe is in form of PAH molecules.
- A substantial fraction of the UV-visible radiative stellar energy in galaxies is “transformed” by PAHs to the mid-IR range.

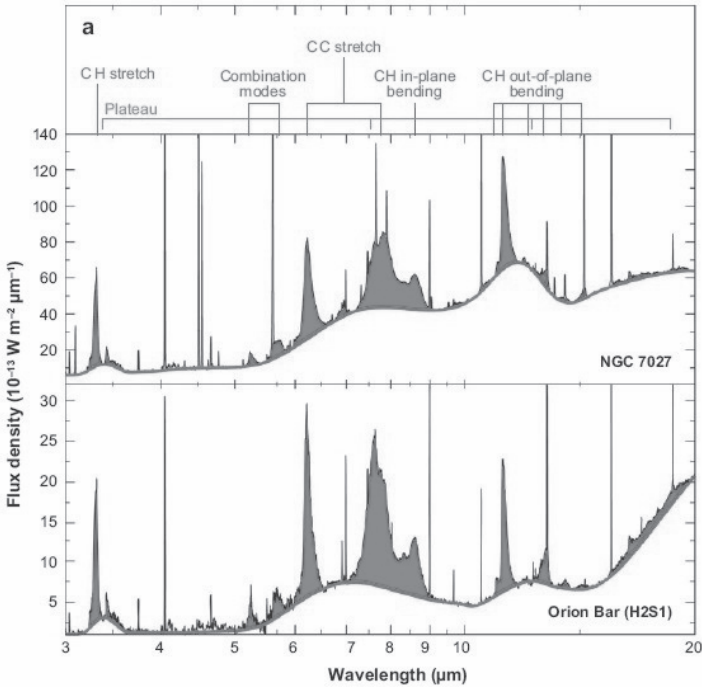


Fig. 2. The mid-infrared spectra of the PhotoDissociation Region in the Orion Bar and in the Planetary Nebulae, NGC 7027 are dominated by a rich set of emission features. Assignments of these features with vibrational modes of PAH molecules are labeled at the top. Figure adapted from Peeters *et al.* (2002).

- PAH molecules may provide observational signatures throughout the full spectral range from the extreme ultraviolet to the radio regime.
- PAHs are destroyed by hard UV radiation and thus they must be at the basis of a complex chemistry in the ISM.
- PAHs contribute to many key physical processes that affect the basic structure and evolution of the interstellar medium of galaxies.

3 The space-based era

The opening of the full infrared window by spectroscopic space missions further increased our knowledge of the interstellar PAHs. The Low Resolution Spectrometer (LRS) – a slitless spectrometer sensitive from 7.5 to 23 μm with a resolving power of $R \sim 20$ – on the InfraRed Astronomy Satellite (IRAS) has provided a first systematic overview (Olmon 1986) of the extent of the UIR bands. The Short Wavelength Spectrometer, SWS (de Graauw *et al.* 1996) on board of the Infrared

Space Observatory (ISO), represented the next big step forward by providing complete 2.5 to 45 μm spectra of essentially all IR-luminous galactic sources with resolutions ranging from ~ 200 up to ~ 2000 (for the brightest sources). The ISO mission also carried the ISOCAM (Cesarsky *et al.* 1996) aboard – which in CVF-mode provided spectral-imaging capabilities over ~ 1 square arcminute areas with pixel sizes of 3–6 arcseconds at a modest spectral resolution of 50 – that produced equally important studies of interstellar PAHs. Together these instruments revealed the dominance of the UIR bands for essentially all bright sources that they could study. The InfraRed Spectrometer (IRS) on board of the Spitzer Space Telescope – operating from 5.2 to 38 μm at low spectral resolution (60 to 130) and from 10 to 37 μm at moderate resolution ($R \sim 600$) but with greatly superior sensitivity over ISO (Houck *et al.* 2004) – allowed systematic spectroscopic studies of large samples of even weak sources in the Milky Way, nearby galaxies and in bright galactic nuclei out to redshifts of ~ 3 . All of these studies together demonstrated that PAHs dominate the spectra of almost all objects, including HII regions, reflection nebulae, young stellar objects, Planetary Nebulae, post-asymptotic-giant-branch objects, nuclei of galaxies, and ultraluminous infrared galaxies (ULIRGs). Moreover, the IR cirrus, the surfaces of dark clouds, and the general interstellar medium (ISM) of galaxies are set aglow in these IR emission features (for a recent review see Tielens 2005).

4 PAHs in the far Universe

The high sensitivity of the Spitzer instruments has demonstrated that PAH emission is present out to redshifts of $z \simeq 3$. Regular and starburst galaxies in the near Universe are readily surveyed with Spitzer and for example the SINGS sample as well as open and guaranteed time programs are rife with galaxies whose spectra are dominated by the mid-IR emission features (*e.g.*, Smith *et al.* 2007). With these studies, reliable criteria could be established that allow the use of the PAH emission strength as tracers of the star formation rate (see Calzetti, elsewhere in this volume). With IRS/Spitzer, galaxies much farther away could still be studied in the case of lens systems. The cloverleaf system at a redshift of 2.58 is a prime example (Fig. 3; Lutz *et al.* 2007) but many more studies exist (Rigby *et al.* 2008; Lutz *et al.* 2005). As a class, the ultraluminous sub-millimeter galaxies were also within reach out to redshifts of ~ 3 with Spitzer (Pope *et al.* 2008).

In a more indirect way, Spitzer probed distant but less luminous systems through source counts. The spectrum of a galaxy will shift further into the infrared as its distance increases. Because the PAH features dominate the mid 5–15 μm region and the continuum due to very small grains does not start to rise until 30 μm , there is a “trough” in the emission from normal or starburst galaxies (*e.g.*, non-ULIRGS). Then, as the PAH features shift into the 24 μm MIPS band at a redshift of $z \simeq 2$, this will lead to a “bump” in the source counts with flux (*e.g.*, distance; Fig. 4; Lagache *et al.* 2004). These studies demonstrate that PAHs are present at abundances of $\simeq 10\%$ of the elemental C in the star forming galaxies as far as Spitzer could probe and that the typical galaxy in these studies

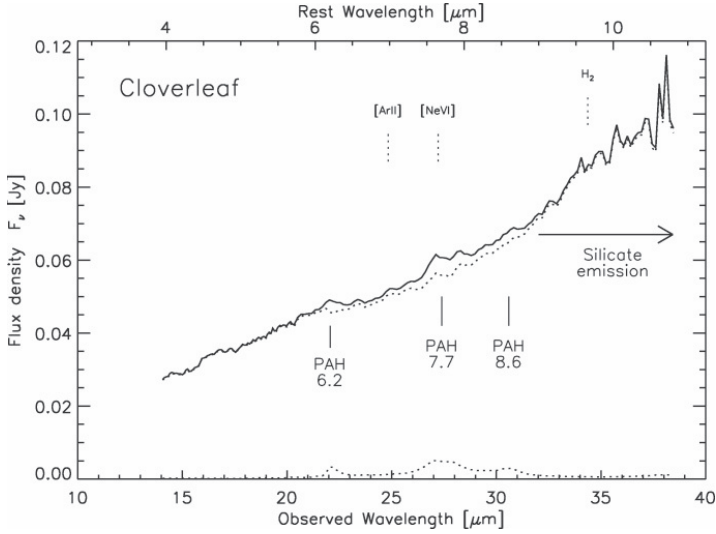


Fig. 3. The infrared spectrum of the Cloverleaf system is characterized by a strong continuum – reminiscent of AGN sources – with distinct PAH features superimposed. The strength of these PAH features indicates a star formation rate of some $10^3 M_{\odot}/\text{yr}$ (Lutz *et al.* 2007).

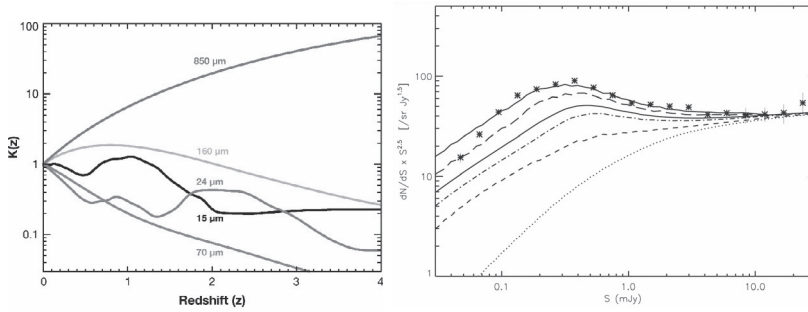


Fig. 4. (a) The K-band correction in different filters shows a “bump” when the PAH emission features shift through the wavelength range covered. (b) Redshift contribution to the number counts at $24 \mu\text{m}$. The dotted, dashed, dash-dotted, tripledot-dashed, and long-dashed lines correspond to the number counts up to redshifts 0.3, 0.8, 1, 1.3, and 2, respectively. Taken from Lagache *et al.* (2006) & (2004).

($L \sim 10^{11} - 10^{12} L_{\odot}$; star formation rates $20 - 130 M_{\odot}/\text{yr}$); $M \simeq 10^{10} - 10^{11} M_{\odot}$ has a mid-IR spectrum dominated by the PAH features. Moreover, the Cosmic InfraRed Background between 24 and $160 \mu\text{m}$ is dominated by these galaxies.

5 The future

With Herschel a new era has arrived and the study of the Universe at far-infrared and sub-millimeter wavelengths has come within reach. First and foremost, Herschel will provide a deeper understanding of the dark and cold or lukewarm local Universe through spectroscopic studies of *e.g.*, [OI], [CII], and CO lines in nearby galactic and extragalactic PAH-bright regions. This will link the mid-IR PAH characteristics in a direct way to the local physical conditions. In addition, spectroscopic studies may reveal far-IR spectral signatures of interstellar PAHs which might provide key information on the individual PAH molecules present in space (see Joblin *et al.*, elsewhere in this volume). Finally, with Herschel, deep source counts at long wavelengths, may reveal the signatures of PAH emission bands as they shift through the 70 μm PACS band at a redshift of ~ 7 . Indeed, at this point it is fair to expand the PAH hypothesis to its strongest version to read:

- PAH molecules formed in the ejecta of the first generation of stars polluting the Universe with heavy atoms in the form of molecules and dust.
- Ever since that time, PAHs are a key component of the “dust” budget of galaxies.
- Ever since that time, PAH molecules have converted a substantial fraction of the UV-visible radiative stellar energy in galaxies to the mid-IR range.
- Ever since that time, PAH molecules are at the basis of a complex chemistry in the ISM of galaxies.
- Ever since that time, PAHs contribute to many key physical processes that affect the basic structure and evolution of the interstellar medium of galaxies.

In short, PAHs are abundant and important throughout the full star forming era of the Universe.

6 Summary

Over the last 25 years, the PAH hypothesis has blossomed thanks to a multitude of observational, experimental, and theoretical studies and the dedicated efforts of many scientists. This conference overviews the current status of the field through the many reviews of key topics related to interstellar PAHs and a cross cut of the active research taking place through the many contributed papers. Overall, the PAH hypothesis has shown to be very robust (or adaptable for the more cynically inclined) and “weathered” the many new observational discoveries and insights that have developed over time. This of course, merely presents a challenge to the younger generation to expand on it so much that the originators might not recognize it anymore or even completely disprove it!

References

- Allamandola, L.J., & Tielens, A.G.G.M., *Interstellar Dust* (Kluwer: Dordrecht)
- Allamandola, L.J., Tielens, A.G.G.M., & Barker, J.R., 1985, *ApJ*, 290, L25
- Allamandola, L.J., Tielens, A.G.G.M., & Barker, J., 1989, *ApJS*, 71, 733
- Cesarsky, C., Abergel, A., Agnese, P., *et al.*, 1996, *A&A*, 315, L32
- Crawford, Tielens, A.G.G.M., & Allamandola, L.J., 1985, *ApJ*, 293, L45
- Duley, W., & Williams, D.A., 1981, *MNRAS*, 196, 269
- Gillett, F.C., Forest, W.J., & Merrill, K.M., 1973, *ApJ*, 183, 87
- de Graauw, Th., Haser, L.N., Beintema, D.A., *et al.*, 1996, *A&A*, 315, L49
- Houck, J., Roellig, T.L., van Cleve, J., *et al.*, 2004, *ApJS*, 154, 18
- Lagache, G., Dole, H., Puget, J.-L., *et al.*, 2004, *ApJS*, 154, 112
- Lagache, G., Puget, J.-L., & Dole, H., 2006, *ARAA*, 43, 727
- Léger, A., & d'Hendecourt, L., 1985, *A&A*, 146, 81
- Léger, A., & Puget, J.-L., 1984, *A&A*, 137, L5
- Lepp, S., & Dalgarno, A., 1988, *ApJ*, 324, 553
- Low, F.J., Young, E., Beintema, D.A., *et al.*, 1984, *ApJ*, 278, L19
- Lutz, D., Yan, L., Armus, L., *et al.*, 2005, *ApJ*, 632, L13
- Lutz, D., Sturm, E., Tacconi, L.J., *et al.*, 2007, *ApJ*, 661, L25
- Olmon, F., Raimond, E., Neugebauer, G., *et al.*, 1986, *A&AS*, 65, 607
- Peeters, E., Hony, S., Van Kerckhoven, C., *et al.*, 2002, *A&A*, 390, 1089
- Pope, A., Chary, R.-R., Alexander, D.M., *et al.*, 2008, *ApJ*, 675, 1171
- Puget, J.-L., Léger, A., & Boulanger, F., 1985, *A&A*, 142, L19
- Puget, J.-L., & Léger, A., 1989, *ARAA*, 27, 161
- Rigby, J.R., Marcillac, D., Egami, E., *et al.*, 2008, *ApJ*, 675, 262
- Russel, R., Soifer, B.T., & Willner, S.P., 1977, *ApJ*, 217, 149
- Sellgren, K., 1984, *ApJ*, 277, 623
- Smith, J.D.T., Draine, B.T., Dale, D.A., *et al.*, 2007, *ApJ*, 656, 770
- Tielens, A.G.G.M., 2008, *ARAA*, 46, 289
- van der Zwet, G., & Allamandola, L.J., 1985, *A&A*, 146, 76
- Verstraete, L., Leger, A., D'Hendecourt, L., Defourneau, D., & Dutuit, O., 1990, *A&A*, 237, 436
- Willner, S.P., Puetter, R.C., Russell, R.W., Soifer, B.T., 1979, *ApSS*, 65, 95

**Rich IR Spectra
of Interstellar PAHs**

ASTRONOMICAL OBSERVATIONS OF THE PAH EMISSION BANDS

E. Peeters^{1, 2}

Abstract. The infrared (IR) spectra of many galactic and extragalactic objects are dominated by emission features at 3.3, 6.2, 7.7, 8.6 and 11.2 μm , generally attributed to the IR fluorescence of Polycyclic Aromatic Hydrocarbon molecules (PAHs). These PAH bands have been found in a wide variety of environments throughout the Universe and contain up to 10% of the total power output of star-forming galaxies.

Ground-based telescopes, the Infrared Space Observatory (ISO) and the Spitzer Space Telescope revealed a plethora of weaker PAH bands and provided extensive evidence for significant variability in the PAH spectrum from source to source and spatially within sources. Here we review the spectral characteristics of astronomical PAHs, their dependence on the local physical conditions and the implications for the physical and chemical characteristics of the carriers.

1 Introduction

The IR spectra of objects associated with dust and gas – including evolved stars, reflection nebulae (RN), the interstellar medium (ISM), star-forming regions, and galaxies – are dominated by emission features at 3.3, 6.2, 7.7, 8.6 and 11.2 μm , the so-called unidentified infrared (UIR) bands. These bands are generally attributed to the IR fluorescence of Polycyclic Aromatic Hydrocarbon molecules (PAHs) and related species³. Observations show without any doubt that PAHs pervade the Universe. A remarkable 20–30% of the galactic IR radiation (and hence ~10–15% of the *total* galactic power budget) is emitted in the PAH bands and 10–20% of the cosmic carbon is locked up in these molecules. Hence, it may not come as a surprise

¹ Department of Physics and Astronomy, University of Western Ontario, London, ON N6A 3K7, Canada

² SETI Institute, 189 N. Bernardo Ave., Suite 100, Mountain View, CA 94043, USA

³In this paper, the term PAH bands/features is used to refer to these IR emission features.

that PAHs play a crucial role in several astrophysical and astrochemical processes as, for example, heating and cooling of the ISM and grain surface chemistry. In addition, PAH intensities are used to determine the star formation rate in galaxies, one of the key indicators for understanding galaxy formation and evolution (*cf.* Calzetti elsewhere in this volume).

Although the presence of PAHs in space is now generally accepted and PAHs are recognized as critical players in various processes, the characteristics of the emitting population remain unclear. Indeed, no single PAH molecule has been firmly identified to date. This identification is hampered by the fact that their main spectral signatures, the UIR bands, are due to vibrational modes primarily governed by the local physical conditions of the molecular environment (which is the same for all PAHs), and only show weak dependence on size and structure. However, there is no reason to despair. Although, to first order, the PAH bands are remarkably similar throughout the Universe, detailed observational studies have revealed a multitude of spectral variations in peak positions, shapes and (relative) intensities. This provides a tool to determine or further constrain the characteristics of the emitting population and to probe the physical conditions in the emitting regions. When properly calibrated, the PAH emission bands can serve as a probe of the physical conditions in regions near and far. Given their omnipresence, a PAH diagnostic toolbox will be extremely powerful.

Here, we give a concise overview of the observational properties of the PAH emission bands. Section 2 describes the astronomical PAH spectrum and Section 3 highlights the observed spectral characteristics of the PAH bands in terms of their intensity, peak position and profile. Section 4 reports on the spectral decomposition of the PAH spectra. The astronomical implications are discussed in Section 5 and Section 6 reviews the application of the PAH bands as a diagnostic tool. We conclude with a short summary and a look into the bright PAH future in Section 7.

2 The rich PAH spectrum

In the early 1970's, new IR instruments on ground-based and airborne telescopes revealed broad emission features at 3.3, 6.2, 7.7, 8.6 and 11.2 μm (*e.g.* Gillett *et al.* 1973; Geballe *et al.* 1985). In the past two decades, the unprecedented views of the IR Universe offered by ground-based telescopes, the Infrared Space Observatory (ISO) and the Spitzer Space Telescope showcased the spectral wealth of the PAH spectrum (see Fig. 1). Besides the main PAH bands, a plethora of weaker bands⁴ may be present. In addition, deuterated PAHs, PADs, have been tentatively detected at 4.4 and 4.65 μm (Peeters *et al.* 2004a). These bands are characteristic for the vibrational modes of PAHs (Fig. 1). In particular, the

⁴This can include bands at 3.4, 3.5, 5.25, 5.75, 6.0, 6.6, 6.9, 7.2-7.4, 8.2, 10.5, 10.8, 11.0, 12.0, 13.5, 14.2, 15.8, 16.4, 16.6, 17.0, 17.4 and, 17.8 μm . A band at 19 μm was originally considered as part of the PAH spectrum. However, its spatial distribution in the reflection nebula NGC 7023 is significantly distinct from that of the PAH bands (Sellgren *et al.* 2007). This feature is recently firmly assigned to C₆₀ (Cami *et al.* 2010; Sellgren *et al.* 2010, elsewhere in this volume).

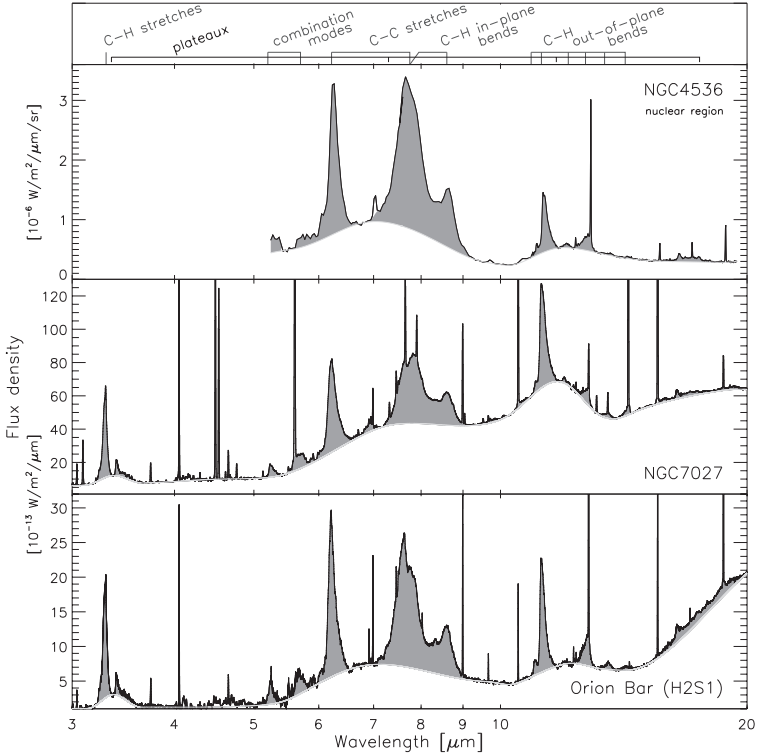


Fig. 1. The ISO-SWS spectra of the planetary nebula NGC 7027 and the Photo-Dissociation Region (PDR) at the Orion Bar and, the Spitzer-IRS spectrum of the nuclear region of NGC 4536, an H II -type galaxy, (SINGS legacy program; Kennicutt *et al.* 2003) illustrate the richness and variety of the PAH spectrum. Also indicated are the aromatic mode identifications of the major PAH bands.

$3.3 \mu\text{m}$ band is due to CH stretching modes and the $6.2 \mu\text{m}$ band to CC stretching modes. C-H in plane bending modes are responsible for the $8.6 \mu\text{m}$ band, coupled CC stretching and CH in-plane bending modes for the $7.7 \mu\text{m}$ complex and the CH out-of-plane bending modes for emission in the $10\text{--}15 \mu\text{m}$ region. At wavelengths longward of $15 \mu\text{m}$, the vibrations involve motions of the entire molecular skeleton and hence are more specific to each molecule. Several PAH bands exhibit highly asymmetric band profiles with a steep blue rise and a red-shaded wing (*e.g.*, 3.4 , 5.25 , 6.2 , $11.2 \mu\text{m}$; Barker *et al.* 1987; Roche *et al.* 1996; Pech *et al.* 2002; Verstraete *et al.* 2001) while other PAH bands exhibit fairly symmetric profiles (*e.g.*, 3.3 , $8.6 \mu\text{m}$ bands). The asymmetry of the $12.7 \mu\text{m}$ band is exceptional as it shows a blue-shaded wing with a steep red decline. The $7.7 \mu\text{m}$ complex is unique and is comprised of at least 2 components: the first peaking at $\sim 7.6 \mu\text{m}$ and the second between $7.8\text{--}8 \mu\text{m}$ (*e.g.* Bregman 1989). Additional substructure

at $8.2 \mu\text{m}$ is fairly common and few sources show substructure near $7.2\text{--}7.5 \mu\text{m}$ (*e.g.* Moutou *et al.* 1999; Peeters *et al.* 2002). The PAH bands are often perched on top of broad emission plateaus at roughly $3.2\text{--}3.6$, $6\text{--}9$, $11\text{--}14 \mu\text{m}$ (note that various methods are applied to distinguish between PAH bands and plateaus; see Sect. 3.1 for details). Several H II regions and planetary nebulae (PNe) also have broad emission between $15\text{--}20 \mu\text{m}$ with sometimes on top the 16.4 and $17.4 \mu\text{m}$ bands. This is quite different from the collection of weaker bands as seen in *e.g.* RNe and galaxies (*e.g.* Van Kerckhoven *et al.* 2000; Werner *et al.* 2004; Peeters *et al.* 2004b; Sellgren *et al.* 2007; Smith *et al.* 2007; Boersma *et al.* 2010).

These emission features are now found in almost all astronomical environments including the (diffuse) interstellar medium (ISM), the edges of molecular clouds, reflection nebulae, some T Tauri stars, several Herbig AeBe stars, H II regions, C-rich post-AGB stars, C-rich PNe, some C-rich WR stars, supernova remnants and, novae. In addition, they have been found throughout the Universe out to redshifts ~ 3 in various type of galaxies: normal galaxies, starburst galaxies, ultra-luminous galaxies (ULIRGs) and AGNs. The PAH emission in galaxies is not just confined to the plane or disk of the galaxy but can also be found in their halo (*e.g.* Engelbracht *et al.* 2006; Irwin *et al.* 2007).

3 Spectral variations

To first order, the PAH bands are remarkably similar notwithstanding the large variety of environments in which they are observed. However, it is clear that the PAH bands show variations in peak positions, shapes and (relative) intensities from source to source and also spatially within extended sources. In the analysis of the PAH bands, various assumptions are made with respect to the characteristics of the different components contributing to the IR emission. Generally, a featureless dust continuum is assumed. However, different methods are applied with regard to the PAH bands themselves. A first method assumes the broad plateaus underlying the individual PAH features to be part of these features. In this case, both plateaus and individual features are fitted together with Lorentzians or Drude profiles (*e.g.* Boulanger *et al.* 1998; Smith *et al.* 2007). Alternatively, the plateaus and the features are considered to be independent and local spline continua are used to separate the components (Fig. 1, *e.g.* Hony *et al.* 2001; Peeters *et al.* 2002). Sometimes, the features are then fitted with Gaussian profiles. Neither approach is technically correct (see Tielens 2008 for a detailed discussion). Although these methods result in different PAH band strengths and profiles, the global trends in spectral variations are independent of the applied method. Some key results are discussed below.

3.1 Intensity variations

Strong variations are observed in the relative strength of the CC and CH in-plane-bending modes in the 6 to $9 \mu\text{m}$ range relative to the CH modes at 3.3 and $11.2 \mu\text{m}$ (Fig. 2, *e.g.* Hony *et al.* 2001; Galliano *et al.* 2008). Specifically, the

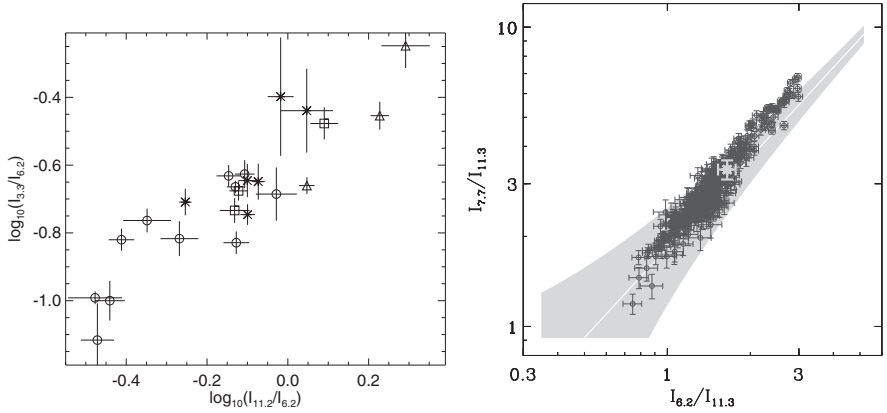


Fig. 2. *Left:* the correlation of the 3.3 and 11.2 μm band strengths normalized to the 6.2 μm band strength. Hexagons are H II regions, stars intermediate mass star-forming regions, squares RNe and triangles are PNe (Figure taken from Honý *et al.* 2001). *Right:* the variation in the CC/CH band ratios within the starburst galaxy M 82. The gray filled area represent the correlation obtained for the integrated spectra of a large sample of galactic and extragalactic sources. The white (gold) symbol is the value of the global measurement over the entire galaxy (Figure taken from Galliano *et al.* 2008).

strength of the 3.3 μm feature correlates with that of the 11.2 μm feature but they both vary considerably with respect to the strengths of the 6.2, 7.7 and 8.6 μm features. Likewise, the latter three PAH bands correlate well with each other. Note however that the CH out-of-plane (CHoop) bending modes (10–15 μm region) do not behave consistently: the 12.7 μm PAH band correlates well with the 6 to 9 μm modes and not with the 11.2 μm PAH band. These relative intensity variations are widespread: they are seen from source to source and spatially within (extra-) galactic sources (Fig. 2). Combined, these studies reveal the interrelationship between the various PAH bands.

PAH ratios in Galactic and Magellanic Cloud H II regions seem to depend on metallicity (Vermeij *et al.* 2002; LeBouteiller *et al.* in prep.). A similar dependence is however not observed towards Galactic and Magellanic Cloud planetary nebulae (Bernard-Salas *et al.* 2009). In addition, several galaxies harboring an AGN exhibit very weak PAH emission in the 6 to 9 μm region relative to the 11.2 PAH band (Smith *et al.* 2007; Bregman *et al.* 2008; Kaneda *et al.* 2005, elsewhere in this volume). Moreover, for these galaxies, the 7.7/11.2 PAH ratio correlates with the hardness of the radiation field. This is in contrast to galaxies with H II region or starburst-like characteristics where the 7.7/11.2 PAH ratio is largely insensitive to the hardness of the radiation field. Even though, the latter include low metallicity systems which typically have a harder radiation field.

The total PAH intensity is highly variable and is generally studied relative to the strength of the dust emission. The latter is commonly determined by either

the dust continuum emission at the wavelength of the considered PAH band, the dust emission at wavelengths around 15–25 μm denoted as Very Small Grains (VSGs), the far-IR (FIR) dust emission or the total IR (TIR) dust emission. The ratio PAH/VSG varies spatially across extended Galactic H II regions such as *e.g.* the Orion Bar and M 17. In particular, the dust emission dominates inside the H II region while in the PDR the PAHs exhibit their peak intensity and the dust continuum at 15–25 μm decreases in strength (due to its lower temperature). Similarly, the PAH/VSG ratio in galaxies depends on the hardness of radiation field and the metallicity (*e.g.* Madden *et al.* 2006; Brandl *et al.* 2006; Engelbracht *et al.* 2006; Gordon *et al.* 2008). These two parameters are related and so it is hard to distinguish between an origin in a less efficient PAH formation process (metallicity effect) or in an increased PAH processing (modification and/or destruction of PAHs by the hard radiation field). For a detailed discussion, we refer to Calzetti, Hunt, Galliano and Sandstrom, elsewhere in this volume.

3.2 Profile variations

From the early days in PAH research, it was realized that i) the 7.7 μm complex is comprised of two components at 7.6 and 7.8 μm which have variable relative strength (Bregman 1989; Cohen *et al.* 1989) and ii) the 3.3 μm PAH band profile showed small variations (*e.g.* Tokunaga *et al.* 1991). However, it is the large amount of PAH spectra provided by ISO and subsequently Spitzer that allowed a systematic study of the PAH band profiles.

These PAH band profiles show pronounced variability, in particular for the CC modes (6.2 and 7.7 μm bands). The variations of the band profiles for the main PAH bands are classified in three classes A, B and C (see Fig. 3; Peeters *et al.* 2002; van Dienenhoven *et al.* 2004). This classification is primarily based upon the peak position of the bands with class C being redshifted from class B which in turn is redshifted from class A. Class C band profiles are significantly different from class A and B. In particular, instead of a 7.7 μm complex with either a dominant 7.6 μm component (class A) or a dominant component peaking between 7.8 and 8 μm (class B), class C objects show a very broad band peaking at ~ 8.2 μm with a weak to absent 8.6 μm PAH band. It should also be emphasized that while class A and C show little variation in their profiles, large differences are present within class B. Some objects have band profiles that encompasses 2 classes (AB: Van Kerckhoven 2002; Boersma *et al.* 2008; BC: Sloan *et al.* 2007) and hence these three classes are not suggestive of three independent groups. Rather, the observed variations in the UIR spectra seem to span a continuous distribution going from class A on one extreme via class B to class C on the other extreme. The observed contrast in the magnitude of the spectral variations for the CH modes versus the CC modes is striking: the peak wavelengths of the features attributed to CC modes (6.2 and 7.7 μm PAH bands) vary by ~ 25 to 50 cm^{-1} , while the variations are smaller for the CH modes (3.3, 8.6 and 11.2 μm PAH bands; ~ 4 to 11 cm^{-1}). In addition, although the classification was applied to each band individually, typically all bands in the 6–9 μm region of a single object belong

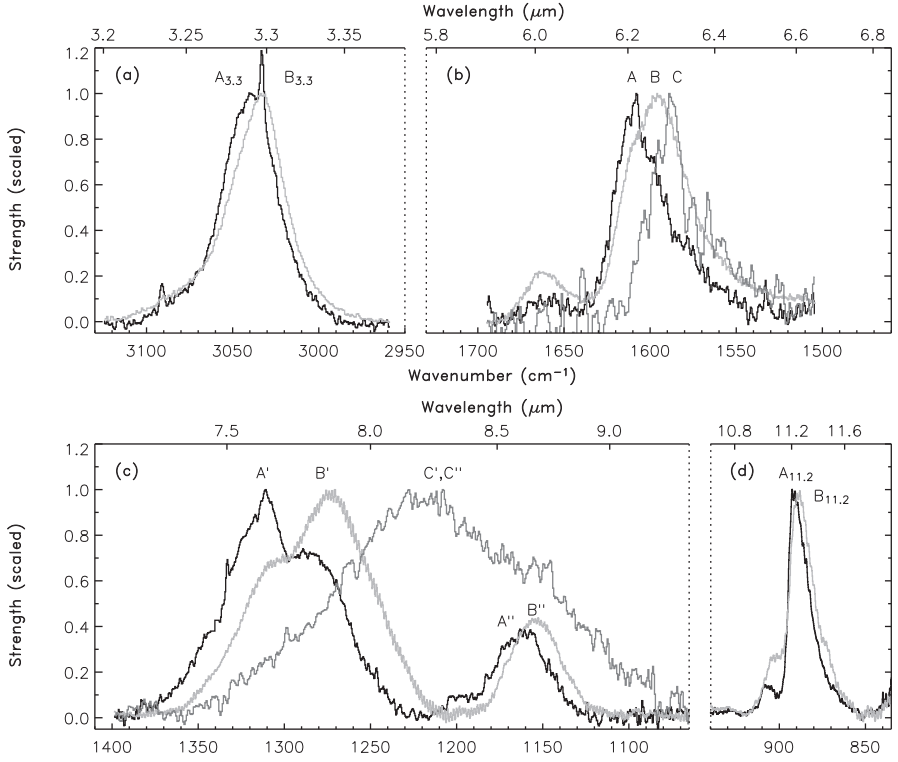


Fig. 3. The source to source variations in position and profile of the main PAH bands. In particular large variations are evident in the 6 to 9 μm . Class A peaks at the shortest, “nominal” wavelengths and class B at longer wavelengths. The CC modes of class C peak at even longer wavelengths (Peeters *et al.* 2002; Figure taken from van Diedenhoven *et al.* 2004).

to the same class while the CH modes at 3.3 and 11.2 μm appear somewhat less connected to each other and/or to the PAH class in the 6–9 μm region.

As already noted by Bregman (1989) and Cohen *et al.* (1989) for the 7.7 μm complex, the specific profile of these PAH bands depends directly on the type of object (Peeters *et al.* 2002; van Diedenhoven *et al.* 2004). Class A represents H II regions, non-isolated Herbig AeBe stars, some PNe, few post-AGB stars, RNe, the (diffuse) ISM and entire galaxies; class B contains most planetary nebulae, isolated Herbig AeBe stars and some post-AGB stars and class C is mainly comprised of post-AGB stars. Few HAeBe and TTauri stars are reported to have class C profiles but their PAH bands are weak and perched on top of both the dust continuum and silicate emission band. Note that post-AGB stars are found in all three classes. From a different perspective, class A profiles are associated with interstellar material (ISM) while class B and C profiles are exhibited by circumstellar material

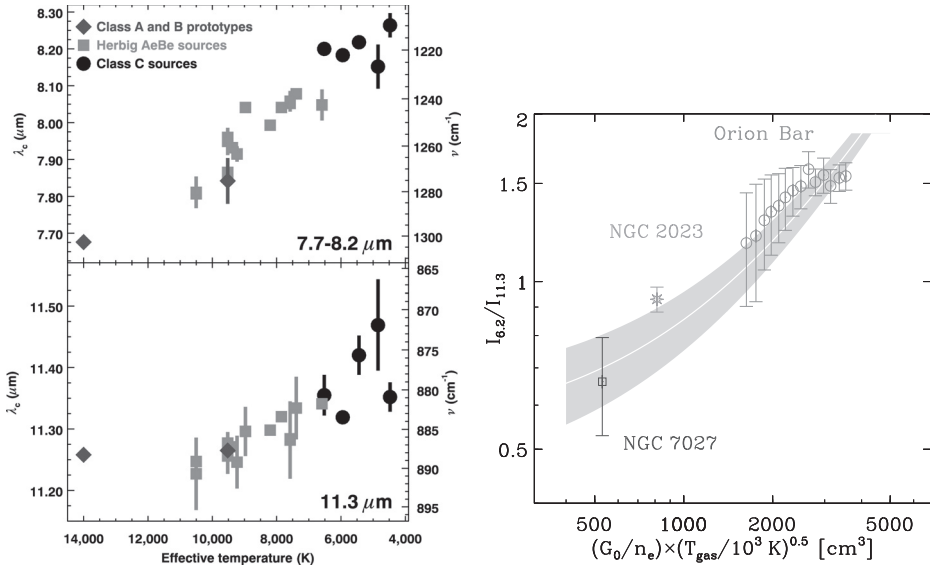


Fig. 4. *Left:* the central wavelengths of the 7.7–8.2 and 11.3 μm PAH features plotted versus the effective temperature of the host star (Sloan *et al.* 2007, Figure taken from Keller *et al.* 2008). *Right:* empirical calibration of the 6.2/11.2 band ratio as a function of the ionization parameter, $G_0 T^{1/2}/n_e$ (Figure taken from Galliano *et al.* 2008).

(CSM). These spectral variations are also seen in the Magellanic Clouds (Bernard-Salas *et al.* 2009). Furthermore, they have also been observed within spatially extended objects such as RNe and evolved stars (Bregman & Temi 2005; Song *et al.* 2007).

Sloan *et al.* (2007) found a remarkable anticorrelation of the band peak position with effective temperature of the exciting star for a sample of post-AGB stars and isolated HAeBe stars, all of class B or C (Fig. 4). This relation does not seem to hold in general because: i) PNe (belonging to class A and B) can have high effective temperatures and class B profiles (*e.g.* NGC 7027), ii) class A objects do not follow the correlation. For example, RNe have class A profiles and a central star with a low effective temperature and iii) the PAH bands of HAeBe stars with the same effective temperature can belong to either class A or B (Van Kerckhoven 2002; Boersma *et al.* 2008). Sloan *et al.* (2007) attributed this relation to different degrees of UV processing and argue that PAHs in reflection nebulae may have been exposed to a stronger radiation field explaining their class A PAH bands. On the other hand, the exceptions may also suggest that in addition to or in contrast with a dependence on effective temperature, other parameters such as *e.g.* history, environment (ISM *vs.* CSM), spatial structure (disk, collapsing cloud; Boersma *et al.* 2008) may play a role.

4 Spectral decomposition

A different and potentially powerful approach to the analysis of PAH observations is the mathematical decomposition of PAH spectra as a linear combination of a basis set of components (Boissel *et al.* 2001; Rapacioli *et al.* 2005, elsewhere in this volume; Joblin *et al.* 2008; Berné *et al.* 2007, 2009, elsewhere in this volume). This method extracts spatially different components from the observations. Originally applied to RNe and edges of clouds, these studies found a basis set of three components – dubbed VSG, PAH⁰ and PAH⁺ – with the VSG located deeper into the PDR while the PAH⁰ and PAH⁺ are found closer to the edge of the PDR. The VSG component is characterized by broad emission bands at wavelengths slightly redshifted to those typical for PAH emission on top of a continuum and is attributed to PAH clusters. Hence, this VSG component is *not* the same as the VSGs discussed earlier. The components PAH⁰ and PAH⁺ do not show continuum emission and are attributed to respectively neutral and ionized PAHs. This neutral PAH component does however exhibit stronger emission in the 6 to 9 μm region than expected from experimental and theoretical PAH spectra. This may indicate the inclusion of some ionized PAH emission in this component. An alternative explanation may be found in the PAH size distribution. In order to fit PAH spectra of class B and C, this basis set has been expanded to include templates exhibiting a very broad band at 8.2, 8.3 and 12.3 μm (thus mimicking class C) and a third PAH template, PAH^x, with peak positions consistent with class B. The latter is attributed to large ionized PAHs and is consistent with theoretical PAH spectra (see Sect. 5). These studies suggest the destruction of the VSGs or PAH clusters by UV photons resulting in the formation of PAHs. These PAH clusters may be reformed in the denser and more shielded environments of molecular clouds. In regions of high UV radiation, the PAH^x component gains in importance due to the destruction of small PAHs and the higher excitation conditions.

5 Astronomical implications

The interpretation of the astronomical PAH spectra strongly relies on theoretical and experimental spectroscopy of PAHs and related species. These studies reveal that intrinsic PAH spectra are determined by parameters such as the PAHs charge, size, the precise molecular (edge) structure and, temperature. Hence, a comparison of astronomical spectra with laboratory and theoretical studies allows to constrain the characteristics of the carriers and to determine the origin of the observed spectral variations. Combined with the observed behavior of PAHs in space, this gives insight into the properties of the astronomical PAH family which can be tied to specific environmental parameters. Here we name a few.

5.1 *The astronomical & the intrinsic PAH spectra: A happy marriage*

One of the strongest criticisms against the PAH hypothesis has been the lack of a good match between a combination of experimental and/or theoretical PAH

spectra and the astronomical PAH spectra. This is now neutralized by the good fits obtained to the three classes A, B and C with the full theoretically calculated NASA Ames PAH spectral database⁵ (Figs. 1b and 2 of Cami elsewhere in this volume). These fits can be broken down according to size, charge and composition unveiling the underlying origin of the different classes. For example, the fit to class C is dominated by emission of small PAHs (number of C-atoms, N_C , ≤ 30).

5.2 The PAH band profiles and the composition of the PAH family

The variations in band profiles reflect primarily a (chemical) modification of the PAH family in different environments. Currently, the precise process is not agreed upon and is further constrained by the following observations. First, the modification of the PAH family needs to be consistent with the observed PAH classes at various stages in the PAH life cycle. Second, the position of the class A 6.2 μm PAH is not reproduced by the strongest pure CC stretching mode of pure PAHs (Peeters *et al.* 2002; Hudgins *et al.* 2005).

To resolve the second issue, various PAH-related species have been proposed. i) *Hetero-atom substituted PAHs* (e.g. Peeters *et al.* 2002; Hudgins *et al.* 2005; Bauschlicher *et al.* 2009). Substitution of a C atom by a N atom in a PAH, *i.e.* PANHs, systematically shifts the position of the strongest pure CC stretching mode towards shorter wavelengths while having no systematic effects on the position of other vibrational modes. This has also been noted in the decomposition of the above mentioned fits (Cami, this volume). ii) *PAH-metal complexes* (e.g. Hudgins *et al.* 2005; Bauschlicher & Ricca 2009; Simon & Joblin 2010; Joalland *et al.* 2009). These are species in which a metal atom is located either below or above the carbon skeleton. See Simon *et al.* (elsewhere in this volume) for specific structures. iii) *PAH clusters* (e.g. Rapacioli *et al.* 2005; Simon & Joblin 2009). For example PAH dimers, see Rapacioli *et al.* (this volume) for specific structures. iv) *Carbon isotope effects* (Wada *et al.* 2003). The presence of ^{13}C in PAHs redshifts the position of the CC stretching modes and thus it will move the band further away from the observed astronomical class A 6.2 μm PAH position. Hence, it cannot resolve the issue.

Additional mechanisms are invoked to interpret the different classes. One mechanism involves variations in the size distribution of the PAH family (Bauschlicher *et al.* 2008; 2009, Cami elsewhere in this volume). It was noticed that small PAHs ($N_C \leq 48$) do emit at 7.6 μm but do not reproduce the 7.8 μm component (e.g. Peeters *et al.* 2002). In contrast, large PAHs ($54 \leq N_C \leq 130$) emit at 7.8 μm and not at 7.6 μm (Bauschlicher *et al.* 2008, 2009). Hence, in order to reproduce the 7.7 μm complex, both small and large PAHs are required and hence the variable strength of the two components (class A *vs.* class B) may then reflect a change of the PAH size distribution in different environments. Similarly, the broad class C component can be produced by small PAHs (Cami, this volume). The PAH classes may then reflect different size distributions of the PAH

⁵<http://www.astrochem.org/pahdb/>; Boersma *et al.* this volume.

family. Alternatively, the classes represent a varying importance of aliphatics *vs.* aromatics (*e.g.* Sloan *et al.* 2007; Boersma *et al.* 2008; Keller *et al.* 2008; Pino *et al.* 2008; Acke *et al.* 2010). Aliphatic carbonaceous species are known to produce broader emission bands compared to PAHs and hence are put forward as the carrier of the class C 7.7 μm complex. An evolution to class B and class A is then obtained by increased UV processing (*e.g.* due to an increase in effective temperature) of these aliphatic carbonaceous species destroying the aliphatic bonds and hence increasing the aromaticity of species. UV processing can also change the PAH size distribution and hence both mechanisms together may lay at the origin of the profile changes. While the second mechanism (towards increased aromaticity) can explain the evolutionary scenario from post-AGB stars to the ISM, it is hard to imagine a reversed process from aromatic material to more fragile aliphatic material when going from the ISM to proto-planetary environments. Hence, Boersma *et al.* (2008) proposed an active chemical equilibrium between aromatic and aliphatic species in all environments through hydrogenation, carbon reactions building (aliphatic) hydrocarbons and UV processing.

5.3 The CC/CH ratio and the charge balance of PAHs

Laboratory and theoretical studies on PAHs have shown the remarkable effect of ionisation on their IR spectra (*e.g.* Hudgins & Allamandola 2004, Pauzat elsewhere in this volume). While peak positions are only modestly affected, the influence on intensity is striking: the bands in the 5–10 μm region grow from the smallest features to become the dominant bands upon ionization. In addition, in the 10–15 μm region, the 11.0 μm PAH band can be attributed to ionized PAHs while the 11.2 μm band is due to neutral PAHs. Besides charge state, there are several other parameters that may influence the CC/CH ratio (*i.e.* the ratio of the 6.2 or 7.7 μm PAH band to the 3.3 or 11.2 μm PAH band) including dehydrogenation, a modification of the temperature distribution (due to a change in the size distribution or the radiation field) and extinction. However, several studies indicate that the observed variation in the CC/CH ratio is dominated by a variation in the degree of ionization of the PAHs in these different environments (Joblin *et al.* 1996; Hony *et al.* 2001; Galliano *et al.* 2008 and Galliano elsewhere in this volume).

5.4 Molecular edge structure of PAHs

The peak wavelength of the CH_{oop} bending modes depends strongly on the number of adjacent peripheral C-atoms bonded to an H-atom (Bellamy 1958; Hony *et al.* 2001). While the exact peak position depends slightly on the charge state, the 11.0 and 11.2 PAH bands originate in solo CH groups (*i.e.* no H-atom is attached to adjacent C-atoms). Both duo and trio CH groups (respectively two and three adjacent C-atoms each with an H-atom attached) contribute to the 12.7 μm band, trio CH groups produce the 13.5 μm band and quatro CH groups the 14.2 μm band. The observed relative intensities of the CH_{oop} bands can then be combined with the intrinsic strengths of these modes to determine possible PAH structures

(Hony *et al.* 2001; Bauschlicher *et al.* 2008, 2009). After all, solo-CH groups decorate the long, smooth straight edges while the other CH groups are characteristics for corners and bays in the (irregular) edge structure. PAHs associated with PNe are characterized by very compact molecular structures with long smooth PAH edges while interstellar PAHs have more corners, either because they are on average smaller or they are more irregular larger species. Similarly, the CH stretching mode of H atoms located in bay regions emit around $\sim 3.22 \mu\text{m}$, a region where little emission is found in astronomical PAH spectra. Therefore, the presence of bay regions in the edge structure of (small) PAHs is very low (Bauschlicher *et al.* 2009).

6 PAHs as a diagnostic tool

The CC/CH ratio is determined by the charge balance of the PAHs. The PAH charge is set by the ratio of the ionization rate to the recombination rate, that is proportional to $G_0 T^{1/2}/n_e$ where G_0 is the UV radiation field, T the gas temperature and n_e the electron density (Tielens 2008). Thus, by coupling the variations in the PAH bands with known variations in the physical conditions (as derived by for example PDR models), an empirical calibration can be established that relates the PAH bands to the local physical conditions. Such a calibration will allow the determination of the physical conditions based upon the omnipresent PAH bands. This can then serve as a diagnostic tool for regions where, for example, the main PDR coolants are not easily observable, such as galaxies at large distances. This approach has been tested for a sample of three well studied objects and has been proven very promising (Fig. 4, Galliano *et al.* 2008; Galliano in this volume). Similarly, combining the observed PAH ionization ratio and H_2 line ratios in dense, highly irradiated PDRs allows to derive the physical conditions (Berné *et al.* 2009, elsewhere in this volume).

Since PAHs are excited by UV radiation, PAH features are also particularly bright in massive star-forming regions. Combined with their omnipresence, this make PAHs a powerful tracer of star formation throughout the Universe (Calzetti and Hunt *et al.* in this volume and references therein). They are widely used to derive star formation rates of galaxies. And in combination with emission lines, they serve as diagnostics for the ultimate physical processes powering galactic nuclei (*e.g.* Genzel *et al.* 1998; Lutz *et al.* 1998; Peeters *et al.* 2004c; Sajina *et al.* 2007; Smith *et al.* 2007). Finally, the presence of PAHs is used to distinguish between shocked gas and PDRs (van den Ancker *et al.* 2000) and to determine redshifts in distant galaxies (*e.g.* Yan *et al.* 2007).

7 Future

This paper reviews the large progress made over the past 25 years in understanding the unidentified infrared bands. Nevertheless, several key questions remain regarding astronomical PAHs including: How do the PAH characteristics (*e.g.*

size, charge state) interact with and reflect the physical conditions of their environment (*e.g.* density, radiation field, temperature, metallicity)?; Do we observe long wavelength counterparts to the well-known mid-IR PAH bands? What are their characteristics?; How can we use the UIR bands as a probe of the physical conditions in regions near and far?; Which specific molecules make up the astronomical PAH family?

The observational future for PAH research is very bright. Currently, we are fortunate to obtain the necessary observations with the Herschel Space Observatory to explore the far-IR modes of the PAHs and to couple the PAH band characteristics to the physical conditions of the environment (*cf.* Joblin *et al.*, elsewhere in this volume). In addition, in the near future, we will use SOFIA and the James Webb Space Telescope (JWST). But the wealth of PAH emission bands and the large variability of the PAH spectrum already prompt more questions than can be answered with the current laboratory and theoretical data. If we intend to make significant progress in our understanding of the PAH bands, the observational effort needs to be balanced with dedicated laboratory and theoretical studies. Indeed, we can only fully exploit the treasure of information hidden in the PAH emission bands by a joint effort of the observational, experimental and theoretical tools.

References

- Acke, B., Bouwman, J., Juhász, A., *et al.*, 2010, ApJ, 718, 558
Barker, J.R., Allamandola, L.J., & Tielens, A.G.G.M., 1987, ApJ, 315, L61
Bauschlicher, C.W.Jr, Peeters, E., & Allamandola, L.J., 2008, ApJ, 678, 316
Bauschlicher, C.W.Jr, Peeters, E., & Allamandola, L.J., 2009, ApJ, 697, 311
Bauschlicher, C.W.Jr, & Ricca, A., 2009, ApJ, 698, 275
Bellamy, L., 1958, The infra-red spectra of complex molecules, 2nd ed. (New York: John Wiley & Sons, Inc.)
Bernard-Salas, J., Peeters, E., Sloan, G.C., *et al.*, 2009, ApJ, 699, 1541
Berné, O., Joblin, C., Deville, Y., *et al.*, 2007, A&A, 469, 575
Berné, O., Fuente, A., Goicoechea, J.R., *et al.*, 2009, A&A, 706, L160
Boersma, C., Bouwman, J., Lahuis, F., *et al.*, 2008, A&A, 484, 241
Boersma, C., Bauschlicher, C.W.Jr, Allamandola, L.J., *et al.*, 2010, A&A, 511, 32
Boissel, P., Joblin, C., & Pernot, P., 2001, A&A, 373, L5
Boulanger, F., Boissel, P., Cesarsky, D., & Ryter, C., 1998, A&A, 339, 194
Brandl, B.R., Bernard-Salas, J., Spoon, H.W.W., *et al.*, 2006, ApJ, 653, 1129
Bregman, J. 1989, in IAU Symp. 135: Interstellar Dust, ed. Allamandola L.J., & Tielens, A.G.G.M., 109
Bregman, J., & Temi, P., 2005, A&A, 621, 831
Bregman, J.D., Bregman, J.N., & Temi, P., 2008, ASPC, 381, 34
Cami, J., Bernard-Salas, J., Peeters, E., & Malek, S.E., 2010, Science, 329, 1180
Cohen, M., Tielens, A.G.G.M., & Bregman, J., *et al.*, 1989, ApJ, 341, 246
Engelbracht, C.W., Kundurthy, K.D., Gordon, K.D., *et al.*, 2006, ApJ, 642, L127

- Galliano, F., Madden, S., Tielens, A.G.G.M., *et al.*, 2008, ApJ, 679, 310
- Geballe, T.R., Lacy, J.H., Persson, S.E., McGregor, P.J., & Soifer, B.T., 1985, ApJ, 292, 500
- Genzel, R., Lutz, D., Sturm, E., *et al.*, 1998, ApJ, 498, 579
- Gillett, F.C., Forrest, W.J., & Merrill, K.M., 1973, ApJ, 183, 87
- Gordon, K.D., Engelbracht, C.W., Rieke, G.H., *et al.*, 2008, ApJ, 682, 336
- Hony, S., Van Kerckhoven, C., Peeters, E., *et al.*, 2001, A&A, 370, 1030
- Hudgins, D.M., Bauschlicher, C.W. Jr., & Allamandola, L.J., 2005, ApJ, 632, 316
- Hudgins, D.M., & Allamandola, L.J., 2004, Astrophys. Dust, ASP Conf. Ser., 309, 665
- Irwin, J.A., Kennedy, H., Parkin, T., & Madden, S., 2007, A&A, 474, 461
- Joalland, B., Simon, A., Marsden, C.J., & Joblin, C., 2009, A&A, 494, 969
- Joblin, C., Szczerba, R., Berné, O., & Szyszka, C., 2008, A&A, 490, 189
- Joblin, C., Tielens, A.G.G.M., Geballe, T.R., & Wooden, D.H., 1996, ApJ, 460, L119
- Kaneda, H., Onaka, T., & Sakon, I., 2005, ApJ, 632, L83
- Keller, L.D., Sloan, G.C., Forrest, W.J., *et al.*, 2008, ApJ, 684, 411
- Kennicutt, R.C.Jr., Armus, L., Bendo, G., *et al.*, 2003, PASP, 115, 928
- Lutz, D., Spoon, H.W.W., Rigopoulou, D., Moorwood, A.F.M., & Genzel, R., 1998, ApJ, 505, L103
- Madden, S., Galliano, F., Jones, A.P., & Sauvage, M., 2006, A&A, 446, 877
- Moutou, C., Sellgren, K., Verstraete, L., & Léger, A., 1999, A&A, 347, 949
- Pech, C., Joblin, C., & Boissel, P., 2002, A&A, 388, 639
- Peeters, E., Hony, S., van Kerckhoven, C., *et al.*, 2002, A&A, 390, 1089
- Peeters, E., Allamandola, L.J., Bauschlicher, C.W.Jr, *et al.*, 2004a, ApJ, 604, 252
- Peeters, E., Mattioda, A.L., Hudgins, D.M., & Allamandola L.J., 2004b, ApJ, 617, L65
- Peeters, E., Spoon, H.W.W., & Tielens, A.G.G.M., 2004c, ApJ, 613, 986
- Pino, T., Dartois, E., Cao, A.-T., *et al.*, 2008, A&A 490, 665
- Rapacioli, M., Joblin, C., & Boissel, P., 2005, A&A, 429, 193
- Roche, P.F., Lucas, P.W., & Geballe, T.R., 1996, MNRAS, 281, L25
- Sajina, A., Yan, L., & Armus, L., *et al.*, 2007, ApJ, 664, 713
- Sellgren, K., Uchida, K.I., & Werner, M.W., 2007, ApJ, 659, 1338
- Sellgren, K., Werner, M.W., & Ingals, J., *et al.*, 2010, ApJ, 722, L54
- Simon, A., & Joblin, C., 2009, J. Phys. Chem. A, 113, 4878
- Simon, A., & Joblin, C., 2010, ApJ, 712, 69
- Sloan, G.C., Jura, M., Duley, W.W., *et al.*, 2007, ApJ, 664, 1144
- Smith, J.D., Draine, B.T., Dale, D.A., *et al.*, 2007, ApJ, 656, 770
- Song, I.-O., McCombie, J., Kerr, T.H., & Sarre, P.J., 2007, MNRAS, 380, 979
- Tielens, A.G.G.M., 2008, ARA&A, 46, 289
- Tokunaga, A.T., Sellgren, K., Smith, R.G., *et al.*, 1991, ApJ, 380, 452
- van den Ancker, M.E., Tielens, A.G.G.M., & Wesselius, P.R., 2000, A&A, 358, 1035
- van Diedenhoven, B., Peeters, E., Van Kerckhoven, C., *et al.*, 2004, ApJ, 611, 928
- Van Kerckhoven, C., 2002, Ph.D. Thesis, Catholic University of Leuven
- Van Kerckhoven, C., Hony, S., Peeters, E., *et al.*, 2000, A&A, 357, 1013

- Vermeij, R., Peeters, E., Tielens, A.G.G.M., & van der Hulst, J.M., 2002, *A&A*, 382, 1042
- Verstraete, L., Pech, C., Moutou, C., *et al.*, 2001, *A&A*, 372, 981
- Wada, S., Onaka, T., Yamamura, I., Murata, Y., & Tokunaga, A.T., 2003, *A&A*, 407, 551
- Werner, M.W., Uchida, K.I., Sellgren, K., *et al.*, 2004, *ApJS*, 154, 309
- Yan, L., Sajina, A., Fadda, D., *et al.*, 2007, *ApJ*, 658, 778

ASTRONOMICAL MODELS OF PAHS AND DUST

B.T. Draine¹

Abstract. Physical dust models which include a PAH component are quite successful in reproducing the measured extinction *vs.* wavelength in the Milky Way, the infrared (IR) emission observed from Milky Way regions and other galaxies, and a number of other observational constraints. Many of the adopted PAH properties are necessarily highly idealized.

The observed variations in the $7.7\ \mu\text{m}/11.3\ \mu\text{m}$ band ratio can be reproduced by varying the PAH ionization balance. Changing the spectrum of the starlight heating the PAHs affects the overall strength of the PAH emission (relative to total IR), but has relatively little effect on the $7.7\ \mu\text{m}/11.3\ \mu\text{m}$ band ratio.

1 Introduction

PAHs are an important component of the dust population. They make a substantial contribution to the overall extinction by dust, accounting for $\sim 20\%$ of the total IR power from a star-forming galaxy like the Milky Way. See Tielens (2008) for a general review of PAHs.

Physical models for dust, including a PAH population, have been developed (Desert *et al.* 1990; Weingartner & Draine 2001; Li & Draine 2001a; Zubko *et al.* 2004; Draine & Li 2007; Draine & Fraisse 2009; Compiegne *et al.* 2010). For application to the Milky Way, these models are subject to an array of observational constraints:

- *Starlight extinction:* The observed extinction of starlight strongly constrains the dust size distribution and composition. Extinction curves have been measured using stars in the Milky Way (MW), Large Magellanic Cloud (LMC), and Small Magellanic Cloud (SMC), and in a limited number of other galaxies using background quasistellar objects (QSOs) and gamma ray burst (GRB) afterglows as the light source. The extinction is best-studied

¹ Dept. of Astrophysical Sciences, Princeton University

in the MW, where spectral features at $10\ \mu\text{m}$ and $18\ \mu\text{m}$ show that amorphous silicates are a major constituent, and a strong extinction “bump” near $2175\ \text{\AA}$ is usually interpreted as due to sp^2 -bonded carbon, as in graphite or PAHs.

- *Starlight polarization:* The extinction is polarization-dependent, requiring that some of the grains be nonspherical and aligned with respect to the Galactic magnetic field.
- *Scattering of starlight:* A substantial fraction of the observed extinction in the optical is due to scattering, requiring that some of the grains must be large enough to efficiently scatter optical light.
- *Abundance constraints:* The grain model should incorporate elements only as allowed by the total abundance of the element minus the fraction observed to be in the gas phase.
- *Infrared emission:* The dust model should reproduce the IR emission spectra observed from regions with different intensities of starlight heating the dust.
- *X-Ray scattering:* The dust composition and size distribution must be such as to reproduce the observed strength and angular distribution of X-ray scattering by interstellar dust.
- *Microwave emission:* Dust-correlated microwave emission is attributed to rotational emission from very small dust grains (Draine & Lazarian 1998a,b). This constrains the abundances of the smallest grains.
- *Dust in meteorites:* Presolar grains with isotopic anomalies are found in meteorites. These were part of the interstellar grain population 4.6 Gyr ago, when the solar system formed.

Models for MW dust are therefore strongly constrained (see Draine 2003, for further discussion).

2 Physical models for dust with PAHs

The Infrared Space Observatory (ISO) discovered, and Spitzer Space Telescope confirmed, that strong PAH emission features are routinely present in the IR spectra of star-forming galaxies. The relative strengths of the PAH features do vary somewhat from galaxy to galaxy, but in fact show surprising “universality”.

Measured extinction curves in the MW, LMC, and SMC have many similarities: (1) A general trend to rise strongly from the near-IR ($\lambda \approx 1\ \mu\text{m}$) to the FUV ($\lambda \approx 0.1\ \mu\text{m}$). (2) A tendency for A_V/N_H to vary in proportion to metallicity – the MW, LMC, and SMC all seem to have similar fractions of “refractory elements” in dust. Models to reproduce the observed A_λ/N_H require a substantial fraction of abundant refractory elements (C, Mg, Si, Fe).

However, significant regional variations in the shape of the extinction curve are observed. The function A_λ/A_V varies from sightline-to-sightline within the MW, and within the LMC and SMC. In particular, the relative strength of the 2175 Å feature decreases as one goes from MW to LMC to SMC. A physical grain model should be able to accommodate these variations.

Contemporary dust models for dust in the MW (and other galaxies) (*e.g.*, Weingartner & Draine 2001; Li & Draine 2001b; Zubko *et al.* 2004; Draine & Li 2007; Draine & Fraisse 2009) have **amorphous silicate** and **carbonaceous material** as the principal dust materials. The specific mix of carbonaceous material (PAH, graphite, various forms of amorphous carbon...) varies from model to model.

A dust model consists of specifying the grain composition and size distribution. The MW, LMC, and SMC extinction curves can be reproduced by models consisting of amorphous silicate + graphite + PAHs, with only changes in the size distributions (and relative abundances) of the 3 components from sightline to sightline (Weingartner & Draine 2001). In galaxies lacking measured extinction curves, it is reasonable to use the size distribution obtained for the MW unless we are *forced* to change some property, such as the relative abundance of PAHs.

For each grain composition and size, we require scattering and absorption cross sections as a function of wavelength. For grains with radii $a > 100$ Å, we calculate the scattering and absorption cross sections by solving Maxwell’s equations for the appropriate grain size and dielectric function, usually assuming either a spherical or spheroidal shape (Draine & Fraisse 2009). To calculate the response to single-photon heating, we also require the heat capacity of each grain.

The PAHs are small enough that scattering is expected to be unimportant, and are also small enough that calculating absorption cross sections using “bulk” optical constants – even if these were available – may be a poor approximation. Instead, we rely on experimental and theoretical studies of PAH absorption cross sections per C atom. The PAH opacity adopted by Draine & Li (2007, hereafter DL07) is shown in Figure 1.

Our knowledge of absorption cross sections for PAHs (neutrals and ions) is limited, especially as regards large species (*cf.* <http://astrochemistry.ca.astro.it/database/pahs.html>). At this time most dust models make the simplifying assumption that the band profiles for PAHs are “universal”. Band positions, widths, and strengths are adopted that appear to be consistent with (1) astronomical observations of band profiles, and (2) laboratory and theoretical studies (to the extent available). In reality, cross sections vary significantly from PAH to PAH, and from region to region (see Peeters 2011, in this volume) but we are not yet in a position to include this in models. Ionization matters: the adopted band strengths depend on whether the PAH is neutral or ionized. A first study on the role of charge state of PAHs in ultraviolet extinction has been recently performed (Cecchi-Pestellini *et al.* 2008; see Mulas *et al.* 2011 in this volume).

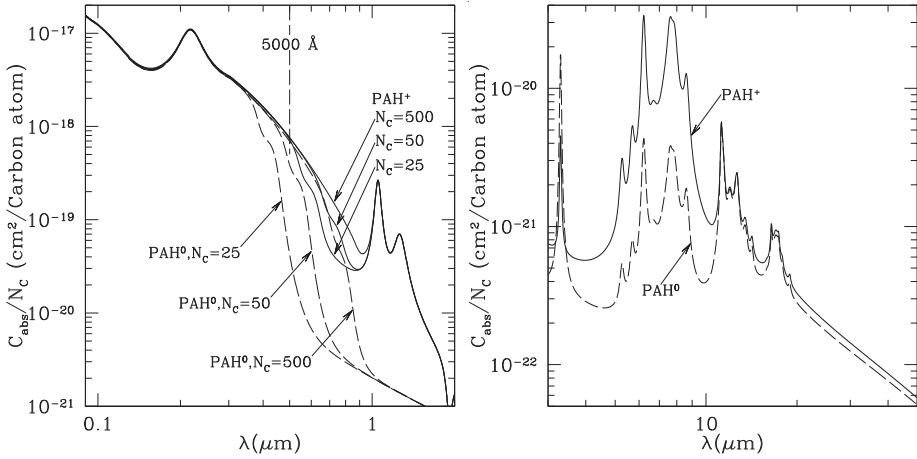


Fig. 1. Radiative cross sections adopted for PAHs (neutral and cations) in the UV-optical (left) and IR (right). After Draine & Li (2007).

3 Modeling the IR emission

In the ISM, grains and PAHs are heated primarily by absorption of starlight photons, and cooled by emission of IR photons. Radiative deexcitation is a quantum process, but $A_\nu(E)d\nu$, the probability per unit time of spontaneous emission of a photon in $[\nu, \nu + d\nu]$ by a PAH with internal energy E , can be approximated by

$$A_\nu(E) \approx \frac{4\pi}{h\nu} C_{\text{abs}}(\nu) B_\nu(T(E))$$

where $B_\nu(T)$ = blackbody function, and $T(E)$ is such that an ensemble of such PAHs at temperature T would have average vibrational energy equal to E . The thermal approximation is valid except at the lowest vibrational energies (Allamandola *et al.* 1989; Leger *et al.* 1989; Draine & Li 2001).

For small PAHs, the time between photon absorptions is in general long compared to the time required for the PAH to deexcite by IR emission, and therefore the PAH temperature T undergoes large excursions. For larger particles, and intense radiation fields, the grain is unable to fully cool between photon absorptions. The PAH temperature distribution function is found by solving the equations of statistical equilibrium, with upward transitions due to photon absorptions, and downward transitions due to spontaneous emission. Figure 2 shows examples of temperature distribution functions for PAH ions.

The temperature distribution function depends on the PAH size, and therefore the total emitted spectrum will be sensitive to the PAH size distribution dn/da . Figure 3 shows dn/da adopted by DL07 for diffuse clouds in the MW, as well as that used by Zubko *et al.* (2004). While both have similar amounts of carbonaceous

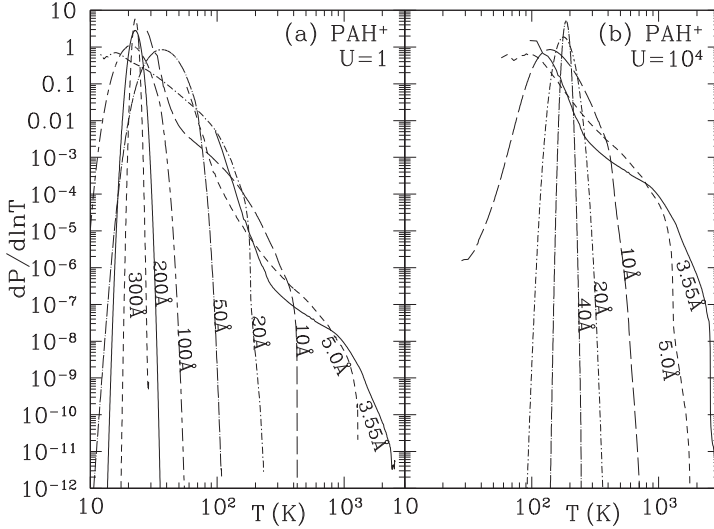


Fig. 2. Temperature distribution functions for PAH^+ particles in (a) the standard ISRF, and (b) a radiation field 10^4 times more intense than the standard ISRF. Curves are labelled by the radius of an equal-volume sphere. After Draine & Li (2007).

material in particles with $< 10^3$ C atoms, the size distributions differ in detail. The differences can be taken as an indication of the uncertainties.

PAHs will in general be rotationally excited. They are expected to have nonzero electric dipole moments, and, therefore, to emit electric dipole radiation in rotational transitions (see Verstraete 2011 in this volume). Draine & Lazarian (1998a) proposed that the PAHs could account for the dust-correlated microwave emission discovered by COBE (Kogut *et al.* 1996). The angular momentum quantum number $J \gtrsim 10^2$, allowing a largely classical treatment of the rotational excitation and damping (Draine & Lazarian 1998b). The rotation rate depends on the PAH size. For the size distribution used to account for the PAH emission features in the infrared results, the predicted rotational emission appears to be in agreement with the observed intensity of dust-correlated microwave emission (*e.g.*, Dobler *et al.* 2009; Ysard *et al.* 2010). There do not appear to be any mechanisms that can effectively align PAH angular momenta with the galactic magnetic field (Lazarian & Draine 2000), and the rotational emission from PAHs is therefore expected to be essentially unpolarized, in agreement with upper limits on the polarization of the dust-correlated microwave emission (Battistelli *et al.* 2006; Mason *et al.* 2009). By contrast, the far-infrared and submm emission from larger grains is expected to have polarizations as large as $\sim 10\%$ (Draine & Fraisse 2009) – soon to be measured by Planck.

Recent theoretical studies have refined the treatment of the rotational dynamics of small particles (Ali-Haïmoud *et al.* 2009; Hoang *et al.* 2010; Silsbee *et al.* 2010; Ysard & Verstraete 2010). The evidence to date supports the view that the PAH

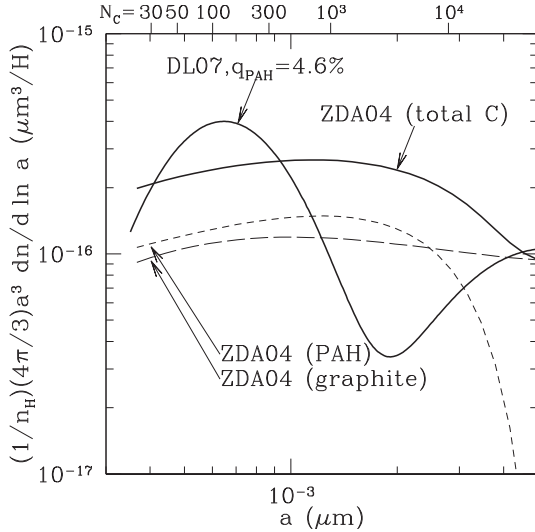


Fig. 3. Volume distributions $\propto a^3 dn/d \ln a$ for small carbonaceous particles. a is the radius of an equal-volume sphere; the number of carbon atoms N_C is shown at the top of the figure. The curve labeled DL07 is the size distribution used by Draine & Li (2007); the curves labeled ZDA04 are for graphite and PAH particles from Zubko *et al.* (2004).

population is responsible for the bulk of the observed dust-correlated microwave emission.

4 PAH ionization balance

The PAH charge state changes due to collisions with electrons, collisions with ions, and photoelectric emission. Rates for these processes can be estimated, and the steady-state charge distribution function can be solved for as a function of size and environment. Figure 4 shows the calculated ϕ_{ion} , the fraction of PAHs that are non-neutral, as a function of size. The solid curve is a weighted sum over the three idealized environments.

5 Comparison of model and observed spectra

The DL07 dust model has been applied to try to reproduce observed IR emission from galaxies. The model is found to reproduce the broad-band photometry from galaxies both globally (*e.g.*, Draine *et al.* 2007) and within galaxies (*e.g.*, Muñoz-Mateos *et al.* 2009). How well does the model compare with observed spectra?

Figure 5 shows the low-resolution spectroscopy and broadband photometry measured in the central few kpc of SINGS galaxies (Smith *et al.* 2007), together

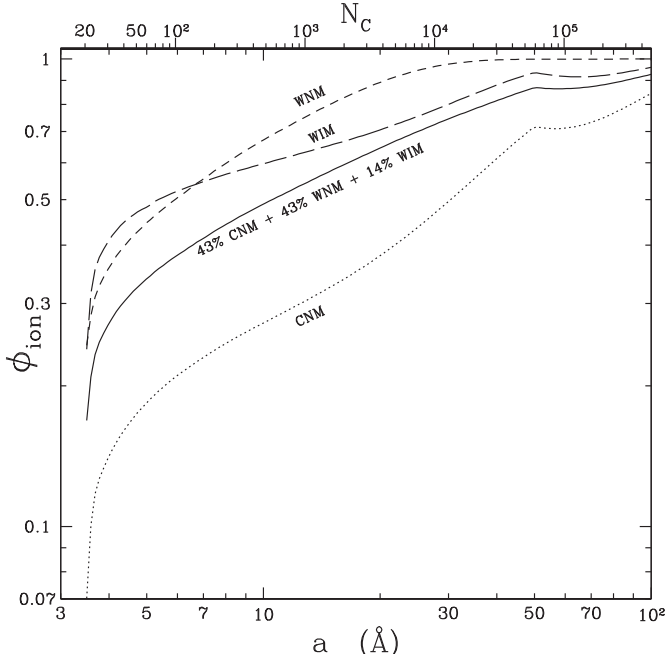


Fig. 4. Calculated ionized fraction ϕ_{ion} for PAHs, as a function of PAH size. **Solid** curve is ϕ_{ion} adopted by DL07 for the overall ISM. From Li & Draine (2001a).

with the spectrum of a best-fit DL07 dust model, where the total dust mass, the PAH abundance (as a fraction of the total grain mass), and the distribution of starlight intensities have been adjusted. The agreement is impressive, particularly since two things that were *not* varied were (1) the PAH ionization fraction $\phi_{\text{ion}}(a)$ (held fixed at the distribution originally estimated to apply to the Milky Way – see Fig. 4), and (2) the spectrum of the starlight heating the dust (taken to be the Mathis *et al.* 1983, hereafter MMP83) ISRF spectrum.

6 Spectral variations

While the overall agreement between model and observations in Figure 5 is excellent, close scrutiny discloses differences. In NGC 5195, the observed ratio of the $7.7 \mu\text{m}$ feature to the $11.3 \mu\text{m}$ feature falls below the model; for NGC 6946 the observed $7.7/11.3$ ratio is slightly higher than the model.

A systematic study of variations in PAH spectra was carried out by Galliano *et al.* (2008). Figure 6a shows examples of variations in the $5\text{--}16 \mu\text{m}$ PAH spectra from galaxy to galaxy, and within M 82. The ratio of the power in the $7.7 \mu\text{m}$ complex to the power in the $11.3 \mu\text{m}$ feature varies considerably. Figure 6b shows that while $I(7.7)/I(11.3)$ varies by up to a factor 6, $I(7.7)/I(6.2)$ and $I(8.6)/I(6.2)$ remain nearly constant.

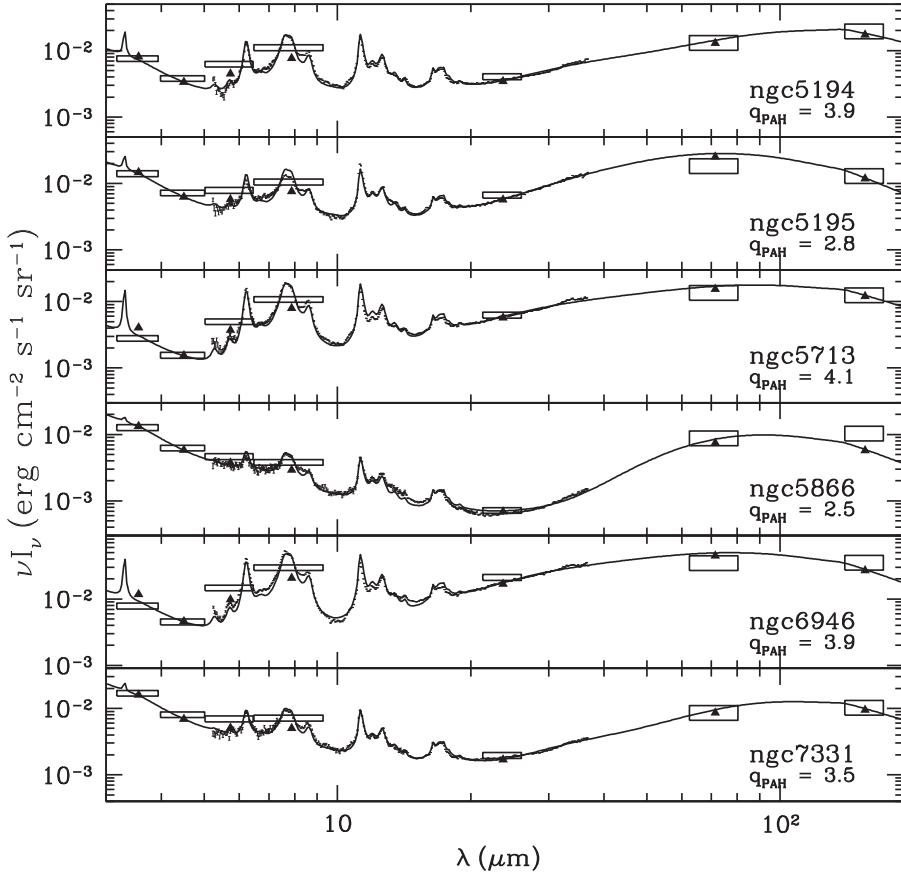


Fig. 5. Spectra of the central regions of SINGS galaxies (Smith *et al.* 2007), reproduced by models of starlight plus IR emission from dust. Numerous (very small) data points with error bars are 5.3 – 38 μm IRS observations, and the rectangles are IRAC and MIPS photometry for the region where the IRS spectrum was extracted. Solid curves are calculated for the dust model; the triangles show the model convolved with the IRAC and MIPS response functions. For each model the value of $q_{\text{PAH}} \equiv$ (the fraction of total dust mass contributed by PAHs with $N_{\text{C}} < 10^3$ C atoms) is given (Reyes *et al.*, in preparation).

Figure 6c shows that for normal galaxies the 7.7/11.3 ratio does not appear to depend on the hardness of the radiation field (using the NeIII/NeII ratio in H II regions as a proxy). However, very low values of 7.7/11.3 can be found for some AGN with high ratios of $[\text{NeIII}]_{15.6 \mu\text{m}}/[\text{NeII}]_{12.8 \mu\text{m}}$.

Can the present dust model accommodate the observed variations in band ratios? Here we consider the effect of changing the PAH ionization, and changing the spectrum of the starlight heating the dust.

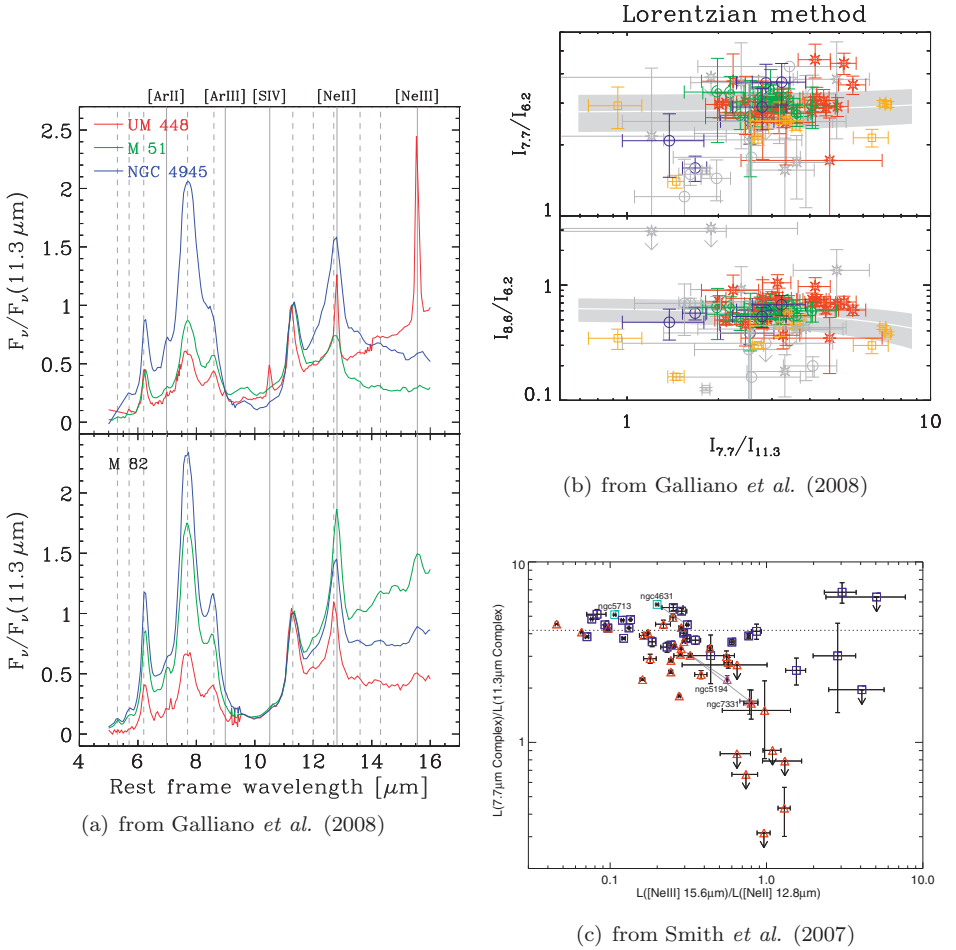


Fig. 6. (a) Variations in spectra from galaxy to galaxy, and within M 82 (from Galliano *et al.* 2008). (b) In a sample of 50 objects, the $I(7.7 \mu\text{m})/I(11.3 \mu\text{m})$ ratio varies by a factor ~ 6 , while $I(7.7)/I(6.2)$ and $I(8.6)/I(6.2)$ remain relatively constant (from Galliano *et al.* 2008). (c) Variations of $I(7.7)/I(11.3)$ among galaxies, as a function of the $[\text{NeIII}]15.6 \mu\text{m}/[\text{NeII}]12.8 \mu\text{m}$ flux ratio. Squares: normal HII-type galaxies; Triangles: AGN (from Smith *et al.* 2007).

PAH ionization

With the ionization-dependent opacities of Figure 1, we can alter the emission spectrum by changing the adopted ionization function $\phi_{\text{ion}}(a)$. Figure 7a shows emission spectra calculated for two extreme assumptions regarding the ionization: $\phi_{\text{ion}} = 0$ and $\phi_{\text{ion}} = 1$, as well as for ϕ_{ion} adopted by DL07 (shown in Fig. 4). It is apparent that the $7.7/11.3$ band ratio increases considerably as the PAH

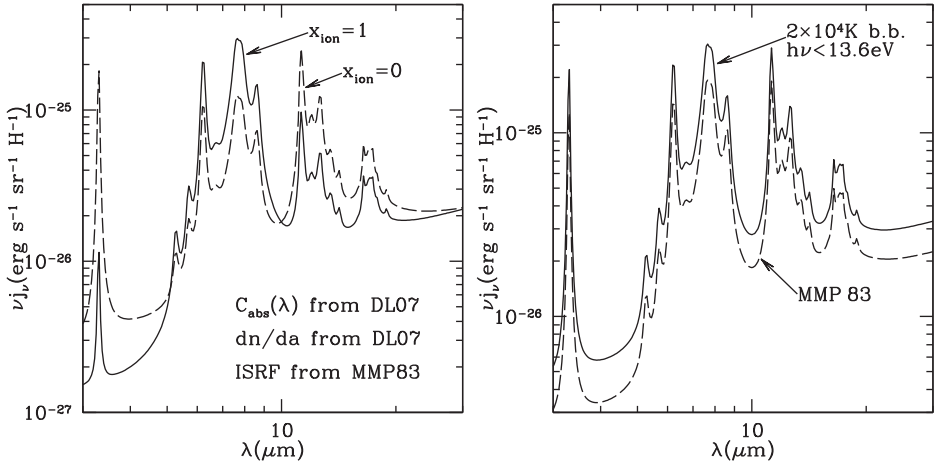


Fig. 7. (a) 3–30 μm emission spectrum for fully-ionized (solid curve) and neutral PAHs (broken curve) heated by the local ISRF (Mathis *et al.* 1983, MMP83). The 7.7/11.3 band ratio changes by a factor ~ 6 . (b) 3–30 μm emission spectrum for fixed ionization $\phi(a)$ used by DL07, but comparing PAHs heated by the MMP83 ISRF (broken curve) *vs.* PAHs heated by a 2×10^4 K blackbody cut off at 13.6 eV (solid curve). The 7.7/11.3 band ratio is essentially unchanged.

Table 1. PAH band ratios calculated for the DL07 model.

ϕ_{ion}	Radiation Field	$(\nu P_\nu)_{7.7 \mu\text{m}} / (\nu P_\nu)_{11.3 \mu\text{m}}$	$(\nu P_\nu)_{7.7 \mu\text{m}} / P(\text{TIR})^a$
$\phi_{\text{ion}} = 0$	MMP83	0.487	0.323
$\phi_{\text{ion}} = 0$	20 kK blackbody	0.512	0.523
DL07	MMP83	1.01	0.499
DL07	20 kK blackbody	1.05	0.783
$\phi_{\text{ion}} = 1$	MMP83	3.08	0.759
$\phi_{\text{ion}} = 1$	20 kK blackbody	3.36	1.162

^a $P(\text{TIR}) = \int P_\nu d\nu$ is the total IR power for the dust model.

ionized fraction is increased. Table 1 shows that for the adopted PAH⁰ and PAH⁺ absorption cross sections (see Fig. 1) *the 7.7/11.3 feature ratio changes by a factor ~ 6.3 as the ionization is varied* – a range comparable to what is actually seen (see Fig. 6b)!

Variations in starlight spectrum?

There will naturally be variations in the spectrum of the starlight heating PAHs, both regionally within a galaxy, and from one galaxy to another. Heating by a harder radiation field will lead to an increase in the fraction of the dust heating contributed by hard photons, and therefore will increase the short wavelength PAH emission. However, Galliano *et al.* (2008) showed that the harder starlight

spectrum of a starburst does not increase the 7.7/11.3 ratio by enough to explain the observed variations. Figure 7 compares the 3–30 μm emission spectrum for PAHs heated by the MMP83 ISRF, *vs.* dust heated by a 2×10^4 K blackbody cut off at 13.6 eV. The 2×10^4 K blackbody is adjusted in intensity to give the same overall power per H absorbed by dust. The harder radiation field does lead to an increase in the PAH emission as a fraction of the total, but has only a small effect on the 7.7/11.3 band ratio (only a 4% change – see Table 1), confirming the finding of Galliano *et al.* (2008).

Changes in the PAH size distribution?

What about the lowest values of 7.7/11.3 found for some AGN (see Fig. 6c)? The smallest PAHs may be susceptible to destruction by X-rays Voit (1992). Suppression of the abundances of PAHs with $< 10^3$ C atoms (while leaving larger PAHs unchanged) would reduce the 7.7/11.3 ratio, lowering it by a factor ~ 1.5 (Galliano *et al.* 2008); however, as noted by Galliano *et al.* (2008), this change to the size distribution would also lower the 6.2/7.7 band ratio, which does not appear to vary in normal galaxies; hence this effect would apply only in unusual objects.

7 What is the relation between PAHs and the 2175 Å feature?

The strength of the interstellar 2175 Å feature requires that the carrier X have $n_X f_X / n_H \approx 9.3 \times 10^{-6}$ (Draine 1989), where f_X is the oscillator strength per X . In general, PAHs have strong absorption near 2200 Å due to $\pi \rightarrow \pi^*$ electronic excitation. For small graphite spheres, the $\pi \rightarrow \pi^*$ excitation has an oscillator strength $f \approx 0.16$ per C atom. If we assume a similar oscillator strength for the $\pi \rightarrow \pi^*$ transition in PAHs, then C/H ≈ 58 ppm in PAHs would be sufficient to account for the observed integrated strength of the 2175 Å feature. The abundance of PAHs required to explain the observed IR emission is 30–60 ppm (Li & Draine 2001a; Draine & Li 2007). Therefore, it seems likely that the 2175 Å feature is due mainly to PAHs (Joblin *et al.* 1992; Li & Draine 2001a).

The sp^2 -bonded carbon in PAHs also has strong absorption in $\sigma \rightarrow \sigma^*$ transitions, resulting in absorption rising steeply beginning at ~ 1200 Å (~ 10 eV) and peaking at ~ 720 Å (~ 17 eV). Thus, any sightline with 2175 Å absorption (if due to PAHs) should also have steeply rising extinction at $\lambda \lesssim 1200$ Å, although other elements of the dust population (*e.g.*, small silicate particles) can also contribute steeply rising far-UV extinction in addition to that provided by the PAHs.

PAH emission features are ubiquitous in IR spectra of star-forming galaxies, including starburst galaxies. However, the 2175 Å feature is weak or absent in spectra of starburst galaxies: the “Calzetti extinction law” for these starbursts shows no 2175 Å feature (Calzetti *et al.* 1994). Conroy (2010) found no evidence of 2175 Å extinction in the spectra of star-forming galaxies at $z \approx 1$. Note, however, that Conroy *et al.* (2010) do find evidence for 2175 Å extinction in GALEX observations of nearby galaxies. Given the ubiquity of PAH emission in star-forming galaxies, the weakness or absence of the 2175 Å feature in the spectra of starburst galaxies, and in the $z \sim 1$ sample of Conroy (2010), is surprising.

Absence of the 2175 Å feature in starburst spectra may be in part the result of complex geometry and radiative transfer – perhaps the regions in the galaxy that dominate the emergent FUV may be regions where the PAHs have been destroyed.

In the SMC, 4/5 sightlines where UV extinction has been measured have no detectable 2175 Å feature (Gordon *et al.* 2003). If PAHs absorb near 2175 Å, then we expect PAH emission to be weak in the SMC. From COBE-DIRBE observations, Li & Draine (2002) argued that PAH emission was strongly suppressed (relative to total IR emission) in SMC (but this was controversial – see Bot *et al.* 2004).

Recently, Sandstrom *et al.* (2010) studied PAH emission in the SMC, finding that the PAH emission, while not zero, is indeed weak, consistent with the 2175 Å extinction feature being due to PAHs. Sandstrom *et al.* also found large regional variations in the PAH abundance within the SMC, with the PAH abundance peaking near molecular clouds.

8 Summary

The principal points are the following:

- Physical models for interstellar dust can reproduce the observed PAH emission features together with other observed properties, including microwave emission, submm and far-IR emission, and extinction and scattering from the near-IR to X-ray energies. Amorphous silicate material accounts for $\sim 75\%$ of the dust mass. Carbonaceous material accounts for $\sim 25\%$ of the mass, with $\sim 5\%$ of the total dust mass in PAHs.
- Lacking detailed knowledge of the physical properties of PAHs, current models use very simplified representations of PAH absorption as a function of wavelength. At present these properties are “tuned” to be able to reproduce astronomical observations, but the adopted opacities appear to be consistent with what is known of PAHs in the IR through ultraviolet.
- PAH band ratios are observed to vary from region to region. The 7.7/11.3 band ratio varies by up to a factor ~ 6 . Model calculations (see Fig. 7) show that this could result from changes in the PAH ionization balance from nearly fully neutral (low 7.7/11.3 ratio) to nearly fully ionized (high 7.7/11.3 ratio).
- The 2175 Å interstellar extinction feature should be due, at least in part, to $\pi \rightarrow \pi^*$ absorption in PAHs. Weakness or absence of the 2175 Å feature would then imply weakness or absence of PAH emission. The 2175 Å feature is observed to be weak in the SMC; recent study of the PAH emission from the SMC confirms that, as predicted, the PAH abundance is very low (Sandstrom *et al.* 2010).
- Existing models use highly simplified descriptions of the PAH absorption cross sections from the UV to the IR, with considerable freedom for adjustment

to reproduce astronomical observations. As both laboratory and theoretical understanding moves forward, modeling will become more strongly constrained.

I am grateful to Christine Joblin and the SOC for organizing this meeting, and for the invitation to speak at it. I thank Xander Tielens for comments and suggestions that helped improve this text. This work was supported in part by NASA through JPL grant 1329088.

References

- Ali-Haïmoud, Y., Hirata, C.M., & Dickinson, C., 2009, MNRAS, 395, 1055
Allamandola, L.J., Tielens, G.G.M., & Barker, J.R., 1989, ApJS, 71, 733
Battistelli, E.S., Rebolo, R., Rubiño-Martín, J.A., *et al.*, 2006, ApJ, 645, L141
Bot, C., Boulanger, F., Lagache, G., Cambrésy, L., & Egret, D., 2004, A&A, 423, 567
Calzetti, D., Kinney, A.L., & Storchi-Bergmann, T., 1994, ApJ, 429, 582
Cecchi-Pestellini, C., Mallocci, G., Mulas, G., Joblin, C., *et al.*, 2008, A&A, 486, L25
Compiegne, M., Verstraete, L., Jones, A., *et al.*, 2010 [ArXiv 1010.2769v1]
Conroy, C., 2010, MNRAS, 404, 247
Conroy, C., Schiminovich, D., & Blanton, M.R., 2010, ApJ, 718, 184
Desert, F.-X., Boulanger, F., & Puget, J.L., 1990, A&A, 237, 215
Dobler, G., Draine, B., & Finkbeiner, D.P., 2009, ApJ, 699, 1374
Draine, B.T., 1989, ed. L. Allamandola & A. Tielens, IAU Symp. 135: Interstellar Dust (Kluwer, Dordrecht), 313
Draine, B.T., 2003, ARAA, 41, 241
Draine, B.T., Dale, D.A., Bendo, G., *et al.*, 2007, ApJ, 663, 866
Draine, B.T., & Fraise, A.A., 2009, ApJ, 696, 1
Draine, B.T., & Lazarian, A., 1998a, ApJ, 494, L19
Draine, B.T., & Lazarian, A., 1998b, ApJ, 508, 157
Draine, B.T., Li, A., 2001, ApJ, 551, 807
Draine, B.T., & Li, A., 2007, ApJ, 657, 810
Galliano, F., Madden, S.C., Tielens, A.G.G.M., Peeters, E., & Jones, A.P., 2008, ApJ, 679, 310
Gordon, K.D., Clayton, G.C., Misselt, K.A., Landolt, A.U., & Wolff, M.J., 2003, ApJ, 594, 279
Hoang, T., Draine, B.T., & Lazarian, A., 2010, ApJ, 715, 1462
Joblin, C., Leger, A., & Martin, P., 1992, ApJ, 393, L79
Kogut, A., Banday, A.J., Bennett, C.L., *et al.*, 1996, ApJ, 464, L5
Lazarian, A., & Draine, B.T., 2000, ApJ, 536, L15
Leger, A., D'Hendecourt, L., & Defourneau, D., 1989, A&A, 216, 148
Li, A., & Draine, B.T., 2001a, ApJ, 554, 778
Li, A., & Draine, B.T., 2001b, ApJ, 550, L213
Li, A., & Draine, B.T., 2002, ApJ, 576, 762
Mason, B.S., Robshaw, T., Heiles, C., Finkbeiner, D., & Dickinson, C., 2009, ApJ, 697, 1187

- Mathis, J.S., Mezger, P.G., & Panagia, N., 1983, *A&A*, 128, 212
- Muñoz-Mateos, J.C., Gil de Paz, A., Boissier, S., *et al.*, 2009, *ApJ*, 701, 1965
- Sandstrom, K.M., Bolatto, A.D., Draine, B.T., Bot, C., & Stanimirovic, S., 2010, *ApJ*, 715, 701
- Silsbee, K., Ali-Haimoud, Y., & Hirata, C.M., 2010 [arXiv1003.4732]
- Smith, J.D.T., Draine, B.T., Dale, D.A., *et al.*, 2007, *ApJ*, 656, 770
- Tielens, A.G.G.M., 2008, *ARAA*, 46, 289
- Voit, G.M., 1992, *MNRAS*, 258, 841
- Weingartner, J.C., & Draine, B.T., 2001, *ApJ*, 548, 296
- Ysard, N., Miville-Deschênes, M.A., & Verstraete, L., 2010, *A&A*, 509, L1
- Ysard, N., & Verstraete, L., 2010, *A&A*, 509, A12
- Zubko, V., Dwek, E., & Arendt, R.G., 2004, *ApJS*, 152, 211

DIALECTICS OF THE PAH ABUNDANCE TREND WITH METALLICITY

F. Galliano¹

Abstract. This paper reviews the various processes that have been proposed to explain the observed trend of PAH strength with metallicity. It summarizes a study showing that, although PAH destruction by hard radiation is important in low-metallicity environments, it is not sufficient to explain their paucity. In these systems, the deficiency of their formation mechanism, related to stellar evolution, has to be invoked.

1 Introduction: An intricate combination of processes

From an extragalactic point of view, the strength of the aromatic features appears to be correlated with the metallicity of the environment. The general trend has been discussed by many authors. It was first demonstrated by Madden *et al.* (2006) using *ISO* spectra, and by Engelbracht *et al.* (2005) with *Spitzer* broadbands.

At the scale of a galaxy, the aromatic-feature-to-mid-IR-continuum intensity ratio appears to be a monotonic rising function of the metallicity of the gas, Z_{gas} . This relation contains a lot of scatter, and the metallicity is uncertain and sometimes difficult to define due to its inherent gradient within large galaxies. However, there is no reason to *a priori* consider that this trend defines two regimes above and below $12 + \log(\text{O}/\text{H}) \simeq 8.0$. The notion of such a threshold was introduced by Engelbracht *et al.* (2005), when studying the $\text{IRAC}_{8\ \mu\text{m}}/\text{MIPS}_{24\ \mu\text{m}}$ ratio. Galliano *et al.* (2008, Figure 1a of the present paper) showed that this was a bias due to the fact that, for low PAH-to-continuum ratios, the $\text{IRAC}_{8\ \mu\text{m}}$ band stops being a good tracer of the PAH strength, as it becomes dominated by the continuum intensity. With such a threshold, several galaxies, which are clearly PAH deficient, would fall in the regime where “normal” galaxies are.

Several scenarios have been proposed to explain the origin of the general trend.

1. PAHs are known to be massively destroyed in regions bathed with hard UV photons. The filling factor of molecular clouds in dwarf galaxies is lower

¹ Service d’Astrophysique – Laboratoire AIM, CEA/Saclay, L’Orme des Merisiers, 91191 Gif-sur-Yvette, France; e-mail: frederic.galliano@cea.fr

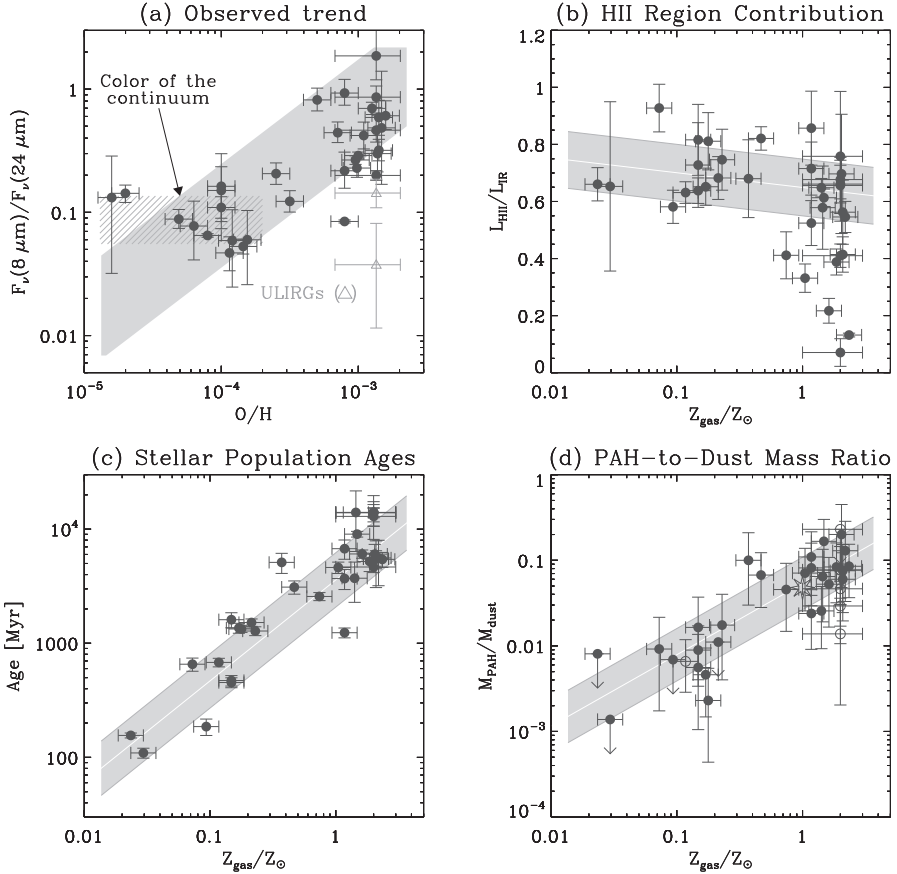


Fig. 1. (a) Ratio of the IRAC $_8 \mu\text{m}$ and MIPS $_{24 \mu\text{m}}$ broadband of our sample, as a function of the observed metallicity. For low PAH-to-continuum ratios, the IRAC $_8 \mu\text{m}$ /MIPS $_{24 \mu\text{m}}$ saturates. (b) Modelled contribution of H II regions to the IR luminosity, as a function of the observed metallicity. (c) Modelled galaxy age (from stellar population synthesis), as a function of the observed metallicity. (d) Modelled PAH-to-dust mass ratio as a function of the observed metallicity. Those 4 panels all come from Galliano *et al.* (2008). On each panel, the grey stripe shows the linear correlation to the data points $\pm 1\sigma$.

than in normal metallicity galaxies (Madden *et al.* 1997). The PAHs could simply be destroyed on large scales in low-metallicity environments, due to the lower opacity of their dust depleted interstellar medium (ISM). This explanation was supported by the anticorrelation of the PAH-to-continuum intensity ratios with $[\text{Ne III}]_{15.56 \mu\text{m}}/[\text{Ne II}]_{12.81 \mu\text{m}}$ (Madden *et al.* 2006). The latter line ratio is a tracer of the very young, ionizing stellar populations.

2. Alternatively, O'Halloran *et al.* (2006) have proposed that PAHs could be destroyed by the numerous supernova (SN) shock waves sweeping the ISM of dwarf galaxies. However, observations of Galactic supernova remnants demonstrate that the blast waves destroy all dust species (PAHs and the other grains; *e.g.* Reach *et al.* 2002) and therefore they do not pose a straightforward explanation for the selective destruction of the PAHs.
3. Finally, Dwek (2005) noted that the contribution to the enrichment of the ISM by the stellar progenitors commonly associated to PAH production, the AGB stars, was also a rising function of metallicity. Therefore the trend discussed in this paper could originate in the fact that PAHs are less abundantly produced in chemically young systems.

Correlation is not causality. Since the different mechanisms invoked above are a function of metallicity, it is difficult to find which one is at the origin of the trend. Looking at only one of these effects independently will always bias the conclusion. To really tackle the origin of this trend, it is needed to confront these various possible processes, and quantify their respective contributions.

2 An estimate of the PAH content of galaxies

To address this issue, we have studied the competition of these various effects within a sample of 35 nearby galaxies ($1/50 Z_{\odot} \lesssim Z_{\text{gas}} \lesssim 2 Z_{\odot}$). We modelled the global UV-to-radio spectral energy distribution (SED) of each galaxy, in order to derive its PAH and dust-to-gas mass ratios. This modelling was done self-consistently, taking into account realistic dust properties, consistent stellar evolution and PAH destruction in H II regions. The detail of this modeling is presented by Galliano *et al.* (2008).

The contribution of H II regions to the IR luminosity is shown in Figure 1b. This contribution is constrained by the observations of the radio free-free and mid-IR thermal continua. We assume that PAHs are fully depleted in H II regions. It therefore quantifies the effect of PAH destruction on the total SED. This effect is important when considering its impact on the $\text{IRAC}_{8 \mu\text{m}}/\text{MIPS}_{24 \mu\text{m}}$ ratio, but is very limited on the $\text{IRAC}_{8 \mu\text{m}}/\text{MIPS}_{160 \mu\text{m}}$ which is the main constraint on the average PAH mass fraction.

Figure 1c shows the galaxy age, derived from stellar population synthesis and fit to the near-IR, as a function of metallicity. It demonstrates that our derived star formation history is consistent with the independent metallicity estimate of the system. This stellar population modelling is important for the subsequent chemical evolution modelling.

Finally, Figure 1d shows the evolution with metallicity of our derived PAH-to-dust mass ratio. Although there is a lot of scatter (partly due to the propagation of the observational uncertainties through the model), this panel shows a clear, relatively smooth, increase with metallicity of the PAH mass fraction.

3 A global point view on PAH evolution in galaxies

To interpret the trend in Figure 1d, we developed a dust evolution model, that takes into account the metal and dust enrichment of the ISM by stars (Galliano *et al.* 2008). Assuming a continuous star formation history (following a Schmidt-Kennicutt law), the model predicts at each time the injection rate of the various elements and dust species. In particular, it computes the evolution of the carbon and silicate dust as a function of metallicity. We independently track the dust production associated with massive and AGB stars. We consider the destruction rate of dust in the ISM by SN blast waves to be proportional to the SN rate.

Figure 2 compares the observed trends of PAH and dust-to-gas mass ratios, with metallicity, to the theoretical evolution of carbon dust produced by AGB stars and dust produced by massive stars. The PAH evolution is strikingly coincident with the production of carbon dust by low-mass stars (see Cherchneff in this volume, for a discussion on PAH condensation in AGB stars). This comparison therefore suggests that the main origin of the PAH trend with metallicity is a result of the delayed injection of these molecules by AGB stars. Indeed, AGB stars start enriching the ISM after their death, $\simeq 400$ Myr after the beginning of the star formation process, when the galaxy has already been enriched by massive stars.

The stellar origin of dust is widely debated (Draine 2009, for a review). Dust is heavily processed in the ISM and reforms in dense clouds. A part of the observed ISM dust content probably does not have a stellar origin. Although our model accounts for the production of dust by various stellar progenitors, there is no assumption made on the actual location and mechanism of condensation. The comparison of our theoretical dust evolution trend to the PAH abundance in galaxies (Fig. 2) would not suffer if the actual dust condensation took place a few 10^7 yr after the metal injection in the ISM. Consequently, our scenario is not in contradiction with dust reformation in the ISM, as long as it occurs on short timescales after the element injection. Dust precursors formed in the stellar envelopes could be injected in the ISM. Although their mass could account for only a few percent of the ISM budget, their presence in the ISM could be crucial to accrete more material and grow the observed ISM grains. That would explain why the dust abundance in galaxies would be closely related to the injection of those grain seeds.

Another concern on these trends is the fact that many dwarf galaxies harbour an old stellar population. It is an indication that these objects had a complex star formation history, and that they are older than indicated by their metallicity. However, the contribution of this old stellar population to the enrichment of the ISM is not significant, otherwise their metallicity would be higher. Moreover, this stellar population does not dominate the integrated SED of these objects (Fig. 1b). Finally, Lee *et al.* (2009) studied a sample of local dwarf galaxies and showed that the star formation bursts were only responsible for about a quarter of the total star formation in the overall population.

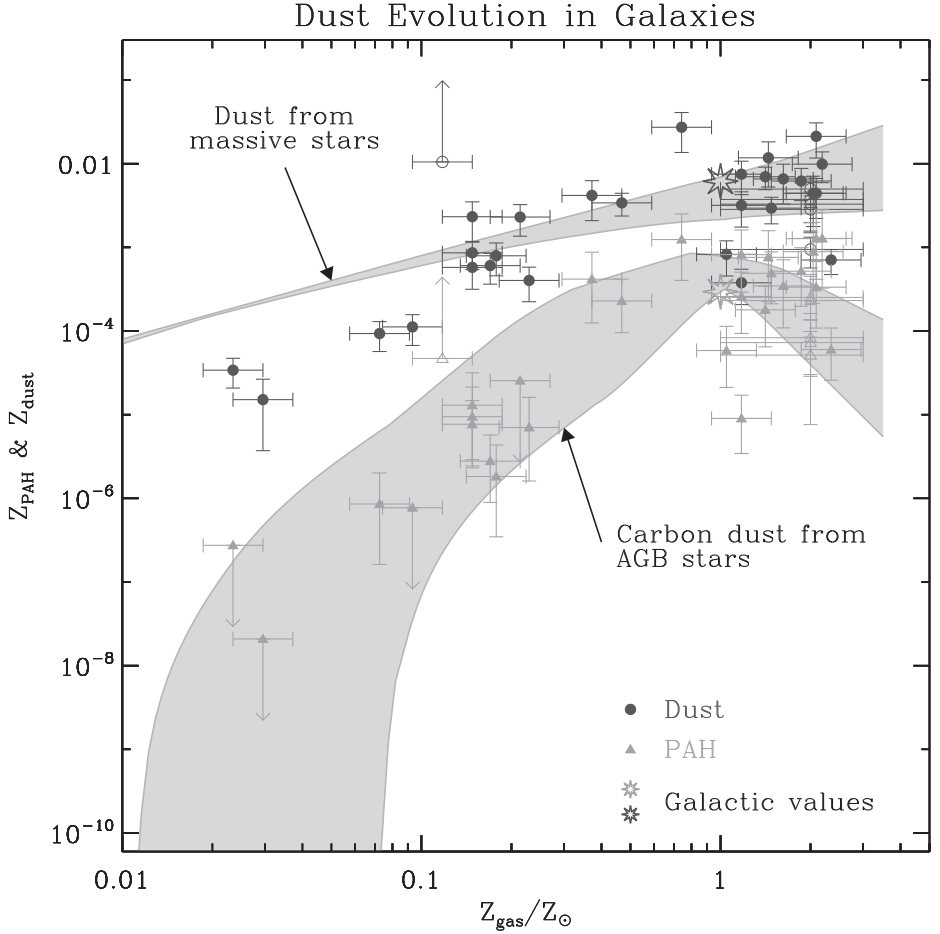


Fig. 2. Comparison between our dust evolution model and the derived trend of PAH and dust-to-gas mass ratios ($Z_{\text{PAH}} = M_{\text{PAH}}/M_{\text{gas}}$ and $Z_{\text{dust}} = M_{\text{dust}}/M_{\text{gas}}$) with the observed gas metallicity. The grey envelopes show the result of our dust evolution model. The various curves within the envelopes represent the spread caused by assuming different star formation rates and different dust destruction efficiencies by SN blast waves. No parameter has been adjusted to fit the dust evolution trends to the observed dust content.

4 Additional confirmations from spatially resolved studies

Although our global approach is relatively crude, because of its lack of spatial resolution, it provides general trends of the various processes and allows a comparison of their respective contributions. Several studies have addressed some of these issues by looking at spatially resolved observations.

Muñoz-Mateos *et al.* (2009) by looking at radial trends within spiral galaxies confirmed the relation between PAH and the evolution of AGB stars. They even found indications of the reversing of the trend at high metallicity, explained by the fact that the enrichment becomes dominated by O-rich low-mass stars (Fig. 2).

In the Large Magellanic Cloud (LMC), the spatial distribution of the PAH mass fraction is associated with the stellar bar (Paradis *et al.* 2009). It has been independently confirmed by Meixner *et al.* (2010). However, this is not the case in the Small Magellanic Cloud (SMC; $\simeq 1/6 Z_{\odot}$; Sandstrom *et al.* 2010, also in this volume). In the SMC, the PAHs appear to be massively depleted in the diffuse ISM, but they are abundant in PDRs, although their abundance is significantly lower than in the Milky Way ($\simeq 0.2\text{--}0.4$ Galactic PAH abundance). Consequently, this study shows, with spatial resolution, that despite the photodestruction effects dominate in the diffuse ISM, the PAHs are underabundant even in regions where they are shielded from the hard radiation field. It therefore supports the idea that the photodestruction processes are not sufficient to account for the trend of PAH abundance with metallicity, and that the deficiency of their production has to be invoked.

References

- Draine, B.T., 2009, ed. in T. Henning, E. Grün, & J. Steinacker, Astron. Soc. Pac. Conf. Ser., 414, 453
- Dwek, E., 2005, ed. in C.C. Popescu, & R.J. Tuffs, AIP Conf. Proc. 761: The Spectral Energy Distributions of Gas-Rich Galaxies, 103
- Engelbracht, C.W., Gordon, K.D., Rieke, G.H., *et al.*, 2005, ApJ, 628, L29
- Galliano, F., Dwek, E., & Charnial, P., 2008, ApJ, 672, 214
- Lee, J.C., Kennicutt, R.C., José G. Funes, S.J., *et al.*, 2009, ApJ, 692, 1305
- Madden, S.C., Galliano, F., Jones, A.P., & Sauvage, M., 2006, A&A, 446, 877
- Madden, S.C., Poglitsch, A., Geis, N., *et al.*, 1997, ApJ, 483, 200
- Meixner, M., Galliano, F., Hony, S., *et al.*, 2010, A&A, 518, L71
- Muñoz-Mateos, J.C., Gil de Paz, A., Boissier, S., *et al.*, 2009, ApJ, 701, 1965
- O'Halloran, B., Satyapal, S., & Dudik, R.P., 2006, ApJ, 641, 795
- Paradis, D., Reach, W.T., Bernard, J., *et al.*, 2009, AJ, 138, 196
- Reach, W.T., Rho, J., Jarrett, T.H., & Lagage, P.-O., 2002, ApJ, 564, 302
- Sandstrom, K.M., Bolatto, A.D., Draine, B.T., *et al.*, 2010, ApJ, 715, 701

THE SHAPE OF MID-IR PAH BANDS IN THE UNIVERSE

O. Berné¹, P. Pilleri^{2, 3} and C. Joblin^{2,3}

Abstract. A large number of galactic and extragalactic sources exhibit a mid-IR spectrum that is dominated by PAH emission. Looking at these spectra in more details reveals a strong variability in the shape/position of the observed features, depending on the observed source, or even the region within a source. In this article, we present the results of an analysis that has allowed us to decompose these spectra into components having a physical meaning. Most, if not all PAH dominated mid-IR spectra of HII regions, PDRs, protoplanetary disks, galaxies etc. can be fitted efficiently using a combination of these components. The results of these fits provide further insight in the composition of the emitting material and the local physical conditions. In the frame of the future IR space missions (JWST, SPICA), this approach can be very useful to probe the physical conditions in distant galaxies.

1 Introduction

The ubiquitous mid-IR emission bands, widely observed in the spectra of dusty astrophysical sources (from protoplanetary disks to starburst galaxies), are commonly attributed to the emission of polycyclic aromatic hydrocarbons (PAHs). However, because these bands are due to nearest neighbor vibrations of the C-C or C-H bonds, they are not specific to individual PAH species. Because essentially any PAH molecule will carry these bonds, the emission bands associated to vibrations are not discriminant to specific PAH molecules, thus preventing from any individual identification. However, these bands do carry some information, in particular their position in wavelength and their relative intensity are known to vary strongly depending on the chemical evolution of their carriers that is driven

¹ Leiden Observatory, Leiden University, Niels Bohrweg 2, 2333 CA Leiden, The Netherlands

² Université de Toulouse, UPS, CESR, 9 avenue du Colonel Roche, 31028 Toulouse Cedex 4, France

³ CNRS, UMR 5187, 31028 Toulouse, France

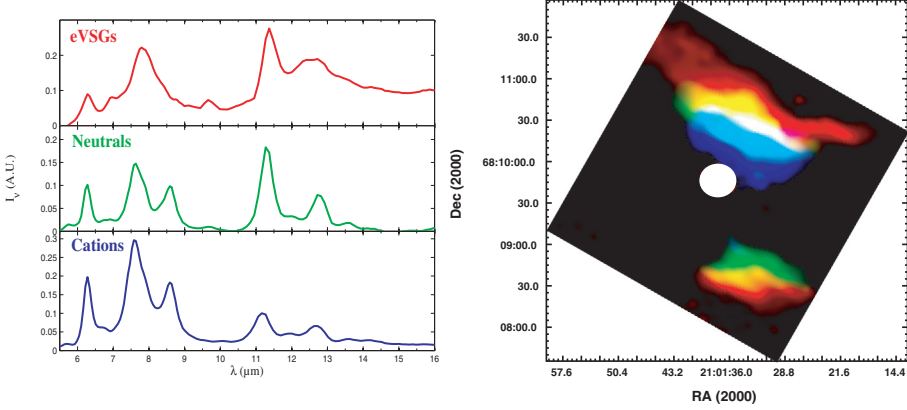


Fig. 1. *Left:* extracted spectra attributed to evaporating VSGs, PAH^0 and PAH^+ in NGC 7023. *Right:* associated distribution maps of the three populations: eVSGs in red, PAH^0 in green and PAH^+ in blue. The white circle shows the position of the exciting star. Colors combine as in an RGB image *i.e.* green (PAH^0)+red (eVSGs)=yellow.

by physical conditions. This has been well demonstrated on the basis of ISO observations (see *e.g.* Peeters *et al.* 2002; Rapacioli *et al.* 2005) and more recently with Spitzer (see *e.g.* Werner *et al.* 2004; Berné *et al.* 2007). The observed IR spectrum usually consists of a set of bands that are most prominent at 6.2, 7.7, 8.6, 11.3, and 12.7 μm . It was established that the modification of the shape of this spectrum can be attributed to the chemical evolution of the emitting populations (Peeters *et al.* 2002; Hony *et al.* 2001) as the local physical conditions change. In particular, models (Tielens 2005) and observations (Joblin *et al.* 1996; Galliano *et al.* 2008) have shown that the variations of the 6.2 (or 8.6) to 11.3 μm band intensity ratio ($I_{6.2}/I_{11.3}$) evolves with the ionization parameter $\gamma = G_0 \times \sqrt{T}/n_H$ where G_0 is the intensity of the UV radiation field in Habing units, T is the gas temperature and n_H the total hydrogen nucleus density. Following this work, Berné *et al.* (2009b) have shown that the combination of the measurement of $I_{6.2}/I_{11.3}$ and of the ratio between the H_2 0-0 S(3) and S(2) line intensities, respectively at 9.7 and 12.3 μm , allows to derive the individual values of T , G_0 and n_H when they fall in the ranges $T = 250 - 1500$ K, $n_H = 10^4 - 10^6 \text{ cm}^{-3}$, $G_0 = 10^3 - 10^5$ respectively.

2 Identification of underlying spectral components

Rapacioli *et al.* (2005) and Berné *et al.* (2007) extracted the “pure” spectra of three different populations of PAH-like grains, namely: neutral PAHs (PAH^0), ionized PAHs (PAH^+) and evaporating very small grains (eVSGs, see

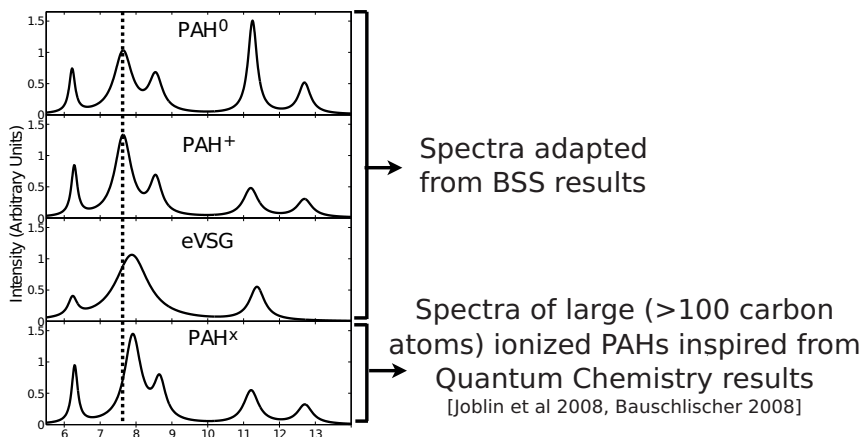


Fig. 2. Template spectra based on the results of Berné *et al.* (2007) and Rapacioli *et al.* (2005). In addition, the PAH^x spectrum introduced by Joblin *et al.* (2008).

Pilleri *et al.* 2010) in the reflection nebula NGC 7023 using blind signal separation methods. This is interpreted as evidence that the evolution of the shape of the mid-IR bands is related to the chemical evolution under the effect of UV photons (see Fig. 1): free PAH molecules are formed from photoevaporation of very small grains (see Rapacioli *et al.* in this volume for a review of possible candidates for eVSGs). The main evolution observed for the PAH population is to get ionized closer to the star. Based on these previous results, Joblin *et al.* (2008) and Berné *et al.* (2009a), were then able to construct a simple model comprising of eVSG, PAH⁰ and PAH⁺ mid-IR template spectra (Fig. 2.). While constructing this model, they found that an additional population of PAHs consisting of large (>100 atoms of carbon) and ionized PAHs (called PAH^x) had to be introduced in order to reproduce the observed spectrum of highly UV-irradiated environments. Other authors (Bauschlicher 2008; Tielens 2008; Geers 2008) have also pointed out the existence of this population of large PAHs.

3 PAHs/eVSGs: Tracers of physical conditions

The templates defined in the previous section can be used to fit observed mid-IR spectra of different astrophysical objects such as planetary nebulae (Joblin *et al.* 2008), protoplanetary disks (Berné *et al.* 2009a), and galaxies (Vega *et al.* 2010). One can then relate the results of the fits to the physical conditions as probed by independent tracers, in order to evidence empirical connections. This was done *e.g.* by Berné *et al.* (2009a) for protoplanetary disks (Fig. 3). The authors have shown that the fraction of emission attributed to eVSGs in the mid-IR spectra of a sample of 12 disks correlates well with decreasing stellar temperature (Fig. 3). This was interpreted as the more efficient destruction of eVSGs in UV-rich environments.

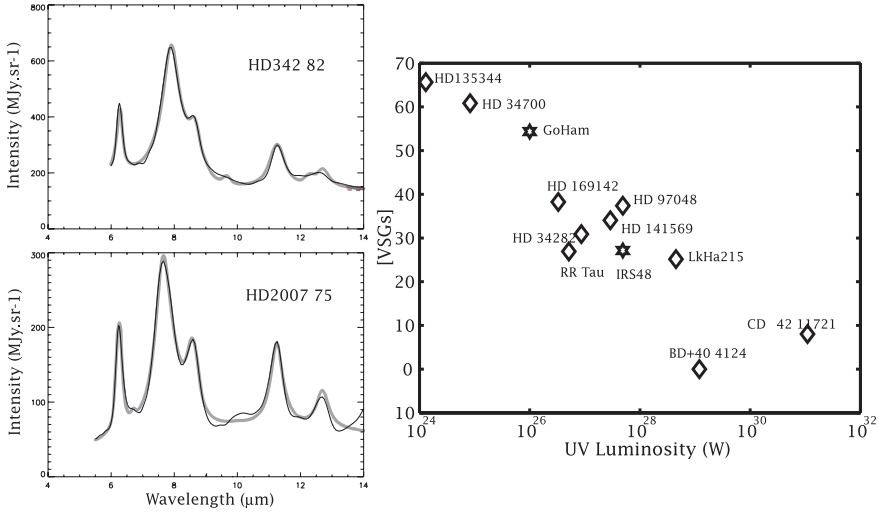


Fig. 3. *Left:* example of fits (gray), using the template spectra of Figure 2 (corrected for extinction on line of sight), to the observed mid-IR spectra of two protoplanetary disks. *Right:* the fraction of “evaporating VSG” emission (%) that was deduced from the fits for a set of 12 observed spectra, as a function of the UV luminosity of the central star (*i.e.* spectral type).

Recently, a detailed and quantitative analysis comparing the results of PDR models to the results obtained by fitting the set template spectra to mid-IR spectral cubes obtained with Spitzer has shown that, indeed, the eVSG abundance can be used as a tracer of the intensity of the UV field (Pilleri *et al.* 2010). The template fitting approach can be applied to the mid-IR spectral cubes of nearby galaxies, which in the end provides the spatial distribution of the different populations of PAHs/eVSGs (Fig. 4). This spatial distribution then informs on the local physical conditions of the ISM in different parts of the galaxy. Here, in the case of M 82, the outflow is PAH⁰-rich, implying the presence of large amounts of molecular gas (as also suggested by Micelotta *et al.* 2010), shielding the PAHs from ionization and allowing quick recombination of PAH⁺ with electrons. The disk, on the other hand, is filled with PAH^{+/x} consistent with the intense star-formation activity producing strong UV fields. Recently, Vega *et al.* (2010) have applied this fitting approach to the Spitzer spectra of spatially unresolved early type galaxies, and shown the pristine nature of their carbonaceous dust content, implying a constant replenishment of dust by carbon stars. Eventually, one could also use this fitting technique to interpret the mid-IR spectra of galaxies at high redshift and derive their properties.

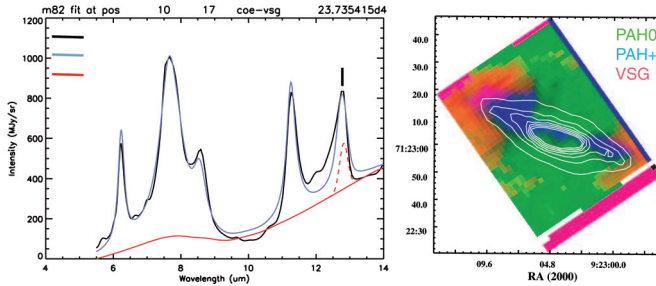


Fig. 4. Example of fit (blue line), using the template spectra of Figure 2 (corrected for extinction on the line of sight), to an observed mid-IR spectrum taken in the cube of M82 in the outflow region. Achieving the fit on all the spatial positions of the spectral cube, the spatial distribution map of the PAH/eVSG populations can be built (inset). In the inset, white contours show the $3.6 \mu\text{m}$ -mostly- stellar emission.

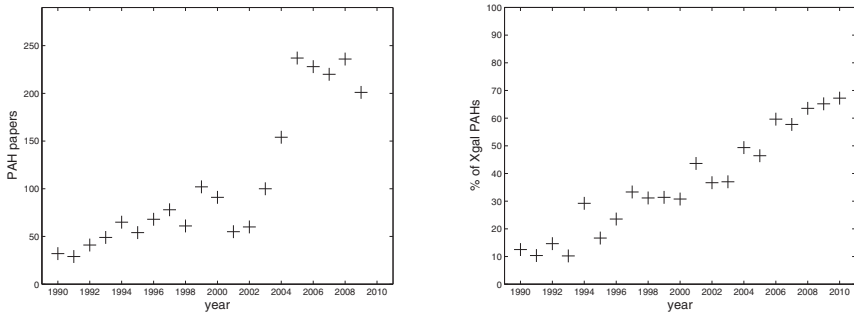


Fig. 5. *Left:* number of published papers each year regarding PAHs in astronomy in the last 20 years. *Right:* percentage of papers regarding PAHs that focus on PAHs observed in external galaxies in the last 20 years. Source: NASA-ADS.

4 Perspectives in astronomical PAH science

The improvement of ground- and space-based instruments in the mid-IR have provided us with an incredible legacy of astronomical PAH spectra. This has, in the last 20 years, motivated each year more studies (Fig. 5). As we have briefly illustrated in the previous section, the PAH spectrum contains a wealth of information on the physical conditions of the emitting source. More and more, these bands are used as a tracer of physical conditions in UV-irradiated astrophysical environments (protoplanetary disks, galaxies, ...) because they are easy to detect (Fig. 5). This is why knowing the detailed composition of PAHs, their evolution and chemistry in space remains one of the key challenges of modern astrophysics. The ISO and Spitzer legacies, the Herschel surveys now (see Joblin *et al.* in this

volume), and the SPICA (Berné *et al.* 2009c), JWST and ELT observations in the future, will contribute to this task.

References

- Berné, O., Joblin, C., Mulas, G., Tielens, A.G.G.M., & Goicoechea, J.R., 2009c, SPICA joint European/Japanese Workshop, July, 2009
- Berné, O., Fuente, A., Goicoechea, J.R., *et al.*, 2009b, *ApJL*, 706, 160
- Berné, O., Joblin, C., Fuente, A., & Ménard, F., 2009a, *A&A*, 495, 827
- Berné, O., Joblin, C., Deville, Y., *et al.*, 2007, *A&A*, 469, 575
- Galliano, F., Madden, S.C., Tielens, A.G.G.M., Peeters, E., & Jones, A.P., 2008, *ApJ*, 679, 310
- Hony, S., Van Kerckhoven, C., Peeters, E., *et al.*, 2001, *A&A*, 370, 1030
- Joblin, C., Szczerba, R., Berné, O., Szyszka, C., *et al.*, 2008, *A&A*, 490, 189
- Joblin, C., Tielens, A.G.G.M., Geballe, T.R., & Wooden, D.H. 1996, *ApJ*, 460, L119
- Peeters, E., Hony, S., Van Kerckhoven, C., *et al.*, 2002, *A&A*, 390, 189
- Rapacioli, M., Joblin, C., & Boissel, P., 2005, *A&A*, 429, 193
- Micelotta, E.R., Jones, A.P., & Tielens, A.G.G.M., 2010, *A&A*, 510, 37
- Tielens, 2008, *ARA&A*, 46, 289
- Tielens, A., 2005 (Cambridge University Press)
- Vega, O., Bressan, A., Panuzzo, P., *et al.*, 2010, *ApJ*, 721, 1090
- Werner, M.W., Uchida, K.I., Sellgren, K., *et al.*, 2004, *ApJS*, 154, 309

AKARI NEAR-INFRARED SPECTROSCOPY OF 3 MICRON PAH AND 4 MICRON PAD FEATURES

T. Onaka¹, I. Sakon¹, R. Ohsawa¹, T. Shimonishi¹, Y. Okada²,
M. Tanaka³ and H. Kaneda⁴

Abstract. Near-infrared (NIR; 2.5–5 μm) low-resolution ($\lambda/\Delta\lambda \sim 100$) spectra were obtained for a number of Galactic and extragalactic objects with the Infrared Camera (IRC) in the AKARI warm mission. These data provide us with the first opportunity to make a systematic study of the 3.3–3.5 μm PAH features in a galactic scale as well as within an object. Whereas the 3.3 μm band is well resolved in most spectra, the 3.5 μm band is not clearly separated from the 3.4 μm band in the IRC spectrum. The intensity ratio of the summation of the 3.4 and 3.5 μm bands to the 3.3 μm band shows a tendency to increase towards the Galactic center, although a large variation in the ratio is also seen in a local scale. A search for deuterated PAH features in the 4 μm region is carried out in IRC NIR spectra. Emission lines originating from the ionized gas together with the detector anomaly hamper an accurate search at certain wavelengths, but little convincing evidence has so far been obtained for the presence of significant features in 4.2–4.7 μm . A conservative upper limit of a few percents is obtained for the integrated intensity ratio of the 4.4–4.7 μm possible features to the 3.3–3.5 μm PAH features in the spectra so far obtained.

1 Introduction

The presence of infrared band features (hereafter PAH bands) in the diffuse Galactic radiation, which are attributed to polycyclic aromatic hydrocarbons (PAHs) or PAH-related materials, has been first confirmed for the 3.3 μm band by the AROME balloon experiment (Giard *et al.* 1988) followed by observations with

¹ Department of Astronomy, Graduate School of Science, University of Tokyo, Tokyo 113-0033, Japan; e-mail: onaka@astron.s.u-tokyo.ac.jp

² I. Physikalisches Institut, Universität zu Köln, 50937 Köln, Germany

³ Center for Computational Sciences, University of Tsukuba, Ibaraki 305-8577, Japan

⁴ Graduate School of Science, Nagoya University, Aichi 464-8602, Japan

the Infrared Telescope in Space (*IRTS*; Tanaka *et al.* 1996). Detection of mid-infrared PAH bands in the interstellar medium (ISM) was made simultaneously with *IRTS* (Onaka *et al.* 1996) and Infrared Space Observatory (*ISO*; Mattila *et al.* 1996). Since then a number of investigations have been carried out for the variations in the MIR PAH bands in Galactic and extragalactic objects including the diffuse Galactic radiation (*e.g.*, Chan *et al.* 2001; Peeters *et al.* 2002; Sakon *et al.* 2004; Rapacioli *et al.* 2005; Berné *et al.* 2007; Smith *et al.* 2007) based on *IRTS*, *ISO* and *Spitzer* observations. However no systematic study has been made for the $3\ \mu\text{m}$ PAH band features in a galactic scale except for the studies of the band variation among a small number of objects and within an object by using ground-based telescopes (*e.g.*, Geballe *et al.* 1989; Joblin *et al.* 1996; Song *et al.* 2003) because of a scarcity of sensitive spectrometers in the $3\ \mu\text{m}$ region.

AKARI, the Japanese satellite mission dedicated to infrared astronomy (Murakami *et al.* 2007), used up 180 liter liquid Helium in 2007 August, 550 days after the launch, and completed its cold mission. However, the on-board cryocooler still keeps the telescope and instrument low enough to continue near-infrared (NIR) observations with the Infrared Camera (IRC; Onaka *et al.* 2007). The IRC has a low-resolution spectroscopic capability (Ohyama *et al.* 2007) in addition to the imaging, which enables us to carry out sensitive spectroscopic observations in the NIR. In this paper we present the latest results of a study of the $3\ \mu\text{m}$ PAH bands based on *AKARI*/IRC spectroscopic observations carried out during the *AKARI* warm mission (Onaka *et al.* 2010) together with the results of a search for features of deuterated PAHs in the $4\ \mu\text{m}$ region.

2 IRC spectroscopy and results

The IRC spectroscopy has the slit and slit-less modes with a choice of the dispersers: prism (NP) and grism (NG) (see Ohyama *et al.* 2007 for details). For slit-less point source spectroscopy with the grism, a small window is used to avoid overlapping with other sources. A number of various types of objects, including young stellar objects, planetary nebulae, and external galaxies, have so far been observed in this mode in the *AKARI* warm mission (*e.g.*, Shimonishi *et al.* 2010).

The IRC slit spectroscopy has a choice of the slit: medium (Ns) and narrow (Nh). The spectral resolution with Ns is about 100, whereas Nh provides about 150. Both are long slits ($\sim 0'.8$) and spatial information can be extracted along the slit. The data used in the present study were taken in the Ns slit spectroscopy. The observations were carried out as part of the *AKARI* mission program Interstellar Medium in our Galaxy and nearby galaxies (ISMGN; Kaneda *et al.* 2009). More than 100 Galactic objects, most of which are HII-PDR complexes, and about 100 positions on the Galactic plane (diffuse Galactic radiation) have been observed in this program, part of which are used in the present investigation.

Figure 1 shows examples of the spectra of the Galactic plane. They clearly detect the 3.3 , 3.4 , and $3.5\ \mu\text{m}$ PAH features together with hydrogen recombination lines originating from the ionized gas (*e.g.*, $\text{Br}\alpha$ at $4.05\ \mu\text{m}$ and $\text{Br}\beta$ at $2.63\ \mu\text{m}$). The $3.3\ \mu\text{m}$ band is well resolved, but the separation of the 3.4 and $3.5\ \mu\text{m}$ bands

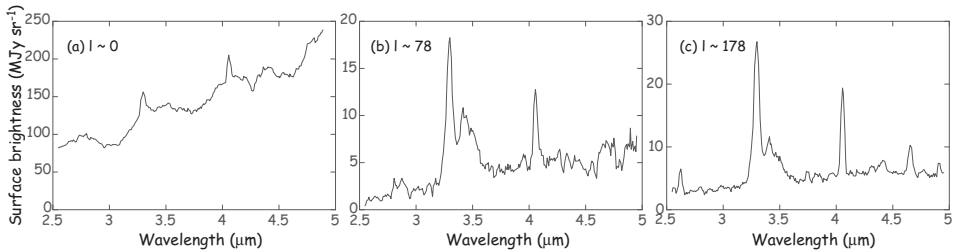


Fig. 1. Examples of AKARI/IRC NIR spectra of the Galactic plane: (a) $l \sim 0^\circ$, (b) $l \sim 78^\circ$, and (c) $l \sim 178^\circ$.

is not always clear. The spectra also indicate a significant variation in the PAH features. The spectrum of the Galactic center region (a) shows the absorption features of H_2O and CO_2 ices at 3.0 and $4.3 \mu\text{m}$, respectively, as well as gaseous CO absorption at $4.6 \mu\text{m}$ and $\text{Br}\alpha$ emission at $4.05 \mu\text{m}$.

To derive the band intensity, we first make a spline fit with the continuum and then fit the PAH features in the $3 \mu\text{m}$ region. A combination of two Lorentzians (for the 3.3 and $3.4 \mu\text{m}$ bands) and one Gaussian (for the $3.5 \mu\text{m}$ band) provides the best fit; however, this does not indicate the nature of the bands because the $3.5 \mu\text{m}$ band consists of more than one components, which are not resolved with the present resolution. Since the separation of the 3.4 and $3.5 \mu\text{m}$ bands is not always clear, only a summation of the two band strengths is discussed in the following.

Figure 2a shows the intensity ratio of the summation of the 3.4 and $3.5 \mu\text{m}$ bands to the $3.3 \mu\text{m}$ band against that of the 3.4 to $3.3 \mu\text{m}$ band. As described above, the horizontal axis may not be well defined and is used here only for the illustration purpose. The compact sources (mostly HII-PDR complexes) have the ratio in a relatively narrow range (0.2 – 0.5), while the ratio of the diffuse Galactic radiation shows a large variation. Figure 2b plots the intensity ratio in the diffuse radiation against the Galactic longitude. It suggests a global trend that the ratio increases towards the Galactic center region, though the scatter is large. The latter is compatible with the variations seen within an object and among objects in previous studies (*e.g.*, Geballe *et al.* 1989; Joblin *et al.* 1996).

3 Search for deuterated PAH features

The abundance of deuterium in the ISM is an important parameter in the study of the galaxy evolution since deuterium was formed at the beginning of the Universe and has been gradually destroyed in the stellar interior (“astration”). Its abundance must be strongly linked to the cosmological parameters and the chemical evolution of the Galaxy. Recent far-ultraviolet observations, however, indicate that the interstellar deuterium abundance is significantly lower than model predictions. In addition they suggest several pieces of evidence that deuterium is depleted onto dust grains (Linsky *et al.* 2006). Draine (2006) proposed that

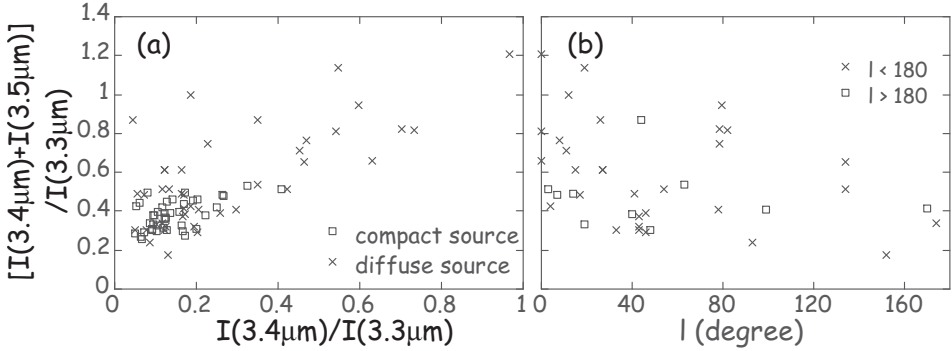


Fig. 2. (a) The intensity ratio of the summation of the 3.4 and 3.5 μm bands to the 3.3 μm band against that of the 3.4 to 3.3 μm band. The open squares indicate “compact” sources, which are mostly HII region-PDR complexes (see text), while the crosses show the diffuse radiation from the Galactic plane. (b) The Galactic longitude dependence of the intensity ratio of the summation of the 3.4 and 3.5 μm bands to the 3.3 μm band for the diffuse Galactic radiation. The crosses indicate those of $0 \leq l < 180^\circ$ and the open squares show those of $180 \leq l < 360^\circ$.

deuterium may be contained in interstellar PAHs since hydrogen in PAHs could be easily replaced by deuterium in low temperature environments. The 3.3 and 3.4 μm PAH bands should be shifted to the 4.3–4.7 μm region once they are deuterated. If the observed depletion can be attributed solely to deuteration of PAHs, then the deuterium fraction in PAHs can be as large as 0.3. Peeters *et al.* (2004) reported a possible detection of the 4.4 and 4.65 μm features in the Orion bar and M17 based on *ISO/SWS* spectra. They derived the integrated intensity ratio of the deuterated PAH features to the 3.3 and 3.4 μm PAH features to be 0.17 ± 0.03 and 0.36 ± 0.08 for the Orion bar and M17, respectively. However, the detection was marginal even for the best case (4.4σ) and needs to be confirmed by further observations. The IRC spectroscopy offers the best opportunity to search for deuterated PAH features in the 4 μm , since the predicted spectral range is strongly blocked by the terrestrial atmosphere.

A couple of problems have to be taken into account before making a reliable search for features in the 4 μm region in IRC spectra. First, the IRC NIR detector array shows fixed patterns in the direction vertical to the dispersion, which could produce spurious features in the spectrum. Appreciable features are in fact seen occasionally at around 3.8, 3.95, and 4.4 μm . The last one unfortunately coincides with the wavelength of one of the predicted deuterated PAH features. For the slit-less spectroscopy this does not make a problem since the spurious features can be removed by dithering operations, but it could be a serious problem for the slit spectroscopy. A spectral flat is created for the slit spectroscopy from the spectra of the central part of M31 by assuming that it is smooth without any appreciable features, and then applied to the observed spectra.

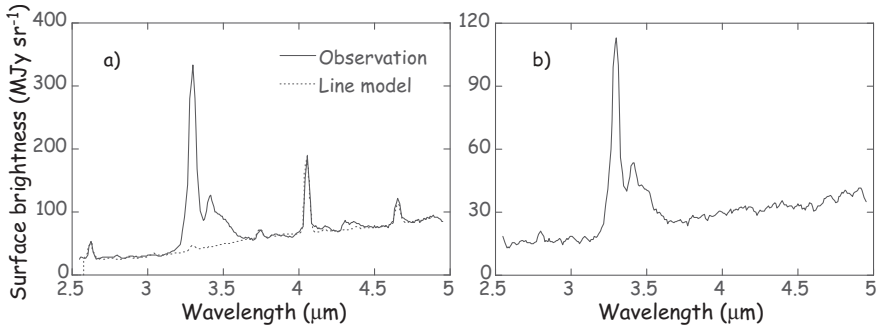


Fig. 3. (a) *AKARI/IRC* spectrum of M17. The solid line shows the observed spectrum corrected for the detector anomaly, whereas the dotted line indicates the spectrum with hydrogen recombination lines that are calculated from $\text{Br}\alpha$ based on the case B conditions (see text). Note that the HeI line at $4.3\ \mu\text{m}$ is not included in the calculation. (b) *AKARI/IRC* spectrum of a region without recombination lines.

The other issue is the evaluation of the contribution of emission lines from the ionized gas. In particular, $\text{Pf}\beta$ at $4.65\ \mu\text{m}$ appears at a wavelength near a predicted feature of deuterated PAHs. Contribution from the ionized gas, if any, must be removed from the spectrum. Assuming the case B conditions with the electron temperature of $7500\ \text{K}$ and the density of $10^4\ \text{cm}^{-3}$, the line intensity of $\text{Pf}\beta$ is estimated from $\text{Br}\alpha$. The intensities of $\text{Br}\beta$ and $\text{Pf}\gamma$ are also used to estimate possible extinction.

Figure 3a shows an IRC spectrum (solid line) of M17 together with the spectrum with the predicted line emission (dotted line). The model well accounts for the observed hydrogen emission lines. The observed $4.65\ \mu\text{m}$ line seems to be slightly stronger than the predicted $\text{Pf}\beta$. There is also excess emission around $4.3\ \mu\text{m}$. Part of the excess can be attributed to the He recombination line at $4.3\ \mu\text{m}$, which is not included in the line calculation. Even taking account of possible features remaining around 4.4 and $4.65\ \mu\text{m}$, however, the summation of the integrated intensities of these features amounts only 3% of the summation of the integrated intensities of the $3\ \mu\text{m}$ PAH features.

Spectra of the regions that do not have appreciable contribution from the ionized gas have a less uncertainty in the removal of $\text{Pf}\beta$ and could impose a more stringent constraint on the possible feature intensities. Figure 3b shows one of the examples, which was obtained towards the Galactic plane of $l \sim 10^\circ$. The spectral flat has been applied. It does not show any significant features in the $4\ \mu\text{m}$ region, while the $3.3\text{--}3.5\ \mu\text{m}$ features are clearly seen. A conservative upper limit for the ratio of the integrated intensities is obtained as 2%.

4 Summary

The IRC NIR spectroscopy in the *AKARI* warm mission provides the first opportunity to make a systematic study of the $3\ \mu\text{m}$ PAH features in various objects.

The intensity ratio of the 3.4 and 3.5 μm bands to the 3.3 μm band is relatively constant for HII-PDR complexes. The intensity ratio of the diffuse Galactic emission, on the other hand, shows a large variation in a galactic scale, suggesting a tendency that the ratio increases towards the Galactic center region, although the scatter is large. A search for deuterated PAH features in the 4 μm region of the IRC spectra of Galactic objects gives a conservative upper limit of 2–3% for the integrated intensity of the deuterated PAH features relative to the 3.3–3.5 μm features. It should be noted that this ratio cannot directly be converted into the abundance ratio because the oscillator strength of isotopic species in the vibration transition could be different. Moreover the difference in the excitation conditions between the 3 and 4 μm regions must also be taken into account properly.

This work is based on observations with *AKARI*, a JAXA project with the participation of ESA. The author thanks all the members of the *AKARI* project for their continuous support. This work is supported by a Grant-in-Aid for Scientific Research and a Grant-in-Aid for challenging Exploratory Research from the JSPS.

References

- Berné, O., Joblin, C., Deville, Y., *et al.*, 2007, *A&A*, 469, 575
Chan, K.-W., Roellig, T.L., Onaka, T., *et al.*, 2001, *ApJ*, 231, 183
Draine, B.T., 2006, *ASP Conf. Ser.*, 348, 58
Joblin, C., Tielens, A.G.G.M., Geballe, T.R., & Wooden, D.H., 1996, *ApJ*, 458, 610
Geballe, T.R., Tielens, A.G.G.M., Allamandola, L.J., Moorhouse, A., & Brand, P.W.J.L., 1989, *ApJ*, 341, 278
Giard, M., Serra, G., Caux, E., Pajot, F., & Lamarre, J.M., 1988, *A&A*, 201, L1
Kaneda, H., Koo, B.-C., Onaka, T., & Takahashi, H., 2009, *Adv. Sp. Res.*, 44, 1038
Linsky, J., Draine, B.T., Moos, H.W., *et al.*, 2006, *ApJ*, 647, 1106
Mattila, K., Haikala, L.K., Laureijs, R., *et al.*, 1996, *A&A*, 315, L353
Murakami, H., Baba, H., Barthel, P., *et al.*, 2007, *PASJ*, 59, S309
Ohyama, Y., Onaka, T., Matsuhara, H., *et al.*, 2007, *PASJ*, 59, S411
Onaka, T., Yamamura, I., Tanabé, T., Roellig, T.L., & Yuen, L., 1996, *PASJ*, 48, L59
Onaka, T., Matsuhara, H., Wada, T., *et al.*, 2007, *PASJ*, 59, S401
Onaka, T., Matsuhara, H., Wada, T., *et al.*, 2010, *Proc. SPIE*, 7731, 77310M
Peeters, E., Hony, S., Van Kerckhoven, C., *et al.*, 2002, *A&A*, 390, 1089
Peeters, E., Allamandola, L.J., Bauschlicher, C.W., Jr., *et al.*, 2004, *ApJ*, 604, 252
Rapacioli, M., Joblin, C., & Boissel, P., 2005, *A&A*, 429, 193
Sakon, I., Onaka, T., Ishihara, D., *et al.*, 2004, *ApJ*, 609, 203
Shimonishi, T., Onaka, T., Kato, D., *et al.*, 2010, *A&A*, 514, A12
Smith, J.D., Braine, B.T., Dale, D.A., *et al.*, 2007, *ApJ*, 656, 770
Song, I.-O., Kerr, T.H., McCombie, J., & Sarre, P.J., 2003, *MNRAS*, 346, L1
Tanaka, M., Matsumoto, T., Murakami, H., *et al.*, 1996, *PASJ*, 48, L53

LABORATORY INFRARED SPECTROSCOPY OF PAHS

J. Oomens^{1, 2}

Abstract. The hypothesis that polyaromatic molecules are the carriers of the infrared interstellar emission bands has spurred the laboratory spectroscopy of this class of molecules. Here we will give an overview of the infrared spectroscopic methods that have been applied over the past two decades to investigate the IR spectra of PAHs, their ions and related species.

1 Introduction

One of the earlier comparisons of a spectrum of the unidentified infrared (UIR) bands – from the Orion Bar region – and an experimental laboratory spectrum of a sample of polyaromatic species was reported by Allamandola *et al.* (1985), who used a low-resolution Raman spectrum of a car exhaust sample as the reference PAH spectrum. In their seminal work, Léger & Puget (1984) used a calculated emission spectrum of coronene as a reference spectrum to explain the UIR bands. These examples illustrate the very limited availability of laboratory spectroscopic data on PAH species at the time the PAHs were first proposed as UIR band carriers. Although some pellet and solution-phase spectra of PAHs had been obtained with grating instruments (Colangeli *et al.* 1992), the PAH hypothesis inspired spectroscopists around the World to record infrared PAH spectra under better defined and more astrophysically relevant conditions.

The interstellar emission spectra are believed to be carried by gas-phase PAH species in complete isolation. Except in highly irradiated environments, their rotational temperature is believed to be below 100 K (Ysard & Verstraete 2010), while the vibrational temperature is estimated to be on the order of 1000 K after the absorption of an interstellar UV photon and subsequent internal conversion releasing the UV photon energy into the vibrational manifold of the electronic ground state. Finally, spectra recorded in emission rather than in absorption are astrophysically more relevant.

¹ FOM Rijnhuizen, Edisonbaan 14, 3439MN Nieuwegein, The Netherlands

² van't Hoff Institute for Molecular Sciences, University of Amsterdam, Amsterdam, The Netherlands

In this contribution, we will briefly review the experimental methods that have been applied over the past 25 years to obtain infrared spectra of isolated PAHs.

2 Neutral PAH infrared spectroscopy

To reduce the effects of the medium on the IR spectra recorded (Flickinger *et al.* 1991; Moutou *et al.* 1996), an inert cryogenic Ar matrix was used instead of the salt pellets or solution (typically CCl_4). This also enabled spectroscopists to obtain spectra at low temperature, which is more relevant to the conditions of dense clouds. But even the rare gas matrix can influence the appearance of the IR spectra (Joblin *et al.* 1994) and hence gas-phase absorption spectra were recorded, although this required heating the samples in an oven as a consequence of the low vapor pressure of the PAHs. The use of molecular beam methods combined with laser spectroscopy allowed spectroscopists to obtain low-temperature gas-phase absorption spectra. It was further realized that emission spectra, as observed from the ISM, may be different from absorption spectra as recorded with the use of (commercial) spectrometers. Various spectroscopists thus set out to record gas-phase IR emission spectra, which perhaps provide the most astrophysically relevant neutral PAH spectra to date.

2.1 Matrix isolation spectroscopy

In matrix isolation, a host molecule (the PAH in this case) and an inert guest (often the rare gas atoms Ar or Ne) are simultaneously condensed onto an optical window, which is kept at a cryogenic temperature in a cryostat. The technique has been widely applied to study reactive species, which are stabilized by the low temperature and inert environment. As a consequence of the low temperature and the quenching of rotational degrees of freedom in the matrix, IR spectra of matrix-isolated PAHs feature sharp absorption bands with FWHM linewidths on the order of 1 cm^{-1} . An extensive database of infrared PAH spectra recorded in cryogenic Ar matrices has been collected by the NASA Ames group¹.

Recent applications include the study of nitrogen containing PAHs (Mattioda *et al.* 2003), which have been suggested to provide a better match for the interstellar $6.2 \mu\text{m}$ emission band (Hudgins *et al.* 2005; Peeters *et al.* 2002), and of complexes of PAHs and atomic Fe, which have been suggested to be stable in interstellar clouds (Klotz *et al.* 1996; Wang *et al.* 2007). The method has also been applied to record PAH spectra in the far-infrared range of the spectrum (Mattioda *et al.* 2009), where very molecule-specific vibrational modes – the so-called “drumhead” modes – are located.

¹See www.astrochem.org/pahdb

2.2 Gas-phase absorption spectroscopy

While the matrix isolation spectra provide high resolution spectra for a large number of PAH molecules, the influence of the matrix on the frequencies and, in particular, intensities remains unknown (Joblin *et al.* 1994). Gas-phase spectra were considered to be more relevant from an astrophysical point of view and could, moreover, shed more light on possible matrix effects. Except for the smallest members of the family, however, the vapor pressure of PAHs is too low to record direct absorption spectra.

This issue was addressed by Joblin *et al.* (1994), who set up a heatpipe oven inside an FTIR spectrometer to record gas-phase IR absorption spectra of PAHs up to the size of ovalene ($C_{32}H_{14}$). This study indicated that while gas-phase and matrix isolated band positions reproduce to within about 1%, band intensities can change by up to a factor of five. While the high temperatures needed to vaporize the molecules lead to substantially larger bandwidths and may appear to be astrophysically unrealistic, interstellar emission occurs from excited PAH molecules which are estimated to possess vibrational temperatures on the order of 1000 K (Joblin *et al.* 1995). Moreover, spectra recorded at different temperatures of the oven yield direct information on the anharmonic frequency shifts of vibrational bands (Pirali *et al.* 2009), which are important in modelling IR emission spectra (Cook & Saykally 1998) and which are hard to estimate computationally for large systems.

Gas-phase spectra recorded at low temperature are expected to give the best values for the intrinsic molecular band positions, free from shifting due to anharmonic interactions or matrix effects. To obtain such low-temperature spectra for low-vapor pressure compounds, molecular beam techniques can be applied. Here, low rovibrational temperatures are achieved by expansion cooling of the molecules in a supersonic beam of rare-gas atoms. Typical rotational temperatures are on the order of 10 K; vibrational cooling can be less efficient. The low densities of molecules in these beams require the application of tunable lasers to obtain (infrared) spectra of the jet-cooled PAHs. Piest *et al.* (2001) applied such methods at the infrared free electron laser facility FELIX (Oepts *et al.* 1995) to obtain IR spectra of small PAH molecules, such as phenanthrene.

2.3 Infrared emission spectra

Interstellar UIR spectra are observed as emission spectra rather than as absorption spectra and hence, laboratory emission spectra are desirable. One of the main difficulties in these experiments is to distinguish the PAH IR fluorescence from the blackbody emission of the environment. Early experiments on UV excited PAH species therefore only recorded spectra in the $3\ \mu\text{m}$ spectral range (Shan *et al.* 1991; Williams & Leone 1995). Thermally heated gas-phase PAH samples were used to increase the number density of emitting molecules so that the infrared PAH emission could be better distinguished from the background allowing various groups to record spectra at higher resolution (Pirali & Vervloet 2006) and further

into the infrared (Joblin *et al.* 1995). The evaporated PAHs, however, form a sample in thermal equilibrium, while UV-excited PAHs combine low rotational excitation with high vibrational excitation, a situation that more closely resembles the assumed conditions in the ISM. Perhaps the most sophisticated emission spectroscopy experiments have been reported by the group of Saykally, who used a cryogenically cooled grating spectrometer to greatly suppress the blackbody background radiation, in combination with an extremely sensitive IR detector (Cook *et al.* 1998, 1996). Thus, emission spectra of UV excited PAHs were recorded over the entire IR range from 3 to 15 μm .

3 IR spectroscopy of ionic PAH species

One of the main conclusions of the emission spectra of Cook *et al.* (1996) was that neutral PAH species would not be able to explain the UIR emission features and the presence of a substantial fraction of ionized PAHs was invoked. In fact, already early on in the history of the PAH hypothesis it was realized that ionized PAHs may play an important role because of the low ionization potentials of PAHs combined with the UV pump fields that are necessary to induce IR emission (Allamandola *et al.* 1989). An important difference between the spectra of neutral and cationic PAHs was first revealed by quantum-chemical calculations on the naphthalene radical cation by Pauzat *et al.* (1992); see also the contribution by Pauzat elsewhere in this volume.

These considerations inspired various laboratory spectroscopists to record spectra of ionized PAH species, again preferably under astrophysically relevant conditions. Because of their mutual repulsion and inherently low gas-phase number densities, direct absorption spectra of (mass-selected) gas-phase ions are difficult, if not impossible, to record. Matrix isolation spectroscopy offers a way around this problem, but also gas-phase “action spectroscopy” schemes have more recently been applied. Here we discuss the different methods applied to date and compare their merits and limitations.

3.1 Matrix isolation spectroscopy

Immediately following the computations of Pauzat *et al.* (1992), the group of Vala at the University of Florida set out to record the naphthalene cation spectrum using a modified matrix isolation set up (Szczepanski *et al.* 1992). The effusive naphthalene beam, which is co-deposited onto the 12-K BaF₂ substrate with an Ar beam, was intercepted by an electron beam with electron energies on the order of 50 – 200 eV. The Ar sample was premixed with CCl₄, which acts as an electron acceptor, reducing the re-neutralization of the naphthalene cations once in the matrix. The IR spectrum of the matrix was then recorded using an FTIR spectrometer. One possible pitfall of this method is the possible recombination or reactivity of the naphthalene cation in the matrix. Observed IR bands of neutral naphthalene are therefore subtracted. Moreover, to assign newly observed IR bands to the cation of interest, their intensity is typically correlated with those of

known bands in a UV/vis spectrum recorded from the same matrix (Szczepanski & Vala 1991).

The experimental naphthalene cation spectrum confirmed the computational results and showed definitively that the relative intensities of the different families of vibrational modes undergo major changes upon ionization. Soon after this first PAH cation spectrum, IR matrix isolation spectra of a whole series of cationic PAHs were reported mainly by the Florida (Szczepanski & Vala 1993a) and NASA Ames (Hudgins & Allamandola 1995a,b; Hudgins *et al.* 1994) groups. These spectra provided the first experimental evidence that ionized PAHs may be abundant in the ISM (Allamandola *et al.* 1999; Szczepanski & Vala 1993b). In addition, these spectra provided the experimental verification for various quantum-chemical studies on the IR properties of ionized PAHs. For the vast majority of the PAH species that have been studied, a good correlation was found between experimental frequencies (and intensities) and values computed at the density functional level of theory (see *e.g.* Langhoff (1996)). This provides confidence in the spectra calculated for species that are experimentally not easily accessible, such as very large PAHs (Bauschlicher *et al.* 2008; Mallocci *et al.* 2007).

Despite the success of matrix isolation spectroscopy and the ever growing database of spectra, the possible unknown effects of the matrix on band frequencies and intensities made that the desire to record true gas-phase PAH ion spectra remained. The main hurdle to record such spectra were the extremely low densities in which gas-phase ions are typically produced as a consequence of their mutual Coulombic repulsion. Spectroscopic methods based on conventional direct absorption techniques are therefore generally not applicable to (mass-selected) molecular ions. Since the 1980's, however, infrared laser-based methods became increasingly successful in recording gas-phase molecular ion spectra (Duncan 2000).

3.2 Messenger atom spectroscopy

One of the most influential laser-based methods was originally introduced by Y.T. Lee and coworkers and became known as “messenger-atom” spectroscopy (Lisy 2006; Okumura *et al.* 1985, 1990). The method is based on a supersonic expansion in which ionized molecular species form weakly bound complexes with neutral molecules or atoms, which are mass-selected typically in a quadrupole mass selector (QMS) or sector magnet. Upon excitation with an IR laser, the complex undergoes pre-dissociation and the now bare molecular ion is detected in a mass analyzer, typically a time-of-flight (TOF) or quadrupole mass spectrometer. In all such combinations of tandem mass spectrometry and laser spectroscopy, monitoring the intensity of the mass peak of the product molecular ion as a function of the IR wavelength then generates an IR spectrum of the ionic complex. While the entire ionic complexes have been the subject of many studies, it was also realized that the neutral partner in the complex could be used solely as the detector of IR photon absorption by the molecular ion, as signalled by its detachment from the ion, hence the term “messenger”. Clearly in this case, the messenger was to have an as small as possible influence on the ionic species of interest – or in the words of Y.T. Lee,

it was to behave as a spy (Okumura *et al.* 1990) – and hence, the use of rare gas atoms rather than small molecules became popular. Messenger atom spectroscopy was for instance used to record the IR spectra of several ionized aromatic systems, particularly benzene and various of its ring-substituted derivatives (Solcà & Dopfer 2004).

The early studies based on messenger spectroscopy focused particularly on the hydrogen stretching vibrations in the $3\ \mu\text{m}$ wavelength range, since tunable radiation can be generated in this range by various methods, including frequency mixing of the output of a tunable dye laser in birefringent crystals. Towards the late 1990's, new widely tunable laser sources became available that covered the astrophysically interesting wavelength range roughly between 6 and $16\ \mu\text{m}$. Novel birefringent materials allowed non-linear frequency down-conversion methods to penetrate further into the IR (Bosenberg & Guyer 1993). Moreover, tunable infrared free electron lasers (O'Shea & Freund 2001), where radiation is generated by a relativistic beam of electrons injected into a periodic magnetic field structure (wiggler), entered the realm of spectroscopy.

Using the free electron laser at the FELIX facility, Meijer and coworkers recorded the gas-phase IR spectra of the naphthalene (Piest *et al.* 1999a) and phenanthrene (Piest *et al.* 2001) cations using a variation of the messenger-atom spectroscopy method (Piest *et al.* 1999b). Van der Waals clusters of the PAH and a rare gas atom (Ar in most cases) were produced in a pulsed molecular beam expansion and they were resonantly ionized using a two-color resonance enhanced multiphoton ionization (REMPI) scheme. The thus formed intact $\text{PAH}^+\text{-Ar}$ complexes were then irradiated by the output of the free electron laser, which was tuned in wavelength across the entire 6 to $16\ \mu\text{m}$ range. IR absorption was signalled as the appearance of the bare PAH^+ ion in a TOF mass spectrometer. Since the influence of the weakly bound Ar atom is assumed to be negligible, the spectra, which feature a resolution of just a few cm^{-1} , can be considered as being due to the cold and isolated PAH cation.

The group of Duncan recently recorded IR spectra of protonated benzene (Douberly *et al.* 2008) and naphthalene (Ricks *et al.* 2009) using an optical parametric oscillator (OPO) source that provides mJ pulse energies down to wavelengths of about $10\ \mu\text{m}$. Argon tagged protonated molecules are produced in the expansion from a pulsed discharge nozzle and mass-selected in the first arm of a reflectron TOF mass spectrometer. The ions are then exposed to the IR radiation in the turning point of the reflectron stack and mass analysis is accomplished in the second arm of the reflectron. Also here, detachment of the messenger (Ar) is used to signal IR absorption by the protonated PAH, giving the spectrum of the ionized PAH at a resolution of a few cm^{-1} .

3.3 IR multiple photon dissociation spectroscopy

In the 1980's, various groups explored the possibilities of gas-phase infrared ion spectroscopy by wavelength selective multiple photon dissociation of ions in storage mass spectrometers using powerful line-tunable CO_2 -lasers (see Eyler 2009 for a

recent review). Although a variety of ionic systems was successfully studied, the limited tuning range of the CO₂-laser (roughly 9 – 11 μm) severely impeded the practical applicability of this method for spectroscopic purposes. More recently, the infrared pulse energies produced by free electron lasers were shown to be high enough to induce photodissociation of vapor-phase PAH cations (Oomens *et al.* 2000). Installation of an ion trap time-of-flight mass spectrometer at the free electron laser facility FELIX thus allowed Oomens *et al.* (2003) to record IR multiple photon dissociation (IRMPD) spectra for a large number of mass selected ionic PAHs. The PAHs are vaporized in an oven and effuse to the center of a quadrupole ion trap, where they are non-resonantly ionized by a UV laser (excimer). Possible UV-induced fragments are mass-selectively removed from the trap and the isolated parent ions are irradiated with the FEL beam. The IR induced fragments and the remaining parent ions are then mass-analyzed in a TOF spectrometer, so that an IRMPD spectrum can be reconstructed by plotting the fragment yield as a function of the FEL wavelength.

Dissociation thresholds for PAH ions are typically in the 6 – 8 eV range, which requires the absorption of tens to hundreds of IR photons. In polyatomic molecules of the size of PAHs, infrared multiple photon excitation typically proceeds via rapid redistribution of the vibrational energy from the excited mode into the bath formed by all vibrations of the molecule. Intramolecular vibrational redistribution (IVR) thus allows the molecule to sequentially absorb multiple photons on the same vibrational transition, because the upper level is constantly being de-excited by quenching to the bath states (Black *et al.* 1977; Eyler 2009; Grant *et al.* 1978). IVR-mediated multiple photon excitation thus avoids vibrational ladder climbing, which is an inefficient process due to the anharmonicity bottleneck. The multiple-photon nature of this spectroscopic technique is reflected in the shape of the spectral features observed, most notably from the increased bandwidth as compared to messenger-atom or matrix isolation spectroscopy. The PAH ion spectra recorded at FELIX using this method display FWHM bandwidths on the order of 30 cm⁻¹ (Oomens *et al.* 2000).

At the free electron laser facilities CLIO and FELIX, the FEL beam has now been coupled to powerful tandem mass spectrometers, so that a variety of ionic PAH-related species can be spectroscopically studied. The ions can be produced by a variety of ion sources, including electrospray ionization (ESI) and laser desorption/ablation methods. Much recent interest has been on protonated PAH species including protonated regular PAHs (Knorke *et al.* 2009; Lorenz *et al.* 2007; Vala *et al.* 2009b) and protonated N-containing PAHs (Alvaro Galué *et al.* 2010; Vala *et al.* 2009a). Clear differences are observed in the spectra of (even-electron) protonated species and (odd-electron) radical cation species. PAHs have long been suggested to efficiently bind to astrophysically abundant metal atoms or ions (Joalland *et al.* 2009; Klotz *et al.* 1996) and such species are now being investigated spectroscopically using IRMPD spectroscopy (Simon *et al.* 2008; Szczepanski *et al.* 2006).

3.4 IR emission spectroscopy

As mentioned in Section 2.3 for neutral PAH species, IR spectra recorded in emission instead of absorption, as is more common, have the advantage that they mimic better the interstellar situation, where the UIR bands are observed in emission as well. However, the difficulty in recording emission spectra in the astrophysically most relevant 6 – 16 μm range lies mainly in distinguishing the weak infrared PAH fluorescence from the blackbody radiation of the environment. This is an even more daunting task for ionic species as compared to neutrals, as the ion densities are intrinsically much lower. Nonetheless, the Saykally group at Berkeley managed to adapt their cryogenically cooled spectrometer so that it could be used to record emission spectra of gas-phase ionic PAHs (Kim & Saykally 2003). To this end, the spectrometer is coupled to an electron impact ion source, which produces high ion currents of more than 6 μA . Electron impact with approximately 70 eV electrons not only ionizes the molecules, but also induces vibronic excitations that are comparable to UV excitation; hence, the IR emission from the ions is assumed to be similar to that from UV excited ions as occurs under interstellar conditions. Using a quadrupole deflector, the ions are injected into a reflectron, which is placed in front of the entrance slit of the spectrometer. A reflectron is used to increase the residence time of the ions in the viewing region of the spectrometer. All ion optics in the line of sight of the spectrometer need to be cryogenically cooled while being electrically isolated, which constituted one of the main design challenges (Kim & Saykally 2003).

IR emission spectra were reported for the pyrene cation ($\text{C}_{16}\text{H}_{10}^+$) and several dehydrogenated derivatives (Kim & Saykally 2002; Kim *et al.* 2001). The pyrene cation spectrum showed a good correspondence with matrix isolation and IRMPD spectra of the pyrene cation. Additional bands observed in the emission spectrum could be attributed to partly dehydrogenated fragments of the pyrene cation.

4 Experimental methods compared

A discussion of the various experimental methods applied for PAH spectroscopy inevitably raises the question as to which of the techniques is superior. This question is, however, not easily answered: each method has its strong and weak points.

Of all spectroscopic methods discussed here, IR emission spectroscopy yields spectra under conditions that are arguably most closely mimicking those of the interstellar PAHs. The gaseous PAHs are electronically excited to energies in the range of the interstellar conditions. The effects of vibrational anharmonicity (Barker *et al.* 1987; Pirali *et al.* 2009) are naturally incorporated into the observed emission bands. This is clearly an advantage over spectra obtained using absorption spectroscopy since for a true comparison to interstellar emission spectra, one would have to convolute the bands using an emission model including the vibrational anharmonicities (Cook & Saykally 1998; Pech *et al.* 2002), which are however largely unknown. However, the experiments are extremely challenging,

particularly for ionic PAHs. The method requires a cryogenically cooled IR spectrometer with a very sensitive IR photon detector; for the ions, a high ion current source is required as well. Thus far, only the group of Saykally have reported IR emission spectra of PAH ions in the 5 – 15 μm spectral range, and only very few spectra (of pyrene and some of its dehydrogenated fragments) have been reported.

Quite in contrast, matrix isolation spectroscopy is experimentally most readily implemented. Indeed, most PAH ion spectra reported to date have been obtained using this method. We may also note that variants of this method are currently being applied to study the spectroscopy and (photo-)chemistry of PAHs and other species in interstellar ices (Bernstein *et al.* 2007; Bouwman *et al.* 2009; Klotz *et al.* 1996). Matrix isolation spectra feature narrow bandwidths induced by the low temperature and the quenching of rotational motion in the rare gas matrix. Experimentally, matrix isolation spectroscopy may suffer from unknown effects of the matrix on the spectrum; in the infrared spectra, it appears that particularly relative intensities are affected (Joblin *et al.* 1994). Moreover, there is some uncertainty as to the exact nature of the species trapped in the matrix, particularly upon electron or UV irradiation, and correlation measurements are usually required to assign bands to specific species (Szczepanski & Vala 1991). This problem may be partly circumvented by mass-selective deposition of ions created *ex-situ*, see *e.g.* Fulara *et al.* (1993).

PAH ion spectra obtained using messenger atom spectroscopy have arguably provided the most reliable linear absorption spectra thus far. Bandwidths of just a few cm^{-1} have been obtained for PAH species that are estimated to be expansion cooled to temperatures on the order of 20 K. These methods require the availability of IR laser sources that are continuously tunable in the 5 – 15 μm spectral range and thus far free electron lasers and optical parametric oscillators have been used. Moreover, the PAHs need to be entrained in a seeded molecular beam expansion to form the weakly bound PAH-rare gas complexes, which has thus far only been possible for the smallest PAHs naphthalene (Piest *et al.* 1999a; Ricks *et al.* 2009) and phenanthrene (Piest *et al.* 2001).

IRMPD spectroscopy has the advantage that it can be conveniently coupled to (commercial) tandem mass spectrometers, providing access to many species beyond regular PAH ions. A tunable laser source with high output powers is required to induce fragmentation of the ions and thus far, mainly the free electron lasers FELIX in The Netherlands (Oomens *et al.* 2000) and CLIO in France (Lorenz *et al.* 2007) have been used for these studies. The spectral band shapes observed are clearly influenced by the process of multiple photon excitation (Oomens *et al.* 2003) resulting in FWHM bandwidths of typically 30 cm^{-1} or more, which tends to produce unresolved spectra for larger, more irregularly shaped species. Nonetheless, PAH ion spectra up to the size of coronene ($\text{C}_{24}\text{H}_{12}$) have been reported (Knorke *et al.* 2009; Oomens *et al.* 2001; Simon *et al.* 2008). In addition, one may note that the broadening of bands is (in part) caused by vibrational anharmonicity; although the processes of IR multiple photon excitation and emission are different, the bandwidths observed in the spectra are comparable (Oomens *et al.* 2003). The use of different ion sources and the capability of mass

selection prior to spectroscopic interrogation makes this method very versatile, which is reflected in the variety of ionic PAH-related species that have been investigated, such as Fe^+ PAH complexes (Simon *et al.* 2008; Szczepanski *et al.* 2006) and protonated PAHs (Knorke *et al.* 2009; Lorenz *et al.* 2007; Vala *et al.* 2009b). We anticipate that mass spectrometry based spectroscopic methods will be ideally suited to investigate structures of PAH photo-products (Ekern *et al.* 1997; Jochims *et al.* 1994), which may provide important information to better understand the chemistry of PAHs in the diffuse ISM.

New technologies to record IR spectra of ionized species are continuously being explored and they may hold great promise for improved PAH ion spectra. Using various spectroscopic schemes, cryogenically cooled multipole ion traps have been recently applied to record spectra of cold gas-phase ions. Laser-induced reactions have been applied to obtain IR spectra of small hydrocarbon ions of astrophysical interest, including the intriguing CH_5^+ (Asvany *et al.* 2005) and hydronium (Asvany *et al.* 2008) ions. Cold ion traps have been applied to record electronic spectra of carbon chain ions of astrophysical interest (Rice *et al.* 2010). Combination of UV and IR lasers in cold ion traps to obtain IR hole-burning spectra of the cryogenically cooled ions has been applied to biomolecules of various sizes (Nagornova *et al.* 2010; Stearns *et al.* 2007). We anticipate that such methods will be applicable to PAH species as well.

Superfluid nanoscopic He droplets are known to provide an extremely non-interacting and cold (0.4 K) matrix to study the spectroscopy of molecular species (Goyal *et al.* 1992; Hartmann *et al.* 1996). Drabbels and coworkers are now applying these methods to study the spectroscopy of ions, including aromatic species, at high resolutions (Loginov *et al.* 2008; Smolarek *et al.* 2010).

5 Concluding remarks

In this review, I have given an overview of the various experimental methods that have been applied to obtain IR spectra of PAHs since the 1980's, when these species were originally hypothesized to occur abundantly in the ISM. The experimental IR spectra provide important benchmarks for theoretical investigations of the spectral properties of PAHs, which are discussed elsewhere in this volume. In addition, theory and experiments to understand PAH spectra in other spectral ranges, particularly in the UV/vis range are addressed elsewhere in this issue. We thus conclude that much progress has been made over the past 25 years in the experimental characterization of the spectra of PAHs, their ions and various of their derivatives.

References

- Allamandola, L., Hudgins, D., & Sandford, S., 1999, *Astrophys. J.*, 511, L115
- Allamandola, L., Tielens, A., & Barker, J., 1985, *Astrophys. J.*, 290, L25
- Allamandola, L., Tielens, A., & Barker, J., 1989, *Astrophys. J. Suppl. Ser.*, 71, 733

- Alvaro Galué, H., Pirali, O., & Oomens, J., 2010, *Astron. Astrophys.*, 517, A15
- Asvany, O., Ricken, O., Müller, H.S.P., *et al.*, 2008, *Phys. Rev. Lett.*, 100, 233004
- Asvany, O., Schlemmer, S., Redlich, B., *et al.*, 2005, *Science* 309, 1219
- Barker, J., Allamandola, L., & Tielens, A., 1987, *Astrophys. J.*, 315, L61
- Bauschlicher, C.W., Peeters, E., & Allamandola, L.J., 2008, *Astrophys. J.*, 678, 316
- Bernstein, M.P., Sandford, S.A., Mattioda, A.L., & Allamandola, L.J., 2007, *Astrophys. J.*, 664, 1264
- Black, J.G., Yablonovitch, E., Bloembergen, N., & Mukamel, S., 1977, *Phys. Rev. Lett.*, 38, 1131
- Bosenberg, W.R., & Guyer, D.R., 1993, *J. Opt. Soc. Am. B*, 10, 17161722
- Bouwman, J., Paardekooper, D.M., Cuppen, H.M., Linnartz, H., & Allamandola, L.J., 2009, *Astrophys. J.*, 700, 56
- Colangeli, L., Mennella, V., Baratta, G.A., Bussoletti, E., & Strazzulla, G., 1992, *Astrophys. J.*, 396, 369
- Cook, D., & Saykally, R., 1998, *Astrophys. J.*, 493, 793
- Cook, D., Schlemmer, S., Balucani, N., *et al.*, 1998, *J. Phys. Chem. A*, 102, 1465
- Cook, D., Schlemmer, S., Balucani, N., *et al.*, 1996, *Nature*, 380, 227
- Douberly, G.E., Ricks, A.M., Schleyer, P.v.R., & Duncan, M.A., 2008, *J. Phys. Chem. A*, 112, 4869
- Duncan, M.A., 2000, *Int. J. Mass Spectrom.*, 200, 545
- Ekern, S., Marshall, A., Szczepanski, J., & Vala, M., 1997, *Astrophys. J.*, 488, L39
- Eyler, J.R., 2009, *Mass Spectrom. Rev.*, 28, 448
- Flickinger, G.C., Wdowiak, T.J., & Gomez, P.L., 1991, *Astrophys. J.*, 380, L43
- Fulara, J., Jakobi, M., & Maier, J., 1993, *Chem. Phys. Lett.*, 211, 227
- Goyal, S., Schutt, D.L., & Scoles, G., 1992, *Phys. Rev. Lett.*, 69, 933
- Grant, E.R., Schulz, P.A., Sudbo, A.S., Shen, Y.R., & Lee, Y.T., 1978, *Phys. Rev. Lett.*, 40, 115
- Hartmann, M., Miller, R.E., Toennies, J.P., & Vilesov, A.F., 1996, *Science*, 272, 1631
- Hudgins, D., & Allamandola, L., 1995a, *J. Phys. Chem.*, 99, 3033
- Hudgins, D., & Allamandola, L., 1995b, *J. Phys. Chem.*, 99, 8978
- Hudgins, D., Bauschlicher, C., & Allamandola, L., 2005, *Astrophys. J.*, 632, 316
- Hudgins, D., Sandford, S., & Allamandola, L., 1994, *J. Phys. Chem.*, 98, 4243
- Joalland, B., Simon, A., Marsden, C.J., & Joblin, C., 2009, *Astron. & Astrophys.*, 494, 969
- Joblin, C., Boissel, P., Leger, A., d'Hendecourt, L., & Defourneau, D., 1995, *Astron. Astrophys.*, 299, 835
- Joblin, C., d'Hendecourt, L., Leger, A., & Defourneau, D., 1994, *Astron. Astrophys.*, 281, 923
- Jochims, H.W., Ruhl, E., Baumgartel, H., Tobita, S., & Leach, S., 1994, *Astrophys. J.*, 420, 307
- Kim, H., & Saykally, R., 2002, *Astrophys. J. Suppl. Ser.*, 143, 455
- Kim, H., & Saykally, R., 2003, *Rev. Sci. Instrum.*, 74, 2488
- Kim, H., Wagner, D., & Saykally, R., 2001, *Phys. Rev. Lett.*, 86, 5691

- Klotz, A., Marty, P., Boissel, P., *et al.*, 1996, *Plan. Space Sci.*, 44, 957
- Knorke, H., Langer, J., Oomens, J., & Dopfer, O., 2009, *Astrophys. J.*, 706, L66
- Langhoff, S.R., 1996, *J. Phys. Chem.*, 100, 2819
- Léger, A., & Puget, J., 1984, *Astron. Astrophys.*, 137, L5
- Lisy, J.M., 2006, *J. Chem. Phys.*, 125, 132302
- Loginov, E., Braun, A., & Drabbels, M., 2008, *Phys. Chem. Chem. Phys.*, 10, 6107
- Lorenz, U.J., Solcà, N., Lemaire, J., Maitre, P., & Dopfer, O., 2007, *Angew. Chem. Int. Ed.*, 46, 6714
- Malloci, G., Joblin, C., & Mulas, G., 2007, *Chem. Phys.*, 332, 353
- Mattioda, A., Hudgins, D., Bauschlicher, C., Rosi, M., & Allamandola, L., 2003, *J. Phys. Chem. A*, 107, 1486
- Mattioda, A.L., Ricca, A., Tucker, J., Bauschlicher, Jr., C.W., & Allamandola, L.J., 2009, *Astron. J.*, 137, 4054
- Moutou, C., Leger, A., & dHendecourt, L., 1996, *Astron. Astrophys.*, 310, 297
- Nagornova, N.S., Rizzo, T.R., & Boyarkin, O.V., 2010, *J. Am. Chem. Soc.*, 132, 4040
- Oepts, D., van der Meer, A.F.G., & van Amersfoort, P.W., 1995, *Infrared Phys. Technol.*, 36, 297
- Okumura, M., Yeh, L.I., & Lee, Y.T., 1985, *J. Chem. Phys.*, 83, 3705
- Okumura, M., Yeh, L.I., Myers, J.D., & Lee, Y.T., 1990, *J. Phys. Chem.*, 94, 3416
- Oomens, J., Sartakov, B.G., Tielens, A.G.G.M., Meijer, G., & von Helden, G., 2001, *Astrophys. J.*, 560, L99
- Oomens, J., Tielens, A.G.G.M., Sartakov, B.G., von Helden, G., & Meijer, G., 2003, *Astrophys. J.*, 591, 968
- Oomens, J., van Roij, A.J.A., Meijer, G., & von Helden, G., 2000, *Astrophys. J.*, 542, 404
- O'Shea, P.G., & Freund, H.P. 2001, *Science*, 292, 1853
- Pauzat, F., Talbi, D., Miller, M.D., DeFrees, D.J., & Ellinger, Y., 1992, *J. Phys. Chem*, 96, 7882
- Pech, C., Joblin, C., Boissel, P., 2002, *Astron. Astrophys.*, 388, 639
- Peeters, E., Hony, S., Van Kerckhoven, C., *et al.*, 2002, *Astron. Astrophys.*, 390, 1089
- Piest, H., von Helden, G., & Meijer, G., 1999a, *Astrophys. J.*, 520, L75
- Piest, H., von Helden, G., & Meijer, G., 1999b, *J. Chem. Phys.*, 110, 2010
- Piest, J., Oomens, J., Bakker, J., von Helden, G., & Meijer, G., 2001, *Spectrochim. Acta A*, 57, 717
- Pirali, O., & Vervloet, M., 2006, *Chem. Phys. Lett.*, 423, 376
- Pirali, O., Vervloet, M., Mulas, G., Malloci, G., & Joblin, C., 2009, *Phys. Chem. Chem. Phys.*, 11, 3443
- Rice, C.A., Rudnev, V., Dietsche, R., & Maier, J.P., 2010, *Astron. J.*, 140, 203
- Ricks, A.M., Douberly, G.E., & Duncan, M.A., 2009, *Astrophys. J.*, 702, 301
- Shan, J., Sutton, M., & Lee, L.C., 1991, *Astrophys. J.*, 383, 459
- Simon, A., Joblin, C., Polfer, N., & Oomens, J., 2008, *J. Phys. Chem. A*, 112, 8551
- Smolarek, S., Vdovin, A., Perrier, D.L., *et al.*, 2010, *J. Am. Chem. Soc.*, 132, 6315
- Solcà, N., & Dopfer, O., 2004, *J. Am. Chem. Soc.*, 126, 1716

- Stearns, J.A., Mercier, S., Seaiby, C., *et al.*, 2007, *J. Am. Chem. Soc.*, 129, 11814
- Szczepanski, J., Roser, D., Personette, W., *et al.*, 1992, *J. Phys. Chem.*, 96, 7876
- Szczepanski, J., & Vala, M., 1991, *J. Phys. Chem.*, 95, 2792
- Szczepanski, J., & Vala, M., 1993a, *Astrophys. J.*, 414, 646
- Szczepanski, J., & Vala, M., 1993b, *Nature*, 363, 699
- Szczepanski, J., Wang, H., Vala, M., *et al.*, 2006, *Astrophys. J.*, 646, 666
- Vala, M., Szczepanski, J., Dunbar, R., Oomens, J., & Steill, J.D., 2009a, *Chem. Phys. Lett.*, 473, 43
- Vala, M., Szczepanski, J., Oomens, J., & Steill, J.D., 2009b, *J. Am. Chem. Soc.*, 131, 5784
- Wang, Y., Szczepanski, J., & Vala, M., 2007, *Chem. Phys.*, 342, 107
- Williams, R.M., & Leone, S.R. 1995, *Astrophys. J.*, 443, 675
- Ysard, N., & Verstraete, L. 2010, *Astron. & Astrophys.*, 509, A12

COMPUTATIONAL IR SPECTROSCOPY FOR PAHS: FROM THE EARLY YEARS TO THE PRESENT STATUS

F. Pauzat¹

Abstract. In the long story of interstellar PAHs, computations have played and are still playing a fundamental role in connection with experiments and observations. From the very first calculations of the IR spectra of small PAHs in the late eighties to the more recent ones, every aspect of the research linked to the PAH hypothesis has evolved dramatically: the size and the variety of the molecules considered, the techniques used, the precision of the astronomical observations . . . The initial landscape has completely changed though the quest is still the same, that is to correlate the so-called UIR bands spectra ubiquitous in the ISM (Inter Stellar Medium) with a chemical family of molecules, the PAHs. An historical review of the 25 years of this quest is presented here, focusing on the computational part.

1 Introduction

Theoretical studies of chemical species and processes in extreme physical conditions are a clear need of the astrophysical community confronted with situations almost impossible to reproduce in laboratory experiments. Many questions arise that do not find experimental answers easily. However, some of them can be obtained from theoretical studies that are the alternative in a number of problems.

One of these questions, which has proved to be a formidable challenge in modern astrophysics, is the interpretation of the infrared emission bands of our galaxy between 2 and 15 μm . These bands, referred to as “Unidentified Infra Red (UIR) bands” in the literature, were first discovered by ground-based observations at the end of the seventies. Since then, their existence has been confirmed in a number of objects by observations using the IRAS, ISO and more recently Spitzer and AKARI space missions. This emission, characterized by a series of bands that are systematically found at 3.3, 6.2, 7.7, 8.6, 11.3 and 12.7 μm , seems to be widely present in various environments of the interstellar medium (ISM). For interpreting

¹ UPMC Univ. Paris 06, UMR - CNRS 7616, LCT, 75005 Paris, France

this emission, Léger & Puget (1984), Allamandola *et al.* (1985) proposed a model based on the similarity between the spectra observed in space and those of neutral polycyclic aromatic hydrocarbons (PAH) obtained in the laboratory. In space, these molecules could become vibrationally excited by absorption of UV photons and then release their excess energy by means of infrared fluorescence (Duley & Williams 1981). This is generally referred to as the *PAH hypothesis*.

Contrary to radio spectra whose interpretation relies on a perfect match between observations and measurements on a single molecule, the observed IR spectra correspond to families of molecules so that the details of the spectral match cannot be satisfactory; furthermore, the relative intensities of the different bands observed may vary significantly from an astronomical object to another. Various interpretations of these differences have been proposed, leading sometimes to contradictory conclusions such as severe dehydrogenation or negligible dehydrogenation of the interstellar PAHs. It has been said that PAHs could be either neutral or positively charged due to ionization by the radiation field and that they could be present in the form of negative ions within dense clouds (Wakelam & Herbst 2008). Given such a diversity of hypotheses, the ideal strategy would have been to measure the IR emission of a selected number of representative species in the gas phase, at temperatures and densities reproducing the interstellar conditions in the laboratory. At that time, it was considered as a practically impossible task, and numerical simulation was the alternative. The main difficulties to be addressed were:

- i) The size of molecules like PAHs, ranging from a few tenths to several hundreds of atoms, which was, when the study began, non tractable for most *ab initio* quantum chemistry codes.
- ii) The number of different types of molecules (ramified, substituted, ionized, hydrogenated, de-hydrogenated, metallic-complexes . . .) to be treated at the same level of accuracy, implying a huge amount of computer time.
- iii) The level of accuracy necessary to connect calculations with observations, which raises two more problems. The first one refers to a real theoretical challenge: one has to compare an emission spectrum (observed) to an absorption spectrum (computed). The second one is not relevant of pure quantum chemistry: the reference being the observed spectrum, *i.e.* a global spectrum emitted by a mixture of molecules from a known family but with an unknown composition, the comparison depends of the composition chosen and there is no theoretical criterion to help designing a unique solution.

The difficult quest for theoretical IR spectra usable by astrophysicists, has been extending from the last eighties to nowadays with successes as well as setbacks. The presentation will be split into three chronological parts. The first part retraces a “learning period”, beginning in the late eighties, with methods whose reliability to efficiency ratio was still to be optimized for such molecules and variables. The options considered at the time are presented and discussed. It allowed to set up

standard procedures and eventually led to some spectacular results. The second part deals with the following period which, for the computation side, turned into a systematic study of all possible PAHs. This mass production was undertaken to get databases available to the PAH community, in order to combine the efforts of theoreticians and experimentalists (*cf.* Sect. 3.1). Indeed, mixing the results of calculations and of experiments turned out to be very fruitful. On top of those calculations, a large amount of work has been performed to produce synthetic spectra with variations of the type and size of the PAHs in order to compare directly with the observations and to deduce information about the population as a function of the environment (see for instance Cami *et al.* in this volume). The third part reports the main theoretical advances made during the last years, aiming at a much more precise insight into the spectroscopy of PAHs. The ongoing developments of new methods and the comparison of their results to astronomical spectra with fine structures of increasing complexity can be regarded as a real challenge. Going beyond the harmonic approximation and taking into account the distinction between emission and absorption spectra are the main points now addressed (see for example Basire *et al.* in this volume).

2 First generation computations: HF vs. DFT electronic calculations

The spectra observed between 2 and 50 μm are the signatures of molecular vibrations. They are characterised by two quantities, namely, their frequencies and their intensities. The frequencies are the energetic signatures of the deformations of the molecular structure whereas the intensities show how the electronic density is distorted with the internal displacements of the nuclei. Together, they constitute a real fingerprint of the molecule, often used for identification in terrestrial laboratories.

Any non-linear molecule composed of N atoms can move along $3N$ degrees of freedom, that can be separated into 3 translations and 3 rotations which do not imply any modification of the geometry, and $3N-6$ vibrations (reduced to $3N-5$ in the case of linear species) that involve periodic structural modifications with well defined frequencies.

Due to the quantum nature of the particles involved, quantum chemistry is most appropriate to describe the behavior of electrons and nuclei within a molecule. It is done by using mathematical functions capable of describing quantum phenomena from first principles and the universal constants of physics. Whatever the choices made, evaluation of wave functions or evaluation of electronic densities, all methods are based on solving the Schrödinger equation in which all the particles and all the interactions between them are taken into account. It is expressed as $H(r, R)\Psi(r, R) = E\Psi(r, R)$

where $H(r, R)$ is the complete Hamiltonian of the system depending on the electronic r and nuclear R coordinates. This operator is expressed as $H(r, R) = T_e + T_A + V_{eA} + V_{ee} + V_{AA}$

where T_e and T_A are the kinetic energy operators for the electrons and nuclei, V_{eA} and V_{ee} the operators describing the Coulomb attraction between electrons

and nuclei and the repulsion between the electrons, V_{AA} the repulsion between the nuclei.

Solving the Schrödinger equation is not a simple process since the energy to be calculated has contributions from various types of movements, motions of electrons, vibrations and rotations of the nuclear frame, all entangled in a subtle way. Rigorously, the Schrödinger equation can be solved exactly only for a two-electron atom. In all other cases, it is necessary to make approximations. Levering on the fact that nuclei are thousands times heavier than electrons, the first and most natural approximation is to uncouple the two types of motions (Born-Oppenheimer principle). Then, the calculations are carried out in the three following steps.

- i) The first step is to determine the geometry of the molecule by minimizing its electronic energy as a function of geometrical parameters such as bond distances, bond angles, dihedral angles. It is a pure electronic calculation in which the wave function in the Schrödinger electronic equation, $\Psi(r, R)$, is a function depending explicitly of all the electronic variables (space and spin) and parametrically of the nuclei coordinates. $\Psi(r, R)$ is developed as a linear combination of suitable functions, known as basis sets. Different types of mathematical functions are currently used, as for example, atomic functions, plane waves or gaussian functions.
- ii) The second step is to describe the movement of the nuclei in the potential previously calculated at fixed positions of the nuclei. Assuming that each vibration can be approximated by a harmonic oscillator, the so-called harmonic frequencies are obtained from the diagonalization of an effective force constant matrix built from the atomic masses and the second derivatives of the energy as a function of the displacements of the nuclei in the vicinity of their equilibrium positions. The eigenvalues lead to the harmonic vibrational frequencies whereas the eigenvectors provide the displacement vectors of the nuclei (normal coordinates). Going beyond the harmonic description would imply the mapping of a multidimensional energy potential allowing the calculation of higher order derivatives and inter-vibration coupling terms (see Sect. 4).
- iii) The third step is the calculation of the vibrations intensities that are directly related to the first multipole moment that has a non vanishing derivative with respect to the normal coordinates previously obtained (Amos 1984; Helgaker *et al.* 1986).

2.1 *Independent electron model versus correlated electron model*

Back to the eighties, the methods of computational chemistry were already elaborated and could be very efficient but only for small sized molecules (3–4 atoms). Confronted to PAHs that are much larger molecules (several tens of atoms) and to the demand for an accurate determination of their IR frequencies and intensities that are wave function derivatives, quantum chemists could only use part of

their codes, taking into account the computer possibilities of the time. Therefore, the first calculations were performed at the Hartree-Fock (HF) level; then came the Density Functional Theory (DFT) option, which is still the major theoretical scheme used today for the treatment of PAHs up to over a hundred of atoms.

In HF theory, electrons are assumed to be independent particles, each one moving in the average field of the others; *there is no correlation between the electrons*. Bringing correlation effects into the electronic wavefunction, *i.e.* taking into account that the movement of one electron is dependent on the instantaneous movement of the others, can be done in several ways. In post HF theories, correlation effects are introduced by mixing the ground state wavefunction with excited configurations. The simplest approach is known as MP2 (Moller Plesset 2nd order) in which only doubly excited configurations are considered in a perturbation treatment. In DFT, electrons are explicitly correlated through what is known as a *correlation functional*, which, by definition, makes it possible to limit the calculation to the ground state only. However, the exact correlation functional not being known, the DFT methods have to rely on approximate functionals. How the HF and DFT approaches are related is presented below.

In the HF theory, the energy as function of the density matrix P , has the form¹:
 $E_{HF} = V + \langle hP \rangle + 1/2 \langle PJ(P) \rangle - 1/2 \langle PK(P) \rangle$
 with:

V : nuclear repulsion energy,

$\langle hP \rangle$: one-electron (kinetic + potential) energy

$1/2 \langle PJ(P) \rangle$: coulomb repulsion of the electrons

$-1/2 \langle PK(P) \rangle$: exchange energy.

In the Kohn-Sham (KS) formulation of density functional theory, the energy has the form:

$$E_{KS} = V + \langle hP \rangle + 1/2 \langle PJ(P) \rangle + E_X[P] + E_C[P]$$

with:

$E_X[P]$: exchange functional

$E_C[P]$: correlation functional.

Within the Kohn-Sham formulation, Hartree-Fock theory can be regarded as a special case of density functional theory, with:

$$E_X[P] = -1/2 \langle PK(P) \rangle \text{ and } E_C = 0.$$

Although the inclusion of electron correlation in DFT can be seen as a qualitative leap in the description of electronic structures, one delicate issue remains when using DFT, namely, the choice of the exchange and correlation functionals. Some depend only of the local value of the density (LDA functionals), others depend not only of the local value of the density, but also of the derivative of this density (GGA functionals). Others, trying to take the best of the HF and DFT approaches use a combination of both (Hybrid functionals). This explains that the results can be rather different depending of the functional used. The most popular and widely

¹The notation $\langle \rangle$, known as the bra-ket Dirac formalism means that the quantity $\langle Q \rangle$ is obtained by integration over the wave function space.

employed functional for the calculation of IR spectra is known under the acronym of B3LYP (Becke 1993; Lee *et al.* 1988). The form initially proposed by Becke for the exchange correlation functional depends on 3 parameters that are adjusted to fit molecular properties of a representative corpus, mostly of organic molecules, which explains the success of this approach in the PAH studies.

At that point, general textbooks (for example: Szabo & Ostlund 1982; Lee & Scuseria 1995; Koch & Holthausen 2001) may help the interested reader to get a better insight into the original developments forming the basis of quantum chemistry as it stands today.

2.2 Correcting the missing effects: Scaling procedures

As mentioned before, all electronic methods are approximate when dealing with correlation, and at least part of the correlation effect is missing. Most of the time, evaluation of the IR frequencies is performed within the harmonic approximation. Thus, two independent effects, correlation and anharmonicity, have to be corrected. In such situations, the most efficient way to proceed is to adjust the raw values as a whole by calibrating on well known experimental data. Several procedures have been employed:

- a direct scaling of the frequencies using a unique scale factor for the entire spectrum or a specific scale factor by frequency range or frequency type,
- an indirect scaling through the force constant matrix, scaling only the diagonal terms (uniformly or not) or scaling also the non-diagonal terms.

The scaling factors depend essentially on the method and the basis set employed, and, in a lesser way, of the type of molecules considered (families). From the original work by Scott & Radom (1996), a number of numerical experiments have been discussed in the literature (see: Yoshida *et al.* 2000; Merrick *et al.* 2007; Johnson *et al.* 2010; Bauschlicher & Langhoff 1997, for the specific case of PAHs). One has to note that, contrary to frequencies, no scaling procedure is available for intensities which are linked to derivatives of observables.

2.3 Successful applications

The approximations detailed above should not mask the fact that an impressive amount of results has been obtained with these methods, allowing a real insight into the PAH spectroscopic features.

For example, a major question was how to justify the weakness of the $3.3 \mu\text{m}$ feature observed, compared to the corresponding experimental value (known only for standard neutral PAHs at that time). Taking into account that this feature corresponds to the CH stretching vibration, the first idea that came in was to argue in favour of dehydrogenated PAHs, assuming the CH intensity to be proportional to the number of CH bonds. However, no spectrum of any dehydrogenated PAH was available and no data could support such an assumption, though it seemed a reasonable one.

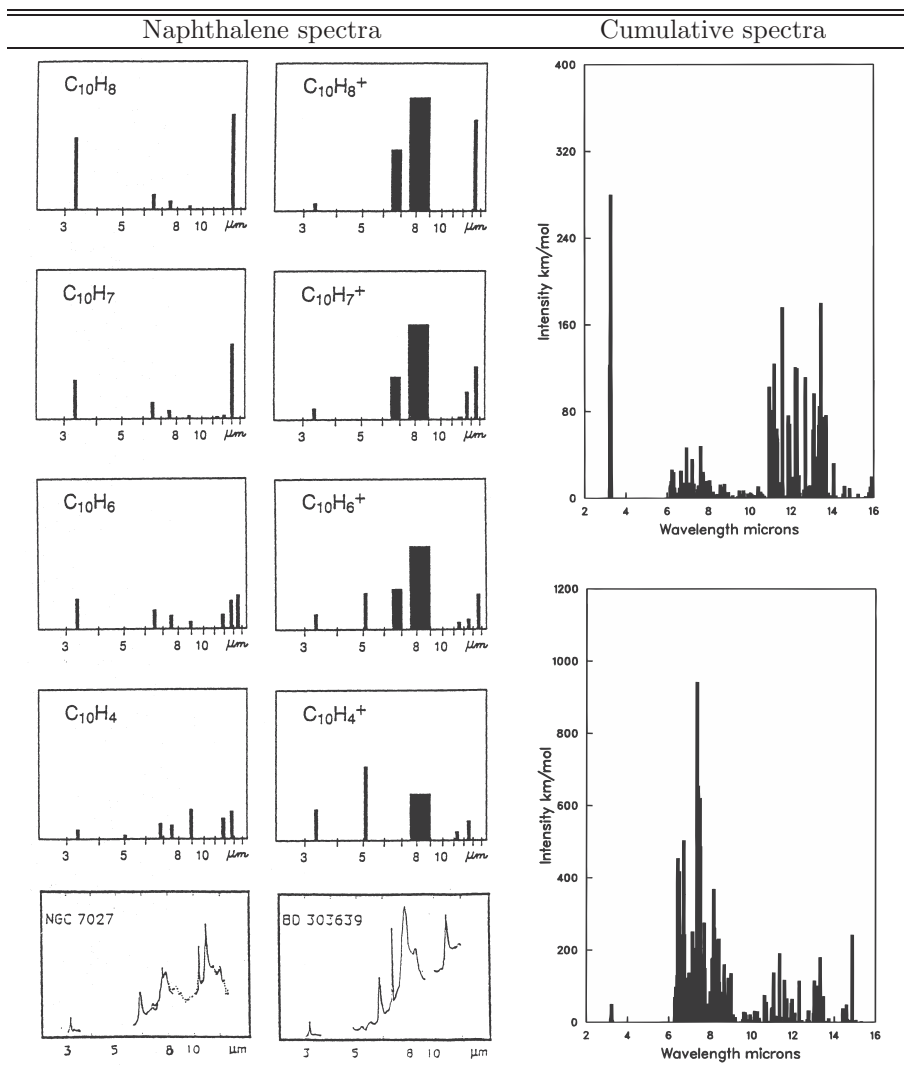


Fig. 1. Absorption spectra of neutral *versus* ionized PAHs. *Left:* effects of dehydrogenation and ionization in the naphthalene family (HF/321G calculations with scaling factor specific of the type of vibration); the bands *FWHM* are the averaged widths of the interstellar bands in the corresponding region of the spectra (adapted from Pauzat *et al.* 1995). *Right:* histogram representations of an equally weighted sum of the IR adsorption band intensities of 13 PAHs (B3LYP/4-31G with uniform scaling): neutrals (top) and cations (bottom) (adapted from Langhoff 1996).

The first breakthrough came from quantum theory simulations showing the spectacular difference between neutrals and cations, in particular for the intensities of the 3.3 μm feature. Suggested in 1988 by HF calculations for the smallest PAHs (Communication by Miller & D. DeFrees, IAU Symp. 135, Interstellar Dust, Santa Clara), it was confirmed in 1992 jointly by computations (Pauzat *et al.* 1992) and experiments (Szczepanski *et al.* 1992). Later on, more extensive studies through HF (DeFrees *et al.* 1993) and DFT calculations (Langhoff 1996) as well as laboratory experiments emphasized this fact (see for example Oomens in this volume). The theoretical spectra reported in Figure 1 summarize the two aspects of that important result. First the compilation of the spectra of a series of 13 PAHs in their neutral and ionized forms (Langhoff 1996) illustrate the general collapse of the 3.3 μm feature obtained by ionisation. Second, the case study of naphthalene (Pauzat *et al.* 1995) demonstrates that the collapse is effectively due to ionization of the PAH and not to some sort of dehydrogenation which would imply the same collapse of the 11.3 μm feature and consequently could not account for the observed intensity ratios. This fact has been confirmed for larger species (Pauzat *et al.* 1997).

It is worth mentioning that the first generation computations have been precise and reliable enough to characterize the fluctuations in frequency positions and relative intensities connected to almost all the different families of PAHs suggested by the various interpretative models. Therefore, all sorts of PAH families have been calculated to support the interpretation of the observed IR spectra (see also Peeters in this volume). In addition to the large body of data obtained on neutral and singly ionized PAHs, more specific calculations were carried out on specifically targeted families. A non exhaustive list of examples is given below focusing on the physical effects, independently of the size of the PAH carriers. Among the effects considered one may cite:

- multiple ionizations (Ellinger *et al.* 1999; Bauschlicher & Bakes 2000; Bakes *et al.* 2001; Mallocci *et al.* 2007)
- negative ions (Langhoff 1996; Bakes *et al.* 2001; Bauschlicher *et al.* 2008, 2009)
- dehydrogenated PAHs (Pauzat *et al.* 1995, 1997)
- hydrogenated PAHs (Pauzat & Ellinger 2001; Bauschlicher *et al.* 2001; Beege *et al.* 2001; Ricks *et al.* 2009)
- substitutions by lateral chains and carbon replacements by heteroatoms (Langhoff *et al.* 1998; Pauzat *et al.* 1999; Hudgins *et al.* 2005)
- irregular structures with 4/5/7 membered rings (Bauschlicher *et al.* 1999; Pauzat & Ellinger 2002)
- deuterated PAHs (Bauschlicher *et al.* 1997; Mulas *et al.* 2003; Peeters *et al.* 2004)
- metal complexation (Fe, Mg, Si) (Ellinger *et al.* 1999; Cassam 2002; Hudgins *et al.* 2005; Bauschlicher & Ricca 2009; Joalland *et al.* 2010; Simon & Joblin 2007, 2010) ...

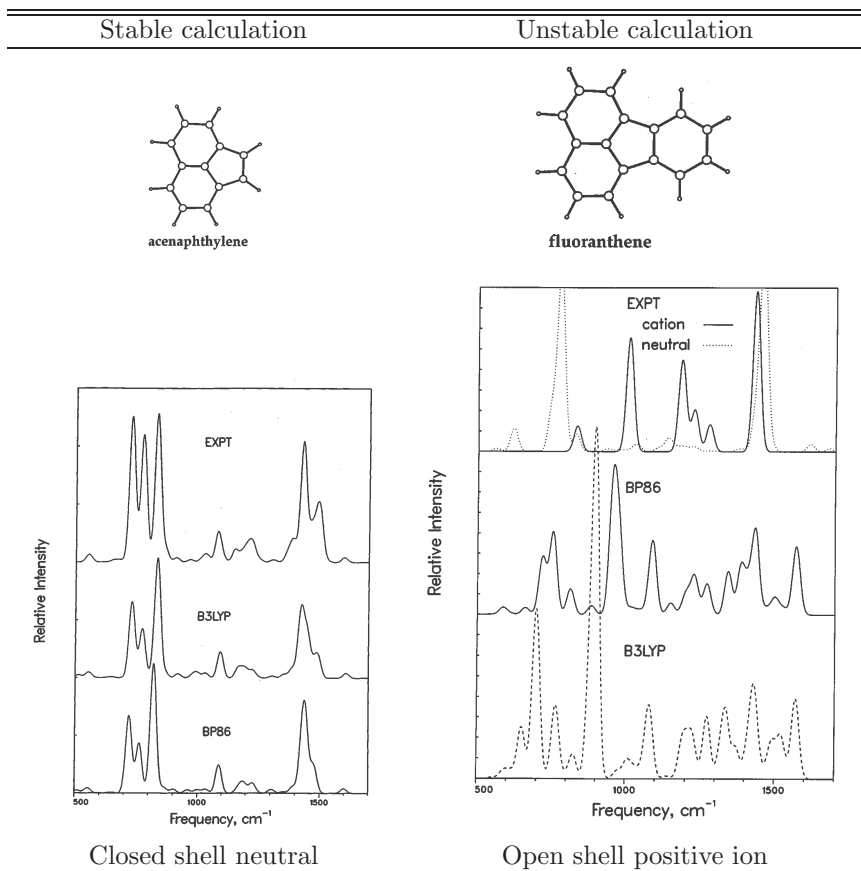


Fig. 2. Examples of successful (*left*) and unstable (*right*) calculations of IR spectra using BP86, B3LYP with the 4-31G basis set and *FWHM* of 30 cm^{-1} (adapted from Bauschlicher *et al.* 1999).

2.4 Limitations

In spite of a number of successes and a satisfactory agreement with the experimental spectra when available (apart from some lack of precision for the intensities), some theoretical problems remain to be solved with electronic calculations. Instabilities, mostly due to symmetry breaking artefacts, may occur *i.e.* when the calculated electronic density has a lower symmetry than the nuclear frame. This happens when two states fall quite close in energy in an open shell structure. Practically, it generates abnormally large intensities as well as inaccurate positions of the bands, especially for in-plane asymmetric CC vibrations. Contrary to what is sometimes advanced, this is true with all methods used for PAHs but hopefully for a few molecules only. It is true for HF methods, especially when using ROHF for open-shells molecules (case of most cations), it is true for Moller Plesset

Perturbation theory (MP2) which has been used sometimes as reference for correlation evaluation, and it is also true of DFT though less often. In this last case, it seems to depend on the choice of the functional. One of those cases, the fluoranthene cation, is discussed by Bauschlicher *et al.* (1999) considering B3LYP and BP86 DFT approaches (Fig. 2). However, the theoretically correct solution of symmetry breaking in open shells relying on high level multiconfigurational calculations (McLean *et al.* 1985) is still out of reach today for most PAHs because of the size of the computational problem.

3 Second generation computations: Databases of PAHs IR spectra

3.1 PAHs databases

Thanks to a quickly increasing power of the computers, systematic calculations of whole families of PAHs, dealing with larger and larger PAHs (Bauschlicher 2002; Pathak & Rastogi 2007; Bauschlicher *et al.* 2008, 2009; Ricca *et al.* 2010), could be currently performed. The time had come for a PAH business, meaning large scale computations implying significant human and computer-time potentials. Such characteristics were available at NASA Ames Research Center. Moreover, experimental setups were available on the same site and cooperation between the two proved very successful. The same objective was also present in the European collaboration between the Cagliari Observatory and the CESR at Toulouse. Two databases are now currently on line:

The Cagliari database: astrochemistry.ca.astro.it/database/

For more details, refer to the review by Mallocci *et al.* (2007):

The NASA database: www.astrochem.org/pahdb/

For more details, refer to the review by Bauschlicher *et al.* (2010) and see also Boersma *et al.* in this volume.

The exploitation of these on line databases of spectra is presented below.

3.2 Modeling interstellar composite IR spectra

Quantum Chemistry calculations give spectra of individual PAHs (free flyers) under a simple form: two numbers per vibration, the frequency and the corresponding absolute intensity; they provide also a vector array which is the normal coordinate describing the movement associated to the vibration in the reference frame of the molecular geometry. It is the analysis of the normal coordinates in terms of elementary displacements (stretching, bending...) that allows structural identification of the vibration. Starting from these data, one has to build a synthetic spectrum to be compared to an observed spectrum. Two issues need to be addressed.

One has to determine the profile of each band to produce a full spectrum for every PAH considered. Then, one has to figure which families of PAHs are concerned, depending of the region of observation, and in which proportions they are to be averaged.

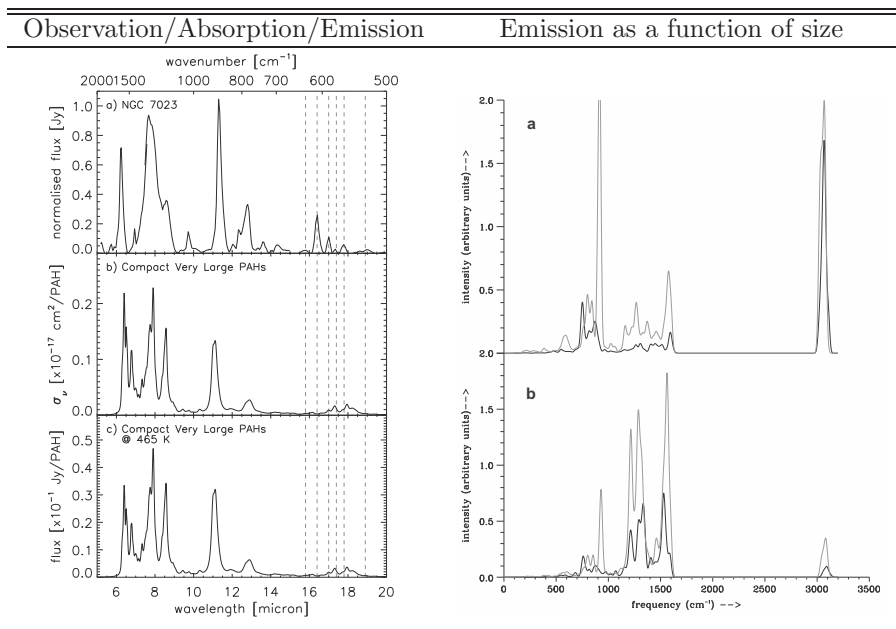


Fig. 3. Composite spectra: *left* – low-resolution spectrum of the reflection nebula NGC 7023 (panel a) compared to the average absorption spectrum of 7 neutral and singly positive ionised very large PAHs (panel b) and the computed emission spectrum of the same PAH mixture at 465 K (panel c) (adapted from Boersma 2009); *right* – comparative emission spectra of PAHs having less than 30 C atoms (black) and more than 30 C atoms (grey) (a) neutrals and (b) cations (adapted from Pathak & Rastogi 2007).

In the case of a single PAH, it is now a priori possible to determine a theoretical profile for each band through elaborate methods implying intramolecular vibrational redistribution, anharmonic shifts and hot bands, rotational broadening, ... It is a highly sophisticated theoretical work, very demanding in man power and computer time. This is hardly an option to be considered when dealing with a mass production of spectra for such oversized molecules as PAHs. Empirical substitutes can be used instead.

Concerning the profile of a band, essentially two simplified representations are available:

- Histograms.
- Curves with Lorentzian / Gaussian shapes.

Then several options are possible for the *FWHM* (full width at half maximum):

- The frequency interval obtained for the calculated vibrations of the same type

- A standard line width
- Different *FWHM* depending on vibration type and deduced from experiments.

The final step is relevant of pure astrochemistry only. The appropriate calculated spectra have to be selected and averaged according variable percentages. Comparison of such composite spectra with the observed spectra allows to deduce information about size, ionization or composition of the PAHs according the environment. Some examples of composite spectra are given in Figure 3.

4 Third generation computations: Current theoretical developments

4.1 Beyond electronic calculations: Anharmonicity

To go beyond the harmonic approximation is not straightforward, but it is essential for understanding hot media in which the temperature influences the band profiles and the intensities as a consequence of the anharmonicity of the potential energy surfaces. Starting from a static quantum chemical calculation, Born Oppenheimer dynamics can be used at two levels of approximation:

- either the vibrations are considered as independent, which takes into account only one-dimension anharmonicity;
- or the vibrations are considered as coupled.

As for electronic calculations, variational or perturbative treatments can be employed, with similar pros and cons all linked to the size and nature of the basis set. A general option is to define a pool of vibrational states that can be populated at the temperature considered and reachable via allowed IR transitions.

The problem of size, in fact the dimension of the basis of vibrational functions so defined, becomes rapidly a bottleneck for the variational methods, especially in terms of computer time. For perturbation methods, it should be reminded that possible bias can be introduced by the perturbative technique used in most available codes, when accidental degeneracy occurs between vibrational levels, which is rather common when the size of the molecule and consequently the number of vibrations increases. The solution is then to resort to degenerate perturbation theory by solving variationally the manifold of quasi degenerate vibrational states in a preliminary step (see for example the case of naphthalene in Cané *et al.* 2007 or Pirali *et al.* 2009).

Using anharmonic parameters deduced from DFT results, it is possible to take the participation of every populated state to the overall profile of each IR band into account. But as the number of transitions and of states to be considered are quickly exploding with temperature, this type of calculation is so far limited to small PAHS. The description of really hot bands has to be done by using a statistical Monte Carlo sampling for example. (G. Mulas *et al.* 2006a; Pirali *et al.* 2009).

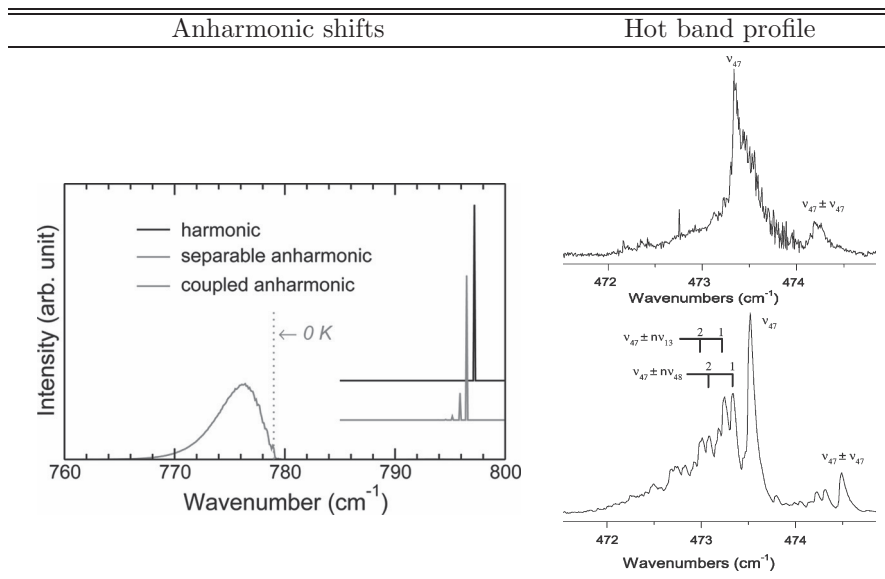


Fig. 4. Computational experiments on the absorption of naphthalene at fixed temperatures. *Left:* calculated partial spectrum near 780 cm^{-1} at 500 K (adapted from Basire *et al.* 2009); *right:* high resolution spectrum near 472 cm^{-1} at 300 K (adapted from Pirali *et al.* 2009); experimental (top); calculated (bottom).

Another theoretical approach is actually proposed to calculate the finite temperature IR absorption spectrum of fully coupled anharmonic systems. The energy levels are described by a second order Dunham expansion and a Wang Landau Monte Carlo procedure is used for the calculation of the quantum densities of states; microcanonical simulations provide an absorption intensity function of both the absorption wavelength and the internal energy of the molecule (Basire *et al.* 2008; Basire *et al.* 2009; see also Basire in this volume). Here too, applications are presently limited to the smallest of the PAHs.

Selected results from both methods are given in Figure 4.

For larger systems, anharmonic effects can be obtained by Born-Oppenheimer or Car-Parrinello molecular dynamics (MD). Though MD methods cannot provide as detailed structures as the preceding methods, it can give the overall band evolution with temperature, and has the advantage of being able to deal with much larger systems efficiently. For even more effectiveness, it can be coupled to computer efficient calculations of the potential energy function, as a parametrized DFT based on a tight binding approach such as SCC-DFTB (Self-Consistent Charge Density Functional Tight Binding (Porezag *et al.* 1995)); such an option used for SiPAH cations can be found in Joalland *et al.* (2010).

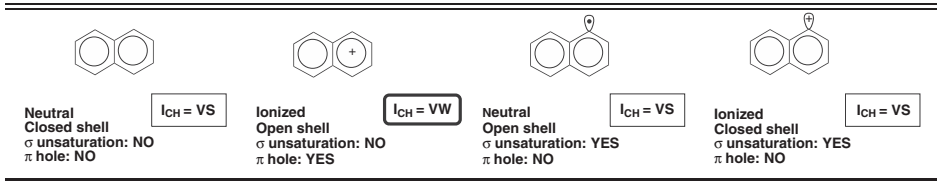


Fig. 5. Typical structures of neutral and ionized PAHs taken from the naphthalene series (adapted from Pauzat *et al.* 2010).

4.2 Emission versus absorption spectra

The *a priori* construction of emission spectra that is the last step toward a direct confrontation of theoretical models to the UIR bands has only been done recently. Two classes of emission models have been proposed.

The thermal emission model describes the IR cooling of PAHs via transitions from levels \mathbf{v} to $\mathbf{v} - 1$ in an emission cascade. The emission in a given vibrational mode from a PAH of internal energy \mathbf{U} is calculated as the average emission of an oscillator connected to a thermal bath, the PAH itself being considered as a heat bath at the temperature \mathbf{T} that corresponds to the average energy \mathbf{E} of the molecule. This kind of model has been employed by Pech *et al.* (2002), using photophysical experimental data, as well as Pathak & Rastogi (2008) using DFT B3LYP calculations ($C_{10}H_8 \rightarrow C_{96}H_{24}$) for the initial adsorption spectra. It has to be noted that this method is efficient but rather approximate: indeed, this canonical formalism is good only when the excitation energy is much larger than all the vibration modes considered, so that the average value of energy \mathbf{E} is a sharply peaked function of \mathbf{T} ; it is a poor approximation in all other cases.

Mulas and co chose a micro-canonical formalism. This approach is based on the conservation of energy between emissions, which insures its validity whatever the excitation energy considered. Though more difficult to implement than the thermal formalism, this option is more rigorous. Practically, the authors use a Monte Carlo technique on top of quantum chemical calculations by extending a preceding Monte Carlo model of photophysics to include rotational and anharmonic band structures and employing molecular parameters calculated by DFT (Mulas 1998; Mulas *et al.* 2006b).

4.3 Origin of the collapse of the CH intensity with ionization

Though the difference between the IR spectra of polycyclic aromatic hydrocarbons (PAH) and those of the corresponding positive ions (PAH⁺) is nowadays a well admitted and documented fact, it remained puzzling and not clearly understood from a theoretical point of view till very recently. Interpreting the origin of these variations has long been neglected, because the production of IR spectra of all sorts of PAHs was considered a matter of urgency in order to support the observations and also because the tools available at the time were considered not reliable enough for such a delicate analysis.

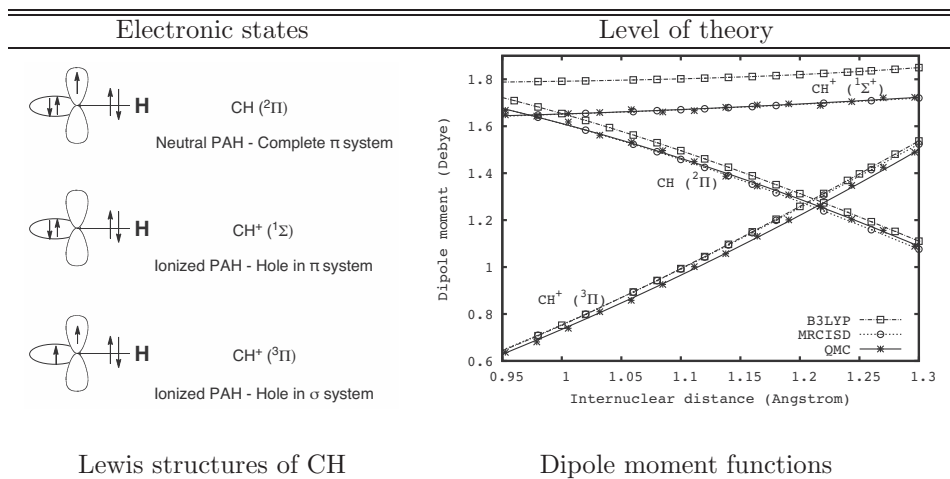


Fig. 6. Variation of the dipole moment of CH with the inter nuclear distance (adapted from Pauzat *et al.* 2010).

When looking more precisely to the large body of data available on PAHs, such a behavior seems to be linked to species with a hole in the system, which is the case of most classic ionized PAHs. A few demonstrative examples built from naphthalene are given hereafter in Figure 5 for a better understanding.

It is well known from vibrational analysis that the CH stretching vibration is a localized mode. Then, a local model of vibrator, namely, the CH fragment can represent the different types of PAHs as shown in Figure 6-left.

The study of the behavior of the dipole moment functions μ calculated with the most elaborate methods available, state of the art *ab-initio* (MRCISD) and Quantum Monte Carlo (QMC), showed that the three model molecules exhibit very different variations of their dipole moment with the CH distance (Fig. 6-right) that are consistent with strong/weak intensities of the CH vibrations in the neutral/ionized PAHs, the key point being the presence, or not, of a hole in the π shell. This can be interpreted as the result of the distortions of the electronic densities, linked to different diabatic dissociation limits.

A topological analysis for the electronic densities (Pauzat *et al.* 2010) shows that the collapse of the CH stretching is directly linked to the compensation between the internal charge transfer contribution and the distortion of the electronic density within the CH bond, which occurs only in the case of CH⁺($^1\Sigma^+$).

5 Conclusion

The PAH hypothesis has been a real source of motivation for several theoretical groups over the last two decades. This is a quasi text book example of creative interaction between space observation, laboratory experiments and theoretical computations. The following summary of the marking theoretical contributions to the

Year	Landmarks	Research groups
1988	<i>Poster IAU Symp. 135, Interstellar Dust naphthalene; anthracene (neutral/cation)</i>	<i>Miller/DeFrees MRI-IBM</i>
92-94	Effects of ionization (\rightarrow C ₁₆ H ₁₀)	<i>Obs. Paris/ENS</i>
93	Anharmonicity and the 3.4 μ m band	"
95-97	Ionization versus dehydrogenation	"
1996	Compilation of 13 PAHs (neutral/cation/anion) \rightarrow C ₃₂ H ₁₄ (ovalene)	<i>NASA Ames</i>
97	Perdeuterated small PAHs	"
98	Effect of O/N substitution on Naphthalene	"
99	PAHs with 5-membered rings	"
99	Effect of double ionization Anthracene-Fe ⁺ complex Effect of aliphatic substitution (3.4 μ m region)	<i>Obs. Paris/ENS</i> " "
2000	PAHs (neutral/cation/anion/ multiple cations) \rightarrow C ₅₄ H ₁₈ (circumcoronene)	<i>NASA Ames</i>
01	Effects of perhydrogenation (3.4 μ m region) Spectra of Perhydrogenated PAHs Large PAHs (neutral/protonated/cation) \rightarrow C ₉₆ H ₂₄ (circumcircumcoronene)	<i>Obs. Paris/ENS</i> <i>NASA Ames</i> "
02	Effects of non-regularity (neutral/cation) PAHs with (4/5/7) membered rings Model for IR emission (band profiles)	<i>Obs. Paris/ENS</i> <i>U. Toulouse</i>
03-05	PANHs (neutral/cation)	<i>NASA Ames</i>
04	Effect of deuteration	"
05	Catacondensed PAHs ((neutral/cation)	<i>U. Gorakpur</i>
06	Pericondensed PAHs ((neutral/cation)	"
07	Far IR of PAHs: emission modeling IR emission of PAHs dications Fe ⁺ PAH complexes	<i>Obs. Cagliari</i> " <i>U. Toulouse</i>
07-08	PAH IR emission modeling and size effects	<i>U. Gorakpur</i>
08	IR emission for PAHs with 10 to 96 carbons	"
09	IR absorption of thermally excited naphthalene (anharmonic levels) IR spectra of Fe ⁺ /Mg ⁺ PAH complexes Mid IR of very large irregular PAHs C ₈₄ H ₂₄ \rightarrow C ₁₂₀ H ₃₆	<i>Obs. Cagliari</i> <i>NASA Ames</i> "
09-10	Anharmonic/temperature effects on IR spectra SiPAH ⁺ π complexes (anharmonicity) Far IR of large to very large PAHs (\rightarrow 130 C) Origin of the collapse of the 3.3 μ m band	<i>U. Paris XI</i> <i>U. Toulouse</i> <i>NASA Ames</i> <i>U. Paris VI^a</i>

^a Formerly *Obs. Paris/ENS*.

Fig. 7. Chronology of the main advances in theoretical studies of PAH infrared spectra.

knowledge of the infrared signatures of PAHs (Fig. 7) is certainly not exhaustive, the individual lonely contributions, except for the historical first one, not being quoted but only those of full groups. Some of these groups, among which the NASA Ames and Toulouse University/Cagliari groups have the particularity and the advantage to have an experimental group also dedicated to the PAH study, which allows them to constructive comparisons. These two groups are at the origin of the two data bases available. During the last years, new young research groups have entered the game and promoted real theoretical advances in particular for the problems of anharmonicity and emission.

The PAH story is still going on!

References

- Allamandola, L.J., Tielens, A.G., & Barker, J.R. 1985, *ApJ*, 290, L25
Amos, R.D., 1984, *Chem. Phys. Lett.*, 108, 185
Bakes, E.L., Tielens, A.G., & Bauschlicher, C.W., 2001, *ApJ*, 556, 501
Basire, M., Parneix, P., & Calvo, F., 2008, *J. Chem. Phys.*, 129, 081101
Basire, M., Parneix, P., Calvo, F., Pino, T., & Bréchnignac, Ph., 2009, *J. Phys. Chem. A*, 113, 6947
Bauschlicher, C.W., & Langhoff, S.R., 1997, *Spectrochim. Acta A*, 53, 1225
Bauschlicher, C.W., Langhoff, S.R., Sandford, S.A., & Hudgins, D.H., 1997, *J. Phys. Chem. A*, 101, 2414
Bauschlicher, C.W., Hudgins, D.M., & Allamandola, L.J., 1999, *Theor. Chem. Acc.*, 103, 154
Bauschlicher, C.W., & Bakes, E.L., 2000, *Chem. Phys.*, 262, 285
Bauschlicher, C.W., Hudgins, D.M., & Allamandola, L.J., 2001, *Theor. Chem. Acc.*, 105, 154
Bauschlicher, C.W., Peeters, E., & Allamandola, L.J., 2008, *ApJ*, 678, 316
Bauschlicher, C.W., Peeters, E., & Allamandola, L.J., 2009, *ApJ*, 697, 311
Bauschlicher, C.W., & Ricca, A., 2009, *ApJ*, 698, 255
Bauschlicher, C.W., Boersma, C., Ricca, A., *et al.*, 2010, *ApJS*, 189, 341
Becke, A.D., 1993, *J. Chem. Phys.*, 98, 5648
Beegle, L.W., Wdowiak, T.J., & Harrison, J.G., 2001, *Spectrochim. Acta A*, 57, 737
Boersma, C., 2009, PhD, U. Groningen
Cané, E., Miani, A., & Trombetti, A., 2007, *J. Phys. Chem. A*, 111, 8218
Cassam-Chenaï, P., *Planet. Space Sci.*, 2002, 50, 871
DeFrees, D.J., Miller, M.D., Talbi, D., Pauzat, F., & Ellinger, Y., 1993, *ApJ*, 408, 530
Duley, W.W., & Williams, D.A., 1981, *MNRAS*, 196, 269
Ellinger, Y., Pauzat, F., & Lengsfeld, B. H., 1999, *J. Mol. Struct.*, 458, 203
Helgaker, T.U., Jensen, H.J.A., & Jorgensen, P., 1986, *J. Chem. Phys.*, 84, 6280
Hudgins, D.H., Bauschlicher, C.W., & Allamandola, L.J., 2005, *ApJ*, 632, 316
Joalland, B., Simon, A., Marsden, C. J., & Joblin, C., 2009, *A&A*, 494, 969
Joalland, B., Rapacioli, M., Simon, A., *et al.*, 2010, *J. Phys. Chem. A*, 114, 5846

- Johnson, R.D., Irikura, K.K., Kacker, R.N., & Kessel, R., 2010, *J. Chem. Theory Comput.*, in press
- Koch, W., & Holthausen, M.C., 2001, *A Chemist Guide to Density Functional Theory*, 2nd ed. (Wiley-VCH, Weinheim, Germany)
- Langhoff, S.R., 1996, *J. Phys. Chem.*, 100, 2819
- Langhoff, S.R., Bauschlicher, C.W., Hudgins, D.M., Sandford, S.A., & Allamandola, L.J., 1998, *J. Phys. Chem. A*, 102, 1632
- Lee, C., Yang, W., & Parr, R.G., 1988, *Phys. Rev. B*, 37, 785
- Lee, T.J., & Scuseria, G.E., 1995, In "Quantum mechanical electronic structure calculations with chemical accuracy", ed. S.R. Langhoff (Kluwer Academic Publishers: Dordrecht, The Netherlands)
- Léger, A., & Puget, J.L., 1984, *A&A*, 137, L5
- McLean, A.D., Lengsfeld, B.H., Pacansky, J., & Ellinger, Y., 1985, *J. Chem. Phys.*, 83, 3567
- Malloci, G., Joblin, C., & Mulas, G., 2007, *Chem. Phys.*, 332, 353
- Malloci, G., Joblin, C., & Mulas, G., 2007, *A&A*, 462, 627
- Martin, J.M.L., El-Yazal, J., & François, J.P., 1994, *J. Phys. Chem.*, 98, 4243
- Merrick, J.P., Moran, D., & Radom, L., 2007, *J. Phys. Chem. A*, 111, 11683
- Miller, M.D., & DeFrees, D.J., 1988, *IAU Symp. 135, Interstellar Dust*, Santa Clara
- Mulas, G., 1998, *A&A*, 338, 243
- Mulas, G., Malloci, G., & Benvenuti, P., 2003, *A&A*, 410, 639
- Mulas, G., Malloci, G., Joblin, C., & Toubanc, D., 2006a, *A&A*, 456, 161
- Mulas, G., Malloci, G., Joblin, C., & Toubanc, D., 2006b, *A&A*, 460, 93
- Pathak, A., & Rastogi, S., 2007, *Advances in Space Research*, 40, 1620
- Pathak, A., & Rastogi, S., 2007, *Spectrochim. Acta Part A*, 67, 898
- Pathak, A., & Rastogi, S., 2008, *A&A*, 485, 735
- Pauzat, F., Talbi, D., Miller, M.D., DeFrees, D.J., & Ellinger, Y., 1992, *J. Phys. Chem.*, 96, 7882
- Pauzat, F., Talbi, & Ellinger, Y., 1995, *A&A*, 293, 263
- Pauzat, F., Talbi, & Ellinger, Y., 1997, *A&A*, 319, 318
- Pauzat, F., Talbi, & Ellinger, Y., 1999, *MNRAS*, 304, 241
- Pauzat, F., & Ellinger, Y., 2001, *MNRAS*, 324, 355
- Pauzat, F., & Ellinger, Y., 2002, *Chem. Phys.*, 280, 267
- Pauzat, F., Pilmé, J., Toulouse, J., & Ellinger, Y., 2010, *J. Chem. Phys.*, 133, 054301
- Pech, C., Joblin, C., & Boissel, P., 2002, *A&A*, 388, 639
- Peeters, E., Allamandola, L.J., Bauschlicher, C.W., *et al.*, 2004, *ApJ*, 604, 252
- Pirali, O., Vervloet, M., Mulas, G., Malloci, G., & Joblin, C., 2009, *Phys. Chem. Chem. Phys.*, 11, 3443
- Porezag, D., Frauenheim, T., Köhler, T., Seifert, G., & Kaschner, R., 1995, *Phys. Rev. B*, 51, 12947
- Ricca, A., Bauschlicher, C.W., Mattioda, A.L., Boersma, C., & Allamandola, L.J., 2010, *ApJ*, 709, 42
- Ricks, A.M., Douberly, G.E., & Duncan, M.A., 2009, *ApJ*, 702, 301

- Scott, A., & Radom, L., 1996, *J. Phys. Chem. A*, 100, 16502
- Simon, A., & Joblin, C., 2007, *J. Phys. Chem.*, 111, 9745
- Simon, A., & Joblin, C., 2010, *ApJ*, 712, 69
- Szabo, A., & Ostlund, N.S., 1982, *Modern Quantum Chemistry* (McGraw-Hill, New York)
- Wakelam, V., & Herbst, E., 2008, *ApJ*, 680, 371
- Yoshida, H., Ehara, A., & Matsuura, H., 2000, *Chem. Phys. Lett.*, 325, 477

MODELING THE ANHARMONIC INFRARED EMISSION SPECTRA OF PAHS: APPLICATION TO THE PYRENE CATION

M. Basire¹, P. Parneix¹, T. Pino¹, Ph. Bréchnignac¹ and F. Calvo²

Abstract. The IR emission cascade from the pyrene cation due to a broad band optical excitation is simulated using kinetic Monte Carlo. Anharmonicities of the ground electronic state potential energy surface are taken into account in the transition energies, the microcanonical densities of states, and the rate of hydrogen loss through various statistical theories. The emission spectral features of the “3.3”, “6.2” and “11.2” μm bands are computed for different blackbody temperatures.

1 Introduction

Unidentified Infrared Bands (UIBs) correspond to intense IR emission bands in the 3–20 μm spectral range. According to the so-called PAH model (Puget & Léger 1989; Allamandola *et al.* 1989); these IR bands, first detected in 1973 (Gillett *et al.* 1973), are attributed to PAH emission bands, although no conclusive identification of molecular carriers has been achieved yet. In the last years, a large number of astrophysical objects has been observed in this IR spectral range and high resolution spectra are now available (Hony *et al.* 2001; Peeters *et al.* 2002; Van Diedenhoven *et al.* 2004; Draine & Li 2007). In the photophysics PAH model, the molecule is initially excited by absorption of a visible/UV photon, after which the intramolecular dynamics is driven by non adiabatic couplings. Subsequently, the PAH molecule is vibrationally heated in the ground electronic state and cools down by emission of several IR photons.

Up to now, only very few experimental data have been collected on the IR emission of neutral (Cherchneff & Barker 1989; Brenner & Barker 1992; Williams & Leone 1995; Cook *et al.* 1996; Cook & Saykally 1998) and cationic (Kim *et al.* 2001;

¹ Institut des Sciences Moléculaires d’Orsay, CNRS UMR 8214, Université Paris-Sud 11, Bât. 210, 91405 Orsay Cedex, France

² LASIM, Université de Lyon and CNRS UMR 5579, 43 Bd. du 11 Novembre 1918, 69622 Villeurbanne Cedex, France

Kim & Saykally 2002) PAHs after an initial excitation provided by a UV laser or an electron gun. These experiments have found evidence that IR emission spectra are shifted with respect to absorption spectra, the vibrational shift being dependent on the amount of internal energy deposited in the molecule.

From the theoretical point of view, IR emission spectra have been mainly computed in the harmonic limit. In these simulations, the IR radiative cooling of the molecule is monitored using thermal approximations (Léger *et al.* 1989; Schutte *et al.* 1993) or a stochastic model (Gillespie 1978; Barker 1983; Mulas 1998; Joblin *et al.* 2002). More recently, in order to reproduce the shape of the spectral profile, anharmonicities were empirically introduced in the spectral simulation (Cook & Saykally 1998; Pech *et al.* 2002), using experimental data on the spectral shifts and broadenings of the IR absorption spectra for neutral PAHs, as a function of increasing temperature (Joblin *et al.* 1995).

In the present article, we describe a novel theoretical approach to determine the IR radiative cascade. In this method, anharmonicities calculated using first-principle methods and second-order perturbation theory are taken into account in all statistical quantities, namely the microcanonical densities of states used in the thermal populations and the dissociation rates, as well as the transition energies themselves.

2 Model and methods

We assume that the initial excitation energy, deposited as visible/UV light, is rapidly converted into vibrational energy in the ground electronic state. Our purpose is then to model the (much slower) radiative decay of the molecule through multiple emission in the infrared domain. In absence of collisional relaxation (low density medium), the internal energy remains constant between two successive IR photon emissions, and the physical conditions are those of a microcanonical ensemble. If the time scale between two such emissions is long with respect to intramolecular vibrational redistribution (IVR), then all vibrational states at the available internal energy E are equiprobable.

Because the excitation energy is large with respect to the emitted IR photons, the energy in the electronic ground state is expected to be initially rather high, hence it is important to account for anharmonicities in the description of transition energies, as well as for counting accurate densities of states (DOS's). We have previously developed a computational procedure based on the Wang-Landau Monte Carlo method (Wang & Landau 2001) to determine the quantum density of vibrational states of fully coupled polyatomic systems. Briefly, the method starts with a perturbative Dunham expansion of the vibrational energy levels in terms of harmonic wavenumbers $\lambda_k^{(h)}$ and anharmonic coefficients $\chi_{k\ell}$, as obtained from quantum chemistry calculations. In the present case, all ingredients were determined using density-functional theory, with the hybrid B3LYP potential and the basis set 4-31G, of modest size because of computer limitations for this rather large molecule. The quadratic force field was then sampled by performing a random walk in energy space, the microcanonical DOS being estimated with

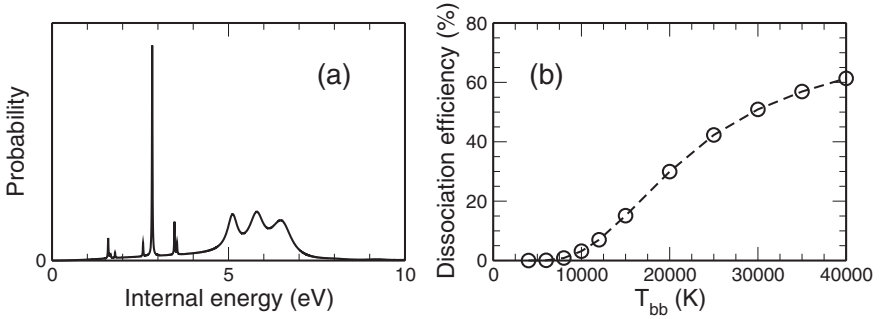


Fig. 1. (a) Distribution of internal excitation energy $P(E^*)$ at blackbody temperature $T_{bb} = 10\,000$ K; (b) dissociation efficiency *versus* blackbody temperature T_{bb} .

increasing accuracy over a broad energy range (Basire *et al.* 2008). Knowledge of the DOS also provides a very convenient way of calculating the infrared emission spectrum at microcanonical equilibrium, by accumulating a two-dimensional histogram $\mathcal{I}_e(\nu; E)$ of emission frequency ν at total energy E along a multicanonical Monte Carlo simulation (Basire *et al.* 2009, 2010). The energy-resolved spectrum is explicated as

$$\mathcal{I}_e(\nu; E) = \frac{1}{\mathcal{N}(\nu; E)} \sum_{\text{MC steps}} \sum_k n_k A_k^{(1 \rightarrow 0)} \delta(h\nu - \Delta E^{(k)}), \quad (2.1)$$

where $\mathcal{N}(\nu; E)$ is the number of entries in the histogram corresponding to the emission of a photon with energy $h\nu$, at total energy E . In this equation, n_k is the vibrational level of mode k with harmonic frequency $\nu_k^{(h)}$, $\Delta E^{(k)}$ is the transition energy associated with the emission of a single photon of mode k , and $n_k A_k^{(1 \rightarrow 0)}$ is the associated oscillator strength, assuming here an harmonic approximation.

In practice, the microcanonical spectra of the pyrene cation have been computed using the above procedure for vibrational energies ranging from the ground state level ($E_{\min} = 0$) to $E_{\max} = 14$ eV, with a resolution $\Delta E = 100 \text{ cm}^{-1}$ in energy and $\Delta\nu = 0.2 \text{ cm}^{-1}$ in emission frequency. Anharmonicities enter the above ingredients through the densities of microcanonical states and thermal populations, and in the transition energies.

Next, a complete IR emission cascade is simulated using a kinetic Monte Carlo (kMC) model (Mulas 1998). At any given energy E , several photon emission processes compete with each other and with molecular dissociation. For simplicity, we only include the lowest (most probable) dissociation channel, namely hydrogen loss, for which the dissociation rate $k_{\text{diss}}(E)$ is accurately modeled using phase space theory (Pino *et al.* 2007). Concerning radiative relaxation, the emission rate $k(\nu; E)$ for a photon $h\nu$ at internal energy E is simply given by $\mathcal{I}_e(\nu; E)$. Starting at time $t = 0$ with an excess energy $E(t = 0) = E^*$, all possible relaxation events are enumerated, including emission of a single photon from mode k with $n_k > 0$,

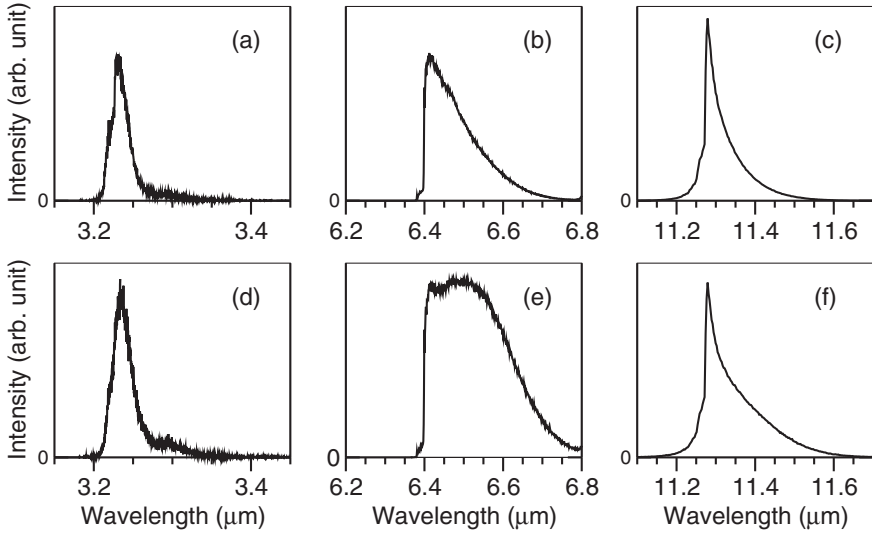


Fig. 2. Simulated emission spectra of the pyrene cation. In panels (a), (b), and (c), the blackbody temperature is $T_{\text{bb}} = 6000$ K; in panels (d), (e), (f), $T_{\text{bb}} = 2 \times 10^4$ K. The spectral ranges considered are $3.1\text{--}3.5 \mu\text{m}$ in panels (a) and (d), $6.2\text{--}6.8 \mu\text{m}$ in panels (b) and (e), and $11.1\text{--}11.7 \mu\text{m}$ in panels (c) and (f).

together with hydrogen dissociation, and one of them is randomly drawn with a probability proportional to its rate. The time and internal energy are updated, and the process is repeated until dissociation occurs or if time exceeds 10 s. 10^7 such kMC trajectories were performed in order to build reasonably smooth IR emission spectra.

In this article, only large band black-body excitations are considered. The absorption cross-section $\sigma(E)$ was adapted from experimental data (Salama & Allamandola 1992; Biennier *et al.* 2004) in the low energy range ($E \leq 4$ eV) and from theoretical works (Mallocci *et al.* 2004) for $4 < E \leq 12$ eV. The initial electronic excitation E^* under the blackbody radiation flux $\Phi(E)$ is randomly drawn at the beginning of each kMC trajectory from the probability $P(E^*) \propto \sigma(E^*)\Phi(E^*)$, after suitable normalization. As an illustration, the visible/UV absorption probability for a black-body temperature $T_{\text{bb}} = 6000$ K is displayed in Figure 1a. At this temperature, absorption mainly occurs near 6 eV due to large cross-sections of excited electronic states in this energy range. The dissociation efficiency is shown in Figure 1b *versus* T_{bb} . Dissociation is found to play a role in the photodynamics of the pyrene cation only when T_{bb} exceeds about 1000 K. In the temperature range considered here, the dissociation efficiency is always lower than 40%. As will be seen below, the dissociation involves hydrogen loss, which significantly alters the infrared emission spectral features.

3 Results and discussion

For the sake of brevity, we focus on the evolution of IR emission spectral features as a function of the blackbody temperature associated to the stellar radiation flux. Three vibrational bands have been considered, namely “3.3” μm (C-H stretchings), “6.2” μm (C-C stretchings) and “11.2” μm (C-H out-of-plane bendings), owing to their astrophysical relevance. A more detailed analysis of the IR emission bands will be given in a forthcoming article. In Figure 2, the emission spectra for these three bands are shown for $T_{\text{bb}} = 6000$ K and 2×10^4 K.

The calculated emission spectra are broad, continuous, and strongly asymmetric, especially for the two softer bands where long wings on the red side are consistent with observations (Van Dienenhoven *et al.* 2004; Peeters *et al.* 2002). This spectral profile is in agreement with previous calculations in which spectral shifts and broadenings due to anharmonicity were extracted from experimental data (Pech *et al.* 2002). The asymmetry also increases with blackbody temperature, and the profile changes significantly in the case of the “6.2” μm band. All these effects originate from anharmonicities of the ground state potential energy surface.

On a more quantitative level, the spectral shift $\langle \lambda \rangle$ and the spectral width $\Delta \lambda$ have been computed as a function of T_{bb} using the first and second moments of the IR emission spectrum, respectively. The variations of $\langle \lambda \rangle$ and $\Delta \lambda$ with T_{bb} are represented in Figure 3 for the same three vibrational bands depicted in Figure 2. Comparing $\langle \lambda \rangle$ to the harmonic wavelength $\lambda_k^{(\text{h})}$, the “11.2” band turns out to be less sensitive to anharmonicities than the two others bands. At very high blackbody temperatures, both the shift and width tend to constant values for the three modes. This is a consequence of hydrogen dissociation, which at high energies becomes an important channel very soon after excitation (see Fig. 1), thus quenching IR emission due to the concomitant strong evaporative cooling.

Finally, we note that the three simulated spectral widths obtained here for cationic pyrene are of the same order of magnitude as those observed in the majority of interstellar sources (Van Dienenhoven *et al.* 2004; Peeters *et al.* 2002). For the three bands considered so far (in decreasing wavelength), the observed widths are approximately equal to 0.20 μm , 0.13 μm , and 0.04 μm , respectively, in agreement with Figure 3.

The observed spectral features seem rather insensitive to the astrophysical objects in the class A (Peeters *et al.* 2002; Van Dienenhoven *et al.* 2004; Galliano *et al.* 2008). The observed IR band broadening is the consequence of the PAH size distribution. However, as demonstrated by the present calculations limited to cationic pyrene, the asymmetric spectral profiles are well reproduced when the PES anharmonicity is properly incorporated, especially for the “11.2” μm band. The observed IR emission spectra could then be strongly influenced by the variety in the intrinsic spectral width of individual PAHs resulting from different anharmonicities. The present computational protocol offers a convenient way to address this issue for larger molecules on a quantitative footing. Work is currently in progress to analyse the corresponding size effects on IR emission spectroscopy.

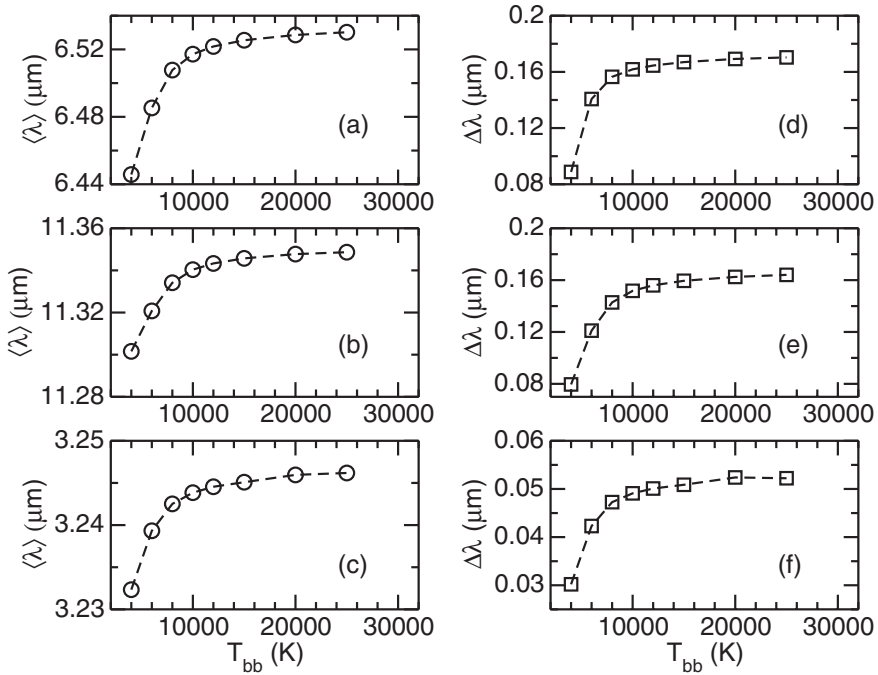


Fig. 3. Variations of the spectral shift $\langle \lambda \rangle$ (left panels) and width $\Delta \lambda$ (right panels) with increasing blackbody temperature, for the same three vibrational bands of the pyrene cation depicted in Figure 2. (a) and (d): 11.10 μm ; (b) and (e): 6.25 μm ; (c) and (f): 3.10 μm .

References

- Allamandola, L.J., Tielens, A.G.G.M., & Barker, J.R., 1989, *ApJS*, 71, 733
 Barker, J.R., 1983, *Chem. Phys.*, 77, 301
 Basire, B., Parneix, P., & Calvo, F., 2008, *J. Chem. Phys.*, 129, 0811019
 Basire, B., Parneix, P., Calvo, F., Pino, T., & Bréchnignac, Ph., 2009, *J. Phys. Chem. A*, 113, 6947
 Basire, B., Parneix, P., & Calvo, F., 2010, *J. Phys. Chem. A*, 114, 3139
 Biennier, L., Salama, F., Gupta, M., & O’Keefe, A., 2004, *Chem. Phys. Lett.*, 387, 287
 Brenner, J., & Barker, J.R., 1992, *ApJ*, 388, L39
 Cherchneff, I., & Barker, J.R., 1989, *ApJ*, 341, L21
 Cook, D.J., Schlemmer, S., Balucani, N., *et al.*, 1996, *Nature*, 380, 227
 Cook, D.J., & Saykally, R.J., 1998, *A&A*, 493, 793
 Draine, B.T., & Li, A.G., 2001, *ApJ*, 551, 807
 Draine, B.T., & Li, A.G., 2007, *ApJ*, 657, 810
 Galliano, F., Madden, S.C., Tielens, A.G.G.M., Peeters, E., & Jones, A.P., 2008, *ApJ*, 679, 310

- Gillespie, D.T., 1978, *J. Comput. Phys.*, 28, 395
- Gillett, F.C., Forrest, W.J., & Merrill, K.M., 1973, *ApJ*, 183, 87
- Hony, S., Van Kerckoven, C., Peeters, E., *et al.*, 2001, *A&A*, 370, 1030
- Joblin, C., Boissel, P., Léger, A., & Défourneau, D., 1995, *A&A*, 299, 835
- Joblin, C., Toubanc, D., Boissel, P., & Tielens, A.G.G.M., 2002, *Mol. Phys.*, 100, 3595
- Kim, H.S., Wagner, D.R., & Saykally, R.J., 2001, *Phys. Rev. Lett.*, 86, 5691
- Kim, H.S., & Saykally, R.J., 2002, *ApJS*, 143, 455
- Léger, A., D'Hendecourt, L., & Défourneau, D., 1989, *A&A*, 216, 148
- Maloci, G., Mulas, G., & Joblin, C., 2004, *A&A*, 426, 105
- Mulas, G., 1998, *A&A*, 338, 243
- Pech, C., Joblin, C., & Boissel, P., 2002, *A&A*, 388, 639
- Pino, T., Parneix, P., Calvo, F., & Bréchnignac, Ph., 2007, *J. Phys. Chem. A*, 111, 4450
- Peeters, E., Hony, S., Van Kerckoven, C., *et al.*, 2002, *A&A*, 390, 1089
- Puget, J.L., & Léger, 1989, *ARA&A*, 27, 161
- Salama, F., & Allamandola, L.J., 1992, *Nature*, 358, 42
- Schutte, W.A., Tielens, A.G.G.M., & Allamandola, L.J., 1993, *ApJ*, 415, 397
- Van Diedenhoven, B., Peeters, E., Van Kerckoven, C., *et al.*, 2004, *ApJ*, 611, 928
- Wang, F., & Landau, D.P., 2001, *Phys. Rev. Lett.*, 86, 2050
- Williams, R.M., & Leone, S.R., 1995, *ApJ*, 443, 675

LABORATORY SPECTROSCOPY OF PROTONATED PAH MOLECULES RELEVANT FOR INTERSTELLAR CHEMISTRY

O. Dopfer¹

Abstract. In this contribution, we summarize the recent progress made in recording laboratory infrared (IR) spectra of protonated polycyclic aromatic hydrocarbon molecules (H^+PAH) in the gas phase. The IR spectra of a large variety of H^+PAH species ranging from benzene to coronene have been obtained by various variants of photodissociation spectroscopy. The employed techniques include single-photon IR photodissociation (IRPD) of tagged H^+PAH ions and IR multiple-photon dissociation (IRMPD) of bare H^+PAH ions. The comparison of the laboratory IR spectra with astronomical spectra supports the hypothesis that H^+PAH ions are possible carriers of the unidentified IR emission (UIR) bands. Moreover, the spectra provide detailed information about the geometric and electronic structure as well as the chemical reactivity and stability of these fundamental hydrocarbon ions.

1 Introduction

The unidentified infrared (UIR) emission bands are observed in a great variety of galactic and extragalactic sources. They are currently attributed to IR fluorescence of UV-excited polycyclic aromatic hydrocarbon (PAH) molecules and their more complex derivatives, such as ionic PAH, (de-)hydrogenated and methyl-substituted PAH, PAH clusters, nitrogen- and silicon-containing PAH, and PAH-metal ion adducts (Léger & Puget 1984; Allamandola *et al.* 1985; Tielens 2008). Recently, also protonated PAH molecules, H^+PAH , have been suggested because laboratory experiments demonstrated that they can readily be formed through efficient protonation of neutral PAH or attachment of H-atoms to PAH^+ radical cations (Snow *et al.* 1998). In addition, their calculated IR spectra identify H^+PAH as promising candidates for UIR band carriers (Hudgins *et al.* 2001).

In order to test the H^+PAH hypothesis, laboratory IR spectra of H^+PAH are required for comparison with astronomical UIR spectra. Such spectra have,

¹ Institut für Optik und Atomare Physik, Technische Universität Berlin, Hardenbergstrasse 36, 10623 Berlin, Germany; e-mail: dopfer@physik.tu-berlin.de

however, been lacking until recently (Lorenz *et al.* 2007), largely due to experimental challenges involved in the generation of high abundances sufficient for spectroscopic interrogation. Recent progress in the development of efficient ion sources and sensitive IR spectroscopic techniques have allowed to obtain the first IR spectra of size-selected protonated aromatic molecules and their weakly-bound clusters in the gas phase by coupling tandem mass spectrometry with resonant vibrational photodissociation spectroscopy (Solca & Dopfer 2001; Solca & Dopfer 2003a). The application of these techniques to protonated aromatic molecules has been reviewed previously (Dopfer 2006). In this contribution, we summarize the results obtained in the past decade for a large variety of H^+PAH ions, ranging from protonated benzene to protonated coronene.

2 Experimental techniques

Several experimental approaches have been used to generate isolated and microsolvated H^+PAH cations in the gas phase for spectroscopic interrogation. Ion and cluster ion generation has been accomplished in an electron-impact or discharge-driven supersonic plasma expansion. This approach was used to produce protonated benzene and naphthalene, C_6H_7^+ and $\text{C}_{10}\text{H}_9^+$, and their weakly-bound clusters with ligands $\text{L} = \text{Ar}, \text{N}_2, \text{CH}_4,$ and H_2O (Solca & Dopfer 2002; Solca & Dopfer 2003b; Douberly *et al.* 2008; Ricks *et al.* 2009). Alternatively, isolated H^+PAH can be generated by chemical ionization of PAH in an ion cyclotron resonance (ICR) mass spectrometer using protonating agents, such as CH_5^+ or C_2H_5^+ , as successfully demonstrated for C_6H_7^+ and $\text{C}_{10}\text{H}_9^+$ (Jones *et al.* 2003; Dopfer *et al.* 2005; Lorenz *et al.* 2007). Larger PAH molecules have low vapour pressure and a feasible option to generate sufficient abundances of their protonated species is electrospray ionization. This technique has been applied to characterize larger H^+PAH ions (Knorke *et al.* 2009), ranging from protonated anthracene, $\text{C}_{14}\text{H}_{11}^+$, to protonated coronene, $\text{C}_{24}\text{H}_{13}^+$.

Two major spectroscopic strategies have successfully been employed to obtain IR spectra of isolated and microsolvated H^+PAH ions. The first technique couples modern low-intensity optical parametric oscillator (OPO) laser systems, typically operating in the $1000\text{--}4000\text{ cm}^{-1}$ range, with tandem mass spectrometers to record single-photon IRPD spectra of cold $\text{H}^+\text{PAH-L}_m$ cluster ions by monitoring the loss of weakly-bound ligands L (Solca & Dopfer 2002; Solca & Dopfer 2003b; Douberly *et al.* 2008; Ricks *et al.* 2009). The low intensities of OPO lasers are usually insufficient to drive multiple-photon processes. The influence of the ligands on the IR spectrum of the central H^+PAH ion can usually be neglected for weakly-bound ligands (*e.g.*, Ar), *i.e.* the IRPD spectra of the tagged species correspond to a very good approximation (to within a few cm^{-1}) to the IR spectra of the bare ion. Moreover, the clusters are cold as they are produced in molecular beams. As a result of the low internal temperature (typically well below 50 K) and the single-photon dissociation process, IRPD spectra display high resolution and sharp transitions with widths of the order of 5 cm^{-1} . Moreover, they display high sensitivity, *i.e.* even transitions with low IR activity can readily be detected.

The IRPD approach has been applied to obtain the first IR spectrum of $C_6H_7^+$ in the gas phase (Solca & Dopfer 2002).

The second spectroscopic strategy couples high-intensity free electron laser (FEL) sources (FELIX and CLIO), operating in the complementary 50–2500 cm^{-1} range, with ion cyclotron resonance (ICR) mass spectrometry to drive IRMPD of isolated, strongly-bound H^+PAH by monitoring either H-atom or H_2 loss (Jones *et al.* 2003; Dopfer *et al.* 2005; Lorenz *et al.* 2007; Zhao *et al.* 2009; Knorke *et al.* 2009). In general, the spectral resolution observed in the IRMPD spectra (circa 30 cm^{-1}) is lower than in IRPD spectra due to the finite bandwidth of the FEL, the broader rotational contour (as the ions probed in the ICR cell are at room temperature), spectral congestion due to overlapping transitions, and spectral broadening arising from the multiple-photon character of the IRMPD process. Typically, several tens of IR photons are required to drive the IRMPD process due to the large dissociation energies for H or H_2 elimination from H^+PAH . As a further consequence of the IRMPD mechanism, weakly IR active transitions with cross sections below a certain threshold are not observed. The IRMPD approach has been utilized to obtain the first IR spectrum of an isolated H^+PAH , namely $C_{10}H_9^+$ (Lorenz *et al.* 2007). Figure 1 compares the IRMPD spectra of a variety of H^+PAH obtained so far, including protonated benzene, naphthalene, anthracene, tetracene, pentacene, azulene, perylene, pyrene, coronene, acenaphthene, and acenaphthylene. While this contribution focuses on the general appearance of the IR spectra and the comparison with an UIR spectrum representative of a highly-ionized region of the interstellar medium (Tielens 2008; Fig. 1), a full account of the potential energy surfaces with structural and vibrational analyses is given elsewhere (Zhao *et al.* 2009; Zhao 2010). Significantly, apart from benzene H^+ , the IRMPD spectra in Figure 1 correspond to the first spectroscopic data of these H^+PAH in the gas phase, providing very valuable information about the geometric and electronic structures as well as the chemical reactivity and stability of these fundamental ions. For an illustration of the information content of these spectra, the reader is referred to a recent analysis of the azulene H^+ spectrum using quantum chemical calculations (Zhao *et al.* 2009). A similar analysis was performed for all H^+PAH spectra in Figure 1 (Zhao 2010) and will be published elsewhere.

3 Results and discussion

Initial IRPD spectra obtained for $C_6H_7^+$ in the CH stretch range using the tagging technique (Solca & Dopfer 2002; Solca & Dopfer 2003b) demonstrated for the first time spectroscopically that the proton is attached to a C-atom (σ -complex) rather than the π electron system of the aromatic ring (π -complex), a conclusion that also holds for larger H^+PAH . In addition, these spectra do not show coincidences with prominent UIR bands. Subsequent IRMPD spectra reported for isolated $C_6H_7^+$ in the fingerprint range (Fig. 1) using CLIO and monitoring H_2 loss (Jones *et al.* 2003; Dopfer *et al.* 2005) and higher-resolution IRPD spectra of Ar-tagged $C_6H_7^+$ ions (Douberly *et al.* 2008) confirm these initial conclusions.

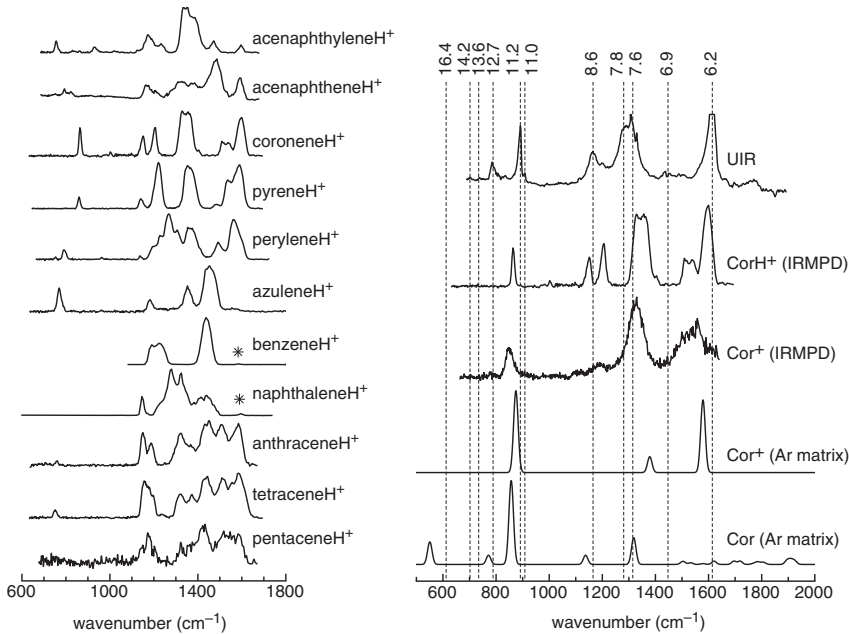


Fig. 1. *Left:* IRMPD spectra of a variety of H^+ PAH ions (Dopfer 2005; Lorenz *et al.* 2007; Dopfer 2008; Knorke *et al.* 2009; Zhao *et al.* 2009); the spectra of benzene H^+ and naphthalene H^+ were recorded using CLIO, whereas all other spectra were obtained using FELIX; bands marked by asterisks are largely suppressed due to reduced laser power. *Right:* IR spectra of coronene, coronene $^+$ and coronene H^+ compared to an UIR spectrum (Knorke *et al.* 2009). The dashed lines indicate positions of UIR bands in μm .

Next, IRMPD spectra were recorded for $C_{10}H_9^+$, the smallest H^+ PAH, using CLIO and the major conclusions can be summarized as follows (Lorenz *et al.* 2007). First, the IRMPD spectra of $C_6H_7^+$ and $C_{10}H_9^+$ are very different (Fig. 1), implying a strong dependence of the IR spectra of H^+ PAH on the number of aromatic rings, at least for small PAH. Second, the IRMPD spectrum of $C_{10}H_9^+$ demonstrates striking coincidences with the UIR spectrum. Both, the positions and IR intensities of the $C_{10}H_9^+$ bands match the astronomical spectrum much better than the IR spectra of neutral and ionized naphthalene. These important conclusions were later confirmed by IRPD spectra of $C_{10}H_9^+$ -Ar (Ricks *et al.* 2009).

The close match of the $C_{10}H_9^+$ and UIR spectra called for laboratory IR spectra of larger H^+ PAH, in order to follow their evolution as a function of PAH size. This was also of importance in the light of astrochemical models, which suggest PAH molecules consisting of 20–80 C-atoms to be photochemically most stable in interstellar clouds (Tielens 2008). To this end, IRMPD spectra of a variety of larger H^+ PAH species (Fig. 1) have been recorded using FELIX (Dopfer 2008).

Figure 1 compares the IRMPD spectra of linear catacondensed H^+PAH featuring n aromatic rings with $n = 1\text{--}5$ (Knorke *et al.* 2009). The $n = 1$ and $n = 2$ spectra are significantly different in appearance, and both differ from those for $n = 3\text{--}5$. However, the IRMPD spectra for $n = 3\text{--}5$ are rather similar, suggesting convergence of the spectral evolution at around $n = 3$. Comparison of the $n = 3\text{--}5$ spectra with an UIR spectrum representative of a highly-ionized region of the interstellar medium (Tielens 2008; Fig. 1) reveals good correspondence for transitions assigned to in-plane CH bend and CC stretch modes. In addition, the highest-frequency CC stretch mode at around 1600 cm^{-1} approaches the $6.2\text{ }\mu\text{m}$ UIR feature with increasing n . The intense, lower-frequency CC stretch modes at 1450 cm^{-1} are characteristic of all linear catacondensed H^+PAH and correlate with the $6.9\text{ }\mu\text{m}$ UIR feature, which is however only weakly observed in the astronomical spectrum. Similar conclusions apply to the 1500 cm^{-1} transition.

Not only are linear catacondensed H^+PAH with $n = 1\text{--}5$ probably too small to be photostable, they are also less stable than pericondensed two-dimensional H^+PAH . To this end, we recorded also the IRMPD spectrum of protonated coronene ($\text{C}_{24}\text{H}_{13}^+$), a pericondensed PAH, which is often considered as the prototypical and representative PAH molecule present in the interstellar medium. Figure 1 compares the available experimental IR spectra for different degrees of ionization and protonation of coronene with the UIR spectrum (Knorke *et al.* 2009). Comparison of the spectra of coronene and coronene⁺ recorded in an Ar matrix demonstrates the significant impact of ionization on the IR intensities. The coronene⁺ spectrum recorded in the cold Ar matrix and via IRMPD in the gas phase are similar but illustrate the typical redshift and broadening of bands induced by the IRMPD process. The IRMPD spectrum of coronene⁺ and coroneneH⁺ are again similar. The redshifts and broadening effects due to IRMPD are, however, less pronounced for the protonated species due to its lower dissociation energy. Moreover, the bands in the $1100\text{--}1200\text{ cm}^{-1}$ range display higher IR activity. Significantly, the intense CC stretch band at 1600 cm^{-1} ($6.25\text{ }\mu\text{m}$) occurs at a higher frequency than for the radical cation and closely approaches the $6.2\text{ }\mu\text{m}$ band observed in the UIR spectrum.

As the UIR bands are caused by IR fluorescence of vibrationally hot species, the vibrational transitions observed are shifted in frequency from the frequencies of fundamental transitions due to vibrational anharmonicities. Similarly, the multiple-photon nature of the IRMPD process also shifts the frequencies to lower values in comparison to fundamental transitions, again via the effect of anharmonicities. Thus, it is indeed meaningful to compare IRMPD spectra with the UIR bands, as both processes and the resulting IR spectra are affected by the same type of vibrational anharmonicity (Oomens *et al.* 2003). In view of this argument, the good agreement between the IRMPD spectrum of coroneneH⁺ and the UIR spectrum in Figure 1 provides for the first time compelling experimental evidence for the hypothesis that H^+PAH indeed contribute to the UIR spectrum. Future efforts include recording IR spectra of even larger H^+PAH ions in order to follow the spectral evolution as a function of PAH size. In addition, electronic spectra of H^+PAH will be recorded, as they are promising candidates for carriers

of the diffuse interstellar bands (Pathak & Sarre 2008; see also Hammonds *et al.*, elsewhere in this volume). First encouraging results have been obtained for $C_{10}H_9^+$ (Alata *et al.* 2010), which strongly absorbs in the visible range, supporting the hypothesis that larger H^+ PAH ions may indeed be carriers of some of the diffuse interstellar bands.

This work was supported by TU Berlin, the *Deutsche Forschungsgemeinschaft* (DO 729/2; 729/3), and the European Community - Research Infrastructure Action under the FP6 Structuring the European Research Area Program (through the integrated infrastructure initiative Integrating Activity on Synchrotron and Free Electron Laser Science).

References

- Allamandola, L.J., Tielens, A.G.G.M., & Barker, J.R., 1985, *ApJ*, 290, L25
- Alata, I., Omidyan, R., Broquier, M., *et al.*, 2010, *Phys. Chem. Chem. Phys.*, 12, 14456
- Dopfer, O., Solca, N., Lemaire, J., *et al.*, 2005, *J. Phys. Chem. A*, 109, 7881
- Dopfer, O., 2006, *J. Phys. Org. Chem.*, 19, 540
- Dopfer, O., 2008, report for project FELIX-030
- Doublerly, G.E., Ricks, A.M., Schleyer, P.V.R., & Duncan, M.A., 2008, *J. Phys. Chem. A*, 112, 4869
- Hudgins, D.M., Bauschlicher, C.W., & Allamandola, L.J., 2001, *Spectrochim. Acta Part A*, 57, 907
- Jones, W., Boissel, P., Chiavarino, B., *et al.*, 2003, *Angew. Chem. Int. Ed.*, 42, 2057
- Knorke, H., Langer, J., Oomens, J., & Dopfer, O., 2009, *ApJ*, 706, L66
- Léger, A., & Puget, J.L., *A&A*, 137, L5
- Lorenz, U.J., Solca, N., Lemaire, J., Maitre, P., & Dopfer, O., 2007, *Angew. Chem. Int. Ed.*, 46, 6714
- Pathak, A., & Sarre, P.J., 2008, *MNRAS*, 391, L10
- Ricks, A.M., Doublerly, G.E., & Duncan, M.A., 2009, *ApJ*, 702, 301
- Snow, T.L., Page, L.V., Keheyen, Y., & Bierbaum, V.M., 1998, *Nature*, 391, 259
- Solca, N., & Dopfer, O., 2001, *Chem. Phys. Lett.*, 342, 191
- Solca, N., & Dopfer, O., 2002, *Angew. Chem. Int. Ed.*, 41, 3628
- Solca, N. & Dopfer, O., 2003, *J. Am. Chem. Soc.*, 125, 1421
- Solca, N., & Dopfer, O., 2003, *Chem. Eur. J.*, 9, 3154
- Tielens, A.G.G.M., 2008, *ARA&A*, 46, 337
- Oomens, J., Tielens, A.G.G.M., Sartakov, B.G., von Helden, G., & Meijer, G., 2003, *ApJ*, 591, 968
- Zhao, D., Langer, J., Oomens, J., & Dopfer, O., 2009, *J. Chem. Phys.*, 131, 184307
- Zhao, D., 2010, Diploma Thesis, TU Berlin, Germany

THE NASA AMES PAH IR SPECTROSCOPIC DATABASE AND THE FAR-IR

C. Boersma¹, L.J. Allamandola¹, C.W. Bauschlicher, Jr.², A. Ricca²,
J. Cami³, E. Peeters³, F. Sánchez de Armas⁴, G. Puerta Saborido⁴,
A.L. Mattioda¹ and D.M. Hudgins⁵

Abstract. Polycyclic Aromatic Hydrocarbons (PAHs) are widespread across the Universe and influence many stages of the Galactic lifecycle. The presence of PAHs has been well established and the rich mid-IR PAH spectrum is now commonly used as a probe into (inter)stellar environments. The NASA Ames PAH IR Spectroscopic Database has been key to test and refine the “PAH hypothesis”. This database is a large coherent set (>600 spectra) of laboratory measured and DFT computed infrared spectra of PAHs from C₁₀H₈ to C₁₃₀H₂₈ and has been made available on the web at (<http://www.astrochem.org/pahdb>). With a new spectral window opening up; the *far-IR*, the study of PAH far-IR spectra and the quest for identifying a unique member of the interstellar PAH family has begun. To guide this research, the far-IR (>20 μm) spectra of different sets of PAHs are investigated using the NASA Ames PAH IR Spectroscopic Database. These sets explore the influence of size, shape, charge and composition on the far-IR PAH spectrum. The far-IR is also the domain of the so-called “drumhead” modes and other molecular vibrations involving low order bending vibrations of the carbon skeleton as a whole. As with drums, these are molecule and shape specific and promise to be a key diagnostic for specific PAHs. Here, the sensitivity of these “drumhead” modes to size and shape is assessed by comparing the frequencies of the lowest drumhead modes of a family of circular shaped (the coronene “family”) and rhombus shaped (the pyrene “family”) PAH molecules. From this study, some consequences for an observing strategy are drawn.

¹ NASA Ames Research Center, MS 245-6, Moffett Field, CA 94035, USA
e-mail: Christiaan.Boersma@nasa.gov

² NASA Ames Research Center, MS 230-3, Moffett Field, CA 94035, USA

³ Department of Physics and Astronomy, PAB 213, The University of Western Ontario, London, ON N6A 3K7, Canada

⁴ SETI Institute, 515 N. Whisman Road, Mountain View, CA 94043, USA

⁵ NASA Headquarters, MS 3Y28, 300 E St. SW, Washington, DC 20546, USA

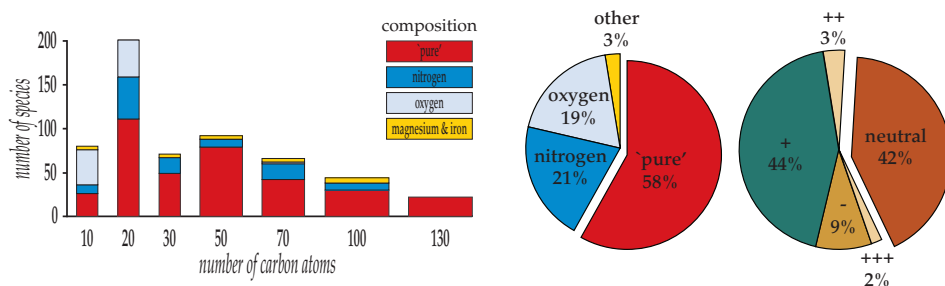


Fig. 1. *Left:* size distribution, in terms of the number of carbon atoms, of the PAHs in the computational database by composition; “pure” PAHs contain only carbon and hydrogen, nitrogen/oxygen/magnesium & iron refer to PAHs containing these elements as well. *Middle:* pie chart showing the breakdown by composition. *Right:* pie chart showing the charge distribution (Bauschlicher *et al.* 2010).

1 Introduction

The astronomical emission features formerly known as the unidentified infrared bands are now commonly ascribed to polycyclic aromatic hydrocarbons (PAHs). The spectra from laboratory experiments and computational modeling done at the NASA Ames Research Center to test and refine the “PAH hypothesis” have been assembled in a spectroscopic database. Here a few highlights are given from a study of PAH far-IR spectra that utilizes this database (Boersma *et al.* submitted). This study, that complements that by Mulas *et al.* (2006) utilizing the Cagliari database of theoretical PAH spectra (Mallocci *et al.* 2007), should prove useful to compare with data obtained by *e.g.*, ESA’s Herschel satellite, the Atacama Large Millimeter Array (ALMA), and NASA’s Stratospheric Observatory For Infrared Astronomy (SOFIA).

2 The NASA ames PAH IR spectroscopic database

The NASA Ames PAH IR Spectroscopic Database now contains over 600 PAH spectra, spanning 2–2000 μm , and is available at www.astrochem.org/pahdb. Tools that allow the user to: 1) interrogate the database; 2) plot, compare and co-add spectra, and 3) adjust parameters such as bandwidth etc. have also been made available online. Additionally, the database can be downloaded along with a suite of IDL tools (the *AmesPAHdbIDL Suite*).

Here the computational data, currently at version 1.11, are utilized and are described in detail by Bauschlicher *et al.* (2010). The experimental data in the database will be described by Mattioda *et al.* (in preparation). Figure 1 shows the distribution of the computational database, broken down by size and composition. Figure 1 also summarizes the charge and PAH type distributions in two pie charts.

Due to improvements in computational methods and in computing power, it is now possible to compute the spectra of PAHs containing more than one hundred

carbon atoms in reasonable amounts of time. When these new sets of spectra become available, they will be added to the database and the version number will be updated accordingly. One promising application is to use the database to directly fit astronomical spectra (see Cami, elsewhere in this volume).

3 PAH far-IR spectroscopy – some highlights

Laboratory experiments and DFT computations show that PAH molecules have bands that span the far-IR from 20 to 1000 μm and, unlike the mid-IR, where fundamental vibrational frequencies are determined largely by vibrations involving the chemical subgroups and specific bonds which make up the molecule, these longer wavelength transitions originate from vibrations of the *entire* molecule. Thus, while the mid-IR spectra of PAHs resemble one another since all PAHs are part of the same chemical class, beyond about 15 μm band positions can depend on *overall* size and structure.

3.1 PAH classes

The influence of PAH shape, charge, composition and size is studied in Figure 2.

Shape: Comparing the effect of structural modifications on neutral circumcoronene ($\text{C}_{96}\text{H}_{24}$) show that with increasing irregularity, far-IR PAH spectra tend to get richer in features.

Charge: The far-IR spectra of $\text{C}_{78}\text{H}_{22}$ in the -1 , 0 , $+$, $+2$ and $+3$ charge states shows that varying charge does not have a strong influence on band positions. However, relative band intensities show some differences.

PAHNs: The far-IR spectra of $\text{C}_{96}\text{H}_{24}^+$ with 8 single nitrogen containing isomers shows that band positions and absolute intensities are hardly affected by the position of the nitrogen atom in the hexagonal network.

Size: The far-IR spectra of ten compact neutral PAHs of increasing size show that the spectra tend to get richer in features and extend further into the far-IR as the molecules get larger.

3.2 PAH “drumhead” frequencies

Figure 3 presents the lowest vibrational mode of four members of both the coronene and pyrene “families”. The plot demonstrates the shift to lower frequencies of the so-called “drumhead” mode as molecular size increases. The vibrational frequencies are well fitted by:

$$\nu = 600 \left(\frac{10^{-15} [\text{cm}^2]}{A} \right) [\text{cm}^{-1}], \quad (3.1)$$

claiming an inverse dependence of frequency on PAH area (A) for the compact PAHs and only a weak dependence on molecular geometry; circular *versus* rhombus shaped.

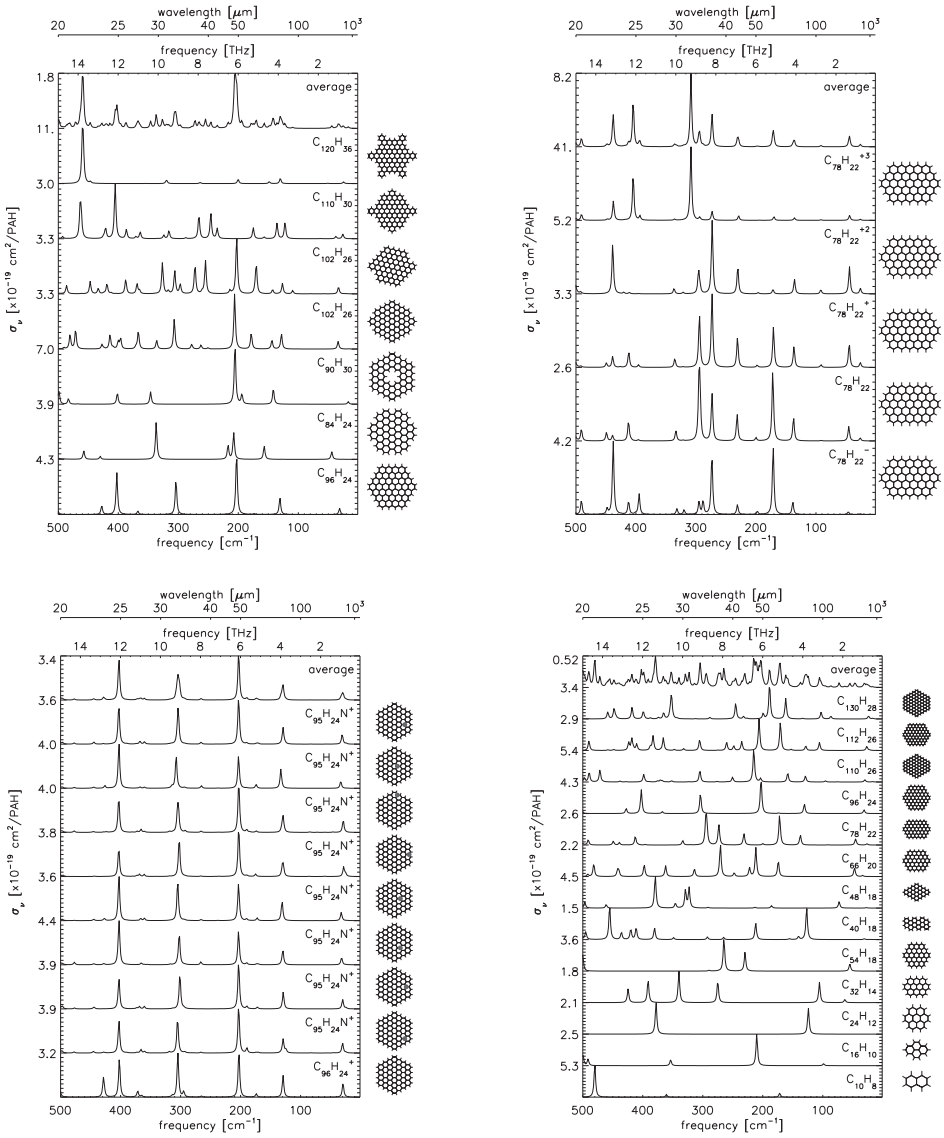


Fig. 2. Series of far-IR PAH spectra (20 – 1000 μm) showing, from top-left-to-bottom-right, the effect of shape, charge, nitrogen substitution, and size. Bands have been given Lorentzian profiles with a FWHM of 6 cm^{-1} . See Boersma *et al.* (submitted) for a detailed discussion.

Considering PAH molecules as a solid plate, this is perhaps not that surprising. The classic solution for the frequency of vibration of “free” plates is given by

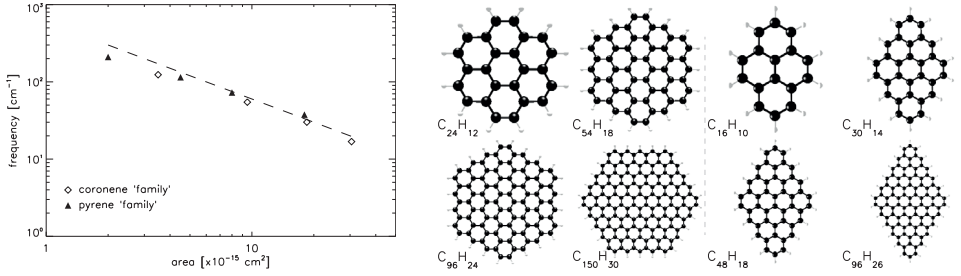


Fig. 3. *Left:* comparison of the predicted (0, 1) frequencies of a solid graphene plate, Equation (3.2), with those found in the database for the coronene (squares) and pyrene (triangles) “families”. *Right:* members of the coronene and pyrene “families”. From Boersma *et al.* (submitted).

(Meirovitch 1997):

$$\nu = \frac{\pi}{2c} \frac{1}{A} \sqrt{\frac{D}{\rho h}} \cdot (n^2 + m^2), \quad (3.2)$$

with c the speed of light, A the surface area, ρ the density, h the plate thickness and D the rigidity. The modes are characterized by m and n ; the number of nodes along both plate-axes. Because of fundamental and commercial interest, there is a rich literature on the mechanical properties of graphene and carbon nano-tubes. The bending rigidity of a graphene sheet has been calculated to be 0.8 – 1.5 eV, depending on the method used (Salvetat *et al.* 2006). Adopting $D = 1.5$ eV and 7.5×10^{-8} g·cm $^{-2}$ for the surface density (ρh), the data are well reproduced.

3.3 PAH temperature

The far-IR *absorption* band strengths are generally an order of magnitude smaller than the mid-IR absorption band strengths. However in the common astronomical case of *emission*, relative band strengths can change significantly depending on the PAH’s internal vibrational energy (temperature).

In the framework of the thermal model, conservation of energy leads to the following expression:

$$4\pi \sum_i \sigma_i \int_{T_i}^{T_{\max}} B(\nu_i, T) \left[\frac{dT}{dt} \right]^{-1} dT = E_{\text{internal}} \quad (3.3)$$

where σ_i is the absorption cross-section in mode i ; $B(\nu_i, T)$, is Planck’s function at frequency ν_i in mode i , at temperature T ; dT/dt is the cooling-rate and E_{internal} is the PAH’s internal vibrational energy after excitation by a FUV photon. The sum is taken over all modes and the integral runs from the initial PAH temperature up to the PAH’s maximum attained temperature ($T_i - T_{\max}$) after absorption of the exciting photon.

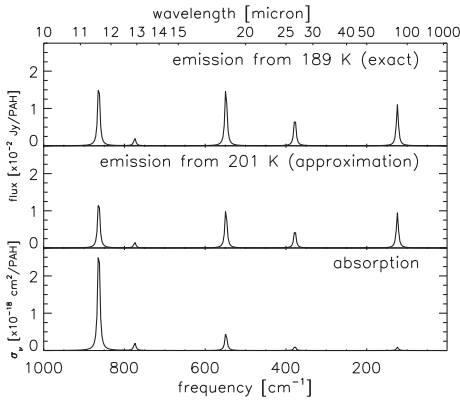


Fig. 4. Comparison of the synthesized *absorption* spectrum (10 – 1000 μm) of coronene (bottom) with the *emission* spectrum produced with an internal vibrational energy of 0.1 eV, both when approximating the calculation of the heat capacity (middle) and exactly calculating the heat capacity (top; see also Boersma *et al.* submitted). Bands have been given Lorentzian profiles with a FWHM of 6 cm^{-1} .

The maximum attained temperature is directly related to the energy of the absorbed photon through the PAH heat capacity, which also effects its cooling-rate. The heat capacity can be calculated exactly by treating the PAH molecule as a molecular system of isolated harmonic oscillators or approximated (see *e.g.*, Dwek *et al.* 1997).

Applying the thermal model to neutral coronene with an internal vibrational energy of 0.1 eV results in a maximum temperature of 189 Kelvin when calculating the full heat capacity *exactly* and 201 Kelvin when using the *approximation*. Comparing both methods in Figure 4 shows the approximation is reasonably.

In absorption the coronene “drumhead” band intensity at 124 cm^{-1} is 2.9% of that of the strongest band at 863 cm^{-1} , whereas at 201 K it has 60% of the intensity of the band at 863 cm^{-1} . However, it should be kept in mind that the intrinsic strength of these bands is still weak.

3.4 Observing PAHs in the far-IR

Far-IR spectra of astronomical objects showing the mid-IR PAH emission features will provide a very different perspective on the PAH population than do the mid-IR bands, *e.g.*, local conditions, chemical history of carbonaceous material, etc. Because the far-IR probes much colder material than the mid-IR, these data will explore the large end of the astronomical PAH-size-distribution and thus expand the scope of astronomical and astrochemical regimes in which PAHs can serve as probes.

The far-IR bands promise to put a firm limit on the size of the emitting PAHs. However, the molecular structure of the PAH does not play a major part in determining the far-IR spectrum and, therefore, identifying specific molecules in the interstellar PAH family likely requires other means. Mulas *et al.* (2006) point to the rotational PQR band structure of the lowest PAH mode as such a means. Joblin *et al.*, elsewhere in this volume, address an observational strategy based on this band structure.

Calculations have shown that the lowest vibrational transitions of interstellar PAHs probably contain a few tenths of a percent of the absorbed FUV energy (Mulas *et al.* 2006). While this is only a tiny fraction, the decrease in background dust continuum emission expected for warm PDRs could enhance the spectroscopic contrast. One first-look observing strategy could be to study the emission from transition zones in harsh environments. Telescope sensitivity will then not be an issue and UV photolysis may have isomerised the PAHs to their most stable form, leaving only a very limited number of *different* species. Given their high stability and likely contribution to the mid-IR (Bauschlicher *et al.* 2008; Mattioda *et al.* 2009), the presented coronene and pyrene “families” are particularly interesting in this regard.

References

- Bauschlicher, C.W., Boersma, C., Ricca, A., *et al.*, 2010, *ApJS*, 189, 341
Bauschlicher, C.W., Peeters, E., & Allamandola, L.J., 2008, *ApJ*, 678, 316
Boersma, C., Bauschlicher, C.W., Ricca, A., *et al.*, *ApJ*, submitted
Dwek, E., Arendt, R.G., Fixsen, D.J., *et al.*, 1997, *ApJ*, 475, 565
Mallocci, G., Joblin, C., & Mulas, G., 2007, *Chemical Phys.*, 332, 353
Mattioda, A.L., Hudgins, D.M., Boersma, C., *et al.*, in preparation
Mattioda, A.L., Ricca, A., Tucker, J., Bauschlicher, C.W., & Allamandola, L.J., 2009, *ApJ*, 137, 4054
Meirovitch, L., 1997, *Principles and techniques of vibrations* (Prentice-Hall International)
Mulas, G., Mallocci, G., Joblin, C., & Toubanc, D., 2006, *A&A*, 460, 93
Salvetat, J.P., Désarmot, G., Gauthier, C., & Poulin, P., 2006, *Lecture Notes in Physics*, Vol. 677, *Mechanical Properties of Individual Nanotubes and Composites* (Springer Berlin/Heidelberg), 439

ANALYZING ASTRONOMICAL OBSERVATIONS WITH THE NASA AMES PAH DATABASE

J. Cami^{1, 2}

Abstract. We use the NASA Ames Polycyclic Aromatic Hydrocarbon (PAH) infrared spectroscopic database to model infrared emission of PAHs following absorption of a UV photon. We calculate emission spectra resulting from the full cooling cascade for each species in the database. Using a least squares approach, we can find out what PAH mixtures best reproduce a few typical astronomical observations representing the different classes of UIR spectra. We find that we can reproduce the observed UIR spectra in the wavelength range 6–14 μm , offering support for the hypothesis that the UIR bands are indeed due to vibrational modes of PAHs and related molecular species. Spectral decompositions of our best fit models confirm and reinforce several earlier results: (i) the 6.2 μm band requires a significant contribution of nitrogen-substituted PAHs (PANHs); (ii) the reported components and their variations in the 7.7 μm band are indicative of changes in the size distribution of the contributing molecules; (iii) there is a significant contribution of anions to the 7.7 μm band; (iv) the 11.2 μm band is due to large, neutral and pure PAHs; (v) the 11.0 μm band is due to large PAH cations.

1 Introduction

The PAH hypothesis that was introduced 25 years ago states that the so-called Unidentified InfraRed (UIR) bands result from PAH molecules that are transiently heated by absorption of a UV photon, and subsequently cool by emission of infrared photons through vibrational relaxation (IR fluorescence). Although this hypothesis has now been generally accepted by the astronomical community, a good and detailed spectral match between a PAH mixture and astronomical observations has not yet been produced. At the same time, it is not clear exactly

¹ Department of Physics and Astronomy, University of Western Ontario, London, Ontario N6A 3K7, Canada

² SETI Institute - 189 Bernardo Ave., Suite 100 - Mountain View, CA 94043, USA

what the properties are of the astronomical PAH population. Such information is vital for astronomers if they are to use the widely observed UIR bands as diagnostic tools for probing the wide variety of astrophysical environments in which the UIR bands are observed.

Here, we present the first results of a program that uses the NASA Ames PAH infrared spectroscopic database to analyze astronomical observations. We show that a mixture of PAHs can indeed reproduce the observed UIR emission bands and their spectral variations. Furthermore, we gain some insight into the nature of astronomical PAHs from spectral decompositions of the best fit models.

2 Modeling the PAH emission

2.1 PAH species

The NASA Ames PAH IR spectroscopic database (Bauschlicher *et al.* 2010; see also Boersma *et al.* elsewhere in this volume) is currently the largest collection of infrared properties of PAHs and some related molecules (*e.g.* the nitrogen-substituted PANHs, see Hudgins *et al.* 2005). The database contains theoretically calculated properties for a much larger set of molecules than is experimentally available; here, we used the theoretical database exclusively.

Amongst others, the theoretical part of the database contains the calculated frequencies and intensities for all the fundamental mode vibrations for a collection of 556 individual species. The database is highly biased toward smaller (≤ 30 C atoms) and pure PAHs that are neutral or singly ionized. We show in Section 4 that reliable conclusions can still be inferred from such a biased database.

2.2 PAH physics

It is well established (see *e.g.* d’Hendecourt *et al.* 1989) that the PAH excitation and IR fluorescent cooling can be adequately described by using the thermal approximation which states that the vibrational energy contained in a large, isolated molecule can be represented by a single parameter – the vibrational excitation temperature. Absorption of a single UV photon will then briefly heat a molecule to very high temperatures, after which it cools by infrared emission that scales with the Planck function at the vibrational temperature (see also Allamandola *et al.* 1989). The total PAH emission following absorption of a single UV photon is then the time-integrated infrared emission as the molecule cools down.

The maximum temperature that can be attained by a PAH molecule after UV absorption depends on the energy of the absorbed photon, and on the molecule capability of distributing the energy over the vibrational states – the “vibrational” heat capacity. Since larger molecules have more vibrational modes, the average energy per vibrational mode is lower for a given photon energy and thus the larger molecules have typically lower temperatures after absorption of the same photon. As a consequence, they will emit much of their energy at longer wavelengths than the smaller PAHs.

To take such effects properly into account, we used the data in the PAH database to first calculate the heat capacities for each individual species. We also calculated the maximum temperature for each species upon absorption of a 10 eV photon, and calculated the cooling rate for each species for temperatures between 0 K and the maximum attained temperature (see *e.g.* Tielens 2005). This then allows to calculate the full fluorescent infrared emission for each molecule in the database by integrating the emission over the cooling curve. A check is performed to ensure energy conservation in the process.

2.3 PAH parameters

The PAH physics described above thus sets the relative intensities for all fundamental modes for each molecular species individually, and the only free parameter is the energy of the absorbed UV photon. However, in order to compare these model spectra to astronomical observations, we need to adopt a band profile shape. Most of the astronomical UIR bands are characterized by asymmetric band profiles that are believed to originate from anharmonicities in the potential energy. This in turn results in hot band transitions that are slightly shifted in frequency compared to the fundamental, and causes the overall profile to be asymmetric.

Since these effects reflect the details of the potential energy surface, they are generally different for each vibrational mode and for each molecule, and the resulting band asymmetry is furthermore a function of the temperature. Unfortunately, the PAH database does not contain information on anharmonicity and integrating anharmonic effects is a very demanding task that is restricted so far to a few small species (see Pirali *et al.* 2009; Basire *et al.* elsewhere in this volume). We thus decided to convolve each of the individual PAH bands with a symmetric Lorentzian profile. We acknowledge that this will necessarily introduce some uncertainty in the wings of the PAH bands; and we will therefore not discuss spectral features at that level.

Finally, we only consider absorption by photons of one single energy – the average photon energy for the environment studied. The above procedures thus result in a set of 556 individual spectra, representing the response of each species in the database to absorption by a photon with the same energy.

3 Fitting the astronomical spectra

3.1 Observations

Peeters *et al.* (2002) and van Diedenhoven *et al.* (2004) have shown that most astronomical observations of the PAH bands can be divided in only a few classes (Class A, B and C; see also Peeters *et al.* elsewhere in this volume). Whereas objects in class A have identical spectra, classes B and C represent a much larger variety in terms of peak positions of individual features and relative intensities of the PAH bands. For this work, we selected a representative object for class A (the HII region IRAS 23133+6050), but somewhat arbitrarily picked an object from

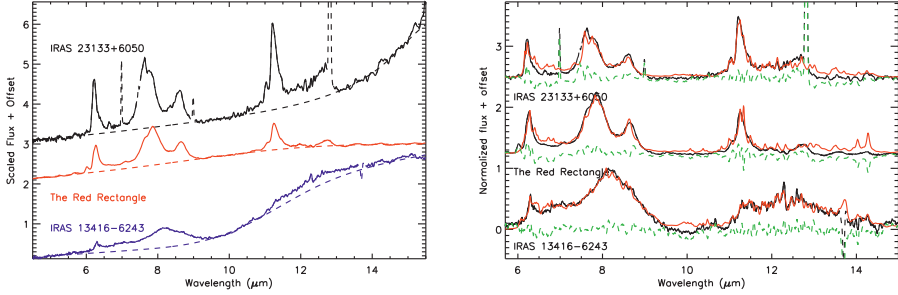


Fig. 1. (a) The three astronomical observations (solid lines) and the adopted dust continua (dashed lines). The HII region IRAS 23133+6050 (top) is a Class A source; the Red Rectangle (middle) a Class B source and the proto-planetary nebula IRAS 13416-6243 (bottom) a Class C object. (b) The astronomical PAH spectra (black) and the best fit PAH model spectra (lighter curves). Residuals are shown as dashed lines.

class B (the Red Rectangle) and another one from class C (the proto-planetary nebula IRAS 13416-6243). If we can reproduce the observable UIR properties for these three objects with PAHs, it stands to reason that we can equally well reproduce most other observations.

All observations used here are ISO/SWS observations; we refer to Peeters *et al.* (2002) for details about the data reduction process. We do note here however that we chose to define a continuum that only represents the thermal emission of dust, and thus does not contain any spectral features to represent possible plateaus underneath the PAH features (see Fig. 1a). For what follows, we will always use the continuum-subtracted spectra.

3.2 Procedures

We calculated individual PAH spectra for each of the species in the database as described above, using an average photon energy of 10 eV. Then, we used a non-negative least squares algorithm to determine “abundances” (weights) for each of those PAHs such that the weighted sum of the PAH spectra provides the best possible fit to each of these astronomical observations.

One issue that needs to be addressed here is the intrinsic widths for each of the PAH bands in our models. Often, it is assumed that the intrinsic PAH bands are fairly broad ($\sim 30 \text{ cm}^{-1}$). However, the astronomical observations of the strong C-H out of plane bending mode at $11.2 \mu\text{m}$ show a band width (FWHM) of only about 4 cm^{-1} . Obviously, the constituent PAH spectra that make up this band cannot be broader than this observed width. The same holds at least for the band at $11.0 \mu\text{m}$. In the $6\text{--}10 \mu\text{m}$ region on the other hand, the observed band profiles are broader (in wavenumber space), and it thus seems unrealistic to adopt a small band width for the PAH profiles in this wavelength range. With some trial and

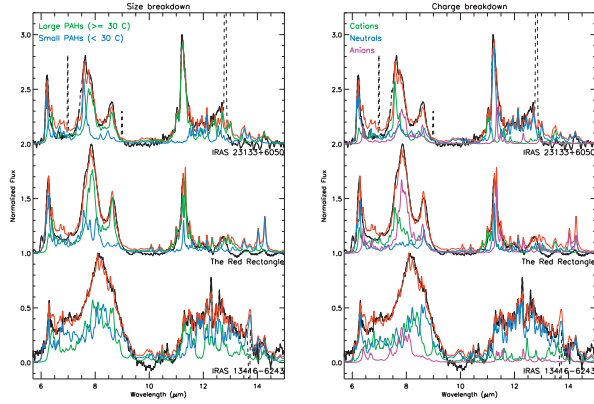


Fig. 2. The spectral decomposition of our best fitting model as a function of molecular size (*left*) and charge state (*right*). Astronomical observations are shown in black; overall fits in red, and decompositions in green, blue or magenta (see legend).

error, we found that in this region, a width (FWHM) of 13 cm^{-1} provides better global results. Thus, we convolved the individual PAH spectra with a Lorentzian profile that has a FWHM of 13 cm^{-1} in the $6\text{--}10 \mu\text{m}$ region, and a width of 4 cm^{-1} in the $10\text{--}14 \mu\text{m}$ region. The resulting best fits are shown in Figure 1b.

4 Results & discussion: Fits & decomposition

Figure 1b clearly shows that a mixture of PAHs can indeed reproduce the observed infrared emission for all three classes of astronomical PAH spectra. Typically, about 50 different molecular species are included in the models presented here.

Much more valuable than the fits themselves is the insight we can gain into the nature of the astrophysical PAH population by breaking down our best fit models into spectral decompositions.

Figure 2 shows just two such examples. In the left panel, the green curve represents the contribution to our total fit of the “large” PAHs, *i.e.* the species in our database with 30 or more carbon atoms; the blue curve represents the small PAHs. This figure shows several interesting results. First, for both the Class A and B sources, the strong $11.2 \mu\text{m}$ PAH band is (almost) exclusively due to *large* PAH species. This is consistent with the band width of 4 cm^{-1} that implies a mean excitation temperature of about 280 K (Pech *et al.* 2002) and thus excludes a significant contribution of small PAHs that are too hot. Note that the NASA Ames PAH database is currently heavily biased toward smaller species, and given that bias, it is somewhat surprising to find that a spectral feature is exclusively due to large PAHs. Clearly, not a single one of the hundreds of small PAH species in the database is able to reproduce the $11.2 \mu\text{m}$ band without causing additional spurious spectral features in this wavelength range. Also the PAH bands at 8.6

and 11.0 μm are due to large PAHs, and the same holds for the red component of the 7.7 μm complex. Variations in the shape of the 7.7 μm complex are then indicative of changes in the size distribution of the PAHs. Note also that the Class C source contains what appears to be a random distribution of both large and small PAHs.

In the right panel, the best fit is decomposed according to the charge state of the contributing species: neutrals are shown in blue, cations in green, and anions in magenta. Neutral PAHs produce the bulk of the emission in the 11.2 μm band, but cations are responsible for the 11.0 μm band. Combined with the left panel, we can thus conclude that the 11.2 μm band is due to large neutral PAHs, while the 11.0 μm band is due to large PAH cations. It is also interesting to see that our best model includes a significant fraction of anions in the mixture. This is especially clear in the 7.7 μm complex. Finally, note that for the class C source, most of the PAH emission arises from neutral molecules.

Many more spectral decompositions are possible, and yield interesting results. One in particular is a decomposition according to the chemical composition which shows that the 6.2 μm band requires a significant contribution of nitrogen-substituted PAHs (called PANHs) – as was shown already by Hudgins *et al.* (2005).

The work presented here illustrates the analytic and diagnostic power that is contained in large spectral databases such as the NASA Ames PAH IR spectroscopy database. The fact that some of our results from the spectral decomposition analysis go against the bias in the database (*e.g.* exclusively large PAHs in the results while the database contains primarily small PAHs) indicates that our results are not driven by the database contents, but rather by the spectral properties of the astronomical PAHs. At the same time, we are somewhat limited by the relatively small number of molecules in the database, and by the uncertainties in the intrinsic band profiles. Nevertheless, the NASA Ames PAH database clearly contains already a significant number of astrophysically relevant PAH species, and future research will undoubtedly increase the diagnostic value of exercises such as the one presented here.

References

- Allamandola, L.J., Tielens, A.G.G.M., & Barker, J.R., 1989, ApJS, 71, 733
Bauschlicher, C.W., Boersma, C., Ricca, A., *et al.*, 2010, ApJS, 189, 341
d'Hendecourt, L., Léger, A., Boissel, P., & Désert, F., 1989, IAUS, 135, 207
Hudgins, D.M., Bauschlicher, C.W. Jr., & Allamandola, L.J., 2005, ApJ, 632, 316
Pech, C., Joblin, C., & Boissel, P., 2002, A&A, 388, 639
Peeters, E., Hony, S., van Kerckhoven, C., *et al.*, 2002, A&A, 390, 1089
Pirali, O., Vervloet, M., Mulas, G., Mallocci, G., & Joblin, C., 2009, Phys. Chem. Chem. Phys., 11, 3443
Tielens, A.G.G.M., 2005, The Physics and Chemistry of the Interstellar Medium (Cambridge University Press)
van Diedenhoven, B., Peeters, E., van Kerckhoven, C., *et al.*, 2004, ApJ, 611, 928

SEARCH FOR FAR-IR PAH BANDS WITH HERSCHEL: MODELLING AND OBSERVATIONAL APPROACHES

C. Joblin^{1,2}, G. Mulas³, G. Mallocci³ and E. Bergin & the HEXOS consortium⁴

Abstract. *Herschel* opens the possibility to detect the low-frequency vibrational bands of individual polycyclic aromatic hydrocarbon (PAH) molecules and therefore to progress in our understanding of the nature of these species and the properties of the environments from which they emit. However, unless one individual molecule dominates the PAH family, this detection will not be straightforward and it is necessary to optimise the observational search with an educated guess of the band profiles and intensities. Such educated guess can be obtained from models that include a detailed description of the molecular properties (anharmonicity, rotation...) in the modelling of the cooling cascade of the emitting species. First results are expected soon from the observation of the Orion Bar as part of the HEXOS *Herschel* key program.

1 Introduction

Polycyclic aromatic hydrocarbons (PAHs) are commonly believed to be the carriers of the aromatic infrared bands (AIBs) that dominate the mid-IR emission between 3.3 and 15 μm in most galactic and extragalactic objects. However the PAH model suffers from the lack of identification of any individual species and different approaches have been pursued over the years to address this question. Diffuse interstellar bands (DIBs), that fall essentially in the visible range (Herbig 1995), are a way to identify individual PAH molecules by their low-lying electronic transitions, which are very characteristic. However, “fishing” for candidates has

¹ Université de Toulouse, UPS, CESR, 9 Av. colonel Roche, 31028 Toulouse Cedex 4, France

² CNRS, UMR 5187, 31028 Toulouse, France

³ INAF – Osservatorio Astronomico di Cagliari – Astrochemistry Group, Strada 54, Loc. Poggio dei Pini, 09012 Capoterra (CA), Italy

⁴ Department of Astronomy, University of Michigan, 500 Church Street, Ann Arbor, MI 48109, USA

not been very successful (see Snow & Destree and Cox and references in these articles, elsewhere in this volume). This approach is a lengthy task considering that each species has specific electronic transitions whose measurement for DIB identification requires dedicated set-ups in the laboratory, to mimic the physical conditions of low pressure and temperature in interstellar space. These experiments are very demanding (see for instance Tan & Salama 2006; Useli–Bacchitta *et al.* 2010; Pino *et al.*, elsewhere in this volume) and the number of candidates that need to be investigated is very large. For a given number of carbon atoms, N_C , there are different isomeric forms as well as a distribution of hydrogenation and ionisation states (*cf.* Bierbaum *et al.* and Montillaud *et al.*, elsewhere in this volume).

Rotational spectroscopy is another technique that has been successful over the years to identify circumstellar and interstellar molecules and radicals with the use of radio telescopes. Dipolar PAHs can display a pure rotational emission spectrum in the radio domain but transitions are expected to be weak; PAHs ought to be rotating suprathermally in photodissociation regions (PDRs), yielding a very large rotational partition function (Rouan *et al.* 1992; Mulas 1998). Combined emissions from different species will lead to forests of weak rotational lines that would merge into a quasi-continuum; PAHs are likely to contribute to the excess microwave emission (Ysard *et al.* 2010). A better characterization of the nature of the carriers of the anomalous emission would allow to constrain their spatial variation that is required to retrieve the cosmic microwave background in the studies that are currently led with the *Planck* mission.

Searches for the vibrational emission features in the far-IR range provide a good alternative to visible (DIB) and radio (rotational) identification methods and that is becoming feasible with the *Herschel* mission. These features involve the whole carbon skeleton of the molecule and are therefore more specific to the exact molecular identity than the ones in the mid-IR, which instead probe functional groups. Experimental data in the far-IR range are still scarce and await for further progress in the coming years (Zhang *et al.* 2010; Mattioda *et al.* 2009; Pirali *et al.* 2006). On the other hand, more and more data are available from quantum-chemistry calculations using density functional theory (DFT; *cf.* Pauzat in this volume) and are collected in databases (Bauschlicher *et al.* 2010; Mallocci *et al.* 2007). This opens the possibility to model the far-IR emission of PAHs in PDRs.

2 Model of the (far-)IR emission spectrum of PAHs

The IR emission from vibrationally excited PAHs can be calculated from fundamental equations (*cf.* Allamandola *et al.* 1989). The main step is to properly describe the populations in all levels v of all modes i during the cooling process. Most of the authors in the literature have used the simplifying assumption of thermal distributions, in which the populations of vibrational levels are described by the Boltzmann equation, with the canonical formalism (*cf.* for instance Désert *et al.* 1990; Pech *et al.* 2002; Draine & Li 2007). Our studies (Mulas 1998; Joblin *et al.* 2002; Mulas *et al.* 2006a) are based on the microcanonical formalism in which the

energy is the well-defined, conserved physical parameter. This more accurately describes the statistical behaviour of a PAH molecule with a given internal energy U but comes at the price of having to explicitly take into account all vibrational modes. A Monte Carlo technique is used to properly solve the master equation and follow the population of states during the cooling of the PAH down to the ground level. Other studies (*cf.* Ysard *et al.* 2010) used the exact-statistical method of Draine & Li (2007). Comparison of results obtained respectively with the micro-canonical formalism and thermal approximation can be found in Joblin & Mulas (2009). Significant differences have been found for the band intensities (a factor of two or more for some of the bands). The emission spectrum of a large sample of PAHs in different charge states (neutrals and cations) and in specific objects (such as the Red Rectangle nebula) has been computed by Mulas *et al.* (2006a). The Monte-Carlo code takes as an input molecular parameters that are available in the theoretical on-line spectral database of PAHs (Mallocci *et al.* 2007): the positions and intensities of all vibrational modes and the photo-absorption cross-sections up to the vacuum-UV. This allows an accurate calculation of the band intensities but the band profiles have to be assumed (*cf.* Fig. 1 and Mulas *et al.* 2006a).

The far-IR bands are emitted mainly at the end of the cooling cascade. Furthermore, at low excitation, it is necessary to consider that at some point the redistribution of energy between vibrational levels (the so-called internal vibrational redistribution, IVR) breaks down; the vibrational states decouple and their quantum numbers cannot be described any more in statistical mechanics terms, but must instead be described explicitly in terms of specific vibrational transitions between specific states. The population of states at decoupling is governed *only* by statistics and therefore does not depend on the Einstein coefficients associated with the far-IR modes. However the latter govern the relaxation rate and play a key role in the competition with the UV absorption rate. If the UV rate is slow compared to the relaxation then the far-IR cooling can further proceed and very weakly active or even inactive modes can relax in a manner analogous to the emission of forbidden atomic lines in nebulae. In other cases, absorption of another UV photon triggers again mid-IR emission from the hot PAH, and this leads to reduced emission in the far-IR. In particular, the “slowest” far-IR modes can be totally suppressed (*cf.* case of IRAS 21282+5050 in Appendix C of Mulas *et al.* 2006a).

3 Detailed calculation of the (far-) IR band profiles

A key aspect in the detection and identification of far-IR bands due to PAHs is related to the exact band profile. During the cooling cascade of the excited PAH, most of the transitions happen between vibrationally excited states. Due to vibrational anharmonicity, the position and width of the emitted bands will depend on the involved states (*cf.* Oomens and Basire *et al.* in this volume). Many far-IR bands are due to out-of-plane vibrational modes, for which one can distinguish two main parts in the ro-vibrational band profile: the Q branch, in which fine structure is expected due to anharmonicity, and the P and R branches, that carry

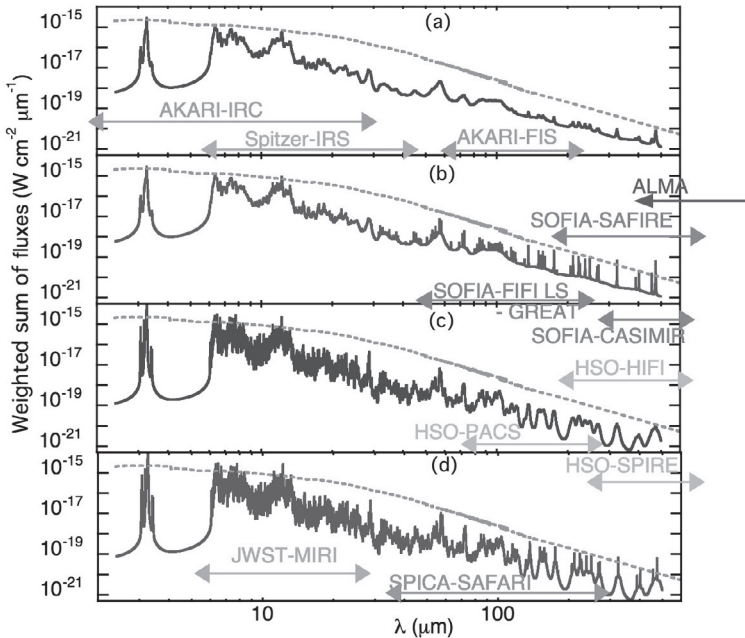


Fig. 1. Calculated infrared emission spectrum from a sample of 40 PAHs ranging in size from $C_{10}H_8$ to $C_{48}H_{20}$ and with neutral or cationic charge, compared with the estimated dust continuum in the Red Rectangle nebula. Different panels correspond to different values for σ_{PR} , the width of the P and R rotational branches, and σ_Q , the width of the central Q branch (*cf.* Mulas *et al.* 2006a for more details). The operation ranges of the relevant astronomical facilities are overlaid for reference. *Herschel* will open the possibility to identify PAHs by their far-IR bands.

the rotational information. The far-IR bands being preferentially emitted near the end of the cooling cascades, the fine structure of these bands should not be washed out by coupling between states, as it happens for mid-IR bands. In particular, for out-of-plane modes, which have sharp Q branches, this enhances spectral contrast, making their detection possible in spite of the expected strong dust continuum background and spectral crowding (*cf.* (b) and (d) in Fig. 1).

The modelling of the band profile requires prior knowledge of several molecular parameters: the χ matrix of anharmonic parameters (including a proper treatment of resonances) and the variations of the rotational constants as a function of the vibrational state. These parameters are not easy to access by experiment or theory; a recent study has been performed on naphthalene, $C_{10}H_8$ (Pirali *et al.* 2009), that illustrates the interplay between high-resolution spectroscopy and numerical simulations of the photophysics of PAHs to access these parameters.

In order to compare with astronomical observations, unless one can use directly experimental results of UV-induced IR fluorescence taken under experimental conditions close to the ones expected in space (but such results are not available yet), some modelling of the emission process is necessary. As previously explained in Section 2, the two commonly used strategies are the simpler, faster, but less accurate thermal approximation, or the more complicated, but more accurate micro-canonical approach that we implemented in the form of Monte Carlo simulations (*cf.* Mulas *et al.* 2006a, 2006b). In our Monte Carlo model, the cooling cascades of the PAHs were simulated assuming collisions to be negligible, and furthermore neglecting photodissociation. While photodissociation is expected to be relevant in the ISM, it still occurs on a relatively small fraction of the UV absorption events, resulting in a small correction to the estimated IR emission. Photoionisation is a bit more frequent for neutrals and negative ions, and was taken into account. A large enough number of UV absorption events and relative IR cascades were simulated, to accumulate sufficient statistics on the emission process. The population of rotational modes (in the semirigid rotor approximation), and the statistics of anharmonic shifts were recorded in the simulations, enabling us to produce full rovibrational structures.

4 PAH far-IR spectroscopy with Herschel

From an observational point of view, the search for the far-IR bands of PAHs is now becoming possible with the Herschel space observatory (Pilbratt *et al.* 2010) that has been launched in 2009. *Herschel* is equipped with three instruments that cover the far-IR and sub-mm ranges from typically 50 to 600 μm . Detailed presentations of the three instruments, the Photodetector Array Camera and Spectrometer (PACS; Poglitsch *et al.* 2010), the Spectral and Photometric Imaging REceiver (SPIRE; Griffin *et al.* 2010) and the Herschel-Heterodyne Instrument for the Far-Infrared (HIFI; de Graauw *et al.* 2010) can be found elsewhere. The best strategy to detect the PAH far-IR bands is to search for the Q branches associated with the out-of-plane modes. The PACS and SPIRE instruments provide the best compromise between resolving power and sensitivity to evidence these features. Follow-up observations at very high resolution with the heterodyne spectrometer HIFI will allow us to resolve the hot band structure of the Q branches and may be also some structure in the P and R branches. These structures, if detected, carry detailed information on the emitting molecule as well as on the local physical conditions that prevail in the emitting environments. To retrieve this information it is necessary to model these features as described in Section 3.

As an example, we present here new calculations of band profiles performed on the large molecule neutral circumovalene ($\text{C}_{66}\text{H}_{20}$). These calculations were motivated by the Herschel observations of EXtra-Ordinary Sources (HEXOS; Bergin *et al.* 2010) key program. In particular, observations are performed on the prototype bright PDR, the Orion Bar, following the strategy explained above. For the molecular parameters, realistic χ matrices were built based on the knowledge of the smaller molecules C_{10}H_8 and $\text{C}_{14}\text{H}_{10}$ studied by Mulas *et al.* (2006b). A

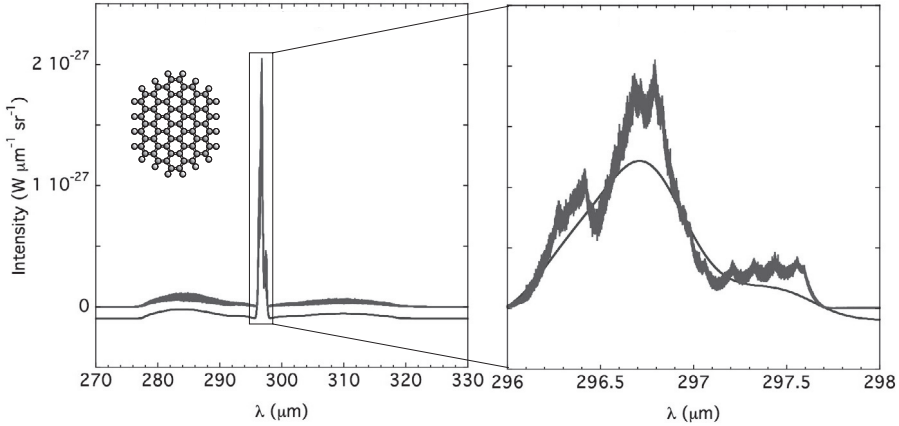


Fig. 2. One example of the calculated structure of the low energy IR-active band of circumvalene ($C_{66}H_{20}$), computed for one molecule embedded in the Orion Bar radiation field assumed to be $G_0 = 5 \times 10^4$ in Habing units. Full PQR structure (*left*) and zoom in on the Q branch (*right*). Green (*upper*) spectrum is at full resolution and illustrates the complex structure that could be revealed by the *Herschel* HIFI heterodyne spectrometer. Blue (*lower*) spectrum has been convolved at the highest resolution of the *Herschel* SPIRE instrument.

similar educated guess was performed for the variations of the rotational constants. The radiation field of the Orion Bar was calculated using the Meudon PDR code (Le Petit *et al.* 2006) with a stellar spectrum from the Kurucz library with a temperature of 40 000 K (Kurucz 1991), a distance of 0.25 pc and a gas density of $n_H = 5 \times 10^4 \text{ cm}^{-3}$. The calculated radiation field at the cloud surface has an integrated UV intensity of $G_0 = 5 \times 10^4$ in Habing units (Habing 1968). The cooling cascades of $C_{66}H_{20}$ in the Orion Bar field were then calculated and the band profiles obtained as described in Section 3. The calculated profiles were convolved at the spectral resolution of the instruments onboard *Herschel* (*cf.* Fig. 2).

5 Conclusions and perspectives

The search for the far-IR bands of PAHs is expected to be a difficult subject since the bands are predicted to be weak and our ability to observe them will depend on how diverse is the mixture of interstellar PAHs. *Herschel* offers the possibility to investigate this question thanks to the characteristics and the spectral range covered by its instruments. SOFIA and ALMA that are now entering the scene could also bring new insights into this topic. The next far-IR/sub-mm space mission will then be SPICA (2018). But none of these new missions will allow to cover the full *Herschel* spectral range and we should therefore try hard to search

for these PAH bands with *Herschel*. As we have illustrated, a proper modelling of the cooling cascade including molecular properties (anharmonicity, rotation...) is mandatory for band prediction and analysis. In this regard, there is still a lot of work to do in the laboratory and this not an easy task for either the experiment or the theoretical calculations. From the experimental point of view, there is a need for far-IR spectroscopy of large PAH molecules, but at $T < 300$ K to resolve (some) of the anharmonic structure. The calculations of the matrix of anharmonic parameters with DFT are very heavy and “tricky”. Furthermore, for high temperatures, alternatives have to be found such as molecular dynamics with an approximated DFT scheme (Porezag *et al.* 1995; see also Pauzat and Basire *et al.*, elsewhere in this volume). A lot of effort still needs to be dedicated to this subject both from the observational and laboratory points of view.

References

- Allamandola, L.J., Tielens, A.G.G.M., & Barker, J.R., 1989, *ApJS*, 71, 733
- Bauschlicher, C.W., Boersma, C., Ricca, A., Mattioda, A.L., *et al.*, 2010, *ApJS*, 189, 341
- Bergin, E.A., Phillips, T.G., Comito, C., *et al.*, 2010, *A&A*, 521, L20
- Désert, F.-X., Boulanger, F., & Puget, J.L., 1990, *A&A*, 237, 215
- Draine, B.T., & Li, A., 2001, *ApJ*, 551, 807
- Draine, B.T., & Li, A., 2007, *ApJ*, 657, 810
- de Graauw, T., Helmich, F.P., Phillips, T.G., *et al.*, 2010, *A&A*, 518, L4
- Griffin, M.J., Abergel, A., Abreu, A., *et al.*, 2010, *A&A*, 518, L3
- Habing, H.J., 1968, *BAIN*, 19, 421
- Herbig, G.H., 1995, *ARA&A*, 33, 19
- Joblin, C., Boissel, P., Léger, A., D’Hendecourt, L., & Défourneau, D., 1995, *A&A*, 299, 835
- Joblin, C., Toubanc, D., Boissel, P., & Tielens, A.G.G.M., 2002, *Mol. Phys.*, 100, 3595
- Joblin, C., & Mulas, G., 2009, in: *Interstellar dust properties: from fundamental studies to astronomical models*, ed. F. Boulanger, C. Joblin, A. Jones, & S. Madden, *EAS Pub. Series*, 35, 133
- Kurucz, R.L., 1991, *BAAS*, 23, 1047
- Le Petit, F., Nehmé, C., Le Bourlot, J., & Roueff, E., 2006, *ApJS*, 164, 506
- Mallici, G., Joblin, C., & Mulas, G., 2007, *Chem. Phys.*, 332, 353
- Mattioda, A.L., Ricca, A., Tucker, J., Bauschlicher, C.W., & Allamandola, L.J., 2009, *AJ*, 137, 4054
- Mulas, G., 1998, *A&A*, 338, 243
- Mulas, G., Mallici, G., Joblin, C., & Toubanc, D., 2006a, *A&A*, 460, 93
- Mulas, G., Mallici, G., Joblin, C., & Toubanc, D., 2006b, *A&A*, 456, 161
- Pech, C., Joblin, C., & Boissel, P., 2002, *A&A*, 388, 639
- Pilbratt, G.L., Riedinger, J.R., Passvogel, T., *et al.*, 2010, *A&A*, 518, L1
- Pirali, O., Van-Oanh, N.-T., Parneix, P., Vervloet, M., & Bréchnac, P., 2006, *Phys. Chem. Chem. Phys.*, 8, 3707

- Pirali, O., Vervloet, M., Mulas, G., Mallocci, G., & Joblin, C., 2009, *Phys. Chem. Chem. Phys.*, 11, 3443
- Poglitsch, A., Waelkens, C., Geis, N., *et al.*, 2010, *A&A*, 518, L2
- Porezag, D., Frauenheim, T., Köhler, T., Seifert, G., & Kaschner, R., 1995, *Phys. Rev. B*, 51, 12947
- Rouan, D., Léger, A., Omont, A., & Giard, M., 1992, *A&A*, 253, 498
- Salama, F., Galazutdinov, G.A., Krelowski, J., Allamandola, L.J., & Musaev, F.A., 1999, *ApJ*, 526, 265
- Ysard, N., & Verstraete, L., 2010, *A&A*, 509, A12
- Zhang, J., Han, F., Pei, L., Kong, W., & Li, A., 2010, *ApJ*, 715, 485

**PAHs and Star Formation
in the Near and Far Universe**

POLYCYCLIC AROMATIC HYDROCARBONS AS STAR FORMATION RATE INDICATORS

D. Calzetti¹

Abstract. As images and spectra from ISO and Spitzer have provided increasingly higher-fidelity representations of the mid-infrared (MIR) and Polycyclic Aromatic Hydrocarbon (PAH) emission from galaxies and galactic and extra-galactic regions, more systematic efforts have been devoted to establishing whether the emission in this wavelength region can be used as a reliable star formation rate indicator. This has also been in response to the extensive surveys of distant galaxies that have accumulated during the cold phase of the Spitzer Space Telescope. Results so far have been somewhat contradictory, reflecting the complex nature of the PAHs and of the mid-infrared-emitting dust in general. The two main problems faced when attempting to define a star formation rate indicator based on the mid-infrared emission from galaxies and star-forming regions are: (1) the strong dependence of the PAH emission on metallicity; (2) the heating of the PAH dust by evolved stellar populations unrelated to the current star formation. I review the status of the field, with a specific focus on these two problems, and will try to quantify the impact of each on calibrations of the mid-infrared emission as a star formation rate indicator.

1 Introduction

First enabled by the data of the Infrared Space Observatory (ISO, Kessler *et al.* 1996) and then expanded by the images and spectra of the Spitzer Space Telescope (Spitzer, Werner *et al.* 2004), the mid-infrared, $\sim 3\text{--}40\ \mu\text{m}$, wavelength range has been at the center of many investigations seeking to define handy and easy-to-use Star Formation Rate (SFR) indicators, especially in the context of extragalactic research.

In the Spitzer (cold-phase) era, the MIR emission from galaxies had experienced renewed interest particularly in the high-redshift galaxy populations community (*e.g.*, Daddi *et al.* 2005, 2007; Papovich *et al.* 2006, 2007; Yan *et al.* 2007;

¹ Dept. of Astronomy, University of Massachusetts, Amherst, MA 01003, USA,
e-mail: calzetti@astro.umass.edu

Reddy *et al.* 2010). The Spitzer Multiband Imaging Photometer (MIPS, Rieke *et al.* 2004) and the Spitzer InfraRed Spectrograph (IRS, Houck *et al.* 2004) had proven particularly sensitive at detecting the MIR dust emission from galaxies in the redshift range $z \approx 1-3$. Observations performed with the MIPS 24 μm and 70 μm bands yield the restframe $\sim 8 \mu\text{m}$ and 23 μm emission of a $z=2$ galaxy. An obvious question to ask is whether, and to what degree, the MIR emission traces the recent star formation in galaxies.

The MIR region hosts the rich spectrum of the Polycyclic Aromatic Hydrocarbon (PAH) emission features in the wavelength range 3–20 μm (Léger & Puget 1984), also previously known as Unidentified Infrared Bands or Aromatic Features in Emission (*e.g.*, Sellgren *et al.* 1983; Sellgren 1984; Puget *et al.* 1985), which are the subject of the present Conference. Thus, a corollary to the question in the previous paragraph is how well the PAH emission traces recent star formation in galaxies.

In this Review, I concentrate on results obtained from the investigation of nearby (closer than about 30–50 Mpc) galaxies, where the MIR emission can be typically resolved to sub-kpc scale at the Spitzer resolution in the 3–8 μm range: the 2'' FWHM corresponds to ~ 0.5 kpc for a galaxy at 50 Mpc distance. In this regime, separating the contributing heating effects of various stellar populations become easier than in unresolved galaxies. Throughout this paper, I will refer to “8 μm emission” when indicating the stellar-continuum subtracted emission as detected by Spitzer in the IRAC 8 μm band (Fazio *et al.* 2004) or similar-wavelength bands on the ISO satellite. With the terminology “PAH emission” I will refer to the emission features (after subtraction of both the stellar and dust continuum) at/around 8 μm .

An important assumption when using the infrared emission as a SFR indicator is that galaxies must contain sufficient dust that a significant fraction of the UV-optical light from recently formed stars is absorbed and re-emitted at longer wavelengths by the dust itself. For the “typical” galaxy in the Universe, about half of its energy budget is re-processed by dust in the infrared (*e.g.*, Hauser & Dwek 2001; Dole *et al.* 2006), but a very large scatter on this “mean” value exists from galaxy to galaxy. There tends to be a relation between star formation activity and dust opacity in galaxies, in the sense that more active galaxies also tend to be more opaque (*e.g.*, Wang & Heckman 1996; Heckman *et al.* 1998; Calzetti 2001; Sullivan *et al.* 2001). In general, infrared SFR calibrations will need to take into account that a fraction of the star formation will emerge from the galaxy unprocessed by dust, and this fraction will depend on a number of factors (metal content and star formation activity being two of those, and dust geometry being a third, harder-to-quantify, factor).

2 PAH emission as a SFR indicator

The 8 μm emission represents about 5%–20% of the total infrared (TIR) emission from galaxies; of this, more than half, and typically 70%, can be attributed to PAH emission in metal-rich galaxies (Smith *et al.* 2007; Dale *et al.* 2009;

Marble *et al.* 2010). In this context, “metal-rich” refers to oxygen abundances larger than $12+\log(\text{O}/\text{H})\sim 8.1\text{--}8.2$ (with the Sun’s oxygen abundance being ~ 8.7 , Asplund *et al.* 2009). Although small, the fraction of TIR energy contained in the $7\text{--}8\ \mu\text{m}$ wavelength region is not entirely negligible, and much effort has been devoted to investigating whether the emission in this region could be used as a reliable SFR indicator.

Systematic efforts began with ISO (*e.g.*, Roussel *et al.* 2001; Boselli *et al.* 2004; Forster-Schreiber *et al.* 2004; Peeters *et al.* 2004), and continued with Spitzer, which enabled extending the analysis to fainter systems and to higher spatial detail (*e.g.*, Wu *et al.* 2005; Calzetti *et al.* 2005, 2007; Alonso-Herrero *et al.* 2006; Zhu *et al.* 2008; Kennicutt *et al.* 2009; Salim *et al.* 2009; Lawton *et al.* 2010). In a typical approach, the $8\ \mu\text{m}$ (or similar wavelengths) luminosity or luminosity/area is plotted as a function of other known SFR indicators, to establish whether a correlation exists; an example is shown in Figure 1. In one case, the $8\ \mu\text{m}$ emission has also been combined with tracers of the unattenuated star formation (*e.g.*, H α line emission) to recover an “unbiased” SFR indicator (Kennicutt *et al.* 2009).

Most of these analyses recover a linear (in log–log space) relation with slope of unity, or slightly less than 1, between the $8\ \mu\text{m}$ emission and the reference SFR indicator. A roughly linear trend with unity slope would in general indicate that the $8\ \mu\text{m}$ luminosity is an excellent SFR tracer; however, as we will see in the next two sections, the PAH emission (and, therefore, the $8\ \mu\text{m}$ emission, of which the PAH emission represents typically more than half of the total) shows a strong dependence on the metal content of the region or galaxy, and a less strong, but possibly significant, dependence on the nature of the heating stellar population.

3 The dependence of PAHs on metallicity

Already known for more than a decade (*e.g.*, Madden 2000, and references therein), the dependence of the intensity of the PAH emission on the galaxy/environment metallicity has been quantified in detail by Spitzer data (*e.g.*, Fig. 1). This dependency is *on top* of the general decrease of the TIR intensity for decreasing metallicity, *i.e.* the decrease in overall dust content. Analyses of galaxy samples and of galaxy radial profiles covering a range of metallicity show an additional order-of-magnitude decrease in the $8\ \mu\text{m}$ -to-TIR luminosity for a factor ~ 10 decrease in metallicity, with a transition at $12+\log(\text{O}/\text{H})\approx 8.1$ (Boselli *et al.* 2004; Madden *et al.* 2006; Engelbracht *et al.* 2005; Hogg *et al.* 2005; Galliano *et al.* 2005, 2008; Rosenberg *et al.* 2006; Wu *et al.* 2006; Draine *et al.* 2007; Engelbracht *et al.* 2008; Gordon *et al.* 2008; Muñoz-Mateos *et al.* 2009; Marble *et al.* 2010).

MIR spectroscopy with Spitzer has established that the observed low abundance of PAHs in low metallicity systems is *not* due to the molecules being more highly ionized and/or dehydrogenated than in higher metallicity galaxies (Smith *et al.* 2007), although there is controversy on whether they could be characterized by smaller or larger sizes (Hunt *et al.* 2010; Sandstrom *et al.* 2010; see, also,

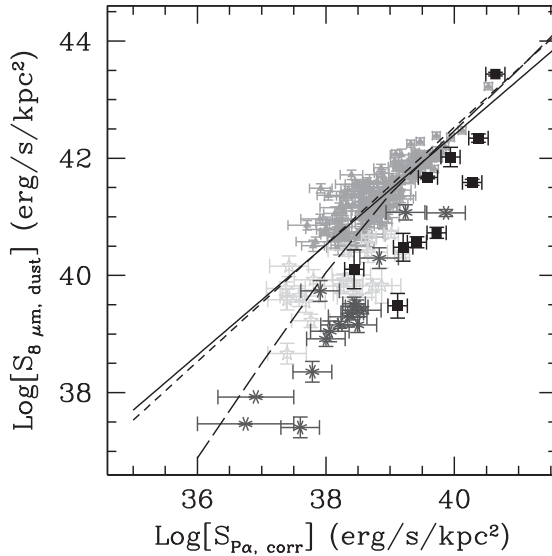


Fig. 1. The surface luminosity density at $8\ \mu\text{m}$ (stellar-continuum subtracted) as a function of the surface luminosity density of the extinction-corrected hydrogen recombination emission line $P\alpha$ ($1.8756\ \mu\text{m}$), for HII knots (red, green, and blue symbols) and low-metallicity starburst galaxies (black symbols). The HII-knots are typically $\approx 0.5\ \text{kpc}$ -size line-emitting regions from 33 nearby galaxies; there are a total of 220 regions in the plot. The starburst galaxies are from the sample of Engelbracht *et al.* (2005). The red symbols show regions hosted in galaxies with oxygen abundance $12+\log(\text{O}/\text{H}) > 8.35$. Regions of lower metal abundance are divided between those with oxygen abundance $8.00 < 12+\log(\text{O}/\text{H}) \leq 8.35$ (green symbols) and those with $12+\log(\text{O}/\text{H}) \leq 8.00$ (blue symbols). The continuous line shows the best linear fit (in the log-log plane) through the high metallicity data points (red symbols). The dash line shows the best linear fit with unity slope. A common result is for the best fit to yield a slope lower than unity. The dot-dash curve shows the locus of a model for which regions/galaxies suffer from decreasing dust attenuation (and, consequently, decreasing dust emission) as their total luminosity decreases, a commonly observed trend in galaxies and star-forming regions (see references in the last paragraph of the Introduction). Even when taking this effect into account, low metallicity regions and starburst galaxies display a depressed $8\ \mu\text{m}$ emission, which has been shown to be due to deficiency of PAH emission. From Calzetti *et al.* (2007).

Hunt *et al.* elsewhere in this volume and Sandstrom *et al.* elsewhere in this volume).

The nature of the correlation between the strength of the PAH emission features and the region's metallicity is still ground for debate. The two main scenarios

that can account for the observed trend are: the “nature” scenario, according to which lower metallicity systems have a delayed PAH formation, and the “nurture” scenario, according to which PAHs are processed and/or destroyed in the harder radiation fields of low metallicity galaxies.

Galliano *et al.* (2008, see, also, Galliano elsewhere in this volume) suggest that the PAH strength–metallicity correlation may be due to the delayed formation of the PAHs themselves, which are thought to form in the envelopes of carbon–rich AGB stars. In a young system, the first dust will emerge from supernovae (timescale < 10 Myr), while AGB–produced dust will emerge at a later stage (timescale ≈ 1 Gyr). This scenario may be difficult to reconcile with the fact that low–metallicity systems in the local Universe contain stellar populations that are typically older than 2 Gyr (Tosi 2009 and references therein), and have median birth parameters that are not drastically different from those of more metal rich galaxies (Lee *et al.* 2007). However, low–mass systems are also thought to lose most of their metals during the sporadic events of star formation that characterize their typical star formation history (*e.g.*, Romano *et al.* 2006). Clearly, self–consistent models for the metal enrichment of dwarf, low–metallicity galaxies that also include their extended star formation histories are needed in order to accept or refute the “nature” scenario.

Alternately, processing of PAHs by hard radiation fields has been proposed as a mechanism for the observed correlation between PAH luminosity and metallicity (Madden *et al.* 2006; Wu *et al.* 2006; Bendo *et al.* 2006; Smith *et al.* 2007; Gordon *et al.* 2008; Engelbracht *et al.* 2008), since low–metallicity environments are generally characterized by harder radiation fields than high–metallicity ones (*e.g.* Hunt *et al.* 2010). Additionally, efficient destruction of PAHs by supernova shocks may also contribute to the observed deficiency (O’Halloran *et al.* 2006). These suggestions agree with the observation that PAHs are present in the PDRs surrounding HII regions, but are absent (likely destroyed) within the HII regions (Cesarsky *et al.* 1996; Helou *et al.* 2004; Bendo *et al.* 2006; Relaño & Kennicutt 2009). A recent study of the SMC finds a high fraction of PAHs within molecular clouds (Sandstrom *et al.* 2010), thus complicating the interpretation of the formation/destruction mechanisms for these molecules. Both production and processing may ultimately be driving the observed trend (Wu *et al.* 2006; Engelbracht *et al.* 2008; Marble *et al.* 2010).

4 The heating populations of PAHs

Outside of HII regions and other strongly ionizing environments, PAHs tend to be ubiquitous. These large molecules are transiently heated by single UV and optical photons, and, therefore, they can be heated by the radiation from the mix of stellar populations that contribute to the general interstellar radiation field, unrelated to the current star formation in a galaxy (Haas *et al.* 2002; Boselli *et al.* 2004; Peeters *et al.* 2004; Mattioda *et al.* 2005; Calzetti *et al.* 2007; Draine & Li 2007; Bendo *et al.* 2008).

Bendo *et al.* (2008) show that the $8\ \mu\text{m}$ emission from galaxies is better correlated with the $160\ \mu\text{m}$ dust emission than with the $24\ \mu\text{m}$ emission, on spatial scales $\approx 2\ \text{kpc}$. Haas Klaas & Bianchi (2002) also find that the ISO $7.7\ \mu\text{m}$ emission is correlated with the $850\ \mu\text{m}$ emission from galaxies. Boselli *et al.* (2004) show that the stellar populations responsible for the heating of the MIR-emitting dust are more similar to those responsible for heating the large grains emitting in the far-infrared, rather than to those responsible for the ionized gas emission in galaxies. This result is similar to that obtained by Peeters *et al.* (2004) for a combined Galactic and extragalactic sample of PAH-emitting sources. All the evidence points to a close relation between the MIR/PAH emission and the cold dust heated by the general (non-star-forming) stellar population.

The presence of heating by evolved stellar populations thus produces a ill-quantified contribution to the total MIR luminosity of a galaxy, affecting the calibration of any SFR indicator using that wavelength range (*e.g.*, Alonso-Herrero *et al.* 2006). We still do not have a clear understanding of dependencies on galaxy morphology, stellar population mix, star formation rate, star formation intensity, etc.

A recent analysis of the nearby galaxy NGC 0628, an almost face-on SAc at a distance of about $7.3\ \text{Mpc}$, shows that its $8\ \mu\text{m}$ emission contains about 20%–30% contribution from a diffuse component unrelated to sites of current star formation (Crocker *et al.* 2010). The 20%–30% range reflects uncertainties in the adopted extinction and [NII] contamination corrections for the $\text{H}\alpha$ emission, used here to trace sites of recent star formation. We can also obtain a rough idea of the amount of diffuse emission in the MIR bands by converting the $8\ \mu\text{m}$ mean luminosity density, $\sim 1.2 \times 10^7\ L_{\odot}\ \text{Mpc}^{-3}$, within the local $10\ \text{Mpc}$ (including emission from both PAHs and dust continuum, see Marble *et al.* 2010) to a volume SFR density, using metallicity-dependent linear calibrations to $\text{SFR}(8\ \mu\text{m})$ from the data of Calzetti *et al.* (2007). The result, $\rho_{\text{SFR}}(8\ \mu\text{m}) \sim 0.019\ M_{\odot}\ \text{yr}^{-1}\ \text{Mpc}^{-3}$, is roughly 30%–60% higher than the commonly accepted values for the SFR density in the local Volume (see references in Hopkins & Beacom 2006).

While the above suggests that the contribution to the $8\ \mu\text{m}$ emission from dust heated by the diffuse stellar populations is not large (less than a factor ≈ 1.5 –2), when galaxies are considered as a whole or as *populations*, we should recall that we don't have a handle on galaxy-to-galaxy variations. Even worse, the diffuse population heating could become a prevalent contribution to the $8\ \mu\text{m}$ emission in some galactic regions, thus potentially affecting any investigation of spatially resolved features within galaxies.

5 Summary and conclusions

Over the past decade, the accumulation of both spectroscopy and high-angular-resolution imaging of the MIR emission from galaxies has paved the road for an accurate investigation of the MIR/PAH luminosity as a SFR tracer. Data have shown that there is generally a linear (with slope of 1 or slightly less than 1 in a log–log plane) correlation between the stellar-continuum-subtracted MIR luminosity

and the SFR, for *high metallicity* systems, *i.e.*, for galaxies and regions that are about 1/5–1/3 solar or higher in oxygen abundance. While a linear correlation would generally indicate that the MIR emission can be considered a reliable SFR indicator, there are at least two caveats to keep in mind: (1) the PAH emission has a strong dependence on metallicity; (2) the MIR-emitting dust can be heated by evolved stellar populations unrelated to the current star formation.

The PAH dependence on metallicity is well established and quantified, and shows an order-of-magnitude deficiency in PAH/TIR emission for a decrease in oxygen abundance by about a factor 10. The nature of this dependency is still debated, and could be due to delayed production of the PAHs in low metallicity systems or to processing/destruction mechanisms in the harder radiation fields of low metallicity galaxies, or a combination of both.

The heating of PAHs by evolved stellar populations is also well established, but less well quantified. It is likely to have a smaller impact on any SFR(PAH) or SFR(MIR) calibration than the metallicity dependence, probably at the level of less than a factor 2. However, potential variations as a function of galaxy morphology, stellar population mix, star formation rate, star formation intensity, etc., and the impact of the diffuse population heating as a function of location for sub-galactic scale analyses have not been quantified yet. This is a virtually unexplored realm with a possibility for major implications as many investigations move from the “global populations” approach to the “sub-kpc regions” approach in the study of star formation in galaxies.

References

- Alonso-Herrero, A., Colina, L., Packam, C., *et al.*, 2006, ApJ, 652, L83
 Aplund, M., Grevesse, N., Sauval, A.J., & Scott, P., 2009, ARA&A, 47, 481
 Bendo, G.J., Dale, D.A., Draine, B.T., *et al.*, 2006, ApJ, 652, 283
 Bendo, G.J., Draine, B.T., Engelbracht, C.W., *et al.*, 2008, MNRAS, 389, 629
 Boselli, A., Lequeux, J., & Gavazzi, G., 2004, A&A, 428, 409
 Calzetti, D., 2001, PASP, 113, 1449
 Calzetti, D., Kennicutt, R.C., Bianchi, L., *et al.*, 2005, ApJ, 633, 871
 Calzetti, D., Kennicutt, R.C., Engelbracht, C.W., *et al.*, 2007, ApJ, 666, 870
 Cesarsky, D., Lequeux, J., Abergel, A., *et al.*, 1996, A&A, 315, L309
 Crocker, A.F., Calzetti, D., *et al.*, 2010, in preparation
 Daddi, E., Dickinson, M., Chary, R., *et al.*, 2005, ApJ, 631, L13
 Daddi, E., Dickinson, M., Morrison, G., *et al.*, 2007, ApJ, 670, 156
 Dale, D.A., Smith, J.T.D., Schlawin, E.A., *et al.*, 2009, ApJ, 693, 1821
 Dole, H., Lagache, G., Puget, J.-L., *et al.*, 2006, A&A, 451, 417
 Draine, B.T., & Li, A., 2007, ApJ, 657, 810
 Draine, B.T., Dale, D.A., Bendo, G., *et al.*, 2007, ApJ, 633, 866
 Engelbracht, C.W., Gordon, K.D., Rieke, G.H., *et al.*, 2005, ApJ, 628, 29
 Engelbracht, C.W., Rieke, G.H., Gordon, K.D., *et al.*, 2008, ApJ, 685, 678
 Fazio, G.G., Hora, J.L., Allen, L.E., *et al.*, 2004, ApJS, 154, 10

- Förster Schreiber, N.M., Roussel, H., Sauvage, M., & Charmandaris, V., 2004, *A&A*, 419, 501
- Galliano, F., Madden, S.C., Jones, A.P., Wilson, C.D., & Bernard, J.-P., 2005, *A&A*, 434, 867
- Galliano, F., Dwek, E., & Chaniel, P., 2008, *ApJ*, 672, 214
- Gordon, K.D., Engelbracht, C.W., Rieke, G.H., *et al.*, 2008, *ApJ*, 682, 336
- Haas, M., Klaas, U., & Bianchi, S., 2002, *A&A*, 385, L23
- Hausser, M.G., & Dwek, E., 2001, *ARA&A*, 39, 249
- Heckman, T.M., Robert, C., Leitherer, C., Garnett, D.R., & van der Rydt, F., 1998, *ApJ*, 503, 646
- Helou, G., Roussel, H., Appleton, P., *et al.*, 2004, *ApJS*, 154, 253
- Hogg, D.W., Tremonti, C.A., Blanton, M.R., *et al.*, 2005, *ApJ*, 624, 162
- Hopkins, A.M., & Beacom, J.F., 2006, *ApJ*, 651, 142
- Houck, J.R., Roellig, T.L., van Cleve, J., *et al.*, 2004, *ApJS*, 154, 18
- Hunt, L.K., Thuan, T.X., Izotov, Y.I., & Sauvage, M., 2010, *ApJ*, 712, 164
- Kennicutt, R.C., Hao, C.-N., Calzetti, D., *et al.*, 2009, *ApJ*, 703, 1672
- Kessler, M.F., Steinz, J.A., Anderegg, M.E., *et al.*, 1996, *A&A*, 315, L27
- Lawton, B., Gordon, K.D., Babler, B., *et al.*, 2010, *ApJ*, 716, 453
- Lee, Janice, C., Kennicutt, R.C., Funes, J.G., Sakai, S., & Akiyama, S., 2007, *ApJ*, 671, L113
- Léger, A., & Puget, J.L., 1984, *A&A*, 137, L5
- Madden, S.C., 2000, in *Massive Stellar Clusters*, ed. A Lançon, & C. Boily, *ASP Conf. Ser.*, 211, 297
- Madden, S.C., Galliano, F., Jones, A.P., & Sauvage, M., 2006, *A&A*, 446, 877
- Marble, A.R., Engelbracht, C.W., van Zee, L., *et al.*, 2010, *ApJ*, 715, 506
- Mattioda, A.L., Allamandola, L.J., & Hudgins, D.M., 2005, *ApJ*, 629, 1183
- Muñoz-Mateos, J.C., Gil de Paz, A., Boissier, S., *et al.*, 2009, *ApJ*, 701, 1965
- O'Halloran, B., Satyapal, S., & Dudik, R.P., 2006, *ApJ*, 641, 795
- Papovich, C., Moustakas, L.A., Dickinson, M., *et al.*, 2006, *ApJ*, 640, 92
- Papovich, C., Rudnick, G., Le Floc'h, E., *et al.*, 2007, *ApJ*, 668, 45
- Peeters, E., Spoon, H.W.W., & Tielens, A.G.G.M., 2004, *ApJ*, 613, 986
- Puget, J.L., Léger, A., & Boulanger, F., 1985, *A&A*, 142, L19
- Reddy, N.A., Erb, D.K., Pettini, M., Steidel, C.C., & Shapley, A.E., 2010, *ApJ*, 712, 1070
- Relaño, M., & Kennicutt, R.C., 2009, *ApJ*, 699, 1125
- Rieke, G.H., Young, E.T., Engelbracht, C.W., *et al.*, 2004, *ApJS*, 154, 25
- Romano, D., Tosi, M., & Matteucci, F., 2006, *MNRAS*, 365, 759
- Rosenberg, J.L., Ashby, M.L.N., Salzer, J.J., & Huang, J.-S., 2006, *ApJ*, 636, 742
- Roussel, H., Sauvage, M., Vigroux, L., & Bosma, A., 2001, *A&A*, 372, 427
- Salim, S., Dickinson, M., Rich, R.M., *et al.*, 2009, *ApJ*, 700, 161
- Sandstrom, K.M., Bolatto, A.D., Draine, B.T., Bot, C., & Staminirović, S., 2010, *ApJ*, 715, 701
- Sellgren, K., Werner, M.W., & Dinerstein, H.L., 1983, *ApJ*, 271, L13

- Sellgren, K., 1984, *ApJ*, 277, 623
- Smith, J.D.T., Draine, B.T., Dale, D.A., *et al.*, 2007, *ApJ*, 656, 770
- Sullivan, M., Mobasher, B., Chan, B., *et al.*, 2001, *ApJ*, 558, 72
- Tosi, M., 2009, *A&A*, 500, 157
- Wang, B., & Heckman, T.M., 1996, *ApJ*, 457, 645
- Werner, M.W., Roellig, T.L., Low, F.J., *et al.*, 2004, *ApJS*, 154, 1
- Wu, H., Cao, C., Hao, C.-N., *et al.*, 2005, *ApJ*, 632, L79
- Wu, Y., Charmandaris, V., Hao, L., *et al.*, 2006, *ApJ*, 639, 157
- Yan, L., Sajina, A., Fadda, D., *et al.*, 2007, *ApJ*, 658, 778
- Zhu, Y.-N., Wu, H., Cao, C., & Li, H.-N., 2008, *ApJ*, 686, 155

PAHS AND THE ISM IN METAL-POOR STARBURSTS

L.K. Hunt¹, Y.I. Izotov², M. Sauvage³ and T.X. Thuan⁴

Abstract. We characterize PAH populations in 22 metal-poor blue compact dwarf galaxies (BCDs), 16 of which have an oxygen abundance $12+\log(\text{O}/\text{H}) \lesssim 8$. This is the largest sample ever studied at such low metallicities. The relative PAH intensities of the 6.2, 7.7, 8.6 and $11.3 \mu\text{m}$ features in these BCDs suggest a deficit of small PAH carriers, or alternatively, an excess of large ones at these low abundances.

1 Introduction

PAH emission dominates the mid-infrared spectra of star-forming galaxies (Brandl *et al.* 2006; Smith *et al.* 2007), and contributes importantly to their IR energy budget. In most star-forming galaxies, PAH emission has a surprisingly narrow range of properties, well characterized by a “standard set” of features (Smith *et al.* 2007). However, first *ISO* and later *Spitzer* have shown that metal-poor star-forming galaxies are deficient in PAH emission (Madden *et al.* 2006; Wu *et al.* 2006; Engelbracht *et al.* 2008), similar to the observed deficit in CO emission (*e.g.*, Taylor *et al.* 1998). Neither PAH nor CO emission is generally detected below $12+\log(\text{O}/\text{H}) \sim 8$, consistent with the idea that PAHs and CO form in similar conditions within molecular clouds (Sandstrom *et al.* 2010, see Sandstrom *et al.* elsewhere in this volume).

Although it has generally been concluded that the reason for this PAH deficiency is low metallicity, it is not yet clear whether it is the metallicity directly, or rather the indirect effects of a low metallicity environment. Previous work with *ISO* (*e.g.*, Galliano *et al.* 2005; Madden *et al.* 2006) examined this question, but the metallicity of the galaxies studied by *ISO* did not go below $12+\log(\text{O}/\text{H}) \sim 8.2$, making it difficult to probe the physical conditions where PAH emission is effectively suppressed. *Spitzer*/IRS added more observations of

¹ INAF-Osservatorio di Arcetri, Firenze, Italy

² Main Astronomical Observatory, Kiev, Ukraine

³ CEA, Saclay, France

⁴ University of Virginia, Charlottesville, USA

the PAHs in low-metallicity dwarf galaxies, but up to now only five objects with $12+\log(\text{O}/\text{H}) \lesssim 8$ (Wu *et al.* 2006) were available for study.

Here, we present observations of PAH features in a new sample of 22 metal-poor blue compact dwarf galaxies (BCDs), 16 of which have $12+\log(\text{O}/\text{H}) \lesssim 8$; this more than triples the number of such dwarfs with PAH spectra. We examine in detail the PAH emission in our sample, and show for the first time that some PAHs can survive even in extremely metal-poor environments.

2 Observations and analysis

In the context of our GO *Spitzer* program (PID 3139), we obtained IRS spectra in the low- and high-resolution modules (SL, SH, LH: Houck *et al.* 2004). The sample definition and data reduction are described in detail by Hunt *et al.* (2010). In order to directly compare the results for our low-metallicity sample with those of more metal-rich galaxies, we analyzed our IRS spectra with PAHFIT (Smith *et al.* 2007), an IDL procedure which was developed for and applied to the Spitzer Nearby Galaxy Survey (SINGS: Kennicutt *et al.* 2003). PAHFIT is particularly suited for separating emission lines and PAH features (*e.g.*, the PAH blend at $12.6\text{--}12.7\mu\text{m}$ and the $[\text{Ne II}]$ line at $12.8\mu\text{m}$), as well as measuring faint PAH features superimposed on a strong continuum. PAHFIT overcomes this problem by fitting simultaneously the spectral features, the underlying continuum, and the extinction. Drude profiles are fitted to the PAH features, and Gaussian profiles to the molecular hydrogen and fine-structure lines.

3 Results

The $7.7\mu\text{m}$ blend is the most common PAH feature in our sample, detected in 15 of 22 objects. The $7.7\mu\text{m}$ feature is also the strongest one, comprising roughly 49% of the total PAH power. The remaining PAHs are significantly weaker, and less frequently detected: 13 BCDs show the $11.2\text{--}11.3\mu\text{m}$ PAH, 9 the $8.6\mu\text{m}$ feature, and 7 the $6.2\mu\text{m}$ PAH. No $17\mu\text{m}$ PAH features were detected. The 6.2 , 7.7 , 8.6 , 11.3 , and $12.6\mu\text{m}$ features by themselves constitute $\sim 72\%$ of total PAH power in BCDs; the SINGS sample has about $\sim 85\%$ of total PAH power in these bands (Smith *et al.* 2007). The remainder of the emission is in the weaker features.

3.1 Fractional power of strongest features

The fractional power of the four strongest features relative to the total PAH luminosity is illustrated in Figure 1. The horizontal lines in each panel correspond to the SINGS medians (dashed) and the BCD means (dotted). The BCD means are calculated taking into account all galaxies with $7.7\mu\text{m}$ detections; thus they are a sort of weighted average which considers frequency of detection together with intensity. This is why the mean for the $6.2\mu\text{m}$ PAH lies below most of the BCD data points: that feature was detected only in 7 galaxies, while the other features in Figure 1 were detected with a frequency more similar to the $7.7\mu\text{m}$ PAH. The relative PAH strengths for the BCD and SINGS 6.2 and $7.7\mu\text{m}$ features are virtually indistinguishable: 0.10 *vs.* 0.11 for $6.2\mu\text{m}$, and 0.49 *vs.* 0.42 for $7.7\mu\text{m}$ (Smith *et al.* 2007). However, for the longer wavelength PAHs at 8.6

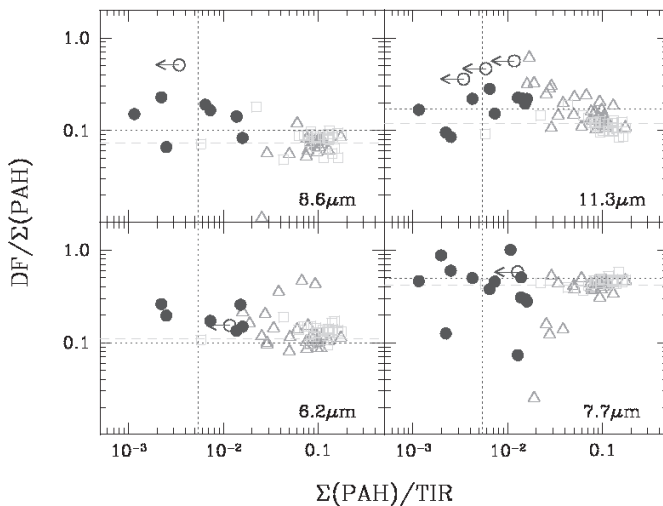


Fig. 1. PAH strengths relative to total PAH luminosity *vs.* total PAH power normalized to total IR luminosity (TIR). The four panels show the the following dust features (DF): top 8.6 μm , 11.3 μm , and 6.2 μm , 7.7 μm features. BCDs are plotted as filled (blue) circles; open (green) squares correspond to SINGS HII nuclei; and open (red) triangles to SINGS AGN (Smith *et al.* 2007). The horizontal dashed lines give the SINGS sample medians (Smith *et al.* 2007), and the dotted ones the means for the BCD sample, taking into account all objects with 7.7 μm detections. The vertical dotted line corresponds to the BCD mean PAH power normalized to TIR.

and 11.3 μm , the BCD fractions are $\gtrsim 40\%$ larger: 0.10 *vs.* 0.07 (8.6) and 0.17 *vs.* 0.12 (11.3). Although with considerable scatter, the BCD mean PAH relative fractions for these features tend to exceed even the 10 to 90th percentile spreads of the SINGS galaxies.

3.2 Profile widths and central wavelengths

Figure 2 shows the mean Drude profile widths and central wavelengths of six aromatic features detected at $\gtrsim 3\sigma$ in our sample; the numbers of BCDs with each feature are given in parentheses. The analogous quantities for the SINGS galaxies are also plotted. In no case, were the PAHFIT profiles fixed to the SINGS galaxy parameters able to fit the BCD data; every BCD was better fitted by allowing the Drude profile widths (FWHMs) and central wavelengths to vary. In some cases, the differences between the χ^2_ν with the SINGS “standard” profile parameters and the best-fit parameters were small, $\lesssim 15\%$; but in others, the improvement of χ^2_ν was almost a factor of 2. The only *systematic* difference between the two samples is the narrower profile width for the 8.6 μm feature; only the very broadest BCD profiles are as broad as those in more metal-rich systems.

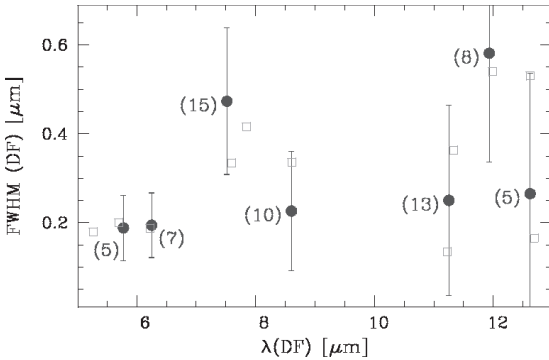


Fig. 2. Median Drude profile widths (FWHM) and central wavelengths for seven aromatic features detected ($\gtrsim 3\sigma$) in our sample. The error bars are the standard deviations of the measurements, and the numbers in parentheses are the BCDs with significant detections. Open squares correspond to SINGS sample means (Smith *et al.* 2007).

3.3 Lack of small PAHs at low metallicity?

The larger relative intensities of the 8.6 and 11.3 μm feature in BCDs and the narrow profile width of the 8.6 μm PAH could be due to a different size distribution of PAH populations at low metal abundances. Bauschlicher *et al.* (2008) find that the 8.6 μm band arises from large PAHs, with $N_{\text{min}} \gtrsim 100$ carbon atoms. Hence, they suggest that the relative intensity of the 8.6 μm band can be taken as an indicator of the relative amounts of large and small PAHs in a given population. The large 8.6 μm intensity relative to total PAH power in BCDs could be a signature of fewer small PAHs (or more larger ones) at low metallicity. The relative lack of small PAHs could also explain the low detection rate of the 6.2 μm feature, since most of its intensity comes from PAHs with less than 100 C atoms (Schutte *et al.* 1993; Hudgins *et al.* 2005). The size of a PAH molecule grows with increasing numbers of carbon atoms (Draine & Li 2007). For a given maximum number of carbon atoms N_{max} , a larger minimum number N_{min} theoretically gives narrower profiles (Joblin *et al.* 1995; Verstraete *et al.* 2001). Although fitting intrinsically asymmetric PAH profiles by symmetric Drude profiles in PAHFIT is a simplification, the narrower width of the 8.6 μm feature could be a signature of relatively larger PAHs at low metallicity. The difference disappears at 7.6 μm and is less pronounced at longer wavelengths than 8.6 μm because both small and large PAH sizes contribute to these bands¹ (Schutte *et al.* 1993; Bauschlicher *et al.* 2009).

Another indication that low-metallicity BCDs may be lacking the smallest size PAHs comes from a correlation analysis. In a detailed study of Galactic HII regions, young stellar objects, reflection and planetary nebulae (RNe, PNe), and evolved stars, Hony *et al.* (2001) found only a few correlations among PAH features. One of these is between 6.2 and the 12.7 μm emission, which is shown for our sample of BCDs in Figure 3; only galaxies with $\gtrsim 3\sigma$ detections in at least two features are plotted. Most galaxies with 6.2 μm PAH detections and $12+\log(\text{O}/\text{H}) \geq 8.1$ (filled circles) are similar to the HII regions studied by Hony *et al.* (2001). On the other

¹The 7.8 μm band may be dominated by larger PAHs only (Bauschlicher *et al.* 2009); but this band is present in only two of the BCDs in our sample, Haro 3 and II Zw 70.

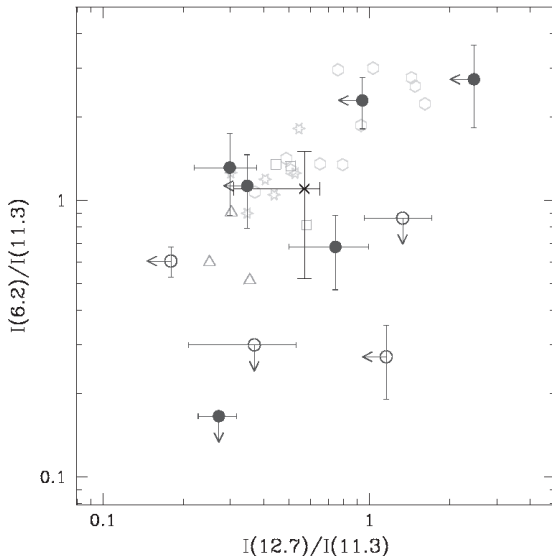


Fig. 3. The integrated flux in the PAH features at $6.2\ \mu\text{m}$, $11.3\ \mu\text{m}$, and $12.7\ \mu\text{m}$, plotted in two sets of ratios: $6.2/11.3$ vs. $12.7/11.3$. Only those BCDs with at least one ratio with $11.3\ \mu\text{m}$ are shown: filled (blue) circles correspond to those BCDs with $12+\log(\text{O}/\text{H})\geq 8.1$; open ones to those objects with lower metallicities. The other data are taken from Hony *et al.* (2001) and correspond to PNe, RNe, intermediate-mass star-forming regions and HII regions. The SINGS average is shown as a \times , with error bars reporting standard deviations over the sample (Smith *et al.* 2007).

hand, BCDs with lower O/H occupy a region of the plot with small $6.2/11.3$ ratios. Although the statistics are poor, small $6.2/11.3$ ratios are found for most of the lowest-metallicity BCDs. Because the $11.3\ \mu\text{m}$ feature arises from non-adjacent or “solo” CH groups, dominant $11.3\ \mu\text{m}$ emission, like $8.6\ \mu\text{m}$ emission, implies large PAH species, with $\gtrsim 100$ – 200 carbon atoms and long straight edges (Hony *et al.* 2001; Bauschlicher *et al.* 2008; Bauschlicher *et al.* 2009). Moreover, fewer small PAHs reduce the intensity of the $6.2\ \mu\text{m}$ emission, as the bulk of this feature comes from PAHs containing less than 100 C atoms (Schutte *et al.* 1993; Hudgins *et al.* 2005). Therefore, small $6.2/11.3\ \mu\text{m}$ band ratios at low metallicities could imply an overall deficit of small PAHs.

A third indication that there is a deficit of small PAHs in a metal-poor ISM is the intensity of the $8.6\ \mu\text{m}$ feature relative to the $7.7\ \mu\text{m}$ blend. As mentioned above, Bauschlicher *et al.* (2008) find that $8.6\ \mu\text{m}$ band arises from large PAHs, with $N_{\text{min}} \gtrsim 100$ carbon atoms. On the other hand, the $7.7\ \mu\text{m}$ feature contains emission from both small and large PAH sizes (Schutte *et al.* 1993; van Dienenhoven *et al.* 2004). For the 9 BCDs with the 7.7 and $8.6\ \mu\text{m}$ PAH features detected at $\gtrsim 3\sigma$, the mean $8.6/7.7$ flux ratio is 0.48 , and the median is 0.33 . This ratio is at least double that in the more metal-rich SINGS galaxies, with $8.6/7.7 \sim 0.18$ in the mean, and a range of 0.11 – 0.21 (Smith *et al.* 2007); 7 of 9 BCDs are outside the upper 90th percentile limit of 0.21 . Again, although the number statistics are small, the large $8.6/7.7\ \mu\text{m}$ flux ratios of the PAHs in these low-metallicity BCDs appear to be dominated by the largest PAH species.

4 Conclusions

In summary, there are three different lines of evidence which tentatively suggest that the PAH populations in low-metallicity BCDs are deficient in the smallest sizes ($N_{\min} \lesssim 50$ C atoms). The IRS spectra show flux ratios typical of the largest PAHs modeled so far, with $N_{\min} \gtrsim 100$ C atoms. Correlations within our sample suggest that the main trend is with radiation field intensity and hardness, rather than with metallicity. Apparently, the ISM environment in the BCD HII regions is too harsh for the smallest PAHs, possibly destroying them through sputtering. Perhaps only the PAH population with the largest species can survive the extreme physical conditions in the low-metallicity HII regions in the BCDs.

We would like to thank the organizers for a very stimulating and well-organized conference.

References

- Bauschlicher, C.W., Jr., Peeters, E., & Allamandola, L.J., 2008, ApJ, 678, 316
 Bauschlicher, C.W., Peeters, E., & Allamandola, L.J., 2009, ApJ, 697, 311
 Brandl, B. R., *et al.*, 2006, ApJ, 653, 1129
 Draine, B. T., & Li, A., 2007, ApJ, 657, 810
 Engelbracht, C.W., Rieke, G.H., Gordon, K.D., *et al.*, 2008, ApJ, 678, 804
 Galliano, F., Madden, S.C., Jones, A.P., Wilson, C.D., & Bernard, J.-P., 2005, A&A, 434, 867
 Hony, S., Van Kerckhoven, C., Peeters, E., *et al.*, 2001, A&A, 370, 1030
 Houck, J.R., *et al.*, 2004a, ApJS, 154, 18
 Hudgins, D.M., Bauschlicher, C.W., Jr., & Allamandola, L.J., 2005, ApJ, 632, 316
 Hunt, L.K., Thuan, T.X., Izotov, Y.I., & Sauvage, M., 2010, ApJ, 712, 164
 Joblin, C., Boissel, P., Leger, A., D'Hendecourt, L., & Defourneau, D., 1995, A&A, 299, 835
 Kennicutt, R.C., Jr., *et al.*, 2003, PASP, 115, 928
 Madden, S.C., Galliano, F., Jones, A.P., & Sauvage, M., 2006, A&A, 446, 877
 Peeters, E., Hony, S., Van Kerckhoven, C., *et al.*, 2002, A&A, 390, 1089
 Peeters, E., Spoon, H.W.W., & Tielens, A.G.G.M., 2004a, ApJ, 613, 986
 Sandstrom, K.M., Bolatto, A.D., Draine, B.T., Bot, C., & Stanimirović, S., 2010, ApJ, 715, 701
 Schutte, W.A., Tielens, A.G.G.M., & Allamandola, L.J., 1993, ApJ, 415, 397
 Smith, J.D.T., *et al.*, 2007, ApJ, 656, 770
 Taylor, C.L., Kobulnicky, H.A., & Skillman, E.D., 1998, AJ, 116, 2746
 van Diedenoven, B., Peeters, E., Van Kerckhoven, C., *et al.*, 2004, ApJ, 611, 928
 Verstraete, L., *et al.*, 2001, A&A, 372, 981
 Wu, Y., Charmandaris, V., Hao, L., *et al.* 2006, ApJ, 639, 157

INTRODUCTION TO AMUSES: AKARI SURVEY WITH A WINDOW OF OPPORTUNITY

J.H. Kim¹, M. Im¹, H.M. Lee², M.G. Lee² and the AMUSES team

Abstract. With advancement of infrared space telescopes during the past decade, infrared wavelength regime has been a focal point to study various properties of galaxies with respect to evolution of galaxies. Polycyclic Aromatic Hydrocarbons (PAHs) have emerged as one of the most important features since these features dominate the mid-infrared spectra of galaxies. These PAH features provide a great handle to calibrate star formation rates and diagnose ionized states of grains. However, the PAH 3.3 μm feature has not been studied as much as other PAH features since it is weaker than others and resides outside of Spitzer capability, although it will be the only PAH feature accessible by JWST for high- z galaxies. AKARI mJy Unbiased Survey of Extragalactic Sources in 5MUSES (AMUSES) intends to take advantage of AKARI capability of spectroscopy in the $2 \sim 5 \mu\text{m}$ to provide an unbiased library of 44 sample galaxies selected from a parent sample of 5MUSES, one of Spitzer legacy projects. For these 3.6 μm flux limited sample galaxies whose redshifts range between $0 < z < 1$, AMUSES will calibrate PAH 3.3 μm as a star formation rate (SFR) indicator while measuring ratios between PAH features. We present preliminary results of AMUSES.

1 Introduction

Infrared (IR) astronomy has progressed tremendously over the past decades thanks to various space missions, such as the Infra-Red Astronomical Satellite (IRAS) (Soifer *et al.* 1987), the Infrared Space Observatory (ISO) (Kessler *et al.* 1996; Genzel & Cesarsky 2000), and the Spitzer space telescope (Werner *et al.* 2004). While providing clues to numerous astrophysical subjects, these space-based observatories also improve extragalactic astronomy since these IR wavelengths carry

¹ CEOU, Department of Physics and Astronomy, Seoul National University

² Department of Physics and Astronomy, Seoul National University

a vast information on galaxies. For example, the shortest IR wavelengths (up to $10\ \mu\text{m}$) represent the photospheric light and are good stellar mass indicators (Regan & The Sings Team 2004). Then, dust grains at different temperatures are represented by different ranges of IR wavelengths (Genzel & Cesarsky 2000). IR wavelengths also carry numerous lines from hydrogen molecule and gas-phase species. However, the most important aspect of IR astronomy on galaxies is probably that IR emission represents dust-obscured star formation activity of galaxies (Genzel & Cesarsky 2000). While other shorter wavelength star formation rate (SFR) proxies, such as hydrogen recombination lines and ultraviolet (UV) emissions rely on the measurement of photoionizing UV photons from heavy stars and, thus, suffer from extinction, the bolometric IR luminosity measures dust-obscured star formation within galaxies and is less affected by extinction. However using the bolometric IR luminosity as a SF indicator has two caveats. First, not only newly formed heavy stars, but also evolved stellar populations can heat dust components within galaxies (*cf.* Calzetti elsewhere in this volume). Then it is extremely tricky to understand the whole range of IR spectral energy distribution (SED) for high- z galaxies.

Therefore, many studies have attempted calibrate reliable IR SF proxies to bolometric IR luminosities in recent years. Among these IR SFR proxies, polycyclic aromatic hydrocarbons (PAHs) have gotten enormous attention due to their ubiquity and strong potential as diagnostics of other properties. On the basis of the aromatic IR band emission, PAHs are considered to be present in a wide range of objects and environments, such as post-AGB stars, planetary nebulae, HII regions, reflection nebulae and the diffuse interstellar medium (Puget *et al.* 1985; Allamandola *et al.* 1989). The PAH mid-IR features are believed to contribute up to 10% of the total IR luminosity of star forming galaxies (Helou *et al.* 2001; Peeters *et al.* 2002; Smith *et al.* 2007).

Numerous recent studies measure PAH band fluxes and equivalent widths (EWs) in order to calibrate these emission features as SFR proxies within the Galactic environments and galaxies at higher redshift. These studies reveal that there exist differences in PAH EWs and L_{PAH}/L_{IR} ratios between local values and high redshift ones (Helou *et al.* 2001; Peeters *et al.* 2002; Smith *et al.* 2007). Since PAH band ratios reflect variations in physical conditions within environments, such as ionization states of dust grains and metallicity (Smith *et al.* 2007; Galliano *et al.* 2008; Gordon *et al.* 2008. See papers by Draine and by Galliano elsewhere in this volume), more detailed study on this subject will put a better constraint on physical conditions of PAH emission sites and calibration of PAH bands as SFR proxies.

Then, most studies on PAH emission features concentrate on stronger bands, such as 6.2, 7.7, and $11.3\ \mu\text{m}$ due to the relatively weaker strength of $3.3\ \mu\text{m}$ feature and lack of wavelength coverage by instruments on board *Spitzer*. The Japanese space-based IR observatory, AKARI can fill this gap (Murakami *et al.* 2007). Launched on February 26th, 2006, AKARI has a 68.5 cm telescope which is cooled down to 65 K. It has two instruments, Far-Infrared Surveyor (FIS) and InfraRed Camera (IRC), whose wavelength coverages range from 1.8 to $180\ \mu\text{m}$.

Developed to carry out all-sky survey, AKARI has two operation modes, survey mode and pointing mode. More details on AKARI, its operation and accomplishments can be found in the literature. Spectroscopic observations of PAHs have also been reported by Onaka *et al.* elsewhere in this volume.

We present one of AKARI mission projects (MPs), AKARI mJy Unbiased Survey of Extragalactic Sources (AMUSES). The main scientific goal of AMUSES is to construct a continuous spectral library over the wavelength window between 2.5 and 40 μm for a subsample of 5 mJy Unbiased Spitzer Extragalactic Survey (5MUSES) (Wu *et al.*, accepted). AMUSES enables to access the 2.5 – 5 μm spectral window which includes the 3.3 μm emission feature. Moreover, the 3.3 μm PAH feature is the only dust emission feature at high redshift ($z > 4.5$) accessible to JWST. Therefore, understanding and calibrating the 3.3 μm feature with respect to the total IR luminosity, the SFR and other PAH emission features for local galaxies is critical for interpreting JWST spectra of dusty galaxies in future.

2 Sample selection

We select our sample from 5MUSES. 5MUSES, one of the Spitzer Legacy surveys, performs a mid-infrared spectroscopic observation of extragalactic sources brighter than 5 mJy at 24 μm in the Spitzer First Look Survey (FLS) field and four subfields of Spitzer Wide-area Infrared Extragalactic (SWIRE) survey with the Infrared Spectrograph (IRS) onboard the Spitzer space telescope. The main scientific goal of 5MUSES is to provide an unbiased library of infrared spectra from 5 to 40 μm of sources which have not been sought after in previous studies. Since the main objective of AMUSES is to detect the 3.3 μm PAH feature, we narrow down our sample to be brighter than 1 mJy at 3.6 μm . Based on the Spitzer IRAC 3.6 μm data for the 5MUSES sample, we find that 60 of the 330 5MUSES galaxies satisfy the flux cut of 1mJy at 3.6 μm . In order to detect the 3.3 μm feature, we limit the redshift range to $z < 0.5$. With this additional cut, we narrow down the sample size to 51 galaxies. In addition to this base sample, we add 10 targets with their 3.6 μm flux brighter than 0.7 mJy whose redshifts could not be determined by optical spectroscopy. After this selection, 60 target galaxies remain.

Then 44 targets are approved for the final program. Based on the SED classification, there are 22 AGNs and 17 starburst galaxies. The rest of the sample shows a composite SEDs. The redshift distribution is presented in Figure 1.

3 Observation and data reduction

The main goal of AMUSES is to detect the PAH 3.3 μm feature with $S/N > 5$ with IRC (Onaka *et al.* 2007). IRC is a workhorse for AKARI and has a field of view of roughly $10' \times 10'$. Pixel scales for three independent cameras range from 1.45'' through 2.5''. Each observation during the pointing mode has a maximum exposure time of ten minutes, but actual exposure times run between six to seven minutes. In order to achieve this S/N for sources with 1 mJy at 3.6 μm ,

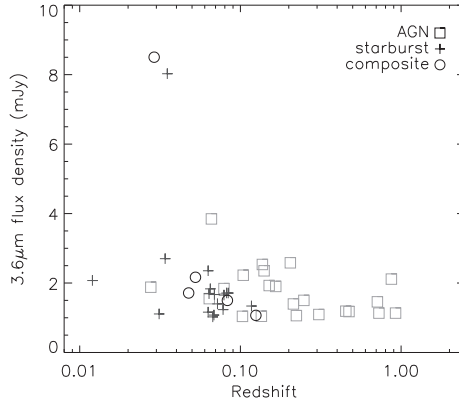


Fig. 1. Redshift distribution of the sample of galaxies of AMUSES plotted against $3.6 \mu\text{m}$ flux. Symbols represent the SED classification of target galaxies based on their MIR colors by 5MUSES collaboration. Open squares represent the AGN-type SED, while crosses represent the starburst-type SED. Open circles represent the composite SED. AGN-type targets are more evenly distributed across the redshift range, while starburst-type targets are more clustered at lower redshifts.

we decided to have three pointings for each target with NIR grism (NG) while adding one pointing with NIR prism (NP) in order to improve continuum extraction. These observations are carried out with a slit aperture whose dimension is $1'$ by $1'$. In total, 51 pointings are observed for 20 target galaxies. Among them, ten sources have completed their scheduled observations. Data reduction is performed with the IRC spectroscopy pipeline¹. Additional cosmic ray removal, stacking multipointing exposures, and sigma clipping during stacking are executed individually after running the IRC spectroscopy pipeline. Final one-dimensional spectra are extracted from two-dimensional spectral images which are binned by three pixels along the wavelength direction.

4 Results

We present several sample spectra in Figure 2. Overall, the $3.3 \mu\text{m}$ PAH emission feature is pretty weak across the sample even if it is detected. However, it is still noticeable that its strength is stronger for galaxies with starburst SED class than for AGN class. Most galaxies in which the $3.3 \mu\text{m}$ PAH feature is detected with a significant S/N are classified as starburst galaxies. The only exceptions are VII Zw353 and 2MASX J16205879+5425127 in which the $3.3 \mu\text{m}$ PAH detection is marginal. The latter is also classified as composite SED.

¹<http://www.ir.isas.jaxa.jp/ASTRO-F/Observation/DataReduction/IRC/>

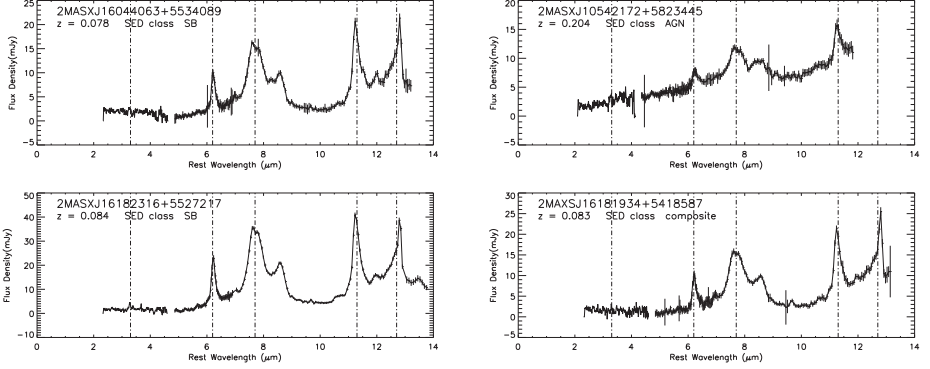


Fig. 2. Sample spectra of AMUSES based on IRC and IRS spectra. Notice the gaps between two instruments around $5 \mu\text{m}$. All spectra are deredshifted. Vertical dashed lines indicate the most notable PAH emission features at 3.3 , 6.2 , 7.7 , 11.2 , and $12.7 \mu\text{m}$. The two galaxies on the left panels are classified as starburst galaxies based on their SEDs while the two galaxies on the right panels are classified as AGN, or have a composite SED. The $3.3 \mu\text{m}$ PAH feature is always the weakest and difficult to detect compared to the other prominent PAH emission features.

We also present a couple of plots showing correlations between EWs of the $3.3 \mu\text{m}$, and $6.2 \mu\text{m}$ features (Fig. 3). Bigger symbols represent samples of AMUSES. Asterisks represent galaxies with starburst SEDs while filled circles represent galaxies with AGN SEDs. A diamond represent a galaxy with composite SED. Overplotted are the data from Imanishi *et al.* (2008). Asterisks represent their samples classified as HII-like galaxies, *i.e.* star-forming galaxies, while filled circles represent AGNs. Within the sample of Imanishi *et al.* (2008), two SED classes do not differ much in correlations between EWs of the $3.3 \mu\text{m}$, and $6.2 \mu\text{m}$ bands. They are relatively well matched, albeit with big scatter. AMUSES sample galaxies, most of which are starburst galaxies, have even bigger scatter while generally following the trend set by the sample of Imanishi *et al.*

5 Summary

We introduce a mission project of AKARI, AMUSES and its preliminary results. With AMUSES, we investigate the $3.3 \mu\text{m}$ PAH feature and its correlation with other PAH features as well as other properties of sample galaxies while constructing an unbiased library of sample galaxies selected from a parent sample of 5MUSES. So far, we have measured fluxes and EW of the $3.3 \mu\text{m}$ PAH feature for 20 target galaxies and have compared their EW to the Imanishi *et al.* (2008) sample.

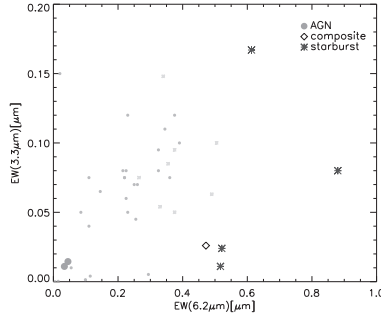


Fig. 3. Correlation between equivalent widths of the $3.3 \mu\text{m}$ PAH line and the $6.2 \mu\text{m}$ PAH line. Asterisks represent galaxies with starburst SEDs while filled circles represent galaxies with AGN SEDs. A diamond represent a galaxy with composite SED. Over-plotted are the data from Imanishi *et al.* (2008). Their AGN samples are represented by small filled circles and their HII-like samples are represented by small asterisks.

This work was supported by the National Research Foundation of Korea(NRF) grant funded by the Korean government(MEST), No. 2009-0063616. This research is based on observations with AKARI, a JAXA project with the participation of ESA.

References

- Allamandola, L.J., Tielens, A.G.G.M., & Barker, J.R., 1989, *ApJS*, 71, 733
 Calzetti, D., *et al.*, 2007, *ApJ*, 666, 870
 Galliano, F., Madden, S.C., Tielens, A.G.G.M., Peeters, E., & Jones, A.P., 2008, *ApJ*, 679, 310
 Genzel, R., & Cesarsky, C.J., 2000, *ARA&A*, 38, 761
 Gordon, K.D., Engelbracht, C.W., Rieke, G.H., *et al.*, 2008, *ApJ*, 682, 336
 Helou, G., Malhotra, S., Hollenbach, D.J., Dale, D.A., & Contursi, A., 2001, *ApJ*, 548, L73
 Imanishi, M., Nakagawa, T., Ohyama, Y., *et al.*, 2008, *PASJ*, 60, 489
 Kessler, M.F., *et al.*, 1996, *A&A*, 315, L27
 Murakami, H., *et al.*, 2007, *PASJ*, 59, 369
 Onaka, T., *et al.*, 2007, *PASJ*, 59, 401
 Peeters, E., Hony, S., Van Kerckhoven, C., *et al.*, 2002, *A&A*, 390, 1089
 Puget, J.L., Leger, A., & Boulanger, F., 1985, *A&A*, 142, L19
 Regan, M., & The Sings Team 2004, 35th COSPAR Scientific Assembly, 35, 4098
 Smith, J.D.T., *et al.*, 2007, *ApJ*, 656, 770
 Soifer, B.T., Neugebauer, G., & Houck, J.R., 1987, *ARA&A*, 25, 187
 Werner, M.W., *et al.*, 2004, *ApJS*, 154, 1
 Wu, Y., *et al.*, 2010, *ApJ*, accepted

**The Lifecycle
of PAHs in Space**

PAH EVOLUTION IN THE HARSH ENVIRONMENT OF THE ISM

H. Kaneda¹, T. Onaka², I. Sakon², D. Ishihara¹, A. Mouri¹,
M. Yamagishi¹ and A. Yasuda¹

Abstract. We review observational results of PAH emission in harsh interstellar environments, which are mostly based on recent works by Spitzer and AKARI. The harsh environments include shock regions in our Galaxy, the ionized superwinds and haloes of external galaxies, and the hot plasmas of elliptical galaxies. Owing to the unprecedented high sensitivity for PAH emission with Spitzer and AKARI, it is found that an appreciable amount of PAHs are present in some cases with such hostile conditions. Some of them exhibit unusual PAH interband strength ratios, reflecting either evolution of PAHs or physical conditions of the ISM. The distribution of the PAH emission, as compared to that of dust emission, is shown to discuss their ways of evolution and survival.

1 Introduction

The evolution and survival of polycyclic aromatic hydrocarbons (PAHs) in the harsh environments of the interstellar medium (ISM) are interesting and important problems to be addressed for understanding the lifecycle of PAHs in space. PAHs are expected to be processed and destroyed quite easily in interstellar shock regions and hot plasmas (*e.g.* Tielens 2008). In general, as observed in our Galaxy and nearby galaxies, most PAHs are associated with neutral gas and their emission is weak in ionized regions with strong radiation field probably due to destruction (*e.g.* Boulanger *et al.* 1988; Désert *et al.* 1990; Bendo *et al.* 2008). However the true destruction efficiency of PAHs has not yet been well understood from astronomical observations because of scarcity of relevant data and their faintness in the mid-IR emission in such conditions, although there are several theoretical studies (Jones *et al.* 1996; Micellota *et al.* 2010a, 2010b). Now the situation has been

¹ G. School of Science, Nagoya University, Chikusa-ku, Nagoya 464-8602, Japan

² Graduate School of Science, The University of Tokyo, Bunkyo-ku, Tokyo 113-0033, Japan

improved with the advent of Spitzer and AKARI; owing to their unprecedented high sensitivity for PAH emission, it is found that PAHs are indeed destroyed quite efficiently as compared to dust grains in most objects with such hostile conditions, but in some cases, an appreciable amount of PAHs are still present. Some of them exhibit unusual PAH interband strength ratios, reflecting either evolution of PAHs or physical conditions of the ISM.

From recent theoretical studies combined with laboratory data, Micellota *et al.* (2010a, 2010b) calculated the collisional destruction efficiency of PAHs in interstellar shocks and hot plasma. According to their results, for shock velocities lower than 100 km s^{-1} , PAHs in shocks are not completely destroyed but their structures are significantly affected. In such a slow shock, PAHs may even be formed by shattering of carbonaceous grains. On the other hand, for shock velocities higher than 200 km s^{-1} , PAHs are completely destroyed in postshock hot plasma.

In hot plasmas with temperatures lower than $3 \times 10^4 \text{ K}$, ion nuclear collisions dominate in the destruction process, which destroy PAHs not so efficiently; for example, in a hot plasma with the density and temperature of 10^4 cm^{-3} and 10^4 K (*e.g.* Orion), small (50–200 C-atom) PAHs can survive against the collisional destruction for a time as long as 10^7 years. For hotter plasma, however, electron collisions dominate in the destruction process, which destroy PAHs very efficiently. For example, in a hot plasma with the density and temperature of 10^{-2} cm^{-3} and 10^7 K (*e.g.* M82 superwinds), small PAHs can survive only for 100 years against collisional destruction (Micellota *et al.* 2010b). It should be noted that these lifetimes of PAHs are two to three orders of magnitude shorter than those for dust grains with the same size, because the sputtering yields of 3-dimensional dust grains are much smaller than unity, while the dissociation yields of 2-dimensional PAHs are close to unity. In HII regions with strong UV radiation field, the photo-dissociation of PAHs is more important, where the lifetimes of PAHs are $\sim 10^5$ year for typical HII regions while they are $\sim 10^8$ years for the diffuse ISM (Allain *et al.* 1996).

Below, we review observational results of PAH emissions in harsh interstellar environments, which are mostly based on recent works by Spitzer and AKARI. The harsh environments include shock around SNRs and intense UV field in a massive cluster in our Galaxy, the ionized superwinds and haloes of external galaxies, and the hot plasmas of elliptical galaxies.

2 PAHs in harsh environments in our Galaxy

According to Spitzer studies of PAH emission from Galactic SNRs by Reach *et al.* (2006), only 4 SNRs, out of 95, indicate the presence of PAH emission from IRAC colors. One example is 3C 396, where the $8 \mu\text{m}$ PAH map shows the presence of filamentary structures inside the radio shell. The Spitzer IRS also detected PAH emission features from the spectra of the SNRs W28, W44, and 3C 391 (Neufeld *et al.* 2007), but their association with the SNRs was not so clear. For the SNR N132D in the Large Magellanic Cloud (LMC), a PAH $17 \mu\text{m}$ broad feature was detected from Spitzer/IRS spectra of the southern rim across the shock front

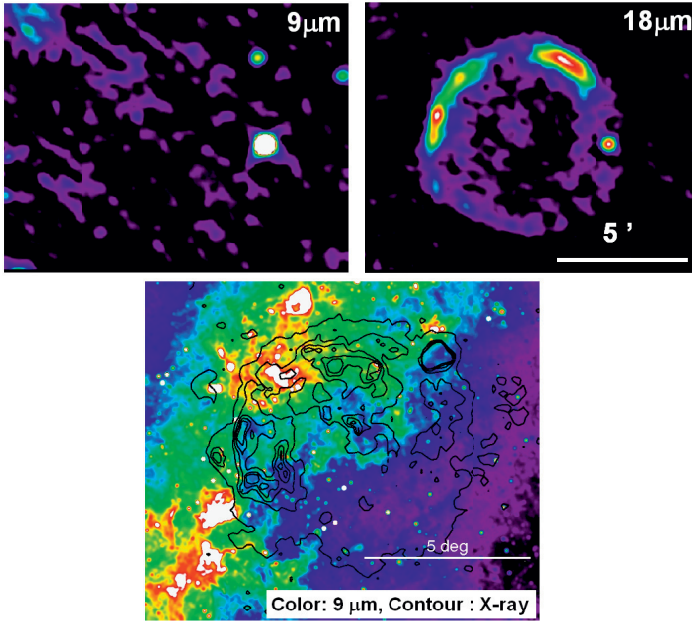


Fig. 1. AKARI 9 μm and 18 μm images of the Tycho SNR on the left and right of the upper panel, respectively (Ishihara *et al.* 2010), and the AKARI 9 μm large-scale image around the Vela SNR in the lower panel, which are created from the AKARI mid-IR all-sky survey data. The ROSAT X-ray contours are superposed on the Vela SNR image.

(Tappe *et al.* 2006). The 17 μm broad feature is interpreted as the emission of larger PAHs with a few thousand carbon atoms in C–C–C in- and out-of-plane bending modes (Van Kerckhoven *et al.* 2000; Peeters *et al.* 2004). The lifetime of large (4000 C-atom) PAHs is estimated to be ~ 200 years (Micellota *et al.* 2010b) while the age of the SNR is ~ 2500 years, and therefore such large PAHs may have been recently swept up by the blast wave and not yet completely destroyed by the shock (Tappe *et al.* 2006).

AKARI mid-infrared (IR) all-sky survey data are useful to discuss the presence of PAHs in SNRs. They consist in photometry in two wide bands centered at wavelengths of 9 μm and 18 μm with effective wavelength ranges of 6.7–11.6 μm and 13.9–25.6 μm , respectively (Onaka *et al.* 2007). The 9 μm band includes the PAH features at 7.7, 8.6, and 11.3 μm , while the 18 μm band traces warm dust continuum emission. The AKARI 9 μm band is relatively broad as compared to the MSX and Spitzer bands for PAH emission, and it is therefore more likely to be dominated by PAH features and less affected by emission lines.

Structures associated with SNRs are often identified in the AKARI 18 μm band, whereas they are not in the AKARI 9 μm . For example, the upper panel of Figure 1 shows the AKARI 9 μm and 18 μm images of the Tycho SNR at an age

of ~ 440 years, where a spherical shell structure is clearly seen in the warm dust continuum emission while it is hardly seen in the PAH emission. The dust emission shows a beautiful spatial correlation with the X-ray and CO emission (Ishihara *et al.* 2010). With the current shock speeds ($\sim 3000 \text{ km s}^{-1}$; Reynoso *et al.* 1997) and the thickness of the dust emission region, we estimate dust residence time in postshock plasma to be ~ 50 years, where the X-ray plasma has temperature and electron density of $8 \times 10^6 \text{ K}$ and 10 cm^{-3} , respectively (Warren *et al.* 2005). Then Figure 1 demonstrates that the dust can survive while the PAHs are almost totally destroyed in the 50 year timescale in a hot plasma with the above plasma parameters, which is consistent with the theoretical prediction. The lower panel of Figure 1 shows an AKARI $9 \mu\text{m}$ image around the Vela SNR ($\sim 1.1 \times 10^4$ years old), on which the X-ray contours are superposed. In this large-scale image, we can clearly see an anti-correlation between the PAH and the X-ray emission, again demonstrating effective destruction of PAHs in the postshock hot plasma.

Other than SNRs, AKARI also reveals the properties of PAHs in harsh environments of clouds with energetic phenomena with the help of large-scale CO data by the NANTEN telescope. One example is RCW49, Wd2, one of the most massive star clusters in our Galaxy. The massive cluster formation was likely triggered by cloud-cloud collision $\sim 4 \times 10^6$ years ago because the NANTEN CO observations revealed two large molecular clouds with a systematic difference in the speed ($\sim 10 \text{ km s}^{-1}$), the crossing point of which exactly corresponds to the position of Wd2 (Furukawa *et al.* 2009). Figure 2 shows the AKARI $9 \mu\text{m}$ and $18 \mu\text{m}$ composite map of RCW49, where the central region is saturated in the $18 \mu\text{m}$ band. In the figure, two examples of the AKARI near-IR $2\text{--}5 \mu\text{m}$ slit spectra are shown together with their observational positions, from each of which a $3.3 \mu\text{m}$ emission is detected. However we should be careful about this interpretation because the $3.3 \mu\text{m}$ emission is also caused by the hydrogen recombination $\text{Pf}\delta$ line at $3.30 \mu\text{m}$ overlapping with the PAH $3.3 \mu\text{m}$ band. Because the intensity of the $\text{Pf}\delta$ line should be $\sim 0.7 \times \text{Pf}\gamma$ for the case B condition, the $3.3 \mu\text{m}$ emission is most likely dominated by the PAH emission only if the $3.3 \mu\text{m}$ line is much stronger than the $\text{Pf}\beta$ and $\text{Pf}\gamma$ lines at $4.66 \mu\text{m}$ and $3.75 \mu\text{m}$, respectively. By taking this into account, the presence of the PAH $3.3 \mu\text{m}$ emission with its subfeatures at $3.4\text{--}3.5 \mu\text{m}$ is confirmed in many regions for which spectroscopic observations have been performed around Wd2 except for its very central region. This physically reflects the presence of very small PAHs because PAHs with the number of C-atoms >100 or the size $>6 \text{ \AA}$ cannot emit the $3.3 \mu\text{m}$ feature efficiently (Draine & Li 2007). It is thus found that even very small PAHs survive for $\sim 4 \times 10^6$ years under intense UV radiation field near very active star-forming region, which shows a striking contrast to the SNRs where PAHs are very easily destroyed.

In general, suppressed PAH emission relative to dust emission (*e.g.* unusually low ratios of the AKARI $9 \mu\text{m}$ to $18 \mu\text{m}$ band intensity) may serve as evidence of shock gas heating rather than radiative heating. For example, the NANTEN CO observations by Fukui *et al.* (2006) revealed the presence of large-scale molecular loops in the Galactic center region. The theoretical simulation by Machida *et al.* (2009) predicted magnetic loops can buoyantly rise due to the Parker instability

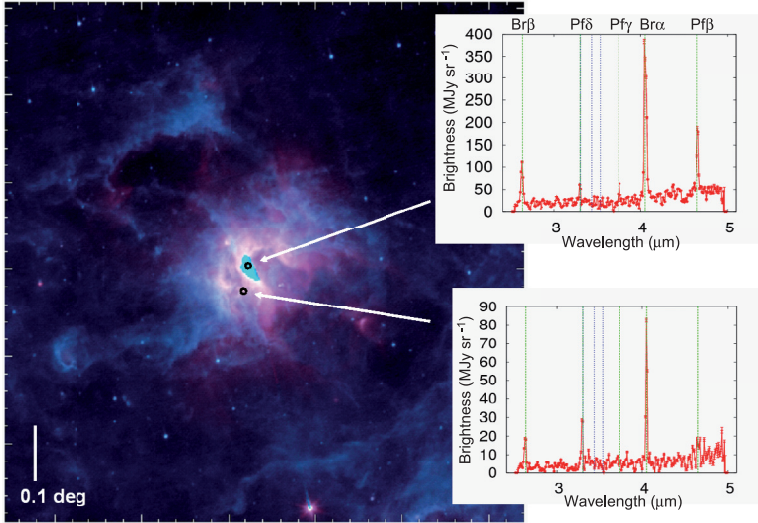


Fig. 2. AKARI 9 μm (blue) and 18 μm (red) composite image of the RCW49 region, where the center is saturated in the 18 μm band. Two examples of AKARI near-IR 2–5 μm slit spectra are shown together with their observational positions.

with disk gas, which cools at the top and then slides down along the loop with a speed of $\sim 30 \text{ km s}^{-1}$, presumably resulting in shock gas heating. If this is the case, we can expect that PAH emission is relatively suppressed at the foot points of the molecular loops.

3 PAHs in the haloes of external galaxies

Several authors have reported the detection of PAH emission in the haloes of nearby edge-on galaxies. As for relatively quiescent normal galaxies, PAH emissions in the haloes of NGC 5529 and NGC 5907 extending up to $\sim 10 \text{ kpc}$ and $\sim 6 \text{ kpc}$ above the disks were detected with ISO by Irwin *et al.* (2007) and Irwin & Madden (2006), respectively. The latter was the first report of the detection of PAHs in the halo of an external galaxy. For NGC 5907, Irwin & Madden (2006) found that the ratio of the PAH 11.3 to 7.7 band increases with distance from the galactic plane and also pointed out that there is a similarity in the spatial distribution between the PAH 6.3 μm and $\text{H}\alpha$ emission. Whaley *et al.* (2009) showed the presence of PAH emission in the halo of NGC 891 extending up to $\sim 3 \text{ kpc}$ above the disk with Spitzer and ISO. They compared the vertical extents of various components and found that the cool dust extends to larger scale heights than the PAHs and warm dust.

For more active galaxies, PAH emission from the galactic superwind of M 82 was observed with Spitzer and was found to widely extend around the halo up to

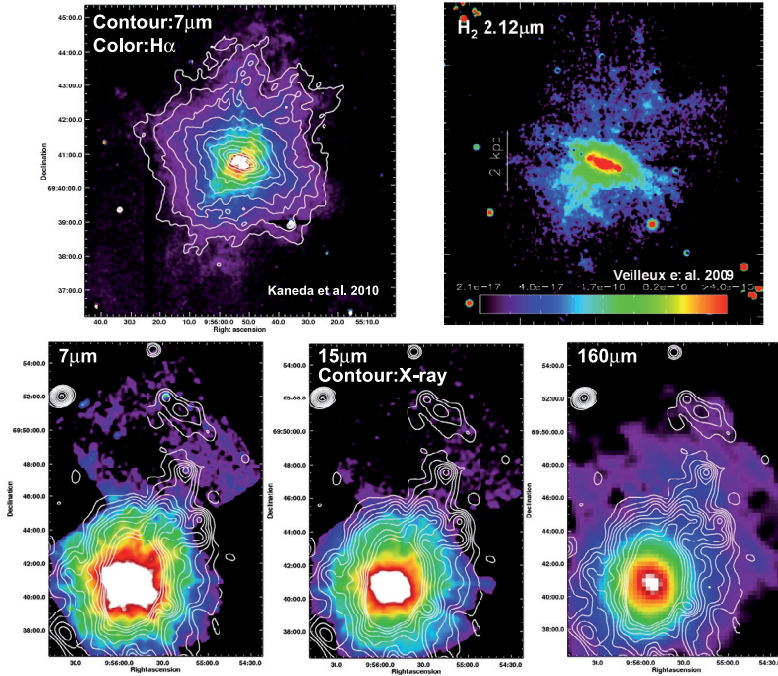


Fig. 3. AKARI 7 μm band contour map of M82 overlaid on the continuum-subtracted $\text{H}\alpha$ image (Kaneda *et al.* 2010a) on the left, and H_2 2.12 μm emission image (Veilleux *et al.* 2009) on the right of the upper panel. In the lower panel, the low-level 7 μm , 15 μm , and 160 μm band images of M82 including the Cap region, overlaid on the XMM/Newton X-ray (0.2–10 keV) contour map (Kaneda *et al.* 2010a).

~ 6 kpc from the center (Engelbracht *et al.* 2006; Beirão *et al.* 2008). However one serious problem is that the central starburst core is dazzlingly bright due to tremendous star-forming activity in the central region of M82 (Telesco & Harper 1980); indeed M82 is the brightest galaxy in the mid- and far-IR after the Magellanic Clouds. Then, instrumental effects caused by saturation made quantitative discussion about the low-surface brightness distribution around the halo rather difficult. Tacconi-Garman *et al.* (2005) performed high-spatial observations of the central region of NGC 253 with the IR camera and spectrograph ISAAC on ESO Very Large Telescope UT1. They found the presence of PAH emission in the galactic superwind of NGC 253 extended on a 0.1 kpc scale on the basis of the 3.28 μm narrow (0.05 μm width) band image, for which, however, the contribution by the $\text{P}\delta$ line may have to be taken into account as mentioned above.

AKARI also observed M82 over a wide area from the center to the halo in the mid- and far-IR in deep pointed observations (Kaneda *et al.* 2010a). One of the AKARI merits is a large dynamic range of signal detection; AKARI has

a special mode to observe bright sources so that the instruments may not suffer saturation effects. The AKARI M82 data consist of four mid-IR narrow-band images at reference wavelengths of $7\ \mu\text{m}$ (effective band width: $1.75\ \mu\text{m}$), $11\ \mu\text{m}$ ($4.12\ \mu\text{m}$), $15\ \mu\text{m}$ ($5.98\ \mu\text{m}$), and $24\ \mu\text{m}$ ($5.34\ \mu\text{m}$), the allocation of which is ideal to discriminate between the PAH emission features ($7\ \mu\text{m}$ band tracing the PAH 7.7 and $8.6\ \mu\text{m}$ features, $11\ \mu\text{m}$ band tracing the 11.3 and $12.7\ \mu\text{m}$ features) and the MIR dust continuum emission ($15\ \mu\text{m}$, $24\ \mu\text{m}$). The data also include four far-IR photometric bands; 2 wide bands at central wavelengths of $90\ \mu\text{m}$ (effective band width: $37.9\ \mu\text{m}$) and $140\ \mu\text{m}$ ($52.4\ \mu\text{m}$) and 2 narrow bands at $65\ \mu\text{m}$ ($21.7\ \mu\text{m}$) and $160\ \mu\text{m}$ ($34.1\ \mu\text{m}$). The left upper panel of Figure 3 shows the AKARI $7\ \mu\text{m}$ band contour map of M82 for a $10\times 10\ \text{arcmin}^2$ area, which reveals filamentary structures widely and faintly extended into the halo. As compared to the $\text{H}\alpha$ distribution in color, a very tight correlation is found between the PAHs and the ionized superwind, providing evidence that the PAHs are well mixed in the ionized superwind gas and outflowing from the disk. In contrast, the $\text{H}_2\ 2.12\ \mu\text{m}$ emission (Veilleux *et al.* 2009) shows a relatively loose correlation with the PAH emission especially in the northern halo (the right upper panel of Fig. 3). The deprojected outflow velocity of the $\text{H}\alpha$ filaments is $525 - 655\ \text{km s}^{-1}$ (Shopbell & Bland-Hawthorn 1998). Therefore the PAHs seem to have survived in such a harsh environment for about 5×10^6 years to reach the observed positions, $\sim 3\ \text{kpc}$ above the disk, in the ionized superwind but not X-ray-emitting hot plasma because the destruction time in a hot plasma should be very short, ~ 100 years (Micelotta *et al.* 2010b).

Far beyond the disk of M82, there is a region called X-ray Cap. The lower panel of Figure 3 shows the AKARI wide-area images of M82 covering the Cap region at $7\ \mu\text{m}$, $15\ \mu\text{m}$, and $160\ \mu\text{m}$, exhibiting the low-brightness distributions of the PAH, warm dust, and cool dust emission, respectively. The X-ray contours are overlaid for each image. Hence PAH emission is widely extended in the Cap region as well, which is presumably caused by the past tidal interaction of M82 with M81 about 10^8 years ago (Walter *et al.* 2002). There is some anticorrelation between the X-ray and PAH emission at the Cap position and also at the upstream of the X-ray superwind. The $15\ \mu\text{m}$ warm dust emission is reasonably weak far beyond the disk, and the $160\ \mu\text{m}$ band clearly shows emission extended to the same direction as the X-ray superwind. Therefore the cool dust is also outflowing, entrained by the hot plasma. By comparing these maps, it is found that the destruction of PAHs in the X-ray plasma is clearly faster than the destruction of far-IR dust.

Another clear example of PAH detection from galactic superwinds is obtained for NGC 1569, a starburst dwarf galaxy possessing a very young (starburst peaked $\sim 5\times 10^6$ years ago) and low-metallicity ($Z \sim 1/4 Z_\odot$) environment; thus we expect a very small contribution from old stars to interstellar PAHs (Galliano *et al.* 2008). The background-subtracted spectra obtained by AKARI revealed the presence of the 3.3 , 6.2 , 7.7 , and $11.3\ \mu\text{m}$ PAH emission features in the prominent X-ray/ $\text{H}\alpha$ filament produced by the galactic superwinds of NGC 1569 (Onaka *et al.* 2010). The filament age is approximately 10^6 years, whereas the destruction timescale

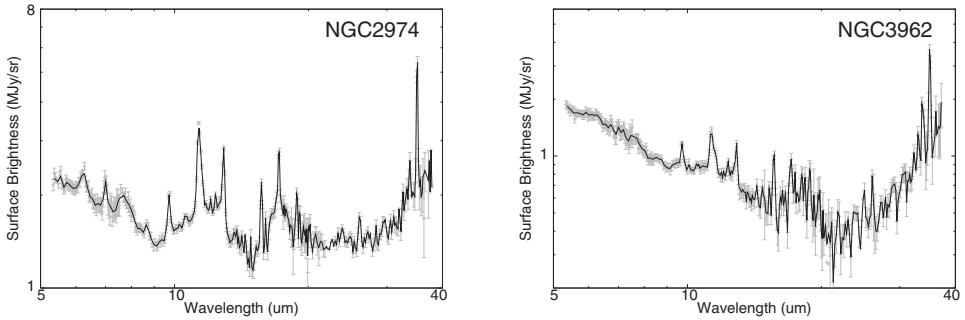


Fig. 4. Mid-IR spectra of the centers of the elliptical galaxies NGC 2974 and NGC 3962 obtained by the Spitzer/IRS staring observations. The figures are taken from Kaneda *et al.* (2008).

of small PAHs must be shorter than 100 years. To reconcile the discrepancy, we expect that PAHs may be produced by fragmentation of carbonaceous grains in shocks (Onaka *et al.* 2010).

4 PAHs in elliptical galaxies

Elliptical galaxies provide a unique environment: little UV from old stars and interstellar space filled by hot plasma, which are hostile conditions for PAH emission. Nevertheless, the early study with ISO by Xilouris *et al.* (2004) showed a hint of PAH emission in the spectral energy distributions of 10 elliptical galaxies out of 18. Then Spitzer/IRS clearly detected PAH emissions from the spectra of 14 elliptical galaxies out of 18 galaxies (Kaneda *et al.* 2008). Figure 4 shows such examples, where the prominent 11.3 μm and the broad 17 μm feature can be seen while usually the strongest 7.7 μm feature is rather weak. The relative weakness of the 7.7 μm feature is almost commonly observed among the elliptical galaxies. Since the 11.3 μm feature is attributed to a C-H out-of-plane bending mode mainly arising from neutral PAHs (*e.g.* Allamandola *et al.* 1989), a natural interpretation is that neutral PAHs are dominant over ionized PAHs due to soft radiation field from old stars, which is typical of elliptical galaxies. As another case supporting this interpretation, from a systematic study of mid-IR spectra of Galactic regions, Magellanic HII regions, and galaxies of various types (dwarf, spiral, starburst) by ISO and Spitzer, Galliano *et al.* (2008) found that the 6.2, 7.7, and 8.6 μm bands are essentially tied together, while the ratios between these bands and the 11.3 μm band vary by one order of magnitude. They concluded that the relative variations of the band ratios are mainly controlled by the fraction of ionized PAHs.

Alternatively, the characteristics of the PAH emission may be regulated by nuclear activities of the galaxies. A significant fraction of local elliptical galaxies are known to harbor a low-luminosity AGN (LLAGN), including a low-ionization nuclear emission region (LINER) nucleus (*e.g.* Ho *et al.* 1997). Smith *et al.* (2007)

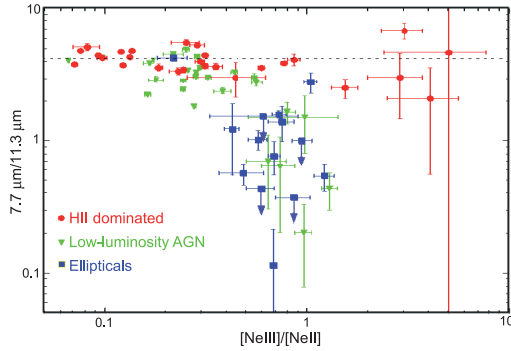


Fig. 5. PAH $7.7 \mu\text{m}/11.3 \mu\text{m}$ ratios plotted against the line ratios of $[\text{NeIII}]/[\text{NeII}]$ taken from Smith *et al.* (2007) for the galaxies with HII-dominated nuclei and LLAGNs, and from Kaneda *et al.* (2008) for the elliptical galaxies.

have reported that the peculiar PAH features with an unusually low ratio of the $7.7 \mu\text{m}$ to the $11.3 \mu\text{m}$ emission strength arise from systems with relatively hard radiation fields of LLAGNs. Figure 5 shows a plot of PAH $7.7 \mu\text{m}/11.3 \mu\text{m}$ versus $[\text{NeIII}]/[\text{NeII}]$ taken from Smith *et al.* (2007) and the elliptical galaxy data from Kaneda *et al.* (2008) are plotted together. Generally, the $[\text{NeIII}]/[\text{NeII}]$ is an indicator of radiation hardness, and the elliptical galaxy data seem to follow a global trend. If this trend is true, PAHs in the elliptical galaxies may be affected by hard radiation from the LINER nuclei through selective destruction of smaller PAHs. Indeed, similar weakness of PAH features in the $5\text{--}10 \mu\text{m}$ range relative to strong $11.3 \mu\text{m}$ features were also obtained for radio galaxies (Leipski *et al.* 2009) and IR-faint LINERs (Sturm *et al.* 2006).

Recent deep spectral mapping with Spitzer/IRS clearly reveals the spatial distributions of PAH emission in elliptical galaxies for the first time (Kaneda *et al.* 2010b). An exemplary case, NGC 4589, is shown in Figure 6, where the upper panel displays the background-subtracted spectra of the central $15''$ region with the slit positions overlaid on the optical image. The lower panel of Figure 6 shows the distribution of the PAH $11.3 \mu\text{m}$ emission in color as well as that of the $5.5\text{--}6.5 \mu\text{m}$ continuum emission in contours. The $5.5\text{--}6.5 \mu\text{m}$ continuum emission shows a smooth stellar distribution, which is consistent with the 2MASS image in the upper panel of Figure 6. However, the PAH $11.3 \mu\text{m}$ emission exhibits a distinctly elongated distribution, possessing an excellent spatial coincidence with the minor-axis optical dust lane (see Fig. 2 of Möllenhoff & Bender 1989). Kaneda *et al.* (2010b) also showed that the molecular hydrogen line emissions come from the dust lane, and that the $[\text{NeII}]$ line emission shows a more compact distribution near the nucleus than the PAH features. Thus the PAH emission comes predominantly from dense gas in the optical dust lane, where the properties of the PAHs are not significantly regulated by hard radiation from the LINER nucleus. Since

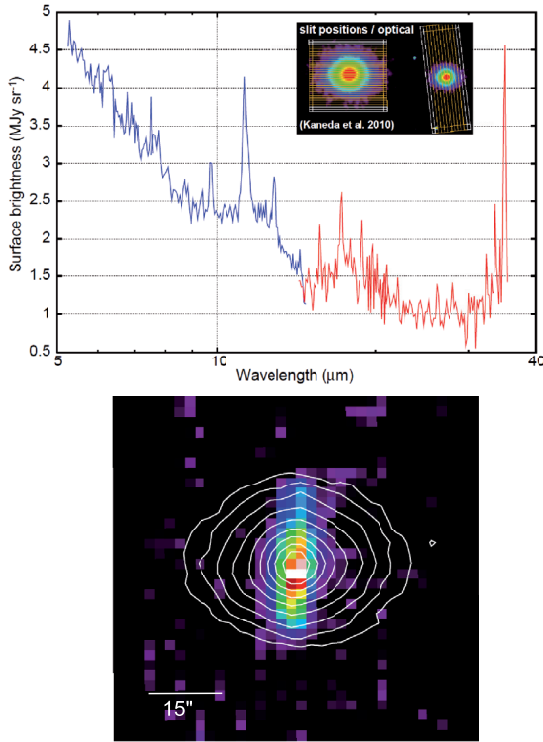


Fig. 6. Upper panel: the background-subtracted IRS SL (blue) and LL (red) spectra of the central $15''$ region of NGC 4589. The inset shows the SL (left) and LL (right) slit positions for the spectral mapping, superposed on the 2MASS image. Lower panel: the distribution of the PAH $11.3 \mu\text{m}$ emission in color as well as that of the $5.5 - 6.5 \mu\text{m}$ continuum emission in contours. For details, see Kaneda *et al.* (2010b).

NGC 4589 is thought to be an about 10^8 year old merger (Kawabata *et al.* 2010), the result may reflect that the PAHs are secondary products from the evolution of the dust brought in by a merger.

As for the signature of interaction of PAHs with hot plasma, no correlation has been found between PAH and X-ray emission among elliptical galaxies, which implies that a large fraction of observed PAHs are not continuously supplied into the interstellar space from old stars, but sporadically from other internal or external sources. A possible major origin of the PAHs is merger events as suggested by the above case. Another interesting possibility was suggested by Temi *et al.* (2007) such that the AGN-assisted feedback outflow from a central dust reservoir may supply PAHs into the interstellar space of elliptical galaxies through residual dust fragments diminished by sputtering.

5 Summary and future prospects

We extensively review observational results of PAH emission in harsh interstellar environments. The observations have indicated that PAHs in the shock regions of SNRs are destroyed very easily on 10–100 year timescales (*e.g.* Tycho SNR), where dust grains survive for a much longer time. There are probably a few exceptional cases (3C 396 and N132D in LMC) where SNR still show PAH emission. In contrast, PAHs survive for 10^6 – 10^7 timescales under very intense UV radiation field in RCW49, one of the most massive star clusters in our Galaxy. The observations have also shown that PAHs are present in the ionized galactic superwinds of starburst galaxies. For M 82, PAHs are widely spread around the halo through the galactic superwind and also probably through past tidal interaction with M 81. For NGC 1569, even very small PAHs emitting the $3.3 \mu\text{m}$ feature exist in the prominent $\text{H}\alpha$ superwind. Finally the observations have revealed that PAHs are present in many elliptical galaxies. The PAH emission from elliptical galaxies is characterized by unusually low ratios of the $7.7 \mu\text{m}$ to the $11.3 \mu\text{m}$ and $17 \mu\text{m}$ emission features, probably reflecting that neutral PAHs are dominant over ionized PAHs due to very soft radiation field from old stars. In particular, for NGC 4589, the PAH emission is found to predominantly come from the optical dust lane. No signatures of interaction between PAHs and hot plasmas have been found among elliptical galaxies, which implies that a large fraction of observed PAHs are sporadically supplied into the interstellar space from internal or external sources other than from old stars.

In future, SPICA (Space Infrared Telescope for Cosmology and Astrophysics; Swinyard *et al.* 2009) will be launched around 2018, covering the wavelength range from 5 to $200 \mu\text{m}$ by imaging spectroscopy with a 3-m aperture, 6 K telescope. Detailed studies of PAH emission in the far-IR regime, such as the ro-vibrational modes (see Joblin *et al.* in this volume), can be carried out with SPICA, which are critical to trace the structural changes of PAH molecules being processed in harsh environments.

Most of the researches presented in this paper are based on observations made with the Spitzer Space Telescope, which is operated by the Jet Propulsion Laboratory, California Institute of Technology under NASA contract 1407, and AKARI, a JAXA project with the participation of ESA.

References

- Allain, T., Leach, S., & Sedlmayr, E., 1996, *A&A*, 305, 602
Allamandola, L.J., Tielens, A.G.G.M., & Barker, J.R., 1989, *ApJS*, 71, 733
Bendo, G.J., Draine, B.T., Engelbracht, C.W., *et al.*, 2008, *MNRAS*, 389, 629
Beirão, P., Brandl, B.R., Appleton, P.N., *et al.*, 2008, *ApJ*, 676, 304
Boulanger, F., Beichman, C., Désert, F.X., *et al.*, 1988, *ApJ*, 332, 328
Désert, F.X., Boulanger, F., & Puget, J.L., 1990, *A&A*, 237, 215
Draine, B.T., & Li, A., 2007, *ApJ*, 657, 810

- Engelbracht, C.W., Kundurthy, P., Gordon, K.D., *et al.*, 2006, ApJ, 642, L12
- Fukui, Y., Yamamoto, H., Fujishita, M., *et al.*, 2006, Science, 314, 106
- Furukawa, N., Dawson, J.R., Ohama, A., *et al.*, 2009, ApJ, 696, 115
- Galliano, F., Madden, S.C., Tielens, A.G.G.M., Peeters, E., & Jones, A.P., 2008, ApJ, 679, 310
- Ho, L.C., Filippenko, A.V., & Sargent, W.L.W., 1997, ApJ, 487, 579
- Irwin, J.A., Kennedy, H., Parkin, T., & Madden, S.C., 2007, A&A, 474, 461
- Irwin, J.A., & Madden, S.C., 2006, A&A, 445, 123
- Ishihara, D., Kaneda, H., Furuzawa, A., *et al.*, 2010, A&A, 521, L61
- Jones, A.P., Tielens, A.G.G.M., & Hollenbach, D.J., 1996, ApJ, 469, 740
- Kaneda, H., Onaka, T., Sakon, I., *et al.*, 2008, ApJ, 684, 270
- Kaneda, H., Ishihara, D., Suzuki, T., *et al.*, 2010a, A&A, 514, A14
- Kaneda, H., Onaka, T., Sakon, I., *et al.*, 2010b, ApJ, 716, L161
- Kawabata, K.S., Maeda, K., Nomoto, K., *et al.*, 2010, Nature, 465, 326
- Leipski, C., Antonucci, R., Ogle, P., & Whysong, D., 2009, ApJ, 701, 891
- Machida, M., Matsumoto, R., Nozawa, S., *et al.*, 2009, PASJ, 61, 411
- Micellota, E.R., Jones, A.P., & Tielens, A.G.G.M., 2010a, A&A, 510, A36
- Micellota, E.R., Jones, A.P., & Tielens, A.G.G.M., 2010b, A&A, 510, A37
- Möllenhoff, C., & Bender, R., 1989, A&A, 214, 61
- Neufeld, D.A., Hollenbach, D.J., Kaufman, M.J., *et al.*, 2007, ApJ, 664, 890
- Onaka, T., Matsuhara, H., Wada, T., *et al.*, 2007, PASJ, 59, S401
- Onaka, T., Matsumoto, H., Sakon, I., & Kaneda, H., 2010, A&A, 514, A15
- Peeters, E., Mattioda, A.L., Hudgins, D.M., & Allamandola, L.J., 2004, ApJ, 617, L65
- Reach, W.T., Rho, J., Tappe, A., *et al.*, 2006, AJ, 131, 1479
- Reynoso, E.M., Moffett, D.A., Goss, W.M., *et al.*, 1997, ApJ, 491, 816
- Shopbell, P.L., & Bland-Hawthorn, J., 1998, ApJ, 493, 129
- Smith, J.D.T., Draine, B.T., Dale, D.A., *et al.*, 2007, ApJ, 656, 770
- Sturm, E., Rupke, D., Contursi, A., *et al.*, 2006, ApJ, 653, L13
- Swinyard, B., Nakagawa, T., Merken, P., *et al.*, 2009, Experimental Astronomy, 23, 193
- Tacconi-Garman, L.E., Sturm, E., Lehnert, M., *et al.*, 2005, A&A, 432, 91
- Tappe, A., Rho, J., & Reach, W.T., 2006, ApJ, 653, 267
- Telesco, C.M., & Harper, D.A., 1980, ApJ, 235, 392
- Temi, P., Brighenti, F., & Mathews, W.G., 2007, ApJ, 666, 222
- Tielens, A.G.G.M., 2008, ARA&A, 46, 289
- Van Kerckhoven, C., Hony, S., Peeters, E., *et al.*, 2000, A&A, 357, 1013
- Veilleux, S., Rupke, D.S.N., & Swaters, R., 2009, ApJ, 700, L149
- Walter, F., Weiss, A., & Scoville, N., 2002, ApJ, 580, L21
- Warren, J.S., Hughes, J.P., Badenes, C., *et al.*, 2005, ApJ, 634, 376
- Whaley, C.H., Irwin, J.A., Madden, S.C., Galliano, F., & Bendo, G.J., 2009, MNRAS, 395, 97
- Xilouris, E.M., Madden, S.C., Galliano, F., Vigroux, L., & Sauvage, M., 2004, A&A, 416, 41

PAH AND DUST PROCESSING IN SUPERNOVA REMNANTS

J. Rho¹, M. Andersen², A. Tappe³, W.T. Reach¹, J.P. Bernard⁴
and J. Hewitt⁵

Abstract. I present observations of shock-processed PAHs and dust in supernova remnants (SNRs). Supernova shocks are one of the primary sites destroying, fragmenting and altering interstellar PAHs and dust. Studies of PAHs through supernova shocks had been limited because of confusion with PAHs in background emission. *Spitzer* observations with high sensitivity and resolution allow us to separate PAHs associated with the SNRs and unrelated, Galactic PAHs. In the young SNR N132D, PAH features are detected with a higher PAH ratio of 15–20/7.7 μm than those of other astronomical objects, and we suggest large PAHs have survived behind the shock. We present the spectra of additional 14 SNRs observed with *Spitzer* IRS and MIPS SED covering the range of 5–90 μm . Bright PAH features from 6.2 to 15–20 μm are detected from many of SNRs which emit molecular hydrogen lines, indicating that both large and small PAHs survive in low velocity shocks. We observe a strong correlation between PAH detection and carbonaceous small grains, while a few SNRs with dominant silicate dust lack PAH features. We characterize PAHs depending on the shock velocity, preshock density and temperature of hot gas, and discuss PAH and dust processing in shocks and implication of PAH and dust cycles in ISM.

¹ SOFIA Science Mission Operations/USRA, NASA Ames Research Center, MS 211-3, Moffett Field, CA 94035, USA; e-mail: jrho@sofia.usra.edu

² Research & Scientific Support Department, European Space Agency, ESTEC, Keplerlaan 1, 2200 AG Noordwijk, The Netherlands

³ Harvard-Smithsonian Center for Astrophysics, MS 83, 60 Garden Street, Cambridge, MA 02138, USA

⁴ Centre d'Étude Spatiale des Rayonnements, CNRS, 9 Av. du Colonel Roche, BP. 4346, 31028 Toulouse, France

⁵ NASA/Goddard Space Flight Center, Code 662, Greenbelt, MD 20771, USA

1 Introduction

Supernova shocks are one of the primary sites destroying, fragmenting and altering interstellar polycyclic aromatic hydrocarbons (PAHs) and dust. Supernovae influence the chemistry and physics in the interstellar medium (ISM) from galactic scales down to the atomic level. Studies of PAHs through supernova shocks had been limited because of confusion with PAHs in background emission. *Spitzer* observations with high sensitivity and resolution allow us to separate PAHs associated with the supernova remnants (SNRs) and unrelated, Galactic PAHs. Moreover, ISO observations of the continuum were limited to wavelengths longer than $40\ \mu\text{m}$ and the dust analysis was focused on the big grains. Shorter wavelength observations are necessary to probe the emission from the very small grains and polycyclic aromatic hydrocarbons (PAHs) in greater details. The ratio of PAH and very small grain (VSG) to big grain (BG) abundance can provide insight of the dust destruction mechanisms.

Dust grains and PAHs control the heating and cooling balance of interstellar gas through absorption of ultraviolet radiation, generation of photoelectrons, and emission of infrared radiation. These processes allow us to use them as diagnostics to probe physical conditions in a range of diverse environments. However, this is hampered by our lack of knowledge of their exact structure and composition, and how these are in turn affected by the physical environment. The PAHs are believed to give rise to the unidentified infrared bands (UIR), well-known emission features near 3.3 , 6.2 , 7.7 , 8.6 , and $11.2\ \mu\text{m}$ attributed to the CC and CH stretching and bending modes of these molecules (Allamandola *et al.* 1989). More recently observed features at 15 – $20\ \mu\text{m}$ are interpreted as PAH CCC out-of-plane bending modes (Peeters *et al.* 2004). Several detections have been reported in a variety of astronomical objects.

We present observations of shock-processed PAHs and dust in SNRs with *Spitzer* IRAC and MIPS imaging and IRS and MIPS-SED spectroscopy covering from $3.6\ \mu\text{m}$ to $95\ \mu\text{m}$. We confirm the PAH detection and its distribution in the young SNR N132D and present GLIMPSE-selected (Reach *et al.* 2006) 14 SNRs, many of which are interacting molecular clouds. We characterize PAHs depending on a shock velocity, preshock density and temperature of hot gas, and discuss correlation of PAH and associated dust composition and dust cycles in ISM.

2 PAH detection from the supernova remnant N132D

N132D is a young SNR in the Large Magellanic Cloud (LMC). The age of N132D is 2500 yr. In the optical, the large-scale morphology of the gas in N132D shows highly red-shifted oxygen-rich ejecta in the center and shocked interstellar clouds in the outer rim. We have previously presented *Spitzer* IRAC, MIPS and an IRS spectrum of N132D (Tappe *et al.* 2006). Here we present IRS-LL mapping of N132D covering the entire SNR, and IRS staring of SL observations toward 4 positions.

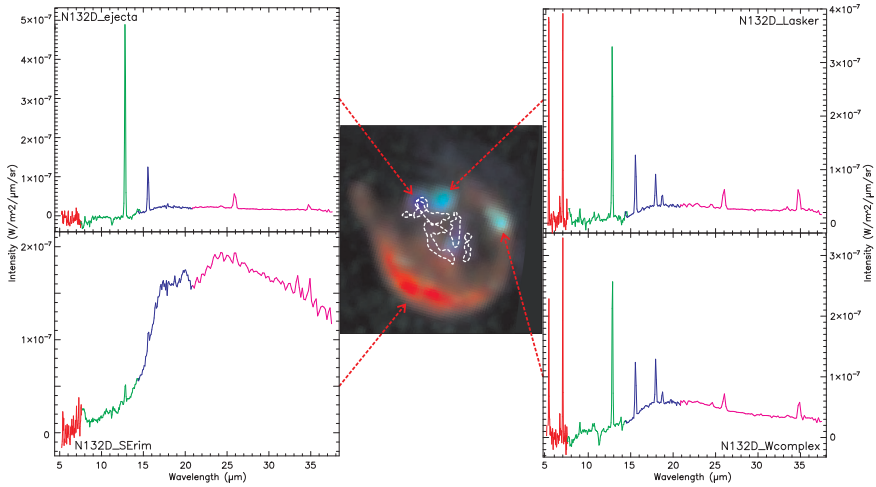


Fig. 1. N132D spectral mapping (center; blue = [Ne III] $15.5 \mu\text{m}$, green = [Fe II] $17.9 \mu\text{m}$, red = MIPS $24 \mu\text{m}$, white dashed line = red and blueshifted high-velocity Ne/O ejecta seen in the optical with HST) and spectra of selected positions.

We detect bright 24 and $70 \mu\text{m}$ emission from shocked, heated dust grains with MIPS. The $5\text{--}40 \mu\text{m}$ IRS mapping was performed, where LL ($13\text{--}40 \mu\text{m}$) covered the entire SNR and SL ($5\text{--}13 \mu\text{m}$) covered a few interesting positions. Figure 1 shows representative sets of spectra from southern rim (bottom left spectrum), the West Complex (bottom right), Lasker Bowl (top right) and an ejecta knot (top left).

IRS spectrum toward the southeastern shell shows a steeply rising continuum with [Ne III] and [O IV] as well as PAH features at ~ 7.7 , 11.3 , and $15\text{--}20 \mu\text{m}$. The PAH bands are from swept-up ISM material, which are processed by the strong shock wave via thermal sputtering and grain-grain collisions (Tielens *et al.* 1994). We found evidence for spatial variations of the PAH features, both in intensity and wavelength, when comparing spectra extracted along the IRS long-low slit from the shell of the remnant and the adjacent molecular cloud/H II region, which confirms the processing of the PAH molecules. These detections, most notably the $15 \sim 20 \mu\text{m}$ features, are the first of its kind for supernova remnants to our knowledge (Tappe *et al.* 2006). The $15 \sim 20 \mu\text{m}$ features in Figure 2a are interpreted as PAH CCC out-of-plane bending modes (*cf.* van Kerckhoven *et al.* 2000; Peeters *et al.* 2004). We generated a PAH map between $15\text{--}20 \mu\text{m}$ (Fig. 2b) after subtracting the continuum at neighboring wavelengths; the morphology is similar to that of the dust continuum in the MIPS $24 \mu\text{m}$ band (Fig. 1). Several detections of $15\text{--}20 \mu\text{m}$ PAH features have been reported in a variety of sources, including H II regions, young stellar objects, reflection nebulae, and evolved stars (see Peeters *et al.* 2004, for references therein). The detections include both broad variable plateaus as well as distinct, narrow features, most notably at 16.4 and $17.4 \mu\text{m}$.

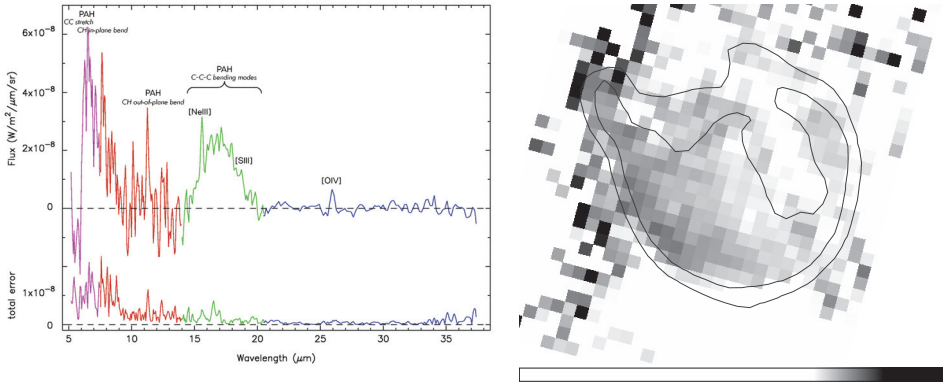


Fig. 2. (a: Left) N132D southeastern rim spectrum (magenta line = SL2, red line = SL1, green line = LL2, blue line = LL1): the local background and the modified blackbody continuum have been subtracted. The total error includes the reduction pipeline delivered errors and an estimate of the variation in the local background (Tappe *et al.* 2006). (b: Right) PAH grey-scale map of N132D between 15–20 μm after subtracting neighboring wavelength dust continuum, superposed on MIPS 24 μm contours from Tappe *et al.* (2006).

3 PAH from slow shocks: Molecular supernova remnants

Interacting SNRs are an ideal laboratory to study the effects of fast shocks on the interstellar material. Shocks can both sputter and shatter interstellar dust and thus potentially modify its abundance and size distribution. Previous observations of interacting SNRs had been limited. Using *Spitzer* GLIMPSE survey data (Reach *et al.* 2006) identified a series of Galactic SNRs in the infrared, a subsample having IRAC colors that indicate shocked H_2 . We present follow-up *Spitzer* IRS low resolution and MIPS SED spectra of a sample of 14 SNRs – G11.2-0.3, G21.8-0.6 (Kes 69), G22.7-0.2, G39.2-0.3 (3C 396), G54.4-0.3, G304.6+0.1 (Kes 17), Kes 20A (G310.8-0.4), G311.5-0.3, G332.4-0.4 (RCW 103), G344.7-0.1, CTB 37A (G348.5+0.1), G348.5-0.0, and G349.7+0.2. Molecular hydrogen detections towards 12 SNRs are presented by Hewitt *et al.* (2009) and Andersen *et al.* (2010), more than doubling the sample of known interacting Galactic SNRs. Here we present an analysis of the continuum and PAH emission. The spectroscopy observations were centered on the emission peaks for each SNR. The wavelength coverage from 5 to 90 μm ensures a good sampling of the three main dust species and enables us to fit the continuum in greater detail.

The dust model fitting of the SEDs (Fig. 3a) is done using the method described in Bernard *et al.* (2008). Three dust components are adopted, PAH molecules, Very Small Grains (VSG) and Big Grains (BG). The abundance of each dust species (Y_{PAH} , Y_{VSG} , Y_{BG}) and the strength of the radiation field (X_{ISRF}) are taken

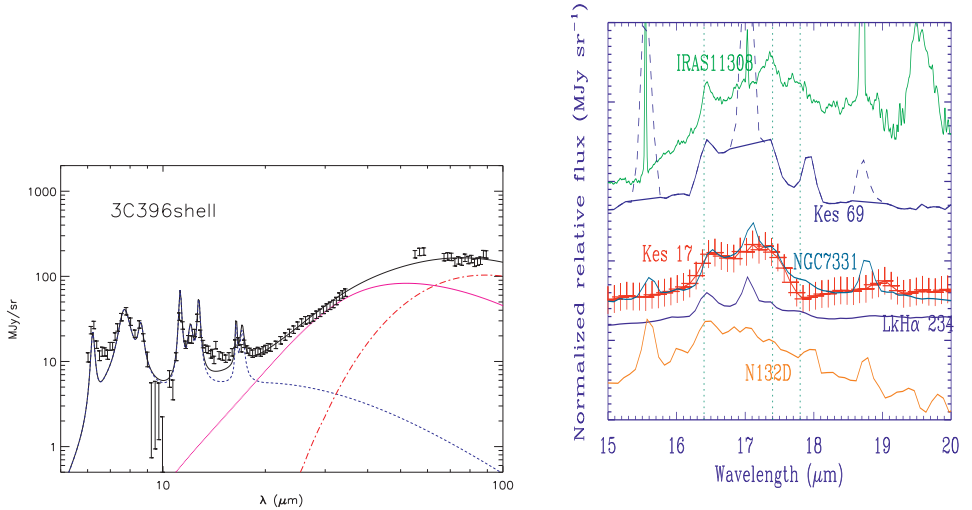


Fig. 3. (a: Left) the DUSTEM fit for 3C 396 superposed IRS and MIPS SED data with 3 component models of PAH, very small grains and big grains. The PAH, very small and large grain contribution are shown as the dotted line, the thin solid line, and the dashed dotted. The total fit is shown as the thick solid line (from Andersen *et al.* 2010). (b: Right) comparison of PAH emission in the SNR Kes 17 (red curve), Kes 69 (dark blue) and N132D (orange) with those of IRAS 11308 (green), LkH α 234 (PDR: blue) and NGC 7331 (yellow).

as free parameters in the fit. For all three dust species, a MRN powerlaw size distribution is assumed. The slopes and size ranges are different than adopted in the original version of DUSTEM due to the updated input physics, mainly the cross sections adopted have changed (Compiègne *et al.* 2008). The reduced χ^2 range between 4–10. Systematically higher reduced χ^2 around the 15–20 μm show that the PAH features in SNRs are significantly different from those in PDRs. The fit results are summarized in Figure 4a, showing that abundances of PAHs and VSGs are higher than those in the Milky Way and the LMC (Bernard *et al.* 2008).

A dust model composed of PAHs, VSGs and BGs provide a good fit to the SEDs of the SNRs. All the SNRs show evidence for PAH emission. Two SNRs, G11.2-0.3, and G344.7-0.1 show no to little evidence for VSGs and a lower PAH/BG ratio than observed in the diffuse interstellar medium and the LMC. We show Kes 17 and Kes 69 as examples (Fig. 3b) to demonstrate the differences in PAH emission between dust processed by a SNR shock and PDR dominated dust. Typically the radiation field is 10–100 times larger than normal interstellar radiation ISRF, the strength of which is consistent with being created from the shock.

The dust spectral fitting indicates the presence of PAH emission in most of SNRs. In Figure 3b, PAH spectra of Kes 17 and Kes 69 are compared with the

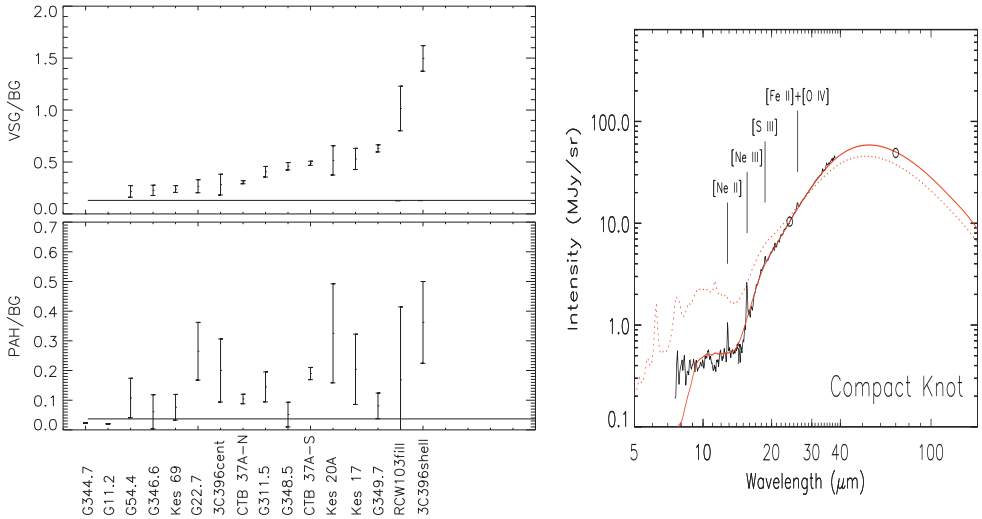


Fig. 4. (a: Left) the ratios of PAHs and very small grains to big grains are higher than those of the Milky Way (solid line). Two young SNRs (G11.2 and G344.2) have the ratios of carbon dust to silicates smaller than the Milky Way value and are associated with a strong radiation field. (b: Right) IRS spectrum of the Puppis A SNR superposed on the best fit (solid line) of the ZDA model (Arendt *et al.* 2010). The dotted line is a model with PAH and VSG, which shows similarity to the N132D spectrum.

emission from LkH α 234 and NGC7331, a PDR and a nearby spiral galaxy with strong PAH emission, respectively. We find that the PAH features of molecular interacting (H_2 emitting) SNRs are very similar to each other as shown for the cases of Kes 17 and Kes 69. The PAH emission is detected in our background spectra since all the SNRs are located in the Galactic plane. However, the PAH emission is clearly enhanced in the shocked region and is present after background subtraction. The 15–20 μm PAH feature in Kes 17 is stronger than that of LkH α 234 whereas the PAH features between 5–14 μm are almost identical. It is similar to that of NGC 7331. The ratio of the emission from the 15–20 μm plateau to the 6.2 μm PAH feature is ~ 0.4 for Kes 17 and other H_2 emitting SNRs, similar to NGC 7331 but larger than for the PDR. This ratio is smaller than that of the young SNR N132D (Tappe *et al.* 2006). The difference in PAH features between molecular SNRs and N132D is due to the environments of SNRs. Many of the interacting SNRs are in a dense molecular cloud environment with a slow shock while N132D is less dense environment and has a strong shock which significantly destroy small PAHs.

3.1 Comparison with Puppis A and other dust model

Figure 3b shows IRS spectrum of a middle-age SNR, Puppis A. Spectral fitting of Puppis A (Arendt *et al.* 2010) was performed based on carbon and silicated grains using Zubko *et al.* (2004; hereafter ZDA), radiatively heated by an ambient interstellar radiation field. The ZDA models are a set of models for the dust grain size (or mass) distributions that are derived to simultaneously fit average interstellar extinction, emission, and abundances. Different models are distinguished by different choices of grain compositions and different sets of abundance constraints. The PAH emission is not evident in Puppis A. In contrast, PAH features are noticeable in N132D, implying that the grains in N132D is less sputtered than those in Puppis A.

References

- Andersen, M., Rho, J., Tappe, A., *et al.*, 2010, submitted
Arendt, R.G., Dwek, E., Blair, W.P., *et al.*, 2010, ApJ, 725, 585
Bernard, J.P., Reach, W.T., *et al.*, 2008, AJ, 136, 919
Compiègne, M., Abergel, A., Verstraete, L., & Habart, E., 2008, A&A, 491, 797
Hewitt, J.W., Rho, J., Andersen, M., & Reach, W.T., 2009, ApJ, 649, 1266
Peeters, E., Mattioda, A.L., Hudgins, D.M., & Allamandola, L.J., 2004, ApJ, 617, L65
Reach, W.T., *et al.*, 2006, AJ, 131, 1479
Tappe, A., Rho, J., & Reach, W.T., 2006, ApJ, 653, 267
van Kerckhoven, C., *et al.*, 2000, A&A, 357, 1013
Zubko, V., Dwek, E. & Arendt, R.G., 2004, ApJS, 152, 211

THE FORMATION OF POLYCYCLIC AROMATIC HYDROCARBONS IN EVOLVED CIRCUMSTELLAR ENVIRONMENTS

I. Cherchneff¹

Abstract. The formation of Polycyclic Aromatic Hydrocarbons in the circumstellar outflows of evolved stars is reviewed, with an emphasis on carbon stars on the Asymptotic Giant Branch. Evidence for PAHs present in their winds is provided by meteoritic studies and recent observations of the Unidentified Infrared bands. We detail the chemical processes leading to the closure of the first aromatic ring as well as the growth mechanisms leading to amorphous carbon grains. Existing studies on PAH formation in evolved stellar envelopes are reviewed and new results for the modelling of the inner wind of the archetype carbon star IRC+10216 are presented. Benzene, C₆H₆, forms close to the star, as well as water, H₂O, as a result of non-equilibrium chemistry induced by the periodic passage of shocks. The growth process of aromatic rings may thus resemble that active in sooting flames due to the presence of radicals like hydroxyl, OH. Finally, we discuss possible formation processes for PAHs and aromatic compounds in the hydrogen-rich R CrB star, V854 Cen, and their implication for the carriers of the Red Emission and the Diffuse Interstellar Bands.

1 Introduction

Upon the suggestion by Léger & Puget (1984) and Allamandola *et al.* (1985) that polycyclic aromatic hydrocarbons (PAHs) were responsible for the emission of a series of unidentified infrared (UIR) bands ubiquitous to the interstellar medium (ISM), large efforts have been devoted to understand the presence of these aromatic molecules in space. PAHs are commonly found on Earth in the exhaust fumes of car engines and are key intermediates in the inception and growth of soot particles in incomplete combustion processes (Haynes & Wagner 1981). They are associated to the fine particles called aerosols released by human activities in the

¹ Departement Physik, Universität Basel, Klingenbergstrasse 82, 4056 Basel, Switzerland

Earth troposphere. PAHs are also mutagens and thus carcinogens. Therefore, PAHs are extensively studied on Earth, providing an abundant and exhaustive scientific literature of great interest to the study of PAHs in space. Cosmic PAHs are observed through their UIR bands in several local, low- and high-redshift environments including HII regions, Proto- and Planetary Nebulae, young stellar objects, and the ISM of high redshift galaxies (Tielens 2008). We can define two populations of PAHs in space: 1) PAHs formed directly from the gas phase in dense media; and 2) PAHs as products of dust sputtering in harsh environments. These two distinct classes require very diverse environments and processes to form, the second class being prevalent in galaxies and most readily observed through the detection of the UIR bands. In this review, we focus on the first class of PAHs, those forming under specific conditions from the gas phase in evolved circumstellar environments. We discuss evidence for PAHs in stardust inclusions in meteorites and PAHs observed in evolved low-mass stars. We detail the formation routes to benzene and its growth to several aromatic rings. We review existing models and present new results on benzene formation in the extreme carbon star IRC+10216. Finally, the PAH synthesis in R CrB stars is discussed.

2 Carbon dust providers in our galaxy

PAHs are intimately linked to the formation of amorphous carbon (AC) dust or soot from the gas phase in combustion processes on Earth. It is thus natural reckoning that similar formation conditions may exist in space that are conducive to the synthesis of PAHs. Those conditions characteristic of the gas phase are: (1) an initial carbon-, hydrogen-rich chemical composition; (2) high densities; (3) and high temperatures. Such conditions are usually found in space in circumstellar environments such as the winds or ejecta of evolved stars. Furthermore, these evolved objects are the prominent providers of dust in our galaxy. Therefore, the formation of PAHs in space from the gas phase is linked to evolved stellar objects synthesising AC dust. The prevalent AC grain makers in our galaxy include the late stages of evolution of low- and high-mass stars. They are the wind of low-mass carbon-rich stars on the Asymptotic Giant Branch (AGB), the ejecta of Type II supernovae, the colliding winds of carbon-rich Wolf-Rayet stellar binaries, and the clumpy winds of R CrB stars. The physical and chemical conditions pertaining to these environments are summarized in Table 1. For carbon AGB stars, the gas layers close to the photosphere that are periodically shocked satisfy the required conditions for PAH formation (Cherchneff 1998). Conversely, the ejecta of supernovae do not as the hydrogen present in the gas is not microscopically mixed within the ejecta layers but is in the form of macroscopically-mixed blobs of gas (Kifonidis *et al.* 2006). Carbon-rich Wolf-Rayet stars have lost their hydrogen envelopes and their wind is H-free. The observed AC dust is thus synthesised by a chemical route that does not involve PAHs but rather bare carbon chains and rings (Cherchneff *et al.* 2000). However, WC stars are part of binary systems in which the companion is usually a OB star characterised by a H-rich wind, thus implying that hydrogen is present in the colliding wind region. But owing to the high gas

Table 1. Most important amorphous carbon (AC) dust stellar providers in our galaxy. Listed in the first column are: (1) the amount of AC dust formed over the star lifetime, (2) the region where dust forms, (3) the presence of hydrogen, (4) the gas density and temperature at which dust forms, and (5) the observed molecules related to AC dust synthesis. Value for supernovae are for SN 1987A (Ercolano *et al.* 2007) and for the SN progenitor of Cas A (Nozawa *et al.* 2010). Value for R CrB stars is an upper limit assuming all carbon condenses in AC dust.

Star	Carbon AGB	Type II Supernova
AC mass (M_{\odot})	$3 \times 10^{-3} - 1 \times 10^{-2}$	$7 \times 10^{-4} - 7 \times 10^{-2}$
Dust locus	Shocked inner wind	Ejecta
Hydrogen	Yes	Yes – not mixed with C
Gas density (cm^{-3})	$10^8 - 10^{13}$	$10^9 - 10^{12}$
Gas temperature (K)	Low: 1000 – 1500	High: 3000
Key species	C_2H_2	CO & SiO
Star	Carbon-rich Wolf-Rayet	R CrB
AC mass (M_{\odot})	0.1	2×10^{-6}
Dust locus	Colliding winds	Episodic clumps
Hydrogen	No	No except V854 Cen
Gas density (cm^{-3})	10^{10}	$10^9 - 10^{11}$
Gas temperature (K)	High: 3000	Medium: 1500 – 2500
Key species	No observation yet	C_2

temperatures, it is unlikely that the chemical routes responsible for PAHs synthesis may be active in these hot regions. Finally, R CrB stars are extremely rare, evolved low-mass stars exhibiting supergiant photospheric conditions and episodically ejecting clumps of gas rich in AC dust. Their wind is H-free but there exists one object, V854 Cen, which is H-rich and for which the UIR bands have been observed with ISO (Lambert *et al.* 2001). PAHs may therefore play a role in the formation process of AC dust in this specific object.

Studies on the formation of PAHs in circumstellar environments have focused on the prevalent AC dust makers, the carbon AGB stars, represented by the well-studied carbon star IRC+10216. We will thus concentrate on these stellar dust providers in the rest of this review.

3 Evidence for circumstellar PAHs in meteorites

Crucial information on the chemical composition, structure, and formation locus of stardust has been gained since the isolation of presolar grains in primitive meteorites and their study by laboratory microanalyses. Graphite grains bearing the isotopic composition resulting from the nucleosynthesis at play in low-mass stars have been isolated implying a formation locus in AGB outflows (Zinner 1997). Two basic graphite spherule morphologies are found, designated by “onion” and

cauliflower' (Bernatowicz *et al.* 2006). Two thirds of the onion-type spherules are characterised by concentric outer shells of well-crystallised graphite surrounding a nanocrystalline carbon core consisting of graphene curled sheets indicative of pentagonal ring insertion. One quarter of this core mass is in the form of small PAHs. Small aromatics including phenanthrene ($C_{14}H_{10}$) or chrysene ($C_{18}H_{12}$) have further been identified in the study of presolar graphite onion spherules. Those aromatics bore similar isotopic anomalies than their parent graphite circumstellar grains, indicating a possible formation in AGB winds (Messenger *et al.* 1998). The cauliflower spherules are formed of contorted graphene sheets with no nanocrystalline core. The morphology of these two types of spherules hint at dust condensation scenarios in AGB winds. The onion morphology indicates that the inner gas layers where dust forms are hotter, with long enough residence times to form dust precursors like PAHs and graphene sheets and allow the outer layers of the newly-formed dust grain to become well graphitised. The cauliflower structure on the other hand is indicative of a lower temperature inner wind and rapid motion outward of the shocked layers above the photosphere. Dust precursors like PAHs have formed and are included into graphene sheets but not enough time is given for these amorphous structures to become crystallised. An amorphous, less structured carbon spherule thus results from these milder inner wind conditions.

Therefore, there exists direct evidence of the presence of PAHs in the dust synthesis zone of carbon-rich AGB stars from the study of presolar grains extracted from meteorites. Moreover, it appears that PAHs do form as precursors before the end of the dust condensation process as found in the pyrolysis of hydrocarbons and in combustion processes like hydrocarbon-fueled flames (Frenklach & Warnatz 1987; Richter & Howard 2000).

4 Evidence for circumstellar PAHs from observations

The common fingerprints of PAHs in space are the emission of the UIR bands through excitation by a single ultraviolet (UV) photon. These bands can be detected in any circumstellar medium, providing the existence of a UV radiation field. The photospheric temperatures of carbon AGB stars are too low to produce a strong UV stellar radiation field capable of exciting PAH molecules in the dust formation zone. Buss *et al.* (1991) and Speck & Barlow (1997) observed the carbon star TU Tauri, part of a binary system with a blue companion providing for UV photons, and detected possible UIR bands. More recently, Boersma *et al.* (2006) analysed the SWS ISO spectra of several carbon stars including TU Tau and found UIR emission bands in the latter only. They ascribed the UIR spectrum to PAH excitation by the UV radiation field of the companion star when other single carbon stars in the sample were devoid of UIR bands in their spectrum. They pointed out that PAHs may be present in any carbon star but not observable due to the lack of exciting radiation. Another probe to the presence of PAHs in AGB stars is the study of S stars, *i.e.*, oxygen-rich AGB stars on the verge of dredging up carbon in their photosphere to become carbon stars. They are characterised by a photospheric C/O ratio less than but ≈ 1 and by the fact that they do not yet

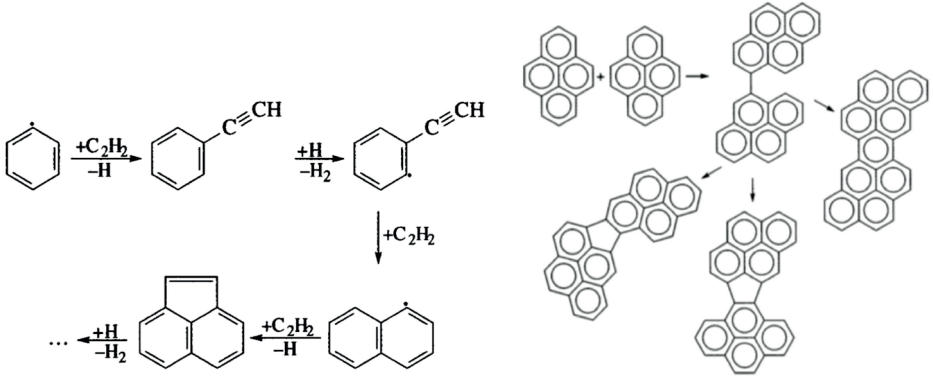


Fig. 1. *Left:* growth of PAHs according to the H abstraction- C_2H_2 addition (HACA) mechanism proposed by Frenklach *et al.* (1984). *Right:* growth of aromatic structures via the dimerisation and coalescence of PAHs proposed by Mukherjee *et al.* (1994).

produce carbon dust. Smolders *et al.* (2010) analysed IR low resolution spectra taken by Spitzer of several galactic S stars. Four of them characterised by C/O ratios very close to 1 show the UIR bands in their spectra. Among those, three stars show weak extended $6.2 \mu\text{m}$ emission bands characteristic of PAHs with a mixture of aliphatic and aromatic bonds excited by a weak UV field. S stars possess a dual chemistry in their dust formation zone due to the pulsation-induced shocks as shown by Cherchneff (2006). As a result of non-equilibrium chemistry, O-bearing molecules form close to the stellar photosphere whereas hydrocarbons (*e.g.* C_2H_2) form at larger radii ($\sim 3 R_\odot$). PAHs may thus form at lower temperatures and densities, favouring small disordered aromatic structures linked by aliphatic bonds. At these radii, the formation of AC dust may be hampered by the low densities and residence time resulting in a population of small aromatic/aliphatic structures that can not turn into dust but are responsible for the observed UIR bands.

5 Chemical routes to PAH formation in flames

Incomplete combustion produces soot particles where PAHs are observed to play a key role in the inception and growth process of AC grains (Richter & Howard 2002). The formation of the single aromatic ring benzene (C_6H_6) represents the rate limiting step to soot synthesis as it is the natural passage from the aliphatic structure of the fuel hydrocarbons to the closed ring aromatic structures which are the backbones of combustion products like soot. Three dominant routes to first ring closure have been identified in flames. The prevalent route involves the recombination of two propargyl radicals (C_3H_3) to form cyclic and linear benzene and the benzene radical phenyl (C_6H_5) according to the following reactions



and

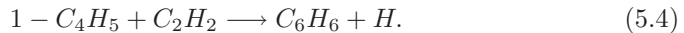


These routes were first studied and proposed by Miller & Mellius (1992) as important sources of aromatic rings in flames. The propargyl recombination into one aromatic ring involves many reactive channels leading to the formation of several intermediates such as fulvene ($C_5H_4CH_2$), observed in flames (Miller & Klippenstein 2003; Tang *et al.* 2006). In pyrolytic shock tube study of propargyl reactions, Scherer *et al.* (2000) show that the direct formation of benzene via Reaction 5.1 is prevalent over 5.2.

The other two chemical pathways to first aromatic ring closure in acetylenic flames involve the reaction of 1-buten-3-ynyl, $1-C_4H_3$ with acetylene proposed by Frenklach *et al.* (1984), and the reaction of 1,3-butadienyl, $1-C_4H_5$ with acetylene proposed by Cole *et al.* (1984). They lead to the following final products via direct pathways involving chemically activated isomerizations (Westmorland *et al.* 1989)



and



In the context of PAH formation in circumstellar outflows, the above pathways will occur if the reactants are present in the gas. The formation of C_3H_3 results from the reaction of C_2H_2 and methylene, CH_2 , whereas vinyl-acetylene, C_4H_4 will form C_4H_3 and C_4H_5 from its reaction with atomic hydrogen.

Once benzene is made available in the gas, larger PAHs may grow according to three different scenarios. The first scenario was proposed by Frenklach *et al.* (1984) and involves the growth of large aromatic structures through sequential hydrogen abstraction and acetylene addition (referred as the HACA mechanism). The formation of radical sites on the aromatic structure enables C_2H_2 to add and finally form a new aromatic ring as depicted in Figure 1. The second route was proposed by Mukherjee *et al.* (1994) in their study of the pyrolysis of pyrene ($C_{16}H_{10}$). In the absence of PAH species arising from the HACA growth pathway, they derive that the dominant weight growth channel was the direct polymerisation of PAHs through the initial formation of PAH dimers, as illustrated in Figure 1 for pyrene. Finally, a third growth pathway was proposed by Krestinin *et al.* (2000) in their study of acetylene pyrolysis and involves the polymerization of polyynes on a surface radical site of any small grain seed as illustrated in Figure 2. This hypothesis is supported by the observation of small polyynes (C_4H_2 , C_6H_2 , C_8H_2) along with PAHs in the sooting zone of flames (Cole *et al.* 1984).

One should bear in mind that there still exists controversy on the prevalent pathways to AC grain growth (for more detail, see Jäger *et al.*, this volume). Despite the fact that the HACA mechanism is largely used to describe the growth of aromatic rings, it does not provide a satisfactory explanation for the early formation in sooting flames of small carbonaceous nanoparticles made of a few aromatic rings linked by aliphatic bonds (Minutolo *et al.* 1998).

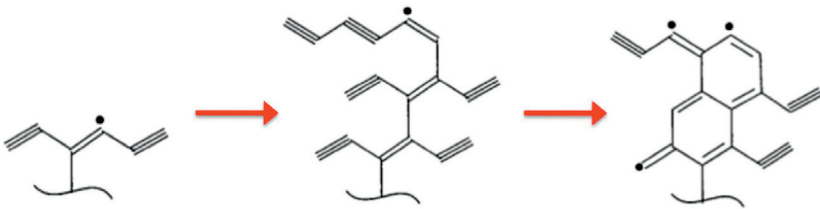


Fig. 2. Polymerization of polyynes on a surface radical site and its transformation into aromatic structures leading to breeding of radical sites and rapid growth (from Krestinin 2000).

6 PAH yields from existing studies

Only a few studies have been conducted to date on the formation of PAHs in the outflows of carbon AGB stars. Frenklach & Feigelson (1989) first applied the HACA mechanism to the steady wind of carbon stars to derive dust masses and PAH yields. They highlighted the existence of a temperature window (900 K – 1100 K) for which PAH growth occurred. However, their treatment of the stellar wind was not taking into account the action of shocks active above the stellar photosphere. Therefore, the gas density dropped by orders of magnitude over short time scales impeding the efficient synthesis of PAHs and dust grains. Cherchneff *et al.* (1992) studied the formation of PAHs using the HACA mechanism for PAH growth but including the newly proposed Reactions 5.1 and 5.2 for first ring closure. They include a treatment of the effects of shocks on the gas above the photosphere but also used a Eulerian treatment for the steady wind. The resulting PAH yields were small for all the various wind models and the shocked layers close to the stars experiencing quasi-ballistic trajectories were proposed as possible loci for a more efficient synthesis of PAHs. Cadwell *et al.* (1994) studied the induced nucleation and growth of carbon dust on pre-existing seed nuclei. Finally Cherchneff & Cau (1992) and Cau (2002) investigated the formation of PAHs and their dimers in the shocked inner wind of IRC+10216, using a Lagrangian formalism that follows the post-shock gas trajectories induced by the periodic shocks and the stellar gravitational field, following a study from Bowen (1988). The formation of PAHs and their dimers occurred at higher temperatures than those of Frenklach & Feigelson, typically for $T \leq 1700$ K, in agreement with a recent laboratory study of soot formation in low-temperature laser-induced pyrolysis of hydrocarbons by Jäger *et al.* (2009). The deduced PAH yields were sufficient to account for the mass of PAHs included in the nanocrystalline cores of graphite spherules. However, they could not account for the total mass of AC dust formed in the wind, indicating that further dust growth mechanisms must occur such as the deposition of acetylene on the surface of dust seeds.

In view of these existing theoretical studies and new observational results, the ubiquity of PAHs in the inner wind of carbon AGB stars is almost certain.

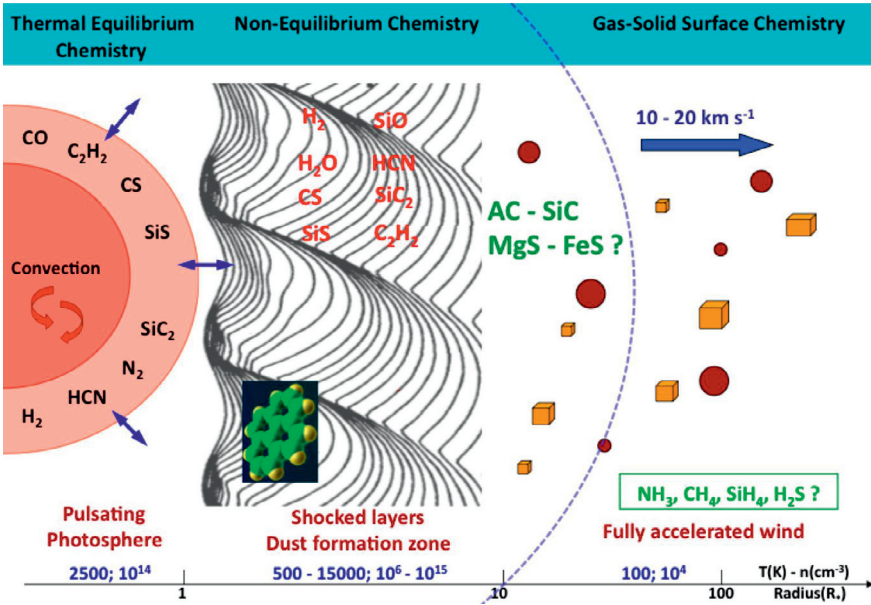


Fig. 3. A schematic representation of the inner envelope of IRC+10216. The gas parameters span the values indicated as a function of radius. The quasi-balistic trajectories of the gas layers are shown according to Bowen (1988). Dust grains are represented by small squares and balls. The mentioned molecules form according to TE and non-TE chemistry depending on their locus. PAHs form in the inner wind between $1 R_*$ and $\sim 5 R_*$.

However, a complete model that includes the various pathways of PAH formation and growth to AC dust as described in Section 5, and applied to the shocked inner layers of carbon stars is still lacking.

7 New results on benzene formation in IRC+10216

The carbon star IRC+10216 has been extensively studied due to its proximity and its stage of evolution that guarantees an extremely rich chemistry in its wind (Olofsson 2006). The dust forms close to the star in gas layers that experience the periodic passage of shocks induced by the stellar pulsation. The energy spectral distribution of IRC+10216 is well reproduced by a dust composition mainly dominated by amorphous carbon with a small contribution from silicon carbide and magnesium sulphide (Keady *et al.* 1988; Ivezić & Elitzur 1996; Hony *et al.* 2002). Acetylene has been detected in the mid-infrared close to the star with high abundances (Keady & Ridgway 1993; Fonfría *et al.* 2008). A schematic representation of the inner wind of IRC+10216 is given in Figure 3 with the gas temperature and density as a function of radius, the various chemical states of the gas and

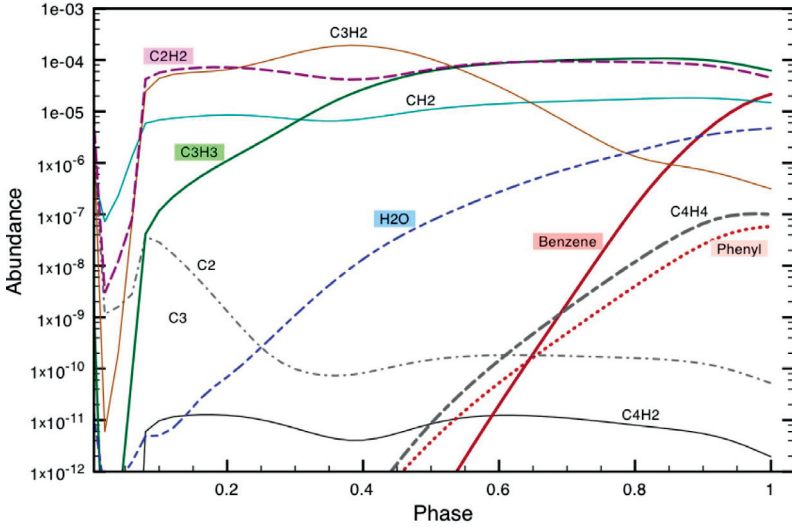


Fig. 4. Molecular abundances with respect to total gas as a function of pulsation period phase at $1.5 R_{\star}$. The shock strength at this radius is 17.9 km s^{-1} .

the molecules observed. Briefly, molecules are formed at chemical equilibrium in the photosphere owing to the high gas temperatures and densities. They are then reprocessed by the periodic passage of shocks induced by the stellar pulsation. In the hot postshock gas, molecules are destroyed by collisions and reform during the adiabatic cooling of the gas as shown in Figure 3. Prevalent species (*e.g.* CO, HCN, CS, C_2H_2) reform with abundances close to their TE values whereas the collisional breaking of CO after the shock front induces a new chemistry responsible for the formation of 'exotic' molecules of lower abundances and not expected to form in C-rich environments. As an example, the radical hydroxyl, OH, quickly forms and triggers the synthesis of O-bearing species like SiO in the inner wind (Willacy & Cherchneff 1998). Thus, an active non-equilibrium chemistry is responsible for the reprocessing of molecules in the dust formation zone of AGB stars (Cherchneff 2006).

PAHs do not escape this shock molecular reprocessing and form once the adiabatic cooling of the shocked gas layers produces the temperature range conducive to the closure of the first aromatic ring (Cherchneff & Cau 1998; Cau 2002). We model the inner wind of IRC+10216 using the Lagrangian formalism of Willacy & Cherchneff (1998) but considering gas densities lower by one order of magnitude than their values for those were slightly overestimated (Agúndez & Cernicharo 2006). An updated chemistry is used that includes the formation of the major O/Si/S/C-bearing molecules as well as the routes to the closure of the first aromatic ring described in Section 5. The results for the adiabatically-cooled post-shock gas layer located at $1.5 R_{\star}$ are shown in Figure 4, where molecular abundances with respect to total gas are presented versus phase of the pulsation

period. As previously mentioned, benzene, C_6H_6 forms once the gas has cooled to temperatures <1700 K, while phenyl, C_6H_5 is consumed in benzene through its reaction with H_2 . The formation of C_6H_5 is triggered by the recombination of propargyl radicals, C_3H_3 , according to Reaction 5.2. The low abundances of C_4H_2 hint at the fact that PAH growth beyond benzene cannot proceed through polyynic polymerization but may rather involve the HACA mechanism and/or the direct coalescence of PAHs. As expected, the abundances of small carbon chains C_2 and C_3 peak at very early phases where the high temperatures precludes the formation of aromatics. However, their abundances are always low for the overabundance of hydrogen favours the formation of hydrocarbons over bare carbon chains.

A secondary important result is the formation of water, H_2O , in the inner wind of IRC+10216. Our results show that H_2O already forms at radius $1.5 R_*$. OH is quickly synthesised after the shock front at early phases by the reaction of atomic oxygen stemming from the partial dissociation of CO with the newly recombined H_2 . H_2O is then synthesised from the reaction of OH with H_2 . Water has recently been detected with Herschel/HIFI in the carbon star V Cygni (Neufeld *et al.* 2010) and the S star Chi Cygni (Justtanont *et al.* 2010), and with Herschel/SPIRE/PACS in IRC+10216 (Decin *et al.* 2010). Those detections imply an inner origin for H_2O . Several mechanisms have been proposed since the first detection of H_2O in IRC+10216 (Melnick *et al.* 2001), and include the vaporisation of icy comets orbiting carbon stars (Melnick *et al.* 2001), the synthesis of water on dust grain surfaces in the intermediate envelope (Willacy 2004), and the photodissociation of ^{13}CO by interstellar UV photons penetrating clumps (Decin *et al.* 2010). Our preliminary results point to a more genuine mechanism for water formation which results from the non-equilibrium chemistry induced by shocks in the inner wind of IRC+10216. The presence of water in the dust formation zone indicates that PAH formation and growth processes may be close to those found in acetylenic flames where oxidation by atomic O and O_2 occurs. While the amounts of atomic O and dioxygen remain low at all phases in the gas layers under study, OH may attack propargyl radicals to form the formyl radical HCO. Therefore, the benzene abundances and yields shown in Figure 3 may be overestimated due to the fact that the oxidation of hydrocarbons has not yet been included in the chemistry. Nevertheless, our preliminary results indicate a rapid conversion of hydrocarbons into monoaromatic rings.

8 Other environments conducive to PAH synthesis

Apart from the winds of carbon AGB stars, there may exist other circumstellar media where PAHs form. One such environment is the wind of one hydrogen-rich R Corborealis star, V854 Centauri. R CrB stars are extremely rare, evolved, low-mass stars showing supergiant photospheric signatures. They have lost their entire hydrogen shell and experience strong fading on periods of the order of a few years. This sudden drop in luminosity is ascribed to the random ejection of AC dust clouds along the line of sight. V854 Cen is a peculiar R CrB as it has retained some hydrogen in its wind. Of particular interest is the detection of red

emission (RE) bands at minimum whose wavelengths match those of a series of emission bands observed in the proto-planetary nebula, the Red Rectangle (Rao & Lambert 1993a). Furthermore, those frequencies almost match some of the Diffuse Interstellar Bands (DIBs) observed in the ISM. The UIR bands were also detected with ISO in V854 Cen pointing to a PAH component in the stellar wind while the Swan and Phillip bands of C_2 were observed during the decline to light minimum (Rao & Lambert 1993b, 2000; Lambert *et al.* 2001). The stellar temperature is high (~ 7500 K) indicating that despite the presence of hydrogen, the formation of bare carbon chains should proceed, as confirmed by the presence of C_2 . As the temperature of the cloud drops with expansion and because of the surrounding hydrogen, polyene molecules could form along with already formed carbon monocyclic and aromatic rings, leading to a growth mechanism for dust involving the polymerization of polyynes on radical sites (Krestinin *et al.* 2000). This growth mechanism should partly result in a left-over population of nanoparticles made of units of one or two aromatic rings linked by aliphatic bonds, as observed at high temperatures in sooting flames (Minutolo *et al.* 1998). Hence the formation of PAHs in V854 Cen occurs along chemical pathways different from those involved in AGB winds (*e.g.*, the HACA mechanism) and these aromatic nanoparticles could be serious contenders as carriers of the RE and the DIBs.

9 Conclusion

The formation of PAHs from the gas phase and their role in the synthesis of carbon dust occurring in hydrogen-rich, low-temperature circumstellar environments like AGB stellar winds are well accepted. Small PAHs act as building blocks in the formation of carbonaceous nanoparticles precursors to dust seeds whereas large ones are direct intermediates to the synthesis of AC grains. A population of small PAHs will survive the AC dust condensation zone and is probably responsible for the UIR bands observed in certain AGB winds. However, most PAHs formed in the inner gas layers will be quickly included into AC dust grains and in this context, carbon AGB stars are not important PAH providers to the ISM. Despite the fact that circumstellar PAHs are less studied than their interstellar ubiquitous counterparts stemming from AC dust processing in the ISM, they are as important, being at the origin of the carbon dust formation process in evolved stars.

References

- Agúndez, M., & Cernicharo, J., 2006, *ApJ*, 650, 374
- Allamandola, L.J., Tielens, A.G.G.M., & Barker, J.R., 1985, *ApJ*, 290, L25
- Bernatowicz, T., Croat T.K., & Daulton, T.L., 2006, *M.E.S.S.*, 943, 109
- Boersma, C., Hony, S., & Tielens, AGGM, 2006, *A&A*, 447, 213
- Bowen, G.H., 1988, *ApJ*, 329, 299
- Buss, R.H. Jr, Tielens, A.G.G.M., & Snow, T., 1991, *ApJ*, 372, 281
- Cadwell, B.J., Wang, H., Feigelson, E.D., & Frenklach, M., 1994, *ApJ*, 429, 285

- Cau, P., 2002, *A&A*, 392, 203
- Cherchneff, I., Barker, J.R., & Tielens, A.G.G.M., 1992, *ApJ*, 401, 269
- Cherchneff, I., 1998, *ISAA*, 4, 265
- Cherchneff, I., & Cau, P., 1999, in *Asymptotic Giant Branch Stars*, IAU Symp. 191, ed. T. Le Bertre, A. Lebre, & C. Waelkens, 251
- Cherchneff, I., LeTeuff, Y., Williams, P.M., & Tielens, A.G.G.M., 2000, *A&A*, 357, 572
- Cherchneff, I., 2006, *A&A*, 456, 1001
- Cole, J.A., Bittner, J.D., Longwell, J.B., & Howard, J.B., 1984, *Combustion and Flame*, 56, 51
- Decin, L., Agúndez, M., Barlow, M.J., *et al.*, 2010, *Nature*, 467, 64
- Ercolano, B., Barlow, M.J., & Sugerman, B.E.K., 2007, *MNRAS*, 375, 753
- Fonfría, J.P., Cernicharo, J., Richter, M.J., *et al.*, 2008, *ApJ*, 673, 445
- Frenklach, M., Clary, D.W., Gardiner, W.C. Jr, & Stein, S.E., 1984, 20th Symp. (Int.) on Combustion, The Combustion Institute, 887
- Frenklach, M., & Warnatz, J., 1987, *Combustion. Sci. Tech.*, 51, 265
- Frenklach, M., & Feigelson, E.D., 1989, *ApJ*, 341, 372
- Haynes, B.S., & Wagner, B.J., 1981, *Prog. Energy Combust. Sci.*, 7, 229
- Hony, S., Waters, L.B.F.M., & Tielens, A.G.G.M., 2002, *A&A*, 390, 533
- Ivezić, J., & Elitzur, M., 1996, *MNRAS*, 279, 1019
- Jäger, C., Huisken, F., Mutschke, H., *et al.*, 2009, *ApJ*, 696, 706
- Jäger, C., Mutschke, H., Henning, T., & Huisken, F., 2011, this volume
- Justtanont, K., Decin, L., & Schoier, F.L., 2010 [[arXiv:1007.1536](https://arxiv.org/abs/1007.1536)]
- Keady, J.J., Hall, D.N.B., & Ridgway, S.T., 1988, *ApJ*, 326, 832
- Keady, J.J., & Ridgway, S.T., 1993, *ApJ*, 199, 214
- Kifonidis, K., Plewa, T., Scheck, L., Janka, H.-Th., & Müller, E., 2006, *A&A*, 453, 661
- Krestinin, A.V., Kislov, M.B., Raevskii, O.I., *et al.*, 2000, *Kinetics and Catalysis*, 41, 90
- Lambert, D., Rao, N.K., Pandey, G., & Evans, I.I., 2001, *ApJ*, 555, 925
- Léger, A., & Puget, J.L., 1984, *A&A*, 137, L5
- Melnick, G., Neufeld, D.A., Ford, K.E., *et al.*, 2001, *Nature*, 412, 160
- Messenger, S., Amari, S. Gao, X., *et al.*, 1998, *ApJ*, 502, 284
- Miller, J.A., & Melius, C.F., 1992, *Combustion and Flame*, 91, 21
- Miller, J.A., & Klippenstein, S.J., 2003, *J. Phys. Chem. A*, 107, 7783
- Minutolo, F., Gambi, G., & D'Alessio, A., 1998, 27th Symp. (Int.) on Combustion, The Combustion Institute, 1641
- Mukherjee, J., Sarofim, A.F., & Longwell, J.P., 1994, *Combustion and Flame*, 96, 191
- Neufeld, D.A., Gonzalez-Alfonso, E., Melnick, G., *et al.*, 2010 [[arXiv:1007.1235](https://arxiv.org/abs/1007.1235)]
- Nozawa, T., Kozasa, T., Taminaga, N., *et al.*, 2010, *ApJ*, 713, 356
- Olofsson, H., 2006, *Rev. Modern Astron.*, 19, 75
- Rao, N.K., & Lambert, D., 1993a, *MNRAS*, 263, L27
- Rao, N.K., & Lambert, D., 1993b, *AJ*, 105, 1915
- Rao, N.K., & Lambert, D., 2000, *MNRAS*, 313, L33
- Richter, H. & Howard, J.B., 2000, *Prog. Energy. Comb. Sci.*, 26, 565

- Richter, H., & Howard, J.B., 2002, *Phys. Chem. Chem. Phys.*, 4, 2038
- Scherer, S., Just, Th., & Frank, P., 2000, *Proc. Comb. Institute*, 28, 1511
- Smolders, K., Acke, B., Verhoelst, T., *et al.*, 2010, *A&A* 514, L1
- Speck, A., & Barlow, M.J., 1997, *Ap&SS*, 251, 115
- Tang, W., Tranter, R.S., & Brezinsky, K., 2006, *J. Phys. Chem. A*, 110, 2165
- Tielens, A.G.G.M., 2008, *ARAA*, 46, 289
- Westmoreland, P.R., Dean, A.M., Howard, J.B., & Longwell, J.P., 1989, *J. Phys. Chem.*, 93, 8171
- Willacy, K., & Cherchneff, I., 1998, *A&A*, 330, 676
- Willacy, K., 2004, *ApJ*, 600, L87
- Zinner, E., 1997, *AIPC*, 402, 3

INSIGHTS INTO THE CONDENSATION OF PAHS IN THE ENVELOPE OF IRC +10216

L. Biennier¹, H. Sabbah^{1,2}, S.J. Klippenstein³, V. Chandrasekaran^{1,4},
I.R. Sims¹ and B.R. Rowe¹

Abstract. The mechanisms of nucleation and growth of carbon dust particles in circumstellar envelopes of carbon-rich stars in the red giant and AGB phases of their evolution are poorly understood. It has been proposed that the transition of gas phase species to solid particles, is achieved by the formation of a critical nucleus composed of two PAHs held together by van der Waals forces. Some insights into the validity of the nucleation of PAH molecules in the envelope can be gained through the investigation of the thermodynamics of dimers, representing the first stage towards condensation. We have performed experiments to identify the temperature range over which small PAH clusters form in saturated uniform supersonic flows. The kinetics of the formation has also been investigated. The experimental data have been combined with theoretical calculations. We unambiguously demonstrate that the association of small PAHs such as pyrene (C₁₆H₁₀) is slower than the destruction of the dimer in warm and hot environments such as IRC +10216. Our findings challenge a formation model based on the physical stacking of small PAH units in circumstellar shells of carbon rich stars.

1 Introduction

The outflows of carbon rich stars in their asymptotic giant branch phase (AGB) are the primary sources of carbon dust (Henning & Salama 1998). AGB stars

¹ Institut de Physique de Rennes, Équipe: “Astrochimie Expérimentale”, UMR CNRS 6251, Université de Rennes 1, Campus de Beaulieu, 35042 Rennes Cedex, France

² *Current address:* Zarelab, Chemistry Department, Stanford University, CA 94305, USA

³ Chemical Sciences and Engineering Division, Argonne National Laboratory, Argonne, IL 60439, USA

⁴ *Current address:* Institut des Sciences Moléculaires, UMR CNRS 5255, Université Bordeaux 1, 33405 Talence, France

lose up to 80% of their original mass in the form of an envelope, with typical loss rates of 10^{-6} to $10^{-4} M_{\odot} \text{ yr}^{-1}$. There is limited observational evidence for the formation of dust in other sources, such as Supernovae (SNe) and novae, but their relative importance as sources of interstellar dust, are still uncertain (Jones 2005).

The determination of the physical conditions under which dust is generated is critical. Estimates of the temperature and pressure of circumstellar envelopes strongly depend on various model assumptions, such as mass loss rates, gas density outflow, and velocity. Observations have revealed that the envelope of evolved stars is huge, extending over 10^4 to 10^5 stellar radii. Close to the photosphere ($< 5 R_{\star}$), the gas is dense ($n \geq 10^{10} \text{ molecule}\cdot\text{cm}^{-3}$) and warm ($T \sim 1500 \text{ K}$). As the matter flows away from the star, it expands ($n \leq 10^5 \text{ molecule}\cdot\text{cm}^{-3}$) and cools rapidly down to 25 K at several hundreds of R_{\star} (Ziurys 2006).

The most refractory material composing the atmosphere, such as carbides, nucleates first in the innermost region, even inside the photosphere. Once formed, they act as nuclei sites for heterogeneous condensation of more volatile carbonaceous molecules. C condensation is delayed until homogeneous nucleation can occur at higher supersaturation levels farther out from the star (Bernatowicz *et al.* 2006). Some complexity is added to this already debated picture, by the propagation of shock waves, produced by stellar pulsations, which greatly enhance the density and temperature just after the shock front. Because of the variety of physical conditions, the chemistry varies substantially throughout the envelope. In the inner shell ($< \text{a few } R_{\star}$), the temperature and density are sufficiently high that thermodynamic equilibrium governs molecular abundances of a number of molecules (Ziurys 2006). This assumption is confirmed by astronomical observations in the infrared, which have shown that stable, closed-shell species such as CS, NH_3 , HCN, and HCCH have high abundances in the inner envelope of the well studied IRC+10216 carbon star ($\approx 10^{-3}$ to 10^{-6} , relative to H_2).

As the density falls with radius, interstellar UV photons penetrate the atmosphere and generate reactive species through photodissociation that subsequently participate in a complex gas-phase chemistry to produce daughter molecules in the outer envelope. Interferometer maps of IRC +10216 reveal radicals such as CN, CCH, C_3H , and C_4H organized in shell-like structures near the envelope edge (Guelin *et al.* 1993).

It is generally accepted that the production pathway determines the resulting structure, chemical composition, and morphology of the grains (Jager *et al.* 2009). However, the formation pathways of carbonaceous grains from molecular components and clusters, evoked by Jager in this volume (2010), are not well understood. From a chemical viewpoint, the high abundance of hot acetylene (Fonfria *et al.* 2008) and the scarcity of oxydizing molecules in circumstellar envelopes of carbon rich stars are expected to lead to the production of carbonaceous particles through processes similar to the ones encountered in terrestrial low pressure flames. The analogy strongly suggests the presence of Polycyclic Aromatic Hydrocarbons (PAHs) as building blocks, intermediates or side products in the generation of carbon dust particles. Remarkably, the aromatic IR emission features, characteristic of PAHs, are generally not seen in the spectra of carbon-rich

AGB stars, but are systematically detected in carbon-rich post-AGB objects and Planetary Nebulae. Two interpretations are contending to explain the infrared emission features in the spectra of the latter sources. It can be the consequence of efficient pumping arising from the increased effective temperature of the central object as it loses its remnant envelope and shifts to the blue in the Hertzsprung-Russell diagram on its way to becoming a white dwarf. Alternatively, it may be the result of photochemical processing of hydrogenated amorphous carbon (HAC) material formed in the outflows. The ground-based and ISO/SWS detection of the aromatic infrared emission features in the spectra of the carbon-rich AGB star TU Tau (Boersma *et al.* 2006), likely irradiated by its blue binary companion, does not provide an unambiguous argument in favor of either of the scenarios. Independent of the formation pathways actually followed, the presence of PAH features in the IR spectra of carbon-rich post-AGB objects and planetary nebulae (PNe) lends indirect support for the importance of late-type stars as sources for PAHs in the interstellar medium (Tielens 2008).

Theoretical studies on the chemical pathways towards PAHs in circumstellar envelopes are reviewed in this conference by Cherchneff (2010). Briefly, the formation of PAHs from small gaseous hydrocarbons in the circumstellar envelopes was initially proposed by Frenklach & Feigelson (1989b). Their study was the first to introduce chemical kinetics in those atmospheres. The chemical scheme considered was largely inspired from combustion studies and relies heavily on the presence of acetylene C_2H_2 and radicals such as C_2H . Reactions involving oxygen were removed, whereas benzyne C_6H_4 was introduced in the network. The dominant PAH formation pathway was identified as the hydrogen abstraction acetylene addition (HACA) route. Cherchneff revised and extended the scheme, explicitly including radicals, such as C_3H_3 and aromatics up to $C_{18}H_{12}$ (Cherchneff *et al.* 1992). In the study, Cherchneff *et al.* considered that the gas density was so low that collisions did not couple efficiently the vibrational and translational degrees of freedom. As a consequence, PAH molecules did end up with vibrational temperatures significantly lower than gas kinetic temperature. Nevertheless, the conclusion was that PAH formation yields were very sensitive to gas density and temperature, and that they were much smaller than values inferred from the observed dust content of late type carbon rich stellar envelopes. They suggested that the PAHs may form instead very close to the photosphere. Allain *et al.* further explored the processes affecting PAH formation and growth (Allain *et al.* 1997). They carried out calculations of the PAH temperature by balancing heating via collisions with gas particles and absorption of stellar emission and cooling via emission from the rotational and vibrational levels. In their work they treated heating processes simultaneously and found that low PAH temperatures enable an efficient formation and growth of PAHs in the circumstellar envelopes of C-stars. The calculated PAH formation rate was large enough to support the idea that PAHs could constitute the first step in the formation of dust grains. The processes, either chemical or physical, that could explain the transition from these large molecules to small dust grains, were however not investigated. Nucleation triggered by association of PAH molecules formed in the gas phase, considered as a key step in

controversial models of soot formation in flames (Frenklach 2002; Frenklach & Wang 1991), was initially discounted as the main mechanism of carbon dust production (Cadwell *et al.* 1994; Cherchneff *et al.* 1992; Frenklach *et al.* 1989a). Astrophysical models were favoring high temperature nucleation of mineral particles in or near the photosphere, onto which PAH molecules could later condense (Cherchneff & Cau 1998). In an attempt to assess alternative pathways of dust formation, which could be potentially competing, Cherchneff (2000) investigated the formation of van der Waals bound PAH dimers in the envelopes, considering species as small as benzene (C_6H_6) and up to coronene ($C_{24}H_{12}$). The conclusion was that PAH dimers could act as dust nuclei in the inner shells (Cherchneff 2000). Cau (2002) later on included periodic shocks in the model and inferred that the amount of PAHs and dimers produced, considering aromatics containing up to 7 rings, is not enough to explain the formation of carbon dust in the atmosphere of the IRC +10216 star, but that it can account for the formation of the small disordered cores of the kind observed in presolar grains (Cau 2002).

In this paper, we re-examine the condensation of PAH molecules in the envelopes of carbon rich stars based on high level theoretical calculations supported by state-of-the-art laboratory experiments related to the thermodynamics and kinetics of the process. Our findings are applied to the envelope of the evolved red giant, IRC +10216.

2 Combined experimental/theoretical approach

Laboratory experiments have been conducted to identify the temperature range under which pyrene ($C_{16}H_{10}$) molecules dimerize (Sabbah *et al.* 2010). Our experimental approach is briefly summarized below to provide the reader with some experimental background (Sabbah *et al.* 2010). The experiments were performed using a continuous flow CRESU apparatus (Canosa *et al.* 2008; Dupeyrat *et al.* 1985), adapted for condensable species such as PAHs (Goulay *et al.* 2006). This chemical reactor is designed to generate dense uniform flows using a Laval nozzle, over a wide range of temperatures (60–470 K) and containing high (supersaturated) concentrations of PAH vapors. The time evolution of the chemical species present in the reactor is monitored by a time of flight mass spectrometer (TOFMS) equipped with a VUV laser for photoionization of the neutral reagents and products. The onset of nucleation is explored for a set of flow temperatures. It is evidenced by the collapse of the PAH ion signal above a certain initial PAH concentration. At these high degrees of supersaturation, dimers may be considered as critical nuclei within the framework of classical nucleation theory. Once they are formed, they go on to react rapidly with more monomer to form trimers and larger clusters. After the identification of the temperature range over which nucleation is occurring, we proceed to kinetics measurements on dimerization within this range, but at lower PAH monomer concentrations. This yields the apparent second order rate coefficient for removal of PAH monomer, according to simple second-order kinetics.

The experimental results are coupled with theoretical calculations that employ careful consideration of the intermolecular interaction energies and intermolecular

dynamics to estimate the binding energy, equilibrium constant, and rate coefficient (Sabbah *et al.* 2010). The theoretical analysis employs a sum of atom-atom potentials to describe the intermolecular interactions. The parameters in this potential are designed to reproduce the equilibrium binding energies from high level calculations for a range of small PAH dimers, while at the same time accurately modeling the interactions for the large separations that span the transition state region for the association. The analysis focuses on the rigid body dynamics of the two PAH molecules, and employs transition state theory and trajectory simulations to examine the high pressure addition kinetics. Predictions for the equilibrium constant are obtained from Monte Carlo integration of the classical phase integral representation of the intermolecular partition function. The intramolecular partition functions of the monomer are assumed to be invariant to the dimerization process. These quantitative coupled anharmonic predictions for the equilibrium constant are used in the following analysis.

3 Astrophysical implications

The stable cluster structures of PAHs ranging from pyrene ($C_{16}H_{10}$) to circumcoronene ($C_{54}H_{18}$) have been explored theoretically recently (Rapacioli *et al.* 2006). Stacking PAH molecules was found to yield the most stable motif. The atomistic model developed in that work was then used in molecular dynamics simulations to study the nucleation and evaporation of coronene ($C_{24}H_{12}$) clusters. Rapacioli *et al.* (2006) found that under cold interstellar conditions, most of the collisions lead to cluster growth. They claimed that PAH clusters could represent the missing link between small carbonaceous grains and free isolated PAH molecules. Here we extend the exploration to the much warmer environment of the envelope of a late carbon star in which PAHs are supposedly generated and the existence of PAH clusters postulated. We first describe below the physical conditions characterizing the extensively studied, albeit not fully understood, envelope of IRC+10216. This late carbon rich star is one of the brightest sources in the infrared sky as a result of thermal re-emission by dust.

The modeling of infrared astronomical observations, led Fonfria *et al.* to divide the envelope in concentric regions (Fonfria *et al.* 2008). They first distinguish the inner shell comprised between the stellar photosphere and about $5 R_{\star}$. The outer edge corresponds to the first grain formation zone. Radiation pressure on grains, together with momentum coupling of gas and grains, strongly accelerate the gas up to $v_{\text{exp}}(r) \sim 11 \text{ km s}^{-1}$. In the intermediate envelope, the gas expands adiabatically until it reaches $\sim 20 R_{\star}$ where it is strongly accelerated for a second time up to its terminal velocity $\sim 14.5 \text{ km s}^{-1}$. The second acceleration zone corresponds to the second dust formation layer.

In this work, we adopt the radial kinetic temperature profile derived from the best fit of observed C_2H_2 lines (Fonfria *et al.* 2008) with an effective stellar temperature, $T_{\text{eff}} \sim 2330 \text{ K}$. The temperature of molecules such as PAHs in the extended atmosphere is governed by balancing heating and cooling processes. PAH molecules are heated by (1) collisions with abundant H_2 gas; and (2) absorption of

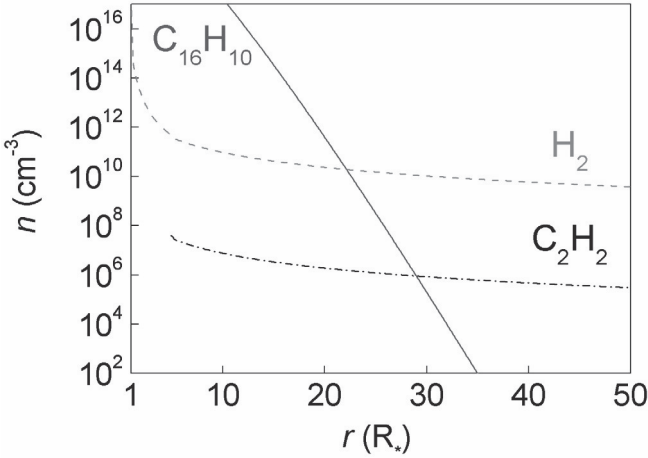


Fig. 1. Minimum pyrene abundance for condensing 10% of the monomers versus the distance from the central star IRC +10216 under a high molecular hydrogen density scenario from Agundez & Cernicharo (2006). Molecular abundances of H_2 (Agundez & Cernicharo 2006) and C_2H_2 (Fonfria *et al.* 2008) are indicated for comparison. The condensation is governed by the PAH temperature which slowly decouples from the gas because of the high number of collisions. The difference between the gas kinetic temperature and the internal pyrene temperature initially null at the photosphere rises up to a maximum of 250 K at around $5 R_*$ and then slowly decreases down to 200 K at $25 R_*$.

central star radiation, which peaks in the near infrared. As small PAH molecules do not absorb efficiently in this energy range, heating is therefore mainly ensured by collisions with molecular hydrogen. Farther from the central star, the total density drops, collisions become less frequent and the vibrational temperature of the PAHs may then decouple from the kinetic temperature of the gas. The main cooling mechanism has been identified as cascade emission of infrared photons. We follow the approach developed by Cherchneff *et al.* to derive the vibrational temperature of pyrene. Adopting a spherical geometry and neglecting bipolar outflow cavities, the density profile, $n(r)$, is given by the law of conservation of mass and therefore depends linearly on the mass loss rate and the expansion velocity:

$$\dot{M} = n(r) \mu m_H v_{\text{exp}}(r) 4\pi r^2 \quad (3.1)$$

with m_H , the mass of the hydrogen atom, and $\mu \sim 2$ assuming that all hydrogen is molecular. Following the work of Agundez (Agundez *et al.* 2006), we consider two different density profiles of the gas across the envelope hence bracketing the range of mass loss rates.

The equilibrium constant for pyrene dimerization (Sabbah *et al.* 2010) determined from the combined experimental/theoretical work is used to calculate the

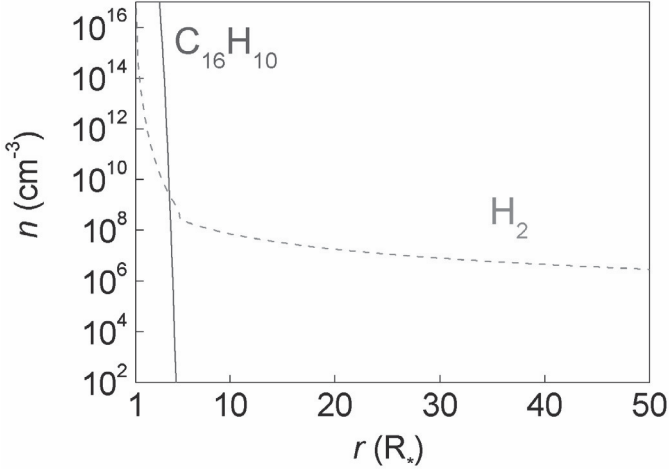


Fig. 2. Minimum pyrene abundance for condensing 10% of the monomers *versus* the distance from the central star IRC +10216 under a low molecular hydrogen density scenario from Agundez & Cernicharo (2006). Molecular abundance of H_2 (Agundez & Cernicharo 2006) is indicated. The condensation is governed by the PAH temperature which decouples from the gas kinetic temperature very close to the star. At the distance of $5 R_\star$, the pyrene internal temperature has already dropped below 100 K.

minimum PAH number density for condensing 10% of the PAH monomers at a given temperature. The resulting minimum abundances are plotted in Figures 1 and 2 along with the molecular hydrogen and acetylene density profiles.

The most striking feature is the high sensitivity of the minimum pyrene abundance to the total gas density. As soon as the gas density drops, collisions are not enough to keep the PAH molecules hot. The PAH vibrational temperature starts to decouple from the gas kinetics temperature, and therefore the association between two cooler PAH molecules becomes faster than the destruction of the dimer. When considering a high relative abundance of 10^{-9} for each of the PAHs, the plots show that condensation may occur $>5 R_\star$ and $35 R_\star$ under the low and high density scenarios, respectively. Based on these observations, we first conclude that under the high gas density scenario, condensation of small PAHs occurs too far from the star ($>35 R_\star$) to represent a key mechanism in the formation of carbon dust particles.

The low gas density scenario seems more favorable. We look now at the kinetics of the association process to extract some time constraints. Collisions between cold PAH molecules above the edge of the inner shell lead to an energized complex which either relaxes by emission of infrared photons, relaxes by collision with a

third body, or breaks apart. Calculations have revealed a surprising decoupling between the inter- and intra-molecular modes in the PAH complex (Sabbah *et al.* 2010). This means that under low pressure environments the excess collisional energy may not be that easily evacuated through infrared emission and may rather cause the complex to break apart, hence reducing its lifetime. Nevertheless, the hypothesis of a 100% sticking efficiency provides an upper limit to the lifetime of the PAH complex. A simple calculation then gives a lower limit for the growth time – corresponding to the inverse of the product of the capture rate and the PAH abundance – of $\sim 10^9$ s. This characteristic growth time is 20 times longer than the period of the shock, ~ 630 days, that strongly affects the inner shell of the carbon star. Based on this kinetics argument, one can then conclude that the formation of PAH clusters is slow and will then be perturbed by the rise in temperature of the environment caused by the propagation of the shock.

4 Conclusion

We have re-examined the condensation of small PAHs in the envelope of IRC+10216. As the distance from the star grows, the gas density drops and the temperature of the PAH molecules decouples from the gas kinetic temperature. Cold PAHs molecules are then more likely to stick to each other and form a dimer. The thermodynamics of pyrene dimers in this environment is explored using the equilibrium constant of the dimer derived from the combined experimental/theoretical work.

Our results show that a low density of gas is necessary for small PAHs such as pyrene to condense at the edge of the inner shell of the star. However, even then the growth of these clusters is expected to be slow and therefore seriously hindered by periodic shocks induced by stellar pulsations. This **rules out** clustering of small PAHs as the main mechanism for generation of carbon particles in these environments. Our conclusions do not contradict the findings of Bernatowicz (2006) as heterogeneous condensation of carbonaceous molecules on carbides is still possible. Alternatively, larger PAHs could stack efficiently under conditions prevailing in high temperatures environments. The chemical pathway leading to these large aromatic units remains to be examined.

In the laboratory, there are a number of challenges to take up to explore the kinetics of dimerization of larger PAHs than pyrene. The most difficult one is probably to evaporate these condensable species and mix them with the buffer gas to produce a uniform continuous flow with a sufficient (and known) amount of reactant, stable over time. An alternative such as laser desorption is not suitable because, although the technique can gently vaporize molecules, the amount of molecules desorbed is unknown and it generally relies on pulsed laser systems.

Future studies will then rather extend the theoretical approach developed here for pyrene to larger species more prone to condensation.

A more complete study would include periodic shocks which boost the density (and therefore the number of collisions) and cause a rise in temperature of the

medium. Other routes based on chemical growth should be explored by chemical kinetics models.

The authors acknowledge funding from the Indo-French Centre for the Promotion of Advanced Research (Project number 3405-3). This work is also supported by the French Programmes of Physique Stellaire and of Physique et Chimie du Milieu Interstellaire. The theoretical work (S.J.K.) has been supported by NASA's Planetary Atmospheres Program through grant NNH09AK24I and by the US Department of Energy, Office of Basic Energy Sciences, Division of Chemical Sciences, Geosciences, and Biosciences under Contract No. DE-AC02-06CH11357.

References

- Agundez, M., & Cernicharo, J., 2006, *ApJ*, 650, 374
- Allain, T., Sedlmayr, E., & Leach, S., 1997, *A&A*, 323, 163
- Bernatowicz, T., Croat, T.K., & Daulton, T.L., 2006, *MESS*, 943, 109
- Boersma, C., Hony, S., & Tielens, A., 2006, *A&A*, 447, 213
- Cadwell, B.J., Wang, H., Feigelson, E.D., & Frenklach, M., 1994, *ApJ*, 429, 285
- Canosa, A., Goulay, F., Sims, I.R., & Rowe, B.R., 2008, In *Low Temperatures and Cold Molecules*, ed. IWM Smith, 55 (Singapore: World Scientific)
- Cau, P., 2002, *A&A*, 392, 203
- Cherchneff, I., Barker, J.R., & Tielens, A., 1992, *ApJ*, 401, 269
- Cherchneff, I., & Cau, P., 1998, *Proceedings of the Asymptotic Giant Branch Stars 191th IAU Symp.*, 251
- Cherchneff, I., 2000, *The Carbon Star Phenomenon*, *Proceedings of the 177th IAU Symp.*
- Cherchneff, I., 2011, *Proceedings of PAHs and the Universe Conference*, this volume
- Dupeyrat, G., Marquette, J.B., & Rowe, B.R., 1985, In *Physics of Fluids*, 1273
- Fonfria, J.P., Cernicharo, J., Richter, M.J., & Lacy, J.H., 2008, *ApJ*, 673, 445
- Frenklach, M., 2002, *Physical Chemistry Chemical Physics*, 4, 2028
- Frenklach, M., Carmer, C.S., & Feigelson, E.D., 1989, *Nature*, 339, 196
- Frenklach, M., & Feigelson, E.D., 1989, *ApJ*, 341, 372
- Frenklach, M., & Wang, H., 1991, *Proceedings of the Combustion Institute*, 23, 1559
- Goulay, F., Rebrion-Rowe, C., Biennier, L., *et al.*, 2006, *JPC A*, 110, 3132
- Guelin, M., Lucas, R., & Cernicharo, J., 1993, *A&A*, 280, L19
- Henning, T., & Salama, F., 1998, *Science*, 282, 2204
- Jager, C., Huisken, F., Mutschke, H., Jansa, I.L., & Henning, T.H., 2009, *ApJ*, 696, 706
- Jager, C., Mutschke, H., Henning, T., & Huisken, F., 2011, *Proceedings of PAHs and the Universe Conference*, this volume
- Jones, A.P., 2005, In *Proceedings of the Dusty and Molecular Universe: a Prelude to Herschel and Alma*, ed. A Wilson, 239 (Ag Noordwijk: Esa Publications Division C/O Estec), 2200
- McCabe, E.M., 1982, *MNRAS*, 200, 71
- Rapacioli, M., Calvo, F., Spiegelman, F., Joblin, C., & Wales, D.J., 2005, *JPC A*, 109, 2487
- Sabbah, H., Biennier, L., Klippenstein, S.J., Sims, I.R., & Rowe, B.R., 2010, *JPC Lett.*, 2962
- Tielens, A., 2008, *ARA&A*, 46, 289
- Ziurys, L.M., 2006, *PNAS*, 103, 12274

FORMATION AND EVOLUTION OF CIRCUMSTELLAR AND INTERSTELLAR PAHS: A LABORATORY STUDY

C.S. Contreras¹, C.L. Ricketts¹ and F. Salama¹

Abstract. Studies of dust analogs formed from hydrocarbon (CH_4 , C_2H_2 , C_2H_4 , C_2H_6) and PAH precursors have been performed using a new facility that we have developed to simulate interstellar and circumstellar processes. The species formed in a plasma are detected, characterized and monitored *in situ* with high-sensitivity techniques, which provide both spectroscopic and ion mass information. From these measurements we derive information on the nature, the size and the structure of dust particles, as well as a better understanding of the growth and destruction processes of extraterrestrial dust.

1 Introduction

The study of the formation, growth and destruction mechanisms of cosmic dust grains is essential for a correct understanding of the physical and chemical evolution of the interstellar medium (ISM). Dust particles span a continuous size distribution from large molecules to nanometer-sized particles to μm -sized particles and influence many processes in the evolution of the ISM such as the energy balance through the photoelectric effect, the ionization balance through recombination with electrons and ions, and the chemical composition of molecular clouds (Tielens 2005, see contributions by Verstraete and Bierbaum *et al.* elsewhere in this volume). The carbonaceous component of cosmic dust plays an important role in the universe (Henning & Salama 1998). Carbon particles are thought to be primarily formed in the outflow of carbon stars, through a combustion-like process where small carbon chains (*e.g.*, acetylene) form polycyclic aromatic hydrocarbons (PAHs) that nucleate into larger-size PAHs and, ultimately, into nanoparticles (Frenklach *et al.* 1989; Pascoli & Polleux 2000; Jäger *et al.* elsewhere in this volume). According to the model, that was developed to account for the formation of carbonaceous meteoritic materials, nucleation occurs above 2000 K, followed by the growth of amorphous carbon on the condensation nuclei in the 2000–1500 K

¹ NASA Ames Research Center, Moffett Field, CA, USA

temperature range. As the temperature falls to around 1100 K, aromatic molecules begin to form in the gas phase and condense onto the growing particles forming graphitic microstructures that will ultimately aggregate into larger structures such as seen in soot formation (Cherchneff *et al.* elsewhere in this volume).

Although a large amount of laboratory data exists on the formation and the properties of solid dust analogs and in particular of Si-based materials (*e.g.*, Michael *et al.* 2003), very little is known, about the specific properties (structure, size and spectral signatures) and the formation mechanisms of the key intermediate range of the size distribution (nanoparticles) of cosmic dust. The scarcity of relevant laboratory data on the transition from gas-phase molecules to solid grains is due to the difficulty of forming and isolating these large species and in tracking their evolutionary path under astrophysically realistic laboratory conditions.

Here we describe new laboratory studies that have been performed to address this key issue. First we describe the experimental set-up that has been developed to measure the formation and destruction mechanisms of carbonaceous grains from molecular precursors in an environment with key physical parameters expected to exist in circumstellar regions where molecular formation is observed. We then present and discuss the preliminary results that were obtained in the laboratory and conclude with a discussion of the implications of these new results.

2 Experimental

2.1 Experimental apparatus

The Cosmic Dust Simulation Chamber (CDSC) was recently set up in our laboratory for the study of cosmic analogs (Fig. 1). The CDSC has been previously used to obtain the first electronic spectra of PAHs and small nanoparticles under conditions that realistically simulate astrophysical environments (for a review see Salama 2008). It combines three complementary techniques: Cavity Ring Down Spectroscopy (CRDS), Pulsed Discharge Nozzle (PDN) Expansion and Reflectron Time-of-Flight Mass Spectrometry (ReTOF-MS) providing both spectroscopic and ion mass information for the identification of the species (large molecules, nano-sized grains) that are formed in the plasma source.

The PDN allows the study of molecules, ions and particles isolated in the gas phase. The species are generated in the hot, confined, plasma from carbonaceous precursors and are suddenly frozen by the expansion (Jost 1996) providing a very efficient cooling over short distances (a few mm) and an ideal simulation tool for astrophysical environments. The current geometry of the PDN leads to a residence time of a few microseconds for the particles in the active region of the discharge. The plasma expansion generated by the PDN is well characterized (Remy *et al.* 2003; Broks *et al.* 2005) and is probed by CRDS several mm downstream with a sub-ppm to ppm sensitivity. CRDS is based on a Nd:YAG pumped tunable pulsed dye laser for the injection of UV-visible photons into a high-finesse cavity (Biennier *et al.* 2003; Tan & Salama 2005). For the ReTOF-MS, in order to

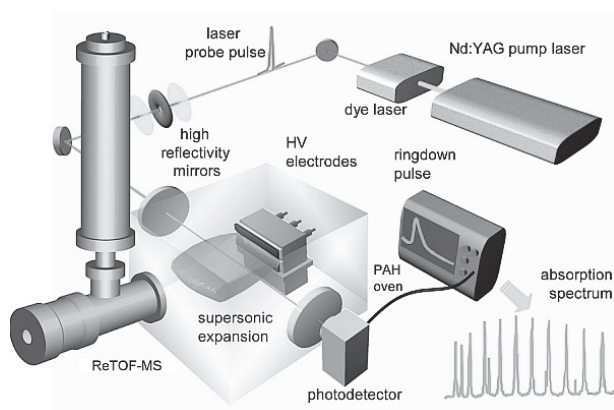


Fig. 1. The Cosmic Dust Simulation Chamber (CDSC) consists of a Pulsed Discharge Nozzle coupled to a Cavity Ring Down Spectrometer apparatus and to an orthogonal, Reflectron time-of-flight mass spectrometer (PDN-CRDS-oReTOFMS).

collect and analyze the ions formed in PDN plasma, a portion of the expansion is skimmed through a 2 mm orifice which is attached to a long tube that leads to a second aperture of 2 mm. The second aperture is polarized (-30 V) in order to attract the positive ions from the plasma. A repelling pulse of $+200$ V is applied when the positively-charged ions have arrived in the extraction region; the ions are steered orthogonally to their original flight path, to minimize noise, and guided into the free flight tube of the ReTOF-MS. The ion pulse is then back reflected with the Reflectron optics toward the MCP detector. The ions are dispersed in time according to their velocity (proportional to their mass-to-charge ratio, m/z) so the discrete packets of different m/z ions are detected (Ricketts *et al.* 2011).

2.2 Experimental procedures

The laboratory species that are generated in the expanding discharge plasma experience a strong temperature gradient that ranges from a few thousand degrees Kelvin to 100 K over a short distance (1.5 – 2.5 mm) from the edge of the plasma chamber to the probing zone where the particles are detected (Remy *et al.* 2003; Broks *et al.* 2005; Biennier *et al.* 2006). This temperature domain corresponds to the domain where aromatic molecules begin to form in the gas phase and condense onto the growing particles forming graphitic microstructures that will ultimately aggregate into larger soot-like structures as we observe. This temperature variation is similar to the temperature variation observed from the surface of a carbon star to the edges of the cooling stellar outflow envelope (Pascoli & Polleux 2000).

Plasma discharges were conducted with small hydrocarbons, methane, ethane, ethylene, and acetylene representative of the alkane, alkene, and alkyne groups, respectively. The formation of larger molecules and carbon grains was probed by the addition of small PAH precursors (naphthalene, 1-methylnaphthalene,

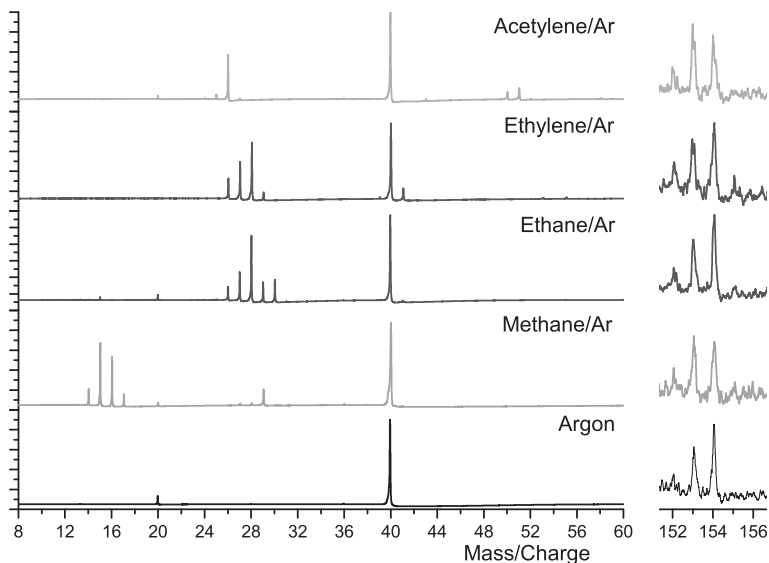


Fig. 2. Representative mass spectra for plasma discharges into Argon seeded with hydrocarbons and/or PAHs. *Left:* hydrocarbons in Argon; *Right:* mixtures of Hydrocarbons and Acenaphthene ($154\ m/z$) in Argon (close-up of the region for the Acenaphthene ion).

acenaphthene) into the hydrocarbon-seeded Ar gas mixture. In all experiments, gases are seeded into Ar and expanded through the PDN. Solid and liquid PAH samples are held in the bottom reservoir of the PDN and are heated to increase their vapor pressure. In typical experiments, the high voltage discharge is $300\ \mu\text{s}$ long and is applied within a gas pulse that lasts 1.2 ms. The ReTOF-MS extraction pulse event is timed to coincide with the discharge and the time it takes the ions to reach the mass spectrometer. The extraction pulse occurred $200\ \mu\text{s}$ after the discharge.

3 Preliminary results

The spectra of the discharge products are shown in Figure 2.

3.1 Linear hydrocarbon precursors:

3.1.1 Alkanes

In the case of methane, a 1-C alkane, carbon build up leads to structures with 2, 3 and 4 carbons. The highest mass ion detected is $C_4H_6^+$. Dehydrogenation (from CH_3 to bare C) is also observed. Carbon build up is also observed in the case of ethane, a 2-C atom alkane, with structures with 2, 3 and 4 carbons. The highest mass ion detected is $C_4H_7^+$. Dehydrogenation (from C_2H_5 to C_2) as well

as fragmentation into 1-C structures is observed. These results seem to indicate that the 1-C alkane precursor (CH_4) exhibits a higher reactivity.

3.1.2 Comparison of the alkane, alkene, and alkyne hydrocarbon classes

Ethylene and acetylene, both unsaturated hydrocarbons, show greater reactivity and propensity to form larger mass ions than ethane. In the case of ethylene, structures up to 5-C atoms are detected and the highest mass ion being $C_5H_9^+$. In the case of acetylene, structures up to 6-C atoms are found with the highest mass ion detected is $C_6H_5^+$. It should be noted that acetylene is routinely stored in acetone and that some of the peaks in the mass spectrum (*e.g.* 58 and 59 m/z) could be due to oxygen containing hydrocarbons (acetone and protonated acetone ions, respectively). The lower reactivity of the alkane, results in lower mass ions formed in the plasma discharge.

3.2 Polycyclic aromatic hydrocarbons

As a basis for the study of the formation of larger PAHs, the naphthalene moiety was used and the reactivity of hydrocarbon-substituted naphthalene was studied. Experiments with naphthalene ($C_{10}H_8$), 1-methylnaphthalene ($C_{11}H_{10}$) and acenaphthene ($C_{12}H_{10}$) were performed. While no evidence for bond formation was found, and therefore no ions with a higher m/z than the PAH precursors were detected in these preliminary runs, an interesting fragmentation pattern was observed to be distinct for each PAH molecule. For example, in the case of naphthalene, the formation of the $C_8H_6^+$ ion corresponds to a loss of C_2H_2 from the precursor. The detection of the $C_4H_4^+$ and its dehydrogenated ions ($C_4H_3^+$, $C_4H_2^+$) demonstrates the loss of C_6H_x fragments, C_6H_4 , C_6H_5 , and C_6H_6 , respectively. The hydrogen loss observed for naphthalene seems to occur in a sequential manner, since both the $C_{10}H_7^+$ and $C_{10}H_6^+$ ions are observed. In the case of 1-methylnaphthalene, the fragmentation process seems to be distinct to that of naphthalene. There is a single H loss ($C_{11}H_9^+$, 141 m/z), and instead of a sequential loss of hydrogen, no peak is observed at 140 m/z . A corresponding fragment ion ($C_9H_7^+$) is observed at 115 m/z , which is a total loss of C_2H_3 . In the acenaphthene spectrum, two clear, sequential hydrogen losses are observed. One possible explanation for this observation is that the hydrogen loss most likely occur at the two adjacent, saturated carbons, thereby forming a double bond between them, with no other fragment ions detected.

3.3 PAHs with hydrocarbons

Plasma experiments with both hydrocarbons and PAHs seeded in Argon indicate minimal reactivity between the two carbon containing species. A notable exception is the formation of the doubly-charged $C_2H_3^{2+}$ ion (13.5 m/z), which only appears in experiments with mixed precursors. With a few exceptions, most of the peaks that are detected in this case follow the trend found for the hydrocarbon-only experiments, with similar relative peaks intensities. PAH molecular ion abundances

(128, 142, 154 m/z for naphthalene, 1-methylnaphthalene, and acenaphthene, respectively) increase when mixed with the hydrocarbons, as opposed to PAHs in Argon experiments. Follow-up studies are on-going to identify the processes responsible for the observed ionization yields.

4 Conclusions

These preliminary experiments have demonstrated that adding a ReTOF-MS to the Cosmic Dust Simulation Chamber (CDSC) constitutes a powerful tool to probe the formation and fragmentation processes of laboratory analogs of interstellar and circumstellar dust. Experiments with hydrocarbon molecule precursors have indicated the formation of larger species through chain growth in all the cases probed so far. The formation of doubly charged ions in the plasma probably contribute to enhancing the reactivity in the plasma chamber. All experiments show fragmentation of the precursors, with losses of H , CH , C_2H_2 , among other fragments specific to each hydrocarbon/PAH combination. The PAHs naphthalene and acenaphthene show subsequent hydrogen loss, with naphthalene dissociating into smaller hydrocarbon fragments. The discharge has been known to induce breakdown of naphthalene in the plasma when the applied voltage on the electrodes is higher than -500 V (Remy *et al.* 2003). For acenaphthene, the loss of two hydrogen atoms most likely occur at the C-C bond that is not part of the aromatic network. Each carbon may lose a hydrogen, forming a double bond between the carbons. The resulting end product is the acenaphthylene ($C_{12}H_8^+$) ion, that is slightly larger than naphthalene. 1-Methylnaphthalene has a total loss of three hydrogens, where two of the hydrogens are lost in one step. The loss of two carbons to form $C_9H_7^+$, and no evidence for the naphthalene cation (127 m/z) in the mass spectrum, tend to indicate that there is ring opening and fragmentation along the ring. No other fragments are detected, possibly due to the stabilization effect of ring opening. There are indicators that multiply-charged ions are being produced in the plasma discharge as indicated by the detection of the $C_2H_3^{2+}$ (13.5 m/z) and $C_2H_5^{2+}$ (14.5 m/z) ions. While $C_2H_5^{2+}$ is only detected when ethane is present, $C_2H_3^{2+}$ is detected in most cases. These observations seem to point to the fact that the presence of the PAHs may facilitate the formation of the doubly-charged species between ions and neutrals from the hydrocarbon gas. More experiments are being performed to further explore these reactions.

This research was supported by the NASA APRA and Cosmochemistry Programs of the Science Mission Directorate. C.S. Contreras and C.L. Ricketts hold NPP fellowships at NASA-Ames Research Center. The authors wish to acknowledge fruitful discussions with L. Biennier and the outstanding technical support of R. Walker.

References

- Biennier, L., Benidar, A., & Salama, F., 2006, *Chem. Phys.*, 326, 445
- Biennier, L., Salama, F., Allamandola, L., & Scherer, J., 2003, *J. Chem. Phys.*, 118, 7863
- Broks, B., Brok, W., Remy, J., *et al.*, 2005, *Phys. Rev., E.*, 71, 36409
- Frenklach, M., Carmer, C., & Feigelson, E., 1989, *Nature*, 339, 196
- Henning, T., & Salama, F., 1998, *Science*, 282, 2204
- Jost, R., 1996, in *Low Temperature Molecular Spectroscopy*, ed. R. Fausto, 483 (Kluwer Academic Publishers, Dordrecht, NL), 249
- Michael, B., Joseph III, A., & Lilleleht, L., 2003, *ApJ*, 590, 579
- Pascoli, G., & Polleux, A., 2000, *A&A*, 359, 799
- Remy, J., Biennier, L., & Salama, F., 2003, *Plasma Sources Sci. Technol.*, 12, 295
- Ricketts, C.L., Contreras, C.S., & Salama, F., 2011, *Int. J. Mass Spectrom. Ion Processes*, 300, 26
- Salama, F., 2008, in *Organic Matter in Space*, IAU Proceedings, ed. Kwok, & Sandford (Cambridge University Press), 357, and references therein
- Tan, X., & Salama, F., 2005, *J. Chem. Phys.*, 122, 084318
- Tielens, A., 2005, *The Physics and Chemistry of the Interstellar Medium* (Cambridge Univ Press, Cambridge, UK)

CONFIRMATION OF C₆₀ IN THE REFLECTION NEBULA NGC 7023

K. Sellgren¹, M.W. Werner², J.G. Ingalls³, J.D.T. Smith⁴,
T.M. Carleton⁵ and C. Joblin^{6, 7}

Abstract. The fullerene C₆₀ has four infrared active vibrational transitions at 7.0, 8.5, 17.5 and 18.9 μm . We have previously observed emission features at 17.4 and 18.9 μm in the reflection nebula NGC 7023 and demonstrated spatial correlations suggestive of a common origin. We now confirm the identification of these features with C₆₀ by detecting a third emission feature at $7.04 \pm 0.05 \mu\text{m}$ at a position of strong 18.9 μm emission in NGC 7023. We also report the detection of these three features in the reflection nebula NGC 2023. We show with spectroscopic mapping of NGC 7023 that the 18.9 μm feature peaks on the central star, that the 16.4 μm emission feature due to PAHs peaks between the star and a nearby photodissociation front, and that the 17.4 μm feature is a blend of a PAH feature and C₆₀. The derived C₆₀ abundance is consistent with that from previous upper limits and possible fullerene detections in the interstellar medium.

1 Introduction

Fullerenes are cage-like molecules (spheroidal or ellipsoidal) of pure carbon, such as C₆₀, C₇₀, C₇₆, and C₈₄. C₆₀ is the most stable fullerene and can account for up to 50% of the mass of fullerenes generated in the laboratory (Kroto *et al.* 1985). Foing & Ehrenfreund (1994) propose that two diffuse interstellar bands at 958 and 963 nm are due to singly ionized C₆₀, or C₆₀⁺, although the identification is debated

¹ Department of Astronomy, Ohio State University

² Jet Propulsion Laboratory, California Institute of Technology

³ Spitzer Science Center, California Institute of Technology

⁴ Ritter Astrophysical Research Center, University of Toledo

⁵ University of Arizona

⁶ Université de Toulouse, UPS, CESR

⁷ CNRS

(Maier 1994; Jenniskens *et al.* 1997). Misawa *et al.* (2009) attribute additional diffuse interstellar bands at 902, 921, and 926 nm to C_{60}^+ . Observational evidence for neutral fullerenes, however, has been elusive to date. No fullerenes have yet been found towards carbon-rich post-AGB stars (Somerville & Bellis 1989; Snow & Seab 1989), carbon stars (Clayton *et al.* 1995; Nuccitelli *et al.* 2005), or R CrB stars (Clayton *et al.* 1995; Lambert *et al.* 2001). Similarly, no neutral fullerenes have yet been found in the diffuse interstellar medium (Snow & Seab 1989; Herbig 2000), dense molecular clouds (Nuccitelli *et al.* 2005), or at the photodissociation front in the reflection nebula NGC 7023 (Moutou *et al.* 1999).

C_{60} has four infrared-active vibrational transitions, at 7.0, 8.5, 17.4, and 18.9 μm (Frum *et al.* 1991; Sogoshi *et al.* 2000). We tentatively identified the 17.4 and 18.9 μm interstellar emission features in the reflection nebula NGC 7023 as due to C_{60} (Werner *et al.* 2004b; Sellgren *et al.* 2007).

We report here the detection of the C_{60} feature at $7.04 \pm 0.05 \mu\text{m}$ in NGC 7023. We also report the detection of C_{60} features at 7.04, 17.4 and 18.9 μm in a second reflection nebula, NGC 2023. The C_{60} 8.5 μm feature is too blended with the strong 8.6 μm PAH feature to yield a useful limit. We have found earlier (Sellgren *et al.* 2007) that the 18.9 μm emission feature in NGC 7023 has a spatial distribution distinct from that of the 16.4 μm emission feature attributed to polycyclic aromatic hydrocarbons (PAHs). We now compare the spatial distributions of the 16.4, 17.4, and 18.9 μm emission features in NGC 7023, and find additional support for the C_{60} identification.

2 Results

We have used the *Spitzer Space Telescope* (Werner *et al.* 2004a) with the Infrared Spectrograph (IRS; Houck *et al.* 2004) to obtain spectra of NGC 7023 and NGC 2023. We used the short-wavelength low-resolution module SL (5–14 μm ; $\Delta\lambda/\lambda = 60\text{--}120$) and the long-wavelength low-resolution module LL2 (14–20 μm ; $\Delta\lambda/\lambda = 60\text{--}120$). Nebular positions were chosen for a strong ratio of the 18.9 μm feature relative to the 16.4 μm PAH feature. We also made a spectroscopic map with the LL2 module of NGC 7023.

We show our 14–20 μm spectrum of NGC 2023 in Figure 1. We mark the wavelengths of C_{60} lines at 17.4 and 18.9 μm , of a PAH feature at 16.4 μm , and of H_2 emission at 17.0 μm .

We show our 5–9 μm spectra of NGC 7023 in Figure 2. We clearly detect an emission feature at $7.04 \pm 0.05 \mu\text{m}$. We detect the 7.04 μm feature also in NGC 2023. This feature is coincident, within the uncertainties, with the wavelength of the expected C_{60} line. We highlight this emission feature by fitting the 5–9 μm spectrum with a blend of PAH emission features in addition to the new emission feature at 7.04 μm . We perform this model fit using PAHFIT (Smith *et al.* 2007a).

In our previous long-slit spectroscopic investigation of NGC 7023 (Sellgren *et al.* 2007), we found that the 18.9 μm feature peaks closer to the central star than either neutral PAHs or ionized PAHs. We now use the LL2 spectroscopic

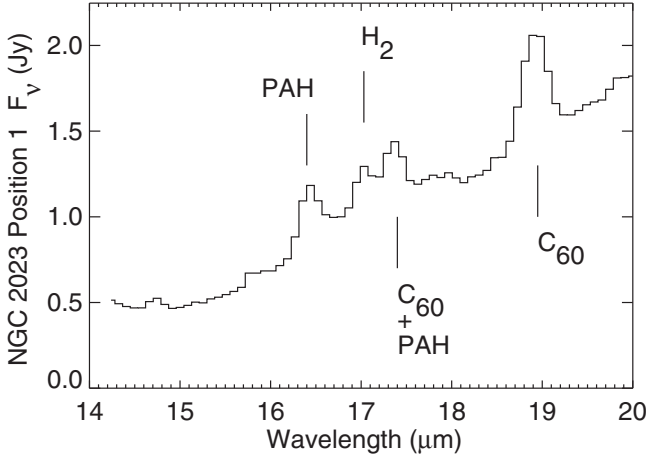


Fig. 1. *Spitzer*-IRS spectrum of NGC 2023 (*solid black histogram*), obtained with the long-wavelength low-resolution module (LL2; 14–20 μm ; $\lambda/\Delta\lambda = 60\text{--}130$). We mark the wavelengths of C₆₀ at 17.4 and 18.9 μm , a PAH feature at 16.4 μm , and H₂ emission at 17.0 μm (*vertical solid lines*).

map extracted in NGC 7023 to illustrate this point more clearly in Figure 3. The 18.9 μm emission is clearly centered on the star. By contrast, the 16.4 μm PAH emission peaks outside the region of maximum 18.9 μm emission, in a layer between the star and the molecular cloud. The photodissociation front at the UV-illuminated front surface of the molecular cloud is delineated by fluorescent H₂ emission at 17.0 μm .

We show an image of the 17.4 μm emission from NGC 7023 in Figure 3, overlaid with contours of 18.9 μm and 16.4 μm emission. The 17.4 μm emission clearly shows one peak on the central star, coincident with the 18.9 μm C₆₀ emission, and a second peak co-spatial with the 16.4 μm PAH emission. We conclude that the observed 17.4 μm emission feature is a blend of a PAH feature at 17.4 μm , whose spatial distribution follows that of the 16.4 μm PAH feature, and of 17.4 μm C₆₀ emission.

3 Discussion

We have detected three lines due to C₆₀, in two reflection nebulae. This is the first detection of neutral C₆₀ in space.

Theorists have suggested that fullerenes might form around stars with carbon-rich atmospheres, such as carbon stars, cool carbon-rich Wolf-Rayet (WC) stars, and C-rich, H-poor R Cr B stars (Kroto & Jura 1992; Goeres & Sedlmayr 1992; Cherchneff *et al.* 2000; Pascoli & Polleux 2000). Fullerenes may also form as

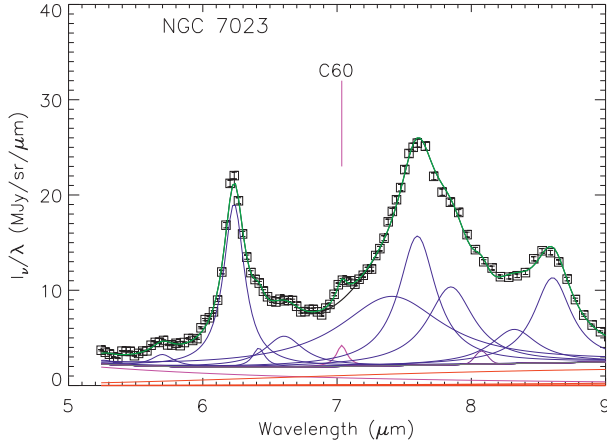


Fig. 2. *Spitzer*-IRS 5–9 μm spectrum of NGC 7023, obtained with the short-wavelength low-resolution module (SL; $\lambda/\Delta\lambda = 60\text{--}120$; solid black histogram). The wavelength of C_{60} at 7.0 μm is marked (vertical solid magenta line). We show the individual contributions of PAH features at 5.3, 5.7, 6.2, 6.4, 6.7, 7.4, 7.6, 7.8, 8.3, and 8.6 μm to the spectrum, by decomposing the spectrum with PAHFIT (Smith *et al.* 2007a) and then overplotting the Lorentzian profile of each feature (thin solid black curves). The Lorentzian fit to the C_{60} feature we detect at $7.04 \pm 0.05 \mu\text{m}$ is highlighted (thick solid magenta curve).

part of the carbon-rich grain condensation process known to occur in the ejecta of Type II supernovae (Clayton *et al.* 2001). Fullerenes might form via interstellar gas-phase chemistry in dense and diffuse molecular clouds (Bettens & Herbst 1996, 1997). Hydrogenated amorphous carbon grains in the interstellar medium may also decompose after interstellar shocks into fullerenes and PAHs (Scott *et al.* 1997).

We compare the relative amounts of stellar flux absorbed and re-radiated by fullerenes and PAHs to derive the abundance of C_{60} in NGC 7023 and NGC 2023. First we compare the sum of the intensities of the 7.0, 17.4, and 18.9 μm features, assumed to be due to C_{60} , to the sum of all other infrared emission features at 5–20 μm , assumed to be due to PAHs. We ignore potential visual fluorescence by C_{60} or PAHs, do not include any potential 8.5 μm C_{60} emission, and do not attempt to correct the 17.4 μm C_{60} emission for any PAH contribution. We used PAHFIT (Smith *et al.* 2007a) to find that the ratio of C_{60} to PAH emission is 0.01–0.03 in NGC 7023 and NGC 2023. We then compare the amount of UV starlight per C atom absorbed by C_{60} (Yasumatsu *et al.* 1996; Yagi *et al.* 2009). and PAHs (Li & Draine 2001). We assume that 9–18% of interstellar carbon is in PAHs (Joblin *et al.* 1992; Tielens 2008). Our preliminary estimate of the percentage of interstellar carbon contained in C_{60} , $p(\text{C}_{60})$, is 0.1–0.6%.

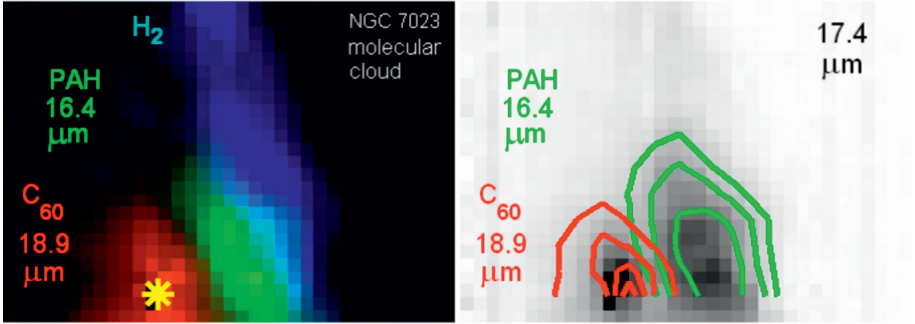


Fig. 3. Spectral map of NGC 7023, obtained with the *Spitzer* IRS 15–20 μm LL2 long-slit module, extracted and analyzed using CUBISM (Smith *et al.* 2007b). Each pixel is $5.1'' \times 5.1''$. *Left:* three-color image of NGC 7023, with the 18.9 μm C₆₀ feature in red, the 16.4 μm PAH feature in green, and the 17.0 μm H₂ line in blue. The position of the central star is marked with a cross. The 18.9 μm C₆₀ feature peaks on the central star. The front surface of the UV-illuminated molecular cloud is traced by H₂ emission, while the 16.4 μm PAH emission peaks between the C₆₀ and H₂ emission. *Right:* gray-scale image of NGC 7023 in the 17.4 μm feature, overlaid with contours of 18.9 μm C₆₀ emission (red), and contours of 16.4 μm PAH feature emission (green). The observed 17.4 μm emission has two spatial components, one co-spatial with C₆₀ emission and the other co-spatial with PAH emission. We conclude that the 17.4 μm emission feature is due to a blend of PAH and C₆₀ emission.

Our preliminary estimate of $p(\text{C}_{60})$ is consistent with published estimates of the percentage of carbon in C₆₀⁺ in diffuse clouds (0.1–0.9%; Foing & Ehrenfreund 1994; Herbig 2000). It is also consistent with previous upper limits on $p(\text{C}_{60})$ towards R Coronae Borealis, massive young stellar objects, and NGC 7023 (<0.3–0.6%; Moutou *et al.* 1999; Nuccitelli *et al.* 2005).

4 Conclusions

We confirm our previous suggestion that emission features at 17.4 and 18.9 μm in NGC 7023 are due to C₆₀, by detecting a third C₆₀ line at 7.04 μm . We detect the 7.04, 17.4, and 18.9 μm C₆₀ lines in NGC 2023 also. The spatial distribution of the 17.4 μm feature in NGC 7023, compared to the spatial distributions of 16.4 μm PAH and 18.9 μm C₆₀ emission, suggests that the observed 17.4 μm feature is a superposition of two lines, one due to PAHs and one due to C₆₀. The abundance we derive for C₆₀ is consistent with previous upper limits on C₆₀ and previous measurements of lines identified with C₆₀⁺. Our observations are the first firm detection of C₆₀ in space.

This work is based on observations made with the *Spitzer* Space Telescope, which is operated by the Jet Propulsion Laboratory, California Institute of

Technology under a contract with NASA. Support for this work was provided by NASA through an award issued by JPL/Caltech.

References

- Bettens, R.P.A., & Herbst, E., 1997, *ApJ*, 478, 585
Bettens, R.P.A., & Herbst, E., 1996, *ApJ*, 468, 686
Cherchneff, I., Le Teuff, Y.H., Williams, P.M., & Tielens, A.G.G.M., 2000, *A&A*, 357, 572
Clayton, D.D., Deneault, E.A.-N., & Meyer, B.S., 2001, *ApJ*, 562, 480
Clayton, G.C., Kelly, D.M., Lacy, J.H., *et al.*, 1995, *AJ*, 109, 2096
Foing, B.H., & Ehrenfreund, P., 1994, *Nature*, 369, 296
Frum, C.I., Engleman, R.J., Hedderich, H.G., *et al.*, 1991, *Chem. Phys. Lett.*, 176, 504
Goeres, A., & Sedlmayr, E., 1992, *A&A*, 265, 216
Herbig, G.H., 2000, *ApJ*, 542, 334
Houck, *et al.*, 2004, *ApJS*, 154, 18
Jenniskens, P., Mulas, G., Porceddu, I., & Benvenuti, P., 1997, *A&A*, 327, 337
Kroto, H.W., Heath, J.R., O'Brien, S.C., Curl, R.F., & Smalley, R.E., 1985, *Nature*, 318, 162
Joblin, C., Léger, A., & Martin, P., 1992, *ApJ*, 393, L79
Kroto, H.W., & Jura, M., 1992, *A&A*, 263, 275
Lambert, D.L., Rao, N.K., Pandey, G., & Ivans, I.I., 2001, *ApJ*, 555, 925
Li, A., & Draine, B.T., 2001, *ApJ*, 554, 778
Maier, J.P., 1994, *Nature*, 370, 423
Misawa, T., Gandhi, P., Hida, A., Tamagawa, T., & Yamaguchi, T., 2009, *ApJ*, 700, 1988
Moutou, C., Sellgren, K., Verstraete, L., & Léger, A., 1999, *A&A*, 347, 949
Nuccitelli, D., Richter, M.J., & McCall, B.J., 2005, *IAU Symp.*, 235, 236
Pascoli, G., & Polleux, A., 2000, *A&A*, 359, 799
Scott, A., Duley, W.W., & Pinho, G.P., 1997, *ApJ*, 489, L193
Sellgren, K., Uchida, K.I., & Werner, M.W., 2007, *ApJ*, 659, 1338
Smith, J.D.T., *et al.*, 2007a, *ApJ*, 656, 770
Smith, J.D.T., *et al.*, 2007b, *PASP*, 119, 1133
Snow, T.P., & Seab, C.G., 1989, *A&A*, 213, 291
Sogoshi, N., Kato, Y., Wakabayashi, T., *et al.*, 2000, *J. Phys. Chem. A.*, 104, 3733
Somerville, W.B., & Bellis, J.G., 1989, *MNRAS*, 240, 41P
Tielens, A.G.G.M., 2008, *ARA&A*, 46, 289
Werner, M.W., *et al.*, 2004, *ApJS*, 154, 1
Werner, M.W., *et al.*, 2004, *ApJS*, 154, 309
Yagi, H., *et al.*, 2009, *Carbon*, 47, 1152
Yasumatsu, H., Kondow, T., Kitagawa, H., Tabayashi, K., & Shobatake, K., 1996, *J. Chem. Phys.*, 104, 899

THE SPITZER SURVEYS OF THE SMALL MAGELLANIC CLOUD: INSIGHTS INTO THE LIFE-CYCLE OF POLYCYCLIC AROMATIC HYDROCARBONS

K.M. Sandstrom¹, A.D. Bolatto², B.T. Draine³, C. Bot⁴ and S. Stanimirovic⁵

Abstract. We present the results of two studies investigating the abundance and physical state of polycyclic aromatic hydrocarbons (PAHs) in the Small Magellanic Cloud (SMC). Observations with ISO and Spitzer have shown that PAHs are deficient in low-metallicity galaxies. In particular, galaxies with $12 + \log(\text{O}/\text{H}) < 8$ show mid-IR SEDs and spectra consistent with low PAH abundance. The SMC provides a unique opportunity to map the PAH emission in a low-metallicity ($12 + \log(\text{O}/\text{H}) \sim 8$) galaxy at high spatial resolution and sensitivity to learn about the PAH life cycle. Using mid- and far-IR photometry from the Spitzer Survey of the SMC (S³MC) and mid-IR spectral mapping from the Spitzer Spectroscopic Survey of the SMC (S⁴MC) we determine the PAH abundance across the galaxy. We find that the SMC PAH abundance is low compared to the Milky Way and variable, with high abundance in molecular regions and low abundance in the diffuse ISM. From the variations of the mid-IR band strengths, we show that PAHs in the SMC are smaller and more neutral than their counterparts in more metal-rich galaxies. Based on the results of these two studies we propose that PAHs in the SMC are formed with a size distribution shifted towards smaller grains and are therefore easier to destroy under typical diffuse ISM conditions. The distribution of PAH abundance in the SMC suggests that PAH formation in molecular clouds is an important process. We discuss the implications of these results for our understanding of the PAH life-cycle both at low-metallicity and in the Milky Way.

¹ Max-Planck-Institute for Astronomy, Königstuhl 17, 69117 Heidelberg, Germany

² Department of Astronomy and Laboratory for Millimeter-Wave Astronomy, University of Maryland, College Park, MD, USA

³ Department of Astrophysical Sciences, Princeton University, NJ, USA

⁴ Observatoire Astronomiques de Strasbourg, Université Louis Pasteur, 67000 Strasbourg, France

⁵ Department of Astronomy, University of Wisconsin, Madison, WI, USA

1 Introduction

Polycyclic aromatic hydrocarbons (PAHs) are a crucial component of interstellar dust. In addition to being responsible for a significant fraction of the total infrared emission of a galaxy, they can be a dominant source of photoelectrons and participate in chemical reactions across a variety of ISM phases. We would like to understand how the amount and characteristics of PAHs vary with galaxy type, star-formation history and ISM environment. All of these issues are tied to the life cycle of PAHs—the balance between their formation, destruction and processing in the ISM. PAH formation is thought to occur in the atmosphere of evolved stars (Latter 1991; Cherchneff *et al.* 1992), although it is not clear that evolved stars alone can account for the abundance of PAHs we observe in the ISM (Matsuura *et al.* 2009). It may also be the case that PAH formation in the ISM can be a significant source of PAHs (for a recent review, see Draine 2009). PAHs are observed to be destroyed in ionized gas in H II regions. Shock waves have been argued to be either a source (via grain shattering; Miville-Deschenes *et al.* 2002) or sink (Micelotta *et al.* 2010) of PAHs.

Although many aspects of the life cycle of PAHs are still poorly understood, we do know that it changes dramatically as a function of metallicity (see contributions by Calzetti *et al.* and Hunt *et al.* in this Volume). Observations with ISO and Spitzer have demonstrated that low metallicity galaxies have a deficit of PAHs relative to the total amount of dust (*e.g.* Engelbracht *et al.* 2005). Draine *et al.* (2007) used SED modeling to determine the PAH fraction q_{PAH} (defined as the fraction of the dust mass contributed by PAHs with sizes less than 10^3 carbon atoms) in the SINGS galaxies. They found that at a metallicity of $12 + \log(\text{O}/\text{H}) \sim 8$, galaxies transition from having a median $q_{\text{PAH}} \sim 3.5\%$, similar to the Milky Way value of 4.6%, to a median of $\sim 1\%$. Spectroscopic (Wu *et al.* 2006; Engelbracht *et al.* 2008) and photometric investigations (Marble *et al.* 2010) of large samples of low-metallicity galaxies provide clear evidence for this deficit.

The cause of the low-metallicity PAH deficit has been the subject of much investigation. Galliano *et al.* (2008) suggest that the deficit is related to PAH production due to the time delay between supernova and evolved star enrichment of the ISM. Others have argued that the deficit is due to destruction of PAHs by harder and more intense UV fields (Madden 2000; Gordon *et al.* 2008) or enhanced supernova shock destruction (O'Halloran *et al.* 2006). The Local Group galaxies, particularly the Small Magellanic Cloud, provide a test case for these scenarios. With a distance of ~ 60 kpc and a metallicity of $12 + \log(\text{O}/\text{H}) \sim 8$, the SMC is a location where we can study PAHs at high spatial resolution and sensitivity in a galaxy right at the metallicity of the transition to PAH deficiency.

We have performed two surveys of the SMC using the Spitzer Space Telescope. The first, the Spitzer Survey of the SMC (S^3MC), imaged the main star-forming areas of the Wing and Bar of the galaxy using all of the photometric bands of IRAC and MIPS. Details of S^3MC and the data processing can be found in Bolatto *et al.* (2007). The second survey, the Spitzer Spectroscopic Survey of the SMC (S^4MC), consisted of extensive spectral mapping observations using the low

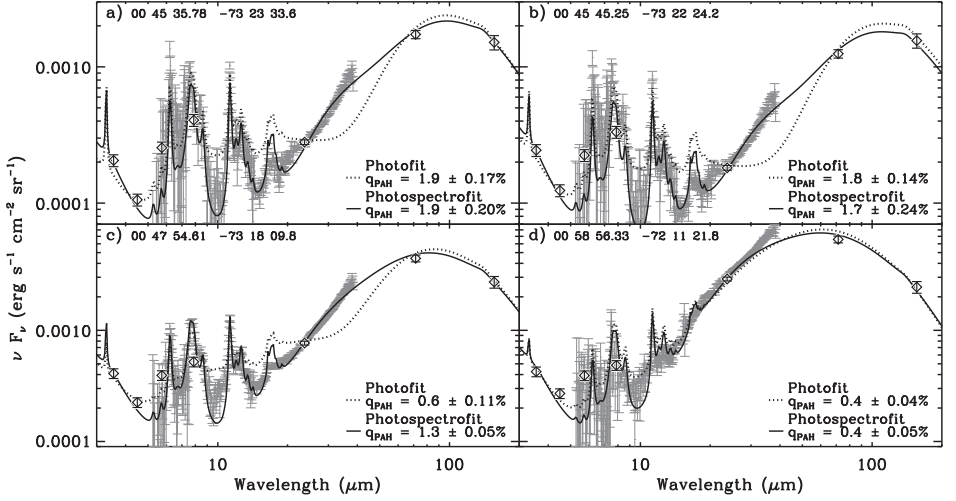


Fig. 1. Best fit models for photometry alone (photofit) and photometry and spectroscopy combined (photospectrofit) for a few selected regions covered by S³MC and S⁴MC.

resolution modules (5–35 μm) of IRS covering six of the main star-forming regions in the galaxy. The details of the survey and the data reduction can be found in Sandstrom *et al.* (2009) and Sandstrom *et al.* (2010, in prep.).

2 The PAH fraction in the SMC

In order to understand the cause of the PAH deficit in low-metallicity galaxies, we would like to answer the following questions about the SMC: 1) is the SMC deficient in PAHs, 2) are there spatial variations in the PAH fraction in the SMC, and 3) if there are spatial variations, with what are they correlated? To answer these questions we have made a map of the PAH fraction q_{PAH} across the galaxy by fitting the SED models of Draine & Li (2007) at every independent pixel in the map. Details of the SED modeling are described in Sandstrom *et al.* (2010) along with a more thorough description of the results. In addition to modeling the SED, we incorporate the S⁴MC spectroscopy in the overlap regions to test whether the photometric determination of q_{PAH} does an adequate job of judging the PAH fraction, with essentially only a measurement of the 8 μm feature. Figure 1 shows the best fit models to the photometry only and combined photometry and spectroscopy for a few locations in our maps. We find that the photometric only determination of q_{PAH} is very close to the best fit q_{PAH} from the combined fit for all of the overlap regions.

In Figure 2 we show the PAH fraction map that results from our SED fits. We find that the SMC has an average $q_{\text{PAH}} = 0.6\%$, significantly below the Milky Way value of $q_{\text{PAH,MW}} = 4.6\%$. There are large spatial variations in the SMC PAH

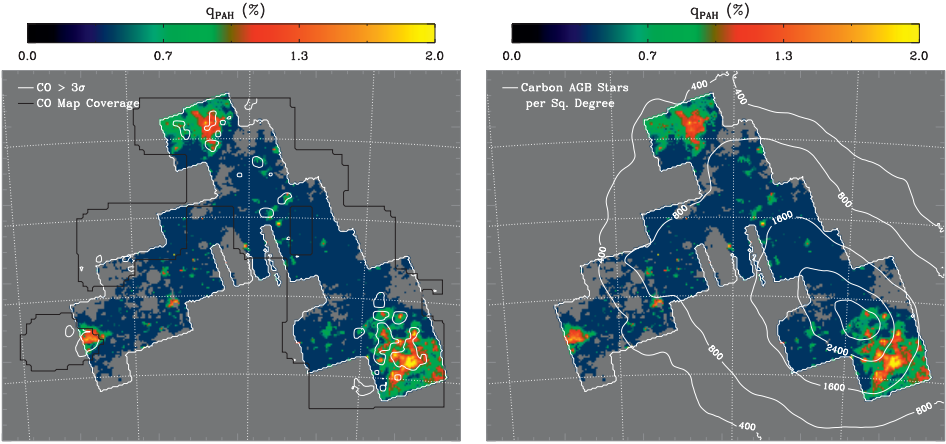


Fig. 2. The PAH fraction maps that result from our SED fitting overlaid with contours of CO $J=(1-0)$ from the NANTEN survey (left) and carbon star surface density (right). It is clear that the PAH fraction is correlated with the locations where molecular gas is present but not with the distribution of evolved stars.

abundance. At maximum q_{PAH} can be within a factor of two of the Milky Way level, but most of the galaxy has $q_{\text{PAH}} = 0.4\%$, which represents the lower limit of our models. For its metallicity, the SMC average q_{PAH} agrees well with the average $q_{\text{PAH}} \sim 1\%$ found by Draine *et al.* (2007) for the SINGS sample.

Next, we compare the PAH fraction to various proposed drivers for the PAH abundance. Evolved stars are thought to be the dominant source of PAHs. We trace the distribution of evolved stars using color selection criteria on the 2MASS catalog to select carbon AGB stars (Cioni *et al.* 2006). The distribution of carbon stars follows the well known spheroidally distributed population of old stars in the SMC (Harris & Zaritsky 2004). There is no correspondence between the evolved star density and the PAH fraction, in contrast to what is seen in the LMC, where the PAH fraction is seen to be enhanced along the stellar bar (Paradis *et al.* 2009). We find that the PAH fraction is correlated with the presence of molecular gas as traced by CO $J=(1-0)$ from the NANTEN survey (Mizuno *et al.* 2001). Since the molecular clouds condense out of the diffuse ISM on timescales of ~ 25 Myr (Fukui *et al.* 1999), there must be some process which allows the molecular clouds and the diffuse ISM they condensed out of to have different PAH fractions. Two possibilities are: 1) a recent (< 25 Myr) event which destroyed PAHs in the diffuse ISM over the whole galaxy after the current generation of molecular clouds condensed; or 2) some component of interstellar PAH material forms in molecular clouds. The SMC star-formation history shows little evidence for a recent event that could have altered the PAH fraction globally, so we consider the latter option more likely.

3 The physical state of PAHs in the SMC

The ratios of the mid-IR PAH bands provide a wealth of information about the physical state of PAHs—charge, size, structure and composition all alter the relative strengths of the mid-IR features. Understanding the physical state of PAHs in the SMC may help us to explain the low-metallicity PAH deficit. For instance, PAHs that are smaller or ionized are easier to photodissociate under typical ISM conditions (Allain *et al.* 1996a, 1996b). To study the physical state of PAHs in the SMC, we have used the S⁴MC spectroscopy and measured the strengths of the various bands. A detailed description of this work can be found in Sandstrom *et al.* (2010, in prep.).

In Figure 3 we show measurements of the band ratios overlaid on theoretical predictions from Li & Draine (2001). The gray lines show neutral (top) and singly-ionized (bottom) PAHs with a variety of sizes (labeled on the bottom plot). Since interstellar PAHs come with a size and charge distribution, the theoretical predictions are only used as a guide for interpreting the ratios relative to other measurements. We also plot the band ratios measured in the SINGS galaxies (without AGN; Smith *et al.* 2007). The SINGS spectroscopy covers regions with approximately solar metallicity. Compared to SINGS, we find that the SMC PAHs tend to be more neutral and smaller, judging from the ratios of their 6 – 12 μm features. In addition, we find that the 17 μm PAH complex is notably weak in the SMC, continuing a trend noted by Smith *et al.* (2007) for the strength of the 17 feature to decrease as a function of metallicity.

4 Insights into the PAH life cycle

To summarize, the Spitzer surveys of the SMC (S³MC and S⁴MC) allow us to study the abundance and physical state of PAHs in a nearby, low-metallicity galaxy. We find that the SMC PAH fraction is significantly below the Milky Way value, but with large spatial variations. High PAH fractions are found in molecular regions, while the diffuse ISM is essentially devoid of PAHs (to the limit of our models). Spectroscopic investigations of a number of the main star-forming regions show that the mid-IR band ratios suggest smaller and more neutral PAHs than found in more metal rich galaxies (for example in the SINGS sample).

These results suggest a scenario where PAH formation in dense regions is important, at least at low-metallicity. The process by which this proceeds is currently uncharacterized, but may depend on the coagulation of material on the surfaces of existing grains. The PAHs that result from this formation channel in the SMC seem to be smaller on average than PAHs in more metal rich galaxies, judging by their band ratios. Smaller PAHs are easier to photodissociate under typical diffuse ISM conditions, perhaps leading to the very low PAH abundance over most of the SMC. PAHs formed in the atmospheres of evolved stars are mainly injected first into the diffuse ISM and may be largely destroyed in the SMC. At higher metallicity, we speculate that PAHs are better able survive in the diffuse ISM, possibly because of softer and less intense UV fields and/or larger average PAH sizes. As

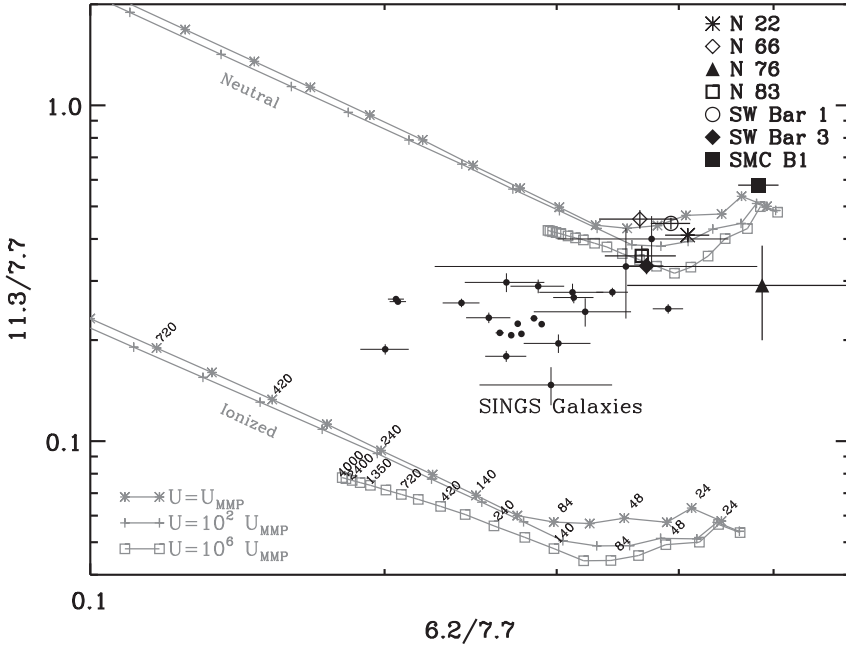


Fig. 3. Ratios of the 6.2, 7.7 and 11.3 μm PAH bands in the SMC compared with the SINGS sample and the theoretical models of Li & Draine 2001. The band ratios suggest that SMC PAHs are smaller and more neutral than PAHs in the SINGS galaxies.

PAHs become able to survive in the diffuse ISM, the overall PAH fraction of a galaxy can build up to Milky Way levels. Resolved studies of the PAH fraction in a larger sample of nearby galaxies that span a range of metallicity will allow us to study these trends.

References

- Allain, T., Leach, S., & Sedlmayr, E., 1996a, *A&A*, 305, 602
 Allain, T., Leach, S., & Sedlmayr, E., 1996b, *A&A*, 305, 616
 Bolatto, A.D., Simon, J.D., Stanimirović, S., *et al.*, 2007, *ApJ*, 655, 212
 Cherchneff, I., Barker, J.R., & Tielens, A.G.G.M., 1992, *ApJ*, 401, 269
 Cioni, M.-R.L., Girardi, L., Marigo, P., & Habing, H.J., 2006, *A&A*, 452, 195
 Draine, B.T., 2009, in *Astronomical Society of the Pacific Conf. Ser.*, 414, ed. T. Henning, E. Grün, & J. Steinacker, 453
 Draine, B.T., & Li, A. 2007, *ApJ*, 657, 810
 Draine, B.T., Dale, D.A., Bendo, G., *et al.*, 2007, *ApJ*, 663, 866
 Engelbracht, C.W., Gordon, K.D., Rieke, G.H., *et al.*, 2005, *ApJ*, 628, L29
 Engelbracht, C.W., Rieke, G.H., Gordon, K.D., *et al.*, 2008, *ApJ*, 678, 804

- Fukui, Y., Mizuno, N., Yamaguchi, R., *et al.*, 1999, PASJ, 51, 745
Galliano, F., Dwek, E., & Charnial, P., 2008, ApJ, 672, 214
Gordon, K.D., Engelbracht, C.W., Rieke, G.H., *et al.*, 2008, ApJ, 682, 336
Harris, J., & Zaritsky, D., 2004, AJ, 127, 1531
Latter, W.B., 1991, ApJ, 377, 187
Li, A., & Draine, B.T., 2001, ApJ, 554, 778
Madden, S.C., 2000, New Astron. Rev., 44, 249
Marble, A.R., Engelbracht, C.W., van Zee, L., *et al.*, 2010, ApJ, 715, 506
Matsuura, M., Barlow, M.J., Zijlstra, A.A., *et al.*, 2009, MNRAS, 396, 918
Micelotta, E.R., Jones, A.P., & Tielens, A.G.G.M., 2010, A&A, 510, A36
Miville-Deschênes, M.-A., Boulanger, F., Joncas, G., & Falgarone, E., 2002, A&A, 381, 209
Mizuno, N., Rubio, M., Mizuno, A., *et al.*, 2001, PASJ, 53, L45
O'Halloran, B., Satyapal, S., & Dudik, R.P., 2006, ApJ, 641, 795
Paradis, D., Reach, W.T., Bernard, J.-P., *et al.*, 2009, AJ, 138, 196
Sandstrom, K.M., Bolatto, A.D., Draine, B.T., Bot, C., & Stanimirović, S., 2010, ApJ, 715, 701
Sandstrom, K.M., Bolatto, A.D., Stanimirović, S., van Loon, J.T., & Smith, J.D.T., 2009, ApJ, 696, 2138
Smith, J.D.T., Draine, B.T., Dale, D.A., *et al.*, 2007, ApJ, 656, 770
Wu, Y., Charmandaris, V., Hao, L., *et al.*, 2006, ApJ, 639, 157

PAH-RELATED VERY SMALL GRAINS IN PHOTODISSOCIATION REGIONS: IMPLICATIONS FROM MOLECULAR SIMULATIONS

M. Rapacioli¹, F. Spiegelman¹, B. Joalland^{1,2}, A. Simon¹,
A. Mirtschink¹, C. Joblin², J. Montillaud², O. Berné³ and D. Talbi⁴

Abstract. The analysis of mid-IR emission suggests that a population of PAH-related very small grains containing a few hundreds of atoms are present in the deep regions of molecular clouds, although no specific species has been identified yet. In this review, we discuss several candidates for these grains: neutral and ionised PAH clusters and complexes of PAHs with Si atoms. The theoretical modelling of the properties of such molecular complexes or nanograins is a challenging task. We first present an overview of quantum chemistry derived models which can be efficiently used on-the-fly in extensive sampling of the potential energy surfaces, as required by structural optimization, classical molecular dynamics or Monte Carlo algorithms. From the simulations, various observables can be determined, such as the binding energies, finite temperature IR spectra, nucleation and evaporation rates. We discuss the relevance of those candidates in the molecular clouds photodissociation regions and propose constraints and perspectives for the nature and size of those very small grains.

1 Introduction

Polycyclic Aromatic Hydrocarbons (PAHs) are usually considered to be at the origin of the Aromatic Infrared Bands (AIBs) observed in emission from

¹ Laboratoire de Chimie et Physique Quantiques, Université de Toulouse (UPS) and CNRS, IRSAMC, 118 route de Narbonne, 31062 Toulouse, France

² Université de Toulouse, UPS, CESR, 9 avenue du colonel Roche, 31062 Toulouse Cedex 4, France and CNRS, UMR 5187, 31028 Toulouse, France

³ Leiden Observatory, Leiden University, Niels Bohrweg 2, 2333 CA Leiden, The Netherlands

⁴ Université Montpellier II - GRAAL, CNRS - UMR 5024, Place Eugène Bataillon, 34095 Montpellier, France

UV-irradiated interstellar matter (Allamandola *et al.* 1985; Léger & Puget 1984, see also Peeters, this volume). Boulanger *et al.* (1990), Bernard *et al.* (1993) analysed the emission in the IRAS photometric bands measured for several molecular clouds, and suggested that free-flying PAHs are produced by photoevaporation of larger grains. The observation of a mid-IR continuum in the reflection nebula Ced 201 has been attributed by Cesarsky *et al.* (2000) to Very Small carbonaceous Grains (VSGs) that have been proposed as precursors of the AIB carriers.

Blind signal separation methods like non-negative matrix factorisation or singular value decomposition (combined with a Monte Carlo search of physical solutions) have been applied to extract three characteristic spectra from mid-IR spectro-imagery data (ISO and Spitzer) of the PhotoDissociation Region (PDR) NGC 7023 (Berné *et al.* 2007; Rapacioli *et al.* 2005, see Berné, this volume). Two spectra have been assigned to PAH populations dominated either by neutral or ionised molecules. The third spectrum is composed of broader AIBs associated with a continuum. As these two characteristic features suggest larger systems, this component has been attributed to a population of PAH-related VSGs. The spatial distribution of these spectra shows that the ionised PAH population is located around the star followed by the neutral PAH population and then by the VSG population when going further from the star and inside the molecular cloud. This suggests a chemical scenario in which PAHs are trapped in VSGs that are photoevaporated at the border of the cloud where the UV flux increases. Closer to the star, the UV flux is strong enough to keep the PAH population mainly positively ionised.

The presence of VSGs related to PAHs has been reported in several PDRs (NGC 7023, ρ Ophiuchi, Ced 201; Berné *et al.* 2007) but also in protoplanetary disks (Berné *et al.* 2009) and in planetary nebulae both in the Milky Way and in the Magellanic clouds (Joblin *et al.* 2008).

A minimal size of these grains can be estimated to 400 carbon atoms from the grain heating process as described in Rapacioli *et al.* (2006). In this paper, we review different hypotheses for PAH-related VSGs and show the capability of theoretical modelling as a tool to investigate these clusters. Three possible species are mostly discussed here: neutral and ionised PAH clusters and complexes of PAHs with Si atoms.

2 Possible candidates for the PAH-related VSGs

Several hypothesis can be made for the PAH-related VSGs. Possible candidates that will be discussed in the following are:

- 1) Neutral PAH clusters: based on the sequential evolution $\text{PAH}^+, \text{PAH}^0$, VSG that is observed in molecular clouds, the most intuitive candidates are PAH clusters. As these clusters are located in deeper regions of molecular clouds than the neutral PAH population, it seems consistent to investigate neutral PAH clusters.
- 2) Ionised PAH clusters: as will be discussed in Section 5, the lowering of the ionisation potential (IP) in PAH clusters compared to PAH could allow the presence of ionised PAH clusters deeper inside molecular clouds. This hypothesis is reinforced

because -(i)- recent calculations (Rhee *et al.* 2007) show that small closed-shell PAH cationic dimers could be at the origin of the Extended Red Emission (ERE) and -(ii)- in NGC 7023N, the ERE spatially correlates with the maximum of VSG emission (Berné *et al.* 2008).

3) Complexes of PAHs with an heteroatom: complexes with Fe atoms can form easily from energetics considerations and have recently been studied both experimentally and theoretically (Simon & Joblin 2007, 2009, 2010; Simon *et al.* 2008) and are the subject of a specific contribution (Simon *et al.*) in this volume. In a similar way, complexes of PAH molecules or clusters with Si atoms could be considered as candidates for the VSGs and are presented in the last section.

This list is of course not exhaustive and the VSGs are most probably made of mixture of various types of grains rather than belonging entirely to one of the previously enumerated families.

3 Theoretical methods adapted to large systems

In the following, we present specific methods that we have used with some theoretical development when needed. The treatment of large clusters containing a few hundreds of atoms is a challenging task for theoretical chemistry. The Density Functional Theory (DFT) is the most widely used method to describe electronic structure, based on a density spanned on molecular orbitals and the solution of a mean-field type single electron Kohn-Sham equation. However, despite fast algorithmic developments, it can presently hardly treat such large clusters, in particular as soon as global Potential Energy Surface (PES) exploration or molecular dynamics (MD) are needed. An alternative for even larger systems and/or larger computational efficiency is provided by approximate schemes of DFT, for instance the Density Functional based Tight-Binding approach (DFTB, Elstner *et al.* 1998; Oliveira *et al.* 2009; Porezag *et al.* 1995; Seifert *et al.* 1996). DFTB is based on a second order Taylor expansion of the DFT energy expression around a reference electronic density and the expression of the second order term as a function of atomic charges. The molecular orbitals are spanned in a minimal set of valence atomic orbitals. All integrals are parametrised and the ground state is found by solving self-consistently the approximate Kohn-Sham secular equation (Self-Consistent-Charge DFTB), including electrostatics self-consistently. In principle, DFTB parametrisation is extracted from DFT calculations on the various atom-pairs and may be expected to show satisfactory transferability. Nonetheless, several parametrisations do exist, adapted to various situations (bulk, biological systems). Parametrisation adjustment may be sometimes needed. In further approximations, the self-consistency can be circumvented, or the electrostatics totally ignored, leading to simple Tight-Binding (TB) schemes. At the present time, DFT (with the most common functionals) and DFTB experience theoretical difficulties such as (i) their failure to describe long-range dispersion forces; (ii) the failure to describe dissociation properly partly screened in the spin-unrestricted formulation; (iii) the difficulty to describe properly open-shell system and multiplets; (iv) the difficulty of today's functionals in the Kohn-Sham formalism to

properly describe systems with strong multi-configurational character. This has motivated the search for new functionals and also *ab initio* hybrid methods based on both the wavefunction for long-range electron-electron correlation and DFT for the short-range correlation (Chabbal *et al.* 2010; Fromager & Jensen 2008; Toulouse *et al.* 2004). The lack of dispersion can also be corrected by addition of empirical atom-atom dispersion potentials in both DFT (Grimme 2006) and DFTB schemes (Elstner *et al.* 2001; Rapacioli *et al.* 2009; Zhechkov *et al.* 2005).

Moreover, in the case of molecular clusters, one can benefit from the partition of the cluster into identifiable units to propose further modelling with different levels of treatments for intra- and intermolecular degrees of freedom. This gives rise to a partition of the level of treatment of the degrees of freedom such as for instance in the case of neutrals: (i) a hybrid approach in which the molecular units (not rigid) are treated via DFT, DFTB or TB (actually developed, see below) and the intermolecular interactions (repulsion, electrostatics and dispersion) are treated via atom-atom classical potentials. This provides a consistent description between intra-molecular charge variations and intermolecular electrostatics. Such model can be considered as a special version of quantum-mechanics/molecular (classical) mechanics (QM-MM, *i.e.* DFTB-MM) schemes. (ii) a more basic rigid molecule approximation (for a review see Stone 1997), where the molecules constituting a cluster are treated as rigid frozen systems and only the intermolecular potential is considered. The rigid body approach obviously is the fastest one and allows global exploration of the intermolecular PES for quite large systems with hundreds of atoms. The advantage of the hybrid (DF)TB/MM approach is its ability to describe energy transfers during collisions or couplings between inter- and intramolecular vibrational modes.

The molecular partition is also relevant for resonance in ionised molecular clusters. Specific approaches consist in expressing the multiconfigurational wavefunction of the ionized cluster as an expansion of charge-localised configurations (Wu *et al.* 2007). A small Configuration Interaction matrix (CI) is then built in this limited valence-bond-like multiconfigurational basis. Such DFT-CI model is clearly very well suited to model charged molecular clusters. It can even be made more efficient in the scope of large systems when using DFTB instead of DFT: benchmark calculations on the benzene, coronene and water dimers show that the DFTB-CI method (Rapacioli *et al.* 2010) is able to correct the wrong behavior of the DFTB dissociation pathway and gives binding energies in agreement with experimental data and reference calculations.

4 Neutral PAH clusters

4.1 Structural properties

4.1.1 PAH dimers

The intermolecular interactions vanish quickly with increasing distance, except for the electrostatic terms which essentially account for interactions between permanent

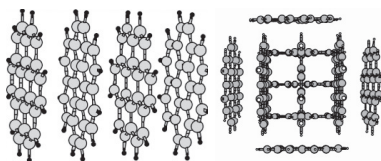


Fig. 1. Stacked coronene clusters of 4 and 10 molecules.

multipoles. The structural growth patterns of PAH clusters are therefore closely related to the dimer structures. Stacks are expected if the most stable dimer structures have sandwich-like configurations. The structures of PAH dimers ranging from benzene to coronene have been optimized at different levels of theory in recent years. The structure of the benzene dimer has been a long-standing discussion until high-level calculations (CCSD(T), SAPT see for instance Podszwa *et al.* 2006) showed that the PES of this dimer has several almost degenerated structures corresponding to T-shaped and sandwich-parallel-displaced geometries. The stacked sandwiches are less stable. For larger PAHs, the T-shaped configurations are strongly destabilised as compared to sandwich structures both in parallel-displaced and stacked configurations. The binding energy increases from about 0.12 eV for the benzene dimer to 0.8-1eV for the coronene dimer (Rapacioli *et al.* 2009; Zhao & Truhlar 2008). The rigid body, TB-MM and DFTB approaches have been parametrised and benchmarked (Rapacioli *et al.* 2005, 2006, 2009) on these high-level calculations on PAH dimers.

4.1.2 Large coronene clusters

A global exploration of the PES using parallel tempering Monte-Carlo methods with the rigid body approach provides the structures of coronene clusters containing up to 32 molecules (Rapacioli *et al.* 2005). As expected from the dimer sandwich structures, the lowest-energy structures of coronene clusters are found to be single stacks for numbers of molecules not exceeding 8. For larger clusters, lower energy structures appear made of two stacks with either parallel axis or in a handshake-like structure (axes almost perpendicular, Fig. 1). The special stability of the “handshake” structure is due to its compactness, while conserving the primary stack structure as basic units. The $(\text{PAH})_{32}$ cluster presents a large number of degenerated isomers which all consist of small units of 4 molecule stacks aggregated to each others. The dissociation energy of these clusters (energy required to remove one molecule) is almost constant (about 1 eV) for clusters above 3 molecules as the less bounded molecules are always at the tip of one stack and interact almost only with their first two neighbors.

In the interstellar medium, PAH clusters are not expected to be made of homogenous units but to aggregate PAHs of different sizes whose structures can also be calculated. The stacks in which the larger PAHs occupy inner sites maximize the number of nearest neighbors between carbon atoms and are energetically favored.

This segregation property remains for larger clusters made of several stacks, the smallest molecules being located at the tips of the stacks.

4.2 *Stability in NGC 7023N*

A key question for astrophysics is whether these clusters can survive in regions such as NGC 7023N where they have been proposed to be present. Their stability results from a competition between formation, upon PAHs/clusters collisions, and destruction by the UV flux. The corresponding rates have been estimated from molecular modelling simulations for clusters made of 4 or 13 coronene molecules (Rapacioli *et al.* 2006). Formation rates were calculated from collision rates between molecules and clusters, which depend on the temperature and density of the cloud, and the probability of sticking at each collision. This last value is calculated from MD simulations using the TB-MM approach combining the TB model of Van Oanh *et al.* (2002) with a classical intermolecular pair potentials as mentioned above. To describe the evaporation which might follow a UV photon absorption, one needs to compare the rate of energy relaxation either by IR emission or by evaporation of one molecule. Both phenomena can occur on relatively long timescales (at low energy) and real-time simulations of these processes are not possible. However these values can be obtained with statistical approaches, namely the Phase Space Theory for the molecular evaporation (Calvo & Parneix 2004) with the rigid body model and a microcanonical IR emission model (Joblin *et al.* 2002) for the IR cooling.

The calculated clustering timescales are typically 10^4 – 8×10^4 years, much longer than the photoevaporation timescales which are below 17 years. Therefore, these clusters should be destroyed by the UV flux much faster than they can be reformed (Rapacioli *et al.* 2006). Such clusters could not survive in UV irradiated clouds like the PDR NGC 7023N. These results do not however rule out completely the hypothesis of neutral PAH clusters as the size of astronomical PAH-related VSGs might be larger (larger clusters or larger units) and this would increase their stability in PDRs.

5 Ionised PAH clusters

Ionised molecular clusters are more strongly bound than the neutrals. The charge resonance at the origin of this strong stabilisation, completed by polarization, is treated with the DFTB-CI method.

5.1 *Energetics considerations*

We have investigated ionised coronene clusters in non-relaxed stacked geometries (Rapacioli & Spiegelman 2009). The charge essentially delocalises over the central molecules: the configurations where the charge is carried by the central molecules have much higher weights in the global CI wavefunction than the configurations where the charge is localised on the edge molecules.

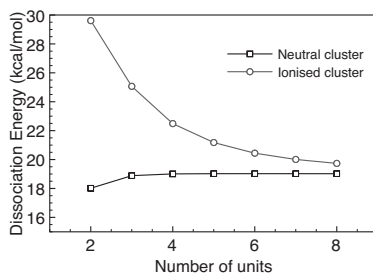


Fig. 2. Dissociation energy of neutral and ionised stacked coronene clusters (Fig. from Rapacioli & Spiegelman 2009).

Figure 2 displays the dissociation energy of neutral and cationic coronene stacks corresponding to the evaporation of a single molecule from one stack side. In the neutral cluster, the dissociation energy reaches a limit for sizes above 3 units as seen previously. The cationic dimer is over 1.5 times more stable than the neutral one. The evaporation rate constant varies approximately exponentially as a function of the dissociation energy, thus cationic clusters will be significantly more resistant to the loss of a neutral molecule. When cluster size increases, the charge distribution is less sensitive to the removal of one unit and the dissociation energy tends to the same limit as observed for neutral clusters.

It should also be noticed that, as the charge delocalisation over the stack stabilises the ionised form, the IP decreases when the cluster size increases. The decrease of the IP with cluster size down to the bulk limit is frequently observed for various families of clusters. For a coronene stack, the IP reaches a limit for clusters above 7–8 units. The IP is then reduced by more than 1 eV compared to that of the isolated molecule. This decrease of the IP could explain the presence of cationic PAH clusters in PDRs regions where isolated PAHs would be neutral. Most of the features will certainly remain valid when achieving full relaxation of the ion geometries. The issues are (i) how large is the core subcluster over which the charge is actually delocalised; (ii) what is the quantitative interplay between geometric relaxation and stability, and the construction of larger clusters; (iii) what is the supramolecular organization of the other units essentially neutral and polarized by this core; and (iv) what are the implications for nucleation and evaporation. Implementation of the analytical gradient in DFTB-CI is underway and should allow to answer precisely these questions.

5.2 Formation rates

Although the complete study of ionised PAH cluster formation would require to perform MD to simulate collisions as done for neutral clusters, the evolution of the collision rate can be estimated. Because the VSGs are observed in regions where PAHs are expected to be neutral, it is consistent to focus on collisions between a neutral molecule with a $(PAH)_n^+$ cluster. In such a collision, the cationic cluster

induces a dipole on the PAH molecule. The long-range ionic clusters/induced dipole interaction is attractive and scales as $1/R^4$. This interaction is much stronger than in the case of neutral clusters, which scales as $1/R^6$. The formation rate can be roughly estimated from a simple Langevin model. The Langevin prediction for the nucleation rate is then given by $k_{nucl} = 2e(\alpha/\mu)^{1/2}$ (see for instance Herbst 2001), where e is the elementary charge, α the polarisability of the PAH, and μ the reduced mass of the reactants. This leads, for the specific case of NGC 7023N, to reformation timescales of a few thousands years, much faster than for neutral clusters. The conclusion that small clusters are destroyed faster than they can be reformed could thus be modified for ionised clusters, but a complete study of their stability, including the calculation of the evaporation rates, necessary to answer this question, is under development.

6 SiPAH complexes

PAH-related VSGs could contain heteroatoms. The case of Fe is discussed in Simon *et al.* (this volume). We discuss here SiPAH complexes. The first step in the study of such systems consists in investigating the smallest dimers, that is a single PAH molecule with a single Si atom. Some characteristic features associated to the coordination of Si can already be derived from these simple model systems, in particular concerning the structures and IR spectra of $[SiPAH]^+$ complexes.

6.1 Structures and binding energies

The structures of $[SiPAH]^{0/+}$ complexes have been optimized at the DFT level by Joalland *et al.* (2009). The SiPAH binding energies in $[SiPAH]^+$ complexes were computed to be at least 1.5 eV. This value being three times higher than for $[SiPAH]^0$, $[SiPAH]^+$ complexes are therefore more likely to survive in the conditions of the ISM than their neutral counterparts. Furthermore, the formation of $[SiPAH]^+$ complexes by radiative association is an exothermic process without any expected activation barrier. These $[SiPAH]^+$ complexes could then represent a significant fraction of PAH-related species and their presence has been suggested to account for the blue-shift of the $6.2 \mu\text{m}$ band (see also Peeter *et al.*, this volume). The exploration of the PES reveals that in the most stable structures, the Si atom is located on top of a C atoms on the edge of the PAH molecular structure. It was furthermore demonstrated that the lowest energy path for the motion of the Si atom parallel to the PAH surface is through the edge of the PAH.

6.2 IR spectroscopy

6.2.1 Harmonic

The IR spectra of such complexes have been calculated with the harmonic approximation at the DFT level. Compared to isolated PAHs, the $[SiPAH]^+$ complexes present very soft modes associated to the motion of the Si atom above the PAH surface. For instance, in $[SiC_{10}H_8]^+$ complex, these modes are located at 202, 240,

and 413 cm^{-1} . The first two correspond to a Si motion parallel to the PAH plane and have very low intensities. The 413 cm^{-1} mode corresponds to a Si motion in a direction perpendicular to the PAH plane with an intensity of about 12% of the maximum intensity.

The mid-IR spectra of $[\text{SiPAH}]^+$ resemble more that of a cationic PAH than that of a neutral PAH. This results from the fact that in the $[\text{SiPAH}]^+$ complexes, most of the charge is actually carried by the PAH. A significant spectral difference stems from the fact that the symmetry is reduced in the complex. For instance, the γ_{CH} band located at 780 cm^{-1} in $\text{C}_{10}\text{H}_8^+$ splits into two subbands at 862 and 786 cm^{-1} in $[\text{SiC}_{10}\text{H}_8]^+$. The first band involves mainly the bending of C-H bonds from the ring neighboring the Si atom whereas the second γ_{CH} band involves the H atoms coordinated to the other rings and is therefore less perturbed. The 1594 cm^{-1} band is assigned to a ν_{CC} mode involving the whole PAH skeleton. It is blue-shifted by 29 cm^{-1} with respect to that in $\text{C}_{10}\text{H}_8^+$. The splitting of the γ_{CH} band into two bands and the blue-shift of the ν_{CC} band are therefore signatures to probe the presence of $[\text{SiPAH}]^+$ complexes in the ISM.

6.2.2 Anharmonic

The spectra calculated at the DFT level are harmonic spectra corresponding to small amplitude motions (spectra at the limit of $T = 0\text{ K}$). In the emission process observed in the ISM, the temperature of such complexes differs from 0 K and anharmonic effects should be taken into account. In the classical motion approximation, these effects can be derived from MD simulations by computing the Fourier transform of the complex dipole autocorrelation function. The use of DFTB on-the fly allows to perform MD simulations on the required long-timescales (Joalland *et al.* 2010) and to explore various ranges of temperatures.

For low temperatures, the Si atom remains on top of the same ring. For higher temperatures, there is sufficient energy for the Si atom to overcome the barrier separating two PES minima (differing by the Si position on top of two adjacent cycles) and the average time spent on a given ring decreases as the temperature increases.

Figure 3 shows the evolution of the γ_{CH} mode in the naphthalene cation. It exhibits a broadening and a red-shift when the temperature increases. The same behavior is observed in the $[\text{SiC}_{10}\text{H}_8]^+$ complex for the two γ_{CH} bands that result from the splitting due to the Si coordination. However, the broadening is much more significant for temperatures larger than 600 K , when the system reaches the high temperature mobility regime. At this temperature, the Si oscillation over the two rings is fast enough to couple the two C-H modes. The two corresponding bands are thus shifted towards each other, each one displaying a broad wing in the interband region.

The study of complexes with increasing sizes shows that this band broadening can be generalized to the spectra of $[\text{SiPAH}]^+$ complexes compared to those of the corresponding bare PAH^+ . Although the spectra calculated for a limited number

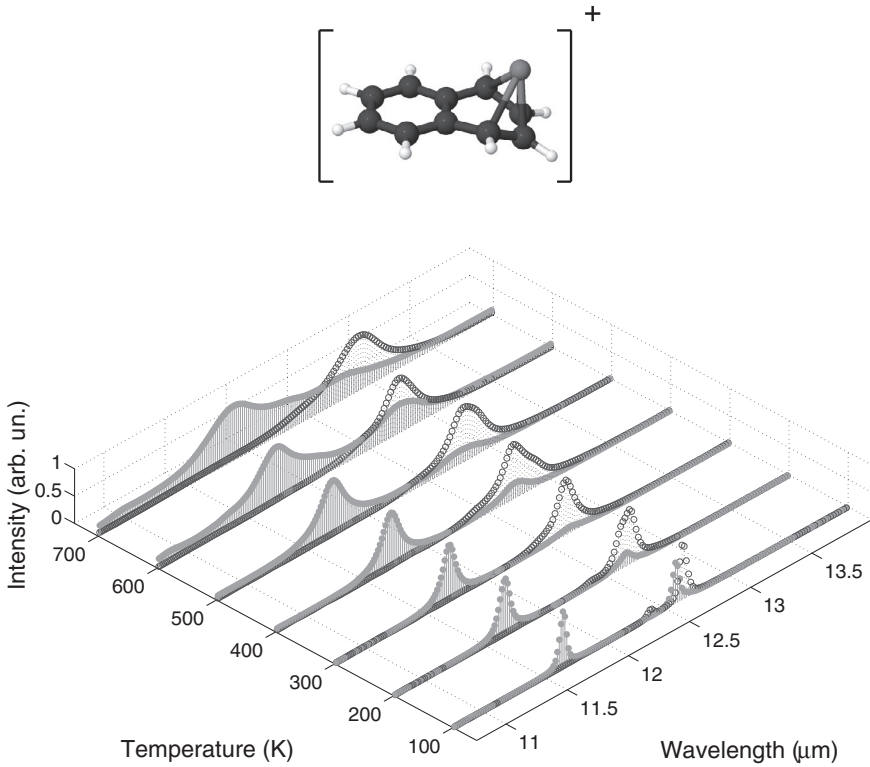


Fig. 3. Evolution of the γ_{CH} band in bare $C_{10}H_8^+$ (blue/open circles) and in the $[SiC_{10}H_8]^+$ complex (red/filled circles) as a function of the temperature.

of SiPAH complexes are not directly able to account the VSG spectrum, this band broadening is consistent with the features observed in the VSG spectrum.

7 Conclusion

The spectral evolution of the AIBs in PDRs provides evidence for PAH evolution in molecular clouds. Inside molecular clouds, the spectra present characteristics of small carbonaceous grains which seem to evaporate, where the UV flux becomes strong enough, to give the free-flying PAHs. The theoretical modelling of these grains requires multiscale approaches combining different levels of theory to model the PES.

Possible candidates for these grains are PAH clusters in their neutral form as they are located in regions where PAHs are expected to be neutrals. A global exploration of the structural properties shows that the most stable structures are

self assemblies of small units made of PAH stacks. The comparison of calculated nucleation rates for clusters of 4 and 13 coronene molecules *versus* their evaporation rates in the physical conditions of NGC 7023N leads to the conclusion that such clusters are photoevaporated faster than they can be reformed. They are thus not the observed VSGs and other hypotheses must be investigated like for instance clusters made of larger PAHs and/or with more units. Other candidates are cationic PAH clusters. The binding energies are larger than that computed for their neutral counterparts and the long-range attraction of the ionic cluster/polarisable molecule strongly increases the formation rate. Finally we investigated the possibility that VSGs could consist of complexes of PAHs with heteroatoms such as Fe or Si. The harmonic spectra of $[\text{SiPAH}]^+$ complexes show the appearance of new bands compared to the spectra of bare PAH⁺. When the temperature increases, these bands are broadened, shifted and mixed to give broad structures. Such effects are in line with the broadening of the AIBs in the VSG spectra.

The question of the VSG nature is still an open question. At the moment, the only conclusion that can be drawn is that these grains are larger than PAHs but strongly related to them. If the small neutral PAH clusters hypothesis has been ruled out, candidates like clusters of larger molecules and/or with more units, ionised PAH clusters and Fe/Si-PAH complexes need further investigations. A global evolution model of PAHs and related species would be very useful to validate/invalidate the various hypotheses (See for instance Montillaud *et al.*, in this volume).

The authors thank F. Calvo and P. Parneix for their contributions in various aspects of the modelling and simulations presented in this overview.

References

- Allamandola, L.J., Tielens, A.G.G.M., & Barker, J.R., 1985, *ApJ*, 290, L25
Berné, O., Joblin, C., Deville, Y., *et al.*, 2007, *A&A*, 469, 575
Berné, O., Joblin, C., Fuente, A., & Menard, F., 2009, *A&A*, 495, 827
Berné, O., Joblin, C., Rapacioli, M., *et al.*, 2008, *A&A*, 479, L41
Calvo, F., & Parneix, P., 2004, *JCP*, 120, 2780
Chabbal, S., Stoll, H., Werner, H.-J., & Leininger, T., 2010, *Mol. Phys.*, submitted
Elstner, M., Hobza, P., Frauenheim, T., Suhai, S., & Kaxiras, E., 2001, *JCP*, 114, 5149
Elstner, M., Porezag, D., Jungnickel, G., *et al.*, 1998, *Phys. Rev. B*, 58, 7260
Fromager, E., & Jensen, H.J.A., 2008, *Phys. Rev. A*, 78, 022504
Grimme, S., 2006, *J. Comp. Chem.*, 27, 1787
Herbst, E., 2001, *Chem. Soc. Rev.*, 30, 168
Joalland, B., Rapacioli, M., Simon, A., *et al.*, 2010, *JPC A*, 114, 5846
Joalland, B., Simon, A., Marsden, C. J., & Joblin, C., 2009, *A&A*, 494, 969
Joblin, C., Szczerba, R., Berne, O., & Szyszka, C., 2008, *A&A*, 490, 189
Joblin, C., Toublanc, D., Boissel, P., & Tielens, A., 2002, *Mol. Phys.*, 22, 3595

- Léger, A., & Puget, J.L., 1984, A&A, 137, L5
- Oliveira, A., Seifert, G., Heine, T., & duarte, H., 2009, J. Braz. Chem. Soc., 20, 1193
- Podeszwa, R., Bukowski, R., & Szalewicz, K., 2006, JPC A, 110, 10345
- Porezag, D., Frauenheim, T., Köhler, T., Seifert, G., & Kaschner, R., 1995, Phys. Rev. B, 51, 12947
- Rapacioli, M., Calvo, F., Joblin, C., *et al.*, 2006, A&A, 460, 519
- Rapacioli, M., Calvo, F., Spiegelman, F., Joblin, C., & Wales, D., 2005, JPC A, 109, 2487
- Rapacioli, M., Joblin, C., & Boissel, P., 2005, A&A, 429, 193
- Rapacioli, M., & Spiegelman, F., 2009, EpJD, 52, 55
- Rapacioli, M., Spiegelman, F., Mirtschink, A., & Scemama, A., 2010, in preparation
- Rapacioli, M., Spiegelman, F., Talbi, D., *et al.*, 2009, JCP, 130, 244304
- Rhee, Y.M., Lee, T.J., Gudipati, M.S., Allamandola, L.J., & Head-Gordon, M., 2007, PNAS, 104, 5274
- Seifert, G., Porezag, D., & Frauenheim, T., 1996, IJQM, 58, 185
- Simon, A., & Joblin, C., 2007, JPC A, 111, 9745
- Simon, A., & Joblin, C., 2009, JPC A, 113, 4878
- Simon, A., & Joblin, C., 2010, ApJ, 712, 69
- Simon, A., Joblin, C., Polfer, N., & Oomens, J., 2008, JPC A, 112, 8551
- Stone, A., 1997, The Theory of Intermolecular Forces, 0198558848, (USA, Oxford: University Press)
- Toulouse, J., Colonna, F., & Savin, A., 2004, Phys. Rev. A, 70, 6
- Van Oanh, N.T., Parneix, P., & Bréchnignac, P., 2002, JPC A., 106, 10144
- Wu, Q., Cheng, S.-L., & Van Voorhis, T., 2007, JCP, 127, 164119
- Zhao, Y., & Truhlar, D. G., 2008, JPC C, 112, 4061
- Zhechkov, L., Heine, T., Patchovskii, S., Seifert, G., & Duarte, H., 2005, JCTC, 1, 841

THE FORMATION OF BENZENE IN DENSE ENVIRONMENTS

P.M. Woods¹

Abstract. PAHs are traditionally thought to form around carbon-rich AGB stars, where the presence of inner-wind shocks and nucleation seeds can aid their formation. However, my recent work has shown that the formation of benzene – thought to be the rate-limiting step in the formation of larger PAHs – can be efficient in other environments, namely the dense tori around the evolved stars of pre-planetary nebulae and in the inner regions of the accretion discs around young stars. I will discuss the chemical pathways to the formation of benzene in these regions and the subsequent formation of larger PAHs.

1 Introduction

The first discovery of benzene outside of the Solar System was made by Cernicharo *et al.* (2001a) towards the carbon-rich pre-planetary nebula², CRL 618. A small absorption at $\sim 14.8 \mu\text{m}$ in the mid-infrared spectrum from the Short-Wavelength Spectrometer on board the *Infrared Space Observatory* was attributed to the Q-branch of the ν_4 band of benzene. These authors also detected lines of diacetylene (C_4H_2) and triacetylene (C_6H_2), and in the companion paper (Cernicharo *et al.* 2001b) detected methylpolyynes and other small hydrocarbons towards CRL 618. The detection of benzene was exciting for several reasons: firstly, this was another molecule to add to the list of 100 or so interstellar and circumstellar molecules detected at that time (the list has since grown to ~ 160). Secondly, benzene (C_6H_6) is a large molecule, and very few molecules of this size have been detected in the interstellar or circumstellar media. Thirdly, benzene is a cyclic molecule, more circular in structure than the “triangular” cyclic molecules,

¹ Jodrell Bank Centre for Astrophysics, School of Physics & Astronomy, University of Manchester, Oxford Road, Manchester M13 9PL, UK

<http://www.jb.man.ac.uk/~pwoods>

²I use the term “pre-planetary nebula” as opposed to “protoplanetary nebula” (both terms describing evolved, post-Asymptotic Giant Branch stars) in order to save confusion with “protoplanetary disc”, which is the accretion disc around a young, low-mass star.

ethylene oxide ($c\text{-C}_2\text{H}_4\text{O}$) and cyclopropenylidene ($c\text{-C}_3\text{H}_2$). As such, its detection heralded the beginnings of an astrochemistry (and an astrobiology) which was not solely dependent on the large linear carbon chain molecules previously seen in the archetypical carbon star, IRC+10216, for example.

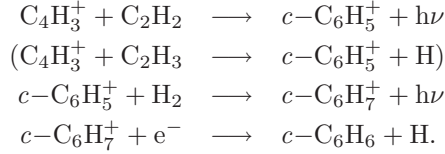
Five years subsequently, Bernard-Salas *et al.* (2006) reported the detection of benzene, diacetylene and triacetylene in another galaxy – the Large Magellanic Cloud. In this case, again, the object in question was a pre-planetary nebula, SMP LMC 11. Herpin & Cernicharo (2000) suggested, for the case of CRL 618, that the molecular richness originates in a circumstellar torus which is sufficiently dense to shield molecules from the intense UV fields in the environments around these proto-White Dwarf stars. Certainly without sufficient shielding complex molecules in the post-AGB phase of evolution are rapidly destroyed (Woods *et al.* 2005). In these proceedings I will summarise work which shows that benzene can form efficiently in the post-AGB phase, in excellent agreement with the observations of Cernicharo *et al.* (2001a). I will also discuss the formation of benzene in a physically and chemically similar environment, the inner regions of protoplanetary discs, where benzene has yet to be detected but PAHs have been seen (Geers *et al.* 2006).

2 Combustion chemistry or interstellar chemistry?

Benzene and polycyclic aromatic hydrocarbons (PAHs) are readily found on Earth in crude oil and coal, and their combustion properties have been well-studied in the laboratory, motivated in part by the petroleum and combustion engine industries and latterly environmental concerns. Both benzene and PAHs are known to form in hydrocarbon flames under terrestrial conditions (*e.g.*, Frenklach 2002), and could potentially form in circumstellar conditions where the chemistry and physics are similar. Such an approach has been used by combustion chemists (*e.g.*, Frenklach & Feigelson 1989) and astrochemists (*e.g.*, Cau 2002; Cherchneff *et al.* 1992, see also Cherchneff, this volume) to explain carbon dust (soot) formation in the inner winds of carbon-rich red giant stars. However, the temperatures reached in flames and in the inner regions of AGB stars (1000–1500K) are not readily found in the interstellar and much of the circumstellar media. Thus we must look to other explanations for the formation of benzene in pre-planetary nebulae, and given the chemical richness that some of these objects display, it seems logical to consider the “bottom-up” route to the formation of benzene and PAHs. (An alternative would be the “top-down” route, where graphitised carbon grains are decimated by shocks or other energetic processes).

Benzene has been detected in the upper atmospheres of Jupiter, Saturn and Titan (*e.g.*, Bézard *et al.* 2001; Waite *et al.* 2007, 2005), environments where ion-molecule reactions dominate over the neutral-neutral reactions which are the mainstay of combustion chemistry. Similarly, if benzene were to form in the interstellar medium (ISM) or the intensely-irradiated environments around post-AGB stars, we would expect it to form via these ion-molecule reactions. Indeed, early

models of dense interstellar clouds by McEwan *et al.* (1999) suggested that benzene was formed thus:



This model produced a fractional abundance of benzene of $\approx 10^{-9}$, several orders of magnitude below that detected in CRL 618. In order, then, to explain the observed abundance and investigate the formation of benzene in CRL 618, we will adopt an interstellar-based chemistry (Le Teuff *et al.* 2000; Millar *et al.* 2000), and a suitable physical model.

3 The formation of benzene in pre-planetary nebulae

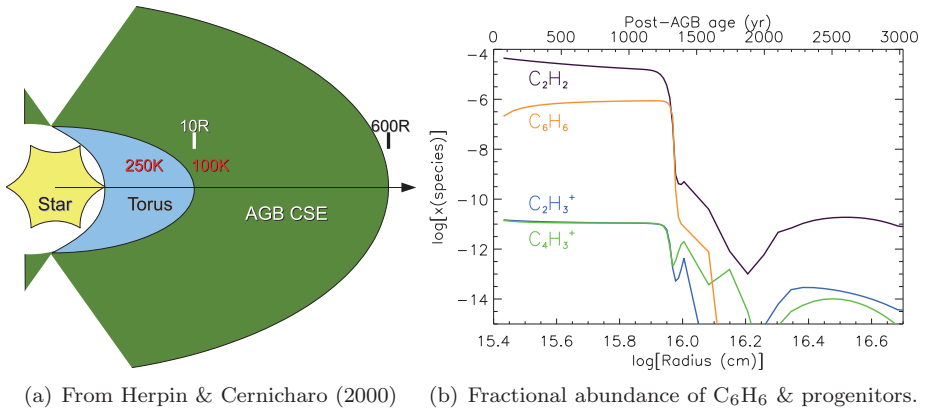
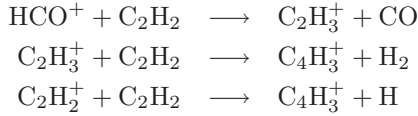


Fig. 1. Physical and chemical models of CRL 618.

Herpin & Cernicharo (2000) were able to determine various physical properties of the circumstellar regions around CRL 618, and some of these are shown in Figure 1a. We choose to model the slowly-expanding (5 km s^{-1}) torus, since the high density of this region ($n \sim 10^{11} \text{ cm}^{-3}$, initially) extinguishes the significant UV radiation ($2 \times 10^5 G_0$) from the central star and allows complex chemistry to develop. We also enhance the cosmic-ray ionisation rate by a factor of 100 in order to account for X-rays from the hot star. At this stage of evolution, mass-loss from the star has ceased, and so we must consider a time-dependent situation. In the thin-shell approximation, we obtain the results shown in Figure 1b.

Benzene in the model is approximately 40 times less abundant than acetylene (a ratio observed by Cernicharo *et al.* 2001a) until about 1300 yr. At this stage,

dilution of the expanding torus means that photodestruction of the molecular matter dominates. The major route to the formation of benzene in this environment is similar to that described in Section 2, except that the route to $C_4H_3^+$ is simpler, *viz.*,



(*cf.*, McEwan *et al.* 1999). This is due to large fractional abundances of HCO^+ (which is generally not abundant in AGB star envelopes but is abundant in the post-AGB phase because of the more intense UV flux from the star) and C_2H_2 (which is generally not abundant in the ISM). Combined with a high degree of UV-shielding and reasonable residence times, large amounts of benzene can form. For further details, see Woods *et al.* (2003, 2002).

4 The formation of benzene in protoplanetary discs

The inner regions of the protoplanetary accretion discs around young stars have a similar temperature and density to the torus modelled in the previous section. In this case, the physical model we use is significantly more complex (see Woods & Willacy 2009, for a complete description) but the chemistry is very similar, although we use solar, oxygen-rich initial abundances, and incorporate gas-grain interactions and grain-surface reactions into the chemical modelling.

Results of the model show that benzene can form at a reasonably high fractional abundance ($\sim 10^{-6} \text{ cm}^{-3}$) in the inner 3 AU of a protoplanetary disc. This is surprising, since protoplanetary discs are not carbon-rich environments; however, the cool midplanes of these discs allow water vapour to freeze out onto the surface of dust grains, effectively removing a major repository of oxygen from the gas-phase chemistry. Small hydrocarbons can then dominate the chemistry until the advecting material is sufficiently warmed to liberate its oxygenous icy mantles. Interestingly, benzene forms in this environment via an odd-carbon-atom pathway rather than through the even-carbon-atom pathway (*i.e.*, acetylene addition) discussed previously:



and this ion-molecule pathway is more efficient than a suggested three-body neutral-neutral reaction:



The abundance of benzene in the gas phase depends on the binding energy of benzene to the grain surface on which it resides after neutralisation (reaction 4.2).

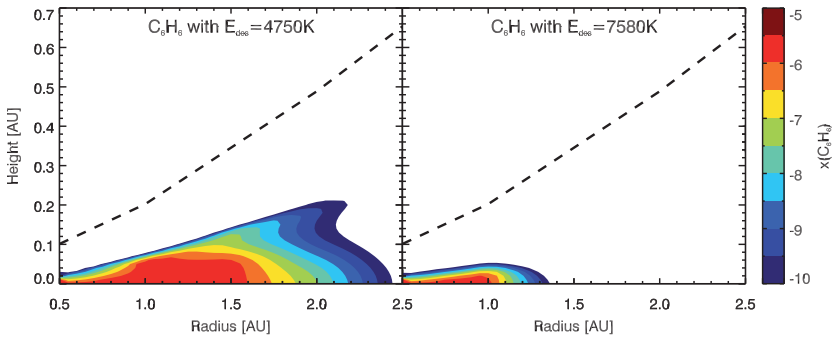


Fig. 2. The fractional abundance of gas-phase benzene in protoplanetary discs, using a low (left) and high (right) value of the binding energy. Dashed lines show the approximate disc surface.

Estimates of this binding energy vary, and thus two extreme cases (4750 K and 7580 K) are shown in Figure 2 for the distribution of gas-phase benzene. A recent experimental result suggests a value of 5600 K (Thrower *et al.* 2009) is appropriate, similar to the binding energy of water. The reaction between C_3H_4 and its ion (reaction 4.1) has been measured in the laboratory, and has been shown to occur for the main isomers of C_3H_4 . These results are discussed in more detail in Woods & Willacy (2007).

5 The formation of PAHs in dense environments

The formation of benzene is thought to be the rate-limiting step in the formation of PAHs, and there is evidence to support this (Wang & Frenklach 1994). Potentially, then, once benzene is formed, PAHs could rapidly form from it, or from related species like phenyl. Second-ring closure (*e.g.*, to form naphthalene from ethylbenzene or similar) is thought to involve an energy barrier which requires temperatures of 900–1100 K to overcome (Frenklach & Feigelson 1989). Temperatures like this are present in the upper regions of protoplanetary discs, and material from the midplane of these discs is mixed to the surface on a timescale of ~ 625 yr (at 3 AU; Ilgner & Nelson 2006). Vertical mixing is neglected in the model of Woods & Willacy (2007), but we can estimate a formation timescale of a generic PAH (say with 40 carbon atoms – a size which is stable to photodissociation) from benzene. Two-carbon (acetylene) units can be added at a rate of one every three years, assuming a density of $\sim 10^{10}$ cm^{-3} and a conservative association rate. Adding 17 of these units to form a stable PAH would take 50 yr, significantly shorter than the mixing timescale calculated by Ilgner & Nelson (2006). Thus it seems reasonable that PAHs could form in protoplanetary discs. Of course, a more detailed treatment is needed, and work is in progress on this topic.

Models of hydrocarbon chemistry in dense environments such as those discussed show that there is a disposition towards the formation of complex species,

including benzene and PAHs. It may be that the destruction mechanisms of these complex molecules are not fully understood, but even if the carbon skeletons of molecules are shattered by some energetic process, the fragments themselves are the constituent building-blocks of PAHs, and can be re-incorporated into the formation process (Ní Chuimín 2009).

PMW would like to thank Tom Millar and Karen Willacy, who have contributed to this work over the past few years.

References

- Bernard-Salas, J., Peeters, E., Sloan, G.C., *et al.*, 2006, *ApJ*, 652, L29
- Bézard, B., Drossart, P., Encrenaz, T., & Feuchtgruber, H., 2001, *Icarus*, 154, 492
- Cau, P., 2002, *A&A*, 392, 203
- Cernicharo, J., Heras, A.M., Tielens, A.G.G.M., *et al.*, 2001a, *ApJ*, 546, L123
- Cernicharo, J., Heras, A.M., Pardo, J.R., *et al.*, 2001b, *ApJ*, 546, L127
- Cherchneff, I., Barker, J.R., & Tielens, A.G.G.M., 1992, *ApJ*, 401, 269
- Frenklach, M., 2002, *Phys. Chem. Chem. Phys.*, 4, 2028
- Frenklach, M., & Feigelson, E.D., 1989, *ApJ*, 341, 372
- Geers, V.C., Augereau, J.-C., Pontoppidan, K.M., *et al.*, 2006, *A&A*, 459, 545
- Herpin, F., & Cernicharo, J., 2000, *ApJ*, 530, L129
- Ilgner, M., & Nelson, R.P., 2006, *A&A*, 445, 223
- Le Teuff, Y.H., Millar, T.J., & Markwick, A.J., 2000, *A&AS*, 146, 157
- McEwan, M.J., Scott, G.B.I., Adams, N.G., *et al.*, 1999, *ApJ*, 513, 287
- Millar, T.J., Herbst, E., & Bettens, R.P.A., 2000, *MNRAS*, 316, 195
- Ní Chuimín, R., 2009, Ph.D. Thesis, Univ. of Manchester
- Thrower, J.D., Collings, M.P., Rutten, F.J.M., & McCoustra, M.R.S., 2009, *MNRAS*, 394, 1510
- Waite, J.H., Young, D.T., Cravens, T.E., *et al.*, 2007, *Science*, 316, 870
- Waite, J.H., Niemann, H., Yelle, R.V., *et al.*, 2005, *Science*, 308, 982
- Wang, H., & Frenklach, M., 1994, *J. Phys. Chem.*, 98, 11465
- Woods, P.M., & Willacy, K., 2009, *ApJ*, 693, 1360
- Woods, P.M., & Willacy, K., 2007, *ApJ*, 655, L49
- Woods, P.M., Nyman, L.-Å., Schöier, F.L., *et al.*, 2005, *A&A*, 429, 977
- Woods, P.M., Millar, T.J., Herbst, E., & Zijlstra, A.A., 2003, *A&A*, 402, 189
- Woods, P.M., Millar, T.J., Zijlstra, A.A., & Herbst, E., 2002, *ApJ*, 574, L167

EXPERIMENTAL STUDIES OF THE DISSOCIATIVE RECOMBINATION PROCESSES FOR THE $C_6D_6^+$ AND $C_6D_7^+$ IONS

M. Hamberg¹, E. Vigren¹, R.D. Thomas¹, V. Zhaunerchyk², M. Zhang³, S. Trippel⁴, M. Kaminska⁵, I. Kashperka¹, M. af Ugglas¹, A. Källberg⁶, A. Simonsson⁶, A. Paál⁶, J. Semaniak⁵, M. Larsson¹ and W.D. Geppert¹

Abstract. We have investigated the dissociative recombination (DR) of the $C_6D_6^+$ and $C_6D_7^+$ ions using the CRYRING heavy-ion storage ring at Stockholm University, Sweden. The dissociative recombination branching ratios were determined at minimal collision energy, showing that the DR of both ions was dominated by pathways keeping the carbon atoms together in one product. The absolute reaction cross sections for the titular ions are best fitted by $\sigma(E_{cm}[\text{eV}]) = 1.3 \pm 0.4 \times 10^{-15} (E_{cm}[\text{eV}])^{-1.19 \pm 0.02} \text{ cm}^2$ ($C_6D_6^+$) and $\sigma(E_{cm}[\text{eV}]) = 1.1 \pm 0.3 \times 10^{-15} (E_{cm}[\text{eV}])^{-1.33 \pm 0.02} \text{ cm}^2$ ($C_6D_7^+$) in the intervals 3-300 meV and 3-200 meV respectively. The thermal rate constants of the titular reactions are best described by: $k(T) = 1.3 \pm 0.4 \times 10^{-6} (T/300)^{-0.69 \pm 0.02} \text{ cm}^3 \text{ s}^{-1}$ for $C_6D_6^+$ and $k(T) = 2.0 \pm 0.6 \times 10^{-6} (T/300)^{-0.83 \pm 0.02} \text{ cm}^3 \text{ s}^{-1}$ for $C_6D_7^+$. These expressions correlates well with earlier flowing after-glow studies on the same process.

1 Introduction

Polyaromatic hydrocarbons (PAHs) are thought to play a central role in astrochemistry. It is suggested that PAHs may contain up to 20% of the available carbon

¹ Department of Physics, Stockholm University, SE-106 91 Stockholm, Sweden;
e-mail: mathias.hamberg@physto.se

² Radboud University Nijmegen, Institute for Molecules and Materials, PO Box 9010, 6500 GL Nijmegen, The Netherlands

³ Institute of Modern Physics, Chinese Academy of Sciences, 509 Nanchang Rd., Lanzhou 730000, China

⁴ Department of Physics, Albert-Ludwigs Universität Freiburg, Hermann-Herder-Str. 3, 79104 Freiburg, Germany

⁵ Jan Kochanowski University, Świętokrzyska 15, 25406 Kielce, Poland

⁶ Manne Siegbahn Laboratory, Frescativägen 26, 114 18 Stockholm, Sweden

in the ISM (Boulanger 1999). Whereas there is strong evidence for the presence of PAHs in various astronomical objects, only the simplest aromatic compound, benzene (C_6H_6) has been unambiguously detected by the *Infrared Space Observatory* in the protoplanetary nebula CRL 618 (Cernicharo *et al.* 2001). Furthermore, benzene is present in the atmospheres of gaseous giant planets and has been found in Titan's atmosphere by the Composite Infra-Red spectrometer (CIRS) on board the Cassini-Huygens mission (Vinatier *et al.* 2007).

Benzene can function as template in the build-up of higher hydrocarbons including PAHs in the interstellar medium. In a recent paper by Le Page *et al.* (2009) it is suggested that PAHs may play a key role as catalyst in forming molecular hydrogen in the interstellar medium. This involves chemical trapping of H atoms on dehydrogenated PAHs, ionisation of the PAH, followed by addition of another H atom with a subsequent release of H_2 through dissociative recombination (DR). This sequence constitutes a circular processes in which a hydrogen molecule is formed from two atoms and the dehydrogenated PAH is recycled. Le Page *et al.* (2009) assume in their model branching fractions of 50% each for the two reaction channels leading to H and H_2 respectively in the DR of $C_6H_7^+$.

Investigation of the synthesis for benzene itself in these environments is therefore a key issue. In interstellar clouds as well as Titan's atmosphere dissociative recombination of the $C_6H_7^+$ ion (which is formed by a sequence of ion-neutral reactions) leading to the unprotonated benzene has been invoked as the final step in the synthesis of this compound (Woods *et al.* 2002; Vuitton *et al.* 2008):



The DR process itself is, however, highly exoergic ($\Delta H = -5.73$ eV for the above-mentioned reaction) and other reaction channels including ejection of carbon-containing fragments may be feasible. In addition, it has recently been shown that ejection of a single H atom can be an only minor reaction channel for protonated molecules (Geppert *et al.* 2005; Hamberg 2010). Therefore knowledge of the branching ratio of the DR of protonated benzene is crucial to validate the postulated formation mechanism in the interstellar medium and planetary atmospheres. This Paper presents an experimental study into the DR rate constant and product branching fractions of $C_6D_6^+$ and $C_6D_7^+$.

2 Experiment

The experiments were carried out at the heavy-ion storage ring CRYRING at Stockholm University, Sweden. The procedure has been explained in detail previously (Neau *et al.* 2000) and will therefore only be summarised here. The ions were formed by a discharge in a mixture of fully deuterated benzene and deuterium gas in a hollow cathode type ion source. The gas was pulsed into the ion source reaching a peak pressure of ~ 1 Torr in order to strive for collisional quenching. The ions were then accelerated by 40 kV and mass selected by the first bending

magnet in the injection line. After a 10-turn multi injection procedure into the storage ring the ions were further accelerated by a RF-system to the maximum kinetic energy of $\sim 96/m_{ion}$ MeV (where m_{ion} is the ion mass in amu). A long storage time of several seconds was ensured due to the low ring pressure of residual gas (typically $\sim 10^{-11}$ Torr). Thus the ions could be left to de-excite for 3 seconds before the measurement sequence started. This left ample time for vibrationally excited inner degrees of freedom to relax. In an electron cooler a cold, monoenergetic electron beam was overlapping the path of the ions over ~ 85 cm which served as DR interaction region. Neutral particles formed in the process were separated from the ion beam, since they are unaffected by the dipole magnet located after the electron cooler and were recorded by an energy sensitive ion implanted silicon detector (IISD).

3 Data analysis and results

3.1 Branching fractions

Branching fraction measurements were performed at 0 eV nominal relative kinetic energy. Neutral fragments deriving from DR-events impinge on the IISD at a timescale (ns) much shorter than the shaping time of the preamplifier (μs). Therefore the detected signal for each event will essentially reflect the sum of the masses of all the incoming fragments and thus yield no information about the branching ratio. To come around this problem a transparent metal grid with a transmission probability of 0.297 ± 0.015 is inserted in front of the IISD. With the grid inserted all fragment masses appear in the energy spectrum and branching ratios can be derived from the intensity distribution of the different mass signals. Fragment energy spectra with and without grid for $C_6D_6^+$ ion are shown in Figure 1. One can see a small signal around energy channel 950 indicating that some fragments containing 3 C-atoms are breaking loose from the rest of the molecule although the majority of DR processes seem to keep all six carbon atoms together. If splitting up of the ions into 2 fragments containing 3 carbon atoms would dominate the reaction flux the spectra measured with the grid inserted would be severely different from the ones recorded without grid. The peak at full energy would then be smaller than the 3C peak found around channel 950 due to the comparatively low transmissibility of the grid. No obvious peaks are found at the energies corresponding to fragments with two or four carbon atoms. The lack of smaller fragments is even more pronounced for the $C_6D_7^+$ ion where the spectrum structure essentially indicates that all fragments keep the six carbon atoms together and no other peaks are distinguishable (see Fig. 1). Rescaling the MCA-channels into mass units (which can only be done in a very approximative way due to the broadness of the features) shows that the difference of the peak centers for the peaks corresponding to the highest masses in Figure 1 with the grid in and out is in the order of one amu. This is well in line with ejection of one or two deuterium atoms and a preservation of the aromatic ring structure during

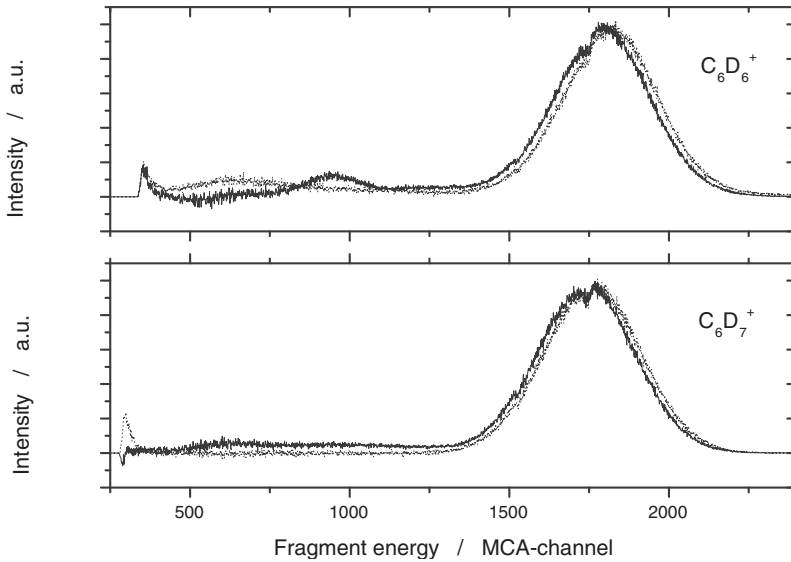


Fig. 1. MCA spectra from branching fraction measurements of the $C_6D_6^+$ (top) and $C_6D_7^+$ (bottom) ions. The data obtained without grid is depicted with a dotted line whereas the ones recorded with the grid inserted are represented with a solid line.

DR. However, further analysis were complicated due to losses of fast deuterium fragments bypassing the active detector area. Possible losses of heavier fragments containing carbon atoms were estimated to be well below 10% using Monte Carlo simulations in a similar fashion as Thomas (2008) and should therefore not affect the obtained spectra much.

3.2 Cross section and rate constant

To measure the DR rate constant the electron velocity was ramped relative to the ion velocity by scanning the electron acceleration voltage in the electron cooler. The neutral particles deriving from the DR-processes were detected by the IISD and counted by a multichannel scaler (MCS) using 2 ms time bins. Each bin corresponds to an interaction energy in the interval between ~ 2 –1000 meV. Background processes from ions interacting with residual gas in the storage ring were simultaneously collected by a micro channel plate (MCP) located at the end of a straight section and recorded by a MCS. The background signal intensity is directly proportional to the ion current and could therefore be scaled to the absolute ion current which was measured with a capacitive pick-up calibrated by an AC transformer directly after acceleration (Paal *et al.* 2006). Therefore the mean ion current throughout the ring-cycle could be determined and fitted by a decay curve. This fit was also used for background subtraction of the DR MCS spectrum before

applying the following formula for calculation of the rate coefficient:

$$k = \left(\frac{dN}{dt}\right) \frac{v_i v_e e^2 r_e^2 \pi}{I_e I_i l}, \quad (3.1)$$

where dN/dt is the measured DR-count rate, I_e , v_e and I_i , v_i are the electron and ion currents and velocities (in the laboratory frame), respectively and e is the elementary charge, r_e is the radius of the electron beam and l is the interaction region length.

Corrections to the data had to be made for: (i) Space charge effects where the electrons experience a drop in the acceleration potential at the cathode in the cooler due to free electrons traveling ahead of them. (ii) Toroidal effects deriving from ion electron collisions at higher energies than the detuning energy in the regions where the electron beam is bent into and out from the interaction region. (iii) The electrons have a non negligible transversal energy spread of 2 meV. The rate constant can therefore be expressed as below through which the DR cross section can be deconvoluted using Fourier methods (Mowat *et al.* 1995):

$$k = \int_0^\infty v_{rel} f(v_\perp) \sigma(v_{rel}) dv_\perp, \quad (3.2)$$

where $f(v_\perp)$ is the transversal electron velocity distribution in the center of mass frame, v_\perp the transversal electron velocity and v_{rel} the relative velocity respectively. The result for the $C_6D_6^+$ ion is displayed in Figure 2 together with the best fit between 3–300 meV giving a cross section of $\sigma(E_{cm}[\text{eV}]) = 1.3 \pm 0.4 \times 10^{-15} (E_{cm}[\text{eV}])^{-1.19 \pm 0.02} \text{ cm}^2$. Applying the same procedure for the $C_6D_7^+$ ion (see Fig. 2) resulted in a best fit over the interval 3–200 meV of: $\sigma(E_{cm}[\text{eV}]) = 1.1 \pm 0.3 \times 10^{-15} (E_{cm}[\text{eV}])^{-1.33 \pm 0.02} \text{ cm}^2$. The thermal rate constant can be obtained from the cross sections by applying the formula:

$$k(T) = \frac{8\pi m_e}{(2\pi m_e k_B T)^{3/2}} \int_0^\infty E_{cm} \sigma(E_{cm}) e^{-E_{cm}/k_B T} dE_{cm}, \quad (3.3)$$

where m_e is the electron mass, k_B is Boltzmann's constant, T is the electron temperature and E_{cm} is the centre of mass energy. The obtained thermal rates are: $k(T) = 1.3 \pm 0.4 \times 10^{-6} (T/300)^{-0.69 \pm 0.02} \text{ cm}^3 \text{ s}^{-1}$ for $C_6D_6^+$ and $k(T) = 2.0 \pm 0.6 \times 10^{-6} (T/300)^{-0.83 \pm 0.02} \text{ cm}^3 \text{ s}^{-1}$ for $C_6D_7^+$. The systematical errors are arising from uncertainties in the ion and electron currents and the length of the interaction region electron density. These errors combined with the statistical uncertainties are estimated to be 25% and 30% for $C_6D_6^+$ and $C_6D_7^+$ respectively.

4 Discussion

For both ions DR experiments have previously been performed using flowing afterglow (FA) technique. The thermal rates at 300 K was found to be $1.0 \pm 0.3 \times 10^{-6} \text{ cm}^3 \text{ s}^{-1}$ ($C_6D_6^+$) and $2.4 \pm 0.4 \times 10^{-6} \text{ cm}^3 \text{ s}^{-1}$ ($C_6D_7^+$), which is in very good

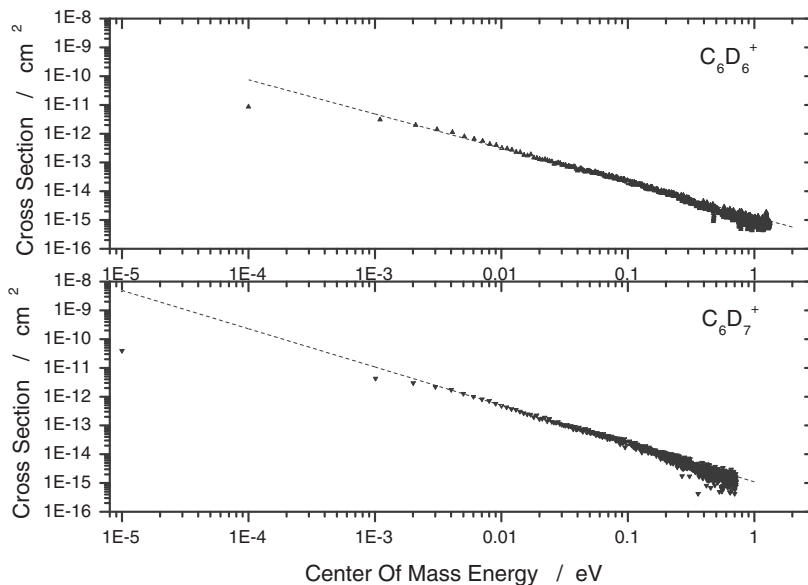


Fig. 2. Cross section of the DR of $C_6D_6^+$ (top) and $C_6D_7^+$ (bottom) versus relative kinetic energy. The triangles shows individually measured spots while the dashed line shows the best fit between 3–300 meV ($C_6D_6^+$) and 3–200 meV ($C_6D_7^+$) respectively.

agreement with previous results for the undeuterated isotopomers (Abouelaziz *et al.* 1993; McLain *et al.* 2004). The lowest formation enthalpy for the undeuterated $C_6H_6^+$ and $C_6H_7^+$ ions are found for their cyclic forms and are $975.8 \text{ kJ mol}^{-1}$ and 854 kJ mol^{-1} respectively (Lias *et al.* 1988). Abouelaziz *et al.* (1993) found in their DR experiment of $C_6H_6^+$ no difference in the results when they formed the ion through charge transfer reaction with C^+ , Xe^+ and Kr^+ suggesting that the structures of the product ions were the same in each case. These charge transfer processes are exoergic with 2 eV, 2.88 eV and 4.75 eV respectively, which can be compared to at least 2.8 eV needed for breaking the benzene ring. Even at higher exoergicities ring opening seems therefore not to occur. In the ion source the $C_6D_6^+$ ions could be formed through charge transfer from D_2^+ and D^+ (exoergic with 6.17 eV and 4.34 eV, respectively (Lias *et al.* 1988)) or charge transfer reaction with D_3^+ leading to D_2 and D (close to thermoneutral, *i.e.* with a reaction enthalpy close to zero). Electron impact and Penning ionization are other processes contributing and one can not rule out formation of other isomers. Nevertheless, we assume that the cyclic structure should dominate the stored ions. In all these thermodynamic considerations the enthalpies of the undeuterated compounds were considered due to the lack of data for the heavier isotopomers.

In our set-up the $C_6D_7^+$ ions should predominantly be formed through protonation by D_3^+ and to some extent reactions with D_2^+ and D^+ (exoergic with 3.48 eV,

5.17 eV and 7.87 eV respectively, Lias & Ausloos 1985). It is also found that the ion can be formed by hydrogen atom abstraction from hydrogen donors. Flowing afterglow experiments were carried out by Milligan *et al.* (2002) and Spanel *et al.* (1995) in which they found that reaction of H_3^+ with benzene leads to $C_6H_7^+$ with unity probability which was described as “a manifestation of the extraordinary stability of this protonated molecule”. Unfortunately however, their type of setup was not sensitive to structural isomers (Spanel & Smith 1998). This is somewhat disadvantageous, since also stable five membered ring and open-chain isomers of $C_6D_7^+$ exist. Kuck (1990) claimed that the cyclic $C_6H_7^+$ was, beyond any doubt, the most stable light hydrogen isomer. In a ICR study, even reactions between aliphatic (neutrals *e.g.* C_3H_4) and ions ($C_3H_4^+$) resulting in the formation of $C_6H_7^+$ at least partly lead to protonated cyclohexene (Lias & Ausloos 1985). This shows that even if the formation process of $C_6D_7^+$ in our ion source to some extent results in open-chain $C_6D_7^+$ isomers, ring closure of these species to deuterated benzene could be possible. Although we cannot exclude different isomeric forms we find it likely that the aromatic form should be dominating. In addition, it should be noted that even protonated benzene has two isomers – a σ and a π -complex. However, Solca & Dopfer (2002) found no presence of the π -complex in a spectroscopic study of $C_6H_7^+$ ions produced by proton transfer to benzene from H_3^+ . This is probably also the major formation process of the $C_6H_7^+$ ion in our experiment, thus we assume the ion present in our experiment to be the σ - $C_6H_7^+$.

Thus, our findings are in line with a formation of benzene in the interstellar medium, circumstellar envelopes and planetary ionospheres through ion-neutral reactions leading to $C_6H_7^+$ followed by DR yielding benzene. Also the rate constant previously measured in flowing afterglow experiments (Abouelaziz *et al.* 1993; McLain *et al.* 2004) and used in models of Titan’s ionosphere (Vuitton *et al.* 2008) has been corroborated in our study, albeit the temperature dependence of the DR rate of $C_6D_7^+$ has been found to be considerably weaker (the exponential factor being -0.83 instead of -1.3). This could be due to a different reactivity of ground and rovibrationally excited states of the ion. In our storage ring, as opposed to afterglow experiments, the distribution between these states is not changed throughout the energy scan. Such different exponential factors of temperature dependence lead to considerably unlike rates at very low temperatures and it has to be seen how model predictions of benzene abundances in very cold environments like dark clouds are affected by that. The effect of the new rate constants on models of warmer environments like planetary ionospheres are, however, probably negligible.

Our results on the DR of $C_6D_7^+$ pose a challenge to neither the invoked formation mechanism of benzene nor to the proposed H_2 formation catalyzed by PAHs. They can, on the contrary, not serve to corroborate them, since we could not establish the branching ratio of the ejection of H_2 and the formation of benzene. If this reaction would only result in production of H_2 , it would render the invoked reaction sequence of benzene formation unfeasible. If on the other hand the branching ratio of the formation of benzene would be close to 1, the catalytic cycle of H_2 formation postulated by Le Page *et al.* (2009) would be impossible. Experiments

on storage rings with higher rigidity, which would enable us to distinguish between H_2 and H ejection are therefore indispensable to clarify the validity of those two reaction sequences.

5 Conclusion

Storage ring technique has for the first time been employed for DR measurements of the simplest aromatic hydrocarbon ions $C_6D_6^+$ and $C_6D_7^+$. The rate constants are in line with previous flowing afterglow measurements at 300 K. Although it was not possible to fully elucidate the branching fractions between the reaction channels, our studies showed that the C_6 -structure is retained almost entirely in both cases. Dissociative recombination of $C_6H_7^+$ therefore still can be regarded as a feasible final step in the synthesis of benzene in the interstellar medium and planetary ionospheres. Our findings also do not disprove the molecular hydrogen formation mechanism by PAHs proposed by Le Page *et al.* (2009).

We thank the staff at the Manne Siegbahn Laboratory for making these experiments possible by excellent technical support. W.D.G. thanks the Swedish Research Council for his Senior Researcher grant (contract number 2006-427) and the Swedish Space Board (grant number 76/06). M.K. thanks the Swedish Institute for financial support and also acknowledges support from the Ministry of Science and Higher Education, Poland, under contract N202 111 31/1194. S.T. acknowledges financing from the COST ACTION (CM0805).

References

- Abouelaziz, H., Gomet, J.C., Pasquero, D., Rowe, B.R., & Mitchell, J.B.A., 1993, *J. Chem. Phys.*, 99, 237
- Boulanger, F., 1999, in *Solid State Matter: The ISO Revolution*, Lecture 2, ed. L. d'Hendecour, C. Joblin, & A. Jones (New York Springer), 19
- Cernicharo, J., Heras, A.M., Tielens, A.G.G.M., *et al.*, 2001, *Astrophys. J. Lett.*, 546, 123
- Geppert, W.D., Thomas, R.D., Ehlerding, A., *et al.*, 2005, *J. Phys. Conf. Ser.*, 4, 26
- Hamberg, M., 2010, *A&A*, 514, A83
- Kuck, D., 1990, *Mass Spectrometry Reviews*, 9, 187
- Le Page, V., Snow, T.P., & Bierbaum, V.M., 2009, *ApJ*, 704, 274
- Lias, S.G., & Ausloos, P., 1985, *J. Chem. Phys.*, 82, 3613
- Lias, S.G., Bartmess, J.E., Liebman, J.F., *et al.*, 1988, *J. Phys. Chem. Ref. Data.*, 17 Suppl. 1
- McLain, J.L., Poterya, V., Molek, C.D., Babcock, L.M., & Adams, N.G., 2004, *J. Phys. Chem.*, 108, 6704
- Milligan, D.B., Wilson, P.F., Freeman, C.G., Meot-Ner, M., & McEwan, M.J., 2002, *J. Phys. Chem. A*, 106, 9745
- Mowat, J.R., Danared, H., Sundtroem, G., *et al.*, 1995, *Phys. Rev. Lett.*, 74, 50

- Neau, A., Al-Khalili, A., Rosén, S., *et al.*, 2000, *J. Chem. Phys.*, 113, 1762
- Paal, A., Simonsson, A., Dietrich, J., & Mohos, I., 2006, *Proceedings of EPAC2006*, 1196
- Solca, N., & Dopfer, O., 2002, *Angew. Chem. Int. Ed.*, 41, 3628
- Spanel, P., & Smith, D., 1998, *Int. J. Mass Spectrom.*, 181, 1
- Spanel, P., Smith, D., & Henchman, M., 1995, *Int. J. Mass Spectrom. Ion Proc.*, 141, 117
- Thomas, R.D., 2008, *Mass Spectrom. Rev.*, 27, 485
- Vinatier, S., Bézard, B., Fouchet, T., *et al.*, 2007, *Icarus*, 188, 120
- Vuitton, V., Yelle, R., & Cui, J., 2008, *J. Geophys. Res.*, 113, E05007
- Woods, P.M., Millar, T.J., Zijlstra, A.A., & Herbst, E., 2002, *Astrophys J. Lett.*, 574, 167

VUV PHOTOCHEMISTRY OF PAHS TRAPPED IN INTERSTELLAR WATER ICE

J. Bouwman¹, H.M. Cuppen¹, L.J. Allamandola² and H. Linnartz¹

Abstract. The mid-infrared emission of Polycyclic Aromatic Hydrocarbons is found in many phases of the interstellar medium. Towards cold dense clouds, however, the emission is heavily quenched. In these regions molecules are found to efficiently freeze-out on interstellar grains forming thin layers of ices. PAHs are highly non-volatile molecules and are also expected to freeze-out. PAHs trapped in interstellar ices are likely to participate in the overall chemistry, leading to the formation of cations and complex molecules in the solid-state. The work presented here aims to experimentally study the chemical reactions that PAHs undergo upon vacuum ultraviolet irradiation when trapped in interstellar H₂O ice.

1 Introduction

PAHs are abundantly present in many phases of the ISM as evidenced by their mid-IR emission bands. Towards dense clouds, however, this emission process is heavily quenched. A possible explanation is that PAHs freeze-out on cold interstellar grains, much like small molecules such as H₂O, CO, CO₂, and CH₃OH, which have been identified in interstellar ices. Once trapped in ices, PAHs are expected to absorb mid-IR photons, rather than emitting them.

Most PAH species have been studied spectroscopically in matrix isolation experiments. Pioneering work has been performed in the past to understand the chemical behavior of PAHs trapped in interstellar ice analogues; the formation of new PAH based products was studied by Bernstein *et al.* (1999) and the efficient ionization of PAHs in H₂O ice was first noted by Gudipati & Allamandola (2003). Here, we build on these first findings by employing near-UV/VIS absorption spectroscopy to present ionization and photoproduct formation rate constants for a

¹ Raymond and Beverly Sackler Laboratory for Astrophysics, Leiden Observatory, Leiden University, PO Box 9513, 2300 RA Leiden, The Netherlands

² NASA-Ames Research Center, Space Science Division, Mail Stop 245-6, Moffett Field, CA 94035, USA

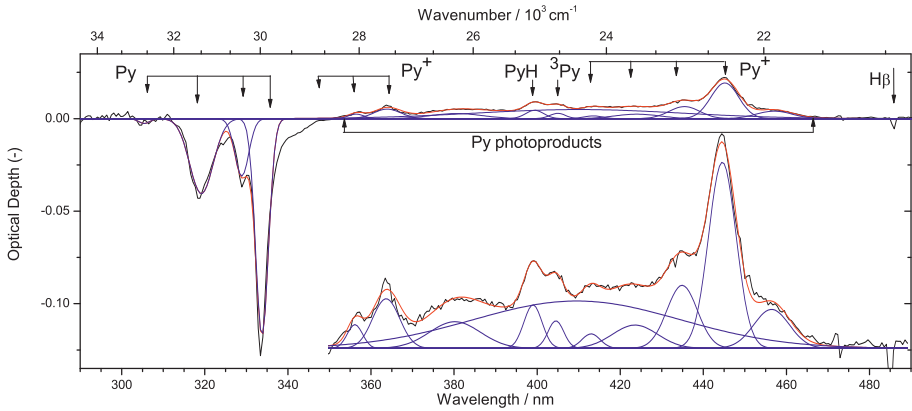


Fig. 1. A typical near-UV/VIS absorption spectrum of the PAH pyrene (Py) trapped in H_2O ice photolyzed for 900 s at a temperature of 125 K. Assignments of the destroyed (negative signal) neutral Py bands and newly formed (positive signal) Py photoproduct bands, the Py cation (Py^+) and 1-hydro-1-pyrenyl radical (PyH) are indicated by arrows. The inset shows a blow-up of the 350 to 490 nm range. Figure is taken from Bouwman *et al.* (2010).

number of PAHs trapped in H_2O ice. Additionally, the photoproducts are also identified *in-situ* by mid-IR spectroscopy. The results are used to derive an upper limit for the possible contribution of PAHs to the 5–8 μm absorption complex towards protostellar objects.

2 Experimental

The PAH: H_2O ice photolysis experiments are performed on two different setups, which have been described in much detail in Bouwman *et al.* (2009) and Hudgins *et al.* (1994) and will only be summarized here briefly. Both setups are based on the same principle and only differ in sample preparation and spectroscopic technique. The systems consist of a high-vacuum chamber pumped down to a pressure of $\sim 10^{-7}$ mbar. A cold finger containing a sample window is suspended in the vacuum chamber and is cooled down to a temperature of 15 K by means of a closed cycle He refrigerator. The sample temperature can be controlled by means of resistive heating.

PAH: H_2O ice samples are grown on the cold sample window by vapor co-depositing milli-Q grade H_2O and the PAH under investigation. The PAHs anthracene (Ant, $\text{C}_{14}\text{H}_{10}$, Aldrich, 99%), pyrene (Py, $\text{C}_{16}\text{H}_{10}$, Aldrich, 99%), or benzo[ghi]perylene ($\text{B}_{\text{ghi}}\text{P}$, $\text{C}_{22}\text{H}_{12}$, Aldrich, 98%) for the mid-IR and additionally coronene (Cor, $\text{C}_{24}\text{H}_{12}$, Aldrich, 99%) for the near-UV/VIS are used as commercially available and brought in the gas phase by heating a sample container to a temperature which is just high enough to create the desired PAH: H_2O sample

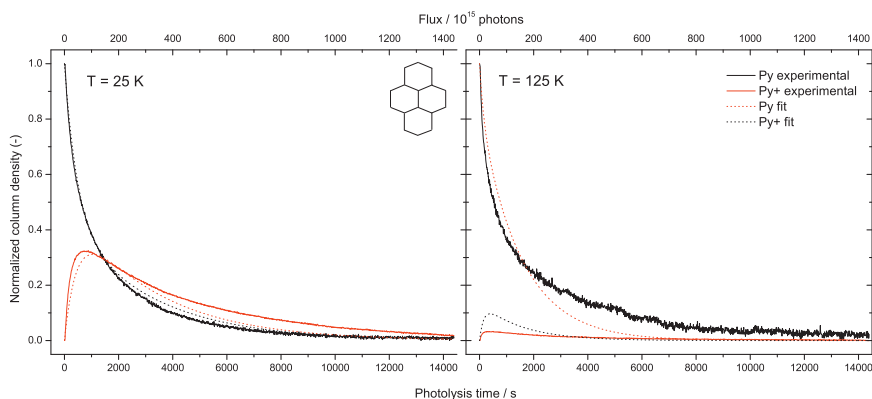


Fig. 2. Time evolution of the relative column density of neutral pyrene (Py) and the pyrene cation (Py⁺) in the ice as a function of photolysis time (VUV fluence). Based on data from Bouwman *et al.* (2010).

ratio. Mixing ratios vary from 1:10 to 1:200 for the mid-IR experiments to 1:500 to 1:10 000 for the optical studies.

The ices for both experimental methods are subsequently irradiated with a vacuum ultraviolet (VUV) H₂ microwave discharge light source to simulate the interstellar radiation field. For the mid-IR spectra, ices are irradiated for 5, 10, 15, 30, 50, 120, and 180 minutes and after each VUV dose one spectrum ranging from 4000 to 400 cm⁻¹ is taken at 0.5 cm⁻¹ resolution. In the near-UV/VIS experiment, spectra are recorded over the spectral range from 280 to 800 nm with a resolution of 0.9 nm.

3 Near-UV/VIS absorption spectroscopy

Near-UV/VIS absorption spectra are obtained for a set of VUV processed PAH:H₂O ices (Bouwman *et al.* 2011a). A typical example of a spectrum is shown in Figure 1. This spectrum is obtained by taking the ratio of a spectrum after photolysis time t and a spectrum taken of the freshly deposited ice $\ln(I_t/I_0)$. The resulting spectrum exhibits positive absorptions arising from the newly formed species and negative absorptions arising from the consumed neutral parent PAH species. Clearly, new bands appear in the spectrum which can be mainly assigned to electronic transitions of the cationic PAH species.

Acquiring a spectrum, such as that displayed in Figure 1, takes 10 s and as many as 1440 spectra are obtained over the course of a single 4 hour photolysis experiment. Currently, optical spectra are available for VUV irradiated Anthracene:H₂O, Pyrene:H₂O, Benzo_{ghi}Perylene:H₂O, and Coronene:H₂O (Bouwman *et al.* 2009, 2010, 2011a) ice mixtures. These data allow us to derive the time evolution of the column density of PAH and PAH⁺ species in the ice as indicated in Figure 2 for a Py containing H₂O ice. Both neutral parent PAH and PAH⁺ cation species

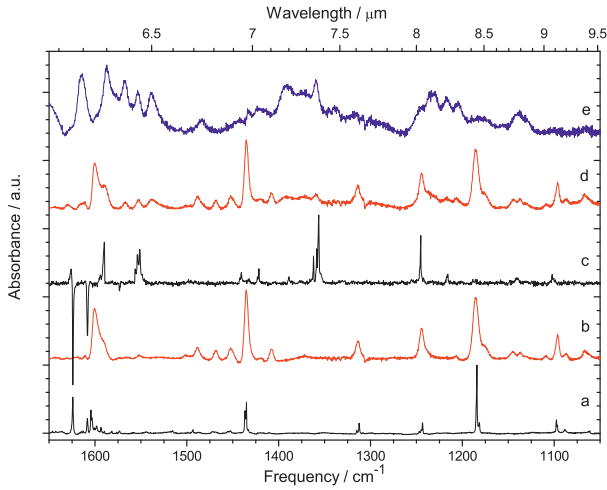


Fig. 3. Comparison between the mid-IR spectra of pyrene (Py) and pyrene cation (Py^+) in an Argon matrix (*a* and *c*) and the same spectra for Py and Py photoproducts trapped in H_2O ice (*b* and *d*). The top spectrum (*e*) indicates the subtraction spectrum ($d - n \times b$) which exhibits photoproducts that appear upon photolysis of a Py: H_2O ice only. Figure is based on data from Bouwman *et al.* (2011b).

are consumed at the end of an experiment. Together with the loss of the PAH and PAH^+ species a broad absorption superposed on the baseline arises, which most likely makes up the absorption by the newly formed photoproducts.

A time-dependent chemical analysis is performed for all PAH species mentioned above. A chemical model is fitted to the experimental data and the rate constants for processing PAHs in an interstellar ice analogue are derived. It is found that the rate constant for ionization of PAHs in H_2O ice is quite similar for all PAHs under investigation here. The derived average PAH ionization rate constant ($\bar{k}_{\text{ion}} \approx 9 \times 10^{-18} \text{ cm}^2 \text{ photon}^{-1}$) can be used to quantify the importance of PAH ionization in the interstellar case by implementing this rate constant in astrochemical models.

4 Mid-IR absorption spectroscopy

Mid-IR spectroscopy is performed on a set of VUV photolyzed PAH containing H_2O ices (Bouwman *et al.* 2011b). Spectra are taken on the freshly deposited ice (spectrum *X*) and after a certain dose of VUV light (spectrum *Y*). A typical spectrum of a neutral PAH in H_2O ice, photolyzed PAH in H_2O ice and a photolyzed PAH in H_2O ice minus the contribution of the remaining neutral PAH species, *n* (photoproducts solely = $Y - nX$) is displayed in Figure 3 for Py: H_2O ice. The factor $(1 - n)$ directly reflects the amount of consumed neutral species.

The spectra of the photoproducts that appear upon photolysis of the PAH in H_2O ice are compared to known spectra of PAH^+ species measured in an Ar

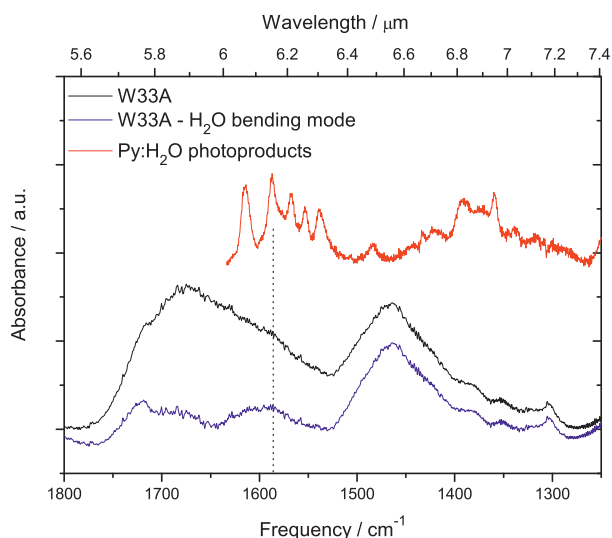


Fig. 4. Comparison between the residuals in the 5–8 μm spectral region towards W33A (Keane *et al.* 2001) and the photoproducts formed by long duration photolysis of a pyrene containing H₂O ice. The dotted line guides the eye to the 6.2 μm interstellar unidentified residual absorption and the cluster of the main pyrene:H₂O photoproduct bands.

matrix (Hudgins *et al.* 1995a, 1995b). In this way, some of the absorption bands can be directly assigned to mid-IR absorptions of the PAH cation. Other bands, however, must be caused by different band carriers.

A comparison of the new absorption bands originating from unknown species with typical mid-IR band positions indicates that the species responsible for the absorptions are likely the parent PAH with side-groups attached. In agreement with an *off-site* analysis of the photoproduct species resulting from the photolysis of PAH:H₂O ices (Ashbourn *et al.* 2007; Bernstein *et al.* 1999), we attribute these absorptions to hydrogenated, hydroxylated and oxydized PAH species.

5 Astrophysical implications

Many interstellar ices have been unambiguously identified by their mid-IR absorption bands observed towards protostellar objects or background stars behind dense clouds. Most of these species are rather simple molecules, such as H₂O, CO, CO₂, NH₃, and CH₃OH (Gibb *et al.* 2000). PAHs frozen out on interstellar grains have not yet been unambiguously identified. Here we derive from the presented spectra an upper limit for the contribution that PAH species may have to the complex absorption in the 5–8 μm mid-IR spectral range towards both high- and low-mass protostars.

The 5–8 μm spectral region is dominated by the strong H_2O bending mode. The residuals that arise after subtraction of the contribution of the H_2O bending mode show that more species are responsible for the overall absorption. As can be seen in Figure 4, there is a clear overlap between the residuals of W33A (taken from Keane *et al.* 2001) and the photoproduct bands that appear upon prolonged irradiation of a PAH: H_2O ice mixture. A band strength can be estimated for the PAH: H_2O photoproduct, because the number of molecules responsible for this band is known. This band strength is used to determine the number of molecules being responsible for the 6.2 μm band (Fig. 4) if these absorption bands are indeed caused by PAH: H_2O photoproducts. In Bouwman *et al.* (2011b), an upper limit of 2–3% with respect to H_2O is derived for the contribution of PAHs to the 5–8 μm absorption complex.

This work is financially supported by NASA’s Laboratory Astrophysics and Astrobiology Programs, “Stichting voor Fundamenteel Onderzoek der Materie” (FOM), and “the Netherlands Research School for Astronomy” (NOVA). J. Bouwman gratefully acknowledges the “Search for Extraterrestrial Intelligence” (SETI) institute for financial support.

References

- Ashbourn, S.F.M., Elsila, J.E., Dworkin, J.P., *et al.*, 2007, *Meteorit. Planet. Sci.*, 42, 2035
- Bernstein, M.P., Sandford, S.A., Allamandola, L.J., *et al.*, 1999, *Science*, 283, 1135
- Bouwman, J., Cuppen, H.M., Allamandola, L.J., & Linnartz, H., 2011a, *A&A*, accepted
- Bouwman, J., Cuppen, H.M., Bakker, A., Allamandola, L.J., & Linnartz, H., 2010, *A&A*, 511, A33+
- Bouwman, J., Mattioda, A.L., Allamandola, L.J., & Linnartz, H., 2011b, *A&A*, 525, A93
- Bouwman, J., Paardekooper, D.M., Cuppen, H.M., Linnartz, H., & Allamandola, L.J., 2009, *ApJ*, 700, 56
- Gibb, E.L., Whittet, D.C.B., Schutte, W.A., *et al.*, 2000, *ApJ*, 536, 347
- Gudipati, M.S., & Allamandola, L.J., 2003, *ApJ*, 596, L195
- Hudgins, D.M., & Allamandola, L.J., 1995a, *J. Phys. Chem.*, 99, 3033
- Hudgins, D.M., & Allamandola, L.J., 1995b, *J. Phys. Chem.*, 99, 8978
- Hudgins, D.M., Sandford, S.A., & Allamandola, L.J., 1994, *J. Phys. Chem.*, 98, 4243
- Keane, J.V., Tielens, A.G.G.M., Boogert, A.C.A., *et al.*, 2001, *A&A*, 376, 254

**PAHs in Regions
of Planet Formation**

OBSERVATIONS OF HYDROCARBON EMISSION IN DISKS AROUND YOUNG STARS

B. Acke^{1, 2}

Abstract. I give an overview of the recent scientific results based on observations of PAH emission from circumstellar disks around young stars. The stellar radiation field plays a key role in the excitation and destruction of the PAH molecules in the disk. The detection rate of PAH emission in disks is optimal for stars of spectral type A. Around stars of similar temperature, the disk structure determines the PAH emission strength: disks with a flared geometry produce stronger PAH emission than flattened disks. The spectral properties of the emission features, indicative of the chemistry of the emitting hydrocarbons, is closely linked to the central star radiation field. The main PAH features shift to redder wavelengths with decreasing stellar effective temperature. This trend has been interpreted as an indication for a higher aliphatic/aromatic ratio of the hydrocarbon mixture around cool stars with respect to hot stars. An alternative explanation may be a more significant contribution to the infrared emission of very small grains around cooler stars.

1 Introduction

As a result of the star-formation process, young stars are surrounded by circumstellar disks. These disks, rich in gas and dust, are believed to be the birthplaces of planetary systems. The disk dissipation timescale is short; In only a few million years, half of the newly formed stars become diskless (*e.g.*, Fedele *et al.* 2010). It is in this short time span that processes such as dust grain growth, crystallisation, sedimentation, photoevaporation, and chemical evolution can take place before the dust is removed. They affect the appearance of the system throughout the electromagnetic spectrum.

¹ Instituut voor Sterrenkunde, University of Leuven, Celestijnenlaan 200D, 3001 Leuven, Belgium; e-mail: bram@ster.kuleuven.be

² Postdoctoral Fellow of the Fund for Scientific Research, Flanders

Young stars are traditionally categorized according to their spectral type. T Tauri stars are young analogues of the Sun, with spectral type later than mid-F and main-sequence masses $M_{\star} \leq 1.5 M_{\odot}$. Higher-mass young stars are called Herbig Ae/Be stars (Herbig 1960). Observations indicate that T Tauri and Herbig Ae stars follow a similar disk evolution. Evidence is growing, however, that disks around Herbig Be stars ($M \geq 3 M_{\odot}$, spectral type earlier than mid-B) are qualitatively different in structure. In the following, it will become clear that the T-Tauri, Herbig-Ae and Herbig-Be classification is also meaningful in the framework of the hydrocarbon emission.

In this Review, I group the scientific results on PAHs in young circumstellar disks in three sections. Section 2 focuses on the detection rates of disk PAH emission features for different types of young stars. In Section 3, it is shown that the strength of the PAH emission is linked to the disk geometry. Finally, I summarize the chemical properties of the hydrocarbons, in relation to the stellar radiation field, in Section 4.

2 PAH detection rates in disks

The detection rate of IR emission features produced by PAH molecules in the circumstellar disk is low for T Tauri stars ($\sim 10\%$) and Herbig Be stars ($< 35\%$). More than two thirds of the intermediate-mass Herbig Ae stars, on the other hand, have detected PAH emission from disks.

2.1 T Tauri stars

Geers *et al.* (2006) and Geers (2007) searched for PAH emission in the spectra of 37 T Tauri stars obtained with the Infrared Spectrograph aboard the Spitzer Space Telescope (Spitzer-IRS; Houck *et al.* 2004). They determined a detection rate of 11–14%, with no detections for stars with spectral type later than G8. Furlan *et al.* (2006) studied Spitzer-IRS spectra of young T Tauri disks in the Taurus star-forming region, whereas Oliveira *et al.* (2010) investigated young stellar objects in the Serpens Molecular Cloud. Only 3–4% of the disk sources have detected PAH features. One could think that the weak UV field of a T Tauri star is insufficient to excite the PAH molecules in the disk. However, Geers *et al.* (2006) compare their data to a simple model for PAH emission in a circumstellar disk. They assume PAH molecules containing 100 carbon atoms ($N_C=100$). To explain the low detection rate, the authors conclude that the abundance of gas-phase PAHs in disks around T Tauri stars must be 10–100 times lower than the PAH abundance of the general interstellar medium (ISM; Cesarsky *et al.* 2000; Habart *et al.* 2001).

Geers *et al.* (2009) searched for PAH emission in low-mass embedded protostars, the evolutionary stage preceding the T Tauri stage, and determined an even lower detection rate (2%). The authors argue that absorption by the envelope surrounding the star and disk is not sufficient to explain the absence of features,

and again suggest that lower PAH abundances are needed. They hypothesize that PAHs enter the disk either frozen out on dust grains, or in agglomerates. Quanz *et al.* (2007) studied the Spitzer-IRS spectra of a sample containing 14 FU Orionis stars. The latter are young low-mass objects that undergo energetic accretion events, leading to strong outbursts at optical and near-IR wavelengths. Only one object, possibly even misclassified as a FU Orionis star, shows hydrocarbon emission features, amongst others the feature at $8.2\ \mu\text{m}$. The low detection rate in this sample ($\leq 7\%$) supports the hypothesis of PAH underabundance in the disks around young low-mass stars.

Siebenmorgen & Krügel (2010) modeled the effect of hard radiation on PAH molecules in a circumstellar disk (see also Siebenmorgen *et al.*, elsewhere in this volume). The authors find that for typical T Tauri X-ray luminosities ($L_X/L_\star \sim 10^{-4}$ – 10^{-3} ; Preibisch *et al.* 2005), PAH molecules in the disk surface are efficiently destroyed at all radial distances, leading to a suppression of the PAH emission. Siebenmorgen & Krügel (2010) suggest that in the few T Tauri disks with detected PAH emission, turbulent vertical mixing brings PAHs to the upper disk layers faster than photodestruction removes the molecules. The hard radiation component in Herbig Ae stars is much weaker ($L_X/L_\star < 10^{-7}$ with a few exceptions; Stelzer *et al.* 2006). A lower destruction rate is expected, consistent with the much higher detection rates (see Sect. 2.3).

However, it may be that the low detection rate is biased because of the focus on the 6.2 and $11.3\ \mu\text{m}$ features. Bouwman *et al.* (2008) find that 5 out of the 7 low-mass young stars in their sample display hydrocarbon emission features. The features are weak compared to the underlying continuum and silicate emission, and a dedicated fit is required to reveal them. Bouwman *et al.* show that the hydrocarbon emission spectrum is different from the spectrum seen in higher-mass young stars. It is dominated by a feature at $8.2\ \mu\text{m}$, and has weak 6.2 and $11.3\ \mu\text{m}$ features. This deviating hydrocarbon spectrum in T Tauri stars is consistent with the picture outlined in Section 4.

2.2 Herbig Be stars

The infrared spectra of roughly half of the Herbig Be stars contain PAH emission features (Acke and van den Ancker, unpublished). Due to the strong UV field of the central star, however, most of the PAH emission comes from surrounding clouds, remnants of the natal cloud, rather than from the disk. Verhoeff *et al.* (A&A submitted) have studied the extended PAH emission in a sample of 30 Herbig Be stars. None of the emission can unambiguously be attributed to the disk, but in 35% of the targets, PAH emission from the disk cannot be excluded either. Verhoeff *et al.* argue that the disks around Herbig Be stars are fundamentally different from those around lower-mass stars in terms of disk geometry: they are radially less extended and vertically flatter. The authors state that, even if PAH molecules are present in the disk surface at ISM abundances, their emission would be insignificant due to the disk geometry, and swamped by the PAH emission from

the extended cloud. Moreover, the hard radiation field of early-type young stars may shift the PAH destruction radius beyond the disk outer radius, suppressing the PAHs in the disk altogether.

2.3 Herbig Ae stars

The intermediate-mass Herbig Ae stars have by far the highest detection rate of PAH emission in disks. Their stellar radiation field is optimal to excite but not destroy the molecules. Acke & van den Ancker (2004) studied the infrared spectra of 46 Herbig Ae/Be stars, mainly based on data obtained with the Short-Wavelength Spectrometer aboard the Infrared Space Observatory (ISO-SWS; de Graauw *et al.* 1996; Kessler *et al.* 1996). The detection rate of PAH emission features is 57%. Recently, Acke *et al.* (2010) investigated a sample of 53 Herbig Ae stars, observed with Spitzer-IRS. The authors detect PAH features in 70% of the targets. The ISO-SWS and Spitzer-IRS sample overlap in 27 sources. A closer look at this subsample shows that the higher detection rate in the Spitzer-IRS spectra is simply due to the superior sensitivity of the latter instrument.

Because of the high detection rate in Herbig Ae stars, most studies of PAHs in young disks focus on these targets.

3 Emission strength and disk geometry

Spatially resolved observations of PAH emission around young stars have clearly demonstrated the disk origin of the emission. Two techniques are commonly used: long-slit spectroscopy (*e.g.*, van Boekel *et al.* 2004; Habart *et al.* 2004b, 2006; Geers *et al.* 2007) and narrow-band imaging (*e.g.*, Lagage *et al.* 2006; Doucet *et al.* 2007). The focus lies on the PAH features that are accessible from the ground, *i.e.* the 3.3 (L-band), 7.7, 8.6 and 11.3 μm (N-band) features. The PAH emission region has a typical extent of tens of AU for the 3.3 μm feature to hundreds of AU for the features at longer wavelengths. Habart *et al.* (2004a) and Visser *et al.* (2007) have modeled PAH emission from a circumstellar disk. These authors conclude that large (*i.e.*, $N_{\text{C}}=100$ as opposed to $N_{\text{C}}=30$) PAHs are needed to explain the observed spatial extent.

Lagage *et al.* (2006) & Doucet *et al.* (2007) have imaged the HD 97048 disk in narrow-band filters containing the 8.6 and 11.3 μm PAH features, and at continuum wavelengths in between, using VLT/VISIR (Lagage *et al.* 2004). They confirm the findings mentioned above. Moreover, the images clearly show the flared geometry of the disk surface: the disk opening angle increases with radial distance to the star, which gives it a bowl-shaped appearance (see Fig. 1). The measured increase of surface height above the midplane with radius follows $H \propto R^{1.26 \pm 0.05}$, in perfect agreement with the predicted value for models in hydrostatic radiative equilibrium (Chiang & Goldreich 1997; Dullemond *et al.* 2001). This provides strong observational support for the physical assumptions underlying the flared-disk models.

The disk geometry plays an important role in the apparent strength of the PAH emission features. Comparison between observations and models shows that the

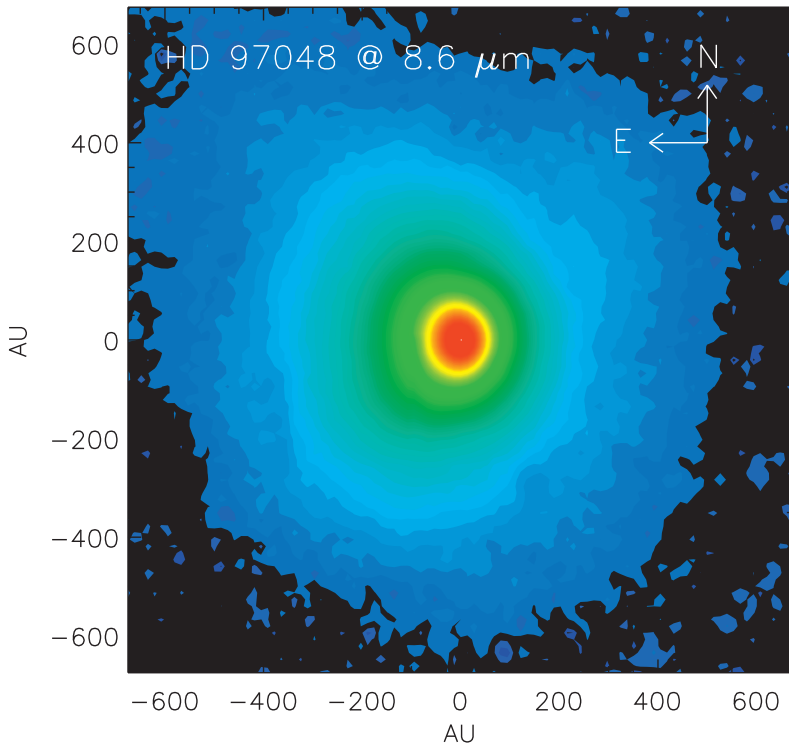


Fig. 1. Image of HD 97048 in a narrow-band filter around the $8.6 \mu\text{m}$ PAH feature (Lagage *et al.* 2006). The scale is the square-root of the flux to enhance the low-flux regions. Courtesy of E. Pantin and P.-O. Lagage.

far-IR excess of Herbig Ae stars is connected to the degree of flaring of the dust disk. The excess is produced by thermal emission of dust grains in the disk. Strong flaring leads to a large far-IR excess (Meeus *et al.* 2001; Dullemond & Dominik 2004; Meijer *et al.* 2008; Acke *et al.* 2009). Dullemond *et al.* (2007) have modeled the effect of dust sedimentation on the appearance of the disk and the strength of the PAH features. Sedimentation makes the dust disk more flattened, and reduces the far-IR excess. However, the gas disk, containing the PAH molecules, remains flared. If dust sedimentation is the dominant process, the models predict stronger PAH emission in flattened disks, both because of an absolute increase in PAH luminosity and an increased feature-to-continuum contrast. Remarkably, the opposite trend is observed: several authors have shown that sources with a flared dust disk have stronger PAH features than those with flattened disks (Meeus *et al.* 2001; Acke & van den Ancker 2004; Habart *et al.* 2004a; Keller *et al.* 2008; Acke *et al.* 2010). In Figure 2, the increase of the feature-to-stellar luminosity ratio of the $6.2 \mu\text{m}$ feature with increasing far-IR excess is shown for a sample of Herbig Ae

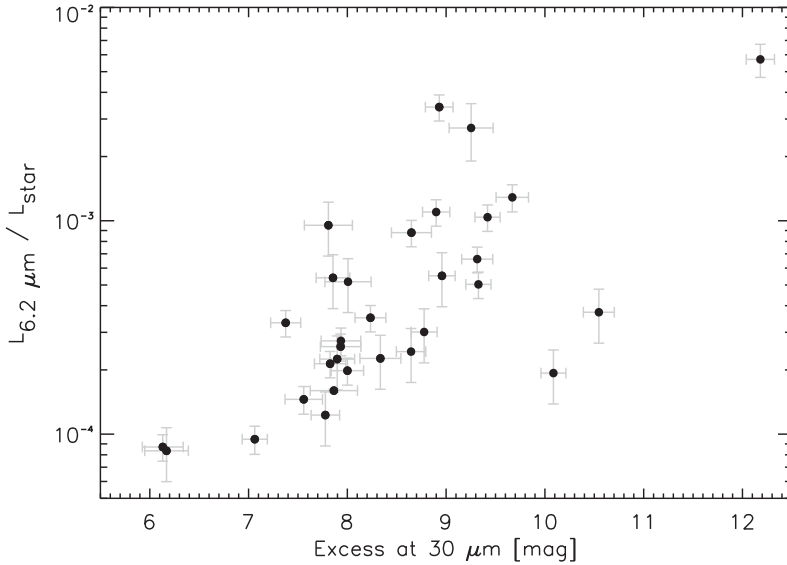


Fig. 2. The feature-to-stellar luminosity ratio of the $6.2\ \mu\text{m}$ feature increases with increasing $30\ \mu\text{m}$ excess above the stellar photosphere (Acke *et al.* 2010). Flattened dust disks are characterized by a low, and flared disks by a high far-IR excess.

stars. This correlation has been interpreted as a simple geometric effect: a flared disk has a larger illuminated surface than a flattened disk. However, the link between disk geometry and PAH emission strength is not necessarily a causal link. PAH molecules in the disk surface layer are an important contributor to the gas thermal balance due the photo-electric effect. Meeus *et al.* (2010) have shown that inclusion of PAH molecules in different charge states can alter the gas temperature considerably. The disk becomes warmer and the degree of flaring larger. PAHs hence help to sculpture the disk structure (see Kamp, elsewhere in this volume).

A few objects with flattened dust disks (*i.e.* low far-IR excesses) are still strong PAH sources (van der Plas *et al.* 2008; Fedele *et al.* 2008; Verhoeff *et al.* 2010). In those targets, the scenario of dust sedimentation could be at work. The general trend, however, shows that sedimentation is not the dominating process in most disks. It indicates that either dust and gas remain well coupled (*e.g.* due to strong turbulent motions), or that the PAH molecules coagulate with dust grains and settle along with the dust (Dullemond *et al.* 2007).

Because of the low detection rate of PAH emission in the lower-mass stars, the statistics in this group of objects is too poor to perform a similar study on disk geometry. Bouwman *et al.* (2008) note that the T Tauri stars *without* detected hydrocarbon emission in their sample have a SED consistent with a flattened disk structure. Geers *et al.* (2006) mention that gaps in the inner dust disk need to be taken into account as well. Such gaps may be formed due to the

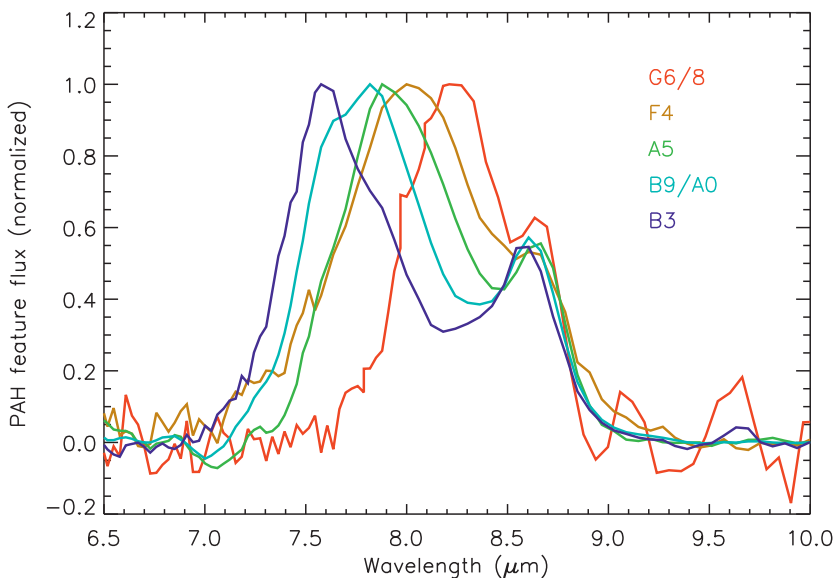


Fig. 3. The $7.7 \mu\text{m}$ feature shifts to longer wavelengths with decreasing stellar effective temperature.

gravitational interaction with a planetary system or a companion star. A gap with an extent of several to tens of AU reduces the thermal continuum emission of the dust at near- and mid-IR wavelengths. This enhances the feature-to-continuum contrast. Moreover, the disk beyond the gap outer radius receives more direct stellar photons. As a result, the disk becomes warmer, giving rise to an increase in scale height, and the surface area exposed to stellar radiation becomes larger than in a gap-less disk. Next to the increased feature-to-continuum contrast, this enhances the absolute PAH luminosity.

4 Chemistry and stellar radiation field

Peeters *et al.* (2002, and elsewhere in this volume) defined three classes of objects based on the peak positions and the relative contribution of the sub-bands of the PAH features in the $6\text{--}9 \mu\text{m}$ range. Class A contains sources with blue 6.2 and $7.7 \mu\text{m}$ features. These are mostly general ISM sources, HII regions, and reflection nebulae, including those around Herbig Be stars. Class C sources are characterized by red features. Very little objects belong to this Class: cool carbon-rich evolved stars, red giant stars and a few T Tauri stars. The Herbig Ae stars belong to Class B (intermediate feature positions), together with most planetary nebulae and a number of binary post-AGB stars. Sloan *et al.* (2005, 2008) note that the

PAH spectra of Herbig Ae stars are different from those of evolved stars belonging to Class B. Herbig Ae stars display a 7–9 μm feature with an extended red wing beyond 8.0 μm . The authors therefore propose to create a new Class (dubbed B') for the latter.

Boersma *et al.* (2008) show that the spatially resolved spectra of two Herbig Ae stars exhibit Class A (ISM-like) characteristics far from the central star, and Class B characteristics closer in. The authors argue that all the emission emanates from the surrounding nebula, and not from the disk. This shows that chemical changes can occur even in the surrounding cloud.

In young stars, the Peeters classification is linked to the radiation field of the central star: the wavelength position of the 6.2 and 7.7 μm features moves to the red with decreasing stellar effective temperature (Sloan *et al.* 2007; Keller *et al.* 2008; Acke *et al.* 2010). In Figure 3, the Spitzer-IRS 6.5–10 μm spectra of five young stars are shown. For clarity, the underlying continuum has been subtracted and the spectra are normalized to the peak flux of the 7.7 μm feature. The figure illustrates the gradual shift of the feature position to shorter wavelengths with increasing stellar effective temperature, from Class C for the T Tauri star to Class A for the Herbig Be star.

The interpretation of this shift is still a matter of debate. Sloan *et al.* (2005) suggested that the redshift of the main features indicates a higher aliphatic/aromatic (sp^3/sp^2) hybridization of the hydrocarbon molecules. This hypothesis is supported by the laboratory measurements of Pino *et al.* (2008). Acke *et al.* (2010) show that in Herbig Ae stars the redshift of the features, or equivalently T_{eff} , is connected to an increase in relative strength of the features at 6.8 and 7.2 μm . The latter features are ascribed to aliphatic CH_2/CH_3 bending modes (*e.g.*, Furton *et al.* 1999; Chiar *et al.* 2000; Dartois *et al.* 2007). Moreover, the strength of the 8.6 μm feature, relative to the CC features at 6.2 and 7.7 μm , decreases with feature redshift.

Rapacioli *et al.* (2005), Berné *et al.* (2007), Joblin *et al.* (2008), and Berné *et al.* (2009) follow a different approach (see also Berné *et al.*, elsewhere in this volume). This group has investigated the spatially resolved IR spectra of photodissociation regions (PDRs) and PNe, and found that they could be decomposed into a few fundamental basis spectra. Based on their fractional contribution to the emission in different spatial regions of PDRs, the fundamental spectra are attributed to different families of hydrocarbon molecules/grains: ionized PAHs, neutral PAHs and very small grains (VSGs; possibly PAH clusters: see Rapacioli *et al.*, elsewhere in this volume). Berné *et al.* (2009) fit the observed PAH spectra of a sample of young stars with the basis spectra. They find that the fraction of the emission ascribed by the authors to VSGs decreases with increasing UV luminosity of the central star. This correlation is very likely the same as the one mentioned above between feature redshift and stellar effective temperature. The VSG spectrum used by Berné *et al.* contains the reddest features in their spectral basis. A reduction in the contributing fraction of the VSG spectrum is therefore equivalent to a blueshift of the features. The link between UV luminosity and T_{eff} is also clear: cooler stars have in general weaker photospheric UV fields. However,

as opposed to the aliphatic/aromatic interpretation outlined above, Berné *et al.* suggest that an increased contribution of VSGs produces the position shift in the feature.

A third possible explanation, which has not been explored sufficiently in the literature, is that the PAH size and charge influence the spectral classification (Bauschlicher *et al.* 2008, 2009). The link between feature position and T_{eff} could then reflect the excitation and charge state of the PAHs with respect to the stellar radiation field.

Keller *et al.* (2008) find that the flux ratios of the 12.7 and 11.3 μm features, and of the 7.7 and 11.3 μm features correlate with stellar effective temperature. The 12.7/11.3 ratio probes the importance of aromatic duo/trio CH modes with respect to solo CH modes (Hony *et al.* 2001). The ratio is expected to be high in small PAHs, or PAHs with jagged edges. The features in the 6–9 μm range are ascribed to ionized PAHs, and those at longer wavelengths to neutrals. The 7.7/11.3 ratio is therefore interpreted as a measure for the ionization of the PAHs. Keller *et al.* (2008) conclude that PAH molecules around hotter stars have rougher edges and are more ionized, as a result of the stellar irradiation.

Finally, Visser *et al.* (2007) point out that the flux ratio of the 3.3 and 6.2 μm features is another strong probe of the PAH charge. The ratio increases by an order of magnitude by going from ionized to neutral species. In the Herbig Ae/Be sample of Acke & van den Ancker (2004), the detection rate of the 3.3 μm feature, given the presence of the 6.2 μm feature, is 44%: half of the PAH spectra are dominated by neutrals, the other half by ionized species. However, no link with stellar UV field or effective temperature is found.

5 Conclusions

The emitting hydrocarbon molecules in disks around young stars are different from those in the ISM, and their chemistry – aliphatic/aromatic hybridization ratio, clustering, size, and/or charge state – is connected to the stellar radiation field. There is an interplay between the disk structure and the strength of hydrocarbon emission. Targets with flared disks have brighter PAH features. In turn, the PAHs in the disk surface contribute to the gas thermal balance, shaping the disk morphology.

References

- Acke, B., & van den Ancker, M.E., 2004, *A&A*, 426, 151
- Acke, B., Min, M., van den Ancker, M.E., *et al.*, 2009, *A&A*, 502, L17
- Acke, B., Bouwman, J., Juhász, A., *et al.*, 2010, *ApJ*, 718, 558
- Bauschlicher, C.W., Peeters, E., & Allamandola, L.J., 2008, *ApJ*, 678, 316
- Bauschlicher, C.W., Peeters, E., & Allamandola, L.J., 2009, *ApJ*, 697, 311
- Berné, O., Joblin, C., Deville, Y., *et al.*, 2007, *A&A*, 469, 575

- Berné, O., Joblin, C., Fuente, A., & Ménard, F., 2009, *A&A*, 495, 827
- Boersma, C., Bouwman, J., Lahuis, F., *et al.*, 2008, *A&A*, 484, 241
- Bouwman, J., Henning, T., Hillenbrand, L.A., *et al.*, 2008, *ApJ*, 683, 479
- Cesarsky, D., Lequeux, J., Ryter, C., & Gérin, M., 2000, *A&A*, 354, L87
- Chiang, E.I., & Goldreich, P., 1997, *ApJ*, 490, 368
- Chiar, J.E., Tielens, A.G.G.M., Whittet, D.C.B., *et al.*, 2000, *ApJ*, 537, 749
- Dartois, E., Geballe, T.R., Pino, T., *et al.*, 2007, *A&A*, 463, 635
- de Graauw, T., Haser, L.N., Beintema, D.A., *et al.*, 1996, *A&A*, 315, L49
- Doucet, C., Habart, E., Pantin, E., *et al.*, 2007, *A&A*, 470, 625
- Dullemond, C.P., Dominik, C., & Natta, A., 2001, *ApJ*, 560, 957
- Dullemond, C.P., & Dominik, C., 2004, *A&A*, 417, 159
- Dullemond, C.P., Henning, T., Visser, R., *et al.*, 2007, *A&A*, 473, 457
- Fedele, D., van den Ancker, M.E., Acke, B., *et al.*, 2008, *A&A*, 491, 809
- Fedele, D., van den Ancker, M.E., Henning, T., *et al.*, 2010, *A&A*, 510, A72
- Furlan, E., Hartmann, L., Calvet, N., *et al.*, 2006, *ApJS*, 165, 568
- Furton, D.G., Laiho, J.W., & Witt, A.N., 1999, *ApJ*, 526, 752
- Geers, V.C., Augereau, J., Pontoppidan, K.M., *et al.*, 2006, *A&A*, 459, 545
- Geers, V.C., 2007, Ph.D. Thesis, Leiden Observatory, Leiden University
- Geers, V.C., van Dishoeck, E.F., Visser, R., *et al.*, 2007, *A&A*, 476, 279
- Geers, V.C., van Dishoeck, E.F., Pontoppidan, K.M., *et al.*, 2009, *A&A*, 495, 837
- Habart, E., Verstraete, L., Boulanger, F., *et al.*, 2001, *A&A*, 373, 702
- Habart, E., Natta, A., & Krügel, E., 2004a, *A&A*, 427, 179
- Habart, E., Testi, L., Natta, A., & Carillet, M., 2004b, *ApJ*, 614, L129
- Habart, E., Natta, A., Testi, L., & Carillet, M., 2006, *A&A*, 449, 1067
- Herbig, G.H., 1960, *ApJS*, 4, 337
- Hony, S., Van Kerckhoven, C., Peeters, E., *et al.*, 2001, *A&A*, 370, 1030
- Houck, J.R., Roellig, T.L., van Cleve, J., *et al.*, 2004, *ApJS*, 154, 18
- Joblin, C., Szczerba, R., Berné, O., & Szyszka, C., 2008, *A&A*, 490, 189
- Keller, L.D., Sloan, G.C., Forrest, W.J., *et al.*, 2008, *ApJ*, 684, 411
- Kessler, M.F., Steinz, J.A., Anderegg, M.E., *et al.*, 1996, *A&A*, 315, L27
- Lagage, P.O., Doucet, C., Pantin, E., *et al.*, 2004, *The Messenger*, 117, 12
- Lagage, P., Pel, J.W., Authier, M., *et al.*, 2006, *Science*, 314, 621
- Meeus, G., Waters, L.B.F.M., Bouwman, J., *et al.*, 2001, *A&A*, 365, 476
- Meeus, G., Pinte, C., Woitke, P., *et al.*, 2010, *A&A*, 518, 124
- Meijer, J., Dominik, C., de Koter, A., *et al.*, 2008, *A&A*, 492, 451
- Oliveira, I., Pontoppidan, K.M., Merín, B., *et al.*, 2010, *ApJ*, 714, 778
- Peeters, E., Hony, S., Van Kerckhoven, C., *et al.*, 2002, *A&A*, 390, 1089
- Pino, T., Dartois, E., Cao, A., *et al.*, 2008, *A&A*, 490, 665
- Preibisch, T., Kim, Y., Favata, F., *et al.*, 2005, *ApJS*, 160, 401
- Quanz, S.P., Henning, T., Bouwman, J., *et al.*, 2007, *ApJ*, 668, 359
- Rapacioli, M., Joblin, C., & Boissel, P., 2005, *A&A*, 429, 193
- Siebenmorgen, R., & Krügel, E., 2010, *A&A*, 511, A6

- Sloan, G.C., Keller, L.D., Forrest, W.J., *et al.*, 2005, ApJ, 632, 956
Sloan, G.C., Jura, M., Duley, W.W., *et al.*, 2007, ApJ, 664, 1144
Sloan, G.C., 2008, in IAU Symposium, ed. S. Kwok & S. Sandford, 251, 191
Stelzer, B., Micela, G., Hamaguchi, K., & Schmitt, J.H.M.M., 2006, A&A, 457, 223
van Boekel, R., Waters, L.B.F.M., Dominik, C., *et al.*, 2004, A&A, 418, 177
van der Plas, G., van den Ancker, M.E., Fedele, D., *et al.*, 2008, A&A, 485, 487
Verhoeff, A.P., Min, M., Acke, B., *et al.*, 2010, A&A, 516, A48
Visser, R., Geers, V.C., Dullemond, C.P., *et al.*, 2007, A&A, 466, 229

EVOLUTION OF PAHS IN PROTOPLANETARY DISKS

I. Kamp¹

Abstract. Depending on whom you ask, PAHs are either the smallest dust particles or the largest gas-phase molecules in space. Whether referred to as gas or dust, these PAHs can contain up to 20% of the total cosmic carbon abundance and as such also play an important role in the carbon chemistry of protoplanetary disks. The interpretation of PAH bands is often a complex procedure involving not only gas physics to determine their ionization stage and temperature, but also radiative transfer effects that can bury these bands in a strong thermal continuum from a population of larger dust particles.

PAHs are most readily seen in the spectral energy distributions (SEDs) of disks around Herbig AeBe stars where they are photoprocessed by the stellar radiation field. Resolved images taken in the PAH bands confirm their origin in the flaring surfaces of circumstellar disks: if the SED is consistent with a flat disk structure (less illuminated), there is little or no evidence of PAH emission. The very low detection rates in the disks around T Tauri stars often require an overall lower abundance of PAHs in these disk surface as compared to that in molecular clouds.

In this review, I will address three aspects of PAHs in protoplanetary disks: (1) Do PAHs form in protoplanetary disks or do they originate from the precursor molecular cloud? (2) Is the presence of PAH features in SEDs a consequence of the disk structure or do PAHs in fact shape the disk structure? (3) How can we use PAHs as tracers of processes in protoplanetary disks?

1 Introduction

Polycyclic aromatic hydrocarbons (PAHs) are considered amongst the smallest dust grains even though their sizes range from macromolecules with 10 carbon atoms, such as naphthalene to large complexes with more than 100 carbon atoms.

¹ Kapteyn Astronomical Institute, University of Groningen, PO Box 9513, 2300 AV Groningen, The Netherlands

They are identified mainly through their near- and mid-IR bands in very different astrophysical environments such as the interstellar medium (ISM), disks around young stars, and the circumstellar environment of AGB stars. I will focus in the following on the role of PAHs in star formation and especially on their relevance in protoplanetary disks.

Protoplanetary disks are complex in nature, because they span a wide range of physical conditions, *i.e.* density and temperature (and irradiation), but also show orders of magnitude different dynamical timescales between the inner and outer disk. Gas and dust in these disks are not necessarily coupled and co-spatial. And a number of processes that operate in protoplanetary disks such as dust coagulation and settling, gas dispersal, and planet formation affect gas and dust often in different ways.

Their nature positions PAHs in terms of their properties somewhere between large gas molecules and small dust grains. Due to their small size, they efficiently couple to the widespread gas in protoplanetary disks and are thus able to escape settling processes that affect the much larger dust grains. Due to their low ionization potentials, PAHs are easily ionized by the stellar UV photons and the ejected electrons can efficiently heat the surrounding gas (photoelectric heating). If they are abundant (23% of carbon dust in the form of PAHs), they can also present an important opacity source and absorb up to 40% of the total radiation (Habart *et al.* 2004). Often the fraction of carbon dust in PAHs is assumed to be much smaller in disks, *e.g.* less than 10% (Geers *et al.* 2006; Dullemond *et al.* 2007a). PAHs are stochastically heated particles and undergo rapid and extreme temperature fluctuations that lead to their emission in the aromatic infrared bands (AIBs).

I start out with a brief summary of PAH observations in protoplanetary disks and their detection frequency (Sect. 2). Section 3 provides a short overview of the PAH excitation mechanism and radiative transfer models. The next two sections then discuss the role of PAHs in disks chemistry (Sect. 4) and physics (Sect. 5) in more detail. The last section will then address three questions concerning PAH evolution in disks: (1) Do PAHs form in protoplanetary disks or do they originate from the precursor molecular cloud? (2) Is the presence of PAH features in SEDs a consequence of the disk structure or do PAHs in fact shape the disk structure? (3) How can we use PAHs as tracers of processes in protoplanetary disks?

2 Some observational facts

PAHs have been rarely observed in embedded low mass protostars. However, as the sources evolve into class II and class III objects, detection rates increase and there is a clear dependency on the UV radiation field of the central star. PAHs are observed in 57% of the Herbig disks (Acke *et al.* 2004), but only in 8% of the T Tauri disks (Geers *et al.* 2006). Various studies (Sloan *et al.* 2007; Boersma *et al.* 2008; Keller *et al.* 2008) noted clear changes in the feature shape and shifts of the central wavelength, which they attribute to signatures of PAH processing in the young star's environment (see Acke, elsewhere this volume, for a more detailed discussion). It seems that the wealth of observational data especially

from *Spitzer* available now for several objects (see below) warrants a much more detailed understanding of the disk structure. For example, Fedele *et al.* (2008) find the PAH emission coming from the upper gas surface in the disk around HD 101412; the PAHs are co-spatial with the [O I] 6300 Å emission of the gas, which is generally thought to be a by-product of the photodissociation of OH in the UV irradiated disk surface. On the other hand, the SED and near-IR visibilities show that the larger dust grains are not directly exposed to the stellar radiation and must reside at lower heights in the disk. This lends support to the idea that PAHs stay well mixed with the gas. Along the same lines, Verhoeff *et al.* (2010) find that the disk around HD 95881 consists of a thick puffed up inner rim and an outer region in which the gas still has a flaring structure, while larger dust grains have settled to the midplane. Such systems are thought to be in a transitional stage between a gas-rich flaring and gas-poor shadowed configuration.

3 PAH emission from disks

A detailed understanding of the PAH emission mechanisms is essential to judge the diagnostic power and impact of PAHs on the disk structure. In the following, the problem is split into the excitation mechanism (ionization state, single *versus* multi-photon excitation) and the radiative transfer in the presence of a strong dust continuum and competing features such as the silicate emission at 10 μm. The combination of these two aspects leads to differences in the spatial appearance of the various PAH emission features (see *e.g.* Fig. 1).

Studies of galactic emission have shown that PAHs contain up to a few percent of the total carbon dust mass (*e.g.* Pendleton *et al.* 1994); the typical PAH carbon abundance found from galactic PDRs and ISM is $[C/H]_{\text{PAH}} \approx 5 \times 10^{-5}$ (Boulanger & Perault 1988; Habart *et al.* 2001; Desert *et al.* 1990; Dwek *et al.* 1997; Li & Draine 2001). For such an extreme case of PAH abundance in disks, Habart *et al.* (2004) find that PAHs reprocess $\sim 30\%$ of the impinging stellar radiation (which is $\sim 0.3\%$ of the total luminosity in the case of a flaring disk surface) in a fiducial Herbig disk model (0.3 – 300 AU, $0.1 M_{\odot}$, $M_{*} = 2.4 M_{\odot}$, $L_{*} = 32 L_{\odot}$); since PAHs then present a significant fraction of the total dust opacity, their presence has a visible effect on the overall SED (see their Figs. 1 and 3). Habart *et al.* (2004) find that $\sim 25\%$ of the flux that PAHs absorb in the inner disk is consumed by their evaporation. Geers *et al.* (2006) found from an extensive comparison of observed PAH features (*Spitzer* spectra) and detailed radiative transfer disk models that the typical PAH abundance in disks must be 10–100 times lower than that in the ISM. Hence, the total dust opacity should be hardly affected by PAHs.

3.1 The excitation mechanism of PAHs

The intensity emitted in a specific AIB roughly scales with the incident FUV radiation provided that the charge state is held constant (Li & Lunine 2003; Habart *et al.* 2004). This directly reflects the single photon excitation mechanism (transiently heated grains) as opposed to the radiative equilibrium that holds for larger

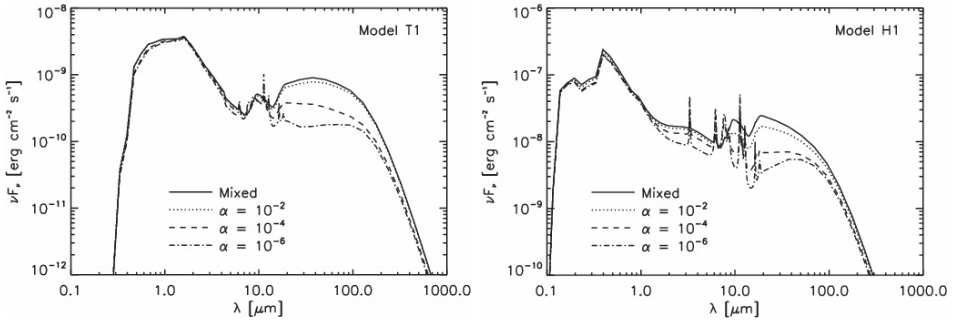


Fig. 1. The SEDs of a T Tauri disk model (Model T1) and a Herbig disk model (Model H1) at an evolutionary age of 10^6 yr (inclination of 45 degrees, $d = 100$ pc). The different curves show the SED before sedimentation (solid), and after sedimentation ($t = 10^6$ yr) for several values of the disk viscosity parameter: $\alpha = 10^{-2}$ (dotted), $\alpha = 10^{-4}$ (dashed) and $\alpha = 10^{-6}$ (dot-dashed). The figure is taken from Dullemond *et al.* (2007a).

grains. Hence, for PAHs one generally defines a temperature distribution function dP/dT that describes the probability of finding a PAH in a particular temperature interval. Due to the single photon excitation mechanism, this temperature distribution depends not on the strength, but on the color of the radiation field. The different PAH bands then require different excitation temperatures, with the short wavelength bands (C-H, C-C stretching modes) requiring higher temperatures than the long wavelength bands (bending modes).

However, spinning of charged dust grains at thermal rates is an alternative excitation mechanism that works at much longer wavelengths Rafikov (2006) (see Draine elsewhere this volume). This microwave emission would trace small dust grains in general (VSGs and PAHs) and it has the potential to trace PAHs even down to the midplane.

3.2 Feature-to-continuum ratios

Manske & Henning (1999) performed a two-dimensional radiative transfer calculation for disk plus envelope systems. They include various grain populations, amongst them also the transiently heated VSGs and PAHs. One of their main results is that the PAH features become weaker with increasing mass fraction of VSGs. However, it proved difficult to entirely suppress the PAHs in the SEDs from Herbig stars with disks and envelopes. The later models by Dullemond *et al.* (2007a) confirm that the VSGs compete with PAHs for the stellar UV photons, thus decreasing the PAH band strength. The SED on the other hand changes only slightly between 20 and 30 μm where VSGs produce a bump in the disk emission.

3.3 Effects of ionization, dehydrogenation and size

The various AIBs are attributed to vibrations of different bonds in the PAH molecule and their strength changes with the PAH ionization, dehydrogenation

state, and size. The following paragraphs summarize our understanding of PAH emission based on results from Habart *et al.* (2004).

The 3.3 μm band is a C-H stretching mode, while the 6.2 and 7.7 μm bands originate from C-C stretching modes. The C-H in-plane and out-of-plane bending modes cause the 8.6 μm band and the 11.3, 11.9, and 12.7 μm features respectively.

The strong effect that the ionization state (neutral or cation) has on the relative PAH band intensities is known from theory and experiment (see references in Pauzat and Oomens, elsewhere in this volume). The 6.2 and 7.7 μm bands are stronger in ionized PAHs; the 8.6 μm band is stronger in cations than in neutrals. On the contrary, the 11.3, 11.9, 12.7 μm bands decrease for charged PAHs. Otherwise, PAH anion band strength is often between that of neutrals and cations.

With strong dehydrogenation, the C-H features would disappear. This is only relevant for the smallest PAHs ($N_C \leq 25$) (Tielens *et al.* 1987; Allain *et al.* 1996). Theory predicts that the C-H features (3.3, 8.6, 11.3, 12.7) become weaker, while the C-C features (6.2, 7.7) become slightly stronger.

In addition to charge and hydrogenation state, the size of the PAH also impacts the excitation state. Small PAHs favor the 3.3 μm band, while larger ones emit preferentially at longer wavelengths. This leads to a degeneracy between charge and size.

3.4 The spatial origin of various PAH features

Habart *et al.* (2006) spatially resolved the 3.3 μm PAH feature using NAOS-CONICA at the VLT (AO providing $\sim 0.1''$ resolution). The emission originates from within 30 AU of the star and is significantly more extended than the adjacent continuum. This is in agreement with the theoretical models that find the higher excitation temperatures required for the 3.3 μm feature mostly in the inner disk ($r < 50$ AU; Habart *et al.* 2004). Geers *et al.* (2007a), (2007b) also report that the disk emission in some targets is more extended within the PAH bands than within the adjacent continuum. Just as a note of caution, the emission from VSGs can also be more extended than that of large dust grains.

4 PAH chemistry in disks

As large gas molecules, PAHs take part in the chemical reaction networks of protoplanetary disks. They can undergo ionization (photoelectric effect), electron recombination and attachment, charge exchange, photodissociation with C or H loss, and H addition reactions. Trapping of PAHs onto dust grains or within ices (Gudipati & Allamandola 2003) are more relevant in the cold dense midplane that does not contribute to the PAH emission features. Reaction rates with heavier elements can be comparable to those of H, H₂, but often the abundances of those heavier elements are much lower. However, in some regions of protoplanetary disks, where H is efficiently converted into water and/or OH, reactions with O and OH can play an important role in breaking PAHs down (Kress *et al.* 2010).

The convention often found in the literature (*e.g.* Le Page *et al.* 2001) is to characterize PAHs by the number of C atoms N_C . The normal number of hydrogen atoms, N_H^0 is the number of hydrogen atoms when one hydrogen atom is attached to each peripheral carbon atom which is bonded to exactly two other carbon atoms. In the following, PAH stands representative for any size PAH and the different charge states are indicated by superscripts, *e.g.* PAH⁺. A recent review on PAH chemistry is given by Tielens (2008) and the formation of PAHs is discussed by Cherchneff (this volume).

4.1 PAH hydrogenation and dissociation

The stability and hydrogenation of PAHs is mainly determined by the strength of the UV environment ($\lambda < 2000 \text{ \AA}$) in which they reside (the ionization potential of PAHs is typically $IP > 6 \text{ eV}$, see Weingartner & Draine 2001). While photons of 3–10 eV can lead to the loss of H (3.2 eV), C₂H₂ (4.2 eV), C (7.5 eV) and C₂ (9.5 eV), X-ray photons are more energetic and can destroy entire PAHs with $N_C = 100$ (Siebenmorgen & Krügel 2009).

Small PAHs ($N_C = 24$) are easily destroyed in protoplanetary disks on short timescales ($< 3 \text{ Myr}$). Larger PAHs survive more easily in the irradiation environment of protoplanetary disks. PAHs with $N_C = 96$ for example survive down to 5 AU in the disk around a Herbig star, while smaller ones ($N_C = 50$) are efficiently destroyed out to a few 10 AU (see Fig. 7 of Visser *et al.* 2007). The weaker radiation field of T Tauri stars is not capable of destroying PAHs unless these stars have a significant UV excess. X-ray and EUV photons are so efficient that they destroy PAHs wherever they can reach them (Siebenmorgen & Krügel 2009).

4.2 Charge distribution of PAHs in disks

The PAH charge state in disks generally has a layered structure with cations being on top, followed by neutrals and anions towards the dense shielded midplane (Visser *et al.* 2007). Figure 2 shows that PAHs get easily double ionized (PAH²⁺) in the surfaces of disks around Herbig stars due to the strong stellar UV radiation field (detailed model description in Sect. 5). This result depends strongly on the size of the PAH. The disk model shown here uses circumcoronene ($N_C = 54$, $N_H = 18$, $IP(1) = 6.243$, $IP(2) = 9.384$, $IP(3) = 12.524$). Due to the weak UV radiation field of T Tauri stars, disks around low mass stars show mostly neutral PAHs and anions ($\sim 50\%$ of the entire population, Visser *et al.* 2007).

4.3 H₂ formation on PAHs

Jonkheid *et al.* (2006) consider that for evolved disks (HD 141569), H₂ might form more efficiently in reactions with PAHs than on the dust grains in the disk ($1 \mu\text{m} < a < 1 \text{ cm}$). Due to the lack of small grains, the total dust surface area available from such a distribution is small compared to the typical ISM size distribution and the H₂ formation rate depends directly on the total available surface area.

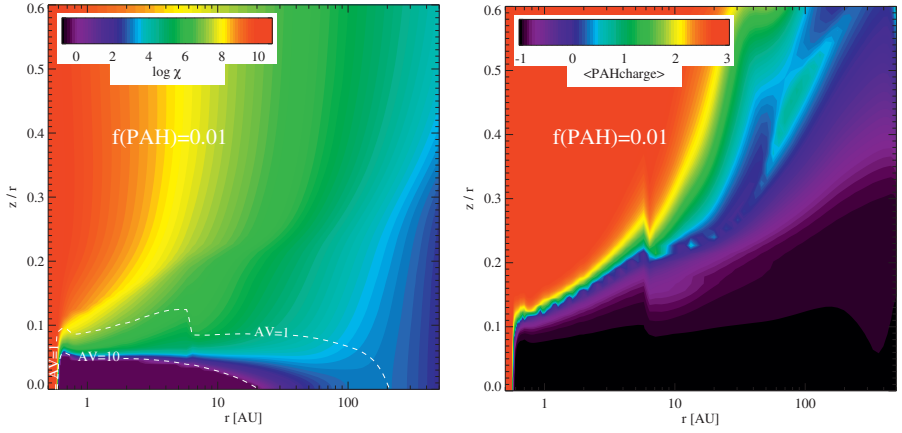


Fig. 2. *Left:* strength of the UV radiation field χ in the protoplanetary disk around a typical Herbig star ($M_* = 2.5 M_\odot$, $T_{\text{eff}} = 10\,000$ K). The main parameters are: $M_{\text{disk}} = 0.025 M_\odot$, a surface density power law profile $\epsilon = 1.0$, a grain size distribution between $a_{\text{min}} = 0.05 \mu\text{m}$ and $a_{\text{max}} = 1$ mm with a power law exponent of 3.5, and a dust-to-gas mass ratio of 0.01, a PAH abundance f_{PAH} of 1% relative to the ISM. χ is defined as the integral of the radiation field between 912 and 2050 Å normalized to that of the Draine field (Draine & Bertoldi 1996). *Right:* charge distribution of PAHs. Note that regions where PAHs carry multiple positive charges have low particle densities (see Fig. 3).

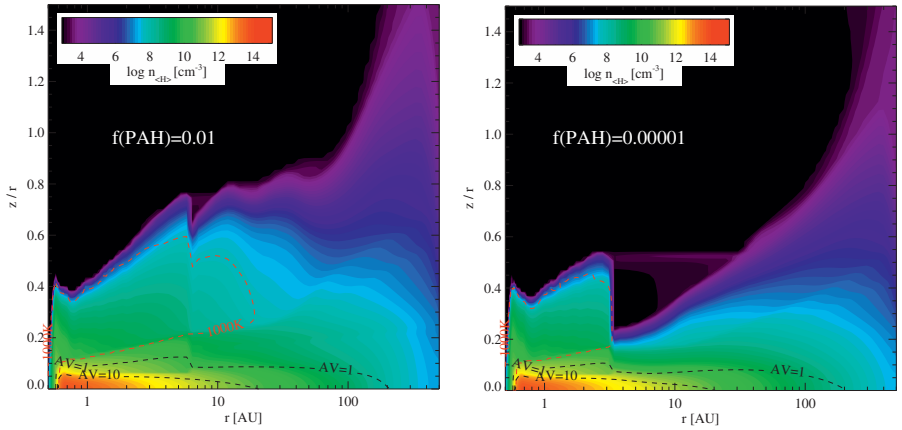


Fig. 3. Density structure of a protoplanetary disk around a $2.5 M_\odot$ Herbig star ($T_{\text{eff}} = 10\,000$ K). The main parameters are: $M_{\text{disk}} = 0.025 M_\odot$, a surface density power law profile $\epsilon = 1.0$, a grain size distribution between $a_{\text{min}} = 0.05 \mu\text{m}$ and $a_{\text{max}} = 1$ mm with a power law exponent of 3.5, and a dust-to-gas mass ratio of 0.01. The left figure shows a model with a PAH abundance relative to the ISM of 0.01 and the right figure one of 10^{-5} . The black dashed lines show the location of the $A_V = 1$ and 10 surfaces, while the red contour line indicates the location of the hot gas ($T_{\text{gas}} > 1000$ K).

5 The role of PAHs in disks physics

PAHs are not relevant for the dust energy balance, *i.e.* they do not present a significant fraction of the dust opacity. However, as large molecules, they efficiently absorb UV radiation and get photoionized. The energetic electrons released in this way efficiently heat the surrounding gas and determine its temperature. Thus the vertical disk structure – as set by the gas temperature – depends sensitively on this heating source.

5.1 The vertical disk structure

The thermo-chemical disk code PRODIMO calculates the vertical hydrostatic disk structure, the chemical composition, and gas & dust temperatures self-consistently. The basic physics and chemistry of the code is summarized in Woitke *et al.* (2009) while additions and new features are described in Kamp *et al.* (2010) (UV radiative transfer and UV-photochemical rates) and Woitke *et al.* (in preparation) (UV pumping, PAH heating and ray tracing of gas lines).

The models shown here (van der Plas *et al.* in preparation) use a chemical network consisting of 10 elements, 76 species and 973 reactions, among them also the five ice species: CO, CO₂, H₂O, CH₄, and NH₃. The inner disk has “soft edges”, *i.e.* soft density gradients at the inner and outer radius.

Figure 3 shows two models of a disk around a Herbig star that differ only in their fractional PAH abundance. The inner disk wall is directly illuminated by the star while the gas behind it is irradiated under a shallow angle; hence, the inner rim has a higher gas temperature than the disk behind it. Under the assumption of vertical hydrostatic equilibrium, this translates into a “puffed-up” inner rim. If the rim has a substantial optical depth, it can cast a shadow on the material behind it and thus cause a “shadow”, *i.e.* a flat disk structure (Dullemond *et al.* 2007b).

The amount of shadowing depends crucially on how efficient the gas is heated by the stellar radiation field. The gas and dust temperatures in these models decouple in the surface layers down to $A_V \sim 1$. For large gas heating efficiencies, it is thus more difficult to cast a shadow. One of the strongest heating processes in the disk surface is photoelectric heating by PAHs. Hence, the disk with very little PAHs has a much lower heating efficiency. The main heating processes in this case are the photoelectric effect on dust grains and the H₂ formation heating. The overall disk structure is cooler and hence much flatter (see *e.g.* the $A_V = 1$ contour lines). In addition, the inner rim now casts a very strong shadow beyond 3 AU.

5.2 PAHs and dust settling

Dullemond *et al.* (2007a) have studied the impact of grain size sorting with height due to dust sedimentation and turbulence equilibrium. They find that the sedimentation enhances the dust features originating from the smallest grains (Fig. 1).

Even though PAHs are potentially destroyed in the irradiated disk surface, rapid turbulent mixing ensures a continuous supply from deeper layers.

As a consequence, the inclusion of sedimentation lowers the required PAH abundances to produce a certain feature-to-continuum ratio. The impact on the SED is twofold: (a) sedimentation suppresses the continuum by letting small grains that are efficiently heated sink down (b) sedimentation lowers the optical depth in surface layers, thereby letting all UV flux be absorbed by PAHs in surface and thus enhancing the feature strength.

6 Conclusions

After an extensive discussion of the PAH chemistry, the role they play in disk physics and their radiative transfer, this section returns to the initially raised three questions and tries to give an answer based on our current understanding.

6.1 Do PAHs form in protoplanetary disks?

The formation of PAHs requires high densities and temperatures (~ 1000 K) and high abundances of organic molecules such as *e.g.* acetylene in a low UV radiation environment. Those conditions could likely exist directly behind the inner rim of a protoplanetary disk. Using various initial abundances of C_2H_2 and CH_4 and CO and (T, P) combinations, Morgan *et al.* (1991) showed that PAH formation can in fact be very efficient in certain temperature/pressure regimes of the early solar nebula. More recently, Woods & Willacy (2007) used a full chemical network (including the formation and destruction of C_2H_2 and CH_4 and CO) to show that in a stationary protoplanetary disk (no mixing), benzene can indeed form inside 3 AU and abundances of other organic species are also high (see Woods, elsewhere this volume). Kress *et al.* (2010) define a soot line for disks, which is the dividing line between the location where carbon compounds readily condense into PAHs at high gas temperatures and that where they rather stay in simpler molecules such as CO, CO_2 , C_2H_2 , CH_4 . The remaining question is how these *in-situ* formed PAHs are mixed to the large radii where they are observed (up to several 10 AU).

Alternatively, PAHs could form in shocks. Desch & Connolly (2002) invoke shocks for the melting of chondrules in the inner solar nebula. If the shocks are associated with the global disk structure *e.g.* because of spiral density enhancements that travel at a lower pattern speed compared to the gas in which they are embedded, those shocks could be recurring on an orbital timescale. The conditions (*e.g.* temperatures and densities) could then be very similar to those in the outer envelopes of AGB stars where PAHs are known to form efficiently (Cherchneff *et al.* 1992; Cherchneff elsewhere this volume).

Important for the question whether PAHs can survive from an earlier ISM phase is the destruction timescale. PAH destruction is mostly driven by UV and X-ray radiation leading to dehydrogenation and photodestruction of the carbon skeleton. In most cases, UV photons can break the weaker C-H bonds thus leading to dehydrogenation. If PAHs absorb more than 21 eV in an interval shorter than

their cooling time, the carbon skeleton breaks up, thereby destroying the PAH (Guhathakurta & Draine 1989). These processes will be most relevant in the surfaces of disks that are exposed to direct UV and X-ray radiation. Another important process is the collisional destruction of PAHs (involving H, O and OH) at high temperatures and pressure ($T \sim 1000$ K, $P \sim 10^{-6}$ bar). Kress *et al.* (2010) find that the overall destruction timescale of PAHs is set by the timescale of the most stable one, since high C_2H_2 abundances are used to convert smaller PAHs back into bigger ones.

Something to keep in mind is that the small dust in the form of VSGs and PAHs presents a very distinct grain population in the ISM. The fact that they do not follow the general power law size distribution (Draine 2004) could indicate that they experience very different processing as compared to the bulk silicate and graphite dust. An alternative production mechanism could thus be a continuous replenishment of PAHs from larger dust grains. Habart *et al.* (2004) suggested an evaporation of icy grain mantles within the disk. Since PAHs are ubiquitous in the ISM, they may have been included into ices during the cold molecular cloud phase. Rafikov (2006) suggested a PAH production through fragmentation of larger grains; a similar process has been discussed by Berné *et al.* (2009) for the VSGs. This could fit into the more recent ideas that the dust grain size distribution in disks reflects the outcome of continuous coagulation and fragmentation processes (Birnstiel *et al.* 2010).

6.2 Do PAHs shape the protoplanetary disk structure?

Photoelectric heating of even small amounts of PAHs is generally more efficient in heating the gas than the rest of the entire dust population. As shown by many authors (*e.g.* Kamp & Dullemond 2004; Jonkheid *et al.* 2004; Nomura & Millar 2005; Gorti & Hollenbach 2008), gas and dust temperature de-couple in the disk surfaces, above $A_V \sim 1$, and the higher gas temperature determines the vertical scale height and hence flaring of the disk. The recently developed disk modeling code PRODiMO solves self-consistently for the gas chemistry, energy balance and disk structure (Woitke *et al.* 2009; Kamp *et al.* 2010) also including PAH chemistry and physics (Woitke *et al.* in preparation). A recent study of PRODiMO disk models around Herbig stars shows that reducing the fractional abundance of PAHs in disks leads in general to much flatter disk structures and even strong shadows (van der Plas *et al.* in preparation).

6.3 How can we use PAHs as tracers of processes in protoplanetary disks?

The ambiguity whether PAHs are very small dust grains or large gas molecules makes them universal tracers of both disks components and widens their diagnostic potential.

As small dust grains, their emission can tell us if and where such small solid particles survive the settling and coagulation processes that lead otherwise to a

rapid grain growth to mm- and cm-sized dust (*e.g.* Natta & Testi 2004). PAHs can also be used to trace the radial disk structure up to ~ 100 AU. Since these grains are stochastically heated, their emission features are generally more extended than that of the continuum. As an example, Geers *et al.* (2007a) imaged IRS48 (previously classified as M dwarf and recently re-classified as A dwarf) in the 8.6, 9, 11.3, 11.9, 18.7 μm filters. The 18.7 μm image shows a gap with a radius of 30 AU, while the shorter PAH bands are all centered on source. Hence, they conclude that the gap cannot be entirely devoid in dust. This object maybe caught in a short lived phase very much related to transitional disks such as HD 141569. Another example for deviations from a simple smooth disk structure observed in PAH band emission are presented in Doucet *et al.* (2005) for the Herbig star HD 97048.

As large molecules, PAHs are thought to remain well mixed with the gas in the disk. As such, the PAH emission can also probe the physical conditions in the disk surfaces such as flaring and irradiation. VISIR imaging of the disk around HD 97048 in the PAH bands has shown that the observed emission, flaring angle and vertical scale height are consistent with the predictions from passive irradiated hydrostatic equilibrium disk models (Lagage *et al.* 2006). This gives support to the idea that PAHs rather belong to the gas than to the dust component of disks.

Along the same lines, Grady *et al.* (2005) show for a sample of 14 Herbig disks that the visibility from STIS coronagraphic imaging (sensitive to $0.5''$ – $15''$ distances from star, hence $r \geq 50 - 70$ AU) is correlated with the strength of PAH features (particularly the 6.2 μm band). They report a correlation with disk flaring, and an anticorrelation with dust settling and the absence of any correlations with SED type, far-IR slope, mass accretion rate or strength of H_2 emission. This could suggest that there is initially a simple stratification with size, very small grains such as PAHs staying up high in the disk. During the disk evolution these small grains should be photodestroyed on short timescales, leaving a rather flat structure behind since photoelectric heating on large grains is generally less efficient. Grady *et al.* (2005) also suggest that settling first occurs in the inner disk, so we should observe some disks that are flat inside and still flaring outside (if sufficient sample size available - since this might be a very short evolutionary phase), *e.g.* HD 163296, DM Tau (faint ring with dark inner disk), which are both around 5 Myr. HD 169142 (~ 6 Myr) is an example, where the inner disk maybe de-coupled from outer disk (Grady *et al.* 2007). The spatially resolved PAH emission and the Meeus group I SED classification are only consistent if the inner disk is substantially flatter than the outer disk.

PAHs are also good diagnostics of the stellar radiation field as the relative band strength indicate the fractional charging and typical sizes of PAHs which is directly related to the strength of the stellar radiation field. The stronger the radiation field, the less small PAHs can survive (*e.g.* Visser *et al.* 2007). This seems to be also confirmed by an analysis of the mid-IR emission of a sample of 12 *Spitzer* sources spread over the spectral ranges F to B (Berné *et al.* 2009).

References

- Acke, B., van den Ancker, M.E., Dullemond, C.P., van Boekel, R., & Waters, L.B.F.M., 2004, *A&A*, 422, 621
- Allain, T., Leach, S., & Sedlmayr, E., 1996, *A&A*, 305, 616
- Berné, O., Joblin, C., Fuente, A., & Ménard, F., 2009, *A&A*, 495, 827
- Birnstiel, T., Ricci, L., Trotta, F., *et al.*, 2010, *A&A*, 516, L14
- Boersma, C., Bouwman, J., Lahuis, F., *et al.*, 2008, *A&A*, 484, 241
- Boulanger, F., & Perault, M., 1988, *ApJ*, 330, 964
- Cherchneff, I., Barker, J.R., & Tielens, A.G.G.M., 1992, *ApJ*, 401, 269
- Desch, S.J., & Connolly, Jr., H.C., 2002, *Meteorit. Planet. Sci.*, 37, 183
- Desert, F., Boulanger, F., & Puget, J.L., 1990, *A&A*, 237, 215
- Doucet, C., Pantin, E., Lagage, P.O., *et al.*, 2005, in *Protostars and Planets V*, 8127
- Draine, B.T., 2004, in *Astron. Soc. Pacific Conf. Ser.*, 309, *Astrophysics of Dust*, ed. A.N. Witt, G.C. Clayton, & B.T. Draine, 691
- Draine, B.T., & Bertoldi, F., 1996, *ApJ*, 468, 269
- Dullemond, C.P., Henning, T., Visser, R., *et al.*, 2007a, *A&A*, 473, 457
- Dullemond, C.P., Hollenbach, D., Kamp, I., & D'Alessio, P., 2007b, *Protostars and Planets V*, 555
- Dwek, E., Arendt, R.G., Fixsen, D.J., *et al.*, 1997, *ApJ*, 475, 565
- Fedele, D., van den Ancker, M.E., Acke, B., *et al.*, 2008, *A&A*, 491, 809
- Geers, V.C., Augereau, J., Pontoppidan, K.M., *et al.*, 2006, *A&A*, 459, 545
- Geers, V.C., Pontoppidan, K.M., van Dishoeck, E.F., *et al.*, 2007a, *A&A*, 469, L35
- Geers, V.C., van Dishoeck, E.F., Visser, R., *et al.*, 2007b, *A&A*, 476, 279
- Gorti, U., & Hollenbach, D., 2008, *ApJ*, 683, 287
- Grady, C.A., Schneider, G., Hamaguchi, K., *et al.*, 2007, *ApJ*, 665, 1391
- Grady, C.A., Woodgate, B.E., Bowers, C.W., *et al.*, 2005, *ApJ*, 630, 958
- Gudipati, M.S., & Allamandola, L.J., 2003, *ApJ*, 596, L195
- Guhathakurta, P., & Draine, B.T., 1989, *ApJ*, 345, 230
- Habart, E., Natta, A., & Krügel, E., 2004, *A&A*, 427, 179
- Habart, E., Natta, A., Testi, L., & Carbillet, M., 2006, *A&A*, 449, 1067
- Habart, E., Verstraete, L., Boulanger, F., *et al.*, 2001, *A&A*, 373, 702
- Jonkheid, B., Faas, F.G.A., van Zadelhoff, G.-J., & van Dishoeck, E.F., 2004, *A&A*, 428, 511
- Jonkheid, B., Kamp, I., Augereau, J., & van Dishoeck, E.F., 2006, *A&A*, 453, 163
- Kamp, I., & Dullemond, C.P., 2004, *ApJ*, 615, 991
- Kamp, I., Tilling, I., Woitke, P., Thi, W., & Hogerheijde, M., 2010, *A&A*, 510, A260000
- Keller, L.D., Sloan, G.C., Forrest, W.J., *et al.*, 2008, *ApJ*, 684, 411
- Kress, M.E., Tielens, A.G.G.M., & Frenklach, M., 2010, *Adv. Space Res.*, 46, 44
- Lagage, P., Doucet, C., Pantin, E., *et al.*, 2006, *Science*, 314, 621
- Le Page, V., Snow, T.P., & Bierbaum, V.M., 2001, *ApJS*, 132, 233
- Li, A., & Draine, B.T., 2001, *ApJ*, 554, 778
- Li, A., & Lunine, J.I., 2003, *ApJ*, 594, 987

- Manske, V., & Henning, T., 1999, *A&A*, 349, 907
- Morgan, Jr., W.A., Feigelson, E.D., Wang, H., & Frenklach, M., 1991, *Science*, 252, 109
- Natta, A., & Testi, L., 2004, in *Astron. Soc. Pacific Conf. Ser.*, 323, *Star Formation in the Interstellar Medium: In Honor of David Hollenbach*, ed. D. Johnstone, F.C. Adams, D.N.C. Lin, D.A. Neufeld, & E.C. Ostriker, 279
- Nomura, H., & Millar, T.J., 2005, *A&A*, 438, 923
- Pendleton, Y.J., Sandford, S.A., Allamandola, L.J., Tielens, A.G.G.M., & Sellgren, K., 1994, *ApJ*, 437, 683
- Rafikov, R.R., 2006, *ApJ*, 646, 288
- Siebenmorgen, R., & Krügel, E., 2009 [[ArXiv e-prints](#)]
- Sloan, G.C., Jura, M., Duley, W.W., *et al.*, 2007, *ApJ*, 664, 1144
- Tielens, A.G.G.M., 2008, *ARA&A*, 46, 289
- Tielens, A.G.G.M., Seab, C.G., Hollenbach, D.J., & McKee, C.F., 1987, *ApJ*, 319, L109
- Verhoeff, A.P., Min, M., Acke, B., *et al.*, 2010, *A&A*, 516, A48
- Visser, R., Geers, V.C., Dullemond, C.P., *et al.*, 2007, *A&A*, 466, 229
- Weingartner, J.C., & Draine, B.T., 2001, *ApJS*, 134, 263
- Woitke, P., Kamp, I., & Thi, W.-F., 2009, *A&A*, 501, 383
- Woods, P.M., & Willacy, K., 2007, *ApJ*, 655, L49

PAH IN VECTORIZED THREE DIMENSIONAL MONTE CARLO DUST RADIATIVE TRANSFER MODELS

R. Siebenmorgen¹, F. Heymann² and E. Krügel³

Abstract. We present a Monte Carlo (MC) radiative transfer code for complex three dimensional dust distributions and include transiently heated PAH. The correctness of the code is confirmed by comparison with benchmark results. The method makes use of the parallelization capabilities of modern vectorized computing units like graphic cards. The computational speed grows linearly with the number of graphical processing units (GPU). On a conventional desktop PC, our code is up to a factor 100 faster when compared to other MC algorithms. As an example, we compute the dust emission of proto-planetary disks. We simulate how a mid-IR instrument mounted at a future 42 m ELT will detect such disks. Two cases are distinguished: a homogeneous disk and a disk with an outward migrating planet, producing a gap and a spiral density wave. We find that the resulting mid-IR spectra of both disks are almost identical. However, they can be distinguished at those wavelengths by coronagraphic, dual-band imaging. Finally, the emission of PAHs exposed to different radiation fields is computed. We demonstrate that PAH emission depends not only on the strength but also strongly on the hardness of the radiation, a fact which has often been neglected in previous models. We find that hard photons (> 20 eV) easily dissociate all PAHs in the disks of T Tauri stars. To explain the low, but not negligible detection rate ($< 10\%$) of PAHs in T Tau disks, we suggest that turbulent motions act as a possible path for PAH survival.

1 Dust model

In the dust model we consider: *large* ($60 \text{ \AA} < a < 0.2 - 0.3 \text{ \mu m}$) silicate (Draine 2003) and amorphous carbon (Zubko *et al.* 2004) grains and *small* graphite

¹ ESO, Karl-Schwarzschild-Str. 2, 85748 Garching b. München, Germany

² Astronomisches Institut, Ruhr-Universität Bochum, Universitätsstra. 150, 44801 Bochum, Germany and ESO

³ MPI für Radioastronomie, Auf dem Hügel 69, Postfach 2024, 53010 Bonn, Germany

($5 < a < 80 \text{ \AA}$) grains. For both, we apply a power law size distribution: $n(a) \propto a^{-3.5}$ and absorption and scattering cross-sections are computed with Mie theory. In addition we include PAHs with 30 and 200 C atoms. For the absorption cross section (Draine 2010; Mallocci 2010; Verstraete 2010) we follow at photon energies between 1.7–15 eV Mallocci *et al.* (2007, their Fig. 4). At low frequency, we take a cross section cut-off given as an average of neutral (Schutte *et al.* 1993) and ionized (Salama *et al.* 1996) species. For hard photons, beyond the 17 eV band, we scale the photo-absorption cross section of PAH up to the keV region to similar sized graphite particles. By computing cross sections above 100 eV, we consider an approximation of kinetic energy losses (Dwek & Smith (1996) and apply it to all dust particles. With the advent of *ISO* and *Spitzer* more PAH emission features and more details of their band structures are detected (Tielens 2008). We consider 17 emission bands and take, for simplicity and as suggested by Boulanger *et al.* (1998) and Siebenmorgen *et al.* (1998), Lorentzian profiles. Parameters are listed in Siebenmorgen & Krügel (2001) and calibrated using mid-IR spectra of starburst nuclei. For starburst galaxies, a SED library is computed (Siebenmorgen *et al.* 2007) and those models provide good fits to the SED of local galaxies and to PAH detected at high red shifts ($z \approx 3$, Efstathiou & Siebenmorgen 2009). In the model, we use dust abundances of $[X]/[H]$ (ppm) of: 31 for [Si], 150 [amorphous C], 50 [graphite] and 30 [PAH], respectively; which is in agreement with cosmic abundance constrains (Asplund *et al.* 2009). We are in the process of upgrading the model to be consistent with the polarisation of the ISM (Voshchinnikov 2004).

2 Monte Carlo method

We compute the radiative transfer with a Monte Carlo (MC) technique, which allows to handle complicated geometries, by following the flight path of many random photons. The basic ideas of our method go back to Lucy (1999) and Bjorkmann & Wood (2001). They are described and extended to the treatment of transiently heated PAHs in Krügel (2006). The space is partitioned into cubes and, where a finer grid is needed, the cubes are further divided into subcubes (cells). The star emits photon packages of constant energy ε , but different frequencies. A package entering on its flight path a cell may be absorbed there or scattered. The probability for such an interaction is given by the extinction optical depth along the path within the cell. When the package is scattered, it only changes direction determined in a probabilistic manner by the phase function. When it is absorbed, a new package of the same energy, but usually different frequency ν_{new} is emitted from the spot of absorption. The emission is isotropic. Each absorption event raises the energy of the cell by ε , and accordingly its temperature.

We were able to increase the computational speed of the code by up to two orders of magnitude by parallelizing it, *i.e.* by calculating the flight paths of a hundred or more photons simultaneously. This allows the treatment of complex geometries which were so far prohibited because of their excessive computer demands. To achieve parallelization, we had to slightly modify the original code. The latter calculates the new frequency ν_{new} of a package that is emitted

after absorption using the cell temperature before absorption, but applies a correction for the new temperature due to Bjorkmann & Wood (2001). We now omit this correction or in, mathematical terms, use Equation (11.67) instead of Equation (11.65) in Krügel (2006). As expected and borne out in tests, the correction may be neglected when the number of photons absorbed in a cell is not small. The vectorized MC code was developed during the PhD project of Heymann (2010). It was verified against benchmarks provided for stellar heated dust spheres by Ivezić *et al.* (1997), the ray tracing code by Krügel (2006) and axi-symmetrical disks by Pascucci *et al.* (2004). Generally, the computed SED agrees with the benchmarks to within a few percent. One example of such comparisons is shown in Figure 1 for a dust sphere with PAHs. The factor by which parallelization speeds up the computation scales almost linearly with the number of graphical processing units. We point out that particular attention had to be given to the choice of the random number generator where we chose the Mersene Twister algorithm (Matsumoto & Nishimura 1998).

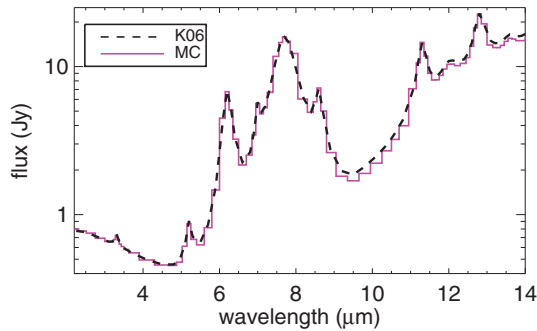


Fig. 1. Comparison of a SED of a stellar heated dust sphere of constant density and visual extinction to the star of $A_V = 10$ mag computed with a ray tracing method, as described in Krügel (2006), and the MC treatment of this work; both methods agree to within a few %.

3 Detection of proto-planetary disk structures

Hydrodynamical simulations of proto-planetary disks with an orbiting planet show particular disk features (Masset *et al.* 2006). We present a three dimensional application of the MC code where a disk heated by a solar type star has a dust density which follows the one as given by Pascucci *et al.*, and has in addition a gap between 3 – 8 AU and a low density spiral structure. The optical depth along the midplane from 0.2 to 75 AU is 10 mag. We simulate if such disk structures can be resolved at a distance of 50 pc with a mid-IR instrument (Brandl *et al.* 2010) mounted at a future 42 m extreme large telescope (ELT); a project under study by ESO. The point spread function (PSF) of the ELT has resolution of 50 milliarcsec at 10 μm . In order to improve the contrast between star and disk, the instrument

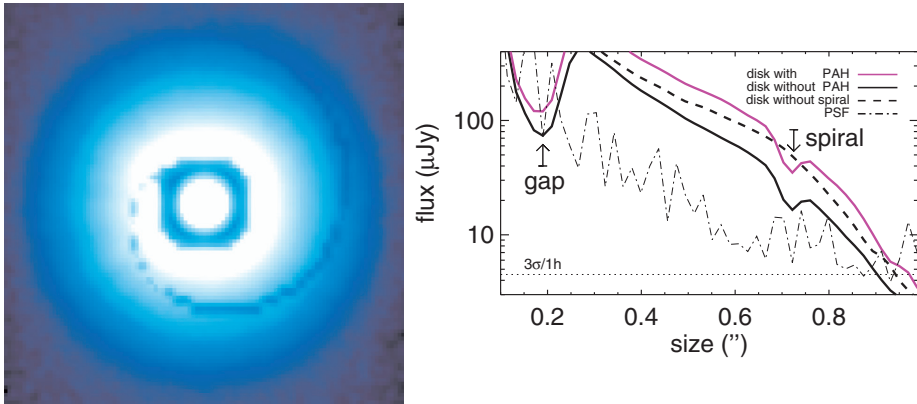


Fig. 2. Image at $11.3 \mu\text{m}$ (left) together with flux profiles along the major axis (right). The 3σ detection limit (dotted) and PSF (dash-dotted) is indicated. For the disk with (magenta) or without (black) PAH the gap and the spiral structure is well preserved. A homogeneous disk including PAHs is shown in dashed for comparison.

will provide coronagraphic and dual band imaging modes. We choose band passes at 11.3 and $10 \mu\text{m}$. The $11.3 \mu\text{m}$ emission is shown in Figure 2 together with the flux profile along the major axis. Profiles of such a disk with and without PAHs and that of a homogeneous disk are computed. The 3σ detection limit after 1h integration is given assuming background limited performance of the instrument. The models predict that the detailed structure of such a proto-planetary disk can be well detected.

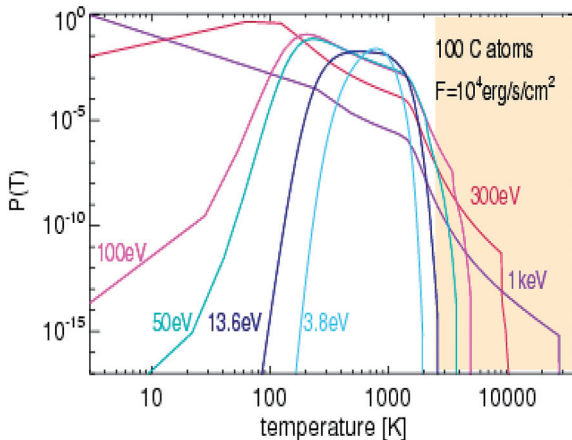


Fig. 3. The temperature distribution $P(T)$ of a PAH with 100 C atoms exposed to monochromatic radiation with $h\nu = 3.8, 13.6, 50, 100, 300 \text{ eV}$ and 1 keV in a constant heating bath of flux $F = 10^4 \text{ erg s}^{-1} \text{ cm}^{-2}$ (Siebenmorgen & Krügel 2010). The shaded area marks temperatures above the sublimation temperature of graphite.

4 Destruction and survival of PAH in T Tauri disks

Despite the fact that from the stellar heating one would expect to detect PAH in the disks of T Tauri, one finds them rather seldom, in less than 10% of T Tauri (Geers *et al.* 2006). In order to explain this fact we present a simplified scheme to estimate the location from the primary heating source at which the PAH molecules become photo-stable (Siebenmorgen & Krügel 2010). T Tauri stars have beside photospheric emission also a far ultraviolet (FUV), an extreme ultraviolet (EUV) and an X-ray component with a fractional luminosity of about 1%, 0.1% and 0.025%, respectively. Such hard photons are very efficient in dissociating PAHs. The temperature distribution, $P(T)$, of PAHs after hard photon absorption is shown in Figure 3. It demonstrates that $P(T)$ depends strongly on the hardness and spectral shape of the exciting radiation field, a fact which is often neglected in computations of the PAH emission. After photon absorption, a highly vibrationally excited PAH may relax through emission of IR photons or, if sufficiently excited, lose atoms (Omont 1986 & Tielens 2005) for a textbook description). We find that hard photons (EUV and X-ray) would destroy all PAHs in the disk of T Tauri stars; whereas soft photons with energies < 20 eV dissociate PAHs only up to short distances from the star (1–2 AU). As a possible path for PAH-survival turbulent vertical motions are suggested. They can replenish or remove PAHs from the reach of hard photons. In our treatment the presence of gas is considered which is ionized at the top of the disk and neutral at lower levels. A view of the scheme is shown as vertical cut along the midplane in Figure 4.

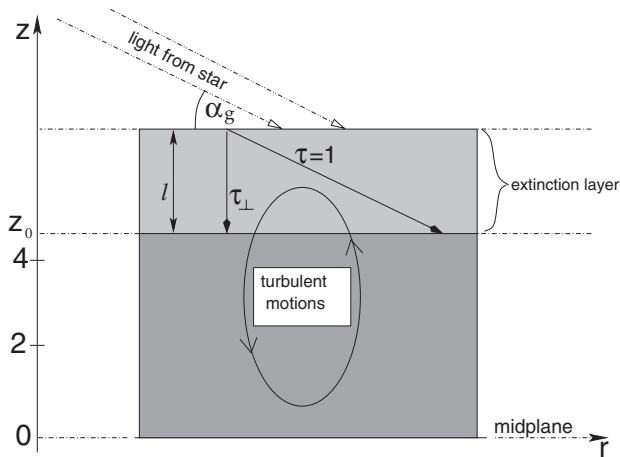


Fig. 4. Of each radiation component (photosphere, FUV, EUV and X-rays) of the fiducial T Tauri star about 90% is absorbed in what we call extinction layer. The optical depth from its bottom to the star is one and in the vertical direction equal to the grazing angle α_g . The height of its lower boundary z_0 declines with the radius, but its geometrical thickness is rather constant ($l \approx 0.5H$, for details see Siebenmorgen & Krügel 2010). Vertical motions may either remove PAH from the extinction layer quickly enough for survival or replenish PAH from below.

References

- Asplund, M., Grevesse, N., Sauval, A.J., & Scott, P., 2009, *ARA&A*, 47, 481
- Bjorkman, J.E., & Wood, K., 2001, *ApJ*, 554, 615
- Boulanger, F., Boissel, P., Cesarsky, D., & Ryter, C., 1998, *A&A*, 339, 194
- Brandl B., *et al.*, 2010, *SPIE*, 7735-86, in press
- Draine, B.T., 2003, *ApJ*, 598, 1026
- Draine, B.T., 2011, this volume
- Dwek, E., & Smith, R.K., 1996, *ApJ*, 459, 686
- Efstathiou, A., & Siebenmorgen, R., 2009, *A&A*, 502, 541
- Geers, V.C., Augereau, J.-C., Pontoppidan, K.M., *et al.*, 2006, *A&A*, 459, 545
- Heymann, F., 2010, Ph.D. Thesis, University of Bochum
- Ivezic, Z., Groenewegen, M.A.T., Menshchikov, A., *et al.*, 1997, *MNRAS*, 291, 121
- Krügel, E., 2006, *An introduction to the Physics of Interstellar Dust (IoP)*
- Lucy, L.B., 1999, *A&A*, 344, 282
- Mallocci, G., Joblin, C., & Mulas, G., 2007, *A&A*, 462, 627
- Mallocci, G., 2011, this volume
- Masset, F.S., Morbidelli, A., Crida, A., & Ferreira, J., 2006, *ApJ*, 642, 478
- Matsumoto, M., & Nishimura, T., 1998, *ACM Trans. Model. Comp. Simul.*, 8, 330
- Micelotta, E.R., Jones, A.P., & Tielens, A.G.G.M., 2010, *A&A*, 510, A36
- Omont, A., 1986, *A&A*, 166, 159
- Pascucci, I., Wolf, S., Steinacker, J., *et al.*, 2004, *A&A*, 417, 793
- Salama, F., Bakes, E.L.O., Allamandola, L.J., & Tielens, A.G.G.M., 1996, *ApJ*, 458, 621
- Schutte, W.A., Tielens, A.G.G.M., & Allamandola, L.J., 1993, *ApJ*, 415, 397
- Siebenmorgen, R., Natta, A., Krügel, E., & Prusti, T., 1998, *A&A*, 339, 134
- Siebenmorgen, R., Krügel, E., & Laureijs, L., 2001, *A&A*, 377, 735
- Siebenmorgen, R., & Krügel, E., 2007, *A&A*, 461, 445
- Siebenmorgen, R., & Krügel, E., 2010, *A&A*, 511, A6
- Tielens, A.G.G.M., 2005, *The Physics and Chemistry of the Interstellar Medium* (Cambridge Univ. Press)
- Tielens, A.G.G.M., 2008, *ARA&A*, 46, 289
- Verstraete, L., 2011, this volume
- Voshchinnikov, N.V., 2004, *Optics of cosmic dust I, ASPR*, 12, 1
- Zubko, V., Dwek, E., & Arendt, R.G., 2004, *ApJS*, 152, 211

**PAHs and Carbonaceous
Grains & Solar System Materials**

FROM PAHS TO SOLID CARBON

C. Jäger¹, H. Mutschke², T. Henning³ and F. Huisken¹

Abstract. Carbonaceous grains represent a major component of cosmic dust. The review will summarize new results in laboratory investigations of carbonaceous dust components. The nanometer-sized carbon particles are supposed to represent a blend of differently structured carbon including graphitic, diamond-like, fullerene-like and chain-like components on a subnanometer or nanometer scale. Recent models used to explain the structure of gas-phase condensed carbon nanoparticles are discussed. Possible formation pathways of carbonaceous grains from molecular components and clusters and the role of polycyclic aromatic hydrocarbons (PAHs) and fullerenes are disclosed.

1 Introduction

Carbonaceous grains belong to the most abundant cosmic dust components. Cosmic dust absorbs and scatters stellar light and radiates the energy in the IR and millimeter range. Very small dust grains influence the heating rate of gas in the interstellar medium (ISM) by the photoelectric effect. In addition, surfaces of dust grains are efficient factories for the formation of molecular hydrogen and larger organic molecules. In the diffuse ISM, grain shattering and sputtering processes can erode and fragment grains into smaller units and therefore grains can act as precursors of organic molecules. Carbon and hydrogen atoms constitute the basis of a rich organic chemistry in the solar system and in the interstellar medium and finally for life on earth and, perhaps, on other planets. However, the problem with the carbon dust component is the huge diversity of allotropes and structures that can be mixed up in one grain. Due to the processing of the dust grains in the interstellar medium, the composition and structure is constantly modified. Large

¹ Max-Planck-Institute for Astronomy, Heidelberg and Institute of Solid State Physics, Friedrich Schiller University, Helmholtzweg 3, 07743 Jena, Germany

² Astrophysical Institute and University Observatory, Friedrich Schiller University, Schillergässchen 2-3, 07745 Jena, Germany

³ Max-Planck-Institute for Astronomy, Königstuhl 17, 69117 Heidelberg, Germany

PAH molecules are involved in these processes both as precursors of condensation and products of grain disintegration. Consequently, the spectral properties of cosmic carbon grains, which are strongly related to the structure and composition of the carbonaceous materials, are changing considerably from circumstellar to interstellar to protoplanetary environments. In order to “understand” the spectral signature of the cosmic carbon component, one has to study the spectral properties of differently structured carbon materials in the laboratory.

2 Solid forms of carbon

For carbon, the possibilities to form solid structures are extremely manifold because of its ability to occur in different hybridization states. Carbon exist in different allotropes including diamond, graphite, polyynes and fullerenes. Further solid forms of carbon are graphene and nanotubes, new forms of solid carbon, which are based on graphitic or fullerene structures.

In the diamond lattice, the tetrahedrally coordinated carbon atoms are covalently bound to each other via four strong σ bonds. Consequently, diamond is an insulator having a large band gap of 5.5 eV. In graphite, the three sp^2 hybrid orbitals have a trigonal planar symmetry and can form σ bonds with the adjacent carbon atoms whereas the nonhybridized p electron is able to form an additional π bond. This results in infinite layers of condensed benzene rings with delocalized π electrons between them. Therefore, graphite represents a zero band gap material.

In polyynes, the carbon atoms are sp hybridized forming two sp hybrid orbitals with two remaining p orbitals. The sp hybridized carbon atoms build up chains with alternating triple bonds. Polyyne molecules or radicals are found to exist in the ISM. These chain-like structures form in gas-phase condensation experiments and they are supposed to be precursors of fullerenes or fullerene-like carbon grains (Ravagnan *et al.* 2002).

Apart from the distinct hybridization states, there exist mixed hybridization states which build up curved structures. In the perfect form, they are closed-shell molecules consisting of only carbon, called fullerenes (the fourth allotrope of carbon). They can be produced in gas-phase condensation reactions such as by laser ablation or arc discharge of carbon electrodes in helium gas atmosphere (Kroto *et al.* 1985; Krätschmer *et al.* 1990). The curvature is achieved by the incorporation of pentagons and heptagons. The deviation of the planar structure results in a higher s-character of the π orbital and a mixed hybridization state (Haddon 1993). C_{60} , C_{70} , or smaller fullerenes are not “superaromatic” as they tend to avoid double bonds in the pentagonal rings. C_{60} behaves like an electron deficient alkene and reacts readily with electron-rich species. Many fullerenes have now been detected in carbon soot, uncovered by electron microscopy, including very small ones such as C_{20} or C_{34} .

Carbon nanotubes (CNTs), the fifth form of solid carbon, can exist as single-walled or multi-walled species with several nested cylinders. Multi-walled forms can be produced in gas-phase condensations together with other particulate carbon

forms (Iijima 1991). Single walled CNTs up to lengths of about 1 μm can be produced using catalysts (Harris 2009). A single-wall CNT can be imagined as a graphene sheet rolled at a certain chiral angle. CNTs can grow up to lengths over 1 μm and with a range of diameters from 1 nm (for single walled) to around 50 nm for multi walled ones. The electronic properties vary from metallic to semiconducting with diameter and chirality.

Since 2004, a sixth form of carbon has been defined that can be considered as a single layer of graphite called “graphene”. The material has been produced by mechanical exfoliation of graphite (Geim & Novoselov 2007). Other methods, developed to produce graphene, are SiC and hydrazine reduction, or chemical vapor deposition. One can consider graphene as an infinite or very large PAH partly hydrogen deficient. The largest molecule chemically synthesized in the laboratory is $\text{C}_{222}\text{H}_{42}$ with a mass of around 2700 u (Wu *et al.* 2007). In gas-phase condensation processes, even larger molecules can be produced, however, to make them visible with analytical methods is rather difficult.

The very large graphene species have to be stabilized either by a substrate or by a scaffold. Graphene can be transformed into a hydrogenated form (graphane) by exposing the sheets to a cold hydrogen plasma (Savchenko 2009; Elias *et al.* 2009). The material transforms from a highly conductive material into an insulator. This process is reversible and can be reversed by annealing in argon. Density-functional-based tight-binding level calculations have shown that the HOMO-LUMO gaps of graphene nanoflakes vary from zero to gap energies typical for insulators (Kuc *et al.* 2010).

3 Structure of gas-phase condensed carbon nano-particles

It is generally assumed that the major fraction of the primary cosmic carbonaceous material is formed as nanometer-sized particles via gas-phase condensation in circumstellar envelopes of carbon-rich asymptotic giant branch (AGB) stars (Henning & Salama 1998). In order to understand the cosmic condensation of carbonaceous grains, gas-phase condensations of carbonaceous grains have to be simulated in the laboratory. Dedicated analytical methods such as high-resolution transmission electron microscopy (HRTEM) and UV/Vis/IR spectroscopy help to understand the structure and composition of condensed carbon grains. Here, we present a brief overview on the structural characteristics of gas-phase condensed nano-particles produced from carbon and hydrogen.

The structural complexity of pure carbon or carbon mixed with hydrogen can be huge in solid carbon. Differently hybridized carbon (sp , sp^2 , and sp^3) and mixed hybridization states may occur in different ratios in one grain. The structure of particulate carbon materials can be characterized on different length scales describing the short-, medium-, and long-range order of the material. The long-range order describes the size and shape of the primary particles and their agglomeration state. The medium-range order characterizes the arrangement, shape and size of the structural subunits and can be derived by HRTEM. So-called basic

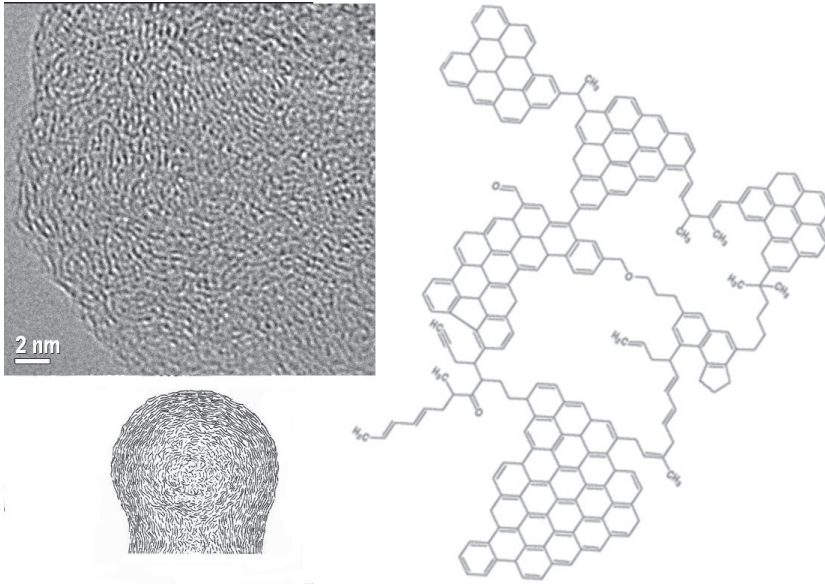


Fig. 1. HRTEM image of a gas-phase condensed particle having a paracrystalline structure. The chemical formula (right) shows one possible amorphous carbon structure which can be considered as a paracrystalline graphene layers.

structural units (BSUs) consisting of small subnanometer- or nanometer-sized graphitic crystallites which can be randomly or concentrically arranged in a grain have been already discussed in the sixties (Heidenreich *et al.* 1968). However, plenty of HRTEM studies of condensed particles show the presence of individual graphene layers that are concentrically arranged. This structure can be described by the more recent paracrystalline model of soot grains (Hess & Herd 1993) which can be characterized by a layer structure of perturbed graphene layers. At present, this concept is the most widely accepted microstructural model for soot.

The hybridization state of the carbon, the nature of the bonds between carbon atoms as well as the incorporation of hydrogen or hetero atoms in the carbon grains can be specified by the short-range order of the material. Analytical methods like electron energy loss, IR, or nuclear magnetic resonance spectroscopy have to be applied to obtain the information on the short range order (Schnaiter *et al.* 1998; Jäger *et al.* 1999). The short- and the medium-range order of carbon grains can be well described by the terms “amorphous carbon” (AC) or “hydrogenated amorphous carbon” (HAC) (see Fig. 1). HACs are frequently used to describe the carbonaceous dust component in astrophysical studies (Jones *et al.* 1990; Duley 1994; Pendleton & Allamandola 2002; Dartois *et al.* 2010). Both terms, “HACs” and ACs, are misleading since they describe groups of carbonaceous materials with different C/H ratios, varying ratios of sp^3 , sp^2 , and sp hybridized carbon, and gap

energies between 0.5 and about 4.0 eV. They represent three-dimensional structures applicable for the characterization of graphitic or paracrystalline structural units in grains. In AC and HAC, the carbonaceous structure can be characterized by aromatic islands of different sizes, which are linked by aliphatic structures including sp, sp², and sp³ carbon atoms. However, there is no clear discrimination between AC and HAC on the basis of the sizes of aromatic and aliphatic units and on their H/C ratios. In astrophysical studies, the term HAC is preferentially used for carbon materials with very small aromatic units (2–8 rings Jones *et al.* 1990). Oxygen in the form of ether bridges (-C-O-C-) or carbonyl groups (-C=O) may also be included. However, the amount of oxygen incorporated into a solid hydrocarbon material present in the diffuse interstellar medium is assumed to be low (Pendleton & Allamandola 2002). According to Robertson (1986), the aromatic as well as the aliphatic structures in HACs tend to cluster. Another acronym for similar materials were “quenched carbonaceous composites” (Sakata *et al.* 1993; Wada *et al.* 1999). The application of natural coals as cosmic dust analogs has been suggested by Papoular *et al.* (1993).

The spectral properties of HACs in the UV/Vis are dominated by electronic transitions. Whereas the $\sigma - \sigma^*$ transitions are located in the far UV, the $\pi - \pi^*$ transitions occur at wavelengths between 190 and 270 nm. Robertson & O’Reilly (1987) claimed that the size of the aromatic units determine the gap energy and the position of the $\pi - \pi^*$ transitions. The gap energy E_g can be derived from the optical spectra by means of the Tauc relation $\sqrt{\epsilon_2 E} = B(E - E_g)$ (Tauc *et al.* 1966). According to the relation $E_g = 2\beta M^{-1/2}$ derived by Robertson & O’Reilly (1987), where β represents a quantum chemically estimated overlapping energy between two adjacent p_z orbitals that has an empirical value of 2.9 eV, the optical gap energy of soot is related to the number M of condensed rings in the graphene layers. However, nowadays it is widely accepted that bent graphene layers can be incorporated into particles. For mixed hybridization states, the electronic transitions are shifted to higher energies proven by using sophisticated spectral measurements such as electron energy loss or near edge X-ray absorption spectroscopy (Ajayan *et al.* 1993; Ravagnan *et al.* 2006; Jäger *et al.* 2010).

In the IR range, the functional groups included in the HAC structure can cause vibrational bands in absorption or emission. In addition, the sizes of aromatic subunits also influence the IR spectral properties due to continuous absorptions by free charge carriers. In particular, the sizes of aromatic subunits affect the conductivity of the material which has a strong influence on the absorptivity in the range between 100 μm and 1 mm.

A special group of gas-phase condensed grains are onion-like or fullerene-like grains including nested buckyonions. Faceted polyhedral onions and onions with not perfectly closed shells are formed during the condensation of carbon vapor at high temperature, for example, in the arc discharge. Completely spherical onions are non-equilibrium structures and self-assemble only under irradiation of graphitic or amorphous carbon precursors (Ugarte 1992; Banhart 1999). Nowadays, defective carbon onions were discussed to be possible carriers of different observational bands such as the 217 nm bump (Tomita *et al.* 2002; Chhowalla *et al.* 2003).

4 Soot formation

4.1 Soot formation in astrophysical environments

Carbon grain condensation in astrophysical environments has been rarely discussed in the astrophysical literature. Gail & Sedlmayr (1985) have applied classical nucleation theory to study the carbon grain formation in stationary, spherical expanding winds. They calculated condensation temperatures of dust between 1260 and 1320 K for optically thin and between 1350 and 1430 K for optically thick shells. The final grain radii were found to be small but very close to the theoretically possible maximum if all condensable material is included in grains. Lodders & Fegley (1999) modeled dust condensation in carbon-rich AGB stars using thermodynamic equilibrium calculations and found that the condensation temperature of graphite is pressure independent but sensitive to the C/O ratio in the circumstellar shells.

Detailed kinetic models for the formation of PAHs from acetylene in AGB stars have been presented by Frenklach & Feigelson (1989), Cherchneff *et al.* (1992), Allain *et al.* (1997), Cherchneff (2010). The authors determined a narrow temperature range of 900 to 1100 K for the formation of PAHs in circumstellar environments strongly dependent on the basic set of conditions such as mass loss, wind velocity, and gas density. Frenklach & Feigelson (1989) found a yield of 1.3% with respect to the amount of carbon initially present in acetylene for the most favorable case (low effective temperature of 1500 K, a mass loss rate as high as $10^{-4} M_{\odot}$ per year and a wind velocity of $10^{-2} \text{ km s}^{-1}$). Cherchneff *et al.* (1992) obtained a maximum yield of 5×10^{-5} . Cherchneff & Cau (1999) reconsidered the modeling of the PAH and carbon dust formation in carbon-rich AGB stars and applied a physico-chemical model, which describes the periodically shocked gas in the circumstellar shells close to the photosphere of the stars. The authors claimed that the formation of the first aromatic ring begins at $1.4 R_{*}$ and, at a radius of $1.7 R_{*}$ corresponding to a temperature of around 1700 K, the conversion of single rings to PAHs begins. The resulting temperature is much higher than the temperature window calculated in previous studies. Cau (2002) investigated the contribution of periodic shocks to the formation of PAHs and their dimers in the inner atmosphere of IRC+10216. He has shown that the amount of PAHs and dimers produced is not enough to explain the formation of carbon dust in the atmosphere of the star, but it can account for the formation of the small disordered cores of the kind observed in presolar grains. These cores might then grow larger through direct chemical reactions with acetylene. The yield of PAHs and dimers obtained was lower than that found by Frenklach & Feigelson (1989).

4.2 Soot formation in terrestrial combustion processes

Most experimental data on the kinetics of soot formation were obtained in flames and shock waves. A rough picture of soot formation in flames has been provided by Richter & Howard (2000) who distinguish three main steps of the soot formation. The process starts with the formation of the molecular precursors of soot which

are supposed to be big PAHs of molecular weights larger than 300 u. The growth process from small molecules such as benzene to larger PAHs comprises both the addition of C₂, C₃ or other small units to PAH radicals and reactions among the growing aromatic species.

The second part of the process is called particle inception. In this process, the conversion from molecular to particulate systems happens. The third part of the soot formation is the particle growth process which can be again sub-divided into the growth of particles by addition of gas-phase molecules, such as PAHs, and coagulation via reactive particle-particle collisions, a process which significantly increases particles sizes. Whereas the first and third step is rather well understood the soot nucleation or particle inception is not yet understood. The first and the second step of soot formation are the most interesting ones for astrophysics.

However, one has to keep in mind that soot formation pathways in flames are more complicated than in the more isothermal laser pyrolysis or laser ablation processes. Within a flame the temperature is rising from the bottom to the top and from the outer edge to the middle of the flame resulting in different formation pathways to soot particles. The application of gas-phase condensation methods which provides higher homogeneity in the temperature distribution are necessary to obtain more general information on carbon grain formation in such processes.

In our laboratory, we have employed gas-phase condensation experiments such as laser pyrolysis and laser ablation in quenching gas atmospheres to condense carbonaceous particles within two different temperature regimes, a high- (HT) and a low-temperature (LT) condensation regime. More experimental details on the techniques can be found in Jäger *et al.* (2008) and (2009). In both cases, the gas-phase condensation is comparable to the grain formation processes suggested to be relevant in astrophysical environments.

The study of the formation pathways has been performed by analytical characterization of the complete carbonaceous condensate, including high-resolution transmission electron microscopy (HRTEM), chromatographic methods, and mass spectroscopy assuming that some fraction of the precursor molecules and intermediate products are preserved in the final condensate due to an efficient quenching of the condensed carbon materials after the formation. In LT condensation processes at temperatures lower than 1700 K, either mixtures of insoluble grains and PAHs or exclusively PAHs are formed. The typical internal structure of the particles can be described by a concentric arrangement of rather plane graphene layers around a kind of disordered core (see Fig. 2). Matrix-assisted laser desorption and ionization combined with time-of-flight (MALDI-TOF) mass spectrometer studies have demonstrated that PAHs up to masses of 3000 u and even higher are formed during the condensation process (see Fig. 3). All sizes of PAHs are formed in such condensations but no saturated hydrocarbon molecules could be identified. LT condensation favors a formation process with PAHs as precursors and particle-forming elements, which condense on the surface of carbonaceous seeds via physis- and chemisorption. As a result, large carbonaceous grains are formed revealing well developed planar or only slightly bent graphene layers in their interior. Since larger PAHs have a lower volatility compared to the smaller ones, a

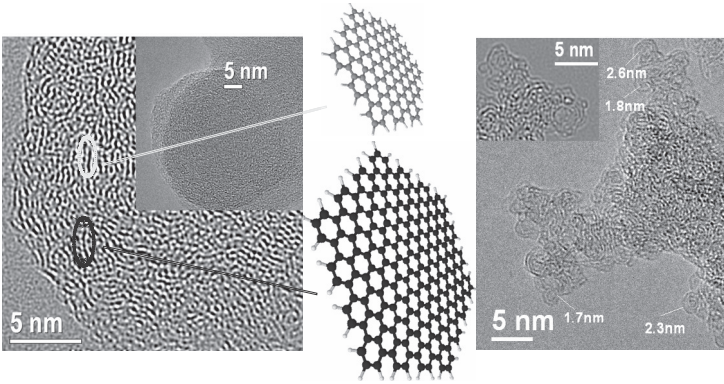


Fig. 2. HRTEM micrograph of a grain formed in a LT (left) condensation process. The average length of graphene layers is around 2 nm comparable to PAHs with masses of around 1300 u (smaller PAH molecule). The largest layers have a size of 3 nm which corresponds to PAHs of about 2700 u (large molecule). The HT condensed grains in the right panel are built of fullerene fragments or bucky onions with nested fullerene cages.

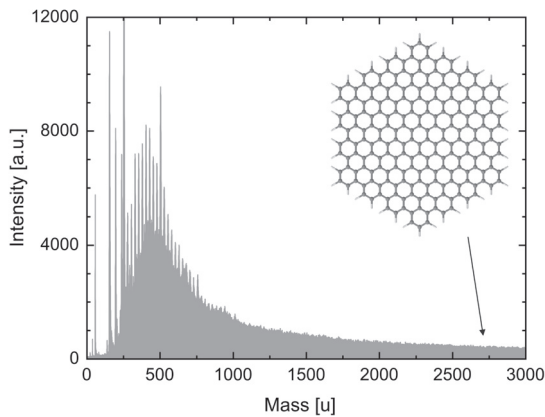


Fig. 3. MALDI TOF spectrum of a LT soot sample showing PAHs with masses up to 3000 u. To exemplify a PAH molecule with comparable mass, a molecule comprising 91 condensed rings is presented.

preferred accumulation of large molecules during the surface growth process can be observed. The accumulation of the large molecules on the surfaces of the seeds can be confirmed by a detailed analysis of the HRTEM micrographs (see Fig. 2) revealing a mean length of the graphene sheets inside the particles of around 2 nm corresponding to PAHs with masses of around 1300 u. The longest graphene layers determined in the soot particles have extensions of about 3 nm corresponding to the highest-mass PAHs detected with MALDI-TOF measurements (Jäger *et al.* 2009).

The generation of fullerenes and fragments of them in the HT condensation process at temperatures higher than 3500 K could be verified by using electron microscopy which can be shown in Figure 2. The presence of symmetric and elongated fullerene molecules with different numbers of carbon atoms is clearly visible in the HRTEM micrographs (Jäger *et al.* 2009). Fullerene fragments, fullerenes and buckyonions serve as building blocks for the very small carbon grains formed in such HT regimes. MALDI-TOF studies of the condensate have shown that no PAHs are formed in this process pointing to a completely different soot formation pathway via polyynes chains, fullerenes and fullerene snatches. The formation pathway is found to be initiated by long and branched carbon macromolecules suggested to be the precursors for cyclic structures (Irle *et al.* 2003). The existence of polyyn structures in the condensate could be verified by *in situ* IR spectroscopy that shows the typical IR stretching bands of triply bound $\equiv\text{CH}$ and $\text{C}\equiv\text{C}$ (Jäger *et al.* 2008).

4.3 The nucleation process

The controversial part of the soot formation even in the combustion community is the so-called inception, the formation of the first stable nuclei, *i.e.* the soot precursor particles.

Most of the combustion models favor the influence of PAHs and the formation of PAH clusters as soot nuclei (Dobbins *et al.* 1998; Richter & Howard 2000; Mansurov 1998). Chen & Dobbins (2000) considered large PAHs and PAH clusters with layer structure as nucleation seeds. Schuetz & Frenklach (2000) discussed the dimerization of PAHs whereas Homann (1998) prefers the theory of PAH oligomerization resulting in the formation of so-called aromers. In PAH dominated soot formation processes, PAH radicals formed by hydrogen abstraction are discussed to be the driving force for the cluster formation (Richter *et al.* 2004). Reactions of PAH radicals with PAHs and between PAH radicals were found to be the dominant pathway to soot nuclei. In flames, the transition from gaseous to solid particles was assumed to depend on the temperature and pressure. Particles heavier than 2000 u and diameters of around 1.5 nm are considered as first solids (Lafleur *et al.* 1996; Harris & Weiner 1988; McKinnon & Howard 1992).

The formation of larger, three-dimensional species with amorphous carbon structure has been proposed by D'Alessio *et al.* (1998) and Minutolo *et al.* (1999). The role of fullerenes as soot nuclei (Zang *et al.* 1990) and the parallel growth of fullerenes and large PAHs in flames (Grieco *et al.* 2000; Lafleur *et al.* 1996) have been favored by other groups.

Generally, the exact transition range from molecules to solid grains is different for different materials and varies between clusters of 100 and 1000 atoms. A nice example for very small solid carbonaceous grains are the meteoritic nanodiamonds with a medium size of 1.3 nm corresponding to number of around 150 atoms. This points to a high stability of these “clusters” consisting of sp^3 hybridized carbon exclusively. Transitional objects between molecules and solids in HT condensates have been observed by using HRTEM. Their structures are similar to the carbon

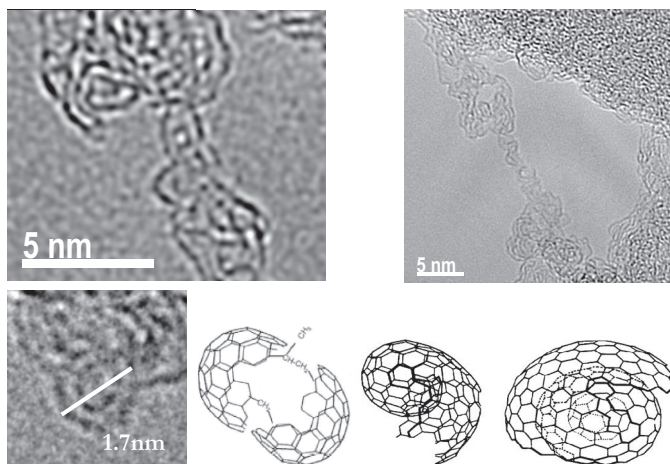


Fig. 4. Small transitional objects between molecules and solid soot grains observed in HT condensation experiments.

cluster with spiral structures (Haberland 1994) which are supposed to be intermediates of the soot formation in condensation processes with high initial carbon atom densities. Three-dimensional fragments of fullerenes, oligomers of fullerenes or fragments and small nested buckyonions have been identified in this condensate (Jäger *et al.* 2009).

5 Conclusion and outlook

Gas-phase condensation studies to uncover the formation process of carbon grains at different condensation conditions are necessary to understand the structural and spectral properties of nanometer-sized carbon grains with respect to an application to cosmic carbon. So far, these studies succeeded in the production and structural characterization of a big variety of carbon structures and in the tuning of special structural and spectral properties of the material.

A first basic understanding of the grain formation process in gas-phase condensations was reached. Laboratory studies have shown that in flames as well as in condensation processes with isothermal conditions, such as laser ablation or pyrolysis, multiple soot formation processes occur. In isothermal condensations, a high- and a low-temperature soot formation process have been identified in which either small fullerene-like carbon grains are produced via carbon chains, fullerenes and fullerene fragments, or soot grains with plane graphene layers are formed via PAHs, respectively. However, we still need more insight into the complicated nucleation process of soot grains, in particular in PAH dominated formation processes. Further laboratory experiments to study the inception or nucleation step have to be developed by coupling selective production methods with sophisticated

analytical tools (Biennier *et al.* 2010). In high-temperature condensation processes, three-dimensional fragments of fullerenes and small nested buckyonions have been identified as transitional objects between molecules and solids.

References

- Ajayan, P., Iijima, S., & Ichihashi, T., 1993, *Phys. Rev. B*, 47, 6859
- Allain, T., Sedlmayr, E., & Leach, S., 1997, *A&A*, 323, 163
- Banhart, F., 1999, *Rep. Prog. Phys.*, 62, 1181
- Biennier, L., Sabbah, H., Chandrasekaran, V., *et al.*, 2011, this volume
- Cau, P., 2002, *A&A*, 392, 203
- Chen, H.X., & Dobbins, R., 2000, *Combust. Sci. Tech.*, 159, 109
- Cherchneff, I., Barker, J., & Tielens, A., 1992, *ApJ*, 401, 269
- Cherchneff, I., & Cau, P., 1999, in ed. T. Le Betre, A. Lèbre, and C. Waelkens, *Asymptotic Giant Branch Stars; Proceedings of the IAU Symposium 191* (San Francisco, ASP), 251
- Cherchneff, I., 2011, this volume
- Chhowalla, M., Wang, H., Sano, N., *et al.*, 2003, *Phys. Rev. Lett.*, 90, 155504
- D'Alessio, A., D'Anna, A., Gambi, G., & Minutolo, P., 1998, *J. Aerosol. Sci.*, 29, 397
- Dartois, E., & Godard, M., 2011, this volume
- Dobbins, R.A., Fletcher, R.A., & Chang, H.-C., 1998, *Comb. Flame*, 115, 285
- Duley, W., 1994, *ApJ*, 430, L133
- Elias, D.C., Nair, R.R., Mohiuddin, T.M.G.J., *et al.*, 2009, *Science*, 323, 610
- Frenklach, M., & Feigelson, E., 1989, *ApJ*, 341, 372
- Gail, H.-P., & Sedlmayr, E., 1985, *A&A*, 148, 183
- Geim, A.K., & Novoselov, K.S., 2007, *Nature Materials*, 6, 183
- Grieco, W.J., Howard, J.B., Rainey, L.C., & Vander Sande, J.B., 2000, *Carbon*, 38, 597
- Haberland, H., 1994, *Clusters of Atoms and Molecules* (Springer Verlag, Heidelberg)
- Haddon, R.C., 1993, in ed. H. Kroto and D. Walton, *The fullerenes* (Cambridge University Press, Cambridge)
- Harris, P.J.F., 2009, *Carbon Nanotube Science* (Cambridge University Press)
- Harris, S.J., & Weiner, A.M., 1988, *Proc. Combust. Inst.*, 22, 333
- Heidenreich, R., Hess, W., & Ban, L., 1968, *J. Appl. Cryst.*, 1, 1
- Henning, T., & Salama, F., 1998, *Science*, 282, 2204
- Hess, W., & Herd, C., 1993, in ed. J. Donnet, R. Bansal, and M. Wang, *Carbon Black* (Marcel Dekker, Inc., New York), 89
- Homann, K.-H., 1998, *Angew. Chem.*, 110, 2572
- Iijima, S., 1991, *Nature*, 354, 56
- Irle, S., Zheng, G., Elstner, M., & Morokuma, K., 2003, *Nano Lett.*, 3, 1657
- Jäger, C., Henning, T., Spillecke, N., & Schlögl, R., 1999, *J. Non-Cryst. Solids*, 258, 161
- Jäger, C., Huisken, F., Mutschke, H., Llamas Jansa, I., & Henning, T., 2009, *ApJ*, 696, 706
- Jäger, C., Kovacevic, E., Mutschke, H., Henning, T., & Huisken, F., 2010, in preparation

- Jäger, C., Mutschke, H., Henning, T., & Huisken, F., 2008, *ApJ*, 689, 249
- Jones, A.P., Duley, W.W., & Williams, D.A., 1990, *QJRAS*, 31, 567
- Krätschmer, W., Lamb, L.D., Fostropoulos, K., & Huffman, D., 1990, *Nature*, 347, 354
- Kroto, H., Heath, J., O'Brien, S., Curl, R., & Smalley, R., 1985, *Nature*, 318, 162
- Kuc, A., Heine, T., & Seifert, G., 2010, *Phys. Rev. B*, 81, 085430
- Lafleur, A.L., Taghizadeh, K., & Howard, J.B. e. a., 1996, *J. Amer. Soc. Mass Spectrom.*, 7, 276
- Lodders, K., & Fegley, B., J., 1999, in ed. T. Le Bertre, A. Lebre, and C. Waelkens, *Asymptotic Giant Branch Stars; Proceedings of the IAU Symposium 191, SAO/NASA Astrophysics Data System*, 279
- Mansurov, Z.A., 1998, *Combust Flame*, 115, 285
- McKinnon, J.T., & Howard, J.B., 1992, *Proc. Combust. Inst.*, 24, 965
- Minutolo, P., Gambi, G., D'Alessio, A., & Carlucci, S., 1999, *Atmospheric Environment*, 33, 2725
- Papoular, R., Breton, J., Gensterblum, G., *et al.*, 1993, *A&A*, 270, L5
- Pendleton, Y.J., & Allamandola, L.J., 2002, *ApJS*, 138, 75
- Ravagnan, L., Bongiorno, G., Bandiera, D., *et al.*, 2006, *Carbon*, 44, 1518
- Ravagnan, L., Siviero, F., & Lenardi, C. e. a., 2002, *Phys. Rev. Lett.*, 89, 285506
- Richter, H., Granata, S., Green, W.H., & Howard, J.B., 2004, *Proc. Combust. Inst.*, 30, 1397
- Richter, H., & Howard, J.B., 2000, *Prog. Energy Combust. Sci.*, 26, 565
- Robertson, J., 1986, *Adv. Phys.*, 35, 317
- Robertson, J., & O'Reilly, E., 1987, *Phys. Rev. B*, 35, 2946
- Sakata, A., Wada, S., Okutsu, Y., Shintani, H., & Nakada, Y., 1993, *Nature*, 301, 493
- Savchenko, A., 2009, *Science*, 323, 589
- Schnaiter, M., Mutschke, H., Dorschner, J., Henning, T., & Salama, F., 1998, *ApJ*, 498, 486
- Schuetz, A.C., & Frenklach, M., 2000, *Combust. Sci. Tech.*, 159, 109
- Tauc, J., Grigorovici, R., & Vancu, A., 1966, *Phys. Status Solid*, 15, 627
- Tomita, S., Fujii, M., & Hayashi, S., 2002, *Phys. Rev. B*, 66, 245424
- Ugarte, D., 1992, *Nature*, 359, 707
- Wada, S., Kaito, C., Kimura, S., Ono, H., & Tokunaga, A.T., 1999, *A&A*, 345, 259
- Wu, J., Pisula, W., & Müllen, K., 2007, *Chem. Rev.*, 107, 718
- Zang, Q.L., O'Brien, S.C., & Heath, J.R. e. a., 1990, *J. Phys. Chem.*, 90, 525

PAHS AND ASTROBIOLOGY

L.J. Allamandola¹

Abstract. In dense molecular clouds, the birthplace of stars and planets, interstellar atoms and molecules freeze onto extremely cold dust and ice particles. These ices are processed by ultraviolet light and cosmic rays forming hundreds of far more complex species, some of astrobiological interest. Eventually, these rain down on primordial planets where they take part in the young chemistry on these new worlds.

Although the IR spectroscopy and energetic processing of interstellar ice analogs have been studied for nearly 30 years, similar studies of PAH containing ices have only just begun. This paper presents recent results from laboratory studies on the vacuum ultraviolet (VUV) photochemistry of PAHs in water ice at low temperatures to assess the roles they play in the photochemical evolution of interstellar ices and their relevance to astrobiology. A number of “surprises” were found in these studies on PAH containing water-rich ices, indicating that PAHs likely play very important, unexpected roles in cosmic ice chemistry, physics and astrobiology.

1 Introduction

The story of PAHs and astrobiology is an important part of a complete revolution in our understanding of chemistry and biochemistry throughout the cosmos. Space was considered chemically barren for most of modern human history. That spell was broken some fifty years ago with the discovery of species such as NH_3 , H_2CO , NH_2CHO , and CO by radio astronomers during the late 1960's and early 1970's (Cheung *et al.* 1968; Snyder *et al.* 1969; Rubin *et al.* 1971; Wilson *et al.* 1970). Today there are almost 120 known interstellar species, the largest of which is HC_{11}N . Add to this the discovery of the Unidentified Infrared (UIR) Emission Band spectra during the 1970's, the suggestion that the UIR bands originated in unbelievably large interstellar PAHs during the 1980's and the growing realization

¹ NASA Ames Research Center, Space Science & Astrobiology Division, MS 245-6, Moffett Field, CA 94035, USA

over the last twenty years that PAHs are widespread and very abundant throughout much of the Cosmos and it is clear that we no longer simply see the Universe as an H dominated physicist's paradise.

While most of the work presented at this wonderful symposium has to do with using the emission from vibrationally excited, gas phase PAHs as probes of different environments, this paper discusses PAHs frozen in ices in dense molecular clouds because it is in these clouds that stars, planets and moons form. These PAHs are part of the extraterrestrial feedstock that contributes to the early chemistry and perhaps biochemistry on the primordial planets and moons.

In dense molecular clouds, atoms and molecules freeze onto the extremely cold dust and ice particles forming mixed molecular ices. Infrared spectroscopy of the clouds reveals the composition of these ices (*e.g.* van Dishoeck 2004). With the occasional exception of CO, the abundance of the identified species is much higher in the ice than in the gas phase. Water is by far the major ice component, with frozen CO, CO₂, and CH₃OH often, but not always, present at concentrations of roughly 10 to 20%. The ices also contain NH₃, H₂CO and CH₄ at about the few percent level. Within these clouds, and especially in the vicinity of star and planet forming regions, these ices are processed by ultraviolet light and cosmic rays forming hundreds of far more complex species, some of biogenic interest. This process is illustrated in Figure 1. Unidentified IR spectral structure indicates that other species are also present at the few percent level (*e.g.* Gibb & Whittet 2002; Boogert *et al.* 2008). Some of these will likely be produced via *in-situ* UV photolysis of the interstellar ices. Although altering only a few percent of the ice, *in-situ* photochemistry favors chemical complexity and produces molecules and chemical groups within the ice that cannot be made via gas phase and gas-grain reactions. As these materials are the building blocks of comets and related to carbonaceous micrometeorites, they are likely to be important sources of complex organic materials delivered to habitable planets such as the primordial Earth. This chapter focuses on the unique roles that PAHs play in the chemical evolution of these cosmic materials and their relevance to astrobiology.

2 Interstellar ice photochemistry and the production of biogenic molecules

This section summarizes the photochemistry of mixed molecular and PAH containing interstellar ice analogs comprised of the most abundant interstellar ice species, with emphasis placed on the production of biogenically interesting molecules.

There is a large body of work on UV driven photochemistry in various low temperature (10–30 K) ice mixtures without PAHs (*e.g.* Allamandola *et al.* 1988; Bernstein *et al.* 1995; Greenberg *et al.* 1995; Gerakines *et al.* 1996, 2001). As these ices are warmed, the starting materials and most volatile photoproducts sublime, leaving non-volatile residues on the substrate. Mass spectroscopic analysis shows that hundreds of complex new species make up these residues (Greenberg *et al.* 2000; Dworkin *et al.* 2004). Of the overwhelming array of compounds produced

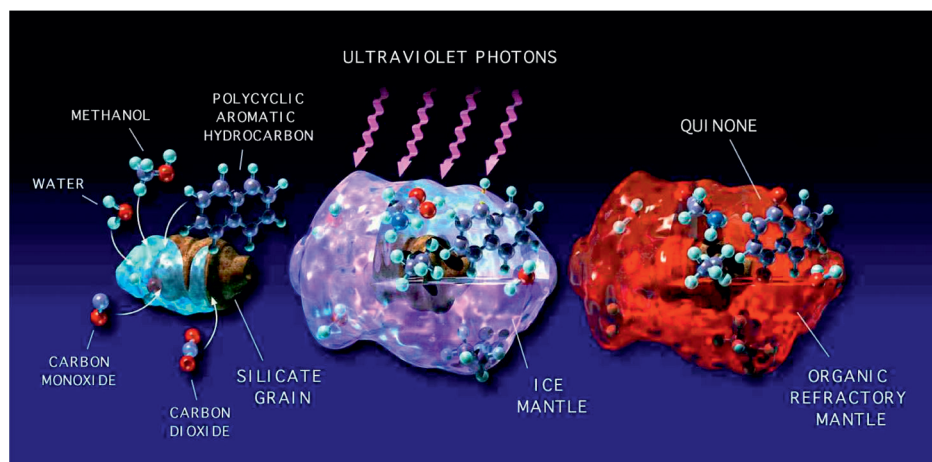


Fig. 1. The Greenberg model of interstellar ice mantle formation and chemical evolution. The mantle grows by condensation of gas phase species onto the cold dust grains. Simultaneously, surface reactions between these species, ultraviolet radiation and cosmic ray bombardment drive a complex chemistry. Figure reproduced from Bernstein *et al.* (1999a).

from even the simplest starting ice (H_2O , CH_3OH , NH_3 , and CO), only a few have been identified (Bernstein *et al.* 1995). In keeping with their expected low concentration and abundance with respect to the simpler ice species, clearcut IR spectroscopic evidence for these types of compounds in interstellar ices is presently lacking although, as mentioned above, weak spectral structure in the $5\text{--}8\ \mu\text{m}$ region of protostars is consistent with their presence (*e.g.* Gibb & Whittet 2002; Boogert *et al.* 2008).

The residue is particularly important for astrobiology because it is quite plausible that this type of material is closely related to that preserved in comets, meteorites and interplanetary dust particles (IDPs), and it is believed that these sources deliver between 12 and 30 tons of organic material to Earth monthly (Love & Brownlee 1993). During the period of great bombardment some 4 billion years ago, the amount of extraterrestrial organic material brought to the early Earth was many orders of magnitude greater. Thus, this organic residue could have played an important role in steering the early chemistry on habitable bodies such as the primordial Earth.

Motivated by the possibility that the residues may contain compounds that impact early Earth biochemistry, experiments have been directed to searching for classes of biogenically important species. Remarkably, although all of the starting compounds are water soluble, as shown in Figure 2, non-soluble droplets spontaneously form when the residues are added to liquid water (Allamandola *et al.* 1997; Dworkin *et al.* 2001). Droplet formation shows that some of the complex organic compounds produced by UV in these interstellar ice analogs are

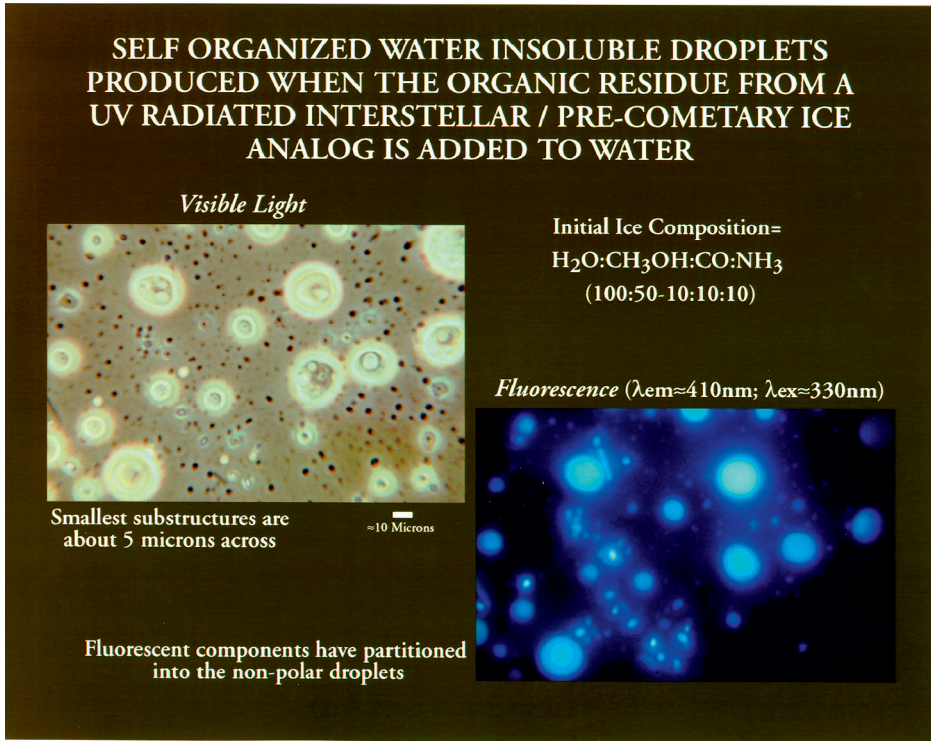


Fig. 2. Water insoluble, fluorescent droplets produced from the residue when it is added to water. The two images are of the same field.

amphiphilic, *i.e.* they have both a polar and non-polar component. These are the types of molecules that make up cell membranes, and membrane production is considered a critical step in the origin of life. These droplets are true vesicles (hollow droplets) with their interiors separated from the surroundings by their lipid multilayer. Vesicle formation is thought critical to the origin of life since vesicles provide an environment in which life can evolve, isolating and protecting the process from the surrounding medium (Deamer *et al.* 2002).

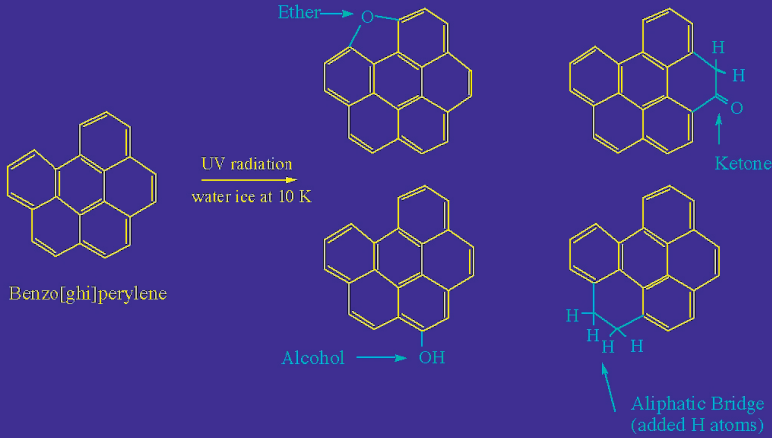
Figure 2 also shows that the membranes trap photoluminescent molecules that are also formed within the ice by UV irradiation (Allamandola *et al.* 1997; Dworkin *et al.* 2001). Thus, not only are vesicle forming compounds produced from the simplest and most abundant interstellar starting materials, complex organics which absorb low energy UV are also made. The ability to form and trap energy receptors within these structures is considered another critical step in the origin of life as it provides the means to harvest energy available outside the system. Interestingly, the vesicles formed from photoproducts of UV irradiated interstellar ice analogs are remarkably similar to those produced by extracts from the Murchison meteorite (Dworkin *et al.* 2001; Deamer *et al.* 2002).

Another class of potentially important organic molecules brought to the Earth by meteorites are amino acids, the molecular building blocks of proteins and enzymes. The amino acids in meteorites are extraterrestrial as demonstrated by their deuterium enrichments – the highest of any species measured in a meteorite (Pizzarello & Huang 2005). Since laboratory photolysis experiments of plausible presolar ice mixtures also produce amino acids and closely related compounds (Bernstein *et al.* 2002; Muñoz Caro *et al.* 2002; Agarwal *et al.* 1985), presolar ice photochemistry may be a source of these extraterrestrial amino acids.

As with other polyatomic interstellar species, PAHs should also become part of the ices in dense clouds. Weak, broad absorption bands in molecular cloud spectra are consistent with PAHs frozen in ice mantles at the few percent level, however they suffer severe blending with the strong absorption bands of the major ice components (Keane *et al.* 2001; Bernstein *et al.* 2005; Sandford *et al.* 2004; Bouwman *et al.* 2011; Bouwman *et al.*, elsewhere in this volume). The chemistry of PAHs in cosmic ice analogs has also been investigated to understand the roles PAHs might play in astrochemistry and astrobiology. Photolysis of interstellar ice analogs containing pure PAHs does not destroy the parent PAH, but decorates it with chemical side-groups formed from the photoproducts of the other ice constituents. For example, in water ice, oxidized products found in the residues include aromatic ethers, alcohols, and ketones with structures as shown in Figure 3 (Bernstein *et al.* 1999b). Hydrogen atom addition transforms some of the edge rings into cyclic aliphatic hydrocarbons, creating molecules with both aromatic and aliphatic character and decreasing the overall degree of aromaticity. Likewise, UV and proton irradiation of PAHs in NH_3 , CH_4 , CH_3OH , HCN and CO_2 ices produces aromatic structures decorated with amino ($-\text{NH}_2$), alkyl ($-\text{CH}_3$, $-\text{CH}_2$), hydroxyl ($-\text{OH}$), cyano ($-\text{CN}$), and carboxy ($>\text{CO}$) side groups, again species similar to the compounds found in meteorites (Bernstein *et al.* 2003, 2002, 2001). Most recently, photolysis of the nitrogenated single ring aromatic molecule, pyrimidine, in water ice produced the nucleobase, uracil (Nuevo *et al.* 2009). These changes open up an aromatic based biogenic chemistry that is not available to the parent PAH or in non-PAH containing ices. For example, compounds closely related to aromatic ketones are widely used in current living systems for electron transport across cell membranes (hardware) while nucleic acids provide the backbone for information coding in DNA and RNA (software).

From both the astrochemical and astrobiological perspective, the production of such an interesting array of aromatic based compounds warranted a deeper understanding of the processes that occur within the ice during the UV irradiation of PAHs in cosmic ice analogs. However, because of severe line blending, the “traditional” laboratory approach using IR spectroscopy to follow chemical change within irradiated ices cannot provide this information (Bernstein *et al.* 2005; Sandford *et al.* 2004; Bouwman *et al.* 2011; Bouwman *et al.*, elsewhere in this volume). It is for this reason that optical studies have been undertaken to follow the stepwise reaction pathways and kinetics of PAHs in water ice and to determine important properties such as ionization efficiencies, onset temperature of

Photolysis of PAHs in Water Ice Produces Alkanes, Ketones, Ethers, and Alcohols.



Both oxidation (alcohol, ether and ketone formation) and reduction (addition of hydrogen) reactions occur on photolysis of water ices containing PAHs. These are the same kinds of compounds observed in meteorites, fit spectra of emission objects and, in some cases, have biochemical significance.

Fig. 3. PAH structures produced by UV irradiation of PAH:H₂O ices at interstellar temperatures.

reaction during warm-up, possible identities of some of the reaction intermediates, and so on. The next section summarizes this work.

3 Photochemistry and photophysics of PAHs in cosmic ice analogs

A number of “surprises” were found in these studies on the photochemical processing of PAH containing water-rich ices. Foremost among these is that rapid photoionization is the dominant process that occurs when dilute, low temperature PAH/H₂O ices are initially exposed to UV radiation (Gudipati & Allamandola 2003; Bouwman *et al.* 2010). As illustrated in Figure 4, a large fraction (generally 50–70%) of the parent PAH is converted to PAH⁺ within minutes of UV onset. If radiation is stopped at this point, the PAH cation appears to be stable indefinitely (on laboratory timescales) as long as the ice temperature is not raised. The PAH cation is also stabilized by the H₂O ice to remarkably high temperatures. This is shown in Figure 5 which compares the spectrum of the quaterylene (QTR, C₄₀H₂₀) cation in water ice at 20 K to that of the same sample at 120 K after a nearly one month, very slow, stepwise warm-up. The QTR⁺ band only starts to weaken after the ice matrix is warmed above 120 K, but the loss is slow up to

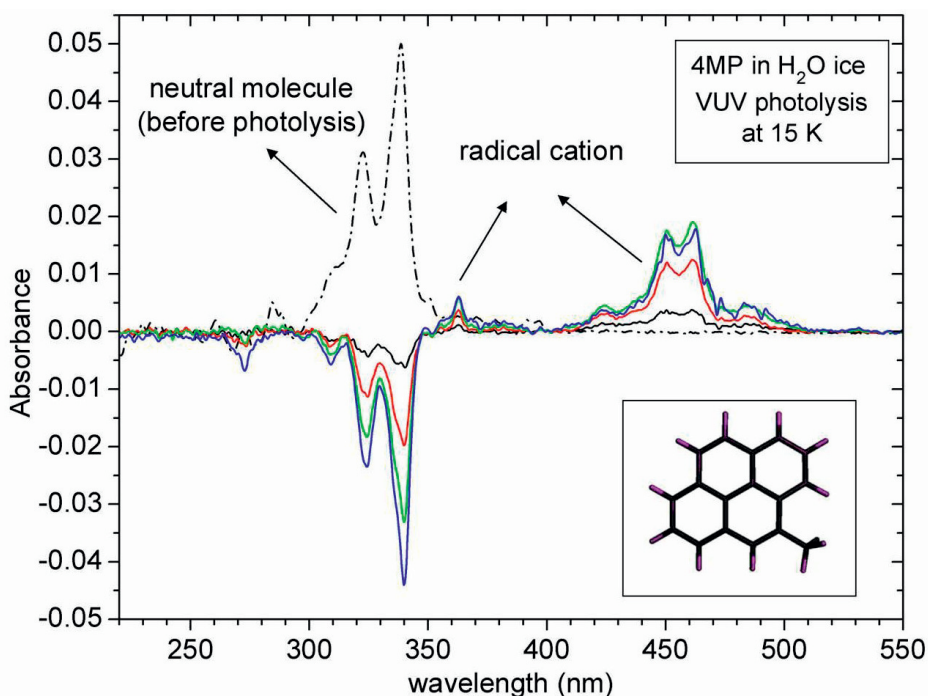


Fig. 4. Spectral evolution of H₂O/4-methylpyrene (4MP, 1500/1) ice at 15 K as a function of VUV irradiation time showing the loss of neutral 4MP and simultaneous growth of 4MP⁺ with VUV exposure. The dot-dashed line shows the absorbance spectrum before photolysis. The black, red, green, and blue solid lines show the loss of the neutral 4MP band and the simultaneous growth of 4MP⁺ after 30, 300, 1200, and 4800 s, respectively, of *in-situ* VUV (vacuum UV) irradiation. The vibronic bands peaking near 340 nm correspond to neutral 4MP, and those near 450 nm to the 4MP⁺ photoproduct (Figure reproduced from Gudipati & Allamandola 2003; see also Bouwman *et al.* 2010).

~140 K. Although the loss increases at higher temperatures, band reduction stops when warm-up stops. Remarkably, the band is still evident at 170 K, the temperature at which the ice sublimates (Gudipati & Allamandola 2006). In addition, the ionization potential (IP) of PAHs trapped in water ice at low temperatures are at least 2 eV lower than the corresponding gas phase IPs (Gudipati & Allamandola 2004; Woon & Park 2004)

These initial studies showed that PAHs likely play important but overlooked roles in cosmic ices, especially regarding the chemistry of charged species. A far more detailed understanding of the processes involved is necessary before one can incorporate these ideas into astrochemical models. To provide this critical information, Bouwman *et al.* (2009, 2010) and Bouwman *et al.* in press, have undertaken a systematic study of several PAHs in H₂O ice, tracking the *in-situ* behavior of each PAH and their photoproducts *within the ice itself* as a function

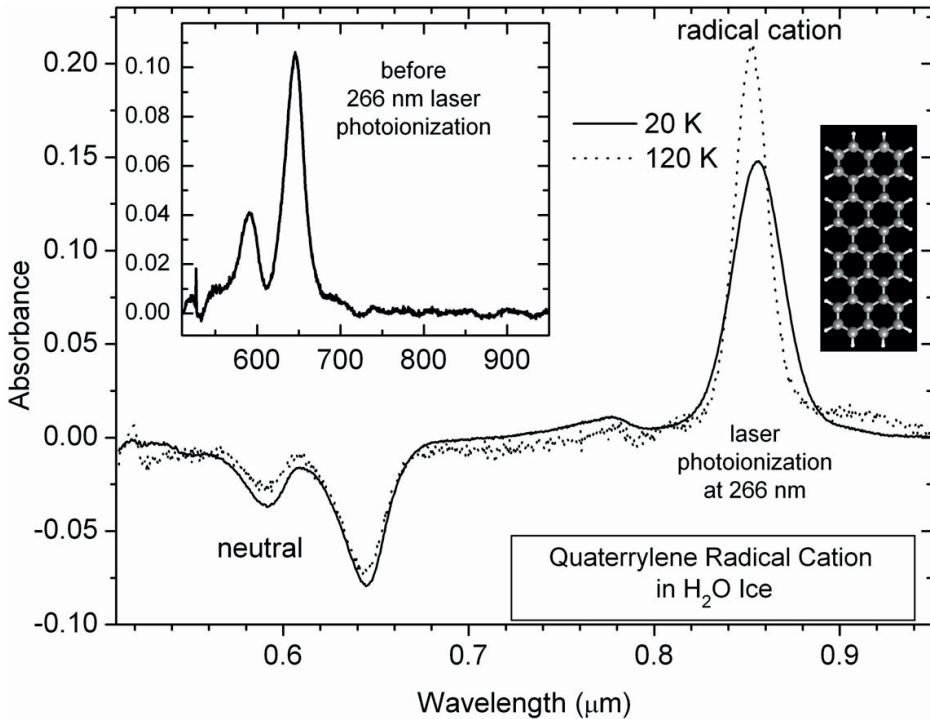


Fig. 5. The 520 to 940 nm (0.52 to 0.94 μm) spectrum of quaterrylene (QTR, $\text{C}_{40}\text{H}_{20}$, upper right insert) in a water ice matrix. The spectrum of the freshly deposited QTR/ H_2O ($\sim 1/500$) ice at 20 K is shown in the upper left insert. The full spectrum (solid line) is that of the same ice after photolysis with 266 nm laser light. Negative bands represent depletion of the parent neutral QTR and positive bands represent generation of QTR^+ . The dotted-line spectrum was recorded at 120 K, after step-wise warm-up over 28 days. The QTR^+ band areas are equal, showing QTR^+ is stable in water-ice at this temperature (Gudipati & Allamandola 2006).

of ice temperature and UV irradiation time with sub-second responsiveness. Figure 6 shows the dramatic effect ice temperature has on the photochemistry of the PAH pyrene (Py, $\text{C}_{16}\text{H}_{12}$) in water ice and Figure 2 in Bouwman *et al.*, elsewhere in this volume, shows the evolution of each band as a function of photolysis time. The ability to measure spectra simultaneously with photolysis and with sub-second time resolution permits kinetic studies previously inaccessible and provides new insights into the processes occurring within the ice during photolysis (Bouwman *et al.* 2009, 2010; Bouwman *et al.* in press). Since these temperatures span the range of dust temperatures in dense clouds in the transition zones with star and planet forming regions and the ranges in the temperatures of icy Solar System bodies beyond the orbit of Jupiter, PAH driven ice photochemistry is likely to impact a variety of cosmic environments.

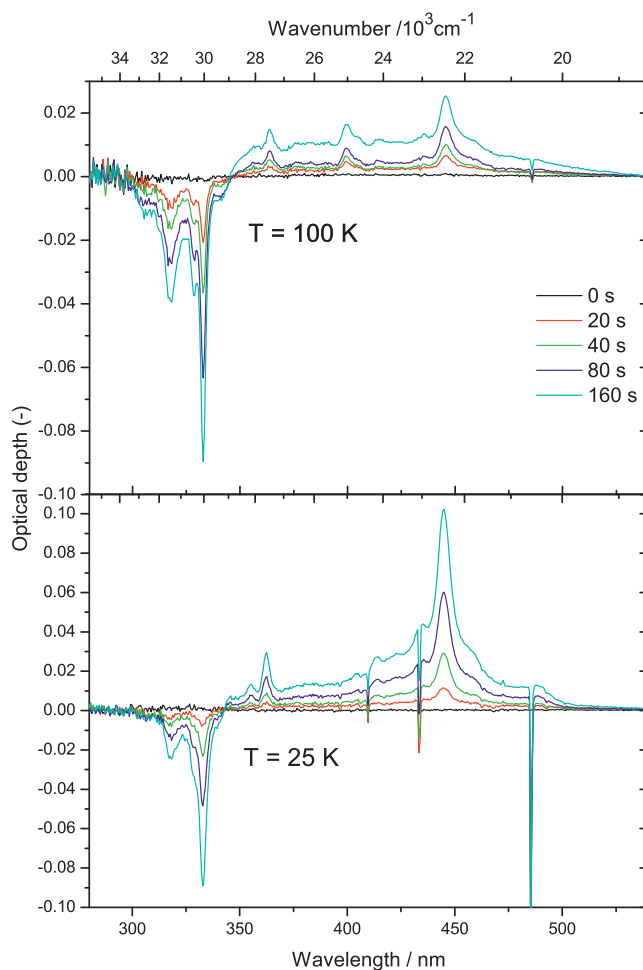


Fig. 6. The VUV induced spectroscopic changes in Pyrene:H₂O ice at 25 (bottom) and 100 K (top) as a function of photolysis time. Temperature plays a critical role in determining photochemical pathways for PAH containing ice. The loss of the neutral pyrene (Py, C₁₆H₁₂) band complex near 330 nm is similar at both temperatures. However, in the 25 K ice, cation formation (~450 nm) is favored over the range of species responsible for the broad, 350 to 500 nm absorption and the 400 and 405 nm band carriers. The opposite holds for the 100 K ice. Figure from Bouwman *et al.* (2010).

4 Astrobiology

The similarities between interstellar ice analog photoproducts with the extraterrestrial materials delivered to the Earth strengthens the case for taking interstellar PAHs and ices into account when pondering the exogenous contribution to the origin of life that is illustrated in Figure 7.

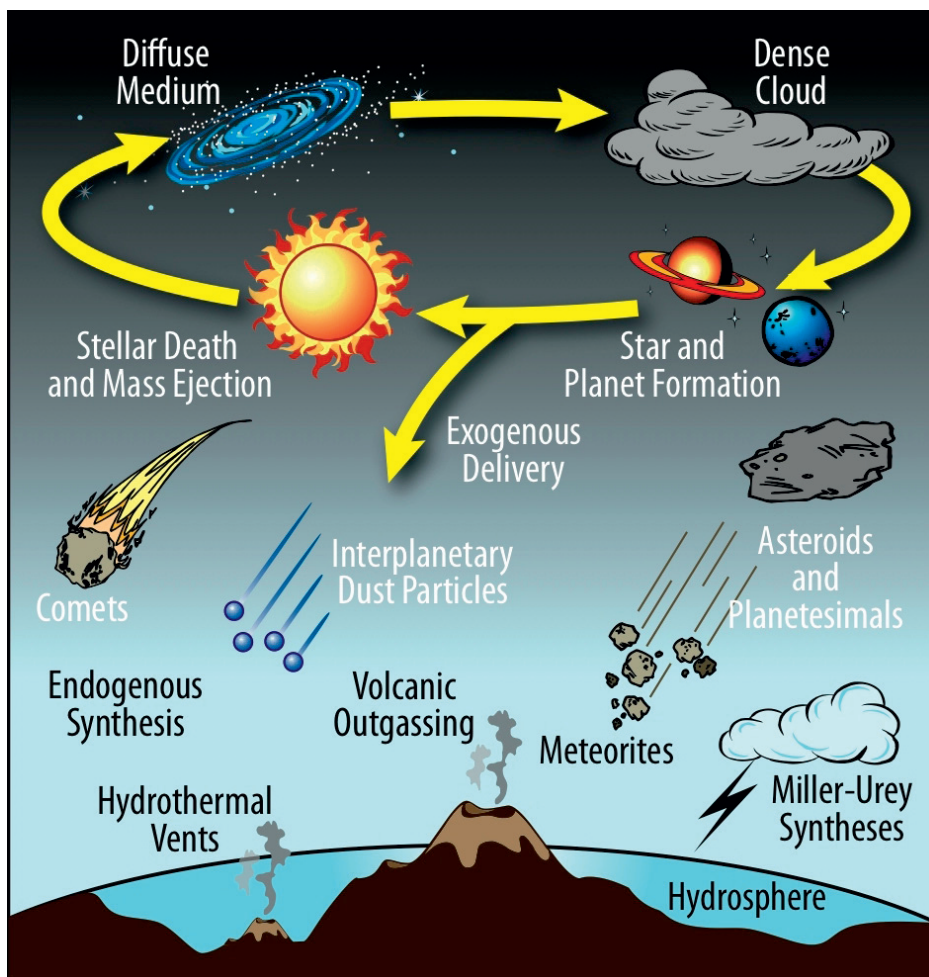


Fig. 7. The cycle of interstellar material that leads to the production and evolution of complex organic compounds that can be delivered intact to, and mixed with, those produced on planets and moons. There they participate in the primordial chemistry on these young objects. Figure courtesy Jason Dworkin, NASA Goddard Space Flight Center, adapted from Deamer *et al.* (2002).

Three possible roles that these interstellar materials might have played in the origin of life on Earth are:

(1) *Supplier of basic, prebiotic raw materials* from which biotic compounds were eventually produced on Earth. Comets, IDPs and meteorites were very likely responsible for raining a rich inventory of prebiotic molecules down onto the early Earth. Recall the variety of species that make up the bulk of interstellar ices.

(2) *Source of complex prebiotic materials* poised to play a direct role once in a favorable environment. The work described here supports the idea that meteorites, dust, and comets could deliver species which are sufficiently complex to play a direct role in the chemistry of the origin of life. From this perspective, comets might represent quite potent prebiotic cocktails. All the complex species discussed above are produced by the irradiation of simple ice mixtures that are widespread throughout dense molecular clouds. Thus, it seems reasonable to hypothesize that wherever a planet or satellite is formed in the habitable zone, it will accrete these chemical remnants from the nascent cloud from infalling IDPs, cometary (formerly interstellar) and meteoritic materials. One of the challenges before us is to understand this chemistry and to assess the relative importance of this input into the origin of life versus an origin from the compounds produced on, or already present on, the primordial planet.

(3) *Fountainhead of species undergoing the basic processes of life.* Going one step further, this article ends on a speculative note. The results summarized here are quite startling when viewed from the perspective held not too long ago that chemistry in space was very limited. We have just started to scratch the surface of this complex chemistry, we know there are hundreds of residue compounds not yet analyzed and we have just realized that ion-moderated processes also play a role in ice chemistry. Given our level of ignorance at this stage, an intriguing possibility is the production, within the processed mixed molecular ices themselves – whether in the interstellar medium or a comet – of species poised to take part in the life process, or perhaps even at the earliest stages of what could be perceived of as rudimentary reactions of a living system.

This “jump-starting” of the life process by the introduction of such marginally biologically active species into the “warm pond” on a habitable planet may not be as far-fetched as it would at first seem. Although one could hardly imagine a better deep freeze than isolation within a comet, with temperatures measured in tens of degrees K, there are repeated episodes of warming for periodic comets. Since these warming episodes, which can be repeated many times in a given comet, can last anywhere from periods of weeks to several months, there is ample time for a very rich mixture of complex organics to develop even though these warming episodes are sandwiched between long periods of extreme cold. At this early stage in our understanding of cometary ices it already appears that comets contain many of the types of compounds which are considered important players in the origin of life, compounds which play central physical roles and compounds which play key chemical roles. Indeed there is evidence for nearly every class of organic chemical thought important in the “RNA world” in these irradiated ices and they are all in close proximity to one another. We are just beginning to appreciate the chemical complexity and possibilities of these ices. Thus, it is no longer inconceivable, at least to this author, that comets played a far more active role in the origin of life than simply that of a spectator-delivery system of raw materials. Perhaps Darwin’s “warm little pond” is a warmed comet.

Summing up, in cold molecular clouds, the birthplace of planets and stars, interstellar molecules freeze into ice particles comprised of water, methanol, ammonia,

carbon monoxide, carbon dioxide and PAHs. In these clouds, especially close to star and planet forming regions, these ices are processed by UV light, cosmic rays, radical surface reactions, etc. forming far more complex species, many of biogenic interest. During star and planet formation, many of these compounds become incorporated in comets and meteorites which eventually seed primordial planets where they take part in the budding chemistry on these young worlds.

While I have been blessed to have worked with many outstanding experimentalists and theoreticians over the years, I particularly wish to thank three exceptionally gifted experimentalists who made this chapter possible: Murthy Gudipati, Jordy Bouwman, and Harold Linnartz. They shined the first light into the microscopic details of PAH/ice processing. I am especially grateful to Harold Linnartz and NASA for making it possible for me to spend six wonderful months working in Leiden once again and Christiaan Boersma who, under severe time pressure, helped LaTeX this article. I also acknowledge support from NASA's Long Term Space Astrophysics, Exobiology, and Astrobiology programs for their continued support throughout this field's blossoming.

References

- Agarwal, V.K., Schutte, W., Greenberg, J.M., Ferris, J.P., *et al.*, 1985, *Orig. Life*, 16, 21
- Allamandola, L.J., Sandford, S.A., & Valero, G.J., 1988, *Icarus*, 76, 225
- Allamandola, L.J., Bernstein, M.P., & Sandford, S.A., 1997, *IAU Colloq. 161: Astron. Bioch. Orig. Search Life Universe*, 23
- Bernstein, M.P., Sandford, S.A., Allamandola, L.J., Chang, S., & Scharberg, M.A., 1995, *ApJ*, 454, 327
- Bernstein, M.P., Sandford, S.A., & Allamandola, L.J., 1999a, *Scient. Amer.*, 281, 26
- Bernstein, M.P., Sandford, S.A., Allamandola, L.J., *et al.*, 1999b, *Science*, 283, 1135
- Bernstein, M.P., Dworkin, J.P., Sandford, S.A., & Allamandola, L.J., 2001, *Meteor. Planet. Sci.*, 36, 351
- Bernstein, M.P., Dworkin, J.P., Sandford, S.A., Cooper, G.W., & Allamandola, L.J., 2002, *Nature*, 416, 401
- Bernstein, M.P., Elsila, J.E., Dworkin, J.P., *et al.*, 2002, *ApJ*, 576, 1115
- Bernstein, M.P., Moore, M.H., Elsila, J.E., *et al.*, 2003, *ApJ*, 582, L25
- Bernstein, M.P., Sandford, S.A., & Allamandola, L.J., 2005, *ApJS*, 161, 53
- Boogert, A.C.A., *et al.*, 2008, *ApJ*, 678, 985
- Bouwman, J., Paardekooper, D.M., Cuppen, H.M., Linnartz, H., & Allamandola, L.J., 2009, *ApJ*, 700, 56
- Bouwman, J., Cuppen, H.M., Bakker, A., Allamandola, L.J., & Linnartz, H., 2010, *A&A*, 511, A33
- Bouwman, J., Mattioda, A.L., Linnartz, H., & Allamandola, L.J., 2010, *A&A*, 511, A33
- Cheung, A.C., Rank, D.M., Townes, C.H., Thornton, D.D., & Welch, W.J., 1968, *Phys. Rev. Lett.*, 21, 1701
- Deamer, D., Dworkin, J.P., Sandford, S.A., Bernstein, M.P., & Allamandola, L.J., 2002, *Astrobiology*, 2, 371
- Dworkin, J.P., Deamer, D.W., Sandford, S.A., & Allamandola, L.J., 2001, *Proc. Nat. Acad. Sci.*, 98, 815
- Dworkin, J.P., Seb Gillette, J., Bernstein, M.P., *et al.*, 2004, *Adv. Space Res.*, 33, 67

- Gerakines, P.A., Schutte, W.A., & Ehrenfreund, P., 1996, *A&A*, 312, 289
- Gerakines, P.A., Moore, M.H., & Hudson, R.L., 2001, *J. Geophys. Res.*, 106, 33381
- Gibb, E.L., & Whittet, D.C.B., 2002, *ApJ*, 566, L113
- Greenberg, J.M., Li, A., Mendoza-Gomez, C.X., *et al.*, 1995, *ApJ*, 455, L177
- Greenberg, J.M., *et al.*, 2000, *ApJ*, 531, L71
- Gudipati, M.S., & Allamandola, L.J., 2003, *ApJ*, 596, L195
- Gudipati, M.S., & Allamandola, L.J., 2004, *ApJ*, 615, L177
- Gudipati, M.S., & Allamandola, L.J., 2006, *ApJ*, 638, 286
- Keane, J.V., Tielens, A.G.G.M., Boogert, A.C.A., Schutte, W.A., & Whittet, D.C.B., 2001, *A&A*, 376, 254
- Love, S.G., & Brownlee, D.E., 1993, *Science*, 262, 550
- Muñoz Caro, G.M., *et al.*, 2002, *Nature*, 416, 403
- Nuevo, M., Milam, S.N., Sandford, S.A., Elsila, J.E., & Dworkin, J.P., 2009, *Astrobiology*, 9, 683
- Pizzarello, S., & Huang, Y., 2005, *Geochim. Cosmochim. Acta*, 69, 599
- Rubin, R.H., Swenson, G.W., Jr., Benson, R.C., Tigelaar, H.L., & Flygare, W.H., 1971, *ApJ*, 169, L39
- Sandford, S.A., Bernstein, M.P., & Allamandola, L.J., 2004, *ApJ*, 607, 346
- Snyder, L.E., Buhl, D., Zuckerman, B., & Palmer, P., 1969, *Phys. Rev. Lett.*, 22, 679
- van Dishoeck, E.F., 2004, *ARA&A*, 42, 119
- Wilson, R.W., Jefferts, K.B., & Penzias, A.A., 1970, *ApJ*, 161, L43
- Woon, D.E., & Park, J.-Y., 2004, *ApJ*, 607, 342

SOLID STATE MOLECULAR REACTORS IN SPACE

M. Maurette¹

Abstract. Lunar minerals and impact glasses, convert the polyatomic beam of solar wind (SW) ions into a flux of small molecules (*e.g.*, H₂, N₂, H₂O, CO, CO₂, CH₄, C₂H₄, C₂H₆, HCN, metal carbides and deuterides, etc.). They thus behave as “Solid State Molecular Reactors”. Moreover, ~100–200 μm size micrometeoroids (μMs) have also been exposed to the SW in the zodiacal cloud, before being captured by the Earth and recovered as Antarctic micrometeorites. They are mostly composed of a PAH-rich hydrous-carbonaceous material, which amplifies their power as molecular reactors. In particular, during the first ~200 Myr of the post-lunar period, about 75% of the μMs have been melted and/or volatilized upon atmospheric entry. The release of their volatile species triggered a cosmic volcanism around the mesopause that ruled the formation of the early Earth’s atmosphere and climate. Furthermore, a fraction of the μMs that survive unmelted upon atmospheric entry did settle on the proto-oceans floors. Upon further burial in sediments their constituent PAH-rich kerogen was cracked into abiotic oil, which generated giant oil slicks that fed prebiotic chemistry. Many stars, of all ages and types, are embedded into a secondary debris-disk loaded with ion implanted μMs. Some of them are expelled to the interstellar medium (ISM) where they behave first as “dormant-invisible” molecular reactors, until they became reactivated by various processes to synthesize interstellar molecules. This short paper only focus on some highlights of this research dealing with the synthesis of important interstellar molecules, including the most abundant ones (H₂ and CO) and H₂O, HCN and PAHs, all involved in prebiotic chemistry.

1 Introduction: Organic geochemistry of lunar molecular reactors

Lunar dust grains are unique reference samples for learning how to extrapolate the results of laboratory simulation experiments to cosmic dust grains, exposed in ultra-high vacuum (~10⁻¹³ torr) to beams of slow and fast ions. Left panel of

¹ CSNSM, University Paris XI, Bâtiment 104, 91405 Orsay-Campus, France

Figure 1 shows the dark-field electron micrograph of a μm -size crystalline lunar feldspar grain, which was observed with a 3 MV high voltage transmission electron microscope by Christian Jouret. Radiation damage features due to the solar wind (SW) and solar energetic particles (SEPs) can be observed, which include -(i)- a darker rim with an average thickness of ~ 40 nm that decorates an amorphous coating (AC) of SW radiation damage, and -(ii)- a high density of latent tracks of SEPs iron-group nuclei that are best observed as faint lines of dark contrast within the dotted yellow ellipse. The right panel of the same figure shows a zoomed-up detail of another grain, with the contrast enhanced to make the ion tracks more visible.

The identification of these features requires artificial ion implantations of terrestrial lunar analogs with both SW type ions (1 keV/amu) and fast Fe ions ($E \sim 1$ MeV/amu). Upon *in-situ* thermal annealing in the HVEM, the fossil SW-ACs and SEPs-tracks, as well as the artificial SW-ACs and Fe-tracks, did anneal at the same temperature (~ 700 – 800°C). Moreover, the average thickness of the fossil ACs, of about 40 nm (see Figs. 1a, 1d, in Maurette 1976), corresponds to both that observed during artificial 1 keV/amu SW-implants, and to the projected damage range, $R_{pd} \sim 40$ nm, of 1 keV/amu SW ions in silicates, as estimated with the SRIM software.

In 1969, organic geochemists discovered that lunar dust grains returned by the Apollo 11 mission did only release small molecules (H_2O , CO , CH_4 , and HCN , etc.) during either pyrolysis at moderate temperature (600°C) or HF etching. They suggested that these molecules were likely produced during the implantation of high fluences of SW ions in the grains. We next helped testing the validity of this assumption while exposing successively ~ 1 cm^2 flat surfaces of terrestrial analogs (ilmenite, oligoclase and a simulated lunar glass) to high fluence implants ($\sim 10^{15}$ to 2×10^{18} cm^{-2}) of “marked” isotopes of hydrogen (^2D), carbon (^{13}C) and nitrogen (^{15}N) ions, at energy of ~ 1 keV/amu. The group of Al Burlingame (Space Science Laboratory, UC Berkeley) next showed (see Bibring *et al.* 1974) that the mixture of small molecules released upon heating and/or HF etching from these targets are very similar to the natural blend released from lunar dust grains (Simoneit *et al.* 1973).

2 Desorption of molecules during ion implants

In 1975, Plasma Desorption Mass Spectrometry (see section 4, last paragraph) was already used to show that ~ 100 MeV fission fragments from ^{252}Cf directly desorb DOH from D-implanted muscovite mica (Maurette *et al.* 1975). To further investigate this stimulated desorption, another set of the pre-implanted lunar analogs have been exposed to the 10 keV primary beam of Ar of the ionic analyzer built by G. Slodzian. This instrument gives the depth concentration profiles of all species released from the targets. J.P. Bibring observed a large variety of synthesized species ranging from ^{13}C -Mg to $^{13}\text{C}_3\text{D}_8$, and including D_2 , $^{15}\text{N}_2$, D_2O , and ^{13}CO . However, ^{15}NO and $^{15}\text{NO}_2$ were not detected ($^{15}\text{NO}/^{13}\text{CD} \leq 10^{-4}$).

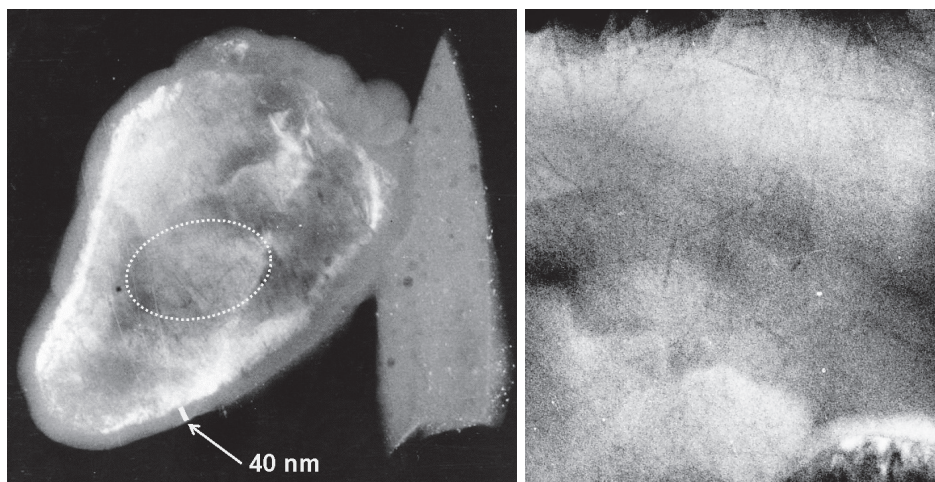


Fig. 1. *Left:* lunar Micron-size molecular reactor. The shard of impact glass stuck to the main grain has not been noticeably eroded by SW sputtering. Thus it has still not reach the critical saturation SW fluence to function as a molecular reactor. *Right:* detail of another dust grain with enhanced contrast to make ion tracks more visible to the untrained eye (the thin dark lines in the image).

This study could be extended to a primary beam of 3 keV deuterium, through the decisive help of W. Möller and his team (Max-Planck-Institute für Plasma-physik, Garching). The three lunar analogs, as well as olivine, silicon, sapphire and a soda-lime glass, have been run with a sophisticated reaction chamber developed for understanding the interactions of a hot DT fusion plasma ($T = {}^3\text{He}$) with the first wall of fusion reactors, at D and T energy in the keV to MeV range. This chamber is equipped with a quadrupole mass spectrometer on-line with both a 30 kV ion accelerator for deuterium implantation, and a 2.5 MV Van de Graaff accelerator for the analysis of the implanted targets with a 750 keV ${}^3\text{He}$ beam, through the $\text{D}({}^3\text{He}, \alpha)\text{H}$ nuclear reaction. This reaction yields the residual concentration and depth concentration profile of the implanted deuterium. The mass spectrometer was tuned to detect simultaneously the release of D_2 and D_2O , which are considered as stumbling blocks in either the gas phase chemistry of the ISM (H_2) or prebiotic chemistry (H_2O).

This on-line study reveals the intimate functioning of the seven molecular reactors (Borgesen *et al.* 1986). In a first group, including ilmenite, olivine, the alkali-poor LSG (0.02% K_2O), sapphire and silicon, a complete retention of D is observed as soon as the deuterium beam is turned on around a fluence of $\sim 10^{15} \text{ cm}^{-2}$. At increasing fluence, a sudden onset of deuterium re-emission (as D_2) is found around $1 \times 10^{17} \text{ cm}^{-2}$, which finally increases to 80–100% of the implanted deuterium around a saturation fluence, $\Phi_s \sim 10^{18} \text{ cm}^{-2}$. These major characteristics of the deuterium release have also been previously reported for metals (at low

temperature), and other targets at room temperature, including semiconductors, fused silica and a sintered powder of graphite, which did release both D_2 , CD, C_2D and CD_4 . During all the re-emission stage in the O-rich targets, the incoming D yields a D_2O / D production ratio of 10^{-4} , 3×10^{-4} and 2×10^{-5} , for ilmenite, oligoclase and the SLG, respectively.

However, both the Na-rich oligoclase and soda-lime glass show a very distinct behavior, as they start losing (*i.e.*, synthesizing) D_2 at the onset of implantation (10^{15} cm^{-2}). They would be the best molecular reactors in a low ion flux environment. On a flat target, perpendicular to the anisotropic SW beam at 1 AU, this fluence is reached in a few months. However, a spherical grain on top of the surface of the Moon would require a longer exposure to accumulate the same fluence on each element of its surface, because the grain is partially shielded from the SW, *e.g.*, during the lunar night.

3 Hydrous-carbonaceous molecular reactors on the early earth

In 1975, we already suspected that lunar type molecular reactors might be effective in the ISM (*cf.*, last section in Maurette & Price 1975). In 1987, a much more powerful family of $\sim 100\text{--}200 \mu\text{m}$ size molecular reactors (*i.e.*, the hydrous-carbonaceous μMs) was discovered as Antarctica micrometeorites (see Maurette 2009, for the most recent review about collects and applications). Their marked similarities with the Wild-2 dust particles returned by the Stardust mission in January 2006 (Dobrica *et al.* 2009), further indicate that they likely originate from comets. This is further supported by IR observations, which revealed that contrarily to previous thoughts, comets are very efficient “dust machine gun” in the solar system (Lisse *et al.* 2004). Observations of comets P/Encke and P/IRAS with IR telescopes on the ISO and MSX spacecrafts show dust-to-gas mass loss ratios about 50 times larger than those inferred from measurement in the visible. These high mass-loss ratios, which were reconfirmed for comet Temple 1 during the Deep Impact mission, clearly show that comets are the major contributors of dust in the interplanetary medium.

After ejection, most of these $100 \mu\text{m}$ size cometary dust grains have been temporarily stored in the Zodiacal Cloud for duration of $\sim 200\,000$ yr (Raisbeck & Yiou 1989), and thus implanted with SW- and SEPs-ions. This cloud is probably a very faint remnant of the secondary debris-disk of the early Sun, which did exponentially decay until about 4 Ga ago, while triggering a period of early heavy bombardment of the Earth-Moon system (Greaves 2005).

About 99% of the Antarctica micrometeorites are only related to the most volatile-rich hydrous-carbonaceous chondrites, which are relatively rare (about 2–3% of the meteorite falls). Their major carbonaceous component is a kerogen composed of a mixture of PAH moieties and aliphatic hydrocarbons, and their constituent water (10 wt.%) is mostly stored in their major hydrous silicate, saponite, that starts dehydrating at $\sim 100^\circ\text{C}$. Upon atmospheric entry μMs would thus release solar wind implanted neon, but also molecules originating from their kerogen (N_2 and CO_2), hydrous silicates (H_2O), and metallic sulfides (SO_2).

These volatiles ended up making the early Earth's atmosphere (*i.e.*, before the formation of O₂), during the first ~200 Myr of the post-lunar period, after the giant impact that did form the Moon (Maurette 2009). This impact did also close the formation time interval of the Earth, and blew-off the intractable pre-lunar atmosphere of the young Earth at a time when the Earth's mantle has already been extensively degassed. Therefore, after the impact, there was not enough volatile species left in the mantle to feed the formation of the massive early Earth's atmosphere, which required the delivery of total amounts of H₂O, CO₂ and SO₂ corresponding to partial pressures of about 270, 60 and 80 bars, respectively (today, CO₂ and SO₂ are mostly stored as carbonates in the crust and metallic sulfides in the upper mantle, respectively). This μ Ms origin of the atmosphere is strongly supported by the Ne/N₂ and the D/H ratios of Antarctic micrometeorites. They best fit the corresponding ratios observed in the air and the oceans, respectively, which are incompatible with all other models of atmosphere formation.

Moreover, a fraction of the μ Ms that did survive unmelted upon atmospheric entry with their full load of PAH-rich kerogen landed on the proto-oceans floors. They well fit the definition of good "source rocks" for the "economic exploitation" of petroleum, *i.e.*, fine clays with at least 0.5 wt.% of kerogen (Rondeel 2002). Therefore, they likely generated giant abiogenic oil slicks that assisted prebiotic chemistry (Dias & Maurette 2007). In 1971, Dave Holland and collaborators (Lasaga *et al.* 1971) proposed a distinct type of primordial oil slick. But their oil was produced during the solar UV irradiation of a primordial methane and nitrogen atmosphere, which had soon to be disregarded.

4 Kerogen-rich molecular reactors in the ISM

Frank Shu (1982) pointed out that the extinction of visible starlight could be caused by "bricks". However, he cautioned that bricks cannot produce a reddening of starlight. The combination of true absorption and reddening of this starlight is thus attributed to grains that are slightly smaller ($\leq 0.4 \mu\text{m}$) than the wavelengths of visible light in order to scatter blue light more efficiently than red light. This general extinction does not exclude the presence of $\geq 100 \mu\text{m}$ size "bricklets", which were injected from various stellar sources in the ISM. They could be made of the large diversity of solids that have the potential of desorbing molecules upon ion implants (Sect. 2), including hydrous carbonaceous micrometeoroids (see Sect. 3). All of them would start as somewhat dormant and invisible molecular reactors in the ISM, until they are re-activated by various processes (see next section).

In 1994, 15 Antarctica micrometeorites (*i.e.*, μ Ms) have been ranked on a scale of increasing thermal metamorphism upon atmospheric entry (Clemett *et al.* 1996). The PAH moieties of their constituent kerogen have been desorbed with the IR laser pulses of a double laser microscope equipped with a reflectron time-of-flight mass spectrometer ($\mu\text{L}^2\text{MS}$). A great diversity of PAH mass spectra were observed, from the simplest spectra of unmelted μ Ms (similar to that of the CM2-type Murchison chondrite) to the complex spectra of partially melted μ Ms that

mimic that of soot particles (see Figs. 4a to 4d, in Clemett *et al.* 1996). “Exotic” PAHs were also observed, such as vinyl PAHs that might have promoted interesting organometallic reactions.

McFarlane and co-workers invented the ^{252}Cf plasma desorption mass spectrometer, which allowed the determination of the molecular weight of large organic molecules, such as insulin, which desorbs “intact” from thin deposits irradiated with ~ 100 MeV ^{252}Cf -fission fragments (Torgeson *et al.* 1974). Therefore, fast ions should also softly desorb PAHs from kerogen, like the IR laser pulses of the $\mu\text{L}^2\text{MS}$. We commented (Maurette *et al.* 2003) on the *in-situ* FTIR analysis of five organics irradiated with 10 MeV/amu ^{40}Ar ions, under oxygen free conditions (Reynaud *et al.* 2001). These materials lose the memory of their initial properties when the radiation dose exceeds ~ 300 Mega-Grays, *i.e.*, after an exposure of about 10^4 yr to SEPs at 1 AU. They are all converted into an insoluble material dubbed as kerogen, which might desorb its PAH moieties in the ISM.

5 Summary and prospects

In the last 70 yr, an abundant literature was published about the main ingredients of dust evolution models in galaxies, including the synthesis of interstellar molecules (*cf.*, Dwek *et al.* 2009). Our studies show that many reaction channels are opened upon implantation of a **polyatomic** beam of fast ions in a great diversity of Solid State Molecular Reactors. A challenge is to check whether their easy-to-desorb and abundant species (*e.g.*, H_2 , CO and PAHs), can help simplifying the chemical models proposed for the synthesis of interstellar molecules in the gas-phase, “*which contain thousands of reactions, many of which have not been studied theoretically or in the laboratory*” (quote from E.Herbst).

Another challenge is to identify the dominant process that can activate molecular desorption from the “dormant” molecular reactors in the ISM. All previous processes, including those listed by Maurette & Price in 1975, might be fully superseded by the high flux of low energy (2–20 MeV/amu) galactic cosmic rays (LOWs) if McCall and co-workers are right (McCall 2010). They reported challenging papers (*e.g.*, Indriolo *et al.* 2009) dealing in particular with the determination of the high degree of ionization of the diffuse ISM (as inferred from the H_3^+ ion) and the production rates of Li, Be, B and gamma-rays. They tested multiple LOWs energy spectra and found only two spectra that best fitted the corresponding observations.

I selected their simplest “broken power-law” distribution of cosmic rays in relativistic momentum, reproduced in Figure 2, that represents a differential number flux, Φ_p [particles $\text{cm}^{-2}\text{s}^{-1}\text{sr}^{-1} (\text{GeV}/n)^{-1}$]. Nick Indriolo has kindly computed the corresponding integrated flux of protons, in the three energy ranges considered in this paper: Δ_1 (0.002–1 GeV/n); Δ_2 (2–20 MeV/n) and Δ_3 (5–20 MeV/n). The corresponding “integral” proton fluxes (number $\text{cm}^{-2} \text{s}^{-1} \text{sr}^{-1}$) are about 3.7, 1.5, and 0.9, for Δ_1 , Δ_2 , and Δ_3 , respectively. For grains smaller than the projected range of 2 MeV/n LOWs in silicates (about 42 μm and 18 μm for H and

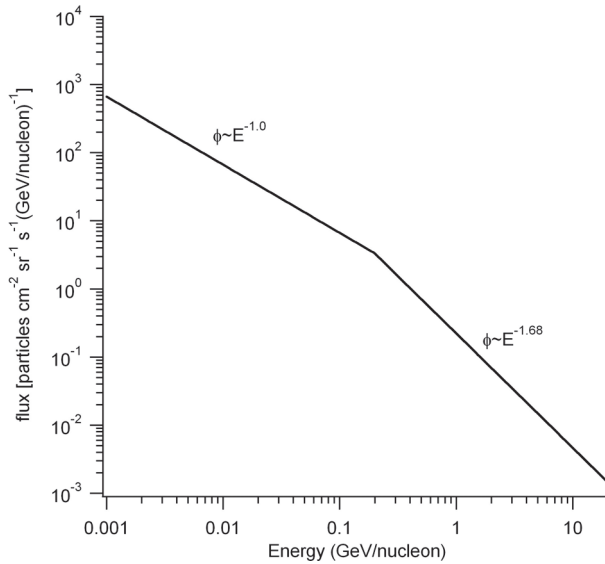


Fig. 2. Possible energy spectrum of low energy cosmic rays in the ISM (Courtesy N. Indriolo).

Fe, respectively), and which include all “visible” grains with sizes $\leq 1 \mu\text{m}$ in the ISM, this value has to be multiplied by 4π because the LOWs flux is isotropic.

The lifetime of a large dust grain in the ISM is about 3×10^7 yr, cycling several times between dense and diffuse clouds (see *e.g.* Tielens 2005). With the resulting flux of 20 protons $\text{cm}^{-2}\text{s}^{-1}$ (in the 2–20 MeV/n range) the kerogen simulation experiments discussed in section 4 predict that the organic component of the visible grains would be transformed into kerogen in $\sim 10^5$ yr of exposure in the diffuse interstellar clouds. Furthermore, artificial implants of Fe and Ar ions, show that crystalline silicates, would be rendered amorphous by a fluence of $\geq 10^{11}$ VH cm^{-2} at the very low temperatures of the ISM, which quench the diffusion induced annealing of atomic defects. Considering a low energy cutoff value of 5 MeV/n required for the penetration of VH ions in the diffuse clouds, the Indriolo predicted proton flux ($11 \text{ cm}^{-2} \text{ s}^{-1}$) corresponds to an exposure of $\sim 3 \times 10^7$ yr and $\sim 10^6$ yr in the ISM, for a solar VH/H ratio (10^{-5}) and the 30 times higher ratio measured for ≥ 1 GeV/n GCRs, respectively. A reasonable VH/H ratio just a few times higher than solar would insure that *in the diffuse ISM, crystalline silicates would be rare but PAHs quite abundant.*

The Mcfarlane desorption mass spectrometer can measure PAH desorption yields of kerogen-rich materials, which are required to extrapolate the desorption model to the ISM. The presence of abundant “bricklets” along the orbits of comets is brightly signaled by meteor showers. However, the ISM bricklets have still to be detected.

I am indebted to: IN2P3 for constant support; A. Burlingame, S. Clemett, C. Hammer, C. Jouret, G. Kurat, W. Möller, N. Indriolo and M. Pouchet for important contributions; E. Dobrica and C. Engrand for their characterization of Antarctic micrometeorites, and; C. Joblin for stimulating thoughts, encouragements and help with LaTeX formatting.

References

- Bibring, J.P., Burlingame, A., Chaumont, J., *et al.*, 1974, *Geochim. Cosmochim. Acta*, 2, 1747
- Borgesen, P., Maurette, M., Möller, W., & Monart, B., 1986, in *Radiation effects in Insulators 3*, ed. I.H. Wilson & R.P. Webb, Gordon and Breach Science Publishers), 711
- Clemett, S.J., Chillier, X.D.F., Gillette, S., *et al.*, 1996, *Origins life Evol. Biosphere*, 28, 425
- Dias, F., & Maurette, M., 2007, *Lunar Planet. Sci.*, 37, A1268
- Dobrica, E., Engrand, C., Quirico, E., Montagnac, G., & Duprat, J., 2009, *MAPS*, 44, 1643
- Dwek, E.E., Galliano, F., & Jones, A., 2009, *ASP Conf. Ser.*, 414, 183
- Greaves, J.S., 2005, *Science*, 307, 68
- Indriolo, N., Fields, B.D., & McCall, B.J., 2009, *ApJ*, 694, 257
- Lasaga, A.C., Holland, H.D., & Dwyer, M.J., 1971, *Science*, 174, 53
- Lisse C.M., VanCleve, J., Adams, A.C., *et al.*, 2004, *Icarus*, 171, 444
- Maurette, M., & Price P.B., 1975, *Science*, 187, 121
- Maurette, M., 1976, *Nucl. Inst. Meth.*, 132, 579
- Maurette, M., Banifatemi, A., Della-Negra, S., & Lebeyec, Y., 1983, *Nature*, 303, 159
- Maurette, M., Balanzat, E., & Duprat J., 2003, *Lunar Planet. Sci.*, 34, A1743
- Maurette M., 2009, *ASP Conf. Ser.*, 414, 137
- McCall, B.J., 2010, in <http://bjm.scs.uiuc.edu/>
- Raisbeck, G.M., & Yiou, F., 1989, *Meteoritics*, 24, A318
- Reynaud, J., *et al.*, 2001, *Spectrochim. Acta*, A57, 797
- Rondeel, H.D., 2002, in www.geol.vu.nl
- Shu F.H., 1982, *The Physical Universe: An Introduction to Astronomy* (University Science Books), 1
- Simoneit, B.R., Wszolek, P.C., Christiansen, P., Jackson, R.F., & Burlingame, A.L., 1973, *Geochim. Cosmochim. Acta*, 37, 1603
- Tielens, A.G.G.M., 2005, "The Physics and Chemistry of the Interstellar Medium" (Cambridge University Press), Section 13
- Torgeson D.F., Skowronsky, R.P., & Macfarlane, R.D., 1974, *Biochem. Biophys. Res. Commun.*, 60, 616

POLYCYCLIC AROMATIC HYDROCARBONS AND THE EXTINCTION CURVE

G. Mulas¹, G. Mallocci¹, C. Joblin^{2,3} and C. Cecchi–Pestellini¹

Abstract. Aromatic carbon, in some form, has been an essential ingredient by and large in all models of the extinction curve, since the original proposal to attribute the bump at 217.5 nm to “astronomical graphite”. This aromatic carbon is most naturally identified, in up to date models, with a population of Polycyclic Aromatic Hydrocarbons (PAHs), free and/or clustered. In all models, this PAH population accounts for the far–UV nonlinear rise in the extinction curve, contributes to the bump and possibly part of the large set of unidentified, discrete absorption features in the visible (the Diffuse Interstellar Bands). We review the current state of our understanding of the contribution of PAHs to interstellar extinction, and what constraints can be imposed on the PAH population by fitting extinction models to observations.

1 Interstellar extinction before PAHs

Interstellar extinction has a long, winding story. It dates as far back in time as 1774, with sir William Herschel noticing a region in the Scorpio constellation remarkably devoid of stars, which he called a “hole in the sky”. The fact that such regions were a common occurrence in the Milky Way was clear in the early years of 1900, with the systematic observations of Barnard, as was stated in a textbook of the time (Clerke 1903), and it began to be hypothesised that they were not actually holes in the fabric of the sky, but instead might be “obscured” by some intervening material. For some decades, this hypothesis was the topic of some heated debates, some of which are on record in the proceedings of academic meetings of the time (Shapley & Curtis 1921). It was only about in 1930 that firm evidence of interstellar extinction became available (Trumpler 1930).

¹ Istituto Nazionale di Astrofisica – Osservatorio Astronomico di Cagliari – strada 54, località Poggio dei Pini, 09012 – Capoterra (CA)

² Université de Toulouse, UPS, CESR, 9 Av. colonel Roche, 31028 Toulouse Cedex 4, France

³ CNRS, UMR 5187, 31028 Toulouse, France

Thus far, interstellar extinction was accessible to study mainly in the visible part of the spectrum, where it was known to increase linearly for decreasing wavelength, when expressed in magnitudes *vs.* wavenumbers (hence the name “reddening” still widely used for it), and was therefore believed to be essentially due to scattering and absorption by some form of classical dust particles. The precise composition and structure of this astronomical dust was not really constrained, as about any distribution of classical particles made of any refractory material would produce a linear extinction curve in the visible. It was only about in the 1940 decade that van de Hulst produced the first full fledged model of interstellar extinction based on well-defined dust particles (van de Hulst 1949). The only structure known at that time in this almost linear behaviour of extinction was a set of optically thin, unidentified features, called the Diffuse Interstellar Bands (DIBs). The first ones were discovered by Merrill (1934), their number has been growing steadily with the increasing sensitivity of instruments and currently exceeds four hundreds (Hobbs *et al.* 2010), still with no unambiguous identification despite some tentative ones. Since DIBs are the subject of some other contributions (Snow & Desheed, Cox in this volume), we will only briefly mention them here. For a beautiful and thorough review of the early studies of interstellar extinction, see *e.g.* Greenberg & Shen (1999).

The opening of the UV section of the spectrum to astronomical observations, with the advent of rocket- (Stecher 1965) and space-based (see *e.g.* Bless & Savage 1970, and references therein) instruments, revealed more structure in the thus far relatively simple extinction curve. The slope of its linear behaviour changed in the near UV, and on top of it appeared two strong features: a broad Drude-like absorption “bump” peaking at about 217 nm, followed by a non-linear additional rise in the extinction at still lower wavelengths in the far-UV. The phenomenological behaviour of the extinction curve in the visible and UV was summarised in the monumental, systematic works by Fitzpatrick & Massa (1986, 1988, 1990, 2005, 2007, 2009). They collected the observed extinction curves for several hundreds of lines of sight, and found that in the UV (*i.e.* for $\lambda < 270$ nm) they could all be parametrised satisfactorily with a relatively simple functional form.

$$k(\lambda - V) = \frac{E(\lambda - V)}{E(B - V)} = \begin{cases} c_1 + c_2x + c_3D(x, x_0, \gamma) & x \leq c_5 \\ c_1 + c_2x + c_3D(x, x_0, \gamma) + c_4(x - c_5)^2 & x \geq c_5 \end{cases} \quad (1)$$

where $x = \lambda^{-1}$ and

$$D(x, x_0, \gamma) = \frac{x^2}{(x^2 - x_0^2)^2 + x^2\gamma^2}.$$

This functional form represents the “normalised” color excess $k(\lambda - V)$, considered as a function of inverse wavelength, with the superposition of a linear contribution, a Drude profile and a quadratic term. At longer wavelengths, $k(\lambda - V)$ is very nearly linear through the visible range, with a change of slope at around 440 nm, and tends to zero for very long wavelengths. The extinction “bump”, which is the single most intense interstellar absorption feature, was found to have an almost invariable peak position, whereas its intensity and full width at half-maximum

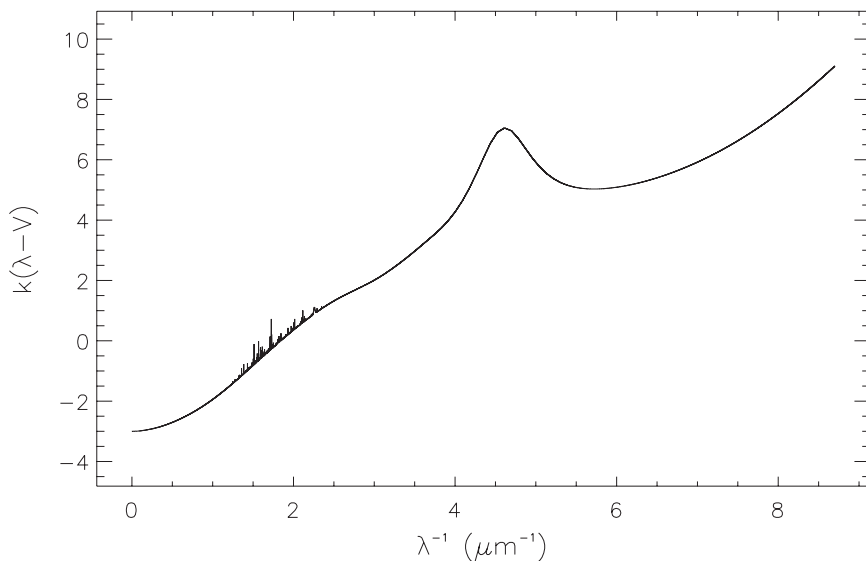


Fig. 1. Average interstellar extinction curve in the galactic plane, as given by Fitzpatrick & Massa (2007). The definition of $k(\lambda - V)$ is given in Equation (1). The weak structure in the visible range is the set of Diffuse Interstellar Bands, taken from Hobbs *et al.* (2010), and arbitrarily enhanced by a large factor to make them visible on the scale of this plot.

vary substantially from one line of sight to another. The average extinction curve in the galactic plane is shown in Figure 1. The overall shape of the extinction curve in the UV suggested the presence of a large population of very small dust particles, the so called “Platt particles” after their original proposer (Platt 1955). It was then suggested, soon after the availability of the first rocket data, that such particles could actually consist of some sort of aromatic carbon (Donn 1968). Indeed, from the integrated intensity of the bump it is straightforward to obtain a robust constraint on the abundance of its carrier (see *e.g.* Draine 1989)

$$\frac{n_x}{n_H} f_x = 9.3 \times 10^{-6},$$

where $\frac{n_x}{n_H}$ is the abundance of the “bump” carrier, and f_x the oscillator strength of the transition producing it. It is apparent that even assuming a very large oscillator strength f_x only the most abundant elements can possibly produce the bump. If one takes $f_x \sim 0.16$, appropriate for intensity per C atom of the very strong $\pi^* \leftarrow \pi$ resonance in graphitic materials, producing the bump observed in the average galactic extinction curve requires about $\frac{1}{4}$ of the available interstellar carbon. No other carriers could realistically produce such a strong feature compatibly with interstellar abundances.

The above argument, together with the resemblance of the observed “bump” profile with the $\pi^* \leftarrow \pi$ bands in graphite, led to the development of dust models attempting to fit the entire interstellar extinction curve (Mathis *et al.* 1977; Lee & Draine 1984; Draine 1987a). These models assumed power-law size distributions of spherical silicate and graphite particles, and used Mie theory, together with “optimised” optical constants (Lee & Draine 1984; Draine 1985; Draine 1987b), obtaining a very successful fit to the observed extinction curves. One drawback was that the “optimised” optical constants did not match any precise known material, but were obtained by collecting the (then available) experimental data, with subtle *ad hoc* changes to make sure that they joined smoothly, that they were consistent with the Kramers–Kronig relations, *and* that they fitted the astronomical observations.

2 PAHs enter the scene

The opening of another previously unavailable spectral window, again with space-based observations, was key to the appearance of PAHs in astronomy. The first IR observations showed a large excess of emission in the 12 μm IRAS band, with respect to the others at longer wavelengths. IR spectra, furthermore, showed an ubiquitous, relatively invariant spectrum of bright emission bands at ~ 3.3 , 6.2, 7.7, 8.6, and 11.3 μm . Sellgren (1984) was the first to notice that especially the 3.3 μm band could not be accounted for by equilibrium thermal emission of dust particles, since it would require unrealistically high temperatures. She hinted, remembering the proposed role of temperature fluctuations in the evaporation of ice mantles of dust grains (Purcell 1976; Greenberg & Hong 1974), that these bands might be due to a population of particles with such a small thermal capacity to be transiently heated to the required high temperatures by a single UV photon. Sellgren’s proposal, in hindsight, was reminiscent of the early suggestion by Platt (1955) and Donn (1968) for extinction (“Platt particles”),

Soon thereafter, two groups independently proposed that these “particles” could be free-flying Polycyclic Aromatic Hydrocarbons (PAHs) (Léger & Puget 1984; Allamandola *et al.* 1985), since they appeared to fit all the required characteristics: they absorb effectively UV radiation, convert it with high efficiency to vibrational excitation, and release it as IR emission, in bands qualitatively matching the observed “Unidentified Infrared Bands” (UIRs). They are also very resistant to photodissociation (provided they are large enough), and can possibly form in C-rich outflows of evolved stars, with chemical pathways inspired from combustion chemistry. Shortly thereafter, it was also realised that since interstellar PAHs, depending on size and charge state, would have also discrete bands in the visible, this made them very plausible candidate carriers for DIBs (van der Zwet & Allamandola 1985; Léger & d’Hendecourt 1985).

Purely energetic considerations, based on the overall integrated emission in the UIRs, assuming unit conversion efficiency and UV absorption cross-sections (Puget & Léger 1989; Joblin *et al.* 1992), led to estimate that about 15–20% of

the available interstellar carbon must be locked in PAHs to produce the observed IR emission fluxes. This led to the consequence that PAHs *must* be taken into account as a necessary ingredient of interstellar extinction models (Puget & Léger 1989).

Indeed, from this point on, all interstellar extinction models got updated to include some sort of “astronomical PAH” component (Désert *et al.* 1990; Siebenmorgen & Kruegel 1992; Li & Greenberg 1997; Dwek *et al.* 1997). In particular, all models use these “astronomical PAHs” to account for the non-linear far-UV rise, very effectively decoupling it from the extinction “bump” at 217 nm. At the time, PAHs were assumed to contribute *only* to the non-linear far-UV rise, while the bump was still entirely attributed to a population of classical small “astronomical graphite” particles. This was very convenient, as it provided a nice physical explanation of the observed behaviour of these two components of the extinction curve, which were known to vary independently in observations.

The assumption that “astronomical PAHs” did not contribute to the bump was due to the following reasons. The bump position is known to be very nearly invariant in all lines of sight, whereas its intensity and width vary. It is also remarkably smooth and no fine structure was detected on it so far. The (few) experimental spectra of PAHs available, almost entirely neutral ones (Joblin *et al.* 1992; Joblin 1992) showed $\pi^* \leftarrow \pi$ transitions with different positions, and with considerable structure on a wavelength scale much smaller than the bump, even when mixtures were considered, making PAHs an unattractive candidate to account for the 217 nm extinction feature (Draine & Malhotra 1993; Mathis 1994).

Moreover, PAHs were believed to be largely ionised (see *e.g.* D’Hendecourt & Léger 1987; Verstraete *et al.* 1990; Salama *et al.* 1995) in the diffuse interstellar medium. In their seminal model, Désert *et al.* (1990) assumed a mixture of ionised PAHs to have no absorption in the bump region, probably reasoning that the variation of the position of $\pi^* \leftarrow \pi$ transitions in different molecules would smooth them out over such a wide wavelength range to make them irrelevant.

Direct measurements of the cross-sections of PAH cations were (and still are) rather complicated, since PAH cations are very reactive species. The first experiments used the technique of matrix isolation, in which a reactive species is included as a trace component in a solid which perturbs it as little as possible (*e.g.* a frozen noble gas like argon or neon). Irradiation of the neutrals by far-UV photons leads to a fraction of ionised species in the matrix.

Experiments like these produced a large amount of good data on the visible spectra of PAH cations (*e.g.* Salama & Allamandola 1992a, 1992b), mainly aiming at the comparison with astronomical spectra of the DIBs. For this spectral region the technique is rather effective, since the neutral PAHs studied have no features in the visible whereas the cations do. Measuring the strong $\pi^* \leftarrow \pi$ transitions in the bump region, however, is much more difficult, since the neutral precursors (also present in the matrix) do have strong and broad transitions there, difficult to disentangle from the features of the cations. This probably misled Lee & Wdowiak (1993, 1994a, 1994b), who interpreted their experiments on irradiated

PAH-containing glasses as showing that the $\pi^* \leftarrow \pi$ transitions were substantially suppressed in cations.

For all these reasons, all interstellar extinction models, for the contribution of PAHs to UV extinction, stuck with the assumption of Désert *et al.* (1990) and adopted an average cross-section of the neutral PAHs from which the $\pi^* \leftarrow \pi$ transitions were simply removed, leaving only the non-linear rise in the far UV due to the onset of $\sigma^* \leftarrow \sigma$ transitions (see *e.g.* Désert *et al.* 1990; Siebenmorgen & Kruegel 1992; Li & Greenberg 1997; Dwek *et al.* 1997).

Several years later, Duley & Seahra (1998) used the discrete dipole approximation (DDA) to study the spectra of PAHs, both single and in clusters, as a function of hydrogenation and ionisation. They found that $\pi^* \leftarrow \pi$ transitions appeared to be almost unaffected by ionisation, in stark contrast with the previous interpretation by Lee & Wdowiak (1993, 1994a, 1994b) and the assumptions of the astronomical PAH models of the time. They also found that the peak of the $\pi^* \leftarrow \pi$ transitions shifts systematically with dehydrogenation, and claimed that heavily dehydrogenated PAHs fit the observed position of the interstellar extinction bump. One year later, Chillier *et al.* (1999) measured the VUV spectrum of the perylene cation with an indirect technique, unambiguously confirming that the strong $\pi^* \leftarrow \pi$ transitions are almost unaffected by ionisation. In hindsight, this is hardly surprising, since, at least for large PAHs, one more or less electron does not overly perturb the π and π^* orbitals.

This awareness that all PAHs have strong $\pi^* \leftarrow \pi$ transitions, and the realisation that they do not leave much room in the interstellar carbon budget for a separate population of carbonaceous particles producing the bump, caused a general update of the photo-absorption cross-sections giving the contribution of PAHs to interstellar extinction models (see *e.g.* Weingartner & Draine 2001; Li & Draine 2001; Draine & Li 2001; Draine in this volume). The far-UV part of the extinction curve, including the bump and the non-linear rise, were assumed to be completely insensitive to charge, and to include a strong $\pi^* \leftarrow \pi$ feature. As a consequence, models lost the flexibility to easily account for independent variation of the bump and the far-UV non-linear rise, since from now on they were assumed to be essentially due to the same population of molecules and to be largely insensitive to size and charge of the PAHs. On the other hand, the onset of absorption by PAHs became dependent on charge, as populations of PAH cations were found to begin absorbing at lower energies with respect to neutrals, reflecting experimental and theoretical results (*e.g.* Ruiterkamp *et al.* 2002, 2005). PAHs became by and large the main carrier of the 217 nm extinction bump (see *e.g.* Draine in this volume).

Since all PAHs were now believed to strongly absorb in the UV, Clayton *et al.* (2003) searched for weak structure in the UV extinction curve, using Hubble Space Telescope observations at high spectral resolution, in the hope of being able to identify some features due to individual PAHs. This resulted in no detection, and in the placement of relatively low upper limits, meaning that no single PAH is very abundant in the diffuse ISM.

As experimental techniques for gas-phase measurements, *e.g.* in cold jets, became more feasible, more and more experimental measurements of PAH spectra became available (see *e.g.* Bréchnignac & Pino 1999; Pino *et al.* 1999; Bréchnignac *et al.* 2001; Biennier *et al.* 2003; Biennier 2004; Tan *et al.* 2005; Staicu *et al.* 2006; Rouillé *et al.* 2007; Salama *et al.* 2008), but mainly in the visible and near-UV, to compare them with observations of the DIBs. PAH spectra in the vacuum UV, especially for cations, being much more difficult and less promising for a direct identification, were left behind. A thorough review of the state of the art of the spectroscopy of PAHs is given in this volume by Pino *et al.*

3 Systematic theoretical spectra come in

In the same years, the steady increase in available computing power brought larger and larger PAHs within reach of quantum chemistry calculations, in particular using the Time-dependent Density Functional Theory (TD-DFT). This technique was proven to hit a sweet spot between computational cost and accuracy, and began to be routinely used both as a complement to experimental measurements, to enable the interpretation of photo-absorption spectra and the identification of bands, and to perform systematic studies on trends of the spectral behaviour of families of PAHs as a function of structure, size, ionisation state etc. (Ruiterkamp *et al.* 2005). However, commonly available implementations of TD-DFT are increasingly ineffective and/or inaccurate for transitions above the ionisation limit of a given molecule. This appears to be not the case for codes which implement TD-DFT in real time and represent wavefunctions by their values on a finite grid in real space, such as the open-source Octopus (Marques *et al.* 2003).

Malloci (2003) and Malloci *et al.* (2004) tested this code against the few experimental photo-absorption spectra available up to the vacuum UV, finding that the accuracy of TD-DFT calculations remained by and large the same up to high energies (a few tenths of an eV for band positions) as for low energies. Moreover, the computational cost, using this kind of implementation, does not change with the spectral range on which the spectrum is computed, making it particularly suitable for computing whole PAH spectra up to (and even beyond) the Lyman limit.

Having validated the approach (*cf.* Fig. 2), Malloci and co-workers (Malloci *et al.* 2005, 2007a, 2007b) proceeded to compute photo-absorption spectra of a large number of PAHs over the whole wavelength range relevant for interstellar extinction, and made their results publicly available on a web-based database¹. This made possible a systematic study of the effect of hydrogenation and charge state. It was confirmed (Malloci *et al.* 2008) that dehydrogenation progressively shifts the $\pi^* \leftarrow \pi$ transitions bluewards, by more than 2 eV upon complete dehydrogenation, confirming the trend previously predicted by Duley & Seahra (1998) and by Duley & Lazarev (2004). However, the increased accuracy of TD-DFT

¹<http://astrochemistry.oa-cagliari.inaf.it/database>

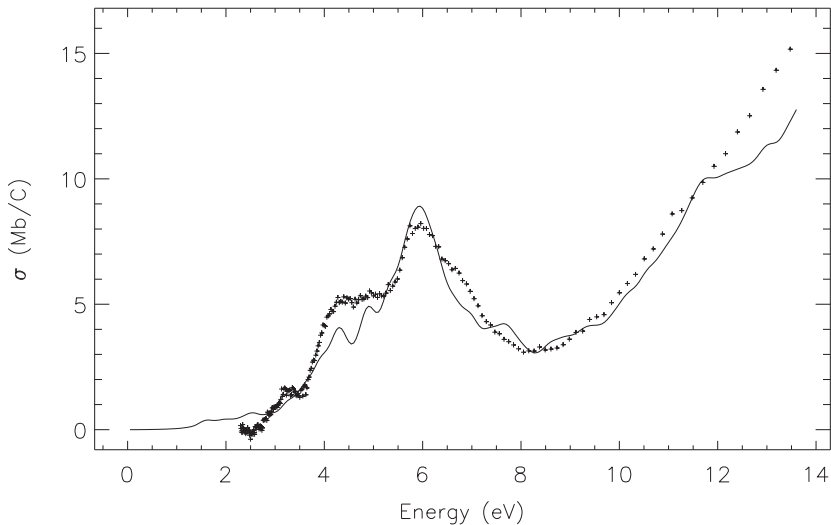


Fig. 2. Average of the photo-absorption cross-sections computed via Time-Dependent Density Functional Theory for a sample of neutral PAHs, normalised to the number of C atoms ($1 \text{ Mb} = 10^{-18} \text{ cm}^2 = 10^{-2} \text{ \AA}^2$). The theoretical curve, in continuous line, is compared with the experimental spectrum (small crosses) of a mixture of small gas-phase PAHs obtained by evaporation of a coal-pitch extract (Joblin *et al.* 1992).

calculations with respect to the DDA technique used by Duley & Seahra (1998) showed that if PAHs were severely dehydrogenated their $\pi^* \leftarrow \pi$ absorption would fall between the “bump” and the onset of the non-linear far-UV rise, placing a strong upper limit on the overall dehydrogenation of PAHs.

As to ionisation, it was demonstrated (Cecchi-Pestellini *et al.* 2008) that there is indeed a relevant systematic effect: going from anions to neutrals to cations and dications it appears that while the $\pi^* \leftarrow \pi$ transitions (in the “bump” region) are almost unchanged, the onset of the large, broad absorption due to $\sigma^* \leftarrow \sigma$ transitions is progressively shifted to higher energies, significantly reducing the absorption in the wavelength range of the non-linear far-UV rise (see Fig. 3). This is important for interstellar extinction models, since it offers a physically sensible parameter which can change the observed independent variation of the “bump” and non-linear far-UV rise.

4 Including actual PAH cross-sections in extinction models?

The availability of a relatively large number of real computed photo-absorption spectra of PAHs made it possible to attempt, for the first time, the construction of an interstellar extinction model including a distribution of classical dust particles

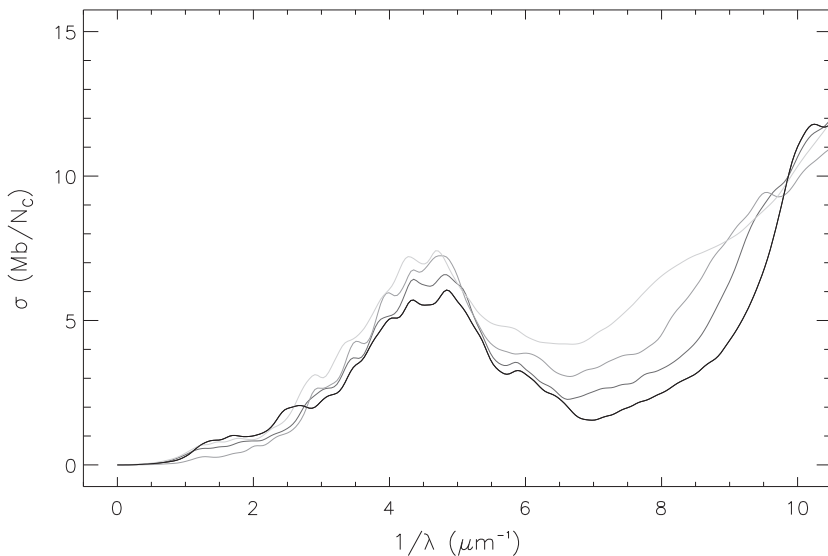


Fig. 3. Systematic variation of the average of the photo-absorption cross-sections of a sample of computed PAHs ($1 \text{ Mb} = 10^{-18} \text{ cm}^2 = 10^{-2} \text{ \AA}^2$), normalised to the number of C atoms, with charge state (anions in light gray, neutrals in medium gray, cations in dark gray, dications in black).

and a linear combination of cross-sections of a sample of PAHs in several charge states (Cecchi-Pestellini *et al.* 2008). This has the obvious advantage of being a more physical approach, and the obvious drawback of introducing a ludicrous number of free parameters (the column density of each species included in the lineal combination).

Comparison with observed extinction curves showed quantitatively several points. The first is that it is indeed practically possible to match the extinction curve very accurately using a mixture of even a relatively small sample of “real” PAHs. Some examples are shown in Figure 4. A few tens of species provide enough chemical diversity to very effectively wash out spectral features of individual species in the UV, resulting in a very smooth extinction curve which matches very accurately the observed one in the UV, including both the “bump” and the far-UV rise. While this would now appear obvious in hindsight, Figures 2 and 3 make it evident that not every mixture of PAH spectra results in washing out spectral structure: an actual fit on real observations was necessary to prove that obtaining a smooth bump with PAHs is not only possible but actually easy (the fit is very strongly underdetermined, see below). On the other hand, at least in some peculiar lines of sight there must be some (probably carbonaceous) component of very small (nanometer sized) particles other than PAHs, as PAHs cannot reproduce extreme cases with a strong non-linear far-UV rise and no bump. Several works showed that one feasible component with the required properties would be

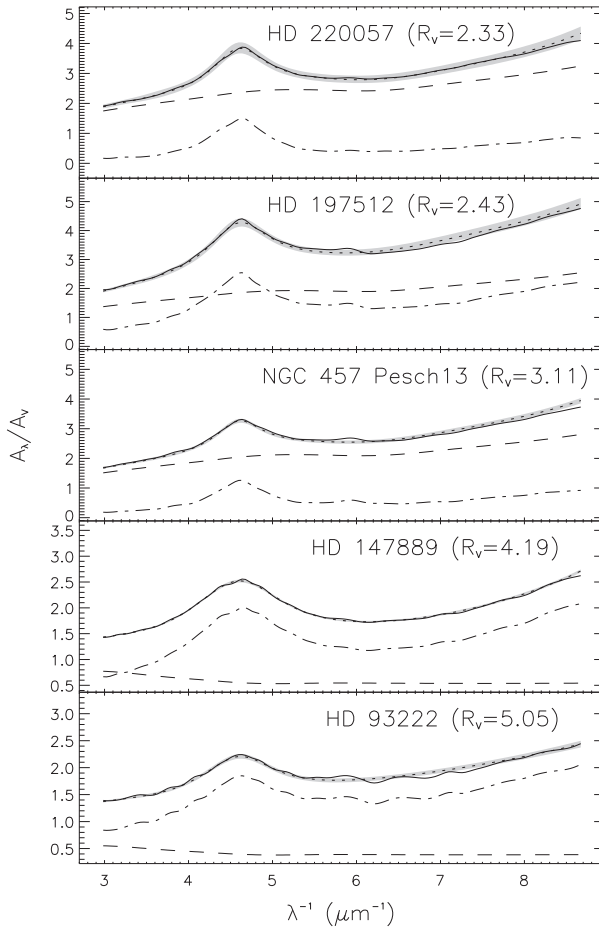


Fig. 4. Comparison between some observed extinction curves (dotted lines, Fitzpatrick & Massa 2007), spanning a large range of values of the total to selective extinction ratio $R_V = \frac{A_V}{E_{B-V}}$, and the fits (solid continuous line) obtained by Cecchi–Pestellini *et al.* (2008). The dashed line shows the contribution of classical dust particles, the dash–dotted lines the contribution of PAHs.

a carbonaceous material in which carbon has an sp^3 structure, such as nanodiamonds or hyperhydrogenated PAHs (see *e.g.* Rai & Rastogi 2010).

The other important point is that it was quantitatively shown that even if a fit of the extinction curve with a mixture of PAHs is severely underconstrained, meaning that there is no uniquely defined composition of PAHs required to produce a given observed interstellar extinction curve, nonetheless some collective properties of the mixture *are* well–determined, *e.g.* the charge per carbon atom, which relates to the relative intensity between the “bump” and the non–linear far–UV rise. This

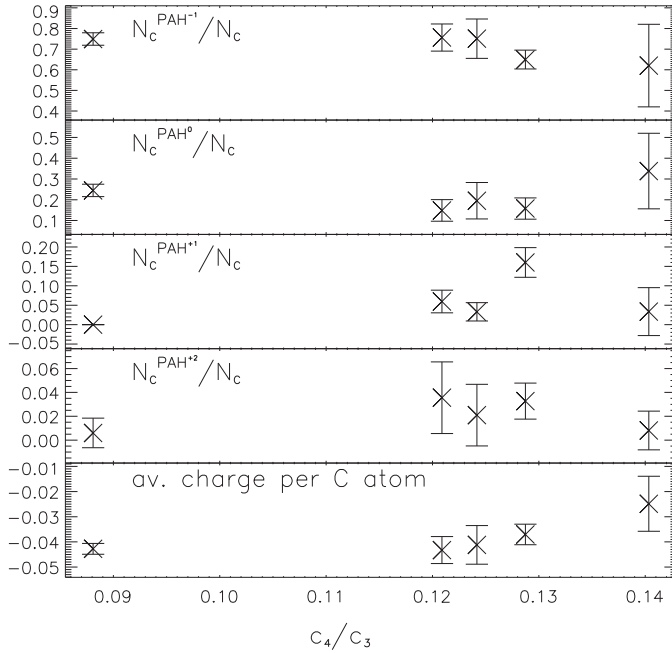


Fig. 5. Correlation between the charge (in units of electron charges) per C atom in PAHs and the c_4/c_3 (c_4 and c_3 are defined in Eq. (1)) ratio. From top to bottom, this is shown for PAH anions, neutrals, cations, dications, and the whole population. A clear trend is visible on the bottom panel.

is illustrated in Figure 5, in which the lowest panel shows that increasing ratios of the c_4 (proportional to the intensity of the non-linear far-UV rise) *versus* c_3 (proportional to the intensity of the bump) parameters in the Fitzpatrick & Massa parametrisation (*cf.* Eq. (1)) correspond to an increasing value of the charge per carbon atom in PAHs. The bottom panel in Figure 5 shows quantitatively that when in an extinction curve the non-linear far-UV rise is more intense with respect to the bump, fitting it requires a mixture of PAHs with less electrons per C atom.

While such a “brute force” approach to the contribution of PAHs to interstellar extinction is probably not *per se* the best way for a comprehensive modelling of dust absorption and emission, it shows that the best currently available such global model (*e.g.* Li & Draine 2001) lose some important information with their (necessary) simplification of PAH absorption, for example disregarding the impact of charge on far-UV extinction. As Einstein liked to say, a model should be made as simple as possible without losing significant physics, but not simpler than that. Some more work still needs to be done to achieve this result for PAHs and extinction, to find an acceptable middle ground somewhere between the nightmare of a poorly defined mixture of too many PAHs and an unrealistic single spectrum of the “average astronomical PAHs”.

References

- Allamandola, L.J., Tielens, A.G.G.M., & Barker, J.R., 1985, *ApJ*, 290, 25
- Biennier, L., 2004, *Chem. Phys. Lett.*, 387, 287
- Biennier, L., Salama, F., Allamandola, L.J., & Scherer, J.J., 2003, *J. Chem. Phys.*, 118, 7863
- Bless, R.C., & Savage, B.D., 1970, *IAU Symp.*, 36, 28
- Bréchnignac, P., Pino, T., & Boudin, N., 2001, *Spectrochim. Acta*, 57, 745
- Bréchnignac, P., & Pino, T., 1999, *A&A*, 343, L49
- Cecchi-Pestellini, C., Malloci, G., Mulas, G., Joblin, C., & Williams, D.A., 2008, *A&A*, 486, L25
- Chillier, X.D.F., Stone, B.M., Salama, F., & Allamandola, L.J., 1999, *J. Chem. Phys.*, 111, 449
- Clayton, G.C., *et al.*, 2003, *ApJ*, 592, 947
- Clerke, A.M., 1903, *Problems in astrophysics* (London, A. & C. Black)
- Désert, F.-X., Boulanger, F., Puget, J.L., 1990, *A&A*, 237, 215
- D'Hendecourt, L.B., & Léger, A., 1987, *A&A*, 180, L9
- Donn, B., 1968, *ApJ*, 152, 129
- Draine, B.T., & Li, A., 2001, *ApJ*, 551, 807
- Draine, B.T., & Malhotra, S., 1993, *ApJ*, 414, 632
- Draine, B.T., 1989, *Interstellar dust*, *Proc. IAU Symp.*, 135, ed. L.J. Allamandola & A.G.G.M. Tielens, 313
- Draine, B.T., 1987, *BAAS*, 19, 1077
- Draine, B.T., 1987, *ApJS*, 64, 505
- Draine, B.T., 1985, *ApJS*, 57, 587
- Draine, B.T., & Lee, H.M., 1984, *ApJ*, 285, 89
- Duley, W.W., & Lazarev, S., 2004, *ApJ*, 612, L33
- Duley, W.W., & Seahra, S., 1998, *ApJ*, 507, 874
- Dwek, E., *et al.*, 1997, *ApJ*, 475, 565
- Ehrenfreund, P., D'Hendecourt, L., Joblin, C., & Léger, A., 1992, *A&A*, 266, 429
- Fitzpatrick, E.L., & Massa, D., 2009, *ApJ*, 699, 1209
- Fitzpatrick, E.L., & Massa, D., 2007, *ApJ*, 663, 320
- Fitzpatrick, E.L., & Massa, D., 2005, *AJ*, 130, 1127
- Fitzpatrick, E.L., & Massa, D., 1990, *ApJS*, 72, 163
- Fitzpatrick, E.L., & Massa, D., 1988, *ApJ*, 328, 734
- Fitzpatrick, E.L., & Massa, D., 1986, *ApJ*, 307, 286
- Greenberg, J.M., & Hong, S.-S., 1973, *BAAS*, 5, 380
- Greenberg, J.M., & Hong, S.-S., 1974, *Galactic Radio Astron.*, 60, 155
- Greenberg, J.M., & Shen, C., 1999, *Ap&SS*, 269, 33
- Hobbs, L.M., York, D.G., Thorburn, J.A., *et al.*, 2010, *A New Atlas of the Diffuse Interstellar Bands: HD 183143*, 65th International Symposium On Molecular Spectroscopy

- Joblin, C., Léger, A., & Martin, P., 1992, *ApJ*, 393, L79
- Joblin, C., 1992, Ph.D. Thesis
- Lee, H.M., & Draine, B.T., 1984, *BAAS*, 16, 446
- Lee, W., & Wdowiak, T.J., 1994, *Molecules and Grains in Space*, 312, 675
- Lee, W., & Wdowiak, T.J., 1994, *The First Symposium on the Infrared Cirrus and Diffuse Interstellar Clouds*, 58, 295
- Lee, W., & Wdowiak, T.J., 1993, *ApJ*, 410, L127
- Léger, A., Verstraete, L., D'Hendecourt, L., *et al.*, 1989, *Interstellar Dust*, 135, 173
- Léger, A., & d'Hendecourt, L., 1985, *A&A*, 146, 81
- Léger, A., & Puget, J.-L., 1984, *A&A*, 137, 5
- Li, A., & Draine, B.T., 2001, *ApJ*, 554, 778
- Li, A., & Greenberg, J.M., 1997, *A&A*, 323, 566
- Malloci, G., Mulas, G., & Joblin, C., 2004, *A&A*, 426, 105
- Malloci, G., 2003, Ph.D. Thesis
- Malloci, G., Joblin, C., & Mulas, G., 2007, *Chem. Phys.*, 332, 353
- Malloci, G., Joblin, C., & Mulas, G., 2007, *A&A*, 462, 627
- Malloci, G., Mulas, G., Cappellini, G., Fiorentini, V., & Porceddu, I., 2005, *A&A*, 432, 585
- Malloci, G., Mulas, G., Cecchi-Pestellini, C., & Joblin, C., 2008, *A&A*, 489, 1183
- Marques, M.A.L., Castro, A., Bertsch, G.F., & Rubio, A., 2003, *Computer Phys. Commun.*, 151, 60
- Mathis, J.S., 1994, *ApJ*, 422, 176
- Mathis, J.S., Ruml, W., & Nordsieck, K.H., 1977, *ApJ*, 217, 425
- Merrill, P.W., 1934, *PASP*, 46, 206
- Pino, T., Boudin, N., & Bréchnignac, P., 1999, *J. Chem. Phys.*, 111, 7337
- Platt, J.R., 1955, *ApJ*, 123, 486
- Puget, J.L., & Léger, A., 1989, *ARA&A*, 27, 161
- Purcell, E.M., 1976, *ApJ*, 206, 685
- Rai, R.K., & Rastogi, S., 2010, *MNRAS*, 401, 2722
- Rouillé, G., Arold, M., Staicu, A., *et al.*, 2007, *J. Chem. Phys.*, 126, 174311
- Ruiterkamp, R., Cox, N.L.J., Spaans, M., *et al.*, 2005, *A&A*, 432, 515
- Ruiterkamp, R., Halasinski, T., Salama, F., *et al.*, 2002, *A&A*, 390, 1153
- Salama, F., Tan, X., Biennier, L., *et al.*, 2008, *BAAS*, 40, 187
- Salama, F., & Allamandola, L.J., 1992, *ApJ*, 395, 301
- Salama, F., & Allamandola, L.J., 1992, *Nature*, 358, 42
- Salama, F., Joblin, C., & Allamandola, L.J., 1995, *P&SS*, 43, 1165
- Sellgren, K., 1984, *ApJ*, 277, 623
- Shapley, H., & Curtis, H.D., 1921, *Bull. Nat. Res. Council*, 2, 217
- Siebenmorgen, R., & Kruegel, E., 1992, *A&A*, 259, 614
- Staicu, A., Krasnokutski, S., Rouillé, G., Henning, T., & Huisken, F., 2006, *J. Mol. Struct.*, 786, 105

- Stecher, T.P., 1965, ApJ, 142, 1683
- Steglich, M., Jäger, C., Rouillé, G., *et al.*, 2010, ApJ, 712, L16
- Tan, X., Biennier, L., Cami, J., & Salama, F., 2005, IAU Symp., 235, 70P
- Trumpler, R.J., 1930, Lick Obs. Bull. XIV, 154
- van de Hulst, H.C., 1957, Light scattering by small particles (Wiley)
- van der Zwet, G.P., & Allamandola, L.J., 1985, A&A, 146, 76
- Verstraete, L., Léger, A., D'Hendecourt, L., Defourneau, D., & Dutuit, O., 1990, A&A, 237, 436
- Weingartner, J.C., & Draine, B.T., 2001, ApJ, 548, 296

THE DIFFUSE INTERSTELLAR BANDS IN HISTORY AND IN THE UV

T.P. Snow and J.D. Destree¹

Abstract. The diffuse interstellar bands (DIBs) have been known of since 1922, but their carrier molecules remain unidentified to this day. We present a brief history of DIB observations, followed by a list of constraints any suggested origin must face, and finally a preview of current research for ultraviolet DIBs using the *Cosmic Origins Spectrograph* on the *Hubble Space Telescope*. We conclude that PAHs are consistent with all the listed constraints, but that PAHs may not be the only molecular species responsible for the DIBs.

1 Introduction

The discovery of the first known diffuse interstellar bands (DIBs) was published in 1922 by Mary Lea Heger, then a graduate student at the Lick Observatory (Heger 1922). After almost a century, the DIBs are now recognized as a main reservoir of organic material in the galaxy – but their origin remains unknown. Some characterize the DIBs as the oldest spectroscopic mystery in all of science. Now, PAHs are among the leading candidate as their carrier molecules.

Recent review papers are Herbig (1995), Snow (2002), Krelowski (2002), and Sarre (2006). An on-line DIB bibliography, listing all published papers on DIBs, can be found at: <http://dibdata.org/>.

This paper is divided into sections as follows: a brief history of DIB observations; the molecular origin of the DIBs; properties of the DIBs; the possible role of PAHs as carriers of the DIBs; and a report of the first search for UV DIBs done with the *Cosmic Origins Spectrograph (COS)* recently installed on the *Hubble Space Telescope (HST)*.

¹ Center for Astrophysics and Space Astronomy, Department of Astrophysical and Planetary Sciences, University of Colorado at Boulder, Campus Box 389, Boulder, CO 80309-0389, USA

2 History of DIB observations

In 1921, while Mary Lea Heger was making observations of “stationary” (*i.e.* interstellar) atomic sodium absorption lines in stellar spectra, she noted the presence of two broad features at 5780 and 5797 Å that appeared to be interstellar in origin (Heger 1922). Heger took little notice of these features, other than to tabulate them, and it was more than a decade later when Paul Merrill began the first of many systematic studies of the bands.

At about the time when Merrill became actively involved in the problem, several noted astronomers from other fields weighed in with comments on the possible origin of the DIBs (Merrill 1934). Henry Norris Russell, Pol Swings, Meghnad Saha, and Otto Struve, all of them among the fathers of modern astrophysics, commented that the DIBs were likely to have molecular origins. Later, Gerhard Herzberg also became interested in the problem and spent significant effort in attempting to identify possible molecular carriers, though nothing definitive came of this.

In the interval between the 1930s and the 1970s, however, most astronomers interested in the DIB problem favored a non-molecular origin. Instead of gas-phase molecules in the interstellar medium (ISM), dust grains with impurity centers came into vogue. The movement away from molecular explanations was based primarily on the good correlation of DIB strength with interstellar dust extinction, and on perceived improbability of forming and maintaining a significant population of molecules in the diffuse ISM where the DIBs reside. Friedman *et al.* (2010) summarized the literature on DIB/dust extinction.

An important point to note is that none of the correlations with dust parameters were perfect, implying there is no simple relation between dust and DIBs.

3 Molecular origins of the DIBs

One of Herzberg’s associates, Alexander E. Douglas, published a very significant paper suggesting that small carbon chain molecules could be the carriers, an idea supported by other authors soon after (Danks & Lambert 1976; and Smith *et al.* 1977).

The impetus for the return to the original idea of molecular origins for the DIBs came from several directions: (1) by the 1960s, astronomers had discovered ion-molecule chemistry (long known by then to atmospheric chemists), whose high reaction rates could explain how significant molecular abundances could persist in the interstellar gas; (2) also starting in the 1960s, radio astronomers were beginning to detect rotational emission transitions from interstellar molecules in dark interstellar clouds, lending credence to the general idea that molecules could form and survive in space; (3) in the 1980s strong evidence was found for very large interstellar molecules, specifically the polycyclic aromatic hydrocarbons (PAHs); (4) at about the same time, accurate linear detectors such as CCDs revolutionized observations of the DIBs, allowing for the measurement of very precise band profiles and strengths, far surpassing the older photographic spectra and settling

a number of issues such as the presence or absence of weak emission wings; and (5) last, but by no means least, in the 1980s scientists from other fields such as chemistry began to take notice of the DIB problem and to lend their expertise to its solution. Chemists are now among the leading users of telescopes for spectroscopic observations of the DIBs, and astronomers have begun to collaborate with chemists in laboratory chemistry experiments on candidate DIB carriers (see the review by Bierbaum *et al.* in this volume).

In short, starting in the 1980s, the DIB problem has achieved a level of celebrity that it lacked for the first 60 years following Heger's discovery, and has risen to a level of awareness that, we can hope, will lead to a timely resolution.

4 Properties of the DIBs

The list below mentions several properties of the DIBs that any successful assignment must explain.

Limited wavelength region: Most are in the red range; almost none are in the blue.

Generally weak strengths: DIBs have very small depths, there are none below 20 percent down from the continuum. Most are less than 5 percent below continuum and less than 30 mÅ in equivalent width.

Specific widths: The broad DIBs are up to 20 Å wide, while the narrow ones are less than 1 or 2 Å wide.

Cloud type dependent: Slightly different sets of DIBs are seen in different environments; they are not constant everywhere. One factor seems to be cloud density, from diffuse to translucent.

Lack of saturation: All DIBs, whether strong or weak, grow linearly with increasing extinction.

Not circumstellar: Several studies of various types of stars with circumstellar material do not show DIBs, despite many searches.

Well-correlated with extinction: All correlations with extinction are good (meaning correlation coefficients are generally above 0.7), but they are far from perfect. This includes UV extinction.

Well-correlated with atomic hydrogen: DIBs are significantly better correlated with atomic hydrogen than with molecular hydrogen.

Poor correlations between DIBs: Different authors have defined different sets or "families" of the DIBs that seem to be well correlated. Only one pair of DIBs comes close to being perfectly correlated.

Invariant central wavelengths: DIB central wavelengths show little to no shift between sightlines, except for Doppler shifts with cloud motion.

Distinct profiles: Many DIBs are asymmetric, though some of the broad ones are symmetric. The profiles are invariant in most lines of sight.

Intrinsic structure: Some narrow DIBs show structure possibly consistent with rotational bands. This is not caused by Doppler shifts, as they are the same everywhere. Broad DIBs generally do not show structure.

Rarely found in emission: DIBs in emission have only been observed in the Red Rectangle and toward one other star.

Lack of emission wings: No DIB has shown emission wings in any environment.

Lack of polarization: Several DIBs have been studied in searches for polarization, with no positive results.

Reasonable elemental composition: Expectations about ISM gas composition should be consistent with the cosmic abundances of common elements.

Lack of UV DIBs: Recent searches have shown that any UV DIBs are weak and do not resemble strong DIBs such as $\lambda 4428$.

5 PAHs as DIB carriers

Neutral PAHs tend to have their spectral lines and bands in the UV, which is one reason for thinking ionized PAHs are reasonable candidates for the DIBs carriers (Crawford *et al.* 1985; Léger & d’Hendecourt 1985; and van der Zwet & Allamandola 1985). The neutral/ion ratio depends in the size of the PAH – the larger the neutral, the greater the tendency to be singly ionized and, thus, to have their spectra in the visible range (Leger & d’Hendecourt 1985; Bakes & Tielens 1994; Salama *et al.* 1996; Le Page *et al.* 2001, 2003).

It could be that ionized PAHs are responsible for most DIBs because of their better correlation with H I than with H₂ (Fig. 1). In this scenario, the C₂ DIBs (A set of several DIBs that correlate well with $N(C_2)/E(B - V)$, Thorburn *et al.* 2003) could be located deeper in clouds, where H₂ dominates.

The differing physical conditions from cloud to cloud could explain the so-called “families” of DIBs. For example, despite several searches (summarized in Luna *et al.* 2008), no DIBs have been found in circumstellar environments, where the physical conditions are different from interstellar clouds.

Since PAHs are composed of common elements, the DIB composition requirements are easily met.

The other criteria listed above apply to almost any hypothesis on DIBs origin, except those involving solid-state transitions in dust grains. Note that molecules adhering to dust grains are still reasonably possible DIB carriers.

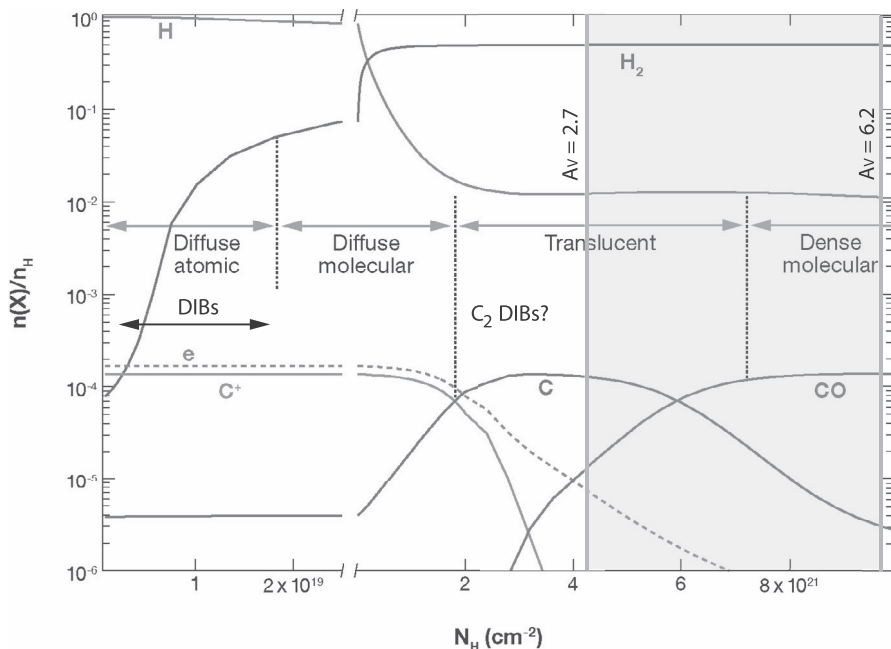


Fig. 1. The physical regimes of the interstellar medium. The ionization levels are shown for hydrogen and carbon, as those species dominate, from diffuse to dense interstellar clouds. The horizontal lines show which types of clouds host the DIBs. The shaded area shows the region now available with the *COS*.

6 UV DIBs

Previous studies have failed to find convincing evidence of DIBs below 3200 \AA (Snow *et al.* 1977; Seab & Snow 1985). These searches were confined to stars no fainter than about fourth magnitude (*Copernicus*) to seventh magnitude (*International Ultraviolet Explorer*). The *COS* can observe reddened stars to tenth magnitude with E_{B-V} values of up to 1.5 magnitudes. Hence the *COS* has a much better chance of finding UV DIBs than any previous instruments.

Details on the design and performance of the *COS* can be found in Green *et al.* (2010, in prep.) and Osterman *et al.* (2010, in prep.). Figure 2 shows the extinction limits of the *COS* and several other UV instruments with comparable spectral resolutions. Depending on cloud type as shown by R_V (which denotes the curvature of the extinction curve, in which small values mean high UV extinction and high values mean low UV extinction), we see that the *COS* is far more sensitive than other instruments in searches for UV DIBs.

We have published one paper on UV DIBs using archival data, finding a few features (Destree & Snow 2009). These unidentified features are all weak and narrow, nothing comparable to the 4428 \AA or 5780 \AA features. But we note that broad DIBs were not included in the search, because the *HST* spectrograph we used

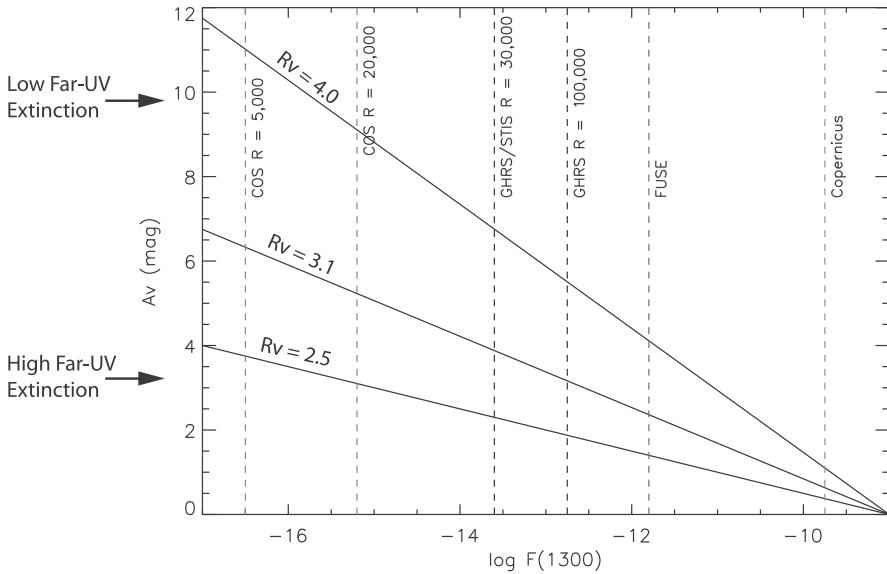


Fig. 2. A comparison of several ultraviolet spectrographs, showing the flux limits (below) and the visual extinction by magnitudes (on the vertical axis). The numbers at the top indicate the spectral resolutions of the various instruments. With low UV extinction (high R_V values), the *COS* can observe dense clouds; with high extinction, the *COS* is more limited, but several magnitudes more sensitive than any previous UV spectrograph.

(the *STIS*) is an echelle design with many spectral orders covering less than 10 \AA each. It is difficult to join orders and match them seamlessly enough to be sure about any broad features. Also, distinguishing between DIBs and instrumental blemishes presents a significant challenge given the current data archive.

The *COS* has similar problems, though not as severe. In the far UV, meaning approximately 1100 \AA to 1700 \AA , there are two wide spectral bands whose central wavelengths are adjustable. Wide DIBs should be seen, if present. In the near UV ($\sim 1900 \text{ \AA}$ to 3200 \AA), the spectrograph is not as efficient and does not lend itself to a search for UV DIBs.

In a preliminary search of *COS* data we found a few unidentified features, which are apparently weak, but we have more work to do before we can make any definitive conclusions. Unfortunately, we have no observation of unreddened stars of the spectral types to use for comparison, a standard technique for finding visible-wavelength DIBs. Comparison stars or stellar models may be necessary if we want to find very weak or broad UV DIBs.

7 Final comments

All the evidence we have so far fits PAHs as the DIB carriers. But PAHs are by no means the only molecular family that might be consistent with the observations.

It is not necessary to assume that only one family is responsible for the DIBs; it could be a mixture of several different species. We should be careful to have open minds.

This research was supported by NASA grant NNX08AC14G.

References

- Bakes, E.L.O., & Tielens, A.G.G.M., 1994, *ApJ*, 427, 822
Crawford, M.K., Tielens, A.G.G.M., & Allamandola, L.J., 1985, *ApJ*, 293, L45
Danks, A.J., & Lambert, D.L., 1976, *MNRAS*, 174, 57, L25
Douglas, A.E., 1977, *Nature*, 269, 130
Destree, J.D., & Snow, T.P., 2009, *ApJ*, 697, 684 (erratum: *ApJ* 702, 823)
Friedman *et al.*, 2010, *ApJ*, submitted
Green, J., *et al.*, 2010, *ApJ*, in preparation
Heger M.L., 1922, *Lick Observatory Bull.*, 10, 337, 146
Herbig, G.H., 1995, *ARA&A*, 33, 19
Herzberg, G., 1955, *Mem. R. Soc. Liege, Serie*, 15, 326
Krelowski J., 2002, *Adv. Space Res.*, 30, 1395
Leger, A., & d'Hendecourt, L., 1985, *A&A*, 146, 81
Le Page, V., Snow, T.P., & Bierbaum, V.M., 2001, *ApJS*, 132, 233
Le Page, V., Snow, T.P., & Bierbaum, V.M., 2003, *ApJ*, 584, 316
Luna, R., Cox, N.L.J., Satorre, M.A., *et al.*, 2008, *A&A*, 480, 133
Merrill P.W., 1934, *PASP*, 46, 206
Osterman, S., *et al.*, 2010, *ApJ*, in preparation
Russell, H.N., 1935, *MNRAS*, 95, 610
Saha, M.N., 1937, *Nature*, 139, 840
Salama, F., Bakes, E.L.O., Allamandola, L.J., & Tielens, A.G.G.M., 1996, *ApJ*, 458, 621
Sarre, P.J., 2006, *J. Molec. Spectr.*, 238, 1
Sarre, P.J., Miles, J.R., & Scarrott, S.M., 1995, *Science*, 269, 674
Seab, C.G., & Snow, T.P., Jr., 1985, *ApJ*, 295, 485
Smith, W.H., Snow, T.P., & York, D.G., 1977, *ApJ*, 218
Snow, T.P., Jr., York, D.G., & Resnick, M., 1977, *PASP*, 89, 758
Snow, T.P., 2002, *Spectrochimica Acta Part A*, 57, 615
Swings, P., 1937, *MNRAS*, 97, 212
Thorburn, J.A., *et al.*, 2003, *ApJ*, 584, 339
van der Zwet, G.P., & Allamandola, L.J., 1985, *A&A*, 146, 76

THE PAH-DIB HYPOTHESIS

N.L.J. Cox¹

Abstract. In this contribution I review the PAH-DIB hypothesis. Firstly, I list several properties of PAHs and their behaviour and expected signatures in space. Next, I give an overview of the current observational insights on the DIB carriers. I conclude with a brief description of recent results on the search for the DIB carriers and the prospects we have for identification.

1 Introduction: The diffuse interstellar band problem

The discovery of stationary absorption lines toward spectroscopic binaries prompted the discovery of the interstellar medium (Hartmann 1904). In the 1930s an increasing number of the narrow absorption bands were identified with *e.g.* ionized titanium, neutral potassium, CH and CH⁺. However, a handful of broader bands could not be identified. Merrill *et al.* (1938) presented the first detailed study of several of these so-called “diffuse” interstellar bands (DIBs). They found these absorption features to correlate roughly with the amount of interstellar dust inferred from the apparent reddening of stars. Also, they found a good correlation with atomic gas phase species. Based on their observations they concluded that indeed these DIBs could not be due to atoms but their carriers would likely be either related to grains or to larger gas-phase molecules (see also Snow & Destree, elsewhere in this volume). Despite many efforts over the last decades, to this date the carriers of the DIBs remain an illusive component of the diffuse interstellar medium (ISM).

2 The PAH-DIB hypothesis

In the May 1985 issue of *A&A* both Van der Zwet *et al.* and Léger *et al.* stipulated explicitly the so-called PAH-DIB hypothesis. Shortly afterwards, June 1st 1985,

¹ Instituut van Sterrenkunde, K. U. Leuven, Celestijnenlaan 200 D, Leuven, Belgium;
e-mail: nick.cox@ster.kuleuven.be

Crawford *et al.* published a paper in similar vein in ApJ. The basic idea of the PAH-DIB hypothesis proposed by these authors states that:

polycyclic aromatic hydrocarbons (PAHs) are predicted to be the carriers of (some of) the diffuse interstellar bands¹.

Essentially this was a direct follow-up on the pioneering work by Allamandola *et al.* (1985) and Puget *et al.* (1985) in which it was shown that PAHs emit in the unidentified infrared (UIR) bands due to excitation upon absorption of optical-UV photons. In this contribution on the connection between PAHs and the DIB carriers I will also consider related large molecules such as fullerenes, nanotubes and carbon rings. Next, I will highlight the different arguments for this connection.

3 Properties of PAHs and their behaviour in space

The arguments favouring PAHs as DIB carriers follow directly from the properties of PAHs (many of which were already listed in the three seminal papers mentioned above):

- PAHs (or more generically aromatics) are very abundant in space as evidenced from the ubiquitous presence in space of the UIR emission bands.
- PAHs, in particular if compact, can be very stable against photo- and thermo-dissociation. Therefore, a significant number density could survive in the harsh ISM.
- PAHs and their ions (cations or anions) have transitions in the near-UV, visible to near-infrared. Wavelengths of the strongest bands depend strongly on the size, the symmetry (shape) and ionization state of the considered PAH. Small to medium sized ionized PAHs have spectra dominated by one strong transition. This can be a broad & strong UV/visible band or a narrow & weak visible/near-IR band, depending whether the ionized PAH is compact or not. This can explain the distribution of DIBs between broad/strong and weak/narrow bands.
- Laboratory spectroscopy of PAHs in Ne/Ar matrix isolation shows indeed strong bands in the DIB range. However, inaccuracies in position and band broadening due to the matrix environment make it impossible to assign specific bands in observations; Theoretical calculations support this conclusion but also lack sufficient accuracy. Unfortunately, laboratory gas-phase spectra of PAHs in interstellar conditions are still very difficult to obtain (Pino *et al.*, elsewhere in this volume).
- Possibly many stable PAH configurations could be formed, and thus give rise to many absorption lines.

¹Historical note: Interestingly, Platt (1956) and Donn (1968) already proposed “PAHs” to explain the reddening curve. Several others proposed polyatomic molecules “carbon chains/rings” as DIB carriers; *e.g.*: Merrill (1938), Danks & Lambert (1976), Smith *et al.* (1977), Douglas (1977). In addition, much was already known about UV/visible spectra and molecular properties of PAHs (*e.g.* Clar 1964; Birks 1970).

- Diffuse cloud models show that PAH ionization and hydrogenation levels are sensitive to the local physical conditions, dust extinction properties, and the effective radiation field (Bierbaum *et al.* and Montillaud *et al.*, elsewhere in this volume). A significant fraction of PAHs will be singly positively ionized (typical ionization potentials of PAHs are between 5 to 8 eV). This provides a natural explanation for the lack of correlation between DIBs.
- PAHs and/or related carbonaceous material can also account for the 2175 Å UV bump (Mulas *et al.*, elsewhere in this volume).

From the inferred presence of PAHs in space (through the UIR emission bands) and the particular chemical and physical properties of PAHs listed above one could already predict that these molecules should also give rise to electronic absorption lines in the UV/visible/near-IR range.

4 Observational insights on the DIB carriers: Are they PAHs?

There is growing observational support to assign the DIB carriers to PAHs (and/or other closely related molecules). This section presents the insights on the DIBs from an observational point of view. The reader is also referred to the excellent reviews by Herbig (1995) and Sarre (2006) for additional details and references.

- DIBs show a large variety of profiles. Widths range from 0.5 to 30 Å (or 2–80 cm⁻¹). These widths exclude atomic or diatomic carriers and suggest polyatomics. Several narrow DIBs have a pronounced substructure. Broad DIBs are not known to show substructure. The 6613 Å DIB substructure (peak separation) changes consistently with temperature. DIB linewidth and line shape can be explained by rovibronic contours and line broadening due to internal conversion for medium sized molecules (*i.e.* PAHs containing 20–30 carbon atoms or the C₆₀ fullerene).
- Searches for polarisation of the DIB profiles have set stringent upper limits to the polarization efficiency of the carriers. This is indicative of a carrier that is not attached or part of (*i.e.* an impurity) the dust grains causing the continuum polarization.
- The signature of these bands can be observed to stunning similarity in galactic and extragalactic regions. DIBs have been observed to reside in most Local Group galaxies (*e.g.* LMC, SMC, M 31, M 33), as well as in more distant spiral galaxies and starburst galaxies and even beyond toward Damped Lyman-Alpha systems (*e.g.* Cox & Cordiner 2008). DIB carriers are therefore ubiquitous (just as the UIR emission bands) throughout the Universe (in space and time). Formation routes and conditions are clearly universal.
- Most DIBs show only a marginal correlation with each other. One of the few exceptions seems to be the 6196 Å and 6613 Å DIB pair. This implies that there is a unique carrier for each diffuse band (*i.e.* 1 DIB for 1 PAH; where the latter can be a specific – ionization/hydrogenation – state of a particular PAH structure).

- DIB strengths are only loosely correlated with the total amount of dust and gas. There appears to be one exception to the rule. The 8620.4 Å “Gaia” DIB shows a strong correlation with reddening, $E(B - V)$, although some intrinsic scatter is still observed. Possibly its carrier is more closely related to dust grains than others. DIB strengths have been compared to many other environmental parameters that give information on the interstellar clouds. Positive correlations are observed for most cases although this may often be simply the result of averaging several individual clouds along distant sightlines. Large variations in DIB strength are observed between single clouds that contain similar amounts of gas and dust.
- Band strength ratios are affected by the effective UV field. In particular the 5780/5797 ratio can be used as a tracer of the effective interstellar radiation field (ISRF) strength.
- DIB families (*i.e.* bands that behave in a similar sense) reflect the interstellar conditions which determine locally the relative importance of neutrals, cations and anions.
- Until this date the DIBs are only observed to reside in the diffuse-to-translucent ISM (probed by sightlines toward stars). No DIBs have been conclusively found to be present in other astrophysical environments. For example, evolved stars are known factories of dust and complex molecules and could therefore contribute to the production of PAHs. However, recent studies show that DIB carriers are very weak, if not absent, in circumstellar environments of post-AGB stars - thus the carriers do not form or conditions to excite these transitions are not met.

5 Search for DIB carriers

The success of laboratory efforts to measure spectra of molecules in the gas-phase has driven the search for carbon chains in the ISM. Maier *et al.* (2001, 2002) obtained laboratory spectra of C_3 and C_5 but only detected the former in a few translucent clouds. In addition, the diacetylene cation (HC_4H^+) is proposed to match with the 5069 Å DIB (Krelowski *et al.* 2010). There have been no other positive results yet for other neutral, cationic and anionic linear carbon-chain radicals measured in gas-phase (Tulej *et al.* 1998; Motylewski *et al.* 2000). Increasingly sensitive astronomical spectra could well reveal these intrinsically weak bands in the future. Further progress in laboratory experiments have yielded the first gas-phase spectra of small PAHs. Iglesias-Groth *et al.* (2008, 2010) found (new) absorption features, toward an interstellar region with anomalous microwave emission, at wavelengths predicted for both naphthalene ($C_{10}H_8^+$) and anthracene ($C_{14}H_{10}^+$) cations. They conclude that 0.008% of the carbon budget is contained in the two molecules. Linnartz *et al.* (2010) studied an acetylene plasma and found a band coinciding with the 5849 Å DIB. A specific molecular assignment of the carbon based carrier could not be made. Similar results by Reilly *et al.* (2007) showed that radical species produced by discharge of benzene give rise to an absorption band coincident with a strong DIB at 4760 Å.

One of the more tentative assignments is perhaps that of C_{60}^+ to two near-infrared bands at 9577 and 9632 Å. Early after its discovery C_{60} was proposed as contributing both to the UIR bands and the DIBs (*e.g.* Kroto *et al.* 1985; Léger *et al.* 1988). Sellgren *et al.* (elsewhere in this volume) report detection and assignment of C_{60} in the IR. Optical laboratory spectra of $C_{60}^{+/-}$ in the gas-phase are needed to detect this molecule in the visual range.

However, it is important to note here that despite identifying several new interstellar features none of the over 200 diffuse bands observed in the visible spectrum has been identified yet.

6 Prospects

- The PAH-DIB proposal provides a plausible working hypothesis to approach the issue of identifying the DIB carrier(s).
- Alternative candidate carriers can not be dismissed, although the carriers are very likely large carbonaceous gas phase molecules that are stable, UV resistant, but sensitive to the local cloud conditions, in particular the ISRF.
- Spectroscopic signatures in both the UV and the near-IR are predicted for many (neutral/cation) PAHs. Surveys with COS/HST (see Snow & Destree, elsewhere in this volume) and X-Shooter/VLT are underway. The presence of electronic absorption bands in the near-IR would be a direct test of the presence of large ionized molecules in space. At present only two interstellar absorption band detections, at 1.18 and 1.32 μm (Joblin *et al.* 1990), have been put forward. The lack of near-IR/UV signatures of PAHs could put severe constraints on the properties of PAHs in the diffuse/dense ISM.
- It is crucial to explore environments other than diffuse/translucent clouds. In particular, circumstellar envelopes of evolved stars (“PAH” factories) are interesting objects.
- Identification of specific PAHs in far-IR could be directly verified in the UV to near-IR (or *vice versa*) as discussed in Joblin *et al.* (elsewhere in this volume).
- The conditions for efficient formation of PAHs are not yet understood. Either this could occur via evolved stars or supernovae that produce the dust content of the Universe or, alternatively, these are produced in-situ in the ISM. The formation process could either happen bottom up starting with small building blocks (C, CH, C_2H_2 , etc.) or alternatively, top down, as fragments from large carbonaceous structures (very small grains).
- Weeding out impossible isomers is another key element to the PAH-DIB hypothesis. Another important point in this respect is the PAH size distribution. Is it dominated by small or larger PAHs, by peri- or catacondensed PAHs?

References

- Allamandola, L.J., Tielens, G.G.M., & Barker, J.R., 1985, *ApJS*, 71, 733
- Birks, J.B., 1970, *Photophysics of Aromatic Molecules* (John Wiley and Sons, Ltd., London)
- Clar, E., 1964, *Polycyclic Hydrocarbons* (Academic Press, London)
- Cox, N.L.J., & Cordiner, M.A., 2008, *IAU Symp.*, 251, 237
- Crawford, M.K., Tielens, A.G.G.M., & Allamandola, L.J., 1985, *ApJ*, 293, 45
- Danks, A.C., & Lambert, D.L., 1976, *MNRAS*, 174, 571
- Donn, B., 1968, *ApJ*, 152, 129
- Douglas, A.E., 1977, *Nature*, 269, 130
- Hartman, J., 1904, *ApJ*, 19, 268
- Herbig, G.H., 1995, *Ann. Rev. Astron. Astrophys.*, 33, 19
- Iglesias-Groth, S., Manchado, A., García-Hernández, D.A., González Hernández, J.I., & Lambert, D.L., 2008, *ApJ*, 685, 55
- Iglesias-Groth, S., Manchado, A., Rebolo, R., *et al.*, 2010 [[arXiv 1005.4388](https://arxiv.org/abs/1005.4388)]
- Joblin, C., D'Hendecourt, L., Leger, A., & Maillard, J.P., 1990, *Nature*, 346, 729
- Krelowski, J., Beletsky, Y., Galazutdinov, G.A., *et al.*, 2010, *ApJ*, 714, 64
- Kroto, H.W., Heath, J.R., O'Brien, S.C., Curl, R.F., & Smalley, R.E., 1985, *Nature*, 318, 162
- Leger, A., & D'Hendecourt, L., 1985, *A&A*, 146, 81
- Leger, A., D'Hendecourt, L., Verstraete, L., & Schmidt, W., 1988, *A&A*, 203, 145
- Linnartz, H., Wehres, N., van Winckel, H., *et al.*, 2010, *A&A*, 511, 3
- Maier, J.P., Lakin, N.M., Walker, G.A.H., & Bohlender, D.A., 2001, *ApJ*, 553, 267
- Maier, J.P., Walker, G.A.H., & Bohlender, D.A., 2002, *ApJ*, 566, 332
- Merrill, P.W., & Wilson, O.C., 1938, *ApJ*, 87, 9
- Motylewski, T., Linnartz, H., Vaizert, O., *et al.*, 2000, *ApJ*, 531, 312
- Platt, J.R., 1956, *ApJ*, 123, 486
- Puget, J.L., Leger, A., & Boulanger, F., 1985, *A&A*, 142, 19
- Reilly, N., Kokkin, D.L., Joester, J.A., *et al.*, 2007, *Molec. Space Lab.*, 85
- Sarre, P.J., 2006, *J. Molec. Spectrosc.*, 238, 1
- Smith, W.H., Snow, Jr., T.P., & York, D.G., 1977, *ApJ*, 218, 124
- Tulej, M., Kirkwood, D.A., Pachkov, M., & Maier, J.P., 1998, *ApJ*, 506, 69
- Van der Zwet, G.P., & Allamandola, L.J., 1985, *A&A*, 146, 76

ELECTRONIC SPECTROSCOPY OF PAHS

T. Pino¹, Y. Carpentier¹, G. Féraud¹, H. Friha¹, D.L. Kokkin²,
T.P. Troy², N. Chalyavi², Ph. Bréchignac¹ and T.W. Schmidt²

Abstract. Polycyclic aromatic hydrocarbons are a class of molecules of broad interest that has long been explored by various spectroscopic techniques. The electronic spectroscopy of these species is of particular interest since it provides a framework for the understanding of the electronic structure of large polyatomic molecules. Such studies also allow the systematic investigation of electronic relaxation mechanisms in large molecules. In this review, we focus on the gas-phase experimental work on such systems and present the latest progress. We also underline the challenges that remain to be tackled. A focus on the understanding of the electronic relaxation pathways at work in gas-phase PAHs will also be presented, as well as their possible manifestation in space.

1 Introduction

Polycyclic Aromatic Hydrocarbons (PAHs) are found in many diverse environments on earth and in space, either from natural or industrial sources. Because of their implication in various physico-chemical phenomena, many studies have been devoted to them. This peculiar class of molecules has also received attention from fundamental studies towards a better understanding of molecular structure and dynamics. A comprehensive review of their electronic structure can be found in Clar's series of books (Clar 1964a; Clar 1964b), where the basic PAH science may also be found. A few examples illustrate the importance of PAH science and their profound impact on molecular science. The study of their quantum yield of fluorescence during the sixties and early seventies (Hunt *et al.* 1962; Siebrand 1967) led to major developments in the understanding of intramolecular dynamics and radiationless transitions in particular (Englman & Jortner 1970). At the beginning of the eighties, with the advances of molecular beam techniques, the first

¹ Institut des Sciences Moléculaires d'Orsay, Univ Paris Sud, CNRS, France

² School of Chemistry, The University of Sydney, NSW 2006, Australia

systematic studies of their gas-phase electronic spectra were performed. Two major breakthroughs in molecular science were thus achieved: the first high-resolution spectrum of a large polyatomic molecule, fluorene, was measured in 1984 (Meerts *et al.* 1984) and the first study of intramolecular vibrational energy redistribution (IVR) in such molecules was measured for anthracene using a picosecond laser (Felker & Zewail 1985; Felker & Zewail 1985b). Such studies mark the birth of time-resolved intramolecular dynamics in large polyatomic systems.

PAHs are thought to carry at least some of the diffuse interstellar bands (DIBs) (Léger & d'Hendecourt 1985), some of the Red Rectangle emission bands (Sarre 2006; Sharp *et al.* 2006), the aromatic infrared bands (AIBs) (Léger & Puget 1984; Allamandola *et al.* 1985) and may have a significant contribution to the “bump” at 217 nm (Joblin *et al.* 1992; Li & Draine 2001). All these spectral features imply electronic absorption and/or intramolecular dynamics such as electronic relaxation and IVR. However, although PAH science may be thought as mature, the experimental data that are of real pertinence for the identification of interstellar or circumstellar PAHs are rather scarce. In fact, the questions posed by the existence of these compounds in space are all real challenges for laboratory astrophysicists and thus the “PAH hypothesis” has triggered many fundamental studies. However, concerning the electronic spectroscopy of PAHs, only few cations have been spectroscopically investigated in the gas phase (see Salama 2007 for a review), even fewer neutral radicals and no anions. Deep-UV spectra around the bump region at 217 nm are available only for few gas-phase neutral species (Joblin *et al.* 1992; Suto *et al.* 1992). This may seem somehow disappointing, but recent progresses on PAH science may be seen as a prelude for many advances in a relatively near future.

In this review, a focus on the recent progress on the electronic spectroscopy of PAHs will be presented. This review mainly concerns works published after the review of Salama (Salama 2007) and is hopefully pedagogical enough to provide the astrophysicist with the background to evaluate the work that has been achieved and that remains to be done in order to make progress on testing the PAH hypothesis in the laboratory, and enable firm identification of some species. The first section will present the experimental methods that are used or developed, followed by a short tour on the main results in the second section. Conclusions and perspectives will be thus given in a third section.

2 Experimental approaches

2.1 *The constraints for laboratory astrophysics studies of the PAHs*

The PAH hypothesis relies on the molecular rather than solid behavior of the carrier of the AIBs (Puget & Léger 1989). It involves the transient heating mechanism, which may be explained within the framework of molecular physics as follows: after absorption of a starlight photon through an electronic transition, electronic

relaxation takes place dominantly by nonradiative processes and subsequent IVR scrambles the resulting vibrational energy over all accessible vibrational states of the electronic ground state. Thus infrared fluorescence proceeds on the ground electronic state. These AIBs imply very large molecules – up to a few hundreds of carbon atoms – completely isolated *in vacuo* on timescales ranging from a few tens of femtoseconds up to a few seconds.

In order to study the astronomical PAHs in the laboratory, generally gas-phase isolation is a strong requirement, in particular when spectroscopy or intramolecular processes are concerned. Thus, depending on the specific timescales of the mechanism being investigated, several methods for isolation are necessary, but also several experimental methods for interrogation of the molecules as well. Most studies use laser technology that permits the study of ultrafast dynamics with femtosecond lasers or high-resolution spectroscopy with continuous lasers. Therefore, laboratory astrophysics devoted to PAHs necessitates the use of state-of-the-art methods taken from molecular and/or cluster sciences that combine gas phase molecules either in a molecular beam or ion trap with different laser sources and detection methods. In addition, it is best to work on cold or even ultracold PAHs in order to avoid spectral congestion.

2.2 Gas-phase PAHs?

PAHs are not naturally available in the gas phase, except when the experiment uses a gas-phase reactor directly coupled to diagnostics. As such, they have to be vaporised before being studied. Many approaches have needed to be developed since a simple heated oven becomes less efficient at sample vaporization beyond the size of coronene. The most successful method for large molecular systems is laser desorption (Haufler *et al.* 1991). Many different protocols may be adapted to each case, using different wavelength, pulse duration and source geometries.

Neutral PAHs are of prime interest, but cations and radicals are also to be studied. In this case additional ingredients have to be added to produce such species. Laser ionisation (Pino *et al.* 1999), laser photolysis and electric discharge (Romanini *et al.* 1999) are favorite tools for this purpose but these additional steps render the experiment much more complex and only few species have been effectively studied.

Before spectroscopic investigation, it is better to cool the PAH. However heating, desorption, ionization, and discharge are all in favor of producing hot PAHs rather than cold ones. As such, these methods are usually coupled to supersonic expansions in order to cool down the target molecule (Haufler *et al.* 1991). When adding all these techniques, one may realize that not all has been effectively experienced yet! Producing a large PAH cold in the gas phase is, in fact, the most limiting problem for experimental investigation, either because the PAH itself is difficult to produce in large enough quantities or because the necessary densities in the gas phase for a given technique cannot be achieved. However, with the advances on new production methods and with the very useful guidance of quantum

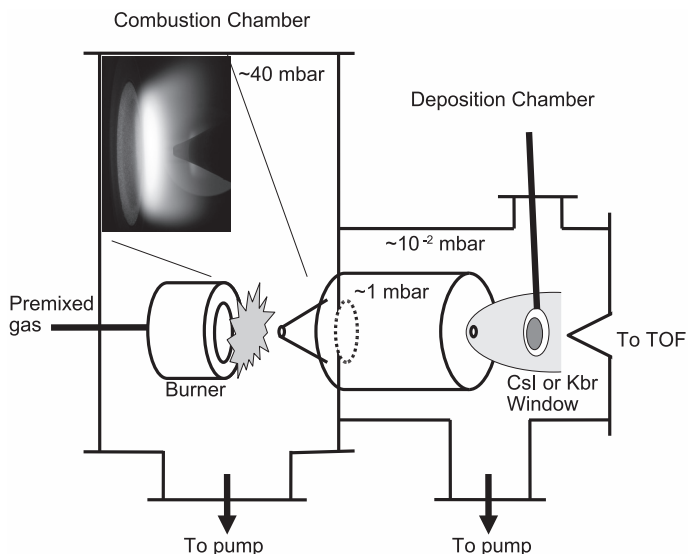


Fig. 1. A schematic view of the experimental set-up that was built at Orsay. The combustion chamber contains the flat burner, cooled by circulating water. The flame is horizontal and the flow (pre-mixed) is maintained at a constant pressure within the chamber, at about a few tens of mbar. The burner is movable along the horizontal axis. The quartz sampling cone (shown) allows species produced at a given distance from the burner to enter the copper thermalisation chamber. This chamber is placed inside the deposition chamber, which is maintained at a pressure of about 10^{-2} mbar under the operating conditions. A window is then placed into the jet that is formed at the end of the thermalisation chamber, where the gas passes through the nozzle. Possible extraction through a skimmer forms a molecular beam at the entrance of a Time-Of-Flight mass spectrometer.

chemical calculations, much progress has been recently reported (Kokkin *et al.* 2008) which may strongly influence our knowledge of PAHs larger than coronene in the near future.

The source of PAHs itself is also of importance. Recent advances in chemical synthesis have led to the production of PAHs up to the $C_{222}H_{42}$ (Simpson *et al.* 2002). In fact, as long as a target PAH is chosen, chemical synthesis is favoured. However gas-phase reactors offer the opportunity to directly produce many of them in the gas phase. Flame and laser pyrolysis are among the most promising of such sources. At Orsay, we have incorporated a low pressure, flat and premixed flame that can be coupled to a time-of-flight mass spectrometer (Fig. 1). Under favorable conditions, a large distribution of PAHs may be produced (Fig. 2). It is remarkable that this PAH distribution is very similar to that obtained in different burning conditions (Apicella *et al.* 2007) and using laser pyrolysis or laser ablation (Jäger *et al.* 2007; Jäger *et al.* 2009).

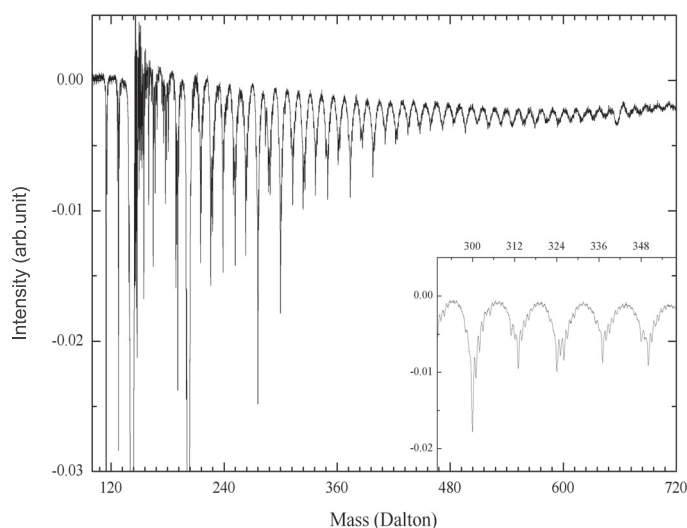


Fig. 2. Mass spectrum measured with the experimental set-up Nanograins at Orsay. The sampled flame was a low pressure (about 80 mbar) of premixed ethylene and oxygen with a C/O ratio of 1.6. Laser ionization was used and the mass spectrum is dominated by PAHs up to a few tens of carbon atoms.

2.3 The experimental techniques

2.3.1 Laser induced fluorescence

Laser Induced Fluorescence (LIF) is the first technique that made the measurement of electronic transitions of PAHs in the gas phase accessible. The first was measured in the group of Smalley and published in 1981 (Beck *et al.* 1981a; Beck *et al.* 1981b). It concerned the naphthalene molecule in its neutral form and presented excitation and dispersed fluorescence spectra. The method is as follows: resonant absorption of a tunable laser through an electronic transition between the electronic ground state and an excited one is measured by collecting the electronic fluorescence from the excited molecule. The fluorescence excitation spectrum is measured by scanning the laser wavelength and monitoring the total fluorescence as a function of the wavelength. It is closely related to the absorption spectrum, only intensity ratios may differ due to differences of the quantum yield of fluorescence of the molecular states. Dispersed fluorescence spectra consist of monitoring the frequency resolved spectra of the fluorescence at a given resonant excitation wavelength. The coupling of both techniques provides information on both ground and excited electronic states, Franck-Condon factors, changes in geometry, dynamics in the excited states and so on. Following advances in CCD technology led by astronomy, two-dimensional fluorescence has been developed.

This consists in measuring excitation and disperse spectra simultaneously (Reilly *et al.* 2006). The strength is a fully allowed characterisation of both states, even from a complex distribution of molecules arising from a gas-phase reactor. Time-resolved fluorescence spectra can also be measured which provides information on the excited state dynamics, such as the contribution of both radiative and nonradiative decay.

2.3.2 Resonant 2-colour 2-photon ionisation spectroscopy

Instead of detecting photons, ions (or electrons) can be measured in combination with a mass spectrometer. In this case, after excitation to a given electronic excited state of the PAH, a second laser (or when possible the same laser) is used to photoionize the molecule, which is the basis of resonant 2-colour 2-photon ionisation spectroscopy – R2C2PI (Duncan *et al.* 1981). The ion or electron current thus traces the resonant absorption during the first tunable step. This method is basically as sensitive as LIF but provides additional information when ions are detected – the mass of the species. This is of importance when dealing with a distribution of PAHs, or unidentified species from a discharge (Reilly *et al.* 2008), for example. If the first laser is tuned to a resonant transition, scanning the second provides the photoionization efficiency curve which reveals the ionization potential (*e.g.* Troy *et al.* 2009). When electrons are detected, the photoelectron spectrum may be used as a projection of the excited state wavefunction onto the cationic molecular states and provides information on the dynamics or the coupling between states in the neutral molecule (Stolow *et al.* 2004). These experiments are generally performed in the time-resolved domain. A similar approach may be performed on anions: The photodetachment rather than the photoionisation is measured, and appearance of the neutral and depletion of the anion must be measured if the detection does not involve the photodetached electrons (Tschurle & Boesl 2006).

2.3.3 Resonant multiphoton dissociation

In the case of the cations, the second ionization potential to access the doubly charged species is generally very high and cannot be easily reached for a R2C2PI technique using benchtop equipment. In addition, aromatic cations are almost all non-fluorescent, *i.e.* the quantum yield of fluorescence is close to zero and electronic relaxation processes are dominated by nonradiative phenomena. Regarding such a situation, mass spectrometry appears as the privileged tool. The signature of the resonant absorption has to be traced through a measurable charge-to-mass ratio change, and involve a change in mass rather than a change in charge via fragmentation of the cation. Actually PAHs are rather stable towards photodissociation. Thus, efficient measurement requires time for measuring slow processes and/or large pulse energies to accelerate the process. To overcome these

limitations, two techniques have been developed: either the cations fragment after absorption of multiple photons (Useli-Bacchitta *et al.* 2010) or the departure of a loosely bound tagging atom (a rare gas atom for example) after absorption of a single photon may be used to trace the absorption spectrum (Bréchnignac & Pino 1999; Pino *et al.* 1999). In the latter case the effect of the presence of the weakly bound rare gas atom has to be carefully investigated in order to properly extract the spectrum of the bare cation. However it has been shown to be the most productive method (Salama 2007) up to now, but the latest developments seem promising to explore and provide novel results on cations (Useli-Bacchitta *et al.* 2010).

2.3.4 Cavity ringdown spectroscopy

Cavity ring down spectroscopy (CRDS) is the only direct absorption method that can be used for any species (O’keefe & Deacon 1988). However, although the sensitivity can be even better than the previously cited methods, the technique suffers from the absence of any two dimensional information which is needed for the identification of the absorbing species if the spectrum is not self-sufficient (via the complete rotational line’s assignment for example). It implies that as long as the spectrum can not be unequivocally assigned, no additional measurements guide the attribution. But, it remains a valuable tool when the other methods are applied, as a cross-check of the absorption spectrum. The principle is as follows: A laser pulse is trapped in an optical cavity and the ringdown time is maximum and defined by the reflectivity of the mirrors, when the laser wavelength is resonant with a transition of the gaseous medium the ringdown time decreases due to cavity loss. Its evolution as a function of laser wavelength traces the absorption spectrum.

2.3.5 Other methods

Other experimental methods do exist and most may be considered as evolutions and improvements upon those cited above. Either the detection or laser scheme changes, offering possibilities for peculiar aspects. Present efforts mainly concern ion or electron imaging for dynamical purposes (Stolow & Underwood 2008), with the development of detectors with time and spatial resolution, as well as optical cavities used under various configurations (Bernhardt *et al.* 2010).

3 Recent progress

3.1 Toward Larger PAHs in the gas phase

Until very recently, the largest molecule conclusively identified in an extraterrestrial environment were the carbon chains HC_{11}N , found in the circumstellar shell of

IRC+10216 by rotational spectroscopy.¹ However, photophysical models of PAHs in interstellar environments conclude that they must contain at least 30 carbon atoms to be sustainable against the weathering photon flux. Prior to 2007, the largest PAH studied as an isolated, free-flying molecule in the vacuum was ovalene, $C_{32}H_{14}$ (Amirav *et al.* 1981). Recently the terrylene $C_{30}H_{16}$, which exhibits a strong transition in the visible range of wavelength, was also studied by LIF in the gas phase (Deperasinska *et al.* 2007). Even these giants are not unambiguously large enough to satisfy the criteria set out by interstellar PAH models.

Troy's all-benzenoid hypothesis motivated the study of those PAHs which can be drawn as isolated benzene rings joined by "single" bonds. A R2C2PI and LIF spectroscopic study of the smallest of these, triphenylene ($C_{18}H_{12}$), was reported by the Sydney laboratory in 2007 (Kokkin *et al.* 2007). By early 2008, an $S_1 \leftarrow S_0$ excitation spectrum of the hexa-*peri*-hexabenzocoronene ($C_{42}H_{18}$: HBC) was obtained (Kokkin *et al.* 2008). This R2C2PI spectrum was recorded following laser desorption of a pressed pellet of HBC in a supersonic expansion of argon. The skimmed beam was interrogated by a pair of laser beams some 30 cm downstream in the extraction region of a TOF-MS. This difficult experiment stands as the record for a PAH studied by gas-phase spectroscopy. Subsequent condensed phase spectra of HBC confirm that these α -bands near 425 nm are extremely weak compared to bands lying in the near ultraviolet (Rouillé *et al.* 2009). It remains for these higher $S_n \leftarrow S_0$ transitions to be recorded in truly isolated molecules. The absence of these signatures in the spectrum of the interstellar gas should provide interesting constraints for interstellar PAH chemistry.

Larger PAHs than HBC have been synthesized. The pioneering organic chemistry of Müllen has produced the monster $C_{222}H_{42}$ - a hexagonal sheet of graphene consisting of 37 separate benzenoid rings whose peripheral carbon are passivated by H (Simpson *et al.* 2002). Before attempting to obtain the R2C2PI spectrum of such a beast, other all-benzenoid PAHs await, such as $C_{78}H_{26}$ and $C_{96}H_{30}$.

3.2 From the visible to the 217 nm bump region absorption of the PAHs

Electronic spectra of PAHs have been generally studied in the vicinity of the first electronic states (Beck *et al.* 1981a). Most of the gas-phase spectra of neutral PAHs were measured in the early 80's by LIF. In the case of the cations, because of the DIBs hypothesis, the electronic absorption spectra were monitored in the visible range (Salama 2007). Of course, matrix isolation spectroscopy provided important measurements, even up to the deep UV. Unfortunately, few were studied in the gas phase around the bump region, most spectra being published in 1992 using synchrotron light sources (Joblin *et al.* 1992; Suto *et al.* 1992). Since that time, nearly no new spectra were published and moreover no cold ones. However

¹Recently, Sellgren *et al.* (2010) reported the detection of the IR emission bands of C_{60} in reflection nebulae (see Sellgren *et al.*, elsewhere in this volume) and Cami *et al.* (2010) reported the detection of C_{60} and C_{70} in a young planetary nebula.

it seems more and more clear that this component of the ISM should contribute significantly to the bump at 217 nm (Mallocci *et al.* 2007).

Recently, using a gas-phase reactor for the production of large PAHs, new insights on their electronic spectra have been obtained. At Orsay, a R2PI experiment coupled to a low-pressure flame has been set up. Electronic spectra of the small aromatics have been recorded from 207 nm up to 330 nm. Nearly 20 spectra have been recorded, assigned to benzene and PAH derivatives with mono- and di-substitution by methyl, vinyl and ethynyl groups (Carpentier *et al.* 2010). Some correspond to known data from vapor phase measurements and others are new. This study focused on species up to pyrene derivatives since the combustion conditions could not produce sufficient and stable enough amounts of larger PAHs for electronic spectra to be recorded. In this experiment, the temperature of the measured PAHs was about 300 K. In the near future, we plan to cool down the extracted PAHs from the flame using a supersonic expansion and extend the study to larger sizes.

Important progress has been performed recently using PAHs produced by laser pyrolysis (Steglich *et al.* 2010). The visible to UV spectra of the molecules dispersed directly on a substrate in the form of thin film and in rare gas matrices were measured. A size dependence could be inferred. Even more the effect of conditions were shown to be very important for the observed band profiles. The matrix isolation spectroscopy data contained considerably more substructures than the thin film. It is clear that gas-phase spectroscopy is a requirement in order to assigned properly the carrier of the bump, even for such a broad and featureless absorption.

3.3 Ultra-high resolution spectroscopy of PAHs

During the last decade, recent advances have allowed ultra-high resolution spectra of some PAHs to be recorded. The developments were performed in the group of M. Baba in Kyoto (Japan). Although the spectra were somehow all known, the unprecedented spectral resolution opened the possibility of a complete analysis, from spectral linewidths to rotational constants and detailed geometries. Azulene, naphthalene, pyrene and perylene, as well as benzene, have all been measured (Baba *et al.* 2009; Yoshida *et al.* 2009; Baba *et al.* 2009b; Semba *et al.* 2009; Kowaka *et al.* 2010). In addition, application of a magnetic field in the laser-molecules interaction zone was performed in order to probe the Zeeman effect. The outcome is a precise measure of the mixing between the first electronic S_1 state with the triplet manifold. All results have revealed that in fact it is very small and that the nonradiative decay is dominated by the internal conversion and not the intersystem crossing.

3.4 The PAHs derivatives: Ions and radicals

As only closed shell PAHs may be purchased from chemical suppliers, these species dominate the spectroscopic PAH literature. However, there exist many PAHs

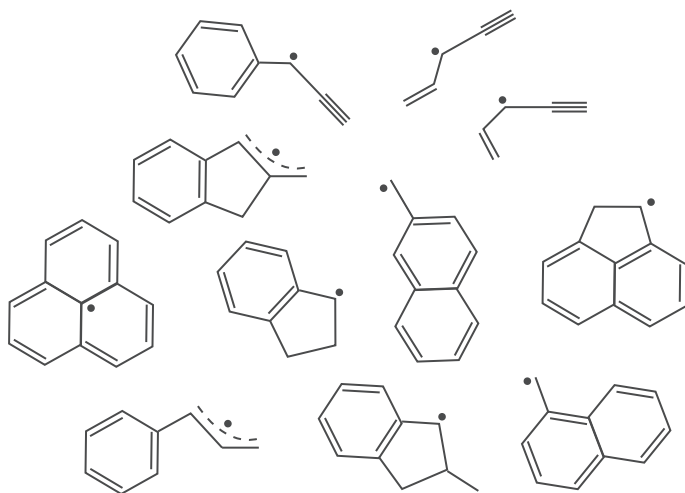


Fig. 3. The collection of aromatic and resonance-stabilized radicals for which excitation spectra have been obtained by the Sydney group. The origin bands lie between 450 nm and 600 nm. While none exhibit a perfect match to any diffuse interstellar band, the naphthylmethyl radicals exhibit spectra in the Red Rectangle emission region (see text).

which are either open-shell or cationic, or both. All of these species have electronic spectra in the visible region, making them especially interesting as DIB candidates. Indeed, many photophysical models predict that a large proportion of interstellar PAHs should be ionized.

3.4.1 Open-shell cations

Most gas-phase spectra of cationic PAHs have been obtained about ten years ago, and have been reviewed in Salama 2007. At Orsay, a new approach is under development with the goal to simplify the photoionisation scheme for the production of the cations. Instead of a R2C2PI process, photoionisation is performed within the supersonic expansion in order to produce cold cationic clusters with a single laser. Test experiments are under progress on naphthalene and its methyl derivatives. In the IRAP (ex-CESR) at Toulouse, thanks to the use of a cold ion trap, investigations of the electronic spectroscopy of cations and their fragments are now possible and should provide challenging data on such species by resonant multiphoton dissociation of the trapped ions, as it was done on the coronene cation (Useli-Bacchitta *et al.* 2010).

3.4.2 PAH radicals

In the past years there have been many new spectra of polycyclic radicals reported, but almost none of radical derivatives. The significance of resonance stability in

aromatic radicals was realized with the observation of the phenylpropargyl radical as the brightest feature, after C_2 , C_3 and CH, in the laser-induced fluorescence spectroscopy of an electrical discharge containing benzene (Reilly *et al.* 2008). Phenylpropargyl is not a true PAH, but could be a precursor to PAH formation in flames and other environments (see Cherchneff 2011 in this volume), given the putative importance of propargyl itself in benzene and subsequently soot formation. The radical can be considered as a benzyl and propargyl radical sharing a carbon, conferring it with a stability, as compared with methyl radical, similar to the sum of those of benzyl and propargyl. Phenylpropargyl, C_9H_7 , which presents an origin transition at 476 nm, is an isomer of the indenyl radical, never reported in the gas phase. An attempt to produce indenyl from indene yielded indanyl radical, C_9H_9 (Troy *et al.* 2009). Indene adds a hydrogen atom barrierlessly, affording the radical presenting a dominant origin at 472 nm, with a true benzylic chromophore. This barrierless addition is of potential interest to interstellar chemistry, where low reaction temperatures predominate. A benzylic chromophore is also presented by 1,2,3-trihydronaphthalene, the spectrum of which was recorded by the Zwier group at Purdue (Sebree *et al.* 2010). This species has its origin near 468 nm, being very similar to indanyl radical in many respects. The Purdue group has also reported the spectra of 1- and 2-hydronaphthalene, the spectra of which are dominated by origins at 528 and 516 nm respectively. Both possess extended conjugation as compared to the benzylic chromophores. The 1-hydronaphthalene is perhaps the more interesting, it being an allylic and a benzylic radical sharing the “radical” carbon. The unligated version, Ph-CHCHCH₂, which is the cinnamyl radical, was observed by the Sydney group very recently (Troy *et al.* 2010). A polycyclic cinnamyl radical, was produced in Sydney by H-loss from the methyl group of 2-methylindene. This radical absorbs principally at 516 nm, in the neighbourhood of the monohydronaphthalenes.

These bicyclic radicals all possess either a benzylic (460–480 nm) or a cinnamylic chromophore (510–530 nm). By extending the naphthalene backbone to one extra carbon we obtain the naphthylmethyl chromophore, with absorptions around 580 nm. The Sydney laboratory has obtained excitation and emission spectra of both CH_2 -Np radicals, $C_{11}H_9$, and the acenaphthyl radical, a tricyclic $C_{12}H_9$ species. The plethora of possible radicals with this chromophore may have a relationship to the emission bands of the red rectangle nebula, which exhibits prominent unassigned emission features in the 580 nm region (Sarre 2006; Sharp *et al.* 2006).

The most symmetric tricyclic PAH radical is the phenalenyl radical, $C_{13}H_9$. Its gas-phase spectrum was recently obtained in the Sydney laboratory, it closely resembles that obtained previously under matrix isolation. The spectrum is not origin dominated as are those of the other aromatic radicals mentioned above. Rather, the origin is small with the spectrum being dominated by e' vibration modes presumably gaining intensity through Herzberg-Teller interactions: the positions are perturbed through Jahn-Teller interactions. A full analysis of this spectrum shall be presented in the near future.

All of these open-shell PAH radicals present an opportunity to produce a different class of PAH cation, closed-shell cations. The closed shell cations possess much higher HOMO-LUMO gaps than similarly sized open-shell cations. As such, their spectra in the visible region should be much sharper than the open-shell cations, and there is the possibility that they emit fluorescence. It will be possible to measure the spectra of such cations in the near future.

3.5 *Nonradiative transitions in PAHs: Present status*

Nonradiative transitions are at the core of the PAH hypothesis. The main concepts should be recalled here. The molecular states are first described within the adiabatic Born-Oppenheimer approximation that separates the electronic and nuclei momenta. This is done at a level beyond the harmonic approximation to account for Fermi resonance at low vibrational energies and wholesale intramolecular vibrational energy redistribution higher up the well. The energy levels are obtained and the overall mechanism may be discussed in term of time-dependent dynamics between bright and dark states. It is noteworthy that such a description belongs to the Bixon and Jortner approach (Bixon & Jortner 1968), while others prefer manipulations of the eigenstates as long as it is possible, which is particularly adapted when ultra-high resolution spectroscopy in the frequency resolved domain provides the complete set of information (Quack 1990). In the case of PAHs, the dominant description is that from Bixon and Jortner. Electronic relaxation can then take place. When it occurs between two states of same multiplicity, the process referred to as internal conversion (IC) and part of (or all) the electronic energy is converted into vibrational energy. Between states of different multiplicity, intersystem crossing (ISC) occurs which relies on spin-orbit coupling. This is generally much slower (by about a million times) for hydrocarbons and the upper (fastest) limit should be found in the nanosecond timescale. Several configurations may be found, depending on the shape of the potential energy surface: The change of geometries and the existence of surface crossings shape the radiationless processes. In the latter case, conical intersections (CI) are thought to play an important role in intramolecular dynamics as it appears more and more than they are more systematic than peculiarities (Yarkony 2001). When relaxation takes place within a particular state, only vibrational energy is concerned and the process is called intramolecular vibrational energy redistribution (IVR). In all cases, the strength of the coupling and the density of states (vibrational and/or electronic) control the nonradiative processes, there being various regimes (weak and strong coupling limit, intermediate case and statistical limit). Very good reviews can be found in the literature for a complete analysis of this topics (Avouris *et al.* 1977; Freed 1978; Medvedev & Osherov 1995).

The PAH family of molecules has long served the exploration of these processes. In particular the energy gap law (EGL) was inferred from measurement of fluorescence lifetime of PAHs in solution and proved to involve ISC (Siebrand 1967). The EGL states that in the statistical limit an exponential dependence of

the nonradiative rates versus the energy gap between the prepared state and the electronic states immediately below is to be found (Englman & Jortner 1970). A summary of nearly all available data is presented in Figure 4. Benzene derivatives, azulene derivatives, neutral and cationic PAHs are reported. Actually, although the EGL was obtained from the ISC rate in neutral PAHs, it is not clear whether in IC such a dependence may be deduced here. The particular role of the CI seems to be very important in the case of ultrafast (below 0.1 ps) electronic relaxation, and recent calculations have shown that these intersections are systematically present in cations (Tokmachev *et al.* 2010). Additionally, in benzene where a CI has long been known to promote IC and quench the electronic fluorescence at a certain excess vibrational energy into the S_1 state (about 4000 cm^{-1}), new insights are becoming available and point to fast ISC as well (Parker *et al.* 2009). In the case of neutral PAHs, the dominant relaxation pathway of the S_1 state was long thought to be ISC, *i.e.* similar to the solution phase. However recent ultra-high resolution measurements of the Zeeman effect point to a weak ISC and a dominant IC (Kasahara *et al.* 2006; Kato *et al.* 2007). In fact the actual strong ground on which electronic relaxation of PAHs were understood is rapidly changing and we expect a new view on this aspect in a near future.

Still, IC is clearly at work in open shell cations and this is completely consistent with the PAH hypothesis. The existence of fast relaxation channels in highly excited states of neutral PAHs remains to be explored, only one study seems to be available Suto *et al.* (1992). The strength of the coupling in radicals or superhydrogenated PAHs is still unknown.

4 Conclusions and outlook

Between our laboratories and others, there has been real progress in obtaining new spectra and sources of PAHs, their radicals and cations since 2007. In Orsay, a new experiment has been built to produce beams of large PAHs from a combustion source, and work progresses on efficiently producing open-shell PAH cations within a molecular beam. The Sydney laboratory has obtained a collection of open-shell PAH radical spectra from electrical discharges, with the view to produce a larger diversity of species. Looking forward, we aim to obtain close-shell PAH cation spectra in the coming years.

The astrophysical PAH hypothesis relies on the concepts of molecular non-radiative processes occurring in the gas phase. Using high-resolution spectroscopy, Baba's group continues to uncover the links between gas phase spectroscopy and the classical ISC studies of PAHs in solution. However, there remains a mismatch in the conditions available to laboratory spectroscopists and astronomers – that of timescale. Unless confined to an ion-trap (where low ion numbers pose their own problems), it is difficult to confine a PAH to the one point in space for longer than a few microsecond – a molecule beam moves at about a millimeter per microsecond. However, the full mechanism underlying the PAH hypothesis takes place on timescales up to seconds. To fully explore the dynamical behaviour of PAHs and

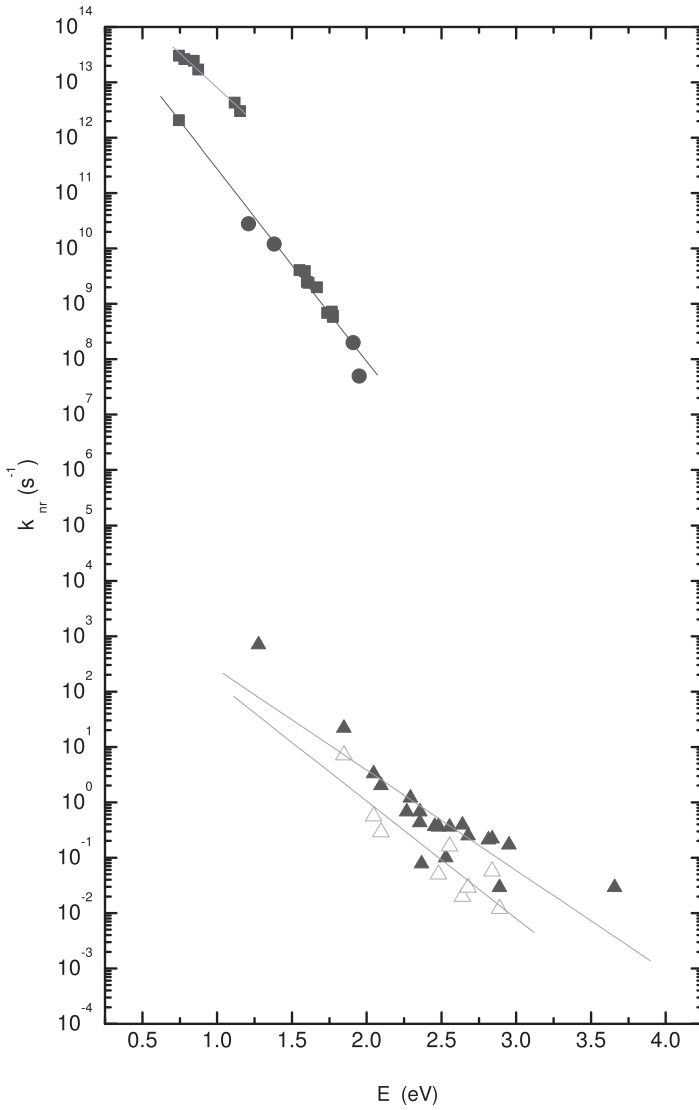


Fig. 4. Nonradiative electronic relaxation rate of the PAHs. Triangles are for the ISC (intersystem crossing) measured in solution for neutral species in their hydrogenated (full) and perdeuterated (open) form (Siebrand 1967), squares are those for IC (internal conversion) measured neutral (azulene derivatives from Murata *et al.* 1972 and phenanthrene from Ohta & Baba 1986) and cationic PAHs (for a detailed list of the references, see Salama 2007). Circles are for the neutral fullerenes. The lines are mainly there to guide the eyes to signify the relative efficiency of the Energy Gap Law and underline the deuterium effect when present. In the case of the azulene derivatives, it was shown to be very weak (Griesser & Wild 1980) unlike for the ISC in the neutral PAHs.

their cations under the full range of timescales available to astronomers, we must perform experiments on larger scales, or slow down our molecular beams. Towards the latter, there have been developments in Stark and Zeeman deceleration for smaller molecules in recent years, but in favour of the former, let us go to space with our molecules. It would certainly be a very interesting experiment to place an artificial small comet into space and observe this with all the spectroscopic tools available to the astronomical community. Such an experiment would produce a wealth of data, of interest to astrochemists, astrophysicists and molecular physicists. Space is still the greatest laboratory of all, where so much more is possible than on Earth.

References

- Allamandola, L.J., Tielens, A.G.G.M., & Barker, J.R., 1985, *ApJ*, 290, L25
Amirav, A., Even, U., & Jortner, J., 1981, *J. Phys. Chem.*, 85, 309
Apicella, B., Carpentieri, A., Alfe, M., *et al.*, 2007, *Proc. of the Comb. Inst.*, 31, 547
Avouris, P., Elbart, W.M., & ElSayed, M.A., 1977, *Chem. Rev.*, 77, 793
Baba, M., Saitoh, M., Taguma, K., *et al.*, 2009, *JCP*, 130, 134315
Baba, M., Saitoh, M., Kowaka, Y., *et al.*, 2009, *J. Chem. Phys.*, 131, 224318
Beck, S.M., Powers, D.E., Hopkins, J.B., & Smalley, R.E., 1981, *J. Chem. Phys.*, 73, 2019
Beck, S.M., Hopkins, J.B., Powers, D.E., & Smalley, R.E., 1981, *J. Chem. Phys.*, 74, 43
Bernhardt, B., Ozawa, A., Jacquet, P., *et al.*, 2010, *Nat. Photon.*, 4, 55
Bixon, M., & Jortner, J., 1968, *J. Chem. Phys.*, 48, 715
Bréchnignac, P., & Pino, T., 1999, *A&A*, 343, L49
Cami, J., Bernard-Salas, J., Peeters E., & Malek, S.E., 2010, *Science*, 329, 1180
Carpentier, Y., *et al.*, in preparation
Cherchneff, I., present volume
Clar, E., “Polycyclic Hydrocarbons vol. I” (Academic Press and Springer Verlag 1964)
Clar, E., “Polycyclic Hydrocarbons vol. II” (Academic Press and Springer Verlag 1964)
Deperasinska, I., Zehnacker, A., Lahmani, F., Borowicz, P., & Sepio, J., 2007, *J. Phys. Chem. A*, 111, 4252
Duncan, M.A., Dietz, T.G., & Smalley R.E., 1981, *J. Chem. Phys.*, 75, 2118
Englman, R., & Jortner, J., 1970, *Mol. Phys.*, 18, 145
Felker, P.M., & Zewail, A.H., 1985, *J. Chem. Phys.*, 82, 2975
Felker, P.M., & Zewail, A.H., 1985, *J. Chem. Phys.*, 82, 2961
Freed, K.F., 1978, *Acc. Chem. Res.*, 11, 74
Glinski, R.J., Michaels, P.D., Anderson, C.M., *et al.*, 2009, *Ap&SS*, 323, 337
Griesser, H.J., & Wild, P.U., 1980, *Chem. Phys.*, 52, 117
Haufler, R.E., Wang, L.S., Chibante, L.P.F., *et al.*, 1991, *Chem. Phys. Lett.*, 179, 449
Hunt, G.R., McCoy, E.F., & Ross, I.G., 1962, *Aust. J. Chem.*, 15, 591
Jäger, C., Huisken, F., Mutschke, H., *et al.*, 2007, *Carbon*, 45, 2981
Jäger, C., Huisken, F., Mutschke, H., Llamas Jansa, I., & Henning, Th., 2009, *ApJ*, 696, 706

- Joblin, Ch., Léger, A., & Martin, P., 1992, *A&A*, 393, L79
- Kasahara, S., Baba, M., & Kato, H., 2006, *Bull. Chem. Soc. Jpn.*, 79, 75
- Kato, H., Baba, M., & Kasahara, S., 2007, *Bull. Chem. Soc. Jpn.*, 80, 456
- Kokkin, D.L., Reilly, N.J., Troy, T.P., Nauta, K., & Schmidt, T.W., 2007, *JCP*, 126, 084304
- Kokkin, D.L., Troy, T.P., Nakajima, M., *et al.*, 2008, *ApJ*, 681, L49
- Kowaka, Y., Suganuma, Y., Ashizawa, N., *et al.*, 2010, *J. Mol. Spec.*, 260, 72
- Léger, A., & Puget, J.L., 1984, *A&A*, 137, L5
- Léger, A., & d'Hendecourt, L., 1985, *A&A*, 146, 81
- Li, A., & Draine, B.T., 2001, *ApJ*, 554, 778
- Malloci, G., Mulas, G., & Joblin C., 2007, *A&A*, 426, 105
- Medvedev, E.S., & Osherov, V.I., 1995, "Radiationless Transitions in Polyatomic Molecules" (Springer Series in Chemical Physics), 57
- Meerts, W.L., Majeski, W.A., & Van Herpen, W.M., 1984, *Can. J. Phys.*, 62, 1293
- Murata, S., Toda, T., Kokubun, H., & Iwanaga C., 1972, *Ber. Bunsen-Gesellschaft Phys. Chem.*, 76, 1176
- Ohta, N., & Baba, H., 1986, *Mol. Phys.*, 59 921
- O'keefe, A., & Deacon, D.A.G., 1988, *Rev. Sci. Inst.*, 59, 2544
- Parker, D.S.N., Minns, R.S., Penfold, T.J., Worth, G.A., & Fielding, H.H., 2009, *Chem. Phys. Lett.*, 469, 43
- Pino, T., Boudin, N., & Bréchnignac, P., 1999, *J. Chem. Phys.*, 111, 7337
- Puget, J.L., & Léger, A., 1989, *ARA&A*, 27, 161
- Quack, M., 1990, *Ann. Rev. Phys. Chem.*, 41, 839
- Reilly, N.J., Schmidt, T.W., & Kable, S.H., 2006, *J. Phys. Chem. A*, 110, 12355
- Reilly, N.J., D.L., Kokkin, Nakajima, M., *et al.*, 2008, *J. Amer. Chem. Soc.*, 130, 3137
- Romanini, D., Biennier, L., & Salama, F., 1999, *Chem. Phys. Lett.*, 303, 165
- Rouillé, G., Steglich, M., Huisken, F., Henning, Th., & Mullen, K., 2009, *J. Chem. Phys.*, 131, 204311
- Salama, F., 2007, "Molecules in Space and Laboratory", ed. J.L. Lemaire and F. Combes, Paris
- Sarre, P.J., 2006, *J. Mol. Spectrosc.*, 238, 1
- Sebree, J.A., Kislov, V.V., Mebel, A.M., & Zwier, T.S., 2010, *J. Phys. Chem. A*, 114, 6255
- Sellgren, K., Werner, M.W., Ingalls, J.G., *et al.*, 2010, *ApJ*, 722, L54
- Semba, Y., Yoshida, K., Kasahara, S., *et al.*, 2009, *J. Chem. Phys.*, 131, 024303
- Sharp, R.G., Reilly, N.J., Kable, S.H., & Schmidt, T.W., 2006, *ApJ*, 639, 194
- Siebrand, W., 1967, *J. Chem. Phys.*, 46, 440
- Simpson, C.D., Diedrich Brand, J., Berresheim, A.J., *et al.*, 2002, *Chem. Eur. J.*, 8, 1424
- Steglich, M., Jäger, C., Rouillé, G., *et al.*, 2010, *ApJ*, 712, L16
- Stolow, A., Bragg, A.E., & Neumark, D.M., 2004, *Chem. Rev.*, 104, 1719
- Stolow, A., & Underwood, J.G., 2008, *Adv. Chem. Phys.*, 139, 497
- Suto, M., Wang, X.Y., Shan, J., & Lee, L.C., 1992, *J. Quant. Spec. Rad. Trans.*, 48, 79

- Tokmachev, A.M., Boggio-Pasqua, M., Mendive-Tapia, D., Bearpark, M.J., & Robb, M.A., 2010, *J. Chem. Phys.*, 132, 044306
- Troy, T.P., O'Connor, G., Chalyavi, N., Nauta, K., & Schmidt, T.W., in preparation
- Troy, T.P., Nakajima, M., Chalyavi, N., *et al.*, 2009, *J. Phys. Chem. A*, 113, 10279
- Tschurle, M., & Boesl, U., 2006, *Int. J. Mass Spec.*, 249, 364
- Useli-Bacchitta, F., Bonnamy, A., Mulas, G., *et al.*, 2010, *Chem. Phys.*, 371, 16
- Yarkony, D.R., 2001, *J. Phys. Chem. A*, 105, 6277
- Yoshida, K., Semba, Y., Kasahara, S., Yamanaka, T., & Baba, M., 2009, *J. Chem. Phys.*, 130, 194304

SPECTROSCOPY OF PROTONATED AND DEPROTONATED PAHS

M. Hammonds¹, A. Pathak², A. Candian¹ and P.J. Sarre¹

Abstract. The spectroscopic properties of protonated and deprotonated PAHs are investigated through Density Functional Theory (DFT) calculations, with reference to their potential astrophysical significance. Attention is focussed on electronic and rotational spectra.

1 Introduction

Evidence for polycyclic aromatic hydrocarbons (PAHs) in the interstellar medium (ISM) is drawn almost exclusively from their infrared emission spectra – the so-called “unidentified” infrared (UIR) emission bands (see Tielens 2008, and references therein). However, it has proved to be very difficult to identify an individual PAH from these spectra as the features are indicative of molecular groups rather than particular molecules; observation of far-IR spectra may alleviate this problem as discussed by Joblin *et al.* elsewhere in this volume. The spectra show significant variation between and within objects so if knowledge of the underlying mix of molecules were available then profile modelling could be very productive and act as a probe of astronomical conditions. In contrast to infrared spectra, electronic and rotational spectra are very dependent on the specific molecule with major differences present even between isomers. For this reason it is of interest to undertake a theoretical investigation of the electronic and rotational spectroscopic properties of PAHs, in part as a guide for laboratory experiments. We present here predicted electronic spectra of protonated and deprotonated PAHs, which are generally closed-shell molecules and have positive and negative charge, respectively (see Fig. 1). The research seeks to contribute to the long-standing problem of the diffuse interstellar bands (DIBs) in the optical region (see Snow & Destree and Cox, this volume), for which PAHs are attractive candidates. We also explore the possibility of detection of specific PAHs through rotational spectroscopy.

¹ School of Chemistry, The University of Nottingham, University Park, Nottingham, NG7 2RD, UK

² Indian Institute of Astrophysics, Koramangala, Bangalore 560034, India;
Present address: Physics Department, Tezpur University, Tezpur - 784 028, India

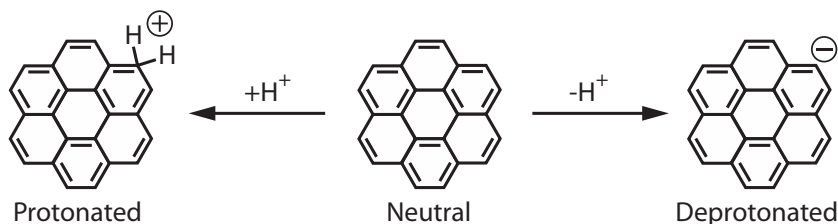


Fig. 1. Illustration of the relation between neutral coronene ($\text{C}_{24}\text{H}_{12}$) and its protonated and deprotonated forms. All three molecules have closed-shell electronic structures. In each case the full aromaticity of the structure is maintained

2 Theoretical methods

We employ Density Functional Theory (DFT) to calculate molecular structures and energetic properties, and its time-dependent form (TD-DFT) for predictions of approximate electronic absorption spectra. Geometry optimisations and TD-DFT calculations were conducted using the B3LYP functional with a 6-31G* basis set for protonated PAHs and a 6-31+G** basis (Hehre *et al.* 1972; Hariharan *et al.* 1973) for deprotonated (anionic) PAHs. The latter basis set is not a standard part of the Q-Chem package used in this work (Shao *et al.* 2006).

3 Protonated PAHs (HPAH⁺)

3.1 Electronic spectroscopy of protonated PAHs

Alongside research on PAHs in connection with the UIR bands, there is long-standing interest in their possible rôle in relation to the DIB band problem (see Herbig 1995 and Sarre 2006, and references therein). The potential significance of protonated PAHs, denoted here HPAH⁺, in connection with this problem was first highlighted by Le Page *et al.* (1997) and both this aspect and the chemistry of HPAH⁺ molecules have been discussed in subsequent papers (Snow *et al.* 1998; Le Page *et al.* 2003). Although small-to-medium sized neutral PAHs generally absorb in the UV or near-UV part of the spectrum, and in principle would be detectable in absorption in the spectra of background stars, no such evidence has yet been found. Larger neutral PAHs such as hexa-peri-hexabenzocoronene ($\text{C}_{42}\text{H}_{18}$) with absorption bands in the 4000–4500 Å range, would appear to be promising candidates, but to date no correspondence with DIBs has been found (Kokkin *et al.* 2008). Consequently attention has also been paid to ionic forms of PAHs and, partly because of ease of production in the laboratory, to radical cations which generally absorb in the visible spectral region. However, being open-shell molecules, they are expected to be reactive and so alternative ionic forms including

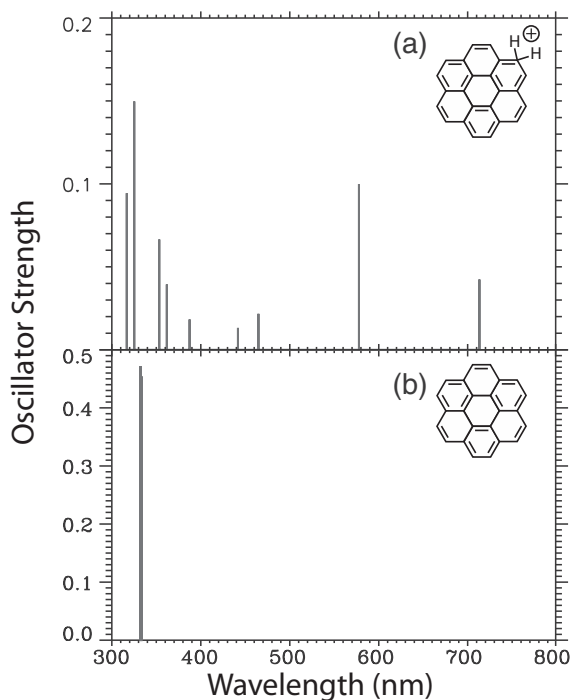


Fig. 2. Calculated electronic transitions of (a) protonated coronene and (b) coronene.

protonated PAHs are worthy of consideration. At present laboratory recording of electronic spectra of HPAH^+ molecules at high-resolution is in its infancy but developing, as outlined in this Symposium. For large systems the only current theoretical method that lends itself to predicting electronic spectra is TD-DFT and the precision is low, being in the region of ± 0.3 eV. However, the results can still be very useful in identifying potential candidates. The calculated electronic absorption spectrum of *e.g.* protonated coronene differs markedly from its corresponding neutral parent molecule as seen in Figure 2. Although the protonated molecule has transitions in the near-UV, as is the case for the neutral molecule, it also has strong transitions in the visible part of the spectrum. Although the effect of protonation on the absorption spectrum of benzene has been known for many years, extension to polycyclic aromatic hydrocarbons is new. The precision of TD-DFT calculations is far too low to discuss any meaningful attribution of DIBs to specific molecules, but the semi-quantitative result is significant. In particular it may assist in planning laboratory experiments in the condensed (inert gas matrix) or, preferably, gas phase. The dissociation energies of protonated PAHs are lower than their neutral counterparts which does raise some question as to their photostability, although for large protonated PAHs fragmentation is expected to be reduced due to the very high density of states.

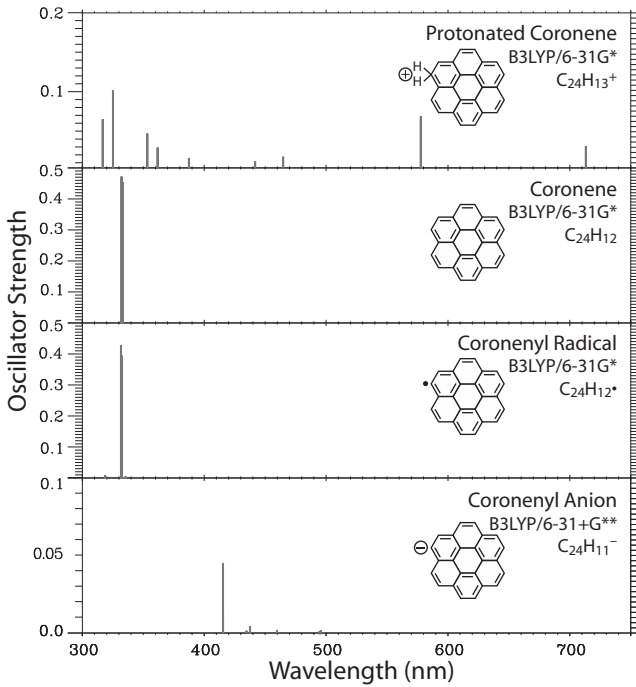


Fig. 3. Calculated transitions of protonated, neutral, radical and deprotonated coronene.

4 Deprotonated PAHs (PAH_{n-1}^-)

As far as we are aware, deprotonated PAHs have not been considered explicitly in an astrophysical context. The analogous deprotonated polyacetylenes such as C_6H^- are the subject of intense current activity as recorded through their laboratory rotational spectra and corresponding studies by radioastronomy (McCarthy *et al.* 2006). PAH anions have been discussed in connection with interstellar chemistry and as possible contributors to the UIR bands, but generally in terms of the radical anion form (Bakes & Tielens 1998). The electron affinities of closed-shell neutral PAHs (Mallocci *et al.* 2005) are a factor of 2–3 lower than those of the neutral radicals of interest here. We have computed using DFT the electron affinities of a number of radicals (values in eV, for the most stable isomer) as follows: pyrenyl (1.57), coronenyl (1.68) and ovalenyl (2.00). While these electron affinities are lower than for the polyacetylenic radicals they are still reasonably high and deprotonated anions should form readily through radiative electron attachment to the radical. Given the special nature of anions a different basis (6-31+G**) was employed. In all cases it is found that the negative charge is very localized at the site of proton removal.

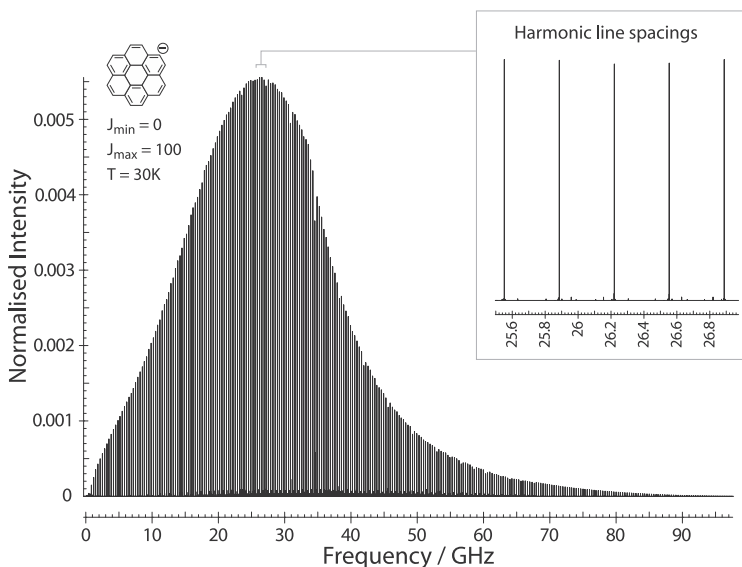


Fig. 4. Computed pure rotational spectrum of the coronenyl anion for J values up to 100 and at 30 K. The inset shows a ~ 1 GHz region of very nearly equally (harmonically) spaced lines.

4.1 Electronic spectroscopy of deprotonated PAHs

An example of a calculated electronic spectrum, for deprotonated coronene, is given in Figure 3 (lowest panel) where it is compared with corresponding spectra of the protonated, closed-shell neutral and neutral radical forms. These are all over-simplifications given that no vibrational band structure is included. The deprotonated coronene molecule exhibits just one significant band in the 300–750 nm region. The astronomical importance of this spectrum is uncertain because in diffuse and translucent clouds it is probable that photodetachment of the electron would destroy the anion; the calculated band at *e.g.* ~ 420 nm corresponds to a photon energy of ~ 3 eV which is well above the ionization energy of ~ 1.7 eV and so autodetachment would occur on photoexcitation. However, in denser regions this restriction is lifted. The possibilities of detection of such species by radioastronomy is now considered.

4.2 Rotational spectroscopy of deprotonated PAHs

The wealth of information gleaned about dense clouds through radioastronomy is reliant on the detected molecules possessing permanent electric dipole moments.

PAHs are very likely present in some form but as the simplest neutral systems are not polar no detection is possible through their rotational spectra. One modification, and one subjected to a radioastronomical search, is corannulene which has a significant dipole moment as it is non-planar (Pilleri *et al.* 2009). PAHs containing heteroatoms may also offer some opportunities. For PAH ions it is likely that protonated forms are present but these molecules are asymmetric tops and so the spectra are extremely complex with huge line-dilution. An alternative that might allow progress is the class of deprotonated PAHs. The removal of one peripheral hydrogen nucleus does affect slightly the centre-of-mass of an otherwise symmetrical PAH, but does not introduce asymmetry to the extent caused by off-plane hydrogens in protonated versions. Deprotonated PAHs are therefore very nearly symmetric top molecules but, crucially, possess large electric dipole moments which fall in the 10–14 Debye range for the coronenyl, ovalenyl, circum-pyrenyl and circumcoronenyl anions. Figure 4 shows a spectrum computed using the pgopher package (Western 2009) where at 30 K there are a large number of apparently barely resolved lines. However, the molecules are very nearly symmetric tops and so the main pattern is a series of equally spaced lines as the finer (K) structure is unresolved (see inset). While the capacity to calculate accurate predicted line positions for deprotonated PAHs is certainly beyond any current theoretical method, identification of harmonically related frequencies has played a significant role in identifying linear molecules in astronomical environments, including C_6H^- , and these could be sought in radio data.

We thank EPSRC (MH) and STFC (AC) for studentships, the Symposium organizers and the Department of Science and Technology, New Delhi, for financial assistance (AP), The Royal Society for travel support (PJS), and The University of Nottingham for support and use of the HPC facility.

References

- Bakes, E.L.O., & Tielens, A.G.G.M., 1998, *ApJ*, 499, 258
Hariharan, P.C., & Pople, J.A., 1973, *Theoret. Chim. Acta.*, 28, 213
Hehre, W.J., Ditchfield, R., & Pople, J.A., 1972, *J. Chem. Phys.*, 56, 724
Herbig, G.H., 1995, *ARA&A*, 33, 19
Kokkin, D.L., Troy, T.P., Nakajima, M., *et al.*, 2008, *ApJ*, 681, L49
Le Page, V., Keheyan, Y., Bierbaum, V.M., & Snow, T.P., 1997, *J. Am. Chem. Soc.*, 119, 8373
Le Page, V., Snow, T.P., & Bierbaum, V.M., 2003, *ApJ*, 584, 316
Mallocci, G., Mulas, G., Cappellini, G., Fiorentini, V., & Porceddu, I., 2005, *A&A*, 432, 585
McCarthy, M.C., Gottlieb, C.A., Gupta, H., & Thaddeus, P., 2006, *ApJ*, 652, L141
Pilleri, *et al.*, 2009 *MNRAS*, 397, 1053

Sarre, P.J., 2006, *J. Mol. Spectrosc.*, 238, 1

Shao, Y., *et al.*, 2006, *Phys. Chem. Chem. Phys.*, 8, 3172

Snow, T.P., Le Page, V., Keheyani, Y., & Bierbaum, V.M., 1998, *Nature*, 391, 259

Tielens, A.G.G.M., 2008, *ARA&A*, 46, 289

Western, C.M., PGOPHER, a Program for Simulating Rotational Structure (version 6.0.111), University of Bristol, <http://pgopher.chm.bris.ac.uk>

OBSERVATIONS OF INTERSTELLAR CARBON COMPOUNDS

E. Dartois¹

Abstract. Infrared absorption and emission features observed spectroscopically in our Galaxy allow to probe the composition of solid dust grains, their evolution and thus follow the cycling of matter in the Galaxy. Many observables do reveal the presence of large amounts of carbonaceous particles in space, other than the PAH-like emission lines. The carbonaceous materials observed include amorphous carbons, diamonoids showing in emission for a few specific sources, and the recently detected fullerenes. An important hydrogenated amorphous carbon component (HAC or a-C:H), traced by the 2940 cm^{-1} structured absorption feature is observed against Galactic background sources. Since the discovery of this feature in the early eighties (Allen 1981), the observation of a-C:H has been extended to the mid-infrared by space observatories, giving insight into additional associated features. They are also observed in external galaxies, showing the ubiquitous nature of these components. We will focus on astronomical observations of organic matter other than PAHs, amorphous carbons and associated laboratory dust analogues relevant to astrophysical applications.

1 Introduction

The nowadays observed dust results from the superposition and mixing of many different galactic environments that participate to the so-called “dust lifecycle”. Dust is produced in several source environments and, as it travels through the galaxy, experiences various physical and chemical processes that will modify its structure and/or composition. Among carbonaceous contributors, additional carbon allotropes, other than the polycyclic aromatic hydrocarbons (PAHs) described abundantly in this volume, participate in the building of the dusty interstellar medium. Organic matter includes various observed structural forms such as amorphous carbons, diamond, hydrogenated amorphous carbons and other materials with aromatic/aliphatic mixed structures.

¹ Institut d’Astrophysique Spatiale, UMR-8617, Université Paris-Sud, Bâtiment 121, 91405 Orsay, France

2 Amorphous carbons

Dust composition in the vicinity of evolved stars flows is constrained from direct observations and modelling. When the stellar wind flowing out reaches a pressure still sufficiently high ($10^{-5} - 10^{-3}$ Pa) and temperature sufficiently low ($\sim 2500 - 1000$ K), atoms and molecules nucleate small dust seeds that start to grow in the expanding flow, until they reach a region where the pressure and temperature regime does not allow to pursue an efficient grain growth (*e.g.* Patzer *et al.* 2003; Gail & Sedlmayr 1999). This dust formation window is the consequence of the competition between the dust formation timescale and the stellar wind ejection speed that freezes the reactivity at some point. Passed this point in the flow, the dust formed leaves the nucleation regime and enters the evolution one. The kind of dust formed is controlled by chemical parameters such as the carbon/oxygen ratio in the flow. The observed circumstellar dust near evolved stars is a mix of oxygen and carbon rich dust. Of particular interest for the carbonaceous world are the so-called “carbon” stars, injecting important amounts of carbon under an amorphous form difficult to observe remotely, as no specific features are associated with them, unlike silicates. This allotrope is clearly observed around extreme carbon stars, as a broad featureless emission in equilibrium with the radiation field (See Fig. 1).

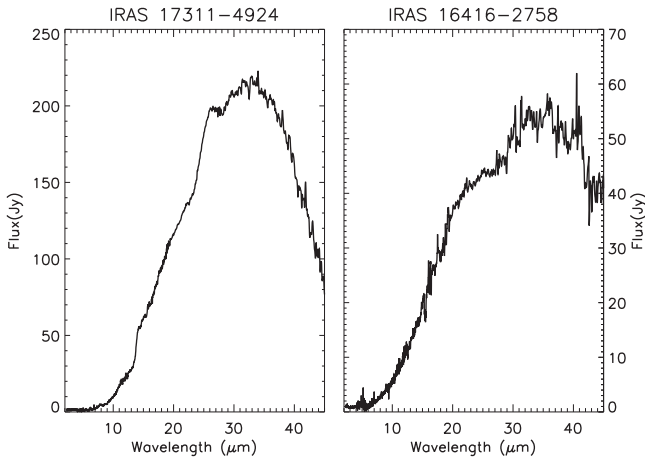


Fig. 1. Emission spectra of two carbon stars extracted from the Infrared Space Observatory database (<http://iso.esac.esa.int/ida/>). They illustrate the almost featureless continuum emission by highly carbonaceous grains in evolved carbonaceous stellar flows (see also Volk *et al.* 2001; Hony 2002; Chen *et al.* 2010 and citations therein).

These stars are likely to be the progenitors of C-rich protoplanetary nebulae (PPNs) such as AFGL 2688 (classified as a Class C by Peeters *et al.* 2002; see also Peeters in this volume), and C-rich planetary nebulae (PNs) such as NGC 7027. They will be involved in the carbon dust cycle although the grains they produced are more difficult to observe in the later phases.

3 (Nano-)diamonds

The presence of high amounts of (nano-)diamonds, up to several thousands ppm (*e.g.* Ott 1993; Anders & Zinner 1993), in the organic extracts from meteorites has led to the search for their plausible infrared signatures in the laboratory, to confront their spectra to those of young stellar objects observed in early evolution phases eventually leading to a protosolar system. They were initially proposed as an alternative explanation for some of the unidentified infrared bands (UIBs) and probably responsible for the “21 microns” astronomical feature, following infrared spectroscopy studies of “Allende” and “Orgueil” meteorite nanodiamonds (Koike *et al.* 1995; Hill *et al.* 1998).

The unambiguous detection of specific CH methine and methylene stretching modes, observed at 3.53 and 3.43 μm , associated with hydrogen atoms chemically bounded to diamond structure was demonstrated by Guillois *et al.* (1999), by comparing emission spectra of astronomical sources to laboratory spectra of nanocrystal diamond films exposed to hydrogen by Chang *et al.* (1995). These sources are different from the ones previously discussed for the 21 “microns” feature. Recently, from a molecular approach, Pirali *et al.* (2007) measured small diamondoids in the gas phase and, reported calculations, as well as attenuated total reflectance spectra for higher diamondoids. Analogues of the measured species with the same symmetry containing around 130 C atoms (*e.g.*, $\text{C}_{136}\text{H}_{104}$) show an intensity ratio of the 3.53 and 3.43 μm bands close to that observed in the interstellar spectra. The inferred size is close to typical sizes of meteoritic diamonds.

Observationally, a survey of 30 Herbig Ae/Be stars, the spectral type of the previously observed stars where the features had been observed, was conducted by Acke & van den Ancker (2006). No new source could be added to the list of diamond emission features, implying that less than 4% of the Herbig targets show the prominent emission features at 3.43 and/or 3.53 μm .

In an effort to resolve spatially the location of these features, Habart *et al.* (2004) marginally resolved the emission intensity profile, showing that it is less extended than the associated 3.3 μm PAH feature. Goto *et al.* (2009), using an adaptive optics system, resolved spatially the PAH and diamond CH emissions. The diamond emission is concentrated, peaking at about 30 AU from the star. The PAH emission is more extended (above 100 AU). The authors speculate on diamond formation in these circumstellar disks, with graphitic grains processed into diamond grains under highly-energetic particle bombardment.

4 Fullerenes

Fullerenes and in particular C_{60} have been searched for intensively via electronic and infrared specific transitions (*e.g.* Foing & Ehrenfreund 1994; Fulara *et al.* 1993; Moutou *et al.* 1999; Herbig 2000). C_{60} was recently detected by Sellgren *et al.* (2009, 2010) and Cami *et al.* (2010). More details can be found in the contribution by K. Sellgren *et al.* in this volume.

5 Hydrogenated amorphous carbons

Hydrogenated amorphous carbons, HAC or a-C:H for amorphous material made of C and H, constitute one important component of interstellar dust. They were observed initially at 3.4 μm against a Galactic center source (Allen & Wickramasenghe 1981). The features contributing to this absorption band were early associated to sp^3 CH_3 and CH_2 stretching modes, as stated in *e.g.* Duley & Williams (1983), “Interstellar amorphous carbon dust with chemisorbed CH_2 and CH_3 groups may be a significant component of interstellar dust in diffuse clouds”. Since then, numerous experiments/observations have been performed to constrain its origin (*e.g.* Jones *et al.* 1983; Butchart *et al.* 1986; Mc Fadzean *et al.* 1989; Ehrenfreund *et al.* 1991; Sandford *et al.* 1991; Sandford *et al.* 1995; Pendleton *et al.* 1994; Tielens *et al.* 1996; Geballe *et al.* 1998; Chiar *et al.* 2002; Mennella *et al.* 2002; Pendleton & Allamandola 2002). A Galactic abundance for a-C:H has been estimated from observed CH stretching modes. Depending on the assumed materials, the associated oscillator strength for CH modes and the degree of hydrogenation, the implied cosmic carbon fraction varies from 2.6% to 35% (Sandford *et al.* 1991), above 2.5 to 4% based on the spectra of alkanes (Pendleton *et al.* 1994) and up to 20–30% for laboratory analogues of a-C:H (Duley 1994; Duley *et al.* 1998).

The constrain on a-C:H was initially set only by the CH stretching modes. Nevertheless, the band profiles of many laboratory analogues were already incompatible with the astronomical absorption profile. It is incompatible with H_2O -dominated photolytic or radiolysis residues obtained starting with an interstellar ice mantle composition (Bernstein *et al.* 1995; Allamandola *et al.* 1988; Greenberg *et al.* 1995; Pendleton & Allamandola 2002). Instead, laboratory analogues using heated carbon rod (Schnaiter *et al.* 1998), laser desorbed carbon (Mennella *et al.* 1999), plasma deposition (Lee & Wdowiak 1993; Furton *et al.* 1999) or photo-produced a-C:H at low temperature (Dartois *et al.* 2005) provide a much better fit to the observed features. The Insoluble Organic Matter (IOM) extracted from meteorites also provides a reasonable fit to the astronomical observations (*e.g.* Ehrenfreund *et al.* 1991) at 3.4 μm .

The discrimination became clearer with the advent of space telescopes, allowing to track the mid-infrared fingerprints of this material. The moderate to high oxygen content in many of the laboratory analogues or IOM does provide strong absorptions in the mid-IR fingerprint region, and the carbonyl band is one of the strongest in the 1650 to 1800 cm^{-1} range. Within the signal-to-noise achieved, these absorptions can at most be a minor contribution to the observed diffuse medium spectra, as shown in Figure 2. For Galactic sources there still exists confusion in the mid-infrared, due to foreground dense clouds ice absorptions (Fig. 2 upper spectra, Dartois *et al.* 2004), or local circumstellar contributions decoupled from the diffuse medium features (Fig. 2 lower spectra, Chiar & Tielens 2001; Chiar *et al.* 2002). However, meaningful upper limits were already set.

In the last years, several extragalactic obscured active galactic nuclei (AGN) sources displaying a-C:H absorptions have been observed, mainly via the stretching

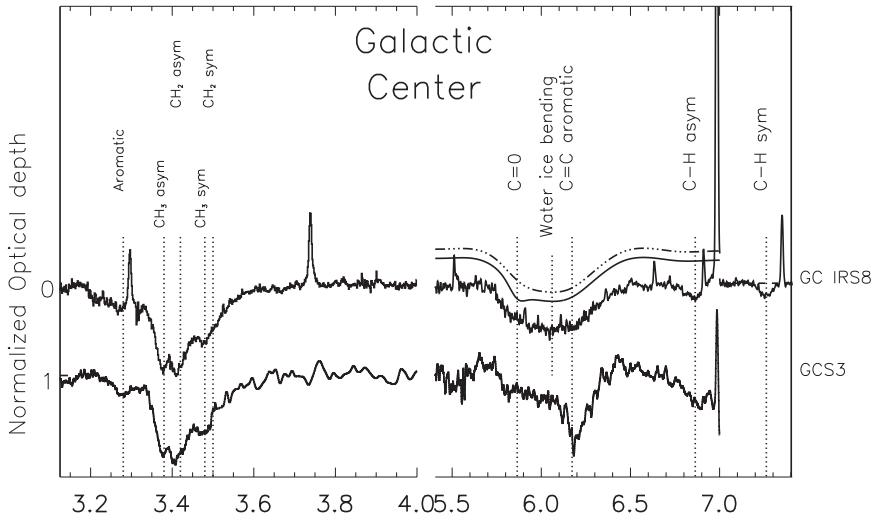


Fig. 2. Continuum extracted transmittance spectra along two Galactic center lines of sight. Both observations supposedly probe the same diffuse interstellar medium absorptions, but display many additional contributions arising from circumstellar and/or dense cloud contributions. Nevertheless, they constrain the mid-infrared counterpart of the $3.4 \mu\text{m}$ absorption from a-C:H. See text for the detailed analysis of these differences.

modes (Pendleton *et al.* 1994; Mason *et al.* 2004; Dartois *et al.* 2004; Imanishi 2006; Risaliti *et al.* 2006; Imanishi *et al.* 2008). In NGC 1068, the hydrocarbon distribution has even been imaged to better constrain its spatial distribution, and foresee its nature (Mason *et al.* 2006; Geballe *et al.* 2009). The extragalactic sources provide a different constrain to get insight into the a-C:H structure and ubiquity. Contrary to Galactic embedded sources used as infrared background to probe the diffuse medium, obscured AGNs probe large dust column densities in front of an extended infrared continuum provided by the active nucleus environment. With a parsec-scale infrared probing pencil, the risk of very local circumstellar contamination is minimised. With a favorable AGN nucleus to diffuse medium alignment geometry, a line-of-sight free from significant dense cloud ice absorptions can be observed, providing a clean mid-infrared continuum to probe a-C:H fingerprints. Another advantage of the extragalactic case is the moderate galaxy red-shift, shifting the wavelength frame to more favourable atmospheric windows for ground-based observations, thus giving a unique access to the aromatic CH stretching mode region, devoid of strong telluric contamination, which are especially important for shallow absorption features.

The IRAS 08572+3915 AGN is such a test case source, with a redshift of $z \sim 0.0583$. An upper limit on the aromatic C-H stretch has been evaluated, and the aromatic *versus* aliphatic C-H content of interstellar a-C:H can be better constrained ($N(\text{CH aromatic}) / N(\text{CH sp}^3) \leq 0.08$; Dartois *et al.* 2007). Using the

$N(\text{H})$ column density relation derived from the observed silicate optical depth combined to an elemental cosmic carbon abundance, about 15% of the cosmic C must be involved in sp^3 bonding. The methyl and methylene C-H observed ratio imply also $x(\text{H}) / x(\text{C } \text{sp}^3) \sim 2.33$. Taking into account that only the infrared moderately active modes are observed, this sets a lower limit to the hydrogen content of the material observed, meaning a fractional hydrogen content in the a-C:H of $x(\text{H}) \geq 0.2$. These constraints can be brought together in a ternary phase diagram where the hydrogen content and the two main bonding types for carbon (sp^2 and sp^3 , as the sp contribution is expected to be small) constitute the poles (Ferrari & Robertson 2000; Dartois *et al.* 2007). Overplotted are the constraints for IRAS 08572+3915, as well as the position for different laboratory produced analogues, including soot, and PAHs lying on the H to sp^2 border. Random Covalent Network models for materials made with olefinic or aromatic $\text{C}=\text{C}$, using the model developed by Angus & Jansen (1988) and extended to aromatic structure by Jones (1990) are displayed. The a-C:H analogues fit perfectly with these constraints as well as the overall infrared spectrum.

In the model structure proposed by Pendleton & Allamandola (2002, Figure 17 in this paper), the aromatic CH component (~ 160 by number) represents more than two times the aliphatic CH component ($\text{CH}_2 + \text{CH}_3 \sim 70$), for a carbonaceous backbone of ~ 540 C atoms. We would expect in principle, with such a structure, an aromatic CH absorption higher than observed for IRAS 08572+3915, even if the lower oscillator strength of the CH aromatic stretch is taken into account.

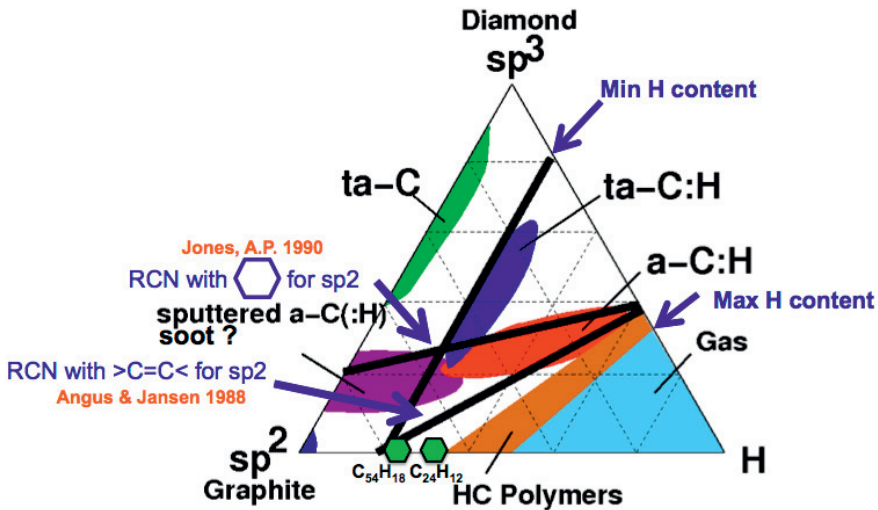


Fig. 3. Ternary phase diagram for analogues made principally from C and H. The constrain from observations of IRAS 08572+3915 is set (min H and max H contents). Several domains for various synthetic materials from the laboratory are shown. Two Random Covalent Network models (Angus & Jansen 1988; Jones 1990) are also displayed, almost enclosing the a-C:H domain.

Based on the observations and ternary diagram, we propose to revise the basic structural unit (BSU) issued from the Pendleton & Allamandola analysis by using a material with a lower aromatic CH contribution¹, such as hydrogenated amorphous carbon or hydrogen rich soot like analogues.

Interstellar a-C:H materials remain difficult to observe as compared to PAHs. Their astrophysical detection requires large column densities, as shown by the visual to band extinction relations ($A_V/\tau(3.4 \mu\text{m}) \sim 250$; *e.g.* Sandford *et al.* 1995; $A_V/\tau(6.85 \mu\text{m}) \sim 640$; Dartois & Munoz Caro 2007). They represent a major ISM component, containing up to 30% of total galactic ISM carbon (typical $\sim 15\%$). Their spectroscopic absorption feature contrast is easily hidden by PAHs when energetic photons are present, as strongly emitting PAH regions require only few tenth of an A_V to be able to record bright emission bands. This explains why their observation is hampered in *e.g.* the interstellar media of Starburst galaxies. It is ubiquitous in the Galactic diffuse ISM and observed in a large number of external galaxies (*e.g.* Dartois & Munoz-Caro 2007). It contains low amount of O heteroatoms. It is in agreement with laboratory plasma produced (microwave, laser) and/or photoproduced a-C:Hs. It may be partly responsible for ISM fluorescence features (*e.g.* Godard & Dartois 2010 and references therein). It is a possible precursor for another form of interstellar carbon (PAHs) upon energetic processing.

6 Mixed aliphatic/aromatic structural units

6.1 Observed classes A, B, C

The relative profile variations of the mid-IR emission among various astrophysical sources has been underlined since a long time from ground-based observations (Joblin *et al.* 1996; Geballe *et al.* 1997) and a classification in various classes was performed when space missions provided a full wavelength infrared coverage (Peeters *et al.* 2002; van Dienenhoven *et al.* 2004, see Peeters elsewhere in this volume). Some of the observed sources, the so-called "class C", display both aromatic and aliphatic emission bands, questioning us on the possible link between hydrocarbons seen in absorption and emission. In few instances, the C-H dust stretching mode is spatially resolved in emission by adaptive optics (Goto *et al.* 2003; Goto *et al.* 2007) and relative variations from the central star suggest a progressive disappearance of aliphatic character to the benefit of the aromatic feature when the distance from the star increases. It has been shown that laboratory analogues thermally annealed at different temperatures, provide a reasonable match to this process (*e.g.* 2005, 2000, 1997, 1990). However one should take into account the possibility to have different emission mechanisms between both phases (solid and molecular), that will depend also on dust particles size in the stellar field. One must not forget that concomittant mechanisms are at work (chemical

¹Note that the constrain is on the aromatic CH. An aromatic backbone structure can still be present but interconnected to other elements via *e.g.* methylene or carbon-carbon bonds like in a-C:H or soot.

modification, emission, stellar versus ISRF photon irradiations) that still need to be further constrained.

A progressive evolution among sources from class A to C has been notably underlined by *Szczerba et al.* (2005). The aromatic C = C stretching mode position is shown to shift from 6.2 to 6.3 μm while the so-called “7.7” feature evolves toward 8 μm . The change in the 6.2 μm feature position has been associated with various hypothesis, such as the formation of PAH metal complexes, the formation of PAH clusters, isotopic shifts, size changes or induced by heteroatoms like nitrogen. In the last case, the band would shift with N atom substitution site within the aromatic structure (*Hudgins et al.* 2005). In the following a simple alternative scenario is proposed to this evolution, based on recent laboratory experiments.

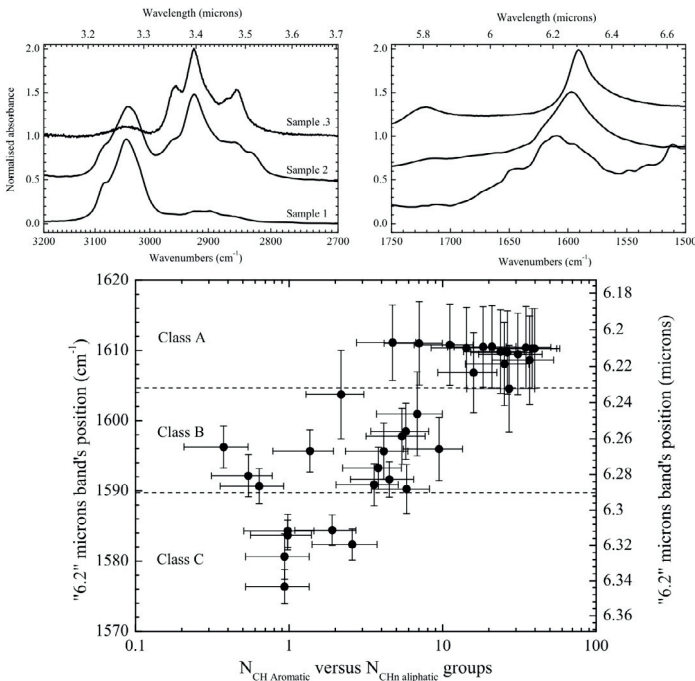


Fig. 4. *Upper panel:* infrared absorption spectra of laboratory soot samples with varying aliphatic to aromatic C-H stretch content and associated C = C mode region. *Lower panel:* evolution of the C = C position in the various samples produced as a function of the aromatic to aliphatic ratio observed in the stretching mode region. Note that the total H/C vary among the samples. The expected astrophysical classes range of 6.2 μm positions are shown for comparison.

6.2 A possible aromatic C = C shift induced by aliphatics

The sources with the “6.2 μm ” feature lying at 6.3 μm also display additional emission lines around 6.85 and 7.25 μm , as well as a more or less pronounced

3.4 μm emission band on the side of the aromatic feature. Sloan *et al.* (2007) had proposed that the observed wavelength shifts are consistent with hydrocarbon mixtures containing both aromatic and aliphatic bonds. More recently, Acke *et al.* (2010) showed the same behaviour with a large set of *Spitzer* spectra (see also Acke, elsewhere in this volume). In order to understand carbon dust nucleation, and the observed astrophysical classes of materials, laboratory soot analogue spectra have been recorded for 50 distinct samples, using a premixed low pressure flame. Varying the flame combustion regime with respect to the stoichiometric conditions, and forcing various sooting conditions allow to produce many different carbonaceous soot materials (Pino *et al.* 2008). The resultant analogues are investigated by FTIR spectroscopy. This spectral analysis, applied to the band shape and position variations, was then used to interpret the diversity and evolution of the features in the astronomical spectra. Strong correlations were evidenced between the spectral regions characteristic of the C = C and C-H modes in these analogs. These shed light on the origin of the infrared emission features. In particular, the observed shift in the position of the 6.2–6.3 μm band is shown to be a key tracer of the evolution of the aliphatic to aromatic component of carbonaceous dust. The produced materials have been characterised by other techniques (Raman spectroscopy, TEM, elemental analysis). These analyses suggest that there is a structural modification of the carbonaceous backbone by aliphatics. The evolution between these extreme positions (6.2 to 6.3 μm) thus appears as tracing the underlying carbon skeleton structure, linked to the presence of aliphatics in the network that favours the development of an alternative basic structural unit as compared to classical aromatic compounds.

References

- Acke, B., & van den Ancker, M.E., 2006, *A&A*, 457, 171
Acke, B., Bouwman, J., Juhász, A., *et al.*, 2010, *ApJ*, 718, 558
Allamandola, L.J., Sandford, S.A., & Valero, G.J., 1988, *Icarus*, 76, 225
Allen, & Wickramasenghe, 1981, *Nature*, 294, 239
Anders, E., & Zinner, E., 1993, *Meteoritics*, 28, 490
Angus, J.C., & Jansen, F., 1988, *J. Vacuum Sci. Technol.*, 6, 1778
Bernstein, M.P., Sandford, S.A., Allamandola, L.J., Chang, S., & Scharberg, M.A., 1995, *ApJ*, 454, 327
Butchart, I., McFadzean, A.D., Whittet, D.C.B., Geballe, T.R., & Greenberg, J.M., 1986, *A&A*, 154, L5
Chang, H.-C., Lin, J.-C., Wu, J.-Y., & Chen, K.-H., 1995, *J. Phys. Chem.*, 99, 11081
Chen, P.-S., Yang, X.-H., & Shan, H.-G., 2010, *Res. Astron. Astrophys.*, 10, 363
Chiar, J.E., & Tielens, A.G.G.M., 2001, *ApJ*, 550, L207
Chiar, J.E., Adamson, A.J., Pendleton, Y.J., *et al.*, 2002, *ApJ*, 570, 198
Dartois, E., Marco, O., Muñoz-Caro, G.M., *et al.*, 2004, *A&A*, 423, 549
Dartois, E., Muñoz Caro, G.M., Deboffle, D., Montagnac, G., & D'Hendecourt, L., 2005, *A&A*, 432, 895

- Dartois, E., *et al.*, 2007, *A&A*, 463, 635
- Dartois, E., & Muñoz-Caro, G.M., 2007, *A&A*, 476, 1235
- Duley, W.W., & Williams, D.A., 1983, *MNRAS*, 205, 67P
- Duley, W.W., Scott, A.D., Seahra, S., & Dadswell, G., 1998, *ApJ*, 503, L183
- Duley, W.W., 1994, *ApJ*, 430, L133
- Ehrenfreund, P., Robert, F., D'Hendecourt, L., & Behar, F., 1991, *A&A*, 252, 712
- Ferrari, A.C., & Robertson, J., 2000, *Phys. Rev. B*, 61, 14095
- Foing, B.H., & Ehrenfreund, P., 1994, *Nature*, 369, 296
- Fulara, J., Jakobi, M., & Maier, J.P., 1993, *Chemical Physics Letters*, 211, 227
- Furton, D.G., Laiho, J.W., & Witt, A.N., 1999, *ApJ*, 526, 752
- Gail, H.-P., & Sedlmayr, E., 1999, *A&A*, 347, 594
- Geballe, T.R., 1997, *From Stardust to Planetesimals*, 122, 119
- Geballe, T.R., Chiar, J., Pendleton, Y.J., & Tielens, A.G.G.M., 1998, *Astrophys. Space Sci.*, 255, 457
- Geballe, T.R., Mason, R.E., Rodríguez-Ardila, A., & Axon, D.J., 2009, *ApJ*, 701, 1710
- Godard, M., & Dartois, E., 2010, *A&A*, forthcoming
- Goto, M., Maihara, T., Terada, H., Kaito, C., Kimura, S., & Wada, S., 2000, *Astron. Astrophys. Suppl.*, 141, 149
- Goto, M., *et al.*, 2003, *ApJ*, 589, 419
- Goto, M., *et al.*, 2007, *ApJ*, 662, 389
- Goto, M., *et al.*, 2009, *ApJ*, 693, 610
- Greenberg, J.M., Li, A., Mendoza-Gomez, C.X., *et al.*, 1995, *ApJ*, 455, L177
- Guillois, O., Ledoux, G., & Reynaud, C., 1999, *ApJ*, 521, L133
- Habart, E., Testi, L., Natta, A., & Carillet, M., 2004, *ApJ*, 614, L129
- Herbig, G.H., 2000, *ApJ*, 542, 334
- Hill, H.G.M., Jones, A.P., & D'Hendecourt, L.B., 1998, *A&A*, 336, L41
- Hony, S., 2002, Ph.D. Thesis
- Hudgins, D.M., Bauschlicher, C.W., Jr., & Allamandola, L.J., 2005, *ApJ*, 632, 316
- Imanishi, M., 2006, *AJ*, 131, 2406
- Imanishi, M., Nakagawa, T., Ohshima, Y., *et al.*, 2008, *PASJ*, 60, 489
- Joblin, C., Tielens, A.G.G.M., Allamandola, L.J., & Geballe, T.R., 1996, *ApJ*, 458, 610
- Jones, T.J., Hyland, A.R., & Allen, D.A., 1983, *MNRAS*, 205, 187
- Jones, A.P., 1990, *MNRAS*, 247, 305
- Koike, C., Wickramasinghe, N.C., Kano, N., *et al.*, 1995, *MNRAS*, 277, 986
- Lee, W., & Wdowiak, T.J., 1993, *ApJ*, 417, L49
- Mason, R.E., Wright, G., Pendleton, Y., & Adamson, A., 2004, *ApJ*, 613, 770
- Mason, R.E., Geballe, T.R., Packham, C., *et al.*, 2006, *ApJ*, 640, 612
- McFadzean, A.D., Whittet, D.C.B., Bode, M.F., Adamson, A.J., & Longmore, A.J., 1989, *MNRAS*, 241, 873
- Mennella, V., Brucato, J.R., Colangeli, L., & Palumbo, P., 1999, *ApJ*, 524, L71
- Mennella, V., Brucato, J.R., Colangeli, L., & Palumbo, P., 2002, *ApJ*, 569, 531
- Moutou, C., Sellgren, K., Verstraete, L., & Léger, A., 1999, *A&A*, 347, 949

- Ott, U., 1993, *Nature*, 364, 25
- Patzer, A.B.C., Chang, C., John, M., Sedlmayr, E., & Sülzle, D., 2003, *Astron. Nachr. Suppl.*, 324, 20
- Pendleton, Y.J., & Allamandola, L.J., 2002, *ApJS*, 138, 75
- Pendleton, Y.J., Sandford, S.A., Allamandola, L.J., Tielens, A.G.G.M., & Sellgren, K., 1994, *ApJ*, 437, 683
- Peeters, E., Hony, S., Van Kerckhoven, C., *et al.*, 2002, *A&A*, 390, 1089
- Pino, T., *et al.*, 2008, *A&A*, 490, 665
- Pirali, O., Vervloet, M., Dahl, J.E., *et al.*, 2007, *ApJ*, 661, 919
- Risaliti, G., *et al.*, 2006, *MNRAS*, 365, 303
- Sakata, A., Wada, S., Onaka, T., & Tokunaga, A.T., 1990, *ApJ*, 353, 543
- Sandford, S.A., Allamandola, L.J., Tielens, A.G.G.M., *et al.*, 1991, *ApJ*, 371, 607
- Sandford, S.A., Pendleton, Y.J., & Allamandola, L.J., 1995, *ApJ*, 440, 697
- Schnaiter, M., Mutschke, H., Dorschner, J., Henning, T., & Salama, F., 1998, *ApJ*, 498, 486
- Scott, A.D., Duley, W.W., & Jahani, H.R., 1997, *ApJ*, 490, L175
- Sellgren, K., Werner, M.W., & Ingalls, J.G., 2009, *Amer. Astron. Soc. Meet. Abs.*, 214, #402.12
- Sellgren, K., Werner, M.W., Ingalls, J.G., *et al.*, 2010, *ApJ*, 722, L54
- Sloan, G.C., *et al.*, 2007, *ApJ*, 664, 1144
- Szczerba, R., Siódmiak, N., & Szyszka, C., 2005, *Planet. Nebulae Astron. Tools*, 804, 214
- Tielens, A.G.G.M., Wooden, D.H., Allamandola, L.J., Bregman, J., & Witteborn, F.C., 1996, *ApJ*, 461, 210
- van Diedenoven, B., Peeters, E., Van Kerckhoven, C., *et al.*, 2004, *ApJ*, 611, 928
- Volk, K., Kwok, S., Hrivnak, B., & Szczerba, R., 2001, *Astrophys. Space Sci. Libr.*, 265, 323

INTERACTION OF ATOMIC HYDROGEN WITH CARBON GRAINS

V. Mennella¹

Abstract. Laboratory studies on the interaction of atomic hydrogen with aliphatic and aromatic hydrogenated carbon grains are discussed. When exposed to atomic hydrogen, both types of hydrogenated carbon grains act as catalysts for molecular hydrogen formation. In the first case, an exchange reaction with hydrogen chemisorbed in aliphatic carbon sites is the formation route to H₂ formation. For aromatic carbon grains, the formation of molecular hydrogen takes place through a two-step reaction sequence: 1) super hydrogenation of the aromatic carbon islands of grains 2) exchange reactions on these islands. This mechanism represents a good approximation of molecular hydrogen formation on large neutral PAHs.

1 Introduction

The evolution of carbon dust in the Interstellar Medium (ISM) is driven by heat, irradiation by cosmic rays and UV photons and interaction with gas. Simulation of carbon dust processing under diffuse and dense medium conditions indicates that the key process for the evolution of the interstellar aliphatic carbon component is its interaction with H atoms. This interaction is able to counteract the destruction of C-H bonds by UV photons and cosmic rays and activates the 3.4 μm absorption band in diffuse interstellar regions and the 3.47 μm feature in dense clouds (Mennella *et al.* 2001, 2002, 2003; Mennella 2008a). The interesting aspect is that the same carbon grain population can absorb at the two different wavelengths as a consequence of evolutionary transformations caused by processing. The transformations are compatible with the time-scale required by fast cycling of materials between dense and diffuse regions of the ISM. Moreover, this carbon component, after the inclusion in a comet during the formation process in the cold outer edge of the solar nebula, may evolve to develop the CH₂ and CH₃ groups (as suggested by laboratory simulations) and contribute to the aliphatic band at

¹ INAF-Osservatorio Astronomico di Capodimonte, Napoli, Italy

3.4 μm of IDPs and in particles of comet Wild 2 collected by the Stardust mission (Mennella 2010).

The interaction of gas with dust grains also plays an important role for the chemical evolution of the ISM. Many molecules observed in the ISM can form as a consequence of gas-phase reactions (Herbst *et al.* 2005 and references therein). However, the formation of important species (*e.g.* H_2 , H_2O and CO_2) requires the presence of dust grain surfaces that act as catalysts. In the case of molecular hydrogen, gas-phase reactions for the conversion of H atoms to H_2 are inefficient to account for the observed abundances of this molecule in the ISM (*e.g.* Williams 2005). The catalytic role of silicates, carbon grains and water ice has been demonstrated at low temperature through experiments performed by several groups (*e.g.* Pirronello *et al.* 1997, 1999; Manicò *et al.* 2001; Hornekaer *et al.* 2003; Perets *et al.* 2005). The recombination efficiency is high only at low temperatures. Laboratory results fail to explain H_2 production at higher grain temperatures such those expected in photodissociation regions (*e.g.* Habart *et al.* 2004), since the residence time of H atoms in physisorption sites on the surface is too short for recombination to take place.

2 H_2 formation on aliphatic hydrogenated carbon grains

To explain H_2 production at high grain temperatures, Cazaux & Tielens (2004) proposed H atom recombination in chemisorption sites of carbon particles. Their model relies on the experimental and theoretical results obtained on aromatic structures such as graphite and coronene-like carbon clusters. H atoms chemisorbed in aliphatic carbon sites were neglected, since their binding energy was considered too high for those atoms to take part to molecular hydrogen formation. Recently, it has been shown experimentally that the formation of H_2 in aliphatic sites of hydrogenated carbon grains occurs (Mennella 2008b). Exposure of fully hydrogenated carbon grains with D atoms and deuterated carbon grains with H atoms has been performed. Figure 1 shows the spectral effects induced by atoms at 300 K interacting with carbon grains at room temperature. The spectrum of hydrogenated carbon grains (Fig. 1A) is characterized by the C-H stretching band at 3.4 μm . Increasing the D atoms fluence, the C-H stretching feature decreases while the corresponding C-D feature increases. The analogous result is obtained when deuterated carbon grains are exposed to H atoms (Fig. 1B). In this case, the C-D feature decreases while the C-H band increases when H atom fluence increases.

The reaction sequence governing the process is an exchange reaction: first, there is abstraction of hydrogen by a D atom with production of a HD molecule in gas phase; the second step is addition of D atom. HD molecules were detected with real-time mass spectroscopy. From the evolution with atom fluence of the stretching band intensity the abstraction and addition cross sections have been estimated. The small value of the abstraction cross section ($3 \times 10^{-18} \text{ cm}^2$) indicates that the formation of HD takes place through an Eley-Rideal process (see Mennella 2008b for more details). Moreover, abstraction is the rate limiting step of the reaction sequence, since the abstraction and addition cross sections

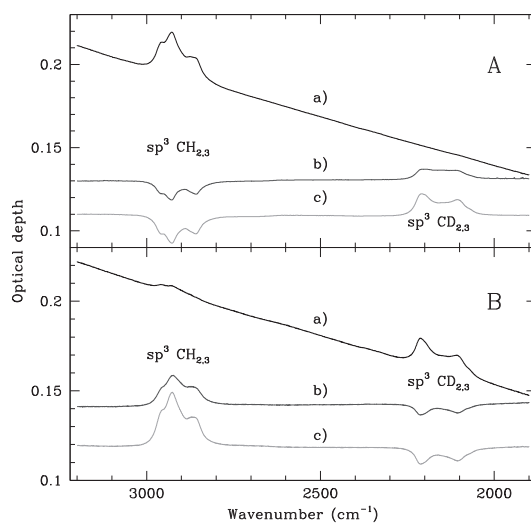


Fig. 1. Evolution of the C-H and C-D stretching bands during D irradiation of hydrogenated carbon grains (A) and H irradiation of deuterated carbon grains (B). In both panels the initial spectrum (a) and those after irradiation (shown after subtraction of the initial spectrum) of 6×10^{17} (b) and 1×10^{19} atoms cm^{-2} (c) are plotted. The difference spectra are offset for clarity. The weak $\text{sp}^3 \text{CH}_{2,3}$ band present in the spectrum of deuterated carbon grains is due to the small fraction (2%) of H_2 present in the D_2 gas used to produce the grains.

are equal, within the errors. These experimental results clearly suggest that H_2 formation occurs on carbon grains even at high grain temperatures since H atoms are bonded to carbon with an energy of about 4 eV, and do not desorb even at high temperatures.

3 H_2 formation on aromatic hydrogenated carbon grains

Theoretical studies have suggested that H_2 can form from abstraction of edge H atoms of PAH cations by incoming H atoms (Cassam-Chenai *et al.* 1994). Alternatively, it has been proposed that H_2 can form on PAH cations in a two-step process: 1) an extra H atom is added to an edge site 2) abstraction of the excess H atom by a second incoming H atom (Bauschlicher 1998). In the case of cations, the formation does not have significant energy barriers. Theoretical studies have shown that low barrier routes to molecular hydrogen formation on neutral coronene exist: H_2 should form by H abstraction on super hydrogenated coronene (Rauls & Hornekaer 2008; Thrower *et al.*, this volume). Laboratory experiments have shown that atomic and molecular hydrogen react with benzene and small PAHs (Petrie *et al.* 1992; Scott *et al.* 1997; Le Page *et al.* 1997; Snow *et al.* 1998). However, the formation of H_2 has not been observed as yet.

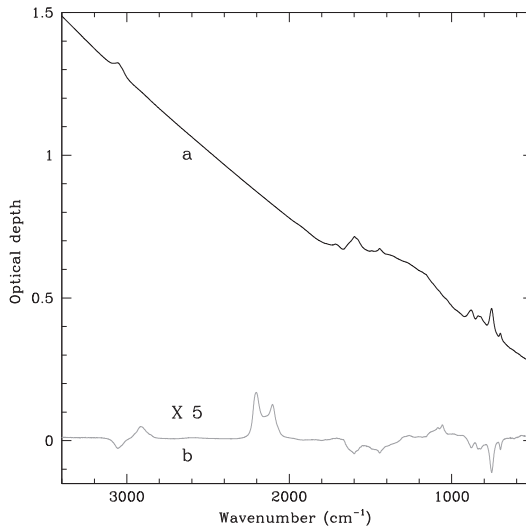


Fig. 2. IR spectrum of BE carbon grains as produced (a). The spectrum is characterized by the C-C and C-O bands at 1600 cm^{-1} ($6.25\text{ }\mu\text{m}$) and 1710 cm^{-1} ($5.85\text{ }\mu\text{m}$) respectively, the weak band at 1442 cm^{-1} ($6.93\text{ }\mu\text{m}$), and by the aromatic C-H bands at 3050 cm^{-1} ($3.28\text{ }\mu\text{m}$) (stretch), the weak mode at 1157 cm^{-1} ($8.64\text{ }\mu\text{m}$) (in plane bend) and the out of plane bend modes between 930 and 670 cm^{-1} . The spectrum after irradiation (shown after subtraction of the initial spectrum) of 1.65×10^{19} D atoms cm^{-2} (b) is also plotted. The intensity of the C-C and C-H bands decreases while the aliphatic C-D stretch bands, falling between 2280 and 2000 cm^{-1} , and the corresponding bending modes, between 1120 and 1020 cm^{-1} , develop with D exposure.

Recently, the interaction of H atoms with a carbon soot (BE) with a marked aromatic character has been studied experimentally (Mennella, in preparation). BE grains have been produced by burning benzene (C_6H_6) in air; they are characterized by a size distribution of ringed sp^2 islands (*e.g.* Colangeli *et al.* 1995). The infrared spectrum of BE (Fig. 2) indicates that, with the exception of the features at $6.25\text{ }\mu\text{m}$ and $5.85\text{ }\mu\text{m}$, all the bands are due to C-H vibrations of hydrogen bonded to aromatic carbon sites. There is no evidence for aliphatic C-H vibrational modes.

Exposure of BE at room temperature to D atoms at 300 K induces significant changes in the spectrum (Fig. 2). The C-C feature at $6.25\text{ }\mu\text{m}$ and all the bands due to the aromatic C-H modes decrease in intensity with D fluence. The formation of the C-D aromatic bands is not observed, while the aliphatic C-D bands develop with D irradiation. The feature at 2912 cm^{-1} is attributed to the C-H stretching mode of CHD. The detailed evolution with D atom fluence of the aromatic C-H and aliphatic C-D stretching band intensity is shown in Figure 3. From the observed trends, it is possible to derive the destruction cross section of aromatic C-H bonds and the formation of the aliphatic C-D bonds. The small

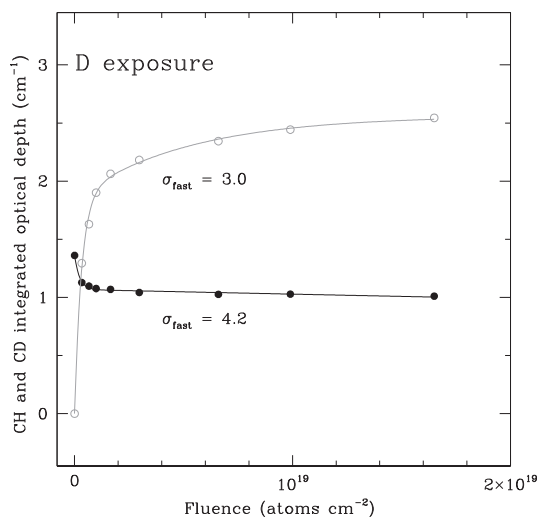


Fig. 3. Evolution with D atom fluence of the aromatic C-H (filled circles) and aliphatic C-D (empty circles) stretch band integrated optical depth. The best fit to the data of the relations $a_1[1 - \exp(-\sigma_{fast}F)] + a_2[1 - \exp(-\sigma_{slow}F)]$ and $b_1 \exp(-\sigma_{fast}F) + b_2 \exp(-\sigma_{slow}F)$, respectively for the C-D and C-H modes, are also shown. The estimated cross sections are expressed in units of 10^{-2} \AA^2 .

values of the cross sections suggest that an Eley-Rideal type process drives the spectral changes produced by D atom irradiation. Unlike the case of D irradiation of aliphatic hydrogenated carbon grains, the spectral changes do not suggest an exchange reaction in the aromatic sites, since the formation of aromatic C-D bonds is not observed. Rather, they indicate super hydrogenation of the aromatic structures of grains as new aliphatic C-D bonds form. In fact, D atoms break a sp^2 double bonds inducing the formation sp^3 C-D bonds.

As one can see in Figure 3, at high fluences the spectral variations are smaller and smaller. To understand which reactions are active in those conditions, at the end of D atom exposure of BE, irradiation has been continued using H atoms at 300 K. H atom exposure determines an increase of the aliphatic C-H stretching and bending modes and a decrease of the corresponding aliphatic C-D bands. On the contrary, there is no variation of the aromatic features. These spectral changes are similar to those observed during H atom irradiation of deuterated aliphatic carbon grains and are indicative of exchange reactions in the aliphatic sites. The exchange reactions form HD molecules. These results clearly show that superhydrogenated aromatic carbon islands act as catalysts for molecular hydrogen formation. Moreover, they represent a good approximation of H_2 formation on neutral PAHs, as the reactions induced by H atoms in aromatic carbon grains are Eley-Reideal type processes.

This work has been supported by ASI research contracts.

References

- Bauschlicher, C.W., Jr., 1998, *ApJ*, 509, L125
- Cassam-Chenaï, P., Pauzat, F., & Ellinger, Y., 1994, *Molec. Grains Space*, 312, 543
- Cazaux, S., & Tielens, A.G.G.M., 2004, *ApJ*, 604, 222
- Colangeli, L., Mennella, V., Palumbo, P., Rotundi, A., & Bussoletti, E., 1995, *A&AS*, 113, 561
- Habart, E., Boulanger, F., Verstraete, L., Walmsley, C.M., & Pineau des Forêts, G., 2004, *A&A*, 414, 531
- Herbst, E., Chang, Q., & Cuppen, H.M., 2005, *J. Phys. Conf. Ser.*, 6, 18
- Hornekær, L., Baurichter, A., Petrunin, V.V., Field, D., & Luntz, A.C., 2003, *Science*, 302, 1943
- Le Page, V., Keheyan, Y., Bierbaum, V.M., & Snow, T.P., 1997, *J. Am. Chem. Soc.*, 119, 8373
- Manicò, G., Ragunì, G., Pirronello, V., Roser, J.E., & Vidali, G., 2001, *ApJ*, 548, L253
- Mennella, V., 2010, *ApJ*, 718, 867
- Mennella, V., 2008a, *ApJ*, 682, L101
- Mennella, V., 2008b, *ApJ*, 684, L25
- Mennella, V., Baratta, G.A., Esposito, A., Ferini, G., & Pendleton, Y.J., 2003, *ApJ*, 587, 727
- Mennella, V., Brucato, J.R., Colangeli, L., & Palumbo, P., 2002, *ApJ*, 569, 531
- Mennella, V., Muñoz Caro, G., Ruiterkam, R., *et al.*, 2001, *A&A*, 367, 355
- Perets, H.B., Biham, O., Manicó, G., *et al.*, 2005, *ApJ*, 627, 850
- Petrie, S., Javahery, G., & Bohme, D.K., 1992, *J. Am. Chem. Soc.*, 114, 9205
- Pirronello, V., Biham, O., Liu, C., Shen, L., & Vidali, G., 1997, *ApJ*, 483, L131
- Pirronello, V., Liu, C., Roser, J.E., & Vidali G., 1999, *A&A*, 344, 681
- Rauls, E., & Hornekær, L., 2008, *ApJ*, 679, 531
- Scott, G.B., Fairley, D.A., Freeman, C.G., *et al.*, 1997, *J. Phys. Chem. A*, 101, 4973
- Snow, T.P., Le Page, V., Keheyan, Y., & Bierbaum, V.M., 1998, *Nature*, 391, 259
- Williams, D.A., 2005, *J. Phys. Conf. Ser.*, 6, 1

NEAR-INFRARED SPECTROSCOPY OF INTERSTELLAR DUST

F. Boulanger¹, T. Onaka², P. Pilleri^{3,4} and C. Joblin^{3,4}

Abstract. Near infrared observations of reflection nebulae have set the historical ground for the discovery of interstellar PAHs, but since, space observations have focused on their mid-IR features, and data shortward of $5\ \mu\text{m}$ have remained scarce. The Spitzer/IRAC images in the 3.6 and $4.5\ \mu\text{m}$ channels do show that the near-IR emission from small dust particles is ubiquitous across the Galaxy, but provide no spectroscopic information. To investigate the nature of this near-IR dust emission, we have obtained AKARI spectroscopic observations, over the $2.5 - 5\ \mu\text{m}$ spectral range, for a set of archetype PDRs mapped with the Spitzer spectrometer at mid-IR wavelengths. These AKARI data supplement earlier observations with the SWS ISO spectrometer, in providing the gain in sensitivity needed to observe low excitation sources, and the spatial information required to spatially correlate near-IR spectroscopic signatures with physical conditions and observed changes in mid-IR spectra. This paper presents the first results of the data analysis, in relation to two open questions on interstellar PAHs. (1) Is there an evolutionary link from aliphatic carbon dust to PAHs? (2) What is the origin of the near-IR dust continuum? The AKARI spectra display features longward of the main $3.29\ \mu\text{m}$ PAH feature, and continuum emission. The intensity ratio between the features ascribed to aliphatic CH bonds and the $3.29\ \mu\text{m}$ aromatic band, varies spatially in a way that may be interpreted as evidence for aromatization of the smallest dust particles by photo-processing. The continuum displays a striking step-increase across the $3.29\ \mu\text{m}$ feature. We also present a spectrum of a photodissociation region with a feature at $4.65\ \mu\text{m}$, which has been speculated to be related to the CD stretch in aliphatic hydrocarbon side-groups on PAHs.

¹ Institut d'Astrophysique Spatiale (IAS), UMR 8617, CNRS & Université Paris-Sud 11, Bâtiment 121, 91405 Orsay Cedex, France

² Department of Astronomy, University of Tokyo, Tokyo 113-0033, Japan

³ Université de Toulouse, UPS, CESR, 9 avenue du colonel Roche, 31028 Toulouse, France

⁴ CNRS, UMR 5187, 31028 Toulouse, France

1 Introduction

The discovery of near infrared (Near-IR) extended emission in reflection nebulae (Sellgren *et al.* 1983) initiated a new field of observations and research on interstellar dust. To account for the $3.3\ \mu\text{m}$ feature and the associated mid-IR features Léger & Puget (1984) proposed that the emission follows stochastic heating of polycyclic aromatic hydrocarbon molecules (PAHs). The PAH emission features have since been observed to be a ubiquitous spectroscopic signature of dust in galaxies. Very small carbon dust particles (PAH molecules and very small grains) are established as a major constituent of interstellar dust that play key roles in the physics and chemistry of the interstellar medium (ISM), but discussions at this conference have shown that the origin and nature of these particles are still debated.

Near-IR wavelengths are of particular relevance to characterize the smallest particles of interstellar dust. First, the near-IR dust emission is thought to arise from the very smallest particles with less than ~ 100 carbon atoms. Second, emission in the C-H stretching modes in the 3.3 to $3.5\ \mu\text{m}$ range are best suited to probe the presence of aliphatic side groups to PAHs. Other characteristic modes of CH_3 and CH_2 bonds that fall at ~ 6.9 and $\sim 7.2\ \mu\text{m}$ are more difficult to observe due to the presence of the 6.2 and $7.7\ \mu\text{m}$ PAH emission band. Third, one may probe the physics of the particle emission by characterizing the emission shortward and longward of the C-H stretch bands.

Despite its specific interest, the near-IR spectral range has been barely explored (Geballe *et al.* 1989). The IRAS, IRTS, ISO and Spitzer space missions have provided us with a wealth of mid-IR observations, but spectroscopy shortward of $5\ \mu\text{m}$ is only available for bright sources with a high UV field (Verstraete *et al.* 2001; van Dienenhoven *et al.* 2004), such as the Orion Bar and the M17SW photodissociation regions (PDRs), and with little spatial information. The AKARI warm mission has provided the opportunity to obtain near-IR spectroscopy of diffuse emission with unprecedented sensitivity (Ohyama *et al.* 2007). In this paper, we briefly present our AKARI observing program, and the first results of the data analysis. This is an early account of on-going work, which will lead to a more thorough publication in a refereed journal.

2 AKARI observations

Our AKARI observing program was designed to investigate dust emission in PDRs. We used the AKARI grating spectrometer with an entrance slit $50''$ long. Our targets comprise 15 slit positions selected within six archetype star forming regions, on the basis of ISO and Spitzer mid-IR spectro-imaging observations. The list of targets includes objects with different excitation conditions (UV radiation field from 100 to a few 1000 times the Solar Neighborhood value), which show strong variation in their mid-IR spectra (C-C to C-H features intensity ratio and band/continuum contrast). It also spans a range of distances, from the local ISM to the 30 Doradus LMC star forming region, to explore a range of physical scales.

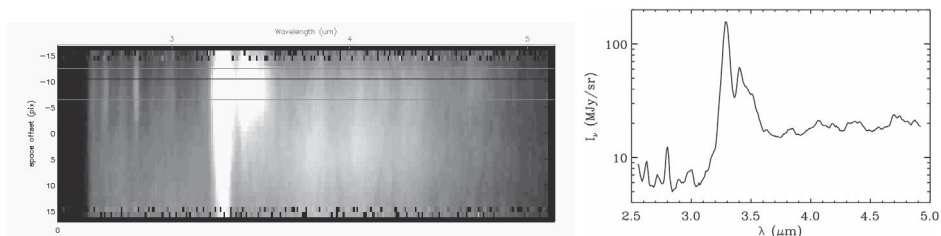


Fig. 1. AKARI observation of one pointing towards the reflection nebula NGC 7023. The spectral image is displayed to the left (wavelengths increasing from the left to the right). To the right, we show the spectrum extracted by averaging data within the two red lines at the top of the image. The log-scale highlights the fainter features at longer wavelengths, and the near-IR continuum with its step-increase across the $3.3 - 3.5 \mu\text{m}$ range.

These AKARI data offer the combination of spatial (along the slit) and spectral information, required to spatially correlate near-IR spectroscopic signatures with physical conditions and mid-IR spectro-imaging observations.

The data have been reduced and calibrated by the Japanese team members using the best knowledge of the instrument (see Onaka *et al.* elsewhere in this volume). The outcome of the data reduction is a spectral image from which spectra can be extracted as a function of position along the slit (Fig. 1). The spectral resolution, measured on hydrogen recombination lines, ranges from 90 to 160. We use an observation of HII gas emission towards 30 Doradus to validate the spectrometer capability to perform photometry of extended emission. This HII spectrum shows 10 hydrogen lines and continuum emission (free-free + free-bound), which are both in agreement with predictions from photo-ionization models. Spectral lines with intensities down to 2–3 MJy/sr, and a 5 MJy/sr continuum, are reliably measured.

3 AKARI dust spectra

To illustrate the initial results of the data analysis, we present spectra measured for one slit position in the reflection nebula NGC 7023 (Figs. 1 and 2), and a spectrum of a molecular cloud in the Large Magellanic Cloud (Fig. 3). This last spectrum obtained towards the massive star forming region 30 Doradus includes several hydrogen recombination lines. In Figure 3, the gas emission, lines and continuum, has been removed using a photo-ionization model. The near-IR emission from dust comprises the prominent $3.29 \mu\text{m}$ feature, a weaker spectrally structured plateau extending to $3.6 \mu\text{m}$, and continuum emission. The step increase of the continuum emission from short to long wavelengths, across the $3.3 - 3.5 \mu\text{m}$ range, is a remarkable result, which is observed in all spectra.

The $3.29 \mu\text{m}$ feature is assigned to the $v = 1 - 0$ aromatic C–H stretch transition. Emission in this feature is predicted to come mainly from neutral PAHs (DeFrees *et al.* 1993). Several types of transitions, most likely the C–H stretch

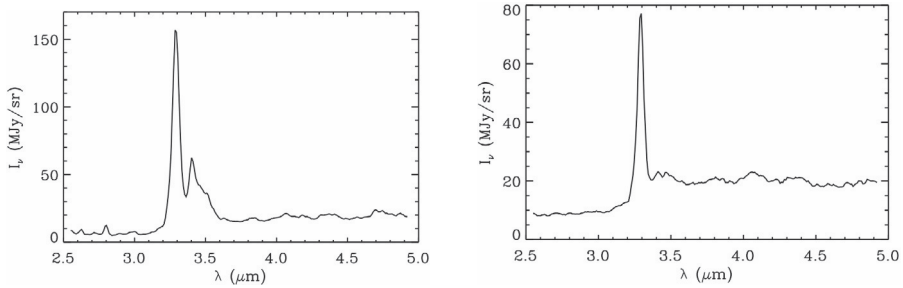


Fig. 2. AKARI spectra at two positions within the reflection nebula NGC 7023. The two positions sample the variation in intensity ratios of the mid-IR PAH features, which has been interpreted as evidence of the transition from neutral to cation PAHs (Rapacioli *et al.* 2005; Berné *et al.* 2007). From the left to the right spectra, the AKARI observations show the disappearance of the $3.4 \mu\text{m}$ emission feature, and an increase by a factor 2 of the intensity of the continuum relative to that of the $3.3 \mu\text{m}$ emission feature.

in aliphatic side groups attached to PAHs or in sur-hydrogenated PAHs, but also possibly, combination bands and hot bands including the $\nu = 2 - 1$ aromatic C–H transition, also contribute to the plateau and superimposed features (Allamandola *et al.* 1989; Joblin *et al.* 1996; Bernstein *et al.* 1996). The near-IR continuum has been observed to be a dominant component of the near-IR emission from the diffuse ISM (Flagey *et al.* 2006), but it has never received a definitive interpretation within the PAH hypothesis. The step-increase in the continuum intensity across the $3.29 \mu\text{m}$ (Fig. 1) band strongly suggests that the continuum is associated with the de-excitation of PAHs, but the emission process has still to be characterized. Allamandola *et al.* (1989) proposed that the continuum represents emission through vibrational modes, which become weakly active in excited PAHs. The combination of a large number of weak overlapping bands would make a quasi-continuum with little spectral structure. Within this interpretation, the step increase of the continuum emission across the C–H $3.29 \mu\text{m}$ feature could reflect the lower coupling efficiency between C–C and C–H modes than between C–C modes. Fluorescence emission from an electronic excited state provides an alternative interpretation (Léger *et al.* 1988). Modelling (private communication from Pino and Schmidt) supported by experimental data suggests that, in PAH cations, the energy gap between the first excited state and the ground state may be small enough for cations to fluoresce in the near-IR. A more detailed analysis of the data will allow us to test this interpretation by looking for a spatial correlation between the continuum emission and that of PAH cations inferred from the decomposition of mid-IR spectra (Rapacioli *et al.* 2005; Berné *et al.* 2007).

4 Evidence for small dust processing

The nature of the small carbon dust particles has to be addressed within the broad context of the evolutionary cycle that can link them to the amorphous

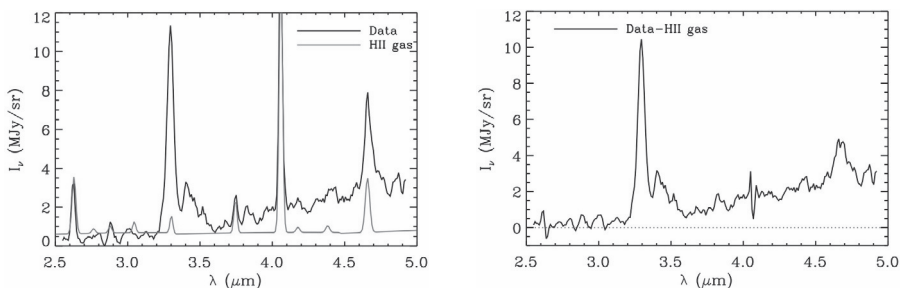


Fig. 3. AKARI spectrum of a molecular cloud in the Large Magellanic Cloud. The plot shows the emission spectrum with the dust and hydrogen lines to the left, and the spectrum obtained after subtraction of the gas emission to the right. We are confident that the $4.65 \mu\text{m}$ feature is real. We have no interpretation for this band at present.

hydrogenated carbon dust seen in absorption spectroscopy (Dartois in this volume). Interstellar PAHs and VSGs could be produced by photo and/or mechanical fragmentation in grain-grain collisions involving amorphous carbon grains (Jones *et al.* 1996) or PAH clusters (Rapacioli *et al.* 2006). The free fragments are expected to be progressively photo-processed by selective dissociation of side groups and loss of non-aromatic CH bonds, when they are exposed to increasing ultraviolet photon fluxes as they move out of the shielded interiors of molecular clouds. This evolutionary scenario can be tested by studying the evolution of the $3.4 \mu\text{m}$ aliphatic band relative to the $3.3 \mu\text{m}$ aromatic band. In particular, we plan to study whether these variations are spatially correlated with variations in emission components inferred from mid-IR spectro-imaging observations (Rapacioli *et al.* 2005; Berné *et al.* 2007).

Onaka *et al.* (elsewhere in this volume) report large variations of the emission ratio, $3.4 + 3.5 \mu\text{m}$ to $3.3 \mu\text{m}$, for the diffuse Galactic emission. We observe similar variations on smaller scales within nearby PDRs. These results extend ground-based observations on brighter sources (Geballe *et al.* 1989; Joblin *et al.* 1996). The two spectra of NGC 7023 in Figure 2 are taken at the opposite ends of the $50''$ long slit, within and out of the dense surface of the molecular cloud (left and right spectra, respectively), marked by bright filamentary structure in PAH and near-IR H_2 images. The disappearance of the $3.4 \mu\text{m}$ emission feature may be interpreted as evidence for aromatization of the smallest dust particles by photo-processing. A thorough analysis of the spatial variations of the aliphatic to aromatic emission ratio across the NGC 7023 PDR is required to ascertain and fully quantify this interpretation.

5 Looking for new spectral features

The AKARI spectra offer an unprecedented opportunity to look for faint near-IR spectral features. The C–D stretching mode around $4.5 \mu\text{m}$ (4.4 and $4.65 \mu\text{m}$ for

the aromatic/aliphatic C–D bond, respectively) is of particular interest to test if PAHs are highly deuterated (Draine 2004; Peeters *et al.* 2004). The C–D in-plane and out-of-plane bending modes, expected at 11.7 and 15.4 μm , cannot be unambiguously identified, because they fall in a spectral region where other PAH features are present.

Analyses of spectra obtained with the Far Ultraviolet Spectroscopic Explorer (FUSE) satellite, together with spectra from the Copernicus space mission and ISM absorption probe spectrograph (IMAPS), have revealed a factor 4 variation in the observed D/H ratios for interstellar gas in the Solar Neighborhood (Linsky *et al.* 2006). Linsky *et al.* argue that spatial variations in the depletion of deuterium onto dust grains can explain the variations in the observed gas-phase D/H ratios. This interpretation is supported by the correlation of D/H with the gas column density and depletions of the refractory metals iron and silicon. Gas-grain reactions could lead to a high deuteration of hydrogenated carbonaceous grains and PAHs (Draine 2004). The gain in sensitivity provided by AKARI permit to look for deuterated PAHs in sources, less excited than the Orion Bar and M17SW PDRs studied in Peeters *et al.* (2004), which are more directly relevant to the deuteration of PAHs in the diffuse ISM (Onaka *et al.* in this volume).

We are presently cautious in reporting new spectral features, but we are not aware of any data artifact that could contaminate the emission feature at 4.65 μm in Figure 3. We are thus confident that this feature is real. Its central wavelength matches that of the aliphatic C–D stretch mode (Peeters *et al.* 2004). However, the absence of the corresponding aromatic band at 4.4 μm , and the intensity of the feature – comparable to that of the 3.4 μm – make the identification with deuterated aliphatic side groups on PAHs unsure.

We thank several participants of the conference, in particular Lou Allamandola, Philippe Bréchnignac, Thomas Pino, Tim Schmidt, Kris Sellgren, and Xander Tielens, for discussions that helped us with the interpretation of the data.

References

- Allamandola, L.J., Tielens, A., & Barker, J.R., 1989, *ApJS*, 71, 733
 Berné O., Joblin, C., Deville, Y., *et al.*, 2007, *A&A*, 469, 575
 Bernstein, M.P., Sandford, S.A., & Allamandola, L.J., 1996, *ApJ*, 472, L127
 DeFrees, D.J., Miller, M.D., Talbi, D., *et al.*, 1993, *ApJ*, 408, 530
 Draine, B.T., 2004, in *Astrophysics in the Far Ultraviolet [Astro-ph/0410310]*
 Draine, B.T., & Li, A., 2007, *ApJ*, 657, 810
 Flagey N., Boulanger F., Verstraete, L., *et al.*, 2006, *A&A*, 453, 969
 Geballe, T.R., Tielens, A.G.G.M., Allamandola, L.J., *et al.*, 1989, *ApJ*, 341, 278
 Joblin, C., Tielens, A.G.G.M., Allamandola, L.J., & Geballe, T.R., 1996, *ApJ*, 458, 610
 Jones, A.P., Tielens, A.G.G.M., & Hollenbach, D.J., 1996, *ApJ*, 469, 740
 Léger, A., & Puget, J.L., 1984, *A&A*, 137, L5
 Léger, dHendecourt, L., & Boissel, P., 1988, *PhRvL*, 60, 921L

- Linsky, J., Draine, B.T., Moos, H.W., *et al.*, 2006, ApJ, 647, 1106
Ohyama, Y., Onaka, T., Matsuhara, H., *et al.*, 2007, PASJ, 59, S411
Peeters, E., Allamandola, L.J., Bauschlicher, C.W., *et al.*, 2004, ApJ, 604, 252
Rapacioli, M., Joblin, C., & Boissel, P., 2005, A&A, 429, 193
Rapacioli, M., Calvo, F., Joblin, C., *et al.*, 2006, A&A, 460, 519
Sellgren, K., Werner, M.W., & Dinerstein, H.L., 1983, ApJ, 271, L13
van Diedenhoven, B., Peeters, E., Van Kerckhoven, C., *et al.*, 2004, ApJ, 611, 928
Verstraete, L., Pech, C., Moutou, C., *et al.*, 2001, A&A, 372, 981

ATYPICAL DUST SPECIES IN THE EJECTA OF CLASSICAL NOVAE

L.A. Helton¹, A. Evans², C.E. Woodward¹ and R.D. Gehrz¹

Abstract. A classical nova outburst arises from a thermonuclear runaway in the hydrogen-rich material accreted onto the surface of a white dwarf in a binary system. These explosions can produce copious amounts of heavy element enriched material that are ejected violently into the surrounding interstellar medium. In some novae, conditions in the ejecta are suitable for the formation of dust of various compositions, including silicates, amorphous carbon, silicon carbide, and hydrocarbons. Multiple dust grain types are sometimes produced in the same system. CO formation in novae may not reach saturation, thus invalidating the usual paradigm in which the C:O ratio determines the dust species. A few novae, such as V705 Cas and DZ Cru, have exhibited emission features near 6, 8, and 11 μm that are similar to “Unidentified Infrared” (UIR) features, but with significant differences in position and band structure. Here, we present *Spitzer* IRS spectra of two recent dusty novae, V2361 Cyg and V2362 Cyg, that harbor similar peculiar emission structures superimposed on features arising from carbonaceous grains. In other astronomical objects, such as star forming regions and young stellar objects, emission peaks at 6.2, 7.7, and 11.3 μm have been associated with polycyclic aromatic hydrocarbon (PAH) complexes. We suggest that hydrogenated amorphous carbon (HAC) may be the source of these features in novae based upon the spectral behavior of the emission features and the conditions under which the dust formed.

1 Introduction

A classical nova (CN) is an eruption arising on the surface of a white dwarf (WD) in a binary system in which the WD is accreting material from a main sequence

¹ Department of Astronomy, School of Physics and Astronomy, University of Minnesota, 116 Church St. SE, Minneapolis, MN 55455, USA;

e-mail: ahelton@astro.umn.edu; chelsea@astro.umn.edu; & gehrz@astro.umn.edu

² Astrophysics Group, Keele University, Keele, Staffordshire ST5 5BG, UK;

e-mail: ae@astro.keele.ac.uk

companion through Roche-lobe overflow. The accreted material accumulates on the surface of the WD until it reaches a density and temperature high enough to initiate a thermonuclear runaway (TNR), resulting in explosive nucleosynthesis and violent ejection of up to 10^{-6} to $10^{-4} M_{\odot}$ of accreted material at velocities exceeding 1000 km s^{-1} . The ejecta are initially optically thick, but as they expand, the density rapidly declines resulting in the recession of the optically thick pseudophotosphere inwards towards the hot underlying WD. This energetic underlying central engine actively photoionizes the ejecta, resulting in the appearance of emission lines from a wide range of isoelectronic species.

CNe frequently produce dust in their ejecta. The dust condensation event is signaled by a rapid decline in the optical light curve due to extinction and a corresponding rise in the infrared luminosity due to thermal emission. Models of the spectral energy distribution (SED) in these systems suggest that the condensation event yields relatively large dust grains with radii up to $\sim 1 \mu\text{m}$ (Gehrz 2008). Unlike most astronomical sources of dust, novae have been observed to produce both carbon rich and oxygen rich dust species simultaneously (*e.g.*, Gehrz *et al.* 1992). Evans & Rawlings (2008) suggest that this chemical dichotomy may be explained by incomplete carbon monoxide formation in the ejecta. If CO does not form to saturation, then neither carbon nor oxygen will be entirely bound up in CO, leaving both available for dust production.

2 Atypical dust species in classical novae

Novae V705 Cas, V842 Cen, and QV Vul exhibited emission features similar to unidentified infrared features (UIRs; Geballe 1997) often attributed to polycyclic aromatic hydrocarbons (PAHs; Allamandola *et al.* 1989) or hydrogenated amorphous carbons (HACs; Duley & Williams 1983). Observations of V705 Cas beginning 157 days after outburst revealed UIR features at 8.2, 8.7, and $11.4 \mu\text{m}$ superimposed on a $10 \mu\text{m}$ silicate emission feature (Evans *et al.* 1997). Subsequent analysis of the $8 \mu\text{m}$ complex by Evans *et al.* (2005) indicated that the band shape and peak wavelength did not match those of standard UIR features and that the peak wavelength drifted bluewards as the system evolved. Simultaneously, the ratio of the 11.4 to $8 \mu\text{m}$ features increased. The $3\text{--}4 \mu\text{m}$ region in the spectrum of V705 Cas showed emission features at 3.28 and $3.4 \mu\text{m}$. These are typically attributed to unsaturated C-H stretching mode oscillations in aromatic molecules and saturated C-H stretching vibrations in aliphatic bonds, respectively. Thus, the $3.28/3.4 \mu\text{m}$ ratio can be used as an indicator of the relative abundance of aromatic to aliphatic structures in the emitting material (Sloan *et al.* 1997). The observed 3.28 to $3.4 \mu\text{m}$ ratio was similar to that seen in post-AGB stars, but an order of magnitude higher than in stars with a high UV photon flux. The behavior of these features in V705 Cas was similar to those observed in V842 Cen and QV Vul. Evans & Rawlings (1994) suggested that during the optically thick stage of dust formation, the rate of H capture is greater than the rate of UV photon absorption. Thus, the conditions are conducive to the growth of aliphatic bonds, *e.g.* HAC grains.

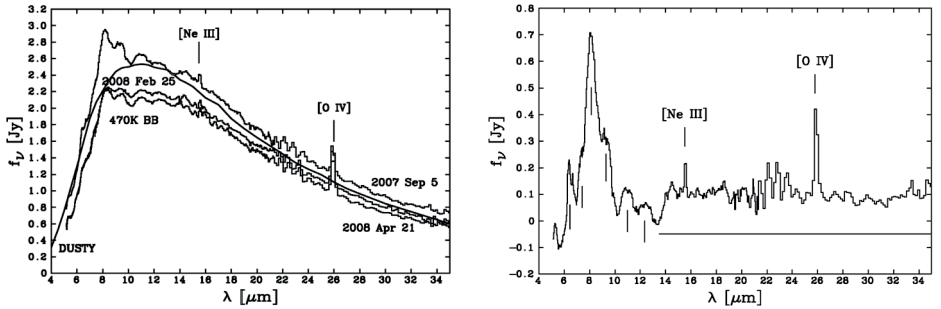


Fig. 1. *Left:* *Spitzer* IRS spectra of DZ Cru with a DUSTY model of AC at 470 K. *Right:* residuals after DUSTY model subtraction showing UIR features.

2.1 DZ Cru

DZ Cru was observed as part of our *Spitzer* Classical Novae Target-of-Opportunity and Monitoring campaign (Evans *et al.* 2010). Due to poor sampling of the light curve, the optical depth of the dust extinction event is not known. Our first *Spitzer* Infrared Spectrograph (IRS) observations commenced nearly 1500 days after eruption. They revealed exceptionally strong emission from amorphous carbon (AC) with superimposed UIR emission features reminiscent of those observed in V705 Cas. The left panel of Figure 1 shows three epochs of *Spitzer* IRS data along with a DUSTY (Ivezić *et al.* 1999) model of AC dust at 470 K. Subtraction of the DUSTY model (Fig. 1, right panel) revealed emission features at 6.5, 7.2, 8.1, 9.3, 11.0, and 12.4 μm . The wavelengths of these features do not correspond with the standard PAH features observed at 6.2, 7.7, 8.6, 11.3, and 12.7 μm .

2.2 V2362 Cyg

V2362 Cyg was a peculiar nova in many respects (see Lynch *et al.* 2008). One of the most interesting characteristics was its optical light curve behavior. After a smooth initial decline the light curve plateaued and subsequently experienced a secondary brightening event, which rivaled its initial outburst luminosity. At the peak of the second outburst, the nova underwent a rapid and extreme dust formation event. The *Spitzer* IRS spectra obtained immediately following dust condensation revealed blackbody emission at 1400 K, near the extreme high end of dust condensation temperatures. At first, low ionization [Ne II], [Ne III], and [O IV] were observed in the spectra alongside a hydrogen recombination spectrum. But within a few days, as the dust emission strengthened, the emission lines disappeared with the sole exception of [O IV], which remained strong throughout.

With the decline in the dust optical depth due to expansion of the ejecta, the emission lines reappeared, but at a much higher ionization level. A range of ionization states was observed including [Ne III], [Ne V], [Ne VI], [Mg V], and [Mg VII], indicating a very energetic ionization field. Indeed, *Swift* observations

from this period indicated a strong, hard X-ray flux that persisted for at least 300 days.

During this same period of optically thin dust emission, strong, broad UIR features near 6–10, 11.5, and 18 μm became evident. We fitted and subtracted a blackbody continuum to isolate the emission components. The results are shown in the left panels of Figure 2. Distinct emission peaks appeared at 6.4, 6.9, 7.9, 9.5, 11.4, 12.5, and 17.9 μm . The features near 9.5 and 18 μm may be associated with silicates. As the ejecta evolved, the central wavelengths of the UIR features varied slightly and irregularly, while the flux ratios changed dramatically. The 6.9, 11.4, and 12.5 μm features declined rapidly and soon disappeared. The fluxes of the 6.4 and 7.9 μm features declined sharply relative to the 9.5 and 17.9 μm features. The 17.9 μm feature began to dominate the spectrum at late times.

2.3 V2361 Cyg

The spectrum of V2361 Cyg was very similar to that of V2362 Cyg. The primary differences were the lack of emission features at 9.5 and 18 μm and additional structure in the 6–10 μm spectral region. Spectra obtained as part of our *Spitzer* program were fitted with blackbody curves. The residuals after blackbody subtraction are shown in the right panels of Figure 2. UIR emission features were observed at 5.4, 6.4, 6.9, 7.1, 7.5, 8.1, 11.5, and 12.4 μm . As the ejecta evolved, the complex of features between 6.4 and 8.1 μm blended together to form a single plateau, while the 6.4 to 8.1 μm flux ratio diminished significantly. The 11.5 and 12.4 μm features joined to produce a broad structure around 13.1 μm .

In Figure 2-h, we compare the observed emission from V2361 Cyg at 102 days post outburst to the Class A, B, and C PAH features described by Peeters *et al.* (2002) and van Dienenhoven *et al.* (2004). The Class A and B PAHs may be excluded as potential contributors due to the poor fit to the emission peaks. The Class C profiles are more consistent with the data. In particular, the 8 μm component of the Class C emission fits the red side of the profile quite well. Sloan *et al.* (2007) have attributed the Class C profiles to carriers with a high fraction of aliphatic bonds.

3 The model

The *Spitzer* IRS observations of DZ Cru, V2362 Cyg, and V2361 Cyg in combination with the previous studies of V705 Cas, V842 Cen, and QV Vul provide the basis for an elementary model for the processing of dust and complex hydrocarbon molecules in classical novae. The dust formation event proceeds quite rapidly with dust grains condensing out of the gas phase and growing to sizes up to $\sim 1 \mu\text{m}$ in a matter of days. In part, this is likely due to the inhomogeneous, clumpy distribution of the ejecta. With the onset of grain formation, the opacity in these regions increases, shielding the rest of the material from the underlying radiation and allowing the acceleration of condensation.

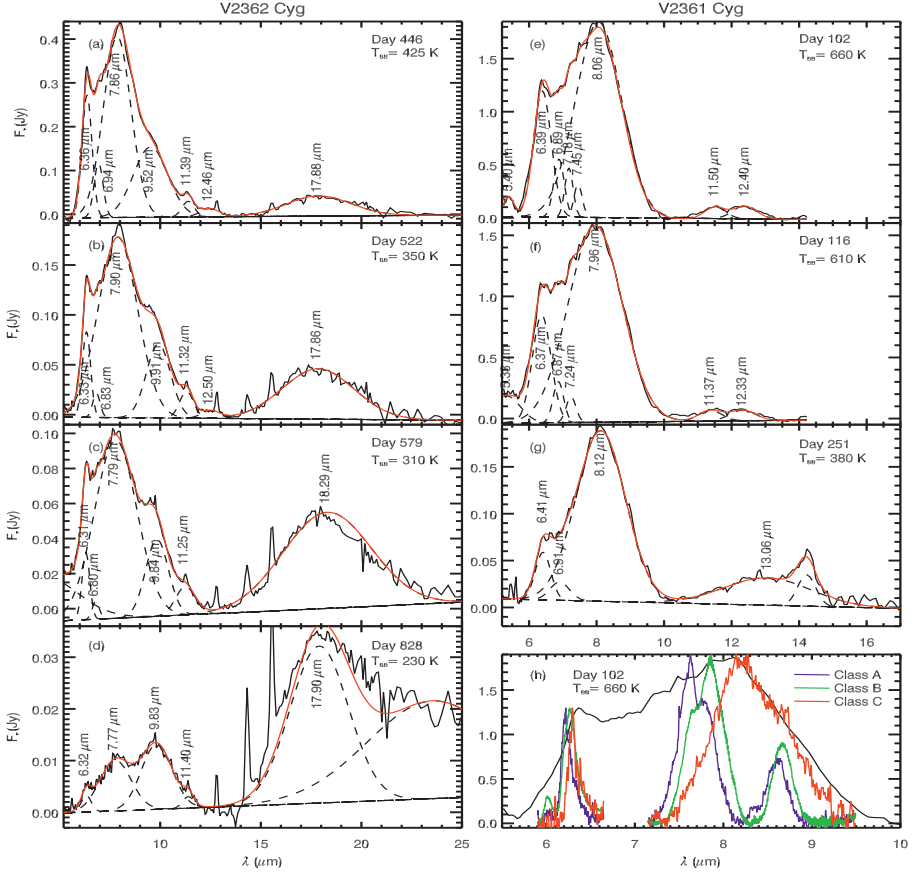


Fig. 2. Residuals for V2362 Cyg, (a)–(d), and V2361 Cyg, (e)–(g). Dashed lines are individual Gaussian components of the composite fit shown in red. Panel (h) shows Class A, B, and C PAH profiles (Peeters *et al.* 2002) overlaid on the V2361 Cyg spectra from Day 102.

The types of dust produced during the condensation event depend on the conditions and abundances in the ejecta. In typical novae, the dust formed is composed of AC, silicates, or some combination thereof. In the novae discussed here, the dominant dust species appears to be carbonaceous. Evans & Rawlings (1994) argued that at the opacities observed during the dust condensation stage in novae, the likelihood for H capture is much higher than the probability of UV photon interaction, thus enhancing the production of aliphatic bonds. This conclusion suggests that the smaller end of the grain size distribution may be due to PAH molecules and larger, more complex HAC agglomerations. However, as the ejecta expand and densities decline, the optical depth of the dust forming regions decreases as the pseudophotosphere recedes, exposing the freshly condensed dust to an increasingly hard and intense radiation field.

Evans & Rawlings (1994) have calculated that small PAHs (*i.e.*, molecules with fewer than 24 C atoms) have a very short lifetime in the environment of a CN. Due to the high UV flux, a free-flying PAH molecule would absorb about one high energy photon every second and would be completely disrupted in less than a day. These same molecules would also be subjected to chemical erosion through collisional interactions in the ejecta. For reasonable densities, temperatures, and abundances in the ejecta, Evans & Rawlings estimated that these PAHs would be destroyed due to chemi-sputtering by H and O in a matter of hours.

If some of the emission features seen in V2361 Cyg, V2362 Cyg, and DZ Cru can be attributed to small PAHs instead of HACs, then there must be a reservoir of material from which the PAHs are being repopulated. This material could be produced by either HACs or the larger AC grains themselves when submitted to energetic processes. Though rapidly destroyed, the transient population of free-flying PAHs could generate some of the observed UIR emission features.

In order to better constrain the carriers of the UIR features observed in CN, it is critical to obtain observations of the expanding ejecta throughout the dust condensation and subsequent stages. If the carrier molecules are being formed during the initial condensation event, they may be observable during or immediately after condensation. Data covering the 3–4 μm region are required in order to determine the relative contributions of aromatic to aliphatic material.

This work was supported in part by *Spitzer*/JPL grants 1294825 and 1289430.

References

- Allamandola, L.J., Tielens, A.G.G.M., & Barker, J.R., 1989, *ApJS*, 71, 733
Duley, W.W., & Williams, D.A., 1983, *MNRAS*, 205, 67P
Evans, A., & Rawlings, J.M.C., 1994, *MNRAS*, 269, 427
Evans, A., Geballe, T.R., Rawlings, J.M.C., Eyres, S.P.S., & Davies, J.K., 1997, *MNRAS*, 292, 192
Evans, A., Tyne, V.H., Smith, O., *et al.*, 2005, *MNRAS*, 360, 1483
Evans, A., & Rawlings, J.M.C., 2008, in *Classical Novae*, 2nd Edition, ed. M.F. Bode & A. Evans (Cambridge Univ. Press: Cambridge)
Evans, A., Gehrz, R.D., Woodward, C.E., *et al.*, 2010, *MNRAS*, 406, 85
Geballe, T.R., 1997, *From Stardust to Planetesimals*, 122, 119
Gehrz, R.D., 2008, in *Classical Novae*, 2nd Edition, ed. M.F. Bode & A. Evans (Cambridge Univ. Press: Cambridge)
Gehrz, R.D., 1992, *ApJ*, 400, 671
Ivezić, Ž., Nenkova, M., & Elitzer, M., 1999 [[arXiv:astro-ph/9910475](https://arxiv.org/abs/astro-ph/9910475)]
Lynch, D.K., Woodward, C.E., Gehrz, R.D., *et al.*, 2008, *AJ*, 136, 1815
Peeters, E., Hony, S., Van Kerckhoven, C., *et al.*, 2002, *A&A*, 390, 1089
Sloan, G.C., Jura, M., Duley, W.W., *et al.*, 2007, *ApJ*, 664, 1144
Sloan, G.C., Bregman, J.D., Geballe, T.R., Allamandola, L.J., & Woodward, C.E., 1997, *ApJ*, 474, 735
van Dienenhoven, B., Peeters, E., Van Kerckhoven, C., *et al.*, 2004, *ApJ*, 611, 928

**The Role of PAHs
in the Interstellar Medium**

THE ROLE OF PAHS IN THE PHYSICS OF THE INTERSTELLAR MEDIUM

L. Verstraete¹

Abstract. In the interstellar medium (ISM), PAHs are abundant and also carry most of the dust surface. They are thus privileged sites for surface reactions such as the formation of H₂. In regions penetrated by UV photons, PAHs loose electrons by the photoelectric effect and efficiently heat the gas. In more shielded regions, PAH recombine and may carry an important fraction of the cloud electronic charge which plays an important role in the gas dynamics and chemistry. We review here processes involving PAHs which control key aspects of the physics of the ISM. We also discuss the corresponding observational constraints. Most of these processes involve a detailed knowledge of the charge of PAHs and we therefore review current models in this area. We argue that more laboratory measurements of the rate of electronic capture on large PAH cations are needed.

1 Introduction

The interstellar lifecycle brings matter from low-density medium (the diffuse ISM or atomic HI gas heated by the standard radiation field) to dense, molecular clouds and eventually protostars. Thanks to the mechanical action of evolved stars (winds, supernovae), molecular clouds are dispersed and restored to the diffuse ISM. Intimately mixed to the gas, dust and in particular the small grains (of radius $a \leq 10$ nm, which include PAHs) play an important role in the thermodynamics, dynamics and chemistry of the ISM. Dust is also the main source of extinction and thus controls the radiative transfer in interstellar clouds.

The primary effect of the interstellar lifecycle on dust is to change the abundance of small grains with respect to larger ones (radii from 10 to a few 100 nm) during fragmentation (by radiation or shocks in the diffuse ISM) and growth (by coagulation in dense regions) episodes. In the vicinity of young stars or in shocks PAHs are observed to be depleted (Geers *et al.* 2006, 2009; Peeters *et al.* 2005;

¹ Institut d'Astrophysique Spatiale, UMR 8617, University Paris-Sud 11, Bât. 121, 91405 Orsay Cedex, France

Lebouteiller *et al.* 2007; see Acke *et al.*; Rho *et al.*, Sandstrom *et al.* and Siebenmorgen this volume). PAH coagulation is suggested by observations of molecular clouds (Boulanger *et al.* 1994; Flagey *et al.* 2009). Conversely, PAHs may be photoevaporated off larger grains when fresh molecular material is exposed to stellar UV radiation thus producing a limb brightening effect (Boulanger *et al.* 1990; Bernard *et al.* 1993; Rapacioli *et al.* 2005; Berné *et al.* 2007; Compiègne *et al.* 2008; Velusamy & Langer 2008; Rapacioli *et al.* this volume).

In the following, we first review interstellar processes where PAHs play an important role and discuss the observational evidence. The next section is devoted to a key property of PAHs: their charge distribution. A brief summary is then given.

2 Physical processes involving PAHs

Interstellar PAHs are abundant (they bear about 20% of the total carbon abundance in diffuse clouds: Joblin *et al.* 1992; Zubko *et al.* 2004; Draine & Li 2007) and are the smallest grains (0.4 to 1 nm in radius) of dust grains. Because of these properties PAHs play a peculiar role in the physics and chemistry of the ISM. While discussing the key interstellar processes which involve PAHs, we will see that most of them require a detailed knowledge of the charge distribution of PAHs.

2.1 Photoelectric heating of the gas

Observations at 21 cm show that the diffuse atomic (HI) gas is at temperatures between 100 and 10^4 K and in rough pressure equilibrium. To explain these temperatures, early models of the gas thermal state proposed that the HI gas was heated by cosmic rays (Field *et al.* 1969) but it was later realized that the flux of energetic nuclei was much (~ 10 times) lower. Watson (1972) then proposed that the heating of HI gas may be due to the photoelectric effect on interstellar grains.

In this process, an UV photon ejects an electron from the grain: this first step is often called *photoemission*. The kinetic energy carried away by the electron (typically 1 to 2 eV) is then rapidly deposited in the gas by inelastic collisions (in less than 10 years for proton densities $n_H > 1 \text{ cm}^{-3}$). To trigger photoemission, the energy of the incident photon must satisfy $h\nu > IP$ where IP is the ionization potential or photoelectric threshold which depends on the charge Z (algebraic number of electron charges carried by the PAH) and size a of the grain. The photoelectric effect is characterized by its probability or yield and its energetic efficiency. The yield Y_{PE} is the ratio of the photoemission cross-section to the absorption cross-section and depends on the energy of the photon¹. Let E_e be the mean energy of the electron ejected, the photoelectric efficiency is given by $\epsilon = Y_{PE} E_e/h\nu_a$ with $h\nu_a$ the mean energy of photons absorbed by the grain.

¹We will quote here Y_{PE} for $h\nu = 10$ eV, roughly the energy of the maximum photoemission rate in the Mathis *et al.* radiation field.

Interstellar grains may also capture electrons from the gas leading to an energy gas loss proportional to $k_B T$ per capture (see Draine 1978, Eq. (10)). This process is called *grain recombination cooling*. Its contribution, particularly important in warm gas, must be subtracted from the photoelectric heating rate to obtain the net photoelectric rate Γ_{PE} ($\text{erg cm}^{-3} \text{s}^{-1}$).

Watson (1973) further pointed out that high yields ($Y_{PE} > 0.1$) were expected for small grains because the mean free path of the electron on its way to the grain surface becomes comparable to the grain size. Early models of photoelectric heating assumed $Y_{PE} \sim 0.1$ and were successful in explaining the cold HI gas but had difficulties in supporting the warm ($T > 5000$ K) gas because of the strong grain recombination cooling (Draine 1978). The photoelectric effect on PAHs does not suffer of this problem because of the higher energy of the ejected electron implying a larger cut-off temperature for the heating rate² (Verstraete *et al.* 1990). Because of their small size, PAHs have a high photoelectric yield ($Y_{PE} \geq 0.4$) and, in the neutral gas, a small mean charge both properties implying a high photoelectric efficiency (*e.g.*, Bakes & Tielens 1994 hereafter BT94)³. Current models of photoelectric heating show that ϵ is maximum (a few percents) in the limit of small size ($a < 1$ nm) and charge ($Z < 1$) (BT94; Weingartner & Draine 2001 hereafter WD01).

Theoretical studies of the gas thermal balance have shown that the photoelectric effect is the dominant heating process over a wide range of conditions in gas density $0.1 \leq n_H \leq 10^4 \text{ cm}^{-3}$ and intensity of radiation field $1 \leq G_0 \leq 10^6$. On the other hand, the gas cools by collisional excitation of optically thin emission lines of major species such as C^+ , O, H, H_2 and CO, depending on the gas density and temperature. The photoelectric heating thus controls the gas temperature and hence the line emissivity and chemistry of interstellar clouds. Moreover, the photoelectric heating also determines the conditions under which the gas becomes thermally unstable, a key process in understanding the structure and evolution of the ISM (Audit & Hennebelle 2005, 2010).

The hypothesis of gas photoelectric heating can be tested observationally. At densities $n_H > 1 \text{ cm}^{-3}$, the gas cools rapidly (in less than 0.1 Myr) and can be assumed to be in thermal equilibrium, *i.e.*, $\Gamma_{PE} = \Lambda$ where Λ is the gas cooling rate in $\text{erg cm}^{-3} \text{s}^{-1}$. Observations of the cooling lines thus directly trace Γ_{PE} . The latter can then be compared to the dust IR emission to determine which grain sizes contribute most to the heating and with which efficiency, in order to check model predictions. Over the last decade, such studies have been performed in different contexts. Habart *et al.* (2001) made a detailed study of an isolated cloud with well-known properties (exciting radiation field, density profile). Using ISO-LWS observations of the major cooling lines ([CII]158 μm and [OI]63 μm) and extracting the emission of each dust population from IRAS data, they found that the gas cooling is well correlated with the IR emission of small grains and

²The temperature at which the photoelectric heating and recombination cooling rates cancel.

³Electrostatic forces bring IP close to 13.6 eV when $Z > 0$.

that the photoelectric heating efficiency for PAHs was 3% and decreases for larger grains. Modelling the [CII]158 μm emission measured by ISO-LWS towards 9 high-galactic latitude translucent clouds ($A_V \leq 5$), Ingalls *et al.* (2002) found an overall photoelectric heating efficiency of 4.3%. They also showed that the decrease of CII emission at high dust emission is due to radiative transfer inside clouds (see also Juvela *et al.* 2003). More recently, Rubin *et al.* (2009) studied the 30 Doradus star forming region in the Large Magellanic Cloud with Spitzer IRAC+MIPS (dust emission) and BICE data (CII emission). They also found that PAHs have the highest photoelectric efficiency, about 5%. Finally, in external normal galaxies, a correlation has been found between the CII line and the 5-to-10 μm ISOCAM emission ascribed to PAHs (Helou *et al.* 2001). All these results are in good agreement with model predictions of the photoelectric effect on dust grains and show the dominant role of PAHs for the gas heating.

2.2 Screening of UV radiation

Aromatic species like PAHs show strong UV absorption in two broad bands centered at 200 nm ($\pi^* \leftarrow \pi$ transitions) and 70 nm ($\sigma^* \leftarrow \sigma$ transitions). PAHs are thus good candidates to explain the 217 nm bump and the far-UV rise of the interstellar extinction curve as suggested by recent theoretical and laboratory studies (see the review by Mulas *et al.* this volume and Cecchi-Pestellini *et al.* 2008; Steglich *et al.* 2009). In particular, PAHs absorb efficiently dissociating photons (at $\lambda \leq 100$ nm) thus controlling the molecular fraction and excitation of interstellar clouds. This UV screen will be enhanced if PAHs are more abundant at cloud boundaries as suggested by observations (the limb brightening effect, see Sect. 1). As discussed by Mulas *et al.* (this volume), the far-UV absorption of PAHs depends on their charge state.

2.3 Ionization of dense gas

The delocalized π -electrons of PAHs are easily polarizable (Omont 1986). Thus due to their high polarizability and abundance PAHs can efficiently capture electrons and, in shielded interstellar regions, PAH anions may be as abundant as electrons ($x = n_e/n_H \sim 10^{-7}$). Charge exchange between positive ions generated by cosmic rays in the gas and PAH anions quenches the ion-molecule chemistry and may reconcile observations and models (Bakes & Tielens 1998; Flower *et al.* 2007; Wakelam & Herbst 2009; Goicoechea *et al.* 2009). The role of PAHs in interstellar chemistry is discussed by Bierbaum *et al.* (this volume). PAH anions may also induce recombination of CII, hence leading to warmer gas in diffuse clouds (Wolfire *et al.* 2008).

Charged PAHs are also important for the ion-neutral coupling and the dynamics. In magnetic C-shocks, PAHs may produce a shortage of electrons leading to the decoupling of larger grains in the shock tail. At a given density, this will increase the Alfvén velocity in the shock and its emissivity by the ion-neutral drift (Ciolek *et al.* 2002, 2004; Guillet *et al.* 2007). In the context of protostars, the

role of PAHs in braking the collapse has been studied by Ciolek and collaborators. At cloud boundaries where UV photons are less shielded, PAHs may carry positive as well as negative charges (see Sect. 3): this could accelerate the coagulation of PAHs together as suggested by the observations of Flagey *et al.* (2009).

2.4 H_2 formation

It has long been known that, at ISM densities, H_2 cannot form efficiently in the gas phase. In 1963, Gould & Salpeter proposed that H_2 may form by catalytic reaction on interstellar grains where an H atom bound to the grain surface recombines with another H. Molecular hydrogen has a profound impact on the physics and chemistry of the ISM: it efficiently cools the gas (Le Bourlot *et al.* 1999) and acts as a shield to photodissociating UV photons, initiating the formation of CO and of chemistry. In spite of many theoretical and experimental studies, the detailed mechanism by which H_2 forms is complex and still debated because it depends on the structure and composition of the grains (surface roughness, presence of chemisorption sites for H) and involves the issue of distributing the 4.5 eV bonding energy of the molecule between excitation energy (grain, H_2 vibrational or rotational) and H_2 kinetic energy (see Bierbaum *et al.*, Throner *et al.* this volume). The rate coefficient for H_2 formation is observed to vary from a few tenths to a few times the standard value of Jura (1975), $R_0 = 3 \times 10^{-17} \text{ cm}^3 \text{ s}^{-1}$ (Gry *et al.* 2002; Browning *et al.*, Habart *et al.* 2003; Gillmon *et al.* 2006; Thi *et al.* 2009). In addition, the observations of H_2 emission in excited regions favor formation routes involving chemisorbed sites for H (Habart *et al.* 2004).

PAHs are attractive candidates for the formation of H_2 because they represent two thirds of the total grain surface, *e.g.*, Habart *et al.* 2004) and carry chemically bonded H atoms. Observations indicate an expected trend between H_2 and PAH integrated emissions (Habart *et al.* 2004) but the corresponding emissivity profiles are not always correlated, (Habart *et al.* 2003; Berné *et al.* 2009; Velusamy & Langer 2008). These results may be related to the radiative transfer of UV photons across cloud borders with different density profiles. Shock excited H_2 emission does not suffer of this limitation and should represent a better test (Guillard *et al.* 2010). Analysing UV absorption data in diffuse clouds, Wolfire *et al.* (2008) modelled in a consistent way the C/C^+ and HI/H_2 transitions with PAH assisted recombination of C^+ and photoelectric heating. Their results also indicate a correlation between the PAH abundance and the H_2 formation rate.

2.5 *Spinning dust emission and microwave polarization*

At centimetric wavelengths (around 30 GHz), an emission component discovered by Kogut *et al.* (1996) in COBE data was later shown to correlate with the emission of large dust grains (Leitch *et al.*; de Oliveira-Costa *et al.* 1997). Unexpected in this spectral range where the free-free, synchrotron and large grain emissions usually dominate, this component was dubbed *anomalous emission*. Due to this mixing, the existence of anomalous emission has long been debated and it is only

recently that it has been extracted in all-sky WMAP data thanks to the constraints on polarization (Miville-Deschênes *et al.* 2008). Understanding this emission is particularly important because it appears in a spectral region where fluctuations of the cosmic microwave background are best measured. It is now further traced by the measurements of the Planck mission.

Several emission mechanisms have been proposed to explain the anomalous emission. Draine & Lazarian (1998a) considered the rotational emission of PAHs (or spinning dust emission). Draine & Lazarian (1999) further proposed magnetic dipole emission of grains with magnetic inclusions and Jones (2009) proposed low-energy transitions arising in disordered grains. The latter two mechanisms involve large grains ($a \sim 0.1 \mu\text{m}$). Recent analysis of observations indicate that the anomalous emission correlates better with the mid-IR emission due to PAHs (Casassus *et al.* 2006, 2009; Ysard *et al.* 2010) than with the emission of larger grains. Another hint comes from polarization: the anomalous emission appears to be weakly polarized (Battistelli *et al.* 2006) as expected for small grains (Lazarian & Draine 2000; Martin *et al.* 2007) thus favoring the spinning dust explanation⁴. These results have stimulated new theoretical studies of PAH rotational dynamics in the ISM (Ali-Haïmoud *et al.* 2009; Ysard & Verstraete; Hoang *et al.*; Silsbee *et al.* 2010) which confirmed the main features of the Draine & Lazarian (1998b) model. Namely, the PAH rotation is mostly controlled by gas-grain collisions and, in irradiated regions, also by their vibrational (IR) emission. In addition, these processes depend on the PAH charge.

The anomalous emission may thus trace the PAH abundance and provide new constraints on PAHs such as their permanent electric dipole moment. Further on, the contribution of spinning PAHs could reduce the polarization fraction measured in the microwave by Planck. Quantitative modelling of this emission component is necessary for the analysis of the Planck polarization data in the cosmological context but also for ISM studies (magnetic field).

3 The charge distribution of PAHs

Most of the processes discussed in the previous section require a detailed knowledge of the PAH charge distribution. This is also true for the spectroscopic properties of PAHs, from the IR to the UV (Pauzat, Pino *et al.*, Mulas *et al.*, Oomens this volume). We therefore review the current state-of-the-art in modelling the charge of interstellar PAHs.

In the ISM PAHs become charged because of photoemission or collisions with charged species. Excluding dark clouds (where PAHs may have coagulated on larger grains), the latter case involves the most abundant species e^- , H^+ and C^+ . Since the characteristic times for charge fluctuations are short, a stationary description is often adopted (see Ivlev *et al.* 2010 however for a discussion of the

⁴Conversely, large grains are known to polarize light in emission (FIR to submm) and extinction (IR to UV), indicating that grains are not spherical and aligned with the magnetic field.

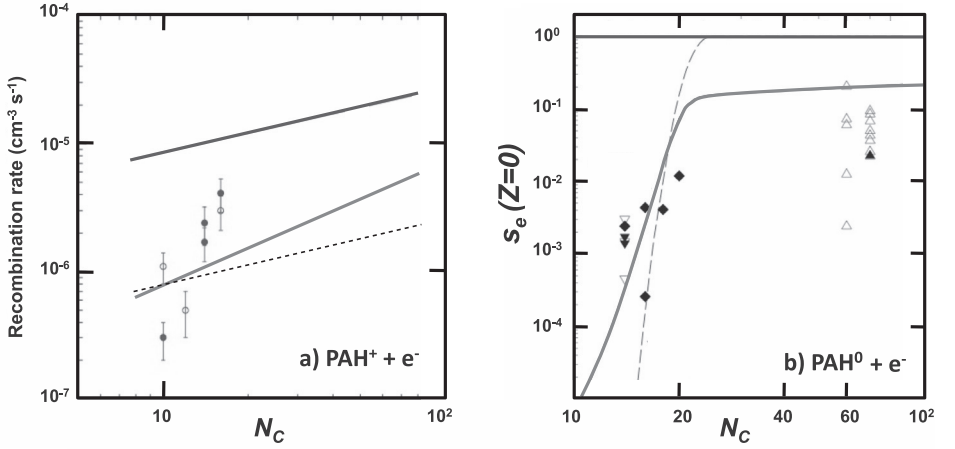


Fig. 1. a) Rate coefficient at 300 K as a function of size (in number of C atoms per molecule) for the electronic recombination of PAH⁺ (adapted from Tielens 2008). The data points are from Biennier *et al.* (2006). The bottom solid line shows the law adopted by WD01 and the top solid line that of BT94 ($s_e = 1$). The dashed line shows the $s_e = 0.1$ -case. b) Sticking coefficient for electronic capture on a neutral PAH as a function of size (adapted from WD01, note that triangles at large sizes are for C₆₀ and C₇₀). Solid lines are as in a). The dashed line shows the law of Dartois & d’Hendecourt (1997).

effect of charge fluctuations). The charge distribution $f(Z)$ is then derived from the balance equation (BT94):

$$f(Z) [J_{PE}(Z) + J_i(Z)] = f(Z + 1) J_e(Z + 1) \quad (3.1)$$

written for a given PAH size and where the J -terms represent charge currents. Estimates of the latter require the knowledge of rate coefficients which depends on intrinsic quantities such as the photoelectric yield, the threshold IP and the electron capture rate coefficient (or sticking coefficient) (see Sect. 2.1). Two types of models have been developed: (i) *molecular models* using the properties measured in the laboratory on small, real molecules (Allain *et al.*, Salama *et al.* 1996; Le Page *et al.* 2001, 2003) and, (ii) *astrophysical models* treating PAHs as generic species whose properties follow size trends based on laboratory measurements (BT94; Dartois & d’Hendecourt 1997; WD01; van Hoof *et al.* 2004). Being more widely applied, we focus here on the models of BT94 and WD01.

The photoelectric (or photoionization) yield for PAHs has been measured on a few, small (containing less than 25C atoms) PAHs (Verstraete *et al.* 1990; Jochims *et al.* 1996). The expressions used by BT94 and WD01 provide a good description of these data and extrapolate well to measurements on larger ($a \geq 100$ nm) grains (Abbas *et al.* 2006). The functions for the photoelectric threshold $IP(Z, a)$ used in both models are also similar with the exception of the electron affinity ($Z = -1$),

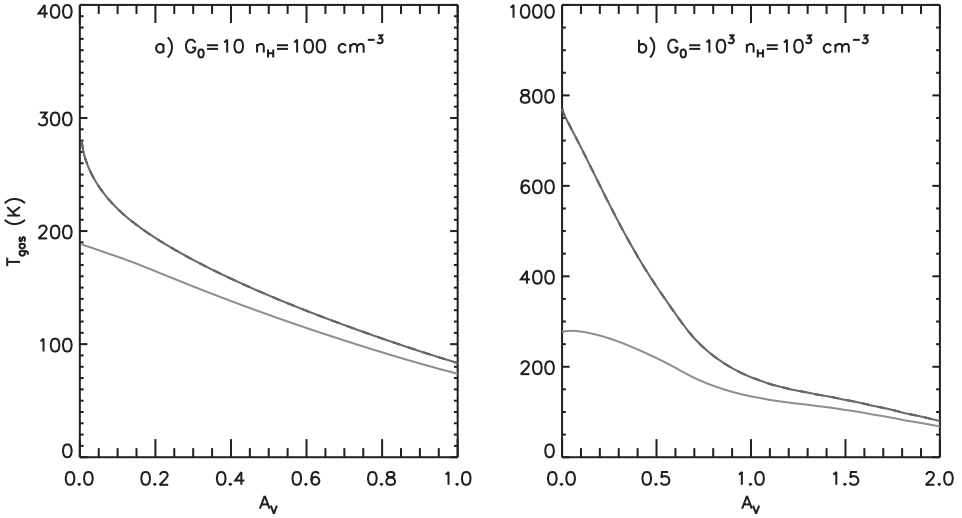


Fig. 2. Temperature profile as a function of optical depth for two PDRs of a) low and b) high excitation. In both panels, the bottom (top) solid line shows the WD01 (BT94) case respectively.

somewhat overestimated by BT94. It is worth noting that these thresholds do not apply to fullerenes such as C_{60} , C_{70} (BT94).

The situation is different for the sticking coefficient (or probability) s_e of the electronic capture: WD01 use a size dependent coefficient whereas BT94 assume $s_e = 1$ for all sizes. These two prescriptions are compared to laboratory data in Figure 1 as a function of molecular size. Note that for interstellar PAHs, one has $N_C > 15$ (Le Page *et al.* 2003). The prescription of BT94 leads to a more efficient electronic capture and hence more abundant neutral or anionic species. We note that the laboratory measurements for PAH^+ recombination fall between the BT94 and WD01 prescriptions which can therefore be seen as extreme cases. Another consequence is that the photoelectric heating rate of BT94 is stronger than that of WD01 because PAHs are less positively charged in the former case (see Sect. 2.1). We illustrate this in Figure 2 by comparing the gas temperature across two photodissociated interfaces or photon-dominated regions (PDR) computed with the Meudon PDR code (Le Petit *et al.* 2006). The physics and chemistry of such regions depend on the gas density n_H and on the intensity of the UV radiation field represented by G_0^5 . We ran isochoric models irradiated on a single side (see Fig. 2) and with the following gas abundances (in ppm): [C]=130, [O]=320, [N]=75, [Mg]=35, [Fe]=28, [Si]=1. As expected, in the BT94 case the mean charge

⁵ G_0 is a scaling factor for the energy density of the radiation field integrated between 6 and 13.6 eV; $G_0 = 1$ corresponds to the standard radiation field of Mathis *et al.* (1983).

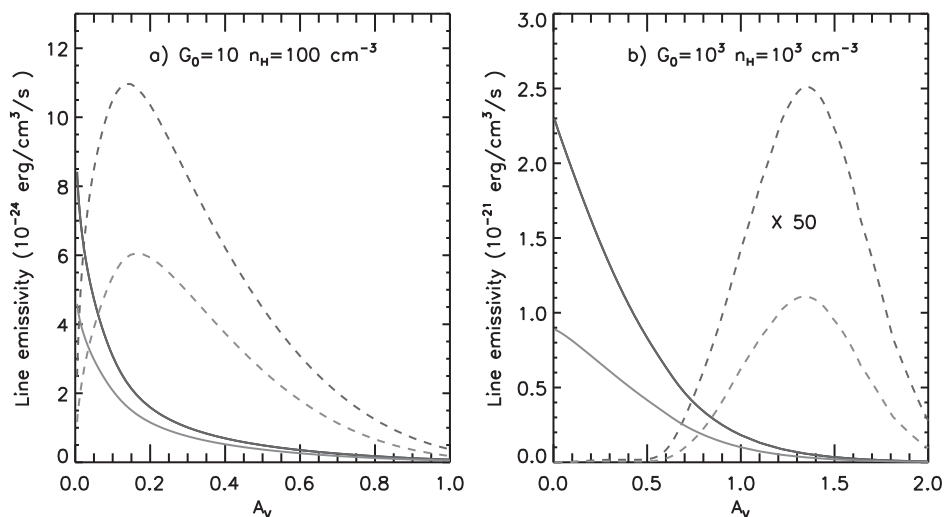


Fig. 3. Line emissivity profiles as a function of optical depth in two PDRs. As in Fig. 2, the bottom (top) solid and dashed lines represent the case of WD01 (BT94). The solid line shows the [OI]63 μm emissivity and the dashed line shows the emissivity in the first 4 rotational lines of H_2 . For clarity the H_2 emissivities have been multiplied by 50.

$\langle Z \rangle$ of a 20C PAH is shifted by -0.5 to -1 with respect to the WD01 case⁶. The photoelectric heating rate of BT94 is correspondingly higher (2 to 4 times higher than WD01 for the present $G_0 = 10$ and 10^3 PDRs respectively). Even for conditions of low excitation ($G_0 = 10$), the BT94 model produces significant column densities of warm gas. In an edge-on geometry, the line emissivity (in $\text{erg cm}^{-3} \text{s}^{-1}$) of major gas coolants is significantly affected as illustrated in Figure 3. Integrated line fluxes (face-on geometry) are less affected (below 30% variations). Such differences will lead to quite different diagnostics of the physical conditions (intensity of the UV radiation field, gas density and temperature) and emphasize the need for more laboratory measurements of the electronic capture on astrophysically relevant PAHs (containing more than 20C). Such measurements should also be carried at different temperatures to check that the classical limit often used provides a reasonable description⁷.

Thanks to the contrasted behaviour of the CC-to-CH ratio of the vibrational band intensities in neutral and ionized PAHs (*e.g.*, Bauschlicher *et al.* 2008 and Pauzat this volume), the charge distribution of PAHs can be constrained from mid-IR observations. Flagey *et al.* (2006) found that, in the diffuse ISM, 40% of PAHs are ionized. Analyzing a sample of galactic and extragalactic excited

⁶With the WD01 model, the mean charge is $+0.5$ ($+0.9$) for the $G_0 = 10$ (10^3) PDR respectively.

⁷Some data suggest a behaviour departing from the classical $T^{1/2}$ (Biennier *et al.* 2006).

regions, Galliano *et al.* (2008 and Galliano this volume) found the expected trend between the fraction of ionized PAHs and excitation conditions.

4 Summary

PAHs have a strong impact on the ISM: they dominate the gas heating in irradiated regions and carry a significant fraction of the dust surface, a potential site for the formation of H_2 and other molecules. In dense clouds, PAHs may become an important sink for electrons and control the ion-molecule chemistry as well as the dynamics of neutrals relative to ionized species in presence of a magnetic field. PAHs are therefore key to understanding the evolution of interstellar gas. Most of the processes involving PAHs depend on their charge state and this is also true of their spectroscopical properties. Quantitative state-of-the-art models of the PAH charge are limited by the lack of data on the rate coefficient for the electronic capture on large species containing more than 20 carbon atoms (see also Montillaud *et al.* this volume). This leads to significant uncertainties in deriving the physical conditions and line emission of interstellar clouds. More laboratory measurements are needed in this area.

The author is grateful to Vincent Guillet and Jacques Le Bourlot for useful discussions and help while preparing this review.

References

- Abbas, M.M., *et al.*, 2006, ApJ, 645, 324
Ali-Haimoud, Y., Hirata, C.M., & Dickinson, C., 2009, MNRAS, 395, 1055
Allain, T., Leach, S., & Sedlmayr, E., 1996, A&A, 305, 616
Audit, E., & Hennebelle, P., 2005, A&A, 433, 1
Audit, E., & Hennebelle, P., 2010, A&A, 511, A76
Bakes, E.L.O., & Tielens, A.G.G.M., 1994, ApJ, 427, 822 (BT94)
Bakes, E.L.O., & Tielens, A.G.G.M., 1998, ApJ, 499, 258
Bauschlicher, C.W., Jr., Peeters, E., & Allamandola, L.J., 2008, ApJ, 678, 316
Battistelli, E.S., Rebolo, R., Rubiño-Martín, J.A., *et al.*, 2006, ApJ, 645, L141
Bernard, J.P., Boulanger, F., & Puget, J.L., 1993, A&A, 277, 609
Berné, O., *et al.*, 2007, A&A, 469, 575
Berné, O., Fuente, A., Goicoechea, J.R., *et al.*, 2009, ApJ, 706, L160
Biennier, L., Alsayed-Ali, M., Foutel-Richard, A., *et al.*, 2006, Chem. Evolu. Universe, Faraday Discuss., 133, 289
Boulanger, F., Falgarone, E., Puget, J.L., & Helou, G., 1990, ApJ, 364, 136
Boulanger, F., Prevot, M.L., & Gry, C., 1994, A&A, 284, 956
Browning, M.K., Tumlinson, J., & Shull, J.M., 2003, ApJ, 582, 810
Casassus, S., Cabrera, G.F., Förster, F., *et al.*, 2006, ApJ, 639, 951
Casassus, S., *et al.*, 2008, MNRAS, 391, 1075

- Ciolek, G.E., & Roberge, W.G., 2002, *ApJ*, 567, 947
- Ciolek, G.E., Roberge, W.G., & Mouschovias, T.C., 2004, *ApJ*, 610, 781
- Compiègne, M., Abergel, A., Verstraete, L., & Habart, E., 2008, *A&A*, 491, 797
- Dartois, E., & D'Hendecourt, L., 1997, *A&A*, 323, 534
- de Oliveira-Costa, A., Kogut, A., Devlin, M.J., *et al.*, 1997, *ApJ*, 482, L17
- Draine, B.T., 1978, *ApJS*, 36, 595
- Draine, B.T., & Lazarian, A., 1998a, *ApJ*, 494, L19
- Draine, B.T., & Lazarian, A., 1998b, *ApJ*, 508, 157
- Draine, B.T., & Li, A., 2007, *ApJ*, 657, 810
- Field, G.B., Goldsmith, D.W., & Habing, H.J., 1969, *ApJ*, 155, L149
- Flagey, N., Boulanger, F., Verstraete, L., *et al.*, 2006, *A&A*, 453, 969
- Flagey, N., *et al.*, 2009, *ApJ*, 701, 1450
- Flower, D.R., Pineau Des Forêts, G., & Walmsley, C.M., 2007, *A&A*, 474, 923
- Geers, V.C., *et al.*, 2006, *A&A*, 459, 545
- Geers, V.C., van Dishoeck, E.F., Pontoppidan, K.M., *et al.*, 2009, *A&A*, 495, 837
- Gillmon, K., Shull, J.M., Tumlinson, J., & Danforth, C., 2006, *ApJ*, 636, 891
- Goicoechea, J.R., Pety, J., Gerin, M., Hily-Blant, P., & Le Boulrot, J., 2009, *A&A*, 498, 771
- Gould, R.J., & Salpeter, E.E., 1963, *ApJ*, 138, 393
- Gry, C., Boulanger, F., Nehmé, C., *et al.*, 2002, *A&A*, 391, 675
- Guillard, P., Boulanger, F., Cluver, M.E., *et al.*, 2010 [[arXiv:1004.0677](https://arxiv.org/abs/1004.0677)]
- Guillet, V., Pineau Des Forêts, G., & Jones, A.P., 2007, *A&A*, 476, 263
- Habart, E., Verstraete, L., Boulanger, F., *et al.*, 2001, *A&A*, 373, 702
- Habart, E., Boulanger, F., Verstraete, L., *et al.*, 2003, *A&A*, 397, 623
- Habart, E., Boulanger, F., Verstraete, L., Walmsley, C.M., & Pineau des Forêts, G., 2004, *A&A*, 414, 531
- Hoang, T., Draine, B.T., & Lazarian, A., 2010, *ApJ*, 715, 1462
- Ingalls, J.G., Reach, W.T., & Bania, T.M., 2002, *ApJ*, 579, 289
- Ivlev, A.V., Lazarian, A., Tsyтович, V.N., *et al.*, 2010 [[arXiv:1003.2633](https://arxiv.org/abs/1003.2633)]
- Jochims, H.W., Baumgaertel, H., & Leach, S., 1996, *A&A*, 314, 1003
- Jones, A.P., 2009, *A&A*, 506, 797
- Jura, M., 1975, *ApJ*, 197, 575
- Juvela, M., Padoan, P., & Jimenez, R., 2003, *ApJ*, 591, 258
- Kogut, A., Banday, A.J., Bennett, C.L., *et al.*, 1996, *ApJ*, 460, 1
- Lazarian, A., & Draine, B.T., 2000, *ApJ*, 536, L15
- Le Boulrot, J., Pineau des Forêts, G., & Flower, D.R., 1999, *MNRAS*, 305, 802
- Lebouteiller, V., Brandl, B., Bernard-Salas, J., Devost, D., & Houck, J.R., 2007, *ApJ*, 665, 390
- Leitch, E.M., Readhead, A.C.S., Pearson, T.J., & Myers, S.T., 1997, *ApJ*, 486, L23
- Le Page, V., Snow, T.P., & Bierbaum, V.M., 2001, *ApJS*, 132, 233
- Le Page, V., Snow, T.P., & Bierbaum, V.M., 2003, *ApJ*, 584, 316
- Le Petit, F., Nehmé, C., Le Boulrot, J., & Roueff, E., 2006, *ApJS*, 164, 506

- Martin, P.G., 2007, EAS Publications Series, 23, 165
- Mathis, J.S., Mezger, P.G., & Panagia, N., 1983, A&A, 128, 212
- Miville-Deschênes, M.-A., Ysard, N., Lavabre, A., *et al.*, 2008, A&A, 490, 1093
- Omont, A., 1986, A&A, 164, 159
- Peeters, E., Martín-Hernández, N.L., Rodríguez-Fernández, N.J., & Tielens, X., 2005, Sp. Science Rev., 119, 273
- Rapacioli, M., Joblin, C., & Boissel, P., 2005, A&A, 429, 193
- Rubin, D., *et al.*, 2009, A&A, 494, 647
- Salama, F., Bakes, E.L.O., Allamandola, L.J., & Tielens, A.G.G.M., 1996, ApJ, 458, 621
- Silksbee, K., Ali-Haimoud, Y., & Hirata, C.M., 2010 [[arXiv:1003.4732](https://arxiv.org/abs/1003.4732)]
- Tielens, A.G.G.M., 2008, ARA&A, 46, 289
- Thi, W.-F., van Dishoeck, E.F., Bell, T., Viti, S., & Black, J., 2009, MNRAS, 400, 622
- van Hoof, P.A.M., Weingartner, J.C., Martin, P.G., Volk, K., & Ferland, G.J., 2004, MNRAS, 350, 1330
- Velusamy, T., & Langer, W.D., 2008, AJ, 136, 602
- Verstraete, L., Léger, A., d'Hendecourt, L., Défourneau, D., & Dutuit, O., 1990, A&A, 237, 436
- Wakelam, V., & Herbst, E., 2008, ApJ, 680, 371
- Watson, W.D., 1972, ApJ, 176, 103
- Watson, W.D., 1973, J. Opt. Soc. Amer. (1917-1983), 63, 164
- Weingartner, J.C., & Draine, B.T., 2001, ApJS, 134, 263 (WD01)
- Wolfire, M.G., Tielens, A.G.G.M., Hollenbach, D., & Kaufman, M.J., 2008, ApJ, 680, 384
- Ysard, N., Miville-Deschênes, M.A., & Verstraete, L., 2010, A&A, 509, L1
- Ysard, N., & Verstraete, L., 2010, A&A, 509, A12
- Zubko, V., Dwek, E., & Arendt, R.G., 2004, ApJS, 152, 211

PAHS AND THE CHEMISTRY OF THE ISM

V.M. Bierbaum¹, V. Le Page¹ and T.P. Snow²

Abstract. This review describes five categories of the reactions of polycyclic aromatic hydrocarbons, including photochemistry, electron attachment/detachment, recombination processes, radical reactions, and ion-neutral chemistry. For each class of reaction, an overview of the studies and their general results are presented, as well as references to the literature. The thermochemistry of PAHs and relevant species is described, including bond dissociation energies, ionization energies, electron affinities, basicities, acidities, and the interrelationships of these quantities. Modeling of the chemistry of PAHs and their ions is discussed for both diffuse and dark clouds. The role of PAH cations in the catalytic formation of molecular hydrogen is considered. Finally, this review concludes with a discussion of current challenges in the chemical characterization of PAHs, and a perspective for future studies.

1 Introduction

The history of polycyclic aromatic hydrocarbons (PAHs) in the universe has been a fascinating saga, beginning with the ground-breaking proposal of their importance in the cosmos twenty-five years ago (Léger & Puget 1984; Allamandola *et al.* 1985). In the intervening years, many scientists have contributed to the unfolding of this story through astronomical observations, laboratory spectroscopy and chemistry, computational characterization, and detailed modeling of astrophysical environments. The integration of these methods and their results has now confirmed the presence of PAHs in many locations throughout the universe. This review will focus on the *chemistry* of PAHs in the interstellar medium (ISM) (Tielens 2008; Snow & Bierbaum 2008). Chemistry can be defined as the interactions of elements and compounds with photons, ions, and neutral species, resulting in the formation and dissociation of bonds, the gain and loss of electrons, and the synthesis of the rich chemical structure of the universe. Thus, although chemistry represents only

¹ Department of Chemistry & Biochemistry; University of Colorado, Boulder, CO 80309, USA

² Department of Astrophysical & Planetary Science; University of Colorado, Boulder, CO 80309, USA

one facet of the complex subject of PAHs in the universe, it is nevertheless an extremely broad and diverse topic, and only a small portion of the literature can be highlighted in this review. Gas phase processes will be discussed at the level of discrete molecules; the chemistry of clusters and grains forms the topics of other manuscripts in this volume.

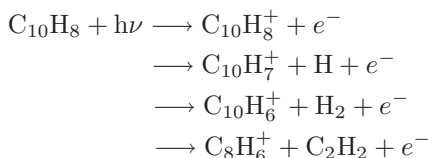
2 Reactions of PAHs

There are several valuable compilations of gas phase reactions: the UMIST Database for Astrochemistry (<http://www.udfa.net/>); the Ohio State Network (http://www.physics.ohio-state.edu/~eric/research_files/osu_01_2009); KIDA, the Kinetic Database for Astrochemistry (<http://kida.obs.u-bordeaux1.fr/>); and the NIST Chemical Kinetics Database (<http://kinetics.nist.gov/kinetics/index.jsp>).

2.1 Photochemistry

Photochemistry involves chemical transformations resulting from the interaction of light with matter. Turro *et al.* (2010) have provided a comprehensive review of the molecular photochemistry of organic molecules that involves a wide array of reactions. This paper will focus on gas phase processes likely to occur in the ISM: the photoionization and dissociation of molecules to form reactive species.

Using naphthalene as an example, photon absorption can result in ionization to form the parent molecular cation; alternatively dissociation can accompany ionization with the loss of hydrogen atom, a hydrogen molecule, or extrusion of a small hydrocarbon such as acetylene.



There have been many experimental and theoretical studies of the photochemistry of PAHs and their cations (Verstraete *et al.* 1990; Jochims *et al.* 1996; Gotkis *et al.* 1993; Banisaukas *et al.* 2004); for example, a comprehensive exploration of the photostability of 33 compounds was carried out using monochromatized synchrotron radiation (Jochims *et al.* 1999). Results from these various studies indicate that there is a rapidly increasing ionization yield above the ionization energy of the PAH, and rules for determining the quantum yield as a function of wavelength have been proposed. These studies have determined the fragmentation channels and the internal energy required for fragmentation; in general, the loss rates for H from alkyl groups exceed those of H from aromatics, which exceed carbon loss as in the form of acetylene.

Photodissociation is being increasingly implemented in Fourier transform ion cyclotron resonance (FT-ICR) experiments to characterize the visible and infrared spectroscopy of PAH cations. The electronic spectra of the pyrene cation, the

1-methylpyrene cation, the coronene cation and its dehydrogenated derivative have been measured in the PIRENEA experiment using a mid-band OPO laser (Useli-Bacchitta *et al.* 2010). The infrared spectra of protonated naphthalene, azulene, anthracene, tetracene, pentacene, and coronene have been determined using a free electron laser (Zhao *et al.* 2009; Knorke *et al.* 2009).

2.2 Electron attachment/detachment

Negative ion formation resulting from low energy (0–15 eV) electron impact of PAHs has been studied in molecular beam experiments (Tobita *et al.* 1992). The electron detachment cross section is a strong function of the electron affinity of the PAH, which generally increases with size. Thus, for naphthalene, phenanthrene, and triphenylene (which have a negative or only slightly positive electron affinity) no long-lived parent anions (M^-) were observed. The transient negative ion autodetaches before stabilization by photon emission (Tielens 2005). However, for molecules where $EA > 0.5$ eV, parent negative ions were detected; these compounds include azulene, anthracene, pyrene, acridine, fluoranthene, perylene, and tetracene. For all ten compounds studied, dehydrogenated anions $(M-H)^-$ were observed at onset electron energies of about 6 eV (Tobita *et al.* 1992).

The room temperature rate coefficient for electron attachment to anthracene was measured in a flowing afterglow-Langmuir probe (FALP) experiment to be 1×10^{-9} cm³ s⁻¹ (Canosa *et al.* 1994). This relatively low value, corresponding to an electron sticking coefficient of only 10^{-4} , suggests the existence of an energy barrier for this process or the absence of accessible negative ion states for attachment. However, the electron attachment rate coefficient is predicted to have a value about 10^{-6} cm³ s⁻¹ for PAHs with 30 carbon atoms (Omont 1986; Allamandola *et al.* 1989). FALP studies indicate that both C₆₀ and C₇₀ efficiently attach electrons above an electron energy of 0.2 eV (Smith & Spanel 1996).

Photodetachment of PAH anions, with energy resolution of the photoelectrons, has been studied for anthracene and perylene (Schiedt & Weinkauff 1997a, 1997b), and for chrysene (Tschurl & Boesl 2006). The electron affinities, vibrational frequencies, and singlet-triplet energy gaps for the neutral molecules can be determined. These relatively limited studies indicate that additional work is needed to fully understand the electron attachment/detachment processes of PAHs.

2.3 Recombination

The recombination of molecular cations with electrons or with negative ions results in neutralization and dissociation. A variety of experimental techniques, including merged beams, ion storage rings, afterglow techniques, and shock-tube methods, have contributed a wealth of data on the recombination of electrons with a variety of cations, from simple diatomics to polyatomic species. Larsson & Orel (2008) have provided an excellent overview of these processes. Many reaction rate constants have been determined, and the temperature dependence and reaction products have been studied for several cations.

However, studies of ion-electron recombination of PAH cations are relatively sparse. Researchers at Rennes University (Biennier *et al.* 2006) have recently used the flowing afterglow/photoions method and the FALP technique to measure the room temperature recombination rate coefficients of seven PAH cations: naphthalene [$0.3 (\pm 0.1) \times 10^{-6} \text{ cm}^3 \text{ s}^{-1}$], azulene [$1.1 (\pm 0.3) \times 10^{-6} \text{ cm}^3 \text{ s}^{-1}$], acenaphthene [$0.5 (\pm 0.2) \times 10^{-6} \text{ cm}^3 \text{ s}^{-1}$], anthracene [$2.4 (\pm 0.8) \times 10^{-6} \text{ cm}^3 \text{ s}^{-1}$], phenanthrene [$1.7 (\pm 0.5) \times 10^{-6} \text{ cm}^3 \text{ s}^{-1}$], fluoranthene [$3.0 (\pm 0.9) \times 10^{-6} \text{ cm}^3 \text{ s}^{-1}$], and pyrene [$4.1 (\pm 1.2) \times 10^{-6} \text{ cm}^3 \text{ s}^{-1}$]. The results indicate an increased reactivity as the number of carbon atoms increases; although the reactions are rapid, they occur below the geometrical limit. Product distributions were not determined; however, these reactions can occur dissociatively to extrude a hydrogen atom or small molecule, or non-dissociatively, especially for larger PAHs.

Hamberg *et al.* (see elsewhere in this volume) report the temperature dependence of the recombination of the benzene cation and of the protonated benzene cation, using the CRYRING. For C_6D_6^+ , $k(\text{T}) = 1.25 \times 10^{-6} (\text{T}/300)^{-0.69} \text{ cm}^3 \text{ s}^{-1}$, and for C_6D_7^+ , $k(\text{T}) = 2.0 \times 10^{-6} (\text{T}/300)^{-0.83} \text{ cm}^3 \text{ s}^{-1}$. These researchers find that the aromatic ring remains largely intact.

Future studies of the dissociative recombination of larger PAH cations, their temperature dependence, and their reaction products are highly desirable. In addition, while positive ion-negative ion reactions have been studied for simple systems, no measurements exist for PAH ions. Due to the positive electron affinity of most PAH molecules, these processes will be less exothermic than the corresponding ion-electron recombination, and therefore less dissociation may occur. The development of DESIREE (Schmidt *et al.* 2008), with two cryogenic ion-storage rings, will make these novel and important studies possible.

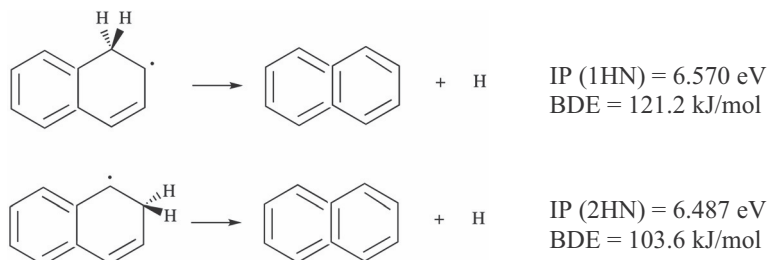
2.4 Radical reactions

Radical-neutral reactions may be important in the interstellar medium even at low temperatures (Ekern *et al.* 2007). Recently, Rowe and coworkers have utilized the CRESU apparatus to measure the rate constants for radicals reacting with anthracene between 58-470 K. For OH radical (Goulay *et al.* 2005), the reaction is rapid and increases as the temperature is lowered: $k = 1.12 \times 10^{-10} (\text{T}/300)^{-0.46} \text{ cm}^3 \text{ s}^{-1}$; formation of the adduct is inferred. For CH radical (Goulay *et al.* 2006a), the reaction exhibits a slight positive temperature dependence: $k = (3.32 \pm 1.00) \times 10^{-10} (\text{T}/298)^{(0.46 \pm 0.14)} \text{ cm}^3 \text{ s}^{-1}$; however, even at the lowest temperature, the reactivity remains high. The products of the reaction were not determined.

There is an extensive literature describing the synthesis of PAHs under various conditions (Tielens 2008); in some environments the reactions of benzene with carbon-containing radicals provide a probable mechanism for the formation of PAHs (see Cherchneff, this volume). For example, the role of the CH_3 radical has been explored, and found to be important in PAH growth (Shukla *et al.* 2010). The rate coefficient for the reaction of the C_2H radical with benzene has

recently been characterized between 105 and 298 K; this value [$k = (3.28 \pm 1.0) \times 10^{-10} (T/298)^{-(0.18 \pm 0.18)} \text{ cm}^3 \text{ s}^{-1}$] indicates that the reaction has no barrier and may play a central role in the formation of large molecules (Goulay & Leone 2006b). Additional T-dependent studies of the reactions of radicals with aromatic molecules are clearly warranted.

An especially challenging aspect of the chemistry of PAHs is the existence of isomeric forms and the resulting differences in reactivity and thermodynamics. There is a recent innovative study of Zwier & co-workers (2010) that explores site-specific thermochemistry of PAH radicals. These workers have determined bond energies and ionization potentials for the C_{10}H_9 isomeric radicals, 1-hydronaphthyl and 2-hydronaphthyl, from their jet cooled vibronic spectra. These studies reveal the intricacies and the richness of the chemistry of the simplest PAH.



2.5 Ion-neutral reactions

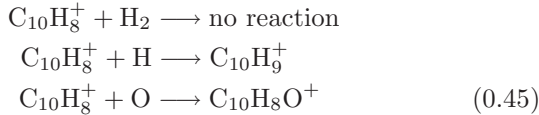
The area of gas phase ion chemistry represents an extremely diverse and complex subject of study. Reactions of cations and anions, both simple and complex, can occur with atoms, radicals, and molecules; a multitude of processes are observed, including charge transfer, proton transfer, addition, carbon insertion/loss, hydrogen addition/abstraction, isotope exchange, and associative detachment. Quantitative rate constants, their temperature dependence, and the product distributions are needed for models of interstellar chemistry (Herbst 2001; Smith 2006). This review will briefly consider three categories of reactions, those involving small organic species, fullerenes, and PAHs.

The reactions of small organic ions, $\text{C}_w\text{H}_x\text{N}_y\text{O}_z^\pm$, with a host of neutral reactants have been characterized by many research groups, using a variety of techniques including flow tubes, ICR instruments, and ion traps. There are several excellent reviews of the field (Smith & Adams 1988; Bohme 2000; Uggerud 2003; Gronert 2005; Nibbering 2006; Gerlich & Smith 2006). These sequential reactions provide the synthesis of complex species, including PAHs. Although past work has focused on positive ions, anions have recently been detected in molecular clouds; thus, the research in our laboratory is currently centered on negative ion chemistry of small carbon-containing species (Eichelberger *et al.* 2007; Yang *et al.* 2010).

Bohme has utilized flow tube mass spectrometry to explore the chemistry of the mono-, di-, and trications of buckminsterfullerene and several substituted cations (Bohme 2009). These ions show remarkable reactivity with a wide variety of

reagents, which form covalent bonds and thereby generate derivatized fullerenes. Although these processes involve three-body stabilization under the experimental conditions, the radiative processes are likely to be rapid. In analogy, large PAH ions are expected to serve as efficient substrates for addition of many atomic or molecular species.

Unfortunately, experimental studies of the ion chemistry of PAHs are relatively limited. Our work (Snow *et al.* 1998; Le Page *et al.* 1999a; Le Page *et al.* 1999b; Betts *et al.* 2006) has employed the flowing afterglow-selected ion flow tube (FA-SIFT) technique to explore the chemistry of the parent molecular cations of benzene, naphthalene, pyrene, and coronene ($C_6H_6^+$, $C_{10}H_8^+$, $C_{16}H_{10}^+$, $C_{24}H_{12}^+$), the monodehydrogenated cations ($C_6H_5^+$, $C_{10}H_7^+$, $C_{16}H_9^+$), as well as protonated benzene, naphthalene, and pyrene ($C_6H_7^+$, $C_{10}H_9^+$, $C_{16}H_{11}^+$). For all of these ions, reactions with H_2 , H, N, and O were characterized; for some ions, reactions with other molecular reagents were also examined (CO, H_2O , NH_3 , N_2 , O_2 , NO, CH_3OH , CS_2 , $(CH_3)_3N$). Consider, for example, the reactions of $C_{10}H_8^+$:



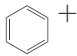
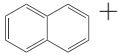
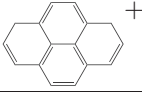
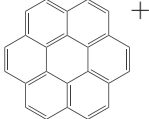
The parent molecular cation of naphthalene does not react with molecular hydrogen. However, this radical cation reacts readily with the radical, H-atom, to form protonated naphthalene. In contrast, singlet cations ($C_6H_5^+$, $C_{10}H_7^+$) have only low reactivity with H atom, but do react with H_2 by addition with moderate rates. Intriguingly, $C_{16}H_9^+$ is computed to have a triplet ground state, and this ion reacts efficiently with H atom but not with H_2 . Our studies suggest that most PAH cations will hydrogenate with either atomic or molecular hydrogen.

Although the addition processes in flow tube experiments involve three-body stabilization, it is expected that radiative stabilization will be facile in the ISM. For example, radiative association of molecular hydrogen with $C_6H_5^+$ and $C_{10}H_7^+$ has been observed (Le Page *et al.* 1999a; Ausloos *et al.* 1989) at low pressure in ICR instruments. Since the radiative process $C_{10}H_7^+ + H_2$ is efficient, the same is likely true for the $C_{10}H_8^+ + H$ reaction; the computed energy content of the intermediate complex [$C_{10}H_9^+$] is almost identical for these processes, and therefore the complex lifetimes are very similar.

The reactions of $C_{10}H_8^+$ with O-atoms and N-atoms illustrated above occur both by association and extrusion of a small stable molecule. This latter channel decreases as the size of the PAH cation increases; this pathway represents less than 5% of the reaction for $C_{16}H_{10}^+$, and is not detectable for $C_{24}H_{12}^+$. Thus, for large PAH cations, only addition is observed.

Table 1 summarizes the rate constants for reactions of four cations with atomic reagents. For both H-atoms and O-atoms, the rate constants are large, and the

Table 1. Comparison of the Reactivity of PAH Parent Molecular Cations with Atomic Reactants. Reaction rate constants are given in units of $\text{cm}^3 \text{s}^{-1}$.

PAH Cations	H	O	N
	2.2×10^{-10}	1.0×10^{-10}	1.2×10^{-10}
	1.9×10^{-10}	1.0×10^{-10}	2.3×10^{-11}
	1.4×10^{-10}	1.0×10^{-10}	1.5×10^{-12}
	1.4×10^{-10}	1.3×10^{-10}	No reaction

reactivity remains high as the PAH increases in size; this suggests that large PAH cations, which might exist in the diffuse ISM, will also be reactive with these atomic reagents. In contrast, the reactivity with N-atoms plummets, and becomes negligible for large PAH cations.

3 Thermochemistry of PAHs

The chemical reactions of PAHs are intimately related to their thermochemistry. Photochemistry is linked with ionization energy, electron attachment/detachment depends on electron affinity, and radical reactivity reflects bond energies; ion-neutral reactions involve these parameters as well as gas phase acidity and basicity values. These quantities are interrelated through thermochemical cycles so that values, which are not easily accessible experimentally, can be computed.

For example, the gas phase acidity of a molecule RH can be measured with flow tube techniques, and the electron affinity of R can be accurately determined with photoelectron spectroscopy; these values can be combined with the well-known ionization energy of the hydrogen atom to yield the R-H bond dissociation energy.

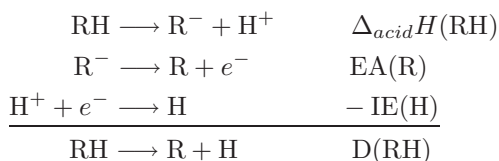


Figure 1 illustrates the relationship of this negative ion cycle with the proton affinity cycle and the appearance energy cycle (Ervin 2001). A comprehensive compilation of thermodynamic quantities for many PAHs is provided in the NIST Chemistry WebBook (<http://webbook.nist.gov/chemistry/>) (NIST 2010).

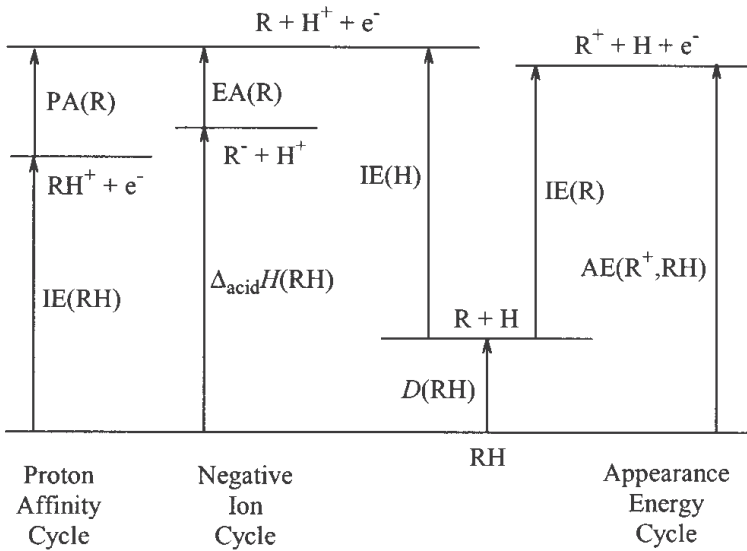


Fig. 1. Thermochemical energy level diagram illustrating the relationship of the proton affinity cycle, the negative ion cycle, and the appearance energy cycle (Ervin 2001).

4 Modeling of the chemistry of PAHs

4.1 Diffuse clouds

Le Page *et al.* (2001) have developed a model of the hydrogenation and charge states of PAHs in diffuse clouds; these studies explore which species are likely to survive in environments where the Diffuse Interstellar Bands are formed. The major processes include ionization and photodissociation in the interstellar UV field, recombination of PAH cations, and chemistry of PAH cations with H_2 and H atoms. The coupled kinetic equations are incorporated into a mathematical framework. Experimental data are employed, and statistical theories are used to estimate properties that are not available from experiments. Other minor processes are considered, including electron attachment, photodetachment, photofragmentation with carbon loss, double ionization, and chemistry with minor species.

Twelve PAH systems were considered, ranging from benzene up to species containing 200 carbon atoms (Le Page *et al.* 2003). For a standard diffuse cloud, the total H density is set as 100 cm^{-3} , the ratio of molecular hydrogen to atomic hydrogen density is 0.5, the scaling of the UV field is unity, the temperature is 100 K, and the ratio of electron density to total H density is 1.4×10^{-4} ; the effects of varying these parameters were examined. Under most diffuse cloud conditions, the density of the cations exceeds that of neutrals, and the density of anions is low. However, the hydrogenation state strongly depends on the size of the molecule. Small PAHs with fewer than about 15–20 carbon atoms

are destroyed in most environments. Intermediate-size PAHs with 20–30 carbon atoms are stripped of peripheral hydrogen atoms, but retain their carbon skeleton. Larger PAHs primarily have normal hydrogen coverage, while very large PAHs may be super-hydrogenated. These studies demonstrate that photodissociation and chemical reactions are critical processes governing the behavior of PAHs in the diffuse ISM.

Recently, Montillaud *et al.* (see elsewhere in this volume) have developed an extended model that includes PAH clusters and PAHs complexed with heavy atoms. Additionally, new reaction rate constants were employed. The first results from this model for coronene appear in this Proceedings volume.

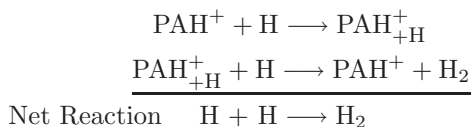
4.2 Dense clouds

Wakelam & Herbst (2008) have recently added PAHs to their gas-phase network of reactions to explore their role in the chemistry of cold dense cores. The processes of radiative electron attachment to form PAH^- , recombination between PAH anions and small cations, and photodetachment of PAH anions by UV radiation were included. A pseudo-time-dependent model, which computes the chemical evolution at a fixed temperature and density, was utilized for three different sets of elemental abundances. The size and abundance of the PAHs were varied to determine the impact of these values on the chemistry. The physical conditions included a temperature of 10 K, a molecular hydrogen density of 10^4 cm^{-3} , a cosmic-ray ionization rate of $1.3 \times 10^{-17} \text{ s}^{-1}$, and a visual extinction of 10.

The abundance of PAH cations was found to be at least two orders of magnitude smaller than the neutral or anionic PAH abundances. A dominant effect in the calculations is that PAH anions replace electrons as the dominant carrier of negative charge; this factor reduces the overall ionization fraction because atomic cations recombine more rapidly with PAH^- than with electrons. In addition, the abundance of many molecular ions and neutrals are strongly influenced by the presence of PAHs. Inclusion of PAHs in the models significantly improves agreement with observational data for TMC-1, but not for L134N; this result suggests that there may be differences in the PAH properties for the two regions.

5 PAHs as catalysts in the synthesis of H_2

Bauschlicher (1998) and Hirama and co-workers (2003) have suggested the possible role of PAH cations in the synthesis of molecular hydrogen:



PAH^+ represents any normally hydrogenated PAH cation, while $\text{PAH}_{+\text{H}}^+$ represents a cation with an additional hydrogen atom. The first step involves the formation of protonated PAH by reaction of H-atom with the parent molecular

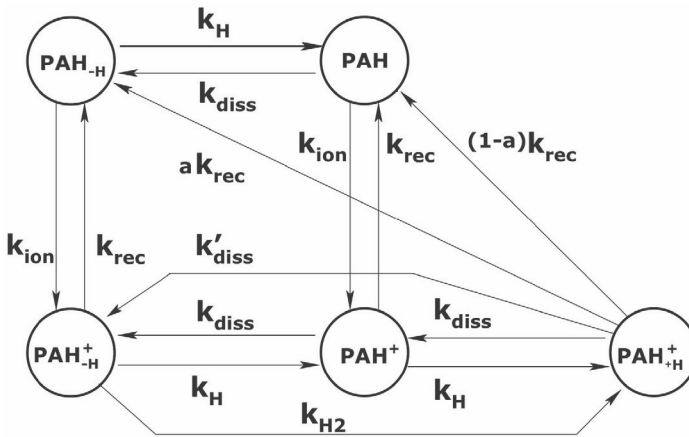
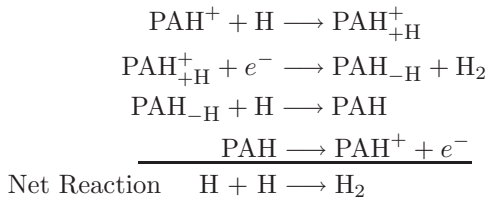


Fig. 2. Chemical mechanism for the catalytic formation of H_2 in the interstellar medium (Le Page *et al.* 2009).

cation; H-atom then abstracts the extra hydrogen to form H_2 . Since the cations are formed and consumed, the net reaction is formation of a hydrogen molecule from two hydrogen atoms. While we have found the first process to be efficient, our experiments indicate that the reactions of protonated PAHs with H are slow. We have therefore proposed an alternate model.

Our proposed mechanism consists of four reactions:



The first step again involves the formation of protonated cations. These species then undergo dissociative recombination with electrons to form the dehydrogenated PAH ($\text{PAH}_{-\text{H}}$) and molecular hydrogen; loss of H_2 is feasible due to the low binding energy of the two hydrogen atoms bonded to the same carbon. Our model also includes formation of $\text{PAH} + \text{H}$, which is not shown here for simplicity. In the third step, the dehydrogenated radical $\text{PAH}_{-\text{H}}$ combines with hydrogen atom to regenerate the neutral PAH; this molecule is then photoionized to complete the cycle. The complete scheme is summarized in Figure 2. The rate coefficient of H_2 production using this process compares well with a widely accepted value of $3 \times 10^{-17} \text{ cm}^3 \text{ s}^{-1}$ for formation on grains in the diffuse ISM. It is inferred that PAHs can contribute significantly to the formation of molecular hydrogen, especially in environments where high grain temperatures impede the recombination of hydrogen atoms on grain surfaces.

Recently, there have been additional novel proposals for the production of H₂ in the ISM. Vala *et al.* (2009) have generated protonated 1,2-dihydronaphthalene by electrospray ionization in an FT-ICR, coupled to an IR-tunable free electron laser; infrared multiphoton dissociation studies, complemented by computations, demonstrate the formation of molecular hydrogen. Thrower *et al.* (see elsewhere in this volume) have used both computational and experimental methods to explore superhydrogenated PAHs; using coronene as an example, these studies indicate efficient routes to H₂ formation that may be important in the ISM.

6 Future perspectives

There have been major advances in the chemical characterization of PAHs during the last 25 years; nevertheless, there are critical questions remaining for each of the chemical processes discussed in this review. Powerful new developments in experimental methods promise to offer new insights into PAH chemistry in the near future; several of the most crucial areas will be briefly highlighted.

Recombination reactions. There are no experimental data on the neutralization reactions of positive ions with negative ions for PAHs. The dual ion-beam storage ring instrument (DESIREE) (Schmidt *et al.* 2008) at Stockholm University will enable the measurement of the cross-sections, rate coefficients, and products distributions for these critical reactions.

Reactions at low temperature and pressure. The CRESU technique (Smith 2006) and variable temperature flow tube systems (Smith 1992) have provided experimental data on a variety of ionic processes at low temperature. The recent development of an FT-ICR with cryogenic cooling of the reaction cell (PIRENEA) (Useli-Bacchitta *et al.* 2010) allows a wide range of ion chemistry experiments under conditions that approach the physical environment of interstellar space ($P \leq 10^{-10}$ mbar, $T_{\text{trap}} \sim 35$ K). In addition, two new experimental methods enable the characterization of ion chemistry involving atomic reactants at low energies. These include the innovative atomic beam 22-pole ion trap (Gerlich & Smith 2006; Luca *et al.* 2006), which can approach temperatures as low as 10 K, and the novel merged beam apparatus at the Columbia Astrophysics Laboratory (Bruhns *et al.* 2010).

Characterization of reactants and products. Even the simplest polycyclic aromatic hydrocarbon, naphthalene, possesses distinct chemical sites for protonation, deprotonation, dehydrogenation, addition, and other reactions. The resulting chemical complexity has largely been uncharacterized. New spectroscopic tools (Knorke *et al.* 2009; Sebree *et al.* 2010) offer a powerful approach for distinguishing isomeric forms of PAHs and their derivatives, including protonated, hydrogenated, and cyclic versus ring-opened species. Similarly, for many reactions, only the rate constants have been determined, and the identification of products and their branching fractions remains an important area for study.

Reactions of negative ions. In general, gas phase ion chemistry has focused on positive ions, since these species are more readily generated, and PAH cations are the probable form in the diffuse interstellar medium. However, the recognition that

PAH anions are important in dense clouds (Wakelam & Herbst 2008) underscores the need for exploring the chemistry of these species. Both electrospray ionization (Fenn *et al.* 1990) and chemical ionization (Vestal 2001) offer promising approaches for the generation and study of PAH negative ions.

Large PAHs. The low volatility of PAH molecules has largely limited their study in the gas phase to the smaller members of this family. However, modeling studies indicate that moderate and large PAHs are likely to exist in the ISM. Laser Induced Acoustic Desorption (LIAD) (Shea *et al.* 2007) offers a new, versatile approach for the study of PAHs and a host of other compounds. We are currently coupling a LIAD source to our FA-SIFT instrument to extend our previous work to large, astrophysically relevant PAHs.

In summary, the field of interstellar chemistry of PAHs has a promising and exciting future; it is fascinating to speculate about the marvelous results that will be presented at the 50th anniversary symposium!

The authors are grateful to the National Aeronautics and Space Administration and the National Science Foundation for financial support. We appreciate the many contributions of our colleagues, students, and research associates. We thank Mr. Oscar Martinez Jr. and Mr. Nicholas Demarais for their help in preparation of this manuscript.

References

- Allamandola, L.J., Tielens, A.G.G.M., & Barker, J.R., 1985, *ApJ*, 290, L25
Allamandola, L.J., Tielens, A.G.G.M., & Barker, J.R., 1989, *ApJS*, 71, 733
Ausloos, P., Lias, S.G., Buckley, T.J., & Rogers, E.E., 1989, *Int. J. Mass Spectrom. Ion Proc.*, 92, 65
Banisaukas, J., Szczepanski, J., Eyler, J., & Vala, M., 2004, *J. Phys. Chem. A*, 108, 3723
Bauschlicher, C.W., 1998, *ApJ*, 509, L125
Betts, N.B., Stepanovic, M., Snow, T.P., & Bierbaum, V.M., 2006, *ApJ*, 651, L129
Biennier, L., Alsayed-Ali, M., Foutel-Richard, A., *et al.*, 2006, *Discuss. Faraday Soc.*, 133, 289
Bohme, D.K., 2000, *Int. J. Mass Spectrom.*, 200, 97
Bohme, D.K., 2009, *Mass Spectrom. Rev.*, 28, 672
Bruhns, H., Kreckel, H., Miller, K., *et al.*, 2010, *Rev. Sci. Instr.*, 81, 013112
Canosa, A., Parent, D.C., Pasquerault, D., *et al.*, 1994, *Chem. Phys. Lett.*, 228, 26
Eichelberger, B.R., Snow, T.P., Barckholtz, C., & Bierbaum, V.M., 2007, *ApJ*, 667, 1283
Ekern, S., Gomez, L., Szczepanski, J., & Vala, M., 2007, *Chem. Phys.*, 331, 219
Ervin, K.M., 2001, *Chem. Rev.*, 101, 391
Fenn, J.B., Mann, M., Meng, C.K., Wong, S.F., & Whitehouse, C.M., 1990, *Mass Spectrom. Rev.*, 9, 37
Gerlich, D., & Smith, M., 2006, *Phys. Scr.*, 73, C25
Gotkis, Y., Oleinikova, M., Naor, M., & Lifshitz, C., 1993, *J. Phys. Chem.*, 97, 12282
Goulay, F., Rebrion-Rowe, C., Garrec, J.L.L., *et al.*, 2005, *J. Chem. Phys.*, 122, 104308
Goulay, F., Rebrion-Rowe, C., Biennier, L., *et al.*, 2006a, *J. Phys. Chem. A*, 110, 3132

- Goulay, F., & Leone, S.R., 2006b, *J. Phys. Chem. A*, 110, 1875
- Gronert, S., 2005, *Mass Spectrom. Rev.*, 24, 100
- Herbst, E., 2001, *Chem. Soc. Rev.*, 30, 168
- Hirama, M., Ishida, T., & Aihara, J.-I., 2003, *J. Comput. Chem.*, 24, 1378
- Jochims, H.W., Baumgartel, H., & Leach, S., 1996, *A&A*, 314, 1003
- Jochims, H.W., Baumgartel, H., & Leach, S., 1999, *ApJ*, 512, 500
- Knorke, H., Langer, J., Oomens, J., & Dopfer, O., 2009, *ApJ*, 706, L66
- Larsson, M., & Orel, A.E., 2008, *Dissociative Recombination of Molecular Ions* (Cambridge University Press: Cambridge)
- Le Page, V., Keheyan, Y., Snow, T.P., & Bierbaum, V.M., 1999a, *J. Am. Chem. Soc.*, 121, 9435
- Le Page, V., Keheyan, Y., Snow, T.P., & Bierbaum, V.M., 1999b, *Int. J. Mass Spectrom.*, 185/186/187, 949
- Le Page, V., Snow, T.P., & Bierbaum, V.M., 2001, *ApJS*, 132, 233
- Le Page, V., Snow, T.P., & Bierbaum, V.M., 2003, *ApJ*, 584, 316
- Le Page, V., Snow, T.P., & Bierbaum, V.M., 2009, *ApJ*, 704, 274
- Léger, A., & Puget, J.L., 1984, *A&A*, 137, L5
- Linstrom, P.J., & Mallard, W.G. (eds.), *NIST Chemistry WebBook*, NIST Standard Reference Database Number 69, National Institute of Standards and Technology, Gaithersburg, MD 20899, <http://webbook.nist.gov>
- Luca, A., Borodi, G., & Gerlich, D., 2006, in "Interactions of Ions with Hydrogen Atoms. In Progress report in XXIV ICPEAC 2005", ed. Colavecchia, F.D., Fainstein, P.D., Fiol, J., Lima, M.A.P., Miraglia, J.E., Montenegro, E.C., Rivarola, R.D. (Rosario, Argentina), 29
- Nibbering, N.M.M., 2006, *Mass Spectrom. Rev.*, 25, 962
- Omont, A., 1986, *A&A*, 164, 159
- Schiedt, J., & Weinkauff, R., 1997a, *Chem. Phys. Lett.*, 266, 201
- Schiedt, J., & Weinkauff, R., 1997b, *Chem. Phys. Lett.*, 274, 18
- Schmidt, H.T., Johansson, H.A.B., Thomas, R.D., *et al.*, 2008, *Int. J. Astrobiology*, 7, 205
- Sebree, J.A., Kislov, V.V., Mebel, A.M., & Zwier, T.S., 2010, *J. Phys. Chem. A*, 114, 6255
- Shea, R.C., Habicht, S.C., Vaughn, W.E., & Kentamaa, H.I., 2007, *Anal. Chem.*, 79, 2688
- Shukla, B., Miyoshi, A., & Koshi, M., 2010, *J. Am. Soc. Mass Spectrom.*, 21, 534
- Smith, D., & Adams, N.G., 1988, *Adv. At. Mol. Phys.*, 24, 1
- Smith, D., 1992, *Chem. Rev.*, 92, 1473
- Smith, D., & Spanel, P., 1996, *J. Phys. B: At. Mol. Opt. Phys.*, 29, 5199
- Smith, I.W.M., 2006, *Angew. Chem. Int. Ed.*, 45, 2842
- Snow, T.P., Page, V.L., Keheyan, Y., & Bierbaum, V.M., 1998, *Nature*, 391, 259
- Snow, T.P., & Bierbaum, V.M., 2008, *Annu. Rev. Anal. Chem.*, 1, 229
- Tielens, A.G.G.M., 2005, "The Physics and Chemistry of the Interstellar Medium" (Cambridge Univ. Press: Cambridge, UK)
- Tielens, A.G.G.M., 2008, *ARA&A*, 46, 289

- Tobita, S., Meinke, M., Illenberger, E., *et al.*, 1992, *Chem. Phys.*, 161, 501
- Tschurl, M., & Boesl, U., 2006, *Int. J. Mass Spectrom.*, 249, 364
- Turro, N.J., Ramamurthy, V., & Scaiano, J.C., 2010, "Modern Molecular Photochemistry of Organic Molecules" (University Science Books: Sausalito, CA)
- Uggerud, E., 2003, *Top. Curr. Chem.*, 225, 3
- Useli-Bacchitta, F., Bonnamy, A., Mulas, G., *et al.*, 2010, *Chem. Phys.*, 371, 16
- Vala, M., Szczepanski, J., Oomens, J., & Steill, J.D., 2009, *J. Am. Chem. Soc.*, 131, 5784
- Verstraete, L., Léger, A., d'Hendecourt, L., Dutuit, O., & Defourneau, D., 1990, *Astron. Astrophys.*, 237, 436
- Vestal, M.L., 2001, *Chem. Rev.*, 101, 361
- Wakelam, V., & Herbst, E., 2008, *ApJ*, 680, 371
- Yang, Z., Eichelberger, B., Carpenter, M., *et al.*, 2010, submitted
- Zhao, D., Langer, J., Oomens, J., & Dopfer, O., 2009, *J. Chem. Phys.*, 131, 184307

[FEPAH]⁺ COMPLEXES AND [FE_xPAH_y]⁺ CLUSTERS IN THE INTERSTELLAR MEDIUM: STABILITY AND SPECTROSCOPY

A. Simon^{1, 2}, M. Rapacioli^{1, 2}, F. Spiegelman^{1, 2} and C. Joblin^{3, 4}

Abstract. The relevance of organometallic complexes in the chemistry of the interstellar medium (ISM) was first suggested in the early 90s. This initial proposal has recently been re-considered in the light of new astronomical data, benefiting from pioneering experimental techniques and theoretical methods. In this article, a review of recent theoretical and experimental results obtained for PAHs coordinated to Fe atoms is presented, focusing on: -(i)- the IR spectra of [FePAH]⁺ and [Fe(PAH)₂]⁺ complexes, found to be in line with the AIBs, with additional specific features in the far-IR range and -(ii)- the photo-evaporation of [Fe_xPAH_y]⁺ clusters as possible candidates for very small grains releasing PAHs in photodissociation regions. These results call for new astronomical data at high spatial resolution. Studies on larger clusters will require further experimental and theoretical developments.

1 Introduction: The Fe-PAH proposal

Serra *et al.* (1992) and Chaudret *et al.* (1991) first proposed that π -adducts of polycyclic aromatic hydrocarbons (PAHs) and Fe atoms are stable species that can form efficiently in the conditions of the interstellar medium (ISM) and play a role in its chemistry. The efficient coordination of Fe atoms on PAHs would then partially account for the significant depletion of elemental Fe from the interstellar gas-phase. Besides, Fe atoms or clusters trapped on carbonaceous grains could play

¹ Université de Toulouse, UPS, LCPQ (Laboratoire de Chimie et Physique Quantiques), IRSAMC, 118 Route de Narbonne, 31062 Toulouse, France

² CNRS, LCPQ, IRSAMC, 31062 Toulouse, France

³ Université de Toulouse, UPS, Centre d'Étude Spatiale des Rayonnements (CESR), Observatoire Midi-Pyrénées, 9 Av. Colonel Roche, 31028 Toulouse Cedex 04, France

⁴ CNRS, CESR, 31028 Toulouse, France

a catalytic role in the formation of large hydrocarbons, and of PAHs in particular. This initial proposal opened a new class of species to be considered and motivated at the time a few experimental (Marty 1996; Marty *et al.* 1996) and theoretical (Klotz *et al.* 1995) studies, along with astrophysical modeling (Marty *et al.* 1994; Ristorcelli & Klotz 1997).

It has recently been reconsidered in the new astrophysical context *e.g.*:

(i)- the search for the carriers of the blue component of the 6.2 μm aromatic infrared band (AIB) assigned to PAH-derived species (Peeters *et al.* 2002) such as substituted PAHs like PANHs^{+0/-} (Bauschlicher *et al.* 2009; Hudgins *et al.* 2005), or PAHs coordinated to an heteroatom such as Mg (Bauschlicher 2009; Bauschlicher & Ricca 2009), Si (Joalland *et al.* 2010, 2009) or Fe (Simon & Joblin 2007, 2010).

(ii)- the search for candidates for the VSGs located in molecular clouds and shown to release PAH molecules at the surface of the cloud (Rapacioli, see elsewhere in this volume): the presence of heteroatoms like Fe (or Si) could stabilize PAH clusters, that are possible candidates for these VSGs (Rapacioli *et al.* 2005). The experimental study, coupled with theoretical modeling, of the photostability of $[\text{Fe}_x\text{PAH}_y]^+$ clusters in the conditions of the ISM, indeed shows that such clusters can be good candidates for these VSGs (Simon & Joblin 2009).

2 Stability of $[\text{FePAH}]^+$ and $[\text{Fe}_x\text{PAH}_y]^+$ in the ISM

Calculations based on Density Functional Theory (DFT) show that $[\text{FePAH}]^+$ complexes are intrinsically more stable than $[\text{FePAH}]^0$ complexes due to larger Fe-PAH binding energies, *e.g.* ~ 2.5 eV for $[\text{FePAH}]^+$ complexes *vs.* ~ 0.6 eV for $[\text{FePAH}]^0$ complexes (Simon & Joblin 2007). They are thus more likely to survive in the conditions of the ISM than their neutral counterparts. $[\text{FeC}_{24}\text{H}_{12}]^+$ and $[\text{Fe}_x(\text{C}_{24}\text{H}_{12})_2]^+$ ($x=1,4$) complexes were formed in the PIRENEA set-up, a cold ion trap dedicated to astrochemistry (Simon & Joblin 2009). Interestingly, complexes with dehydrogenated coronene also form when the number of Fe atoms reaches 3, suggesting the occurrence of intramolecular organometallic reactions. Each $[\text{FeC}_{24}\text{H}_{12}]^+$ and $[\text{Fe}_x(\text{C}_{24}\text{H}_{12})_2]^+$ ($x=1,3$) was isolated and photodissociated under soft irradiation conditions. The major dissociation pathway is a sequential loss of Fe atoms from $[\text{Fe}_3(\text{C}_{24}\text{H}_{12})_2]^+$ and $[\text{Fe}_2(\text{C}_{24}\text{H}_{12})_2]^+$ to lead to $[\text{Fe}(\text{C}_{24}\text{H}_{12})_2]^+$ that loses one coronene molecule under further irradiation. The smallest complex $[\text{FeC}_{24}\text{H}_{12}]^+$ then loses Fe, leaving $[\text{C}_{24}\text{H}_{12}]^+$ as the final charged photofragment. The stoichiometry of these $[\text{Fe}_x(\text{C}_{24}\text{H}_{12})_2]^+$ complexes and their dissociation sequence make them good candidates for the VSGs mentioned in the previous section. The photodissociation kinetics of the smallest complex $[\text{FeC}_{24}\text{H}_{12}]^+$ was simulated using a Monte Carlo kinetic model in order to retrieve, from the fit of the experimental points, data such as the dissociation pre-exponential factor $A_d = 10^{12} \text{ s}^{-1}$ and the mean internal energy at dissociation ($\langle U_d \rangle_{\text{min}} \sim 5$ eV). These data can now be inserted into astrochemical models.

3 Mid- and far-IR features of $[\text{FePAH}]^+$ and $[\text{Fe}(\text{PAH})_2]^+$ complexes

The AIBs are emission features from UV-excited species. Anharmonic effects are therefore expected to play an important role in these spectra. A laboratory approach to study these effects is to perform infrared multiple photon dissociation (IRMPD) spectroscopy experiments (Oomens, see elsewhere in this volume). This technique was applied to $[\text{FeX}_{1,2}]^+$ complexes with small PAHs ($X=\text{C}_6\text{H}_6, \text{C}_{10}\text{H}_8, \text{C}_{13}\text{H}_{10}$ (Szczepanski *et al.* 2006)) and to $[\text{YFeC}_{24}\text{H}_{12}]^+$ heterogeneous complexes ($\text{Y}=\text{C}_5\text{H}_5, \text{C}_5(\text{CH}_3)_5$ (Simon *et al.* 2008)). To our knowledge, no IRMPD experiments have been performed yet on $[\text{Fe}_x\text{PAH}_y]^+$ complexes with large PAHs, the production and dissociation of these species being challenging tasks. Infrared (IR) spectra of neutral FePAH complexes were recorded in cold rare-gas matrices (Elustondo *et al.* 1999; Wang *et al.* 2007). All laboratory spectra have been compared with calculated harmonic IR spectra obtained at the DFT level and the calculations have been extended to larger systems (Simon & Joblin 2010). These calculations remain the most straightforward approach to test the contribution of various PAH-derived species to the AIBs.

3.1 Harmonic spectra

Using DFT calculations, we found that the π -coordination of an Fe atom on an individual PAH⁺ leads to a collapse of the band intensity in the 6.2 μm region – where the CC stretching modes (ν_{CC}) are located – with respect to the 11.2 μm region – where the intense C-H out-of-plane bending modes (γ_{CH}) are found. A blueshift of the ν_{CC} band and a slight redshift of the γ_{CH} band upon coordination of an Fe atom were also put forward (Simon & Joblin 2007). Considering a mixture of cationic PAHs ranging from pyrene $\text{C}_{16}\text{H}_{10}$ to circumcoronene $\text{C}_{54}\text{H}_{18}$ (Simon & Joblin 2010), the π -coordination of an Fe atom was shown to lead to:

- (i)- an increase of the intensity ratio of the C-H stretching (ν_{CH} at $3.25\pm 0.01 \mu\text{m}$) and γ_{CH} bands with respect to the intense ν_{CC} band, and shifts of the ν_{CC} and γ_{CH} band positions ($-0.1 \mu\text{m}$ and $+0.04 \mu\text{m}$ respectively), with characteristic profiles displaying a steep blue rise and an extended red tail,
- (ii)- the occurrence of many new bands in the far-IR range. Some vibrational modes of the PAH skeleton are indeed activated due to symmetry reduction and new modes involving the motion of the Fe atom appear. In particular, an accumulation point due to the activation of the Fe-PAH stretching mode is observed at $\sim 40 \mu\text{m}$. This range is thus suggested to contain the spectral fingerprint for the presence of $[\text{M-PAH}]^+$ ($\text{M}=\text{Fe}, \text{Si}, \text{Mg}$) complexes in the ISM. Additional features in the [60–300] μm range were also found for complexes with large PAHs.

$[\text{Fe}(\text{PAH})_2]^+$ were shown to be stable in low-temperature and low-pressure conditions (Simon & Joblin 2009). The harmonic spectra of mixtures of homogeneous $[\text{Fe}(\text{PAH})_2]^+$ and heterogeneous $[(\text{C}_{66}\text{H}_{20})\text{FePAH}]^+$ for 6 compact PAHs ranging from pyrene ($\text{C}_{16}\text{H}_{10}$) to circumvalene ($\text{C}_{66}\text{H}_{20}$), were computed at the DFT level of theory (Fig. 1). Both mid-IR spectra present very similar features, making them

a prototype for $[\text{Fe}(\text{PAH})_2]^+$ complexes with large PAHs. The 6–9 μm region differs from that of $[\text{FePAH}]^+$ complexes (Simon & Joblin 2010), with an enhanced intensity of the 7.38 μm band in particular. The intensity of the 3.25 μm band is also considerably enhanced with respect to that of the γ_{CH} and ν_{CC} bands. In the far-IR range, bands with reasonable intensities appear at ~ 30 and 100 μm . They are assigned respectively to the Fe-PAH stretching mode coupled to PAH-skeleton deformations, and to the Fe motion parallel to the PAH surface (Simon & Joblin, in preparation).

The mid-IR spectra of $[\text{Fe}(\text{PAH})_x]^+$ ($x=1,2$) are found to be good candidates to account for both positions and profiles of the AIBs. Their rich far-IR spectra call for new astronomical data from space missions such as the Herschel Space Observatory and the future SPICA telescope, that can probe this spectral range with an increased sensitivity.

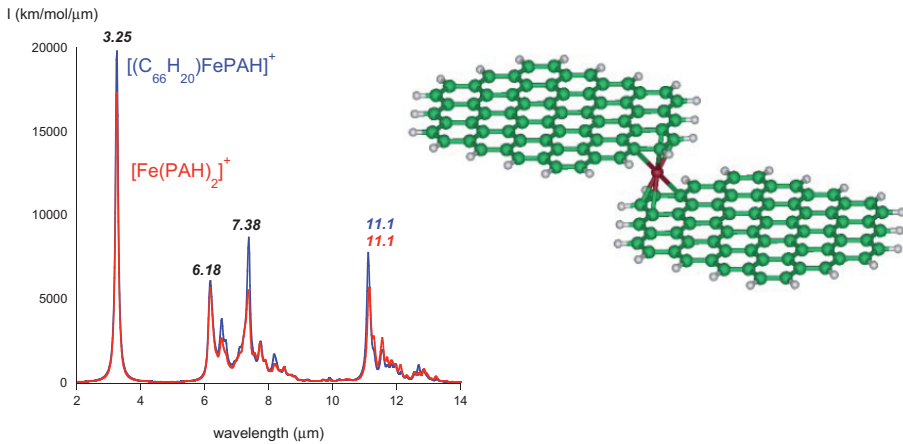


Fig. 1. *Left:* computed mid-IR harmonic spectra of mixtures of $[\text{Fe}(\text{PAH})_2]^+$ (red) and $[(\text{C}_{66}\text{H}_{20})\text{FePAH}]^+$ (blue) complexes. *Right:* stable structure of $[\text{Fe}(\text{C}_{66}\text{H}_{20})_2]^+$ obtained at the DFT level of theory.

3.2 Anharmonic effects on the mid-IR spectra of $[\text{FePAH}]^+$

The anharmonic effects in the mid-IR spectra of various PAH, PAH^+ and $[\text{SiPAH}]^+$ complexes were obtained from classical molecular dynamics (MD) simulations (Joalland *et al.* 2010) on a potential energy surface described at the DFTB (Density Functional Tight Binding) level of theory (Elstner *et al.* 1998). Using a similar approach, we performed a comparative study of the anharmonic effects on the IR spectra of $[\text{FeC}_{24}\text{H}_{12}]^+$ and $[\text{C}_{24}\text{H}_{12}]^+$ (Simon *et al.* submitted), showing in particular that:

(i) the anharmonicity of the γ_{CH} band is decreased upon coordination of an Fe atom, resulting in the merging of the γ_{CH} bands of $[\text{FeC}_{24}\text{H}_{12}]^+$ and $[\text{C}_{24}\text{H}_{12}]^+$ at ~ 700 K (Fig. 2),

(ii)- the anharmonicity of the ν_{CC} band is also decreased, enhancing the blueshift of the ν_{CC} band of $[\text{FeC}_{24}\text{H}_{12}]^+$ with respect to that of $[\text{C}_{24}\text{H}_{12}]^+$.

The band positions were shown to have a linear dependence on temperature. Extrapolating these dependences to the mixture of $[\text{FePAH}]^+$ complexes with large PAHs studied by Simon & Joblin (2010), we found that the γ_{CH} band shifts from $11.02 \mu\text{m}$ at 0 K to $11.23 \mu\text{m}$ at 800 K whereas the ν_{CC} band shifts from $6.16 \mu\text{m}$ to $6.31 \mu\text{m}$. These results show that the assignment of the $6.2 \text{ vs. } 6.3 \mu\text{m}$ components of the AIBs should be done with caution.

MD simulations also show that the diffusion of the Fe atom on the $[\text{C}_{24}\text{H}_{12}]^+$ surface is observed at $T \sim 850 \text{ K}$, *e.g.* for an energy excess of $\sim 4 \text{ eV}$, which is below the dissociation energy determined to be 5 eV (*cf.* Sect. 2). This DFTB/MD method also allows us to probe high-temperature chemistry and will be used for reactivity studies in a very near future.

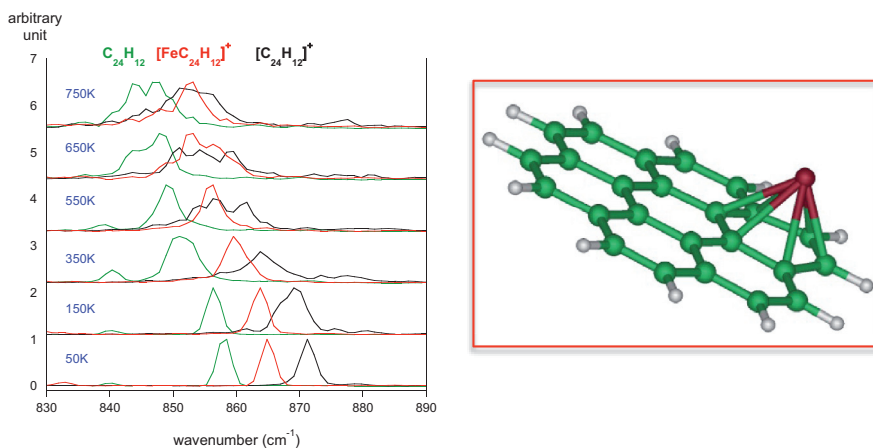


Fig. 2. *Left:* DFTB/MD simulated anharmonic IR spectra (zoom on the CH out-of-plane bending mode γ_{CH}) of $[\text{FeC}_{24}\text{H}_{12}]^+$ (red) and $[\text{C}_{24}\text{H}_{12}]^{0/+}$ (green/black). *Right:* most stable structure of $[\text{FeC}_{24}\text{H}_{12}]^+$ obtained at the DFT level of theory.

4 Conclusions and future work

The computed harmonic mid-IR spectra of $[\text{FePAH}]^+$ and $[\text{Fe}(\text{PAH})_2]^+$ complexes with large PAHs show that these species could contribute to the AIBs. The far-IR spectra of these complexes present specific features that need to be searched for in astronomical spectra. Experimental results show that $[\text{Fe}_x\text{PAH}_y]^+$ complexes are likely candidates for astronomical VSGs releasing PAHs at the surface of molecular clouds. These studies have benefited from recent experimental and theoretical developments that will be pursued to improve our knowledge of larger clusters. Future work will include the study of the stability and spectroscopy of complexes of Fe atoms with dehydrogenated PAHs and the investigation of the role of FePAH complexes in the formation of H_2 .

References

- Bauschlicher, C.J., 2009, *Mol. Phys.*, 107, 809
- Bauschlicher, C.W., Peeters, E., & Allamandola, L.J., 2009, *Astrophys. J.*, 697, 311
- Bauschlicher, C.W., Jr., & Ricca, A., 2009, *Astrophys. J.*, 698, 275
- Chaudret, B., Le Beuze, A., Rabaa, H., Saillard, Y., & Serra, G., 1991, *New J. Chem.*, 15, 791
- Elstner, M., Porezag, D., Jungnickel, G., *et al.*, 1998, *Phys. Rev. B*, 58, 11, 7260
- Elustondo, F., Dalibart, M., Derouault, J., & Mascetti, J., 1999, *Phys. Chem. Earth C*, 24, 583
- Hudgins, D.M., Bauschlicher, C.W., & Allamandola, L.J., 2005, *Astrophys. J.*, 632, 1, 316
- Joalland, B., Rapacioli, M., Simon, A., *et al.*, 2010, *J. Phys. Chem. A*, 114, 5846
- Joalland, B., Simon, A., Marsden, C.J., & Joblin, C., 2009, *Astron. Astrophys.*, 494, 969
- Klotz, A., Marty, P., Boissel, P., *et al.*, 1995, *Astron. Astrophys.*, 304, 520
- Marty, P., 1996, *Chem. Phys. Lett.*, 256, 669
- Marty, P., de Parseval, P., Klotz, A., Serra, G., & Boissel, P., 1996, *Astron. Astrophys.*, 316, 270
- Marty, P., Serra, G., Chaudret, B., & Ristorcelli, I., 1994, *Astron. Astrophys.*, 282, 916
- Peeters, E., Hony, S., Van Kerckhoven, C., *et al.*, 2002, *Astron. Astrophys.*, 390, 1089
- Rapacioli, M., Joblin, C., & Boissel, P., 2005, *Astron. Astrophys.*, 429, 193
- Ristorcelli, I., & Klotz, A., 1997, *Astron. Astrophys.*, 317, 962
- Serra, G., Chaudret, B., Saillard, Y., *et al.*, 1992, *Astron. Astrophys.*, 260, 489
- Simon, A., & Joblin, C., 2007, *J. Phys. Chem. A*, 111, 9745
- Simon, A., & Joblin, C., 2009, *J. Phys. Chem. A*, 113, 4878
- Simon, A., & Joblin, C., 2010, *Astrophys. J.*, 712, 69
- Simon, A., & Joblin, C., in preparation
- Simon, A., Joblin, C., Polfer, N., & Oomens, J., 2008, *J. Phys. Chem. A*, 112, 8551
- Simon, A., Rapacioli, M., Lanza, M., Joalland, B., & Spiegelman, F., *Phys. Chem. Chem. Phys.*, submitted
- Szczepanski, J., Wang, H., Vala, M., *et al.*, 2006, *Astrophys. J.*, 646, 666
- Wang, Y., Szczepanski, J., & Vala, M., 2007, *Chem. Phys.*, 342, 107

MODELLING THE PHYSICAL AND CHEMICAL EVOLUTION OF PAHS AND PAH-RELATED SPECIES IN ASTROPHYSICAL ENVIRONMENTS

J. Montillaud^{1,2}, C. Joblin^{1,2} and D. Toubanc^{1,2}

Abstract. An active carbon chemistry is observed at the border of photo-dissociation regions (PDRs), involving small hydrocarbons, polycyclic aromatic hydrocarbon (PAH) macromolecules and evaporating very small grains (VSGs). In this context, we aim at quantifying the physical and chemical evolution of PAHs (hydrogenation and charge states, aggregation, and complexation with heavy atoms) as a function of the local physical conditions (radiation field, temperature, density, abundances of atomic and molecular hydrogen, electrons and heavy atoms). We have developed a numerical model that follows the time dependency of the abundance and internal energy of each species. In this paper, we use this model to calculate the hydrogenation and charge states of coronene C₂₄H₁₂ as an interstellar PAH prototype. We take advantage of recent results on photodissociation and reaction rates and provide guidelines for future laboratory studies. Reaction rates of coronene-derived radical cations with H and H₂ are found to be sufficiently constrained by experiments, whereas the absence of experimental data for neutral species is critical.

1 Introduction

During the two last decades, polycyclic aromatic hydrocarbons (PAHs) have been extensively studied as candidate carriers for the so-called aromatic infrared bands (AIBs). In order to test this hypothesis, models of increasing complexity and accuracy have been developed. Bakes & Tielens (1994) described the charge state of PAHs and their contribution to the photoelectric heating. Allain *et al.* (1996a, 1996b) modelled the photodissociation rates of PAHs, taking into account the loss of H, H₂, and C₂H₂, and discussed their lifetime in the interstellar medium (ISM).

¹ Université de Toulouse, UPS, CESR, 9 Av. du Colonel Roche, 31028 Toulouse Cedex 4, France

² CNRS, UMR5187, 31028 Toulouse, France

Le Page *et al.* (2001, 2003) further improved the description of the photophysical and chemical processes of PAHs and discussed the hydrogenation and charge states of PAHs in the diffuse ISM. Visser *et al.* (2007) built a model based on previous studies to describe the evolution of PAHs in protoplanetary disks.

The accuracy of the results provided by these models depends on how well photophysical and chemical processes can be quantified. Experimental data are often scarce and studies on fundamental processes are needed, which in general involve interdisciplinary collaborations between physicists, chemists, and astrophysicists.

In this paper, we analyse the question of the charge and hydrogenation states of coronene ($C_{24}H_{12}$) taking advantage of experimental data obtained with the cold ion trap PIRENEA (Joblin *et al.* 2002a). Section 2 presents the model that was developed to perform this study. The chemical and physical data are discussed in Section 3. Results are given and discussed in Section 4.

2 Presentation of the model

The model includes all hydrogenation states from fully dehydrogenated to super-hydrogenated coronene (0 to 24 H). We do not consider PAH anions since there is so far no clear evidence for their presence in the ISM and we are facing a lack of information in particular on their reactivity with hydrogen. The processes driving the evolution of charge and hydrogenation states are discussed in Section 3.

The time evolution of the species is computed using the rate equation formalism. Typical environments are PDRs in which the physics and chemistry are driven by UV photons. In order to describe as properly as possible the physical conditions in these PDRs, we use the Meudon PDR code (Le Petit *et al.* 2006) that provide a self-consistent set of physical parameters, as a function of depth inside the cloud.

3 Charge and hydrogenation states

3.1 Charge balance

In the scope of this work, we focus on the most external layers of PDRs. The PAH charge state is determined by the balance between the photoionization and the electron recombination with PAH cations. The photoionization rate for a given energy of the UV photon $h\nu$ is computed as the product of the absorption cross-section $\sigma_{abs}(h\nu)$ by the photon flux $F_{photon}(h\nu)$ and by the ionization yield $Y_{ion}(h\nu)$. The values of σ_{abs} are from Mallocci *et al.* (2004) and those of Y_{ion} from Verstraete *et al.* (1990).

Electron recombination rates have been measured for a few small PAH cations, up to the pyrene cation $C_{16}H_{10}^+$ (see Biennier *et al.* 2006). The classical law for a thin conducting disk (*e.g.* Verstraete *et al.* 1990) overestimates the rates for these small species, but is expected to be relevant for large PAH cations ($N_C \approx 100$). For species of intermediate size like coronene cation $C_{24}H_{12}^+$, we assume the recombination rate to be between the value of pyrene ($4.1 \times 10^{-6} \text{ cm}^3 \text{ s}^{-1}$ at

300 K) and the value predicted by the classical law ($1.6 \times 10^{-5} \text{ cm}^3 \text{ s}^{-1}$ at 300 K). We choose the mean value $k_{rec} = 1.0 \times 10^{-5} \text{ cm}^3 \text{ s}^{-1}$ at 300 K and also consider the extreme cases $k_{rec} = 4.1 \times 10^{-6} \text{ cm}^3 \text{ s}^{-1}$ and $k_{rec} = 1.6 \times 10^{-5} \text{ cm}^3 \text{ s}^{-1}$. A dependence of k_{rec} on $T^{-1/2}$ is used (Bakes & Tielens 1994).

For the sake of simplicity, the photoionization and electron recombination rates were supposed not to depend on the hydrogenation state.

3.2 Reactivity of PAHs with hydrogen

Only few studies have been dedicated to the reactivity of PAH cations with H or H₂, and we found no data for the reactivity of neutral PAHs. We use no temperature dependence for neutral-ion reactions, and use reaction rates $k \propto T^{1/2}$ for neutral-neutral reactions. All the values hereafter are given at 300 K except when mentioned.

The reactivity of PAH cations with H has been studied experimentally for a few PAH cations (Bierbaum, see elsewhere in this volume) including coronene ($k_{+H} = 1.4 \pm 0.7 \times 10^{-10} \text{ cm}^3 \text{ s}^{-1}$, Betts *et al.* 2006). We generalized the latter value to all coronene derivative species missing an even number of hydrogens, *i.e.* radical dehydrogenated cations. Cations missing an odd number of hydrogens are expected to be less reactive. This was demonstrated on naphthalene by Le Page *et al.* (1997), who measured $k_{+H} = 1.9 \times 10^{-10}$ and $< 5 \times 10^{-11} \text{ cm}^3 \text{ s}^{-1}$ for C₁₀H₈⁺ and C₁₀H₇⁺, respectively. Since no experimental data are available for closed-shell dehydrogenated coronene cations, we follow Le Page *et al.* (2001) and use a reaction rate of $k_{+H} = 5 \times 10^{-11} \text{ cm}^3 \text{ s}^{-1}$.

Betts *et al.* (2006) have evaluated an upper limit for the reactivity of C₂₄H₁₂⁺ with H₂ of $5 \times 10^{-13} \text{ cm}^3 \text{ s}^{-1}$. We generalize this result to all radical dehydrogenated cations. Similarly, recent measurements using the cold ion trap PIRENEA (Joblin *et al.* 2002a) have shown no reactivity of C₂₄H₁₁⁺ with H₂ at low pressure ($\sim 10^{-8}$ mbar) and temperature ($T \approx 80$ K). An upper limit of $4 \times 10^{-12} \text{ cm}^3 \text{ s}^{-1}$ was derived. Here again, we generalize this value to all closed-shell dehydrogenated coronene cations.

Superhydrogenated naphthalene and pyrene were measured not to react with H₂, and to react slowly with H at rates around $\sim 10^{-12} \text{ cm}^3 \text{ s}^{-1}$ (Snow *et al.* 1998). Hence we assume superhydrogenated coronene to react with H only, at a rate of $10^{-12} \text{ cm}^3 \text{ s}^{-1}$. More informations concerning superhydrogenated PAHs can be found in Thrower *et al.* (see elsewhere in this volume).

3.3 Photodissociation of coronene by hydrogen loss

After absorption of a UV photon, a PAH can either dissociate or cool down radiatively. Allain *et al.* (1996a) showed that the relaxation cascade is dominated by IR photons. The IR emission rates were calculated in a microcanonical formalism (Joblin *et al.* 2002b).

Using the PIRENEA set-up, Joblin *et al.* studied the photodissociation of C₂₄H_{*p*}⁺ species ($p = [1, 12]$) and derived dissociation rates as a function of the

Table 1. Summary of the reaction rates ($\text{cm}^3 \text{s}^{-1}$) at 300 K used in our model for coronene derivatives and their origin. The neutral counterparts are assumed to react neither with H nor with H_2 . (a) Betts *et al.* (2006); (b) Le Page *et al.* (2001); (c) Snow *et al.* (1998); (d) No detection with the PIRENEA set-up.

Species	$C_{24}H_n^+$ (even $n \leq 12$)	$C_{24}H_n^+$ (odd $n < 12$)	$C_{24}H_n^+$ ($n > 12$)
$+H$	1.4×10^{-10} (a)	5.0×10^{-11} (b)	1.0×10^{-12} (c)
$+H_2$	$< 5 \times 10^{-13}$ (a)	$< 4 \times 10^{-12}$ (d)	- (b)
$+e^-$	1.0×10^{-5} (extrapolation)		

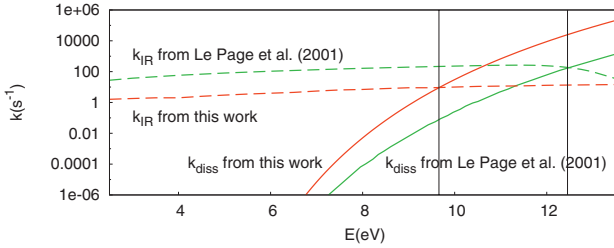


Fig. 1. Comparison of the IR cooling (dashed lines) and photodissociation (solid lines) rates from Le Page *et al.* (2001) (green lines) and from this work (red lines) for the coronene cation $C_{24}H_{12}^+$, as a function of its internal energy. Vertical lines indicate the threshold energy above which the dissociation is faster than the IR emission.

internal energy (Joblin *et al.* 2010a). Only H loss was observed for these species, the destruction of the carbon skeleton occurring only after complete dehydrogenation (C_{24}^+ ; Joblin *et al.* 2003; Joblin *et al.* 2010b). The reaction rates derived by Joblin *et al.* differ significantly from the values from Le Page *et al.* (2001; *cf.* Fig. 1).

4 Results

Using our numerical model, we compute the hydrogenation and charge states of coronene for the northern PDR in NGC 7023. For the incident radiation field, we used the stellar spectrum from the Kurucz library (Kurucz 1991) for a star with a temperature of 15 000 K and an integrated UV intensity of 2600 Habing. The density was set to $n_H = 2 \times 10^4 \text{ cm}^{-3}$ (Gerin *et al.* 1998).

General behaviour. The hydrogenation state of coronene adopts four possible regimes: (1) totally dehydrogenated ($C_{24}^{0/+}$ dominates), (2) partially dehydrogenated with a roughly equivalent abundance for each $C_{24}H_p^+$, species ($p = [1, 11]$), (3) normally hydrogenated ($C_{24}H_{12}^{0/+}$ dominates) and (4) superhydrogenated ($C_{24}H_{13}^{0/+}$ dominates).

Hydrogenation and charge state of coronene in NGC 7023. As shown in Figure 2, coronene is found to be essentially neutral throughout the PDR. Despite

the high intensity of the radiation field, PAHs are ionized only in the first layers of the cloud. The totally dehydrogenated species, C_{24} , dominates inside the PDR up to a depth of $A_V \approx 5$, where $G_0 \approx 20$ in Habing units. For equivalent conditions, *i.e.* $G_0/n_H \approx 1/1000$, Le Page *et al.* found the normal hydrogen coverage to dominate. This difference is consistent with our model using larger photodissociation rates, and lower reaction rates with H_2 .

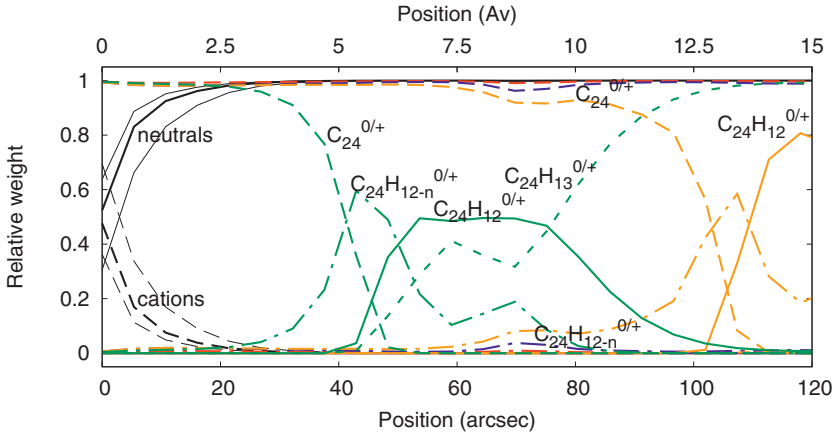


Fig. 2. Evolution of the charge and hydrogenation states of coronene through the northern PDR of the reflection nebula NGC 7023. Black lines: evolution of the abundances of cations (dashed lines) and neutrals (solid lines), for different electron recombination rates (thick lines: $k_{rec}(300\text{ K}) = 1.0 \times 10^{-5} \text{ cm}^3 \text{ s}^{-1}$; thin lines: $k_{rec}(300\text{ K}) = 0.4$ and $1.6 \times 10^{-5} \text{ cm}^3 \text{ s}^{-1}$). Color lines: abundances of $C_{24}^{0/+}$ (dashed lines), partially dehydrogenated species $C_{24}H_{12-n}^{0/+}$ with $n=[1,11]$ (dot-dashed lines), $C_{24}H_{12}^{0/+}$ (solid lines) and $C_{24}H_{13}^{0/+}$ (dotted lines) derived with (i) our standard model (red), (ii) maximum values for reactivity between cations and H_2 (blue), (iii) reaction rates of neutral radicals with H set to $1.4 \times 10^{-11} \text{ cm}^3 \text{ s}^{-1}$ at 300 K (orange) and (iv) reaction rates of neutrals with H set at 300 K to $1.4 \times 10^{-11} \text{ cm}^3 \text{ s}^{-1}$ (radicals) and $5.0 \times 10^{-12} \text{ cm}^3 \text{ s}^{-1}$ (closed-shells) (green).

Influence of the uncertainties. The uncertainty on the electron recombination rate affects the ionization fraction to at most a factor of 2. Tuning the reaction rates of PAH cations with H_2 from their upper limit to zero does not change significantly the results. The abundances are also not strongly affected by the experimental uncertainty of 50% on the reactivity of $C_{24}H_{12}^{0/+}$ with H. On the contrary, tuning the reactivity of neutral PAHs, which was set to 0 in our standard model, leads to substantial changes. If neutral radicals $C_{24}H_{2n-1}$ react with H at a rate at 300 K ten times lower than cation radicals, the hydrogenation state differs only deep in the cloud ($A_V > 10$), where PAHs are very likely in solid phase. However, if neutral closed-shell species $C_{24}H_{2n}$ are also considered to react with H, with a rate at 300 K ten times lower than for closed-shell cations, then $C_{24}H_{12}$ dominates between $A_V = 6$ and 9, while $C_{24}H_{13}$ dominates deeper.

5 Conclusion

We present the first results of a model dedicated to the study of the evolution of PAHs in astrophysical environments. We examine the case of coronene hydrogenation and charge states, in the northern PDR of NGC 7023, using the latest available physical and chemical data. Coronene was found to be much more dehydrogenated than calculated in previous studies. Reaction rates of coronene-derived radical cations with H and H₂ were found to be sufficiently constrained by experiments, whereas the absence of experimental data for the reactivity of neutral species appears to be critical. A first theoretical study is presented elsewhere in this volume (Thrower *et al.*).

References

- Allain, T., Leach, S., & Sedlmayr, E., 1996a, *A&A*, 305, 602
Allain, T., Leach, S., & Sedlmayr, E., 1996b, *A&A*, 305, 616
Bakes, E.L.O., & Tielens, A.G.G.M., 1994, *ApJ*, 427, 822
Betts, N.B., Stepanovic, M., Snow, T.P., & Bierbaum, V.M., 2006, *ApJ*, 651, L129
Biennier, L., Alsayed-Ali, M., Foutel-Richard, A., *et al.*, 2006, *Faraday Discussions*, 133, 289
Draine, B.T., & Sutin, B., 1987, *ApJ*, 320, 803
Gerin, M., Phillips, T., Keene, J., Betz, A.L., & Boreiko, R.T., 1998, *ApJ*, 500, 329
Joblin, C., Pech, C., Armengaud, M., Frabel, P., & Boissel, P., 2002a, *EAS Publication Series*, 4, 73
Joblin, C., Toubanc, D., Boissel, P., & Tielens, A.G.G.M., 2002b, *Mol. Phys.*, 100, 3595
Joblin, C., 2003, in *SF2A-2003*, ed. F. Combes *et al.* (EDP-Sciences), 175
Joblin C., Toubanc D., Pech C., Armengaud M., Frabel P., & Boissel P., 2010a, in preparation
Joblin C., Armengaud M., Frabel P., & Boissel P., 2010b, in preparation
Jochims, H.W., Ruhl, E., Baumgartel, H., Tobita, S., & Leach, S., 1994, *ApJ*, 420, 307
Kurucz, R.L., 1991, *BAAS*, 23, 1047
Leger, A., d'Hendecourt, L., Boissel, P., & Desert, F.X., 1989, *A&A*, 213, 351
Le Page, V., Keheyan, Y., Bierbaum, V.M., & Snow, T.P., 1997, *JACS*, 119, 35
Le Page, V., Keheyan, Y., Snow, T.P., & Bierbaum, V.M., 1999a, *IJMS*, 185, 949
Le Page, V., Keheyan, Y., Snow, T.P., & Bierbaum, V.M., 1999b, *JACS*, 121, 9435
Le Page, V., Snow, T.P., & Bierbaum, V.M., 2001, *ApJS*, 132, 233
Le Page, V., Snow, T.P., & Bierbaum, V.M., 2003, *ApJ*, 584, 316
Le Petit, F., Nehme, C., Le Bourlot, J., & Roueff, E., 2006, *ApJS*, 164, 506
Mallocci, G., Mulas, G., & Joblin, C., 2004, *A&A*, 426, 105
Snow, T.P., Le Page, V., Keheyan, Y., & Bierbaum, V.M., 1998, *Nature*, 391, 259
Verstraete, L., Leger, A., D'Hendecourt, L., Defourneau, D., & Dutuit, O., 1990, *A&A*, 237, 436
Visser, R., Geers, V.C., Dullemond, C.P., *et al.*, 2007, *A&A*, 466, 229

SUPERHYDROGENATED PAHS: CATALYTIC FORMATION OF H₂

J.D. Thrower¹, L. Nilsson¹, B. Jørgensen¹, S. Baouche¹, R. Balog¹,
A.C. Luntz¹, I. Stensgaard¹, E. Rauls² and L. Hornekær¹

Abstract. The possible role of neutral PAHs as catalysts for H₂ formation in the interstellar medium is investigated by a combined experimental and density function theory study of the superhydrogenation of coronene (C₂₄H₁₂). The calculations suggest efficient hydrogenation of both edge and centre sites, along with competing abstraction reactions to form H₂ in a series of catalytic cycles. Scanning tunneling microscopy and thermal desorption measurements have been used to provide direct evidence of the formation of superhydrogenated coronene as a result of exposure to D atoms. Lower limit estimates for the cross-sections of 1.8×10^{-17} , 5.5×10^{-18} and 1.1×10^{-18} cm² for the formation of singly, doubly and triply hydrogenated coronene are derived. The results suggest that superhydrogenated PAHs may play an important role in H₂ formation in the ISM.

1 Introduction

The interstellar formation of H₂ remains the subject of intense research effort given the importance of this molecule as a cooling agent and as a key precursor for chemical processes in interstellar dust and molecular clouds. The present consensus is that molecular hydrogen forms on the surface of interstellar dust grains by reactions between hydrogen atoms (Hollenbach & Salpeter 1971). Experiments and theoretical calculations have shown that surface reactions involving physisorbed H atoms are efficient at temperatures below approximately 20 K (Pirronello *et al.* 1997b; Pirronello *et al.* 1997a; Pirronello *et al.* 1999; Katz *et al.* 1999; Manico *et al.* 2001; Roser *et al.* 2002; Hornekær *et al.* 2003; Cuppen & Herbst 2005).

¹ Department of Physics and Astronomy, Aarhus University, 8000 Aarhus C, Denmark
e-mail: liv@phys.au.dk

² Department of Theoretical Physics, Faculty of Natural Sciences, University of Paderborn, 33098 Paderborn, Germany

In regions with gas temperatures of several hundred kelvin surface reactions involving chemisorbed H atoms have been shown to be efficient (Zecho *et al.* 2002; Cazaux & Tielens 2004; Hornekær *et al.* 2006a, 2006b). However, at intermediate temperatures, no efficient routes for H₂ formation have been identified (Cuppen & Herbst 2005).

A possible alternative route to interstellar H₂ formation is provided by PAH molecules. Observations of spatial correlations between vibrationally excited H₂ and PAHs in photo dissociation regions provide indications of PAHs acting as catalysts for H₂ formation (Habart *et al.* 2003; Habart *et al.* 2004). PAHs in the ISM are thought to exhibit a range of hydrogenation and charge states depending on the environment, especially the UV flux (Le Page *et al.* 2001; Le Page *et al.* 2003; Montillaud *et al.* 2011). At high UV fluxes small PAHs will be dissociated, whilst at intermediate fluxes H loss and ionization dominate, resulting in dehydrogenated and cationic PAHs. Under low UV flux conditions neutral, anionic and superhydrogenated PAHs are likely to be present in the gas phase or frozen out on dust grain surfaces. For example, observations of the 3.4 μm emission aliphatic band in low UV flux regions compare well with laboratory spectra of superhydrogenated neutral PAHs (Bernstein *et al.* 1996). To date, investigations of H₂ formation on PAHs have focussed primarily on cationic states, see, for example, (Le Page *et al.* 1997; Bauschlicher 1998; Betts *et al.* 2006; Le Page *et al.* 2009; Bierbaum 2011). However, formation of H₂ on PAH anions (Bauschlicher & Bakes 2001) and neutral PAHs (Stein & Brown 1991; Bauschlicher 1998; Rauls & Hornekær 2008; Rodriguez *et al.* 2010), as well as on PAH coated grains (Duley & Williams 1993) has also been discussed.

Here we investigate in detail the possible role of neutral PAH molecules and PAH covered dust grains as catalysts for H₂ formation. Density functional theory (DFT) calculations on the hydrogenation of the coronene molecule reveal a relatively small barrier to the addition of a single H atom to coronene. Interestingly, subsequent hydrogenation and abstraction reactions can proceed with little or no barrier, suggesting a catalytic cycle which results in H₂ formation (Rauls & Hornekær 2008). Experimental observations of superhydrogenated coronene formed through exposure to atomic D are also presented. These combined experimental and theoretical results suggest that superhydrogenation of PAHs may provide an important additional route to H₂ formation in intermediate, as well as high temperature environments in the ISM. Similar experimental results for the case of aromatic carbon grain mimics are provided by Mennella (2011).

2 Methods

The DFT calculations were carried out using the plane wave based DACAPO code (Hammer *et al.* 1999; Bahn & Jacobsen 2002) and the PW91 exchange correlation (xc) functional (Perdew *et al.* 1992). Spin polarization was included in all calculations. Potential energy curves were constructed by performing single

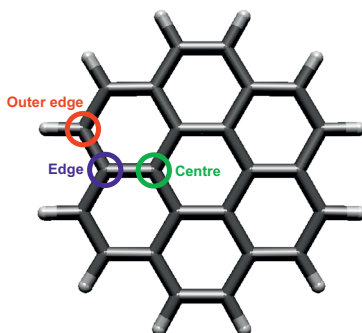


Fig. 1. The possible hydrogenation sites on the coronene molecule. The sites are referred to as outer edge (oe), edge (e) and centre (c).

point calculations with constrained distances between either one H and one C atom, or two H atoms in the case of hydrogenation and abstraction reactions respectively. Barrier heights were obtained by iterative energy calculations within close proximity of the critical geometry. As a result, all barriers can be considered to be upper bounds for the activation energies. See Rauls & Hornekær (2008) for further details.

Scanning tunneling microscopy (STM) and thermal desorption measurements were performed under ultrahigh vacuum (UHV) conditions in two separate chambers. In both chambers, $C_{24}H_{12}$ films were grown by placing the substrate close to an evaporation source in which the $C_{24}H_{12}$ sample was held at 180°C . The coronene films were then exposed to atomic D, which was produced using a hot capillary thermal cracker source of the Jülich type (Tschersich & von Bonin 1998). Temperature programmed desorption (TPD) experiments employed a highly oriented pyrolytic graphite (HOPG) substrate, cleaved prior to mounting in the UHV chamber. TPD spectra were acquired using a quadrupole mass spectrometer (QMS) and a heating ramp of 1 K s^{-1} . A Cu(100) single crystal substrate was used for the STM measurements to exploit the improved imaging conditions provided by the stronger binding between coronene molecules and this substrate.

3 Results

There are three possible sites for the addition of a single H atom to coronene as shown in Figure 1. The most stable product is obtained through addition to a carbon atom in an outer edge site. The additional H atom has a binding energy in excess of 1.4 eV, twice that found for graphite. There is a barrier to addition of 60 meV which is significantly smaller than the 200 meV found for H adsorption on the basal plane of graphite (Sha & Jackson 2002). This indicates that hydrogenation of $C_{24}H_{12}$ is likely to occur in cooler environments than for graphite and that the hydrogenated species thus formed will be stable.

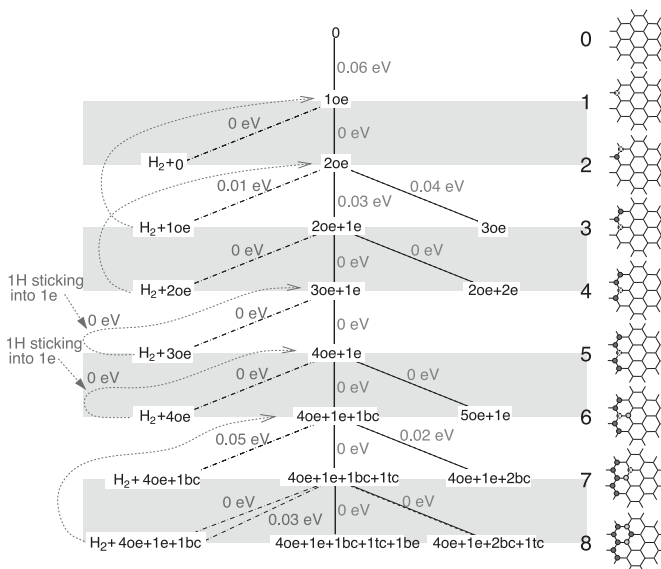


Fig. 2. A summary of the results of the DFT calculations. The central line shows the most favourable addition reactions. The sites involved are indicated. The abstraction reactions and catalytic loops are shown on the left. All energies are the associated reaction barriers. The top and bottom sides of the molecule are labelled t and b respectively. Reproduced by permission of the AAS from Rauls & Hornekær (2008).

Further addition reactions were also considered. The results of these DFT calculations for up to 8 additional H atoms, as well as abstraction reactions from each hydrogenation state, are summarized in Figure 2. Individual potential energy surfaces for these reactions, along a more detailed discussion, can be found elsewhere (Rauls & Hornekær 2008). Addition of a second H atom is most favourable to the outer edge site adjacent to that involved in the first hydrogenation step. This reaction is barrierless and results in a binding energy for the second H atom of 3.2 eV which gives a combined binding energy for the outer edge dimer of *ca.* 4.7 eV. Comparing this value with the H₂ binding energy of 4.5 eV indicates that direct recombination of two bound H atoms to form gas phase H₂ is not energetically favourable. H₂ formation is likely to occur, however, through Eley-Rideal abstraction reactions. Indeed, abstraction by, rather than addition of, the second H atom is also found to be barrierless revealing a competition between these two processes. Similarly, for subsequent incoming H atoms there exist reaction pathways for both addition and abstraction that are thermodynamically viable and have small or even vanishing activation barriers.

Interestingly, not only outer edge and edge sites can be accessed, but a favourable addition to a centre site is also possible with the addition of a sixth H atom.

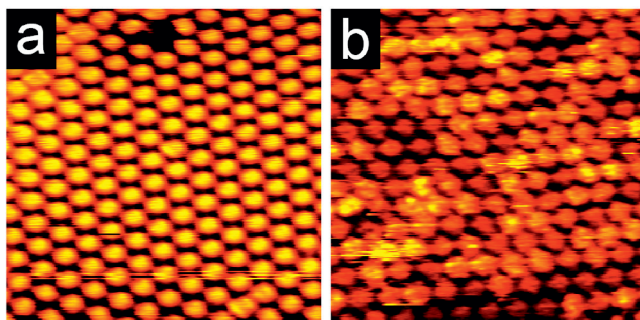


Fig. 3. STM images ($150 \times 150 \text{ \AA}^2$) of a monolayer of coronene adsorbed on Cu(100) (a) prior to and (b) after exposure to D atoms ($4 \times 10^{13} \text{ cm}^{-2}$). The bright protrusions of diameter *ca.* 11.5 \AA are identified as individual coronene molecules. Imaging parameters: (a) $V_t = -2460 \text{ mV}$, $I_t = -0.21 \text{ nA}$ (b) $V_t = -784 \text{ mV}$, $I_t = -0.17 \text{ nA}$.

Addition to centre sites occurs such that adjacent H atoms are bound on opposite faces of the molecule. This is consistent with the molecular structure approaching that of the fully hydrogenated coronene molecule, perhydrocoronene ($\text{C}_{24}\text{H}_{36}$) which exhibits this arrangement of hydrogen atoms. It is clear that the most important step in the hydrogenation process is the addition of the first hydrogen atom. This opens up a series of reaction pathways in which further H atoms may be added with H_2 formation occurring *via* catalytic loops, re-forming lower hydrogenated states. The branching ratios for the competing addition and hydrogenation reactions are not known and will be essential for a full understanding of the efficiency of H_2 formation.

In Figure 3a an STM image of a self-assembled monolayer of $\text{C}_{24}\text{H}_{12}$ deposited on the clean Cu(100) surface is displayed. An ordered structure of circular protrusions of diameter *ca.* 11.5 \AA is observed. These bright protrusions are identified as individual coronene molecules adsorbed flat on the surface. A single vacancy defect is observed in the top part of the image. The coronene covered surface was subsequently exposed to D atoms with a fluence of $4 \times 10^{13} \text{ cm}^{-2}$. An STM image of the surface after exposure is shown in Figure 3b. The image clearly shows variations in imaging intensity between coronene molecules, as well as within individual coronene molecules. These variations are attributed to the formation of hydrogenated coronene. The range of different intensity variations in the image suggests the presence of coronene molecules with differing degrees of hydrogenation. Comparison between STM images and theoretical calculations should make it possible to determine the number and position of deuterium atoms added to individual coronene molecules in the near future.

Thermal desorption measurements have also been conducted using a layer of $\text{C}_{24}\text{H}_{12}$ grown on the HOPG substrate and subsequently exposed to D atoms with a fluence of $9 \times 10^{15} \text{ cm}^{-2}$. The substrate was then heated linearly and the desorbing

Table 1. Contributions to the desorption signal from the different hydrogenation states along with estimated lower limits for the associated addition reaction cross-sections.

m/z	% of desorption signal	cross-section / cm^2
300	77	—
302	16	1.8×10^{-17}
304	5	5.5×10^{-18}
306	1	1.1×10^{-18}

species detected. Desorption signals (not shown) for $m/z = 300, 302, 304$ and 306 corresponding to coronene and singly, doubly and triply hydrogenated (with D) products were observed. Table 1 shows the relative contributions to the total desorption signal for the individual hydrogenation states observed. The estimated reaction cross-sections are based on the following assumptions: only contribution from one coronene layer (correct within a factor of 2–3), no saturation effects, detection of all hydrogenated species. For the doubly and triply hydrogenated coronene the values derived are the effective overall cross-sections obtained using the total initial coronene coverage. Since the electron impact ionization employed in the QMS is likely to lead to fragmentation and dehydrogenation, the calculated cross-sections are only lower limits. The cross-sections thus derived are larger than those found previously for the irradiation of carbon grain mimics (*ca.* $2 \times 10^{-18} \text{ cm}^2$) with H atoms at temperatures of 80–300 K (Mennella *et al.* 2002; Mennella 2006). This is consistent with the use of significantly higher D atom temperatures in the present study. At higher D atom fluences, even higher degrees of superhydrogenation of coronene are observed.

4 Conclusions

DFT calculations indicate the presence of energetically favourable pathways to H_2 formation through catalytic cycles of hydrogenation and abstraction. The barrier to addition of the first H atom is of the order of 60 meV and small or vanishing barriers are found for all subsequent reactions. The hydrogenation of coronene has been observed directly using STM through the appearance of sub-molecular structure following exposure to D atoms. There is evidence for the presence of several different hydrogenated species, although comparison with theory will be required to determine the degree of hydrogenation and the sites involved. Thermal desorption measurements show that very high levels of superhydrogenation can be attained. Hence, both theoretical calculations and experimental results indicate that PAHs might well play a role as catalysts for H_2 formation in intermediate and high temperature environments.

The authors gratefully acknowledge financial support from the European Research Council under ERC starting grant HPAH, No. 208344. The research leading to these results has received funding from the European Community's Seventh Framework Programme under grant agreement No. 238258.

References

- Bahn, S.R., & Jacobsen, K.W., 2002, *Comput. Sci.*, 4, 56
- Bauschlicher, C.W., 1998, *ApJ*, 509, L125
- Bauschlicher, C.W., & Bakes, E.L.O., 2001, *Chem. Phys.*, 274, 11
- Bernstein, M.P., Sandford, S.A., & Allamandola, L.J., 1996, *ApJ*, 472, L127
- Betts, N.B., Stepanovic, M., Snow, T.P., & Bierbaum, V.M., 2006, *ApJ*, 651, L129
- Bierbaum, V.M., 2011, this volume
- Cazaux, S., & Tielens, A.G.G.M., 2004, *ApJ*, 604, 222
- Cuppen, H.M., & Herbst, E., 2005, *MNRAS*, 361, 565
- Duley, W.W., & Williams, D.A., 1993, *MNRAS*, 260, 37
- Habart, E., Boulanger, F., Verstraete, L., *et al.*, 2003, *A&A*, 397, 623
- Habart, E., Boulanger, F., Verstraete, L., Walmsley, C.M., & des Forets, G.P., 2004, *A&A*, 414, 531
- Hammer, B., Hansen, L.B., & Norskov, J.K., 1999, *Phys. Rev. B*, 59, 7413
- Hollenbach, D., & Salpeter, E.E., 1971, *ApJ*, 163, 155
- Hornekær, L., Baurichter, A., Petrunin, V.V., Field, D., & Luntz, A.C., 2003, *Science*, 302, 1943
- Hornekær, L., Rauls, E., Xu, W., *et al.*, 2006a, *Phys. Rev. Lett.*, 97, 186102
- Hornekær, L., Sljivancanin, Z., Xu, W., *et al.*, 2006b, *Phys. Rev. Lett.*, 96, 156104
- Katz, N., Furman, I., Biham, O., Pirronello, V., & Vidali, G., 1999, *ApJ*, 522, 305
- Le Page, V., Snow, T.P., & Bierbaum, V.M., 2001, *ApJS*, 132, 233
- Le Page, V., Snow, T.P., & Bierbaum, V.M., 2003, *ApJ*, 584, 316
- Le Page, V., Snow, T.P., & Bierbaum, V.M., 2009, *ApJ*, 704, 274
- LePage, V., Keheyang, Y., Bierbaum, V.M., & Snow, T.P., 1997, *J. Am. Chem. Soc.*, 119, 8373
- Manico, G., Raguni, G., Pirronello, V., Roser, J.E., & Vidali, G., 2001, *ApJ*, 548, L253
- Mennella, V., 2006, *ApJ*, 647, L49
- Mennella, V., Brucato, J.R., Colangeli, L., & Palumbo, P., 2002, *ApJ*, 569, 531
- Mennella, V., 2011, this volume
- Montillaud, J., Joblin, C., Toublanc, D., *et al.*, 2011, this volume
- Perdew, J.P., Chevary, J.A., Vosko, S.H., *et al.*, 1992, *Phys. Rev. B*, 46, 6671
- Pirronello, V., Biham, O., Liu, C., Shen, L.O., & Vidali, G., 1997a, *ApJ*, 483, L131
- Pirronello, V., Liu, C., Roser, J.E., & Vidali, G., 1999, *A&A*, 344, 681
- Pirronello, V., Liu, C., Shen, L., & Vidali, G., 1997b, *ApJ*, 475, L69
- Rauls, E., & Hornekær, L., 2008, *ApJ*, 679, 531

- Rodriguez, L.S., Ruetter, F., Sanchez, M., & Mendoza, C., 2010, *J. Mol. Catal. A*, 316, 16
- Roser, J.E., Manico, G., Pirronello, V., & Vidali, G., 2002, *ApJ*, 581, 276
- Sha, X.W., & Jackson, B., 2002, *Surf. Sci.*, 496, 318
- Stein, S.E., & Brown, R.L., 1991, *J. Am. Chem. Soc.*, 113, 787
- Tschersich, K.G., & von Bonin, V., 1998, *J. Appl. Phys.*, 84, 4065
- Zecho, T., Güttler, A., Sha, X., Jackson, B., & Küppers, J., 2002, *J. Chem. Phys.*, 117, 8486

Summary of the Meeting

SUMMARY OF THE MEETING

A. Omont¹

Abstract. This symposium has shown that the field of astrophysical PAHs remains extremely active and lively. Thanks to *Spitzer* Space Telescope, the number of PAH papers has spectacularly increased, including now up to the young Universe. Laboratory and theoretical works have progressed in proportion. Salient features of the six sessions of the symposium are briefly reviewed. Comprehensive analyses of the rich and complex infrared spectra of interstellar PAHs are now well established, based on a large database of observational data. PAHs are fully confirmed as excellent tracers of star formation, but their emission strongly depends on metallicity. Various observations, especially in harsh environments, have confirmed the complexity of the lifecycle of PAHs in space, and the need for multiple formation modes. Electronic properties remain a major issue for astronomical PAHs, including their possible connection with the diffuse interstellar bands, and the possible importance of protonated PAHs. Progress in studying complex carbonaceous compounds, such as those of various soots, and in synthesizing very large PAHs may give important clues for understanding interstellar PAHs. Significant progress was also reported in modeling the important role of PAHs in the physics and chemistry of the interstellar medium.

1 Introduction

Coming back to this field after some time, I am not surprised to find it quite mature for its 25th anniversary. However, I am also struck seeing it so active and lively. Of course, as any well established field, after the explosion of its opening, it had to face renewal and serious challenges. But this symposium has shown that new directions are constantly opened, while older ones are renewed and benefit from breakthroughs in observational, laboratory and theoretical capabilities. The size of the attendance of this meeting including a very lively, enthusiastic and

¹ Institut d'Astrophysique de Paris, UMR 7095, CNRS, UPMC Univ. Paris 06, 98bis Bd. Arago, 75014 Paris, France

outstanding new generation is the best proof of the current impact of the field and its appeal to young researchers.

Before spotting various highlights of the meeting, I would like to stress two major features that we may agree on being the main drivers of many of the new achievements that we heard about in the last days

First, after ISO, *Spitzer* and its mid-infrared spectrometer have considerably widened the field of PAH studies, especially the extragalactic world up to amazingly large distances close to ten billion light years. This is strikingly demonstrated by the figure displayed by O. Berné showing the rapid increase in papers on PAHs in the last ten years, and furthermore that the number of papers on PAHs in extragalactic systems increased even more rapidly.

The other major trend is the amazing strength of the synergy between astrophysics, laboratory and theory in the works which were reported. Indeed, very large efforts have been invested in ambitious, astronomy orientated laboratory projects exploiting sophisticated techniques. At the same time, the development of a variety of theoretical and computing techniques has spectacularly improved the efficiency of quantum chemistry methods, as reviewed by F. Pauzat and others.

Astrophysical PAHs remain highly appealing even outside the strict realm of astronomy, because of their strong connection with astrochemistry and exotic interstellar organic molecules, and also with interstellar dust and thus with the origin of planetary systems as traced by the presence of PAHs in meteorites and comets. With SOFIA, JWST and SPICA, exciting new instrumentation will come on line to probe the many mysteries associated with interstellar PAHs. I will thus list in turn the most salient features of each of the six sessions of the symposium.

2 Rich (IR) spectra of interstellar PAHs

The interpretation of the rich and complex interstellar mid-IR PAH spectra remains difficult, even for the main classical features from 6.2 to 12.7 μm , and *a fortiori* the weaker features although many of them are now well established, especially in the 15–20 μm range. However, we have now a very comprehensive general analysis of PAH mid-IR spectra, mainly from the Ames-Dutch group, as reported by E. Peeters. It is based on a rich set of observational data of a broad variety of astronomical sources, and PAH spectroscopic data that is now available in the impressive Ames database. The main classes of spectra are well established for various classes of sources including interstellar HII regions, reflection nebulae, circumstellar material of most post-AGB stars, planetary nebulae, Herbig Ae-Be stars, plus peculiar objects. Various characteristics of the spectra reflect first the ionization state and the size of the PAHs. In addition, specific interpretations for various details have been proposed, involving mainly chemical modifications such as hetero-atoms - mainly N - metal compounds, carbon isotopes, aliphatic fraction, etc.

PAH band ratios have been further analysed in detail in various observations, and in models *e.g.* by F. Galliano. An interesting spectral decomposition of PAH emission has been proposed by O. Berné and the Toulouse group. It is based

on the identification of a few main spectral components, attributed to specific compounds. The addition with various weights of these components may account for the spectra observed in different spatial regions.

Although overwhelming, the infrared range is by no way the only spectral range where PAHs show up in the interstellar medium. I will discuss optical bands below. PAHs have long been proposed to be main contributors to the major band seen around 2175 Å in the UV extinction curve. B. Draine very convincingly reviewed the arguments in favor of this natural key attribution. As reported by C. Joblin, a major effort is undertaken to detect far-IR modes of PAHs with Herschel. Detection of such modes would represent a major breakthrough because these modes should be more specific than in the mid-IR. However, as she discussed, it is not an easy task. Finally I note the absence in the meeting of a specific discussion of the likely important contribution of PAH rotation to the radio emission of the interstellar medium around 30 GHz.

3 PAHs, star formation and metallicity

Because of their UV excitation, it is well established that the mid-IR features of PAHs are major tracers of star formation, as shown by their ubiquitous presence in star formation regions of various types of galaxies. The correlation between 8 μm PAH emission and the ionizing photons produced by star formation was comprehensively and quantitatively reviewed by D. Calzetti, with the conclusion that it is almost perfect. This emission can thus be used as a star formation rate indicator. However, the 8 μm emission is heavily dependent on metallicity, and the 8 μm emission may also be triggered by evolved (non star-forming) stellar populations.

Detailed evidence for the correlation of PAHs and metallicity was given by several other communications and posters, including E. Peeters, F. Galliano, L. Hunt and K. Sandstrom. This utilizes large samples of galaxies, as well as the SMC where the PAH fraction is especially low and spatially variable.

4 The lifecycle of PAHs in space. PAH evolution and processing

PAHs are relatively stable and natural carbonaceous products in hydrogen-rich environment. However, they are submitted to various destruction processes. Still they exist in a diversity of environments including hostile ones. This implies that they can form easily by a variety of processes.

PAHs are much faster destroyed in hot plasmas than dust, as seen in the halo of M 82; this confirms that they are efficiently dissociated in each collision with energetic particles, while dust is only slowly sputtered (H.Kaneka). However, PAHs are observed in a significant fraction of the supernova remnants of the comprehensive study reported by J. Rho. Such shocked processed PAHs are strongly correlated with carbon dust and shock conditions. PAHs also evolve as a function of the UV

intensity in photo-dissociation regions, possibly in connection with PAH clusters (M. Rapacioli).

As reported by I. Cherchneff, the inner envelope of carbon stars is a natural location of PAH formation as intermediates to the amorphous carbon dust synthesis. In this context, it is important to note the finding of PAHs and onion-like graphene sheets in meteorite nanograins. Understanding the characteristics of dust formation in carbon star may give interesting clues to the relationship between PAHs and carbonaceous dust products.

However, direct formation and growth of PAHs from large molecules or carbon dust in molecular clouds remains very likely a crucial process to explain the ubiquity of interstellar PAHs as discussed by P. Woods, W. Geppert and V. Menella.

The frequent detection of PAHs in many circumstellar disks, including most Herbig Ae stars, also shows their importance in the process of formation of planets and comet nuclei. In such cases, the well defined geometrical conditions allow a precise modeling of their interaction with the UV field and their destruction, as developed in sophisticated models by R. Siebenmorgen.

5 Electronic properties

Electronic properties remain a major issue for astronomical PAHs in many respects. Research about these properties justify a good part of the major laboratory projects across the world. A good knowledge of excited state properties is needed for understanding the complex cascade and relaxation processes resulting in interstellar IR emission induced by UV absorption. Major efforts address the spectroscopy of PAHs in difficult laboratory conditions of cold temperature and gas phase isolated PAHs, relevant for astrophysical conditions. They aim at determining not only spectral characteristics – accurate positions, widths and intensities of spectral lines – but also fluorescence and relaxation pathways. As reported by T. Pino, laser spectroscopy is especially useful, including multi-photon processes, induced fluorescence, etc., both in gas phase and matrix isolation spectroscopy.

A major challenge for astrophysical PAHs is that their dominant forms may be a variety of species that are unstable in usual laboratory conditions – ionized, protonated, deprotonated, dehydrogenated – rather than regular neutral PAHs. P. Sarre especially stressed the importance of protonated and deprotonated PAHs, and their fast reactions, providing calculations of their electronic properties and spectra.

The identification of the carriers of the **Diffuse Interstellar Bands (DIBs)** is still the main issue in the field of interstellar compounds possibly associated with PAHs. Ted Snow gave a comprehensive summary of the state of the DIB problem. He stressed that while more than 600 DIBs have now been catalogued, with more coming, not one DIB has been definitively identified, after almost 90 years of trying! However, almost certainly carbon-based molecules are responsible, and candidates include linear chains, buckyballs, PAHs, and others. There is some hope that UV COST/HST spectroscopy gives important clues about this identification.

Nick Cox further reviewed the hypothesis that DIBs are connected with PAHs or other large “related” molecules such as fullerenes, nanotubes or carbon rings.

Some significant progress in this field was reported during the symposium, especially the confirmation of C_{60} in reflection nebulae through mid-IR detection of several lines by K. Sellgren.

6 PAHs and carbonaceous grains

The connection of PAHs with carbonaceous grains is obvious from the similitude of their basic graphene structure, and the possibility to exchange carbonaceous matter through PAH accretion onto grains and PAH generation in grain shattering.

Furthermore, PAHs could also condensate onto water rich ices in dense clouds. As discussed by Bouwman *et al.*, the UV induced PAH-grain photochemistry may then play an important role in interstellar chemistry.

However, the relationship of PAHs with carbonaceous grains is much more intimate because of their similitude of structure and possible family ties. C. Jaeger gave a fascinating review of the various solid forms of carbon and carbonaceous particles. Compared to diamond and even graphite, amorphous hydrogenated carbon and soot particles are much more likely akin to PAHs.

Among various topics, she reported Matrix-Assisted-Laser Desorption and Ionization combined with mass spectrometry to produce and characterize amazingly heavy PAHs up to ~ 3000 atomic mass units, such as $C_{222}H_{42}$!

Her summary about soot formation and its multiple processes may give important clues for interstellar PAHs. She described how different may be soot formation at high temperature, leading to fullerene-like carbon, and at low temperature ending with soot with plane layers. It is clear that carbonaceous transition objects between molecules and solids may have an amazing diversity including: PAH clusters, PAH oligomers, 3D fragments of fullerenes, oligomers of fullerene fragments, and small nested buckyonions!

7 The role of PAHs in the physics and chemistry of the interstellar medium

When seeing the important contribution of PAHs in the electromagnetic emission of the interstellar medium of galaxies, it is not surprising that they also play a crucial role in its physics and chemistry.

Talks and posters by L. Verstraete, J. Montillaud and others showed that PAHs intervene in many physical processes. Their determining contribution to the ionization of the interstellar gas is the most well known. It is also now agreed that their rotation emission may dominate the radio continuum emission of galaxies at wavelengths around 1 cm. However, there are still many pending questions to be further investigated by observations, modelling, laboratory and theory.

The role of PAHs in the chemistry of the interstellar medium is probably at least equally important, as discussed in many talks and posters, and especially in

the comprehensive review by V. Bierbaum. It was also stressed by A. Simon that metallic compounds, especially Fe-PAH, may be important.

8 Conclusion

To conclude, there is no doubt that the symposium was timely and highly successful. The field is blooming and will continue for long. Certainly, the symposium, its dense scientific program and its wonderful organization by Christine and the local organizing committee will significantly contribute to a new start of the exploration of galaxies through their PAHs. Exciting new instrumentation is coming for probing their many mysteries, with SOFIA, JWST, SPICA, etc, and one may again anticipate an excellent synergy with the major progress expected in laboratory and theoretical techniques.

Author Index

- Acke B., 259
af Ugglas M., 241
Allamandola L.J., 109,
251, 305
Andersen M., 169
- Balog R., 453
Baouche S., 453
Basire M., 95
Bauschlicher C.W., 109
Bergin E., 123
Bernard J.P., 169
Berné O., 49, 223
Biennier L., 191
Bierbaum V.M., 427
Boersma C., 109
Bolatto A.D., 215
Bot C., 215
Boulanger F., 399
Bouwman J., 251
Bréchnignac Ph., 95, 355
- Calvo F., 95
Calzetti D., 133
Cami J., 109, 117
Candian A., 373
Carleton T.M., 209
Carpentier Y., 355
Cecchi-Pestellini C., 327
Chalyavi N., 355
Chandrasekaran V., 191
Cherchneff I., 177
Contreras C.S., 201
Cox N.L.J., 349
Cuppen H.M., 251
- Dartois E., 381
Destree J.D., 341
- Dopfer O., 103
Draine B.T., 29, 215
- Evans A., 407
- Féraud G., 355
Friha H., 355
- Galliano F., 43
Gehrz R.D., 407
Geppert W.D., 241
- Hamberg M., 241
Hammonds M., 373
Helton L.A., 407
Henning T., 293
Hewitt J., 169
Heymann F., 285
Hornekær L., 453
Hudgins D.M., 109
Huisken F., 293
Hunt L.K., 143
- Im M., 149
Ingalls J.G., 209
Ishihara D., 157
Izotov Y.I., 143
- Jäger C., 293
Joalland B., 223
Joblin C., 49, 123, 209,
223, 327, 399, 441, 447
Jørgensen B., 453
- Källberg A., 241
Kaminska M., 241
Kamp I., 271
Kaneda H., 55, 157
Kashperka I., 241
- Kim J.H., 149
Klippenstein S.J., 191
Kokkin D.L., 355
Krügel E., 285
- Larsson M., 241
Lee H.M., 149
Lee M.G., 149
Le Page V., 427
Linnartz H., 251
Luntz A.C., 453
- Mallocci G., 123, 327
Mattioda A.L., 109
Maurette M., 319
Mennella V., 393
Mirtschink A., 223
Montillaud J., 223, 447
Mouri A., 157
Mulas G., 123, 327
Mutschke H., 293
- Nilsson L., 453
- Ohsawa R., 55
Okada Y., 55
Omont A., 463
Onaka T., 55, 157, 399
Oomens J., 61
- Paál A., 241
Parneix P., 95
Pathak A., 373
Pauzat F., 75
Peeters E., 13, 109
Pilleri P., 49, 399
Pino T., 95, 355
Puerta Saborido G., 109

- Rapacioli M., 223, 441
Rauls E., 453
Reach W.T., 169
Rho J., 169
Ricca A., 109
Ricketts C.L., 201
Rowe B.R., 191
- Sabbah H., 191
Sakon I., 55, 157
Salama F., 201
Sánchez de Armas F., 109
Sandstrom K.M., 215
Sarre P.J., 373
Sauvage M., 143
Schmidt T.W., 355
Sellgren K., 209
- Semaniak J., 241
Shimonishi T., 55
Siebenmorgen R., 285
Simon A., 223, 441
Simonsson A., 241
Sims I.R., 191
Smith J.D.T., 209
Snow T.P., 341, 427
Spiegelman F., 223, 441
Stanimirovic S., 215
Stensgaard I., 453
- Talbi D., 223
Tanaka M., 55
Tappe A., 169
Thomas R.D., 241
Thrower J.D., 453
- Thuan T.X., 143
Tielens A.G.G.M., 3
Toublanc D., 447
Trippel S., 241
Troy T.P., 355
- Verstraete L., 415
Vigren E., 241
- Werner M.W., 209
Woods P.M., 235
Woodward C.E., 407
- Yamagishi M., 157
Yasuda A., 157
- Zhang M., 241
Zhaunerchyk V., 241

Astronomical Object Index

- | | | |
|---|--|---|
| <p>BD+303639 81</p> <p>3C 396 (G39.2-0.3) 173</p> <p>Ced 201 224</p> <p>Chi Cygni 186</p> <p>Cloverleaf galaxies 7, 8</p> <p>CRL 618 235, 237, 242</p> <p>CRL 2688 382</p>
<p>D7 Cru 409, 410</p> <p>DM Tau 281</p> <p>30 Dor 400, 401, 418</p>
<p>Galactic Center 384,
385</p>
<p>HD 10412 273</p> <p>HD 14154 276</p> <p>HD 34282 52</p> <p>HD 95881 273</p> <p>HD 97048 262, 263,
281</p> <p>HD 141569 281</p> <p>HD 163296 281</p> <p>HD 169142 281</p> <p>HD 200775 52</p>
<p>IRAS 11308 173,
174</p> <p>IRAS 08572+3915
385</p> <p>IRAS 13418-6243 120,
121</p> <p>IRAS 23133+6050 120,
121</p> | <p>IRC+10216 179, 184,
185, 186, 192, 194,
195-198, 236, 298,
362</p> <p>IRS 48 281</p>
<p>Jupiter 236</p>
<p>Kes 17 (G304.6+0.1)
173, 174</p> <p>Kes 69 (G21.8-0.6)
173, 174</p>
<p>Large Magellanic
Cloud 17, 20, 48,
158, 170, 173,
236, 351, 418</p> <p>Lick Hα 234 173, 174</p>
<p>M17 18, 58, 59, 400,
404</p> <p>M31 58, 351</p> <p>M33 351</p> <p>M81 163</p> <p>M82 17, 35, 52, 53,
161, 162, 163</p> <p>2MASX
J16205879+5425127
152</p> <p>Magellanic clouds 29,
30, 31, 40, 137, 162,
167, 216ff, 224, 236,
351, 403</p> <p>Milky Way 29, 30</p>
<p>N132D 170, 173</p> | <p>NGC 253 162</p> <p>NGC 628 138</p> <p>NGC 891 161</p> <p>NGC 1068 385</p> <p>NGC 1569 163</p> <p>NGC 2023 20, 210</p> <p>NGC 2974 164</p> <p>NGC 3962 164</p> <p>NGC 4536 15</p> <p>NGC 4589 165, 166</p> <p>NGC 5194 36</p> <p>NGC 5195 35, 36</p> <p>NGC 5529 161</p> <p>NGC 5713 36</p> <p>NGC 5866 36</p> <p>NGC 5907 161</p> <p>NGC 6946 36</p> <p>NGC 7023 50, 51, 85,
210-213, 224, 225,
228, 230, 233, 401,
403, 450</p> <p>NGC 7027 4, 6, 15, 20,
81, 382</p> <p>NGC 7331 36, 173, 174</p>
<p>Orion Bar 6, 15, 18,
20, 58, 127, 128,
400, 404</p>
<p>P/Encke 322</p> <p>P/IRAS 322</p> <p>Puppies A supernova
remnant 174, 175</p>
<p>QV Vul 408, 409, 411</p>
<p>RCW 29 160, 161</p> |
|---|--|---|

- Red Rectangle 120, 121, 126, 365
Rho Oph 224
RW Leo, see IRC+10216
- Saturn 236
Serpens molecular cloud 260
Small Magellanic Cloud 137, 215ff, 351
- SMP LMC 11 236
- Titan 236, 242, 247
Tycho supernova remnant 159
- V2361 Cyg 409
V2362 Cyg 409, 410
V Cygni 186
Vela supernova remnant 160
VII Zw 353 152
- V705 Cas 408, 409, 411
V842 Cen 408, 409, 411
V854 Cen 179, 186, 187
- W33A 255
Wild-2 322

Chemical Compound Index

- Acenaphthene (C₁₂H₁₀) 105, 106, 205, 206, 430
Acenaphthyl (c-C₁₂H₉) 365
Acenaphthylene (C₁₂H₁₈) 83, 105, 106, 206
Acetylene (C₂H₂) 184, 185, 192, 193, 195, 196, 201, 205, 206, 237, 238, 279, 280
Acridine (C₁₃H₉N) 429
Ammonia (NH₃) 192, 305, 306, 307
Anthracene (C₁₄H₁₀) 104-106, 253, 352, 356, 429, 430
Azulene (C₁₀H₈) 105, 106, 363, 429, 430

Benzene (C₆H₆) 104-106, 181, 182, 184, 186, 194, 227, 235, 236, 237, 238, 242ff, 279, 299, 363, 395, 430, 432
Benzo(g,h,i)perylene (C₂₂H₁₂) 253
Benzene, protonated (C₆H₇⁺) 66, 103ff, 430
Benzynes (C₆H₄) 193
1,3-butadienyl (l-C₄H₅) 182
1-buten-3-ynyl (l-C₃H₃) 182

Carbon chain 70
Carbondioxide (CO₂) 306, 323
Carbon monoxide (CO) 185, 186, 279, 305, 306, 307, 320
Carbon nanotube 113
Carbon sulfide (CS) 185, 192
CH₅⁺ 70
C₃ 299, 352, 365
C₃H₂ 355
C₃H₄ 238
C₄H 192
C₄H₃⁺ 237, 238
C₅ 352
C₆H⁻ 376
C₇₈H₂₆ 362, 363
C₉₆H₃₀ 362, 363
C₂₂₂H₄₂ 295, 358, 362

Chrysene (C₁₈H₁₂) 180
Circumcoronene (C₅₄H₁₈) 195, 443
Circumovalene (C₆₆H₂₀) 127, 128
CN 192
Coranulene (C₂₀H₁₀) 378
Coronene (C₂₄H₁₂) 61, 69, 104-106, 113, 114, 194, 195, 227, 233, 253, 357, 364, 376, 377, 395, 429, 430, 437, 448, 449, 450, 455, 457, 458
coronene, deprotonated (C₂₄H₁₁⁻) 376
coronene, protonated (C₂₄H₁₃⁺) 375
Cyclopropenyldiene (c-C₃H₂) 235

Diacetylene (C₄H₂) 235, 236
Dicarbon radical (C₂) 187, 299, 344, 365
Dihydronaphthalene (C₁₀H₁₀) 436
Diamondoids 383

Ethane (C₂H₆) 203, 204
Ethylene (C₂H₄) 203, 204
Ethylene oxide (c-C₂H₄O) 236
Ethyl-naphthalene (C₂₂H₁₈) 239
Ethylnyl radical (C₂H) 192, 193, 430

Fluoranthene (C₁₆H₁₀) 83, 84, 429, 430
Fluorene (C₁₃H₁₀) 356
Formaldehyde (H₂CO) 305
Formamide (NH₂CHO) 305
Formyl ion (HCO⁺) 238
Fullerene (C₆₀ and others) 209ff, 297, 301, 302, 351, 353, 383, 429, 431, 432
Fulvene (C₆H₆) 181

Graphene 113
Graphite 30

H₂ 244, 247, 276, 321, 322, 394, 419
HC₄H⁺ 352
HC₁₁N 305, 361
Hexa-peri-hexabenzocoronene (C₄₂H₁₈) 362, 374
Hydrogen cyanide (HCN) 185, 192, 320
Hydronaphthalene (C₁₀H₉) 365
Hydronaphthyl (C₁₀H₉) 431

- Hydronium (H_3O^+) 70
Hydroxyl (OH) 186, 430
- Indanyl (C_9H_9) 365
Indynyl (C_9H_7) 365
- Methane (CH_4) 203, 204, 279, 280, 306, 320
Methanol (CH_3OH) 306, 307
Methyl (CH_3) 430
Methylene (CH_2) 182
Methyldiyne (CH) 349, 353, 365, 430
Methyldiyne cation (CH^+) 349
Methylnaphthalene ($\text{C}_{11}\text{H}_{10}$) 205
- Naphthalene (C_{10}H_8) 64, 65, 66, 69, 81, 82, 86, 88, 104, 106, 126, 127, 203, 205, 231, 239, 352, 359, 363, 364, 428, 429, 430, 432, 449
Naphthalene, protonated ($\text{C}_{10}\text{H}_9^+$) 104-106
Naphthylmethyl (C_{11}H_9) 365
- Ovalene ($\text{C}_{32}\text{H}_{14}$) 362
- Pentacene ($\text{C}_{22}\text{H}_{14}$) 105, 106, 429
Perhydrocoronene ($\text{C}_{24}\text{H}_{36}$) 457
Perylene ($\text{C}_{20}\text{H}_{12}$) 105, 106, 363, 429
- Phenanthrene ($\text{C}_{14}\text{H}_{10}$) 63, 180, 429, 430
Phenyl (C_6H_5) 181, 186, 239
Phylpropargyl (C_9H_7) 365
Polyyne 182, 186, 187, 294, 301
Propargyl (C_3H_3) 181, 182, 186, 193, 238
Propynylidene (C_3H) 192
Pyrene ($\text{C}_{16}\text{H}_{10}$) 68, 69, 97, 98, 105, 106, 113, 127, 182, 193, 194, 195, 198, 252, 253, 312, 363, 428, 430, 432, 443
Pyrimidine ($\text{C}_4\text{H}_4\text{N}_2$) 309
- Quaterrylene ($\text{C}_{40}\text{H}_{20}$) 310
- Silicon monoxide (SiO) 186
Sulfur dioxide (SO_2) 323
- Terrylene ($\text{C}_{30}\text{H}_{16}$) 362
Tetracene ($\text{C}_{18}\text{H}_{12}$) 105, 106, 429
Triacetylene (C_6H_2) 235, 236
Trihydronaphthalene ($\text{C}_{10}\text{H}_{11}$) 365
Triphenylene ($\text{C}_{18}\text{H}_{12}$) 362, 429
- Uracil ($\text{C}_4\text{H}_2\text{N}_2\text{O}_2$) 309
- Vinylacetylene (C_4H_4) 182
- Water (H_2O) 186, 306, 307, 320, 323

Subject Index

- Absorption feature, aliphatics 384, 394
- Active Galactic Nuclei, see Galaxies, AGN
- AKARI 49ff, 143ff, 401
- Aliphatic hydrocarbons 23, 266, 384, 387, 395, 396, 402, 403, 408
- Amino acids 309
- Amorphous carbon 178, 184, 296, 382, 409, 411
- Amphiphilic compound 308
- Anharmonicity 68, 80, 86, 87, 95ff, 107, 119, 125, 444
- Anomalous radio emission 30, 33, 124, 274, 419
- Aromatic carbon 30, 329, 394, 408
- Astrobiology 305
- Asymptotic Giant Branch stars 46, 137, 178, 179, 180, 192, 194, 210, 211, 216, 218, 219, 236, 279, 295, 298, 382
- Astration 57
- Band gap 294, 295
- Bay region 24
- Blue Compact Dwarfs, see Galaxies, Blue Compact Dwarf
- Big Grains (BG) 173
- Canonical ensemble 88, 125, 127
- Carbide 192
- Carbonaceous material 31, 46, 47, 294ff
- Carbonate 323
- Carbon chain 70, 201, 352
- Carbon dust 294ff
- Carbon onion 297, 301, 302
- Carbon star, see Asymptotic Giant Branch stars
- Cavity ring-down spectroscopy 361
- C-C modes 18, 80, 82, 99, 107
- C-H modes 17, 18, 23, 66, 80, 82, 99, 105, 107
- Chemistry models 183-186, 237-239, 279, 433-435, 448-451
- Chemistry, non-equilibrium 185, 186
- Cloverleaf galaxies 7, 8
- Cluster, see also PAH, clusters
- Cluster, dissociation energy 227, 229
- Cluster, ionization energy 229
- Cluster, structure 227
- Coal 5, 297
- Combustion 178, 236, 298
- Comets 307, 312, 314, 315, 322
- Complexes, see PAH, complexes
- Cosmic infrared background 8
- Cosmic Rays 324, 325
- Database 84, 109ff, 122ff
- Dehydrogenation, see PAH, dehydrogenation
- Density Functional Theory (DFT) 79, 110, 118, 129, 225, 333, 442-444
- Density-of-states 96
- Depletion 30, 404
- Destruction, see PAH, destruction & dust, destruction
- Deuterium 57, 403
- Diamond 294, 301, 336
- Diamondoids 383
- Diffuse Interstellar Bands (DIBs) 5, 123, 187, 209, 328, 331, 341ff, 356, 373, 374
- Diffuse Interstellar Bands, families 343, 344
- Diffuse Interstellar Bands, polarization 351
- Diffuse Interstellar Bands, properties 343, 344
- Diffuse Interstellar Medium 19, 416-418
- Dimer, see PAH, dimer
- Dipole moment 378
- Dissociative recombination 242ff
- Drumhead modes 62, 111-113
- Dust 29ff, 160

- Dust, annealing 320
- Dust, carbon 294ff, 329, 381ff, 394ff
- Dust, destruction 170, 173
- Dust, evolution 46, 47, 170, 173, 415
- Dust, formation 177ff, 192, 197, 198, 201, 202, 212, 236, 365, 382, 408, 410
- Dust, H₂ formation 321, 322, 394, 395
- Dust, IR emission 30, 32, 34-36, 134
- Dust, lifecycle 381
- Dust, Lunar 319, 320
- Dust, models 29ff, 43ff, 285, 286, 331, 332
- Dust, nova 407ff
- Dust, shattering 158, 164, 216, 236
- Dust, size distribution 31, 32, 158, 164, 172, 173, 286, 415
- Dust, structure 294, 295-297
- Dust, surface reactions 238, 393ff
- Dust-to-gas ratio 45
- Dwarf galaxy, see galaxies, dwarf

- Electron affinity, see PAH, electron affinity
- Electron attachment 429
- Electron correlation 80
- Electronic spectroscopy 327ff, 355ff, 374ff
- Electron recombination 429, 430, 434, 437
- Elliptical galaxy, see Galaxies, elliptical
- Emission model, see PAH, emission model
- Extinction 29
- Extinction curve 328ff
- Extinction bump (2175Å) 30, 31, 39, 40, 328-330, 331, 332, 351, 362, 418
- Extinction, far-UV 331, 332, 334, 418
- Evolved star, see Asymptotic Giant Branch star

- Far-infrared absorption 111-113
- Fluorescence 359, 360, 365
- Free electron laser 67, 69
- Fullerene 209ff, 297, 301, 302, 351, 353, 383, 429, 431, 432

- FU Orionis star 261
- Fused silica 322

- Galactic halo 161, 161
- Galactic plane 57
- Galactic superwind 158, 161, 162, 163
- Galaxies 7, 19
- Galaxies, AGN 152, 164, 165, 384
- Galaxies, Blue Compact Dwarf 144
- Galaxies, dwarf 46, 137, 144, 163
- Galaxies, elliptical 164
- Galaxies, evolution 46, 152
- Galaxies, high redshift 133, 134
- Galaxies, LINERS 164, 165
- Galaxies, low metallicity 216
- Galaxies, star formation 134
- Galaxies, starburst 7, 30, 39, 143, 150, 152, 153, 387
- Galaxies, submillimeter 7
- Gas, cooling 417, 423
- Gas, ionization 418
- Gas phase spectroscopy 63
- Giant planets 236, 242
- Graphane 295
- Graphene 113, 180, 294, 295, 296, 299
- Graphite 30, 179, 294, 322, 330

- H₂ formation 244, 247, 276, 321, 322, 394, 395, 419, 435, 436
- HAC, see Hydrogenated amorphous Carbon
- HACA mechanism 182, 186, 187, 193
- Hartree-Fock method 79
- Herbig AeBe star 17, 19, 20, 260, 261, 262, 263, 264, 272, 273, 276, 278, 383
- Herschel Space Observatory 127
- Heteroatom substitution 22
- HII region 17, 19, 147
- Hot plasma 158, 163
- Hydrogenated Amorphous Carbon 4, 5, 193, 212, 296, 297, 384-387, 394, 403, 408

- Ice, interstellar 251, 280, 306
- Ice, photochemistry 307-312
- Ilmenite 321

- Infrared cirrus 5, 7
 Infrared emission spectroscopy 63, 68
 Infrared features, emission plateau 16
 Infrared features, peak position 18, 272
 Infrared features, profile 18, 85, 98, 99, 114, 119, 125, 128, 145, 265, 272, 387
 Infrared features, relative intensities 16-18, 144
 Infrared features, spatial variations 16-18
 Infrared features, substructure 15
 Infrared features, variations 16-18, 35, 37, 56, 57, 121, 442, 443
 Infrared Multiphoton Dissociation Spectroscopy 66, 67, 69, 105ff, 360, 361
 Infrared spectroscopy 61ff, 251ff
 Internal Conversion (IC) 366, 367
 Interplanetary dust particle 307, 314, 315
 InterSystem Crossing (ISC) 366, 367
 Ion irradiation 320, 321
 Ionization parameter 50
 Ion-neutral reactions 431, 437
 IRAS LRS 6
 ISOCAM 7
 ISO SWS 7
 Intramolecular Vibrational Redistribution 67, 96, 125, 356, 357, 366, 367
 Kerogen 322-325
 Laboratory method 61ff, 103ff, 203-205, 241ff, 251ff, 427ff, 357-361
 Magnesium Sulfide 184
 Matrix isolation spectroscopy 62, 69, 106, 107, 252-255
 Membrane 308
 Meteorites 179, 307, 309, 314, 315, 322, 323, 383, 384
 Messenger-atom spectroscopy 65, 66, 69, 361
 Metallicity 17, 18, 43, 135-137, 143, 163, 216
 Methylpolyynes 235
 Microcanonical ensemble 88, 97, 125, 127
 Micrometeorite 322, 323
 Molecular beam 68
 Molecular cloud 218
 Molecular ions 64-68
 Molecular structure, see PAH, molecular structure
 Nanodiamonds 336, 383
 Nanotubes 113, 294, 295
 Nova 407ff
 Olivine 321
 oop modes 17, 18, 23
 Origin of life 314, 315
 PAH, abundance 13, 43ff, 135, 217, 271, 273, 330, 416
 PAH, anion 429, 43§1, 437
 PAH, cation 122, 267
 PAH, charge balance 23, 24, 31, 34, 37
 PAH, chemical model 183-186, 237-239, 279, 433-435, 448-451
 PAH, chemistry 177ff, 191ff, 201ff, 235ff, 251ff, 278, 427ff
 PAH, chemical evolution 50
 PAH, chemical growth 181
 PAH, clusters 21, 22, 104, 182, 186, 194, 198, 266, 301, 388, 441ff
 PAH, complexes 22, 62, 67, 70, 82, 388, 441ff
 PAH, database 84, 109ff, 117ff
 PAH, dehydrogenation 23, 76, 80, 82, 97, 98, 99, 242, 275, 276, 279, 332, 333, 334, 351, 434, 436, 442, 448, 449, 450
 PAH, deprotonated 373
 PAH, destruction 43, 48, 137, 157ff, 170, 173, 216, 289
 PAH, deuteration 57-59, 82, 403
 PAH, dimer 183, 194, 195, 298, 301
 PAH, dissociation 67, 428, 434, 447, 449
 PAH, dissociation threshold 67
 PAH, dissociative recombination 242ff
 PAH, electron affinity 376, 421, 429
 PAH, electronic transition 124

- PAH, emission model 29ff, 88, 98, 99, 118, 119, 124, 125
- PAH, evolution 46, 157ff
- PAH, family 22
- PAH, far-infrared 109ff, 123ff
- PAH, formation 45, 137, 177ff, 191-194, 201, 216, 218, 236, 279, 295, 298, 299
- PAH, fragmentation 428
- PAH, H₂ formation 244, 247, 276, 419, 435, 436, 453ff
- PAH, hydrogenated 82
- PAH, hypothesis 3ff
- PAH, ice 251ff, 261, 309-311
- PAH, identification 111ff, 123ff, 341ff, 349ff
- PAH, infrared cascade 97
- PAH, infrared spectroscopy 61ff, 75ff, 109ff, 441ff
- PAH, ionization 23, 31, 34, 37, 50, 51, 164, 219, 275, 276, 344, 351, 353, 420, 428, 434, 448
- PAH, metal complex 22, 62, 67, 70, 82, 388, 441ff
- PAH, molecular structure 23, 24
- PAH, negative ion 82, 122,
- PAH, neutral 122
- PAH, nitrogen substitution 22, 62, 67, 110, 118, 122, 388
- PAH, photochemistry 253, 254, 289, 428, 447, 449
- PAH, photo-detachment 360
- PAH, photo-ionization 360
- PAH, photolysis 251
- PAH, protonated 67, 70, 103ff, 242, 245-247, 373, 432
- PAH, reaction 427ff, 449
- PAH, recombination 448
- PAH, rotational emission 33, 420
- PAH, rotational excitation 61, 127, 377
- PAH, sidegroup 309
- PAH, size 22, 23, 32, 34, 39, 146, 260, 267, 275
- PAH, spectral classes 18-20, 111, 121
- PAH, spectral variations 14, 16-20, 144, 442, 443
- PAH, sputtering 148, 158
- PAH, superhydrogenated 431, 435, 436, 448, 453ff
- PAH, temperature 32, 33
- PAH, UV feature (2175Å) 39, 327ff
- PAH, UV processing 20, 51
- PAH, UV spectrum 330ff
- PAH, vibrational modes 14, 15
- PAHfit 144
- PANHs 22, 62, 67
- Photochemistry, see PAH, photochemistry
- PhotoDissociation Region (PDR) 224, 228, 229, 266, 400, 422, 423, 448, 450, 457
- Photo-detachment 360, 429
- Photo-electric heating 280, 416
- Photo-ionization 360, 416, 421
- Planetary nebula 17, 19, 24, 193, 224, 266
- Plasma discharge 203-205
- Platt particles 329, 330
- Polarization 30, 357
- Post-AGB object 19, 20, 46, 193, 210, 236
- Prebiotic molecules 307-309, 314, 315
- Presolar grains 30, 179, 194
- Protoplanetary disk 238, 260, 261, 271
- Protoplanetary disk, models 278, 280
- Protoplanetary disk, structure 263-365, 273, 281, 287, 288
- Protoplanetary disk, sedimentation 263, 264, 278, 279, 281
- Pyrolysis 180
- Quantum chemistry 75ff, 333, 454
- Quenched Carbonaceous Compound (QCC) 5, 297
- Radiation damage 320
- Radiation field, hardness 17, 18, 36, 37, 39, 137, 138, 148, 164, 165, 262, 266, 289
- Radiation field, intensity 148, 172, 180, 281, 352
- Radiation field, interstellar 35, 39
- Radiative transfer 286
- Radical reactions 430

- RCrB stars 178, 179, 186, 210, 211, 213
- Reflection nebula 17, 19
- Rotational spectroscopy 124, 377, 378
- Ro-vibrational profile 127
- Sapphire 321
- Scattering 30, 170, 172
- SED, see Spectral Energy Distribution
- Shock 158, 170, 171, 183-186, 192, 194, 216, 298
- Silica 321
- Silicates 30, 31, 411
- Silicon carbide 184, 295
- Sodalime glass 322
- Spectral decomposition 21
- Spectral Energy Distribution 217, 273, 274, 287
- Spinning dust 419
- Spitzer IRS 7
- Sputtering 170, 172
- S Star 180, 181
- Starburst galaxy, see Galaxies, starburst
- Star formation history 45
- Star formation rate 14, 24, 133ff, 150
- Stellar ejecta 178, 192
- Stellar population model 45
- Stellar pulsation 185
- Stellar wind 178, 183-186, 195-197, 237
- Submillimeter galaxy, see Galaxies, submillimeter
- Sulfide 323
- Supernova 45, 137, 178, 179
- Supernova remnant 158, 169ff
- Tauc relation 297
- Temperature, radiative equilibrium 4
- Thermal approximation, see canonical ensemble
- Thermochemistry 433
- T-Tauri star 19, 20, 260, 261, 264, 272, 276, 289
- UIR bands 4, 6,7, 75
- UV absorption 350
- UV bump (2175Å) 30, 31, 39, 40, 328-330, 331, 332, 351, 356, 362, 418
- UV extinction 39, 345, 346, 418
- Very Small Grains (VSG) 18, 21, 50, 172, 173, 223ff, 266, 274, 275, 280, 403, 442
- Very Small Grains, evaporating 50, 228
- Vesicles 308
- Wolf Rayet stars 178, 179, 211
- X-ray 261, 410
- Zodiacal cloud 322

EAS Publications Series

- Volume 1** AGN in their Cosmic Environment (JENAM'99)
September 7-9, 1999 • 30 €
- Volume 2** GAIA: A European Space Project
May 14-18, 2001 • 60 €
- Volume 3** Star Formation and the Physics of Young Stars
(Summer School on Stellar Physics X)
September 18-22, 2000 • 40 €
- Volume 4** Infrared and Submillimeter Space Astronomy
June 11-13, 2001 • 65 €
- Volume 5** Radiative Transfer and Hydrodynamics in Astrophysics (GRETA)
November 28, 2001 • 25 €
- Volume 6** Observing with the VLT Interferometer (EuroWinter School)
February 3-8, 2002 • 47 €
- Volume 7** Final Stages of Stellar Evolution (Summer School on Stellar Physics XI)
September 16-21, 2001 • 52 €
- Volume 8** Astronomy with High Contrast Imaging
May 13-16, 2002 • 56 €
- Volume 9** Magnetism and Activity of the Sun and Stars
September 17-21, 2002 • 56 €
- Volume 10** Galactic & Stellar Dynamics (JENAM 2002)
September 3-6, 2002 • 36 €
- Volume 11** The Future Astronuclear Physics
August 20-22, 2003 • 47.50 €
- Volume 12** Astronomy with High Contrast Imaging II
October 6-10, 2003 • 56 €
- Volume 13** Evolution of Massive Stars, Mass Loss and Winds
(Summer School on Stellar Physics XII-XIII)
October 13-18, 2002 and October 6-10, 2003 • 50 €
- Volume 14** Dome C: Astronomy and Astrophysics Meeting
June 28-30, 2004 • 63 €
- Volume 15** Radio Astronomy from Karl Jansky to Microjansky (JENAM 2003)
August 27-30, 2003 • 72 €
- Volume 16** Teaching and Communicating Astronomy (JENAM 2004)
September 13-17, 2004 • 44 €

- Volume 17** Element Stratification in Stars: 40 Years of Atomic Diffusion Meeting in Honour of Georges Michaud
June 6-10, 2005 • 60 €
- Volume 18** Radiative Transfer and Applications to Very Large Telescopes (GRETA)
May 11-13, 2005 • 47 €
- Volume 19** Stars and Nuclei: A Tribute to Manuel Forestini
March 4-5, 2004 • 36 €
- Volume 20** Mass Profiles and Shapes of Cosmological Structures (IAP 2005)
July 4-9, 2005 • 47 €
- Volume 21** Stellar Fluid Dynamics and Numerical Simulations: From the Sun to Neutron Stars
September, 2004 and May, 2005 • 55 €
- Volume 22** Astronomy with High Contrast Imaging III: Instrumental Techniques, Modeling and data Processing
May 16-19, 2005 • 55 €
- Volume 23** Sky Polarisation at Far-Infrared to Radio Wavelengths: The Galactic Screen before the Cosmic Microwave Background
September 12-15, 2005 • 39 €
- Volume 24** CRAL-2006. Chemodynamics: From First Starts to Local Galaxies
July 10-14, 2006 • 47 €
- Volume 25** 1st ARENA Conference on “Large Astronomical Infrastructures at CONCORDIA, prospects and constraints for Antarctic Optical/IR Astronomy”
October 16-19, 2006 • 47 €
- Volume 26** Stellar Evolution and Seismic Tools for Asteroseismology
November 20-23, 2006 • 32 €
- Volume 27** The Third European Summer School on Experimental Nuclear Astrophysics
October 2-9, 2005 • 39 €
- Volume 28** Perspectives in Radiative Transfer and Interferometry
May 14-16, 2007 • 25 €
- Volume 29** Tidal Effects in stars, Planets and Disks
September 5-9, 2005 • 47 €
- Volume 30** Spanish Relativity Meeting – Encuentros Relativistas Españoles ERE2007
September 10-14, 2007 • 63 €
- Volume 31** Far-Infrared Workshop 2007
November 5-7, 2007 • 39 €

- Volume 32** Stellar Nucleosynthesis 50 Years after B²FH
December 4-8, 2006 • 63 €
- Volume 33** 2nd ARENA Conference on “The Astrophysical Science Cases at Dome C”
September 17-21, 2007 • 55 €
- Volume 34** Astronomy in the Submillimeter and Far Infrared Domains
with the Herschel Space Observatory
April 23-May 4, 2007 • 47 €
- Volume 35** Interstellar Dust from Astronomical Observations to Fundamental Studies
May 1st-5, 2006 • 47 €
- Volume 36** Dark Energy and Dark Matter
and Theories
July 7-11, 2008 • 55 €
- Volume 37** Astrophysics Detector Workshop 2008
November 17-20, 2008 • 63 €
- Volume 38** Nonlinear Pulsations and Hydrodynamics of Cepheids
July 9-13, 2007 • 32 €
- Volume 39** Stellar Magnetism
September 24-28, 2007 • 39 €
- Volume 40** 3rd ARENA Conference on “An Astronomical Observatory at CONCORDIA
(Dome C, Antarctica)”
May 11-15, 2009 • 87 €
- Volume 41** Physics and Astrophysics of Planetary Systems
February 18-29, 2008 • 95 €
- Volume 42** Extrasolar Planets in Multi-Body Systems: Theory and Observations
August 25-29, 2008 • 79 €
- Volume 43** Non-LTE Line Formation for Trace Elements in Stellar Atmospheres
July 30 – August 03, 2007 • 43 €
- Volume 44** JENAM 2008: Grand Challenges in Computational Astrophysics
September 8-11, 2008 • 26€
- Volume 45** GAIA: At the Frontiers of Astrometry
June 7-11, 2010 • 78€

Order directly to EDP Sciences

17 av. du Hoggar • BP. 112 • P.A. de Courtabœuf • 91944 Les Ulis Cedex A • France
Tel.: 33 (0)1 69 18 75 75 • Fax: 33 (0)1 69 86 06 78 • books@edpsciences.org



Assembling the puzzle of the Milky way

Le Grand-Bornand, France
April 17-22, 2011

<http://mw2011.obs-besancon.fr>

SOC :

Timothy Beers (USA)
James Binney (UK)
Horwig Dejonghe (Belgium)
Sofia Feltzing (Sweden)
Francisca Figueras (Spain)
Ken Freeman (Australia)
Masha Haywood (France)
Annika Helmi (Netherlands)
Daizuko Kawata (UK)
Xavier Luri (Spain)
Dante Minniti (Chile)
Daniel Pfenniger (Switzerland)
Alice Quillen (USA)
Céline Salyé (France)
Annie Robin (France)
Mathias Schulz (France)
Manuela Zoccali (Chile)

Topics

- ✧ Insight in early times
- ✧ Installation of the disc and dense regions
- ✧ In place and up-coming tools

IAU Symposium 279

Death of Massive stars: Supernovae & Gamma-Ray Bursts

Nikko, Japan, 18-22 April 2011

<http://www.hp.phys.titech.ac.jp/iau279/>

mail: contact_iau279@hp.phys.titech.ac.jp

Topics:

- Progress in our understanding of Core Collapse (CC) SNe & GRBs
- GRB-SNe connection
- Environments of CCSNe & GRBs
- Progenitors of CCSNe & GRBs
- CCSN & GRB mechanism and subsequent evolution
- CCSNe & GRBs as cosmological tools
- Explosive Nucleosynthesis in CCSNe and GRBs

SOCs:

Peter Roming (Southwest Research Inst., USA; chair)
Nobuyuki Kawai (Titech., Japan; chair)
Elena Pian (SNS Pisa, Italy; chair)
Zi-Gao Dai (Nanjing U., China)
Massimo Della Valle (INAF, Italy)
Johan Fynbo (Univ. Copenhagen, Denmark)
Neil Gehrels (NASA GSFC, USA)
Sheila McBreen (U. Coll. Dublin, Ireland)
Maryam Modjaz (UC Berkeley, UK)
Ehud Nakar (Tel Aviv U., Israel)
Ken'ichi Nomoto (IPMU, Japan)
Paul O'Brien (U. Leicester, UK)
Sandra Savaglio (MPE, Germany)
Brian Schmidt (Australian National U., Australia)
Stephen Smartt (Queen's U. Belfast, UK)
Alicia Soderberg (CfA, USA)
Shoichi Yamada (Waseda U., Japan)

LOCs:

Keiichi Maeda (IPMU; chair)
Katsuaki Asano (Tokyo Tech.)
Aya Bamba (DIAS/ISAS)
Kei Kotake (NAOJ)
Takeo Minezaki (IoA, Univ. Tokyo)
Takuya Ohkawa (Tokyo Tech.)
Toru Tamagawa (RIKEN)
Masaomi Tanaka (IPMU)
Yoichi Yatsu (Tokyo Tech.)



Exploring Strange New Worlds: From Giant Planets to Super Earths

May 1 -6, 2011
Flagstaff, Arizona

Planet Formation and Disks
What Can We Learn from Our Solar System
Characterization of Exoplanets using JWST
Architecture of Planetary Systems
Planets and Non-Solar Type Stars

<http://nexsci.caltech.edu/conferences/Flagstaff>

Confirmed Speakers:

J. C. Augereau, T. Barman, J. Bean, A. Boccaletti, A. Boss, M. Brown, M. Clampin, D. Deming, S. Dodson-Robinson, R. Doyon, K. Enya, D. Fischer, M. Fridlund, A. Gould, T. Greene, T. Guillot, O. Guyon, H. Hammel, J. Johnson, L. Kaltenegger, D. Kirkpatrick, J. Krist, H. Knutson, H. Levison, G. Marcy, M. Meyer, C. Mordasini, R. Murray-Clay, D. Pourbaix, I. N. Reid, D. Rouan, S. Seager, A. Sivaramakrishnan, K. Su, M. Tamara, G. Tinetti, W. Traub, D. Valencia, J. Valenti, E. van Dishoek,



BLUE DOTS

LOCKHEED MARTIN

NORTHROP GRUMMAN

Images: Xiaohong J. Shan (Milky Way) / Tenji (Grand Canyon; distributed under the GNU Free Documentation License)